

Multi-Component Metallo-Supramolecular Assemblies

DISSERTATION

zur Erlangung des Grades eines Doktors
der Naturwissenschaften

vorgelegt von

Venkateshwarlu Kalsani, M.Sc

geb. am "10-06-1973" in "Gudur, A.P, India"

eingereicht beim Fachbereich 8

der Universität Siegen

Siegen 2005

Dedicated to my Parents

Gutachter:

1. Professor Dr. Michael Schmittel
2. Professor Dr. Heiko Ihmels
3. Professor Dr. Hans-Jörg Deiseroth

Eingereicht am: 06th April 2005
Tag der mündlichen Prüfung: 13th May 2005

urn:nbn:de:hbz:467-2242

Acknowledgements

First I wish to thank my supervisor Professor Michael Schmittel, Department of Chemistry, University of Siegen, Germany, for giving me the opportunity to carry out this research at his laboratory and for his constant supervision and guidance throughout my stay. He always had time for discussions during this work and supported me with his immense theoretical and practical knowledge. His extensive knowledge in many fields and his patience in helping me understand have not only driven me to complete my research projects, but also fueled my passion for pursuing future scientific endeavors in a variety of subjects. I fondly remember his kind hospitality and the time spent with Elias Schmittel and Elisabeth Schmittel. I also extend my thanks to Mrs. Gabriele Schmittel for her hospitality as well.

I am very grateful to all my collaborators during my doctoral studies at the University of Siegen. I wish to thank Professor Dieter Fenske (University of Karlsruhe), Dr. Marc Schlosser, Professor Hans-Jörg Deiseroth (University of Siegen), Professor Martin U. Schmidt (Johann Wolfgang Goethe-University, Frankfurt) for their collaboration with crystal structure measurements. In particular, special thanks goes to Dr. Jan W. Bats (Johann Wolfgang Goethe-University, Frankfurt) for his very fruitful and fast collaboration on X-ray structures. I also wish to thank Dr. Frank Jäckel, Professor Jürgen P. Rabe (Humboldt University of Berlin, Berlin) for their collaboration with the STM imaging of oligophenanthrolines. I thank Professor Nicola Armaroli (Institute for Organic Synthesis and Photoreactivity, Bologna, Italy) for his cooperation in studying the photophysical properties of copper(I)/Zn(II) based supramolecular aggregates.

I wish to thank Professor Heiko Ihmels for allowing me to access the fluorescence spectrometer. I also thank Professor Karl-Heinz Drexhage for his help with fluorescence measurements.

I am very grateful to Frau Ulrike Utsch for her timely help during my stay at the University of Siegen. I am indebted to her patience for always taking the time to help with my documentation procedures. I wish to thank Dr. Wolfgang Demuth for his technical expertise with a variety of instruments and also, helping with my Ph.D thesis writing. I extend my thanks to Heinrich Bodenstedt for his meticulous analysis of elements and osmometry

Acknowledgements

measurements. I feel very fortunate to be able to work with people who have such a helping nature.

Furthermore, I would like to extend my thanks to the members of our group, Dr. Guido Morbach, Dr. Andreas Haeuseler, Dr. Michael Maywald, Dr. Jens-Peter Steffen, Wolfgang Henn, Dr. Mukul Lal, Dr. Thomas Koy, Ravuri Kishore, Vavilala Chandrasekar, Atul Mahajan, Emin Cinar, Rochus Breuer, Hengwei Lin for their help and friendship during my stay at Siegen, Germany. I thank Andreas Wiegrefe, Christoph Michel and Bice He for their fruitful cooperation. I enjoyed the good working climate and the fun during our Monday presentations followed by coffeebreaks. Also, I wish to thank Dr. Nampally S. Chary and Dr. Annie Marquis, Strasbourg, France for their kind hospitality and help.

I wish to thank my parents and sister for their never-ending love and support. I wish to extend my thanks to Nadia for her friendship during my Ph.D.

On a final note, I want to give credit to the financial support from the Deutsche Forschungsgemeinschaft (DFG) that has made my research possible.

Table of Contents

I	Introduction	1-2
II	State of Knowledge Taken in part from Functional, Discrete, Nanoscale Supramolecular Assemblies <i>M. Schmittel, V. Kalsani, Top. Curr. Chem. 2005, 245, 1-53</i>	3-41
III	The HETPHEN Approach	42-58
III-1	The HETPHEN Approach: Interplay of π - π Interactions, Solvent Association, and Steric Hindrance <i>M. Schmittel, A. Ganz, M. Schlosser, H. J. Deiseroth, S. X. Liu, V. Kalsani, 2005, manuscript ready for submission</i>	59-96
III-2	Towards a Kinetically Stable Bisphenanthroline Copper Complex <i>V. Kalsani, M. Schmittel, A. Listorti, G. Accorsi, N. Armaroli. Inorg. Chem. 2006, 45, 2061-2067.</i>	97-113
IV	Synthesis, Structures and Surface Patterning of Bisphenanthrolines. Versatile Precursors For Heteroleptic/Heterometallic Supramolecular Rack and Grids	114-132
IV-1	Synthesis of Soluble, linear BisPhenanthrolines For the construction of Heteroleptic Nanogrids and Nanoboxes <i>M. Schmittel, C. Michel, A. Wiegrefe, V. Kalsani, Synthesis 2001, 1561-1567</i>	133-149
IV-2	Rigid Bisphenanthrolines: Their Synthesis, Structure and Self-Assembly at the Solid-Liquid Interface and in Solution <i>M. Schmittel, V. Kalsani, F. Jäckel, J. P. Rabe, D. Fenske, J. W. Bats. Eur. J. Org. Chem. 2006, in early view.</i>	150-173
IV-3	Supramolecular Copper Phenanthroline Racks: Structures, Mechanistic Insight and Dynamic Nature <i>V. Kalsani, H. Bodenstedt, D. Fenske, M. Schmittel, Eur. J. Inorg. Chem. 2005, 1841-1849.</i>	174-192
IV-4	Self-Assembly of Heteroleptic [2x2] and [2x3] Nanogrids <i>M. Schmittel, V. Kalsani, D. Fenske, A. Wiegrefe, Chem. Commun. 2004, 490-491</i>	193-207
IV-5	Metal-Driven and Covalent Fabrication of Supramolecular Grids from Racks: A Convergent Approach to Heterometallic and Heteroleptic Nanostructures <i>M. Schmittel, V. Kalsani, J. W. Bats, Inorg. Chem. 2005, 44, 4115-4117.</i>	208-227
V	Multicomponent Aggregates of a Rigid Exotopic Bisphenanthroline Macrocycle and their Characterization in Solution and at Surfaces	228-240
V-1	Synthesis and Self-Assembly of a Rigid Exotopic Bisphenanthroline Macrocycle: Surface Patterning and a Supramolecular Nanobasket <i>V. Kalsani, H. Ammon, F. Jäckel, J. P. Rabe, M. Schmittel, Chem. Eur. J. 2004, 10, 5481-5492</i>	241-269
V-2	Quantitative Formation and Clean Metal Exchange Processes of Large Void (~5000 Å ³) Nanobox Structures <i>M. Schmittel, H. Ammon, V. Kalsani, A. Wiegrefe, C. Michel, Chem. Commun. 2002, 2566-2567</i>	270-276
V-3	Heteroleptic Bisphenanthroline Metallo-Nanoscaffolds – A Model Case for the Solution State Characterisation of Supramolecular Nano Edifices <i>M. Schmittel, V. Kalsani, C. Michel, A. Wiegrefe, 2005, manuscript ready for submission</i>	277-303

V-4	Simple and Supramolecular Copper Complexes as Precursors in the HRTEM Induced Formation of Crystalline Copper Nanoparticles <i>M. Schmittel, V. Kalsani, L. Kienle, Chem. Commun. 2004, 1534-1535</i>	304-309
VI	The HETTAP Approach	310-326
VI-1	The HETTAP Approach: Self-Assembly and Metal Ion Sensing of Dumbbell-Shaped Molecules and A Clip Molecule <i>M. Schmittel, V. Kalsani, J. W. Bats, 2005, manuscript ready for submission</i>	327-342
VI-2	A Facile Approach to Dynamic and Fluorescent Nanoscale Phenanthroline/Terpyridine Zinc(II) Ladders <i>M. Schmittel, V. Kalsani, R. S. K. Kishore, J. W. Bats, H. Cölfen, 2005, J. Am. Chem. Soc. 2005, 127, 11544-11545</i>	343-351
VI-3	Zn(II)/Ag(I) Nanoscale 2D Ladders Containing Pyrene Units <i>M. Schmittel, V. Kalsani, B. He, J. W. Bats, 2005, manuscript ready for submission</i>	352-364
VI-4	A Functional Nanoscale Ladder Containing Ferrocene Units <i>M. Schmittel, V. Kalsani, B. He, J. W. Bats, 2005, manuscript ready for submission</i>	365-375
VII	Crystal Structure Data	376-436
VIII	Summary	437-441
IX	Resume	442-444

CHAPTER 1

Introduction:

Supramolecular chemistry is one of the actively pursued areas of research in chemistry. The concepts and the term of “supramolecular chemistry” were introduced in 1978 by Lehn¹ and it was defined in words, “just as there is a field of molecular chemistry based on the covalent bond, there is a field of supramolecular chemistry, the chemistry of molecular assemblies and of the intermolecular bond”.

Over decades covalent chemistry has produced countless molecules which are capable of exhibiting interesting functions. However, with increasing scale and complexity of target molecules increases, the step-wise construction (covalent) of large, discrete, super-molecules becomes increasingly difficult and often low-yielding. The self-assembly of molecular synthons to large multicomponent supramolecular systems, capable of performing specific functions is one of the basic formula for success in biology.² Recently, major chemistry research activities are devoted to the development of chemical tools for the self-assembly of structurally rich supramolecular arrays.³ Several strategies, such as the mutual complementary approach (based on hydrogen bonded assemblies), directional bonding, weak-link and HETPHEN approaches (based on metal coordination chemistry) have been designed to fabricate self-assembled architectures using bio-inspired noncovalent interactions, such as hydrogen bonds, π - π stacking, donor-acceptor interactions, and metal coordination chemistry (see second chapter). As a result, supramolecular chemistry was able to produce spectacular architectures possessing various functionalities.

As witnessed by the available supramolecular tools (see second chapter), it is quiet evident that very few general strategies are at hand when compared to the covalent chemistry and general strategies for the construction of multitopic aggregation is at rudimentary levels when compared to biologically occurring assemblies (*ex. cell*). It is therefore, highly important to address these general strategies to construct a defined supramolecular aggregates possessing interesting functionalities. Among the all supramolecular aggregates produced to date the homoleptic (one ligand-assemblies) aggregates are the most common ones and has been a choice of strategy for long time. It is largely because of the complexity arising from the competing homo-ligand assemblies and therefore, it is a difficult task to control hetero-ligand aggregation. However, few heteroleptic aggregates are also reported, which are very unique not only in the structural sense but also in the sense of having access to multiple functionalities containing self-assembled arrays (see second chapter).

In view of these developments, the aim of this thesis is to develop supramolecular tools for multicomponent aggregation and study the properties of the resulting assemblies. This thesis is divided into eight chapters: After this brief introduction, the second chapter will summarize the state of knowledge in the area of supramolecular chemistry. In the third chapter the HETPHEN (**h**eteroleptic bis**p**henanthroline complexes) concept is presented. The fourth chapter addresses the synthesis of bisphenanthrolines and their self-assembly to multicomponent rack and grid motifs. The fifth chapter deals with nanoscaffold structures and their characterization by several spectroscopic means. The generation of copper nanoparticles is also included in this chapter. The sixth chapter will present the HETTAP (**h**eteroleptic **t**erpyridine **a**nd **p**henanthroline) concept and photo and electroactive supramolecular ladder structures synthesized there from. The seventh chapter is dedicated to single crystal structures. The discussion of structures which have already been published will be kept short. The eighth chapter will summarize the results and provide outlooks. Each of these chapters will contain a brief introduction (highlights of the work) that is followed by subchapters (termed as Supp) being written as manuscripts. Hence, all experimental data will be available in the subchapters (Supp).

-
- ¹ J.-M. Lehn, Cryptates: inclusion complexes of macropolycyclic receptor molecules, *Pure. Appl. Chem.* **1978**, *50*, 871-892.
- ² J. E. Vaener, Ed. Self-Assembly Architecture; Alan R. Liss, New York, **1988**.
- ³ a) reviews: M. Schmittel, V. Kalsani, Functional, Discrete, Nanoscale Supramolecular Assemblies, *Topics in Current Chemistry*, **2005**, *245*, 1-54. b) B. J. Holliday, C. A. Mirkin, Strategies for the Construction of Supramolecular Compounds through Coordination Chemistry, *Angew. Chem. Int. Ed.* **2001**, *40*, 2022-2043. c) L. J. Prins, D. N. Reinhoudt, P. Timmerman, Noncovalent Synthesis Using Hydrogen Bonding, *Angew. Chem. Int. Ed.* **2001**, *40*, 2382-2426.

CHAPTER 2**State of Knowledge**

In this chapter recent developments in the area of supramolecular chemistry will be highlighted.¹

2.1 Introduction	4
2.2 Supramolecular Nanoscale Structures	4
2.3 Hydrogen Bond Driven Supramolecular Nanoscale Assemblies.....	5
2.3.1 2D and 3D Motifs	6
2.4 Coordination Driven Supramolecular Nanoscale Assemblies	9
2.4.1 Design	9
2.4.2 Nanoscale Self-Assemblies Built Using Monodentate Ligands.....	9
2.4.2.1 2D Nanoscaffolds.....	10
2.4.2.2 3D Nanoscale Architectures (Polyhedra)	12
2.4.3 Nanoscale Self-Assemblies Built from Bidentate and Tridentate Ligands.....	14
2.4.3.1. 2D Assemblies (Homo and Heteroleptic aggregation).....	15
2.4.3.2. 3D (Heteroleptic) assemblies	16
2.5 Functional Devices.....	18
2.5.1 Supramolecular Catalysis	18
2.5.2 Photoactive Assemblies.....	22
2.5.3 Molecular Recognition.....	25
2.5.4 Switching the Molecular Shape of Assemblies	29
2.5.5 Electroactive and Magnetic Assemblies.....	32
2.6 Conclusions	35
2.7 References	36

Comments:

For clarity purposes in schemes several nanostructures have been depicted without unnecessary alkyl or other groups.

2.1 Introduction

For billions of years, nature has capitalized on self-assembly strategies based on non-covalent interactions, such as hydrogen bonds, salt bridges, solvation forces and even metal coordination, to organise biological systems. Hence, such forces had been exploited long before the terms "supramolecular chemistry" and "self-assembly" were introduced.² It is well known that the protein function largely depends on the global conformation and the folding process is governed by a multitude of reversible non-covalent interactions.³ The folding is guided by several elements of control, such as recognition and self-sorting, which lead the way to the desired shape (correct folding). By learning these lessons from biology, chemists are now starting to compose highly complex chemical systems from components that interact *via* noncovalent intermolecular forces.

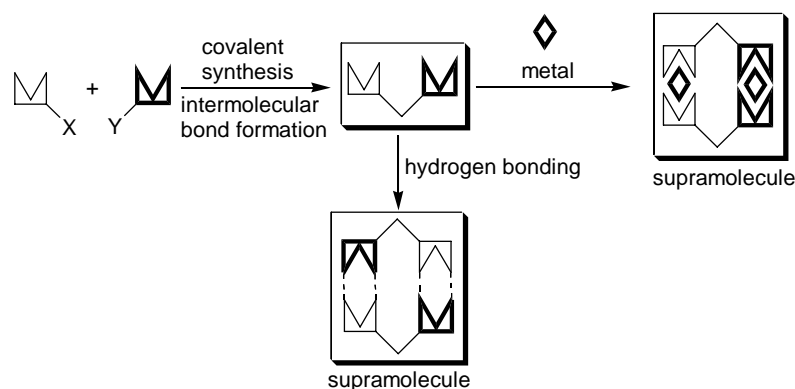
The *de-novo* preparation of complex and large structures relying on covalent synthesis is often a very difficult and time consuming chore. In contrast, supramolecular chemistry offers a convergent entrée to the creation of nanoscale systems for a wide range of applications.

The construction of nanostructures is of great interest not only because of their biological archetypes, but also because of their potential to revolutionize novel technologies such as the development of molecular level devices. Over the last few decades numerous supramolecular aggregates have been studied thus revealing the principles that guide the needed critical balance of weak interactions. As described by Lehn the supramolecular architecture is a sort of molecular sociology in which non-covalent interactions and the individual properties of the molecules define the intermolecular bond. In this article, we highlight the most often used synthetic strategies to nanoscale assemblies (> 2 nm) and their chemical and physical properties in view of their potential applications as molecular devices. The vast area of inorganic and organic/inorganic cluster chemistry with strong M–M or M–ligand bonds will not be covered here, although also nanoscopic aggregates have equally been realised by such strategy.^{4,5,6}

2.2 Supramolecular Nanoscale Structures

The self-assembly process driven by non-covalent interactions that are prominent in biological systems (electrostatic, hydrogen bonding, π - π stacking, etc.) offers a great tool to

engineer nanoscale structures. Using elaborated non-covalent protocols several groups have created sparkling architectures, such as *e.g.* rosette aggregates,^{7,8} self-assembled capsules,⁹ and ordered hydrogen bonded arrays.^{7,10}



Scheme 2-1

Formation of nanoscale supramolecular arrays was also achieved using coordination chemistry. This protocol has been adopted by several groups to yield spectacular discrete architectures, such as grids, squares, nanoboxes, ring-in-ring structures, catenanes and rotaxanes, etc., that will be discussed below.

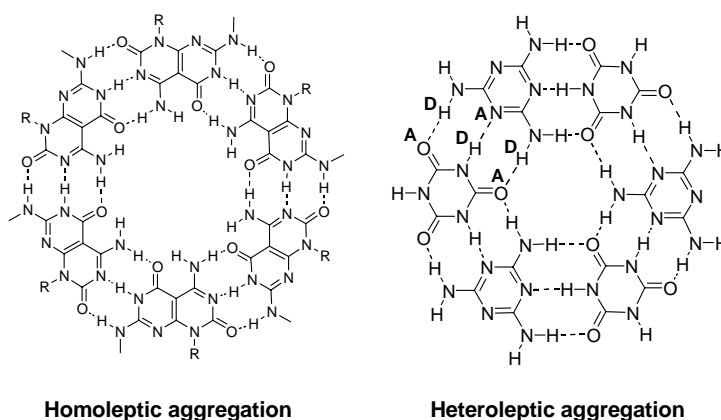
A detailed analysis of synthetic protocols leading to discrete nanoscopic self-assembled systems (>2 nm) reveals clearly that two motifs dominate the scene: hydrogen bonding and metal coordination driven approaches. This review will therefore highlight some recent developments in this field including a discussion about functional devices.

2.3 Hydrogen Bond Driven Supramolecular Nanoscale Assemblies

As indicated above, hydrogen bonding motifs play an important role in biological systems, which adds a bio-mimetic flavour to all artificial hydrogen bonded 2D and 3D assemblies. A thorough analysis of the size of known aggregates reveals that relatively few discrete hydrogen bonded assemblies are known with dimension above 2 nm, to which this article is restricted.

2.3.1 2D and 3D Motifs

All larger (> 2 nm) hydrogen bonded assemblies are based on a multitude of hydrogen bonding interaction in order to compensate entropic losses by enthalpic gains. Sessler *et al.* elaborated the assembly of artificial dinucleotide modules to yield homoleptic 2D-scaffolds.¹¹ The stability of these homodimers is improved with respect to their monomer units when a rigid linker is used. A later report by the same group further illustrated the importance of structural rigidity and cooperativity.¹² Along those lines Fenniri *et al.* utilised heteroaromatic bases possessing both the Watson-Crick **DDA** pattern of guanine (**A** = acceptor, **D** = donor) and **AAD** design of cytosine to mastermind homoleptic rosette aggregates in water (Scheme 2-2, left). These homoleptic rosette-assemblies further aggregate into nanotubes through hierarchical self-assembly.^{8a} Analogously, the **ADA** H-bonding arrays of isocyanuric acid are mutually complementary with **DAD** arrays of melamine. A detailed study of these interactions initiated the engineering of nanoscale scaffolds based on these two building blocks.¹³ Hence, the combination of isocyanuric acid and melamine led to several sparkling architectures such as 2D and 3D rosette motifs (Scheme 2-2, right). Timmerman, Reinhoudt *et al.* reported on the self assembly of a [2x2] heteroleptic grid architecture through the cooperative formation of 24 hydrogen bonds.¹⁴

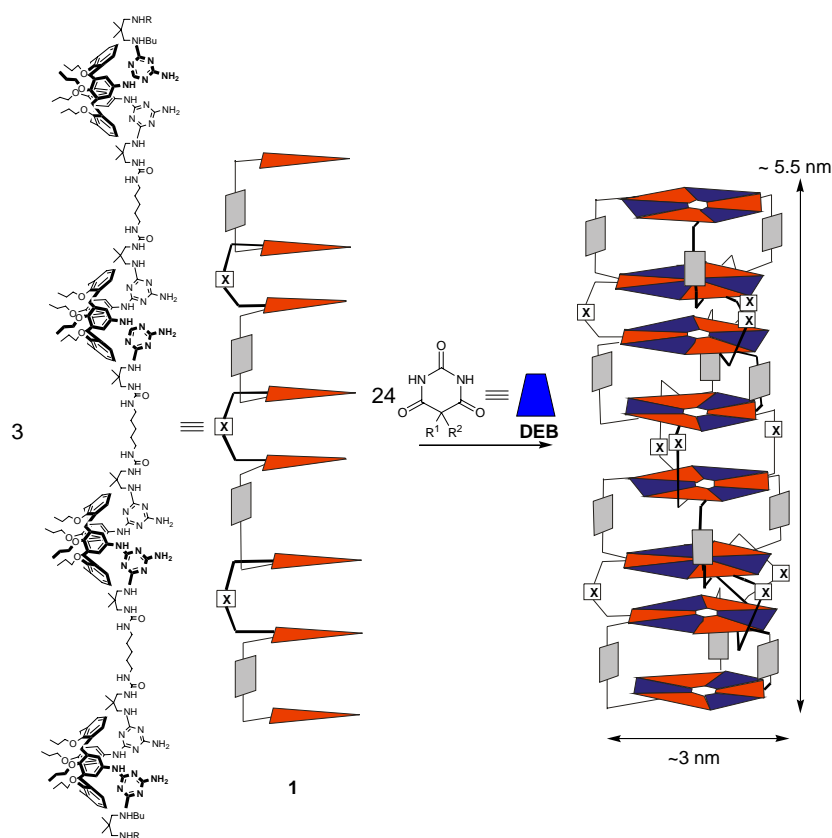


Scheme 2-2. Strategies used to construct homoleptic and heteroleptic 2D-rosette aggregates.^{7, 8a}

Whitesides *et al.* developed two different approaches to nanoscale 2D and 3D rosette motifs: peripheral crowding¹⁵ and covalent preorganization.¹⁶ In the first approach, due to the increasing size of substituents at the melamine unit the formation of 2D rosettes over linear tapes is favoured as repulsions between substituents are reduced in rosette structures. Whereas, the covalent preorganization approach uses covalently linked melamine or cyanurate units thus generating a much more favourable entropic situation for rosette

scaffolds. The latter approach was further explored to create nanoscaffolds with internal cavities.¹⁷ A combination of the two approaches was used to obtain two extremely stable rosette assemblies.¹⁸ Calix[4]arene linked melamine and cyanurate units were used by Reinhoudt *et al.* to build a family of 3D-double-rosette assemblies.¹⁹ Their equilibria were investigated and their growth on gold surface was studied.²⁰

In a remarkable study by the same group, the quantitative formation of a 15-component 3D-tetra-rosette nanoscale assembly held together by 72 hydrogen bonds was demonstrated.²¹ Self-sorting, well known from metallosupramolecular aggregates,²² is an important phenomenon in these assemblies. Spontaneous generation of discrete nanoscale motifs was further explored to generate 3D-heteroleptic hexa-²³ and octa-rosette assemblies (Scheme 2-3).²⁴ One equivalent of the octamelamine ligand **1** forms well-defined assemblies (**1**)₃(**DEB**)₂₄ with eight equivalents of 5,5-diethylbarbituric acid (**DEB**). The spontaneous formation of this 27 component octa-rosette structure (~20 kDa) demonstrates the huge potential of this approach in engineering nanoscale 3D-heteroleptic aggregates. The resultant assemblies are expected to have a height of 5.5 nm, which makes them alike in size to DNA oligomers used for conductivity measurements.²⁵



Scheme 2-3 Hydrogen bond self-assembly of 27 components leading to a heteroleptic rosette aggregate.

Capsule assemblies have received special attention due to their high potential in the field of host-guest chemistry and catalysis (*vide infra*). As a result of the difficulties in constructing capsules by covalent synthesis²⁶ several groups have explored the fabrication of capsules relying on non-covalent synthesis. Most of the self-assembled capsules reported to date are homoleptic in nature^{9a,c,27} with only a couple of heteroleptic capsules being known. As shown in Figure 2-1 six strategies to capsule-like assemblies are explored. While calix[4]arenes, resorcinarenes and cavitands are amongst the most extensively used building blocks, homoleptic capsule formation from calix[4]arenes is hampered due to its high conformational flexibility. Calix[4]arenes with four urea moieties at the upper rim, that allow for side way directed urea hydrogen bonds, form well defined homoleptic capsules in solution (Figure 2-1, **d**).²⁸ A similar strategy was used to construct homodimers from cyclocholates,²⁹ cyclotrimeratrylenes³⁰ and a heterodimer from complementary cyclodextrin and porphyrin moieties.³¹ Rebek *et al.* prepared homoleptic capsules of tennis ball shape using the hydrogen bonding properties of glycoluril moieties (Figure 2-1, **b** and **f**).³² A like strategy was explored to construct capsules using glycoluril and sulfamides as complementary hydrogen bonding blocks (Figure 2-1, **a**) and self-assembly of the tetramide block (Figure 2-1, **c**). For heteroleptic hydrogen bonded capsules the versatile approach **d** (Figure 2-1) was used by Reinhoudt,³³ Rebek³⁴ and others³⁵. To construct heteroleptic capsules two cavitands with carboxylic acid groups serve as end-caps and four 2-aminopyridine molecules act as connectors.³⁶ These heteroleptic capsules are of particular interest because one can readily introduce multiple functionalities. All these capsules range from ~ 2-3 nm in size.

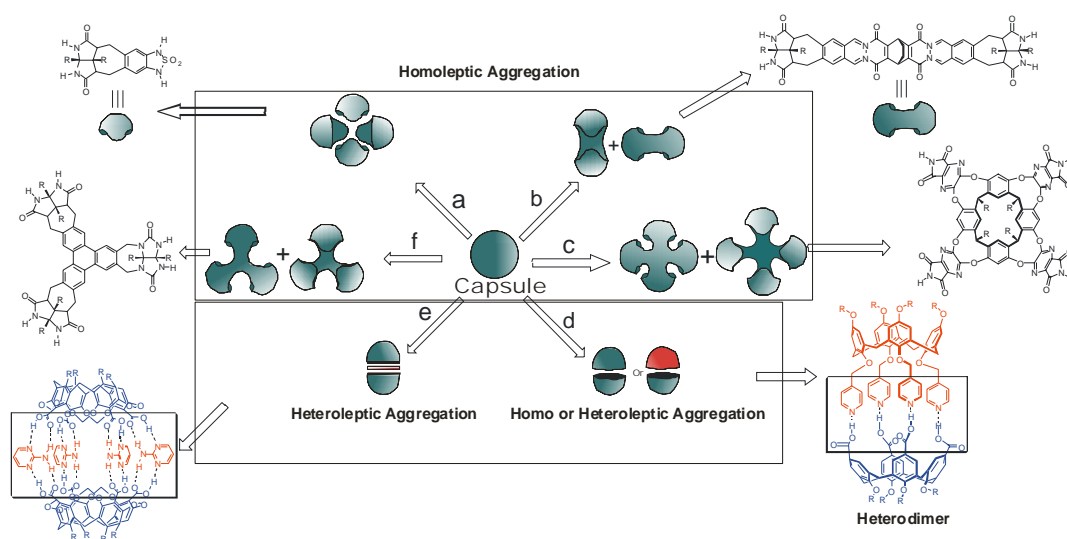
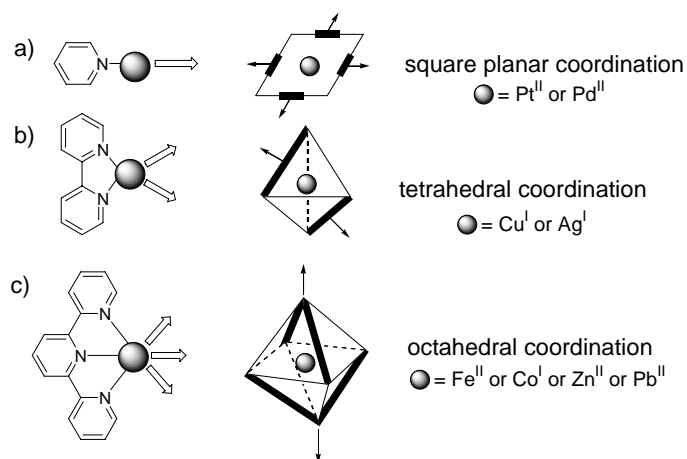


Figure 2-1 Strategies used to construct homo and heteroleptic capsule like nanoscale assemblies.²⁸⁻³⁶

2.4 Coordination Driven Supramolecular Nanoscale Assemblies

2.4.1 Design

The metal coordination geometry and the information stored in the ligands should provide the construction manual for any self-assembly. Therefore, the selection of appropriate metal ion(s) and ligand(s) is very crucial, as witnessed in a multitude of publications, reviews, and books. In this chapter, we will concentrate on nanoscale architectures built from monodentate (pyridine), bidentate (bipyridine, phenanthroline, catechol) and tridentate (terpyridines) ligands. The dentate term used here is purely referred to describe the interaction of the ligand with one single coordination centre. As depicted in a simplified way in Scheme 2-4 most literature-known self-assemblies are constructed about Pd^{II} or Pt^{II} ions in a square planar arrangement using monodentate ligands, at Cu^I or Ag^I ions in a tetrahedral fashion making use of bidentate ligands, and at Co^{II}/Cu^{II}/Fe^{II}/Zn^{II}/Hg^{II} in an octahedral grouping by employing terpyridine chelating motifs.

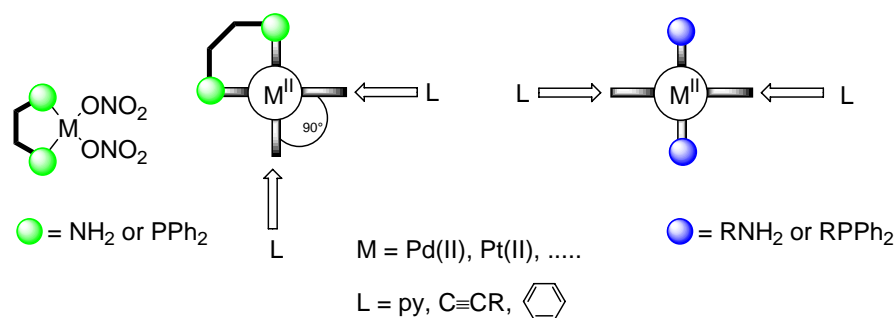


Scheme 2-4 Cartoon representation of preferred coordination geometry of a) monodentate, b) bidentate, and c) tridentate ligands.

2.4.2 Nanoscale Self-Assemblies Built Using Monodentate Ligands

Stang,³⁷ Fujita³⁸ and Hupp³⁹ have shown the utility of monodentate ligands in developing nanoscale supramolecular architectures. As emphasised by Stang^{37a} the important factors to be

considered are the coordination angles at the metal-ion equipped with a kinetically inert ligand and at the incoming labile multitopic ligand. This design is usually termed as directional bonding approach. Metal ions can readily provide free *cis* (90°) or *trans* coordination sites depending on the inert ligand. Therefore, the careful selection and design of labile ligand(s) is a prerequisite for a rational approach to any desired supramolecular assembly.

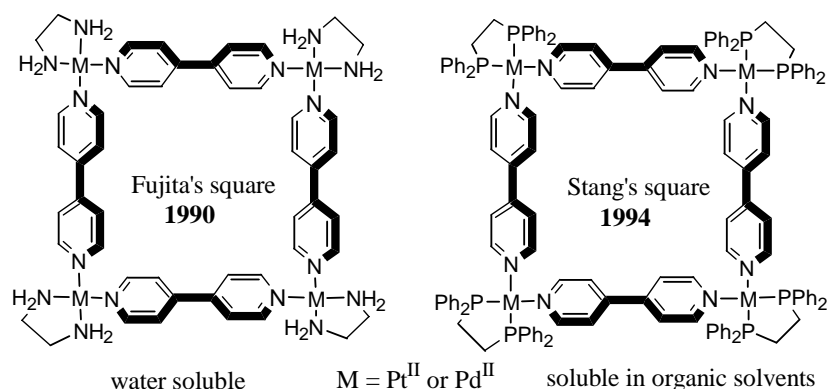


Scheme 2-5 Cartoon representation of the *cis*- and *trans*-coordinating metal ions (Pt^{II} or Pd^{II}).

2.4.2.1 2D Nanoscaffolds

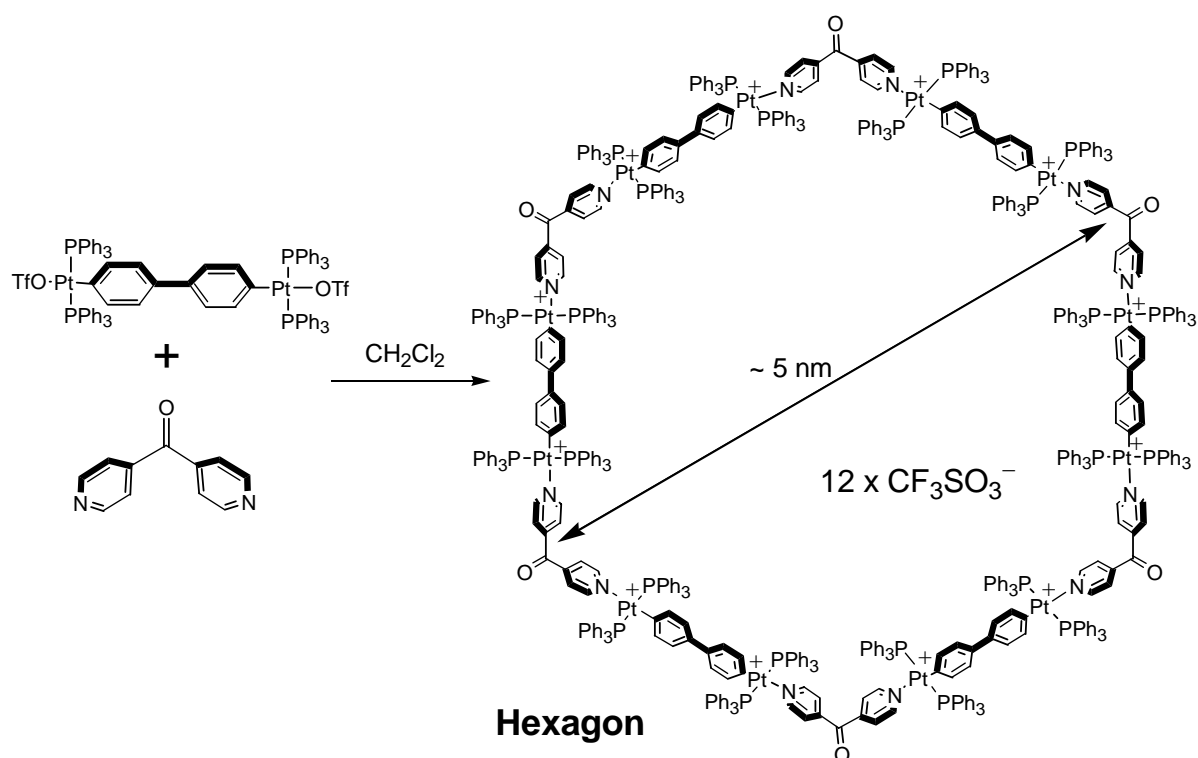
A molecular square requires 90° metal corners (Scheme 2-5, left) to define its specific shape. Pioneering work in this area by Fujita *et al.* described the construction of tetranuclear squares, the structure of which was confirmed by NMR, ESI MS and the solid state structure.⁴⁰ When the square motif was expanded to the nanoscale by incorporating phenylene or acetylene spacers into the bis-pyridine backbone,^{40d} an equilibrium resulted between squares and triangles depending on the concentration. Later, Hong *et al.* could control this equilibrium by induced-fit molecular recognition.⁴¹ Over the years, a large variety of molecular squares was reported³⁷⁻³⁹ and even the gas phase chemistry of these assemblies was investigated.⁴²

After the initial stage had been set, Stang *et al.* modified the structure of the metal ion corners by using Pt(II) or Pd(II) -phosphane units in the directional bonding approach.^{43,44} This allowed to dissolve the molecular nanoscale squares in organic solvents and to analyse the structures by ^{31}P NMR.⁴⁵



Scheme 2-6 Supramolecular squares as developed by Fujita and Stang.^{40a}

Larger polygons of nanoscale, such as a heteroleptic hexagon of about 5 nm diameter, were accessible by using *trans*-coordinating metal fragments (Scheme 2-7). 12 individual building blocks were assembled in a cooperative manner to yield the desired macrocycle as a single entity.^{44a, 45a} Such authoritative examples illustrate the utility of the metal-driven self-assembly approach to 2D nanoscale structures.



Scheme 2-7 A supramolecular heteroleptic hexagon.^{45c}

Analogous self-assembly strategies were employed to produce a large variety of 2D nanoscale polygons (using Pt(II), Pd(II), Hg(II), Ru(II), Re(I)^{39a,46} coordination), such as porphyrin squares,⁴⁷ ferrocene,⁴⁸ 1,1'-bi-2-naphthol (BINOL)^{49,50} and anthracene⁵¹ containing squares,

and molecular necklaces.⁵² Depending on the conditions and the metal centres used these structures are dynamic. Würthner *et al.* reported on the dynamics of interconverting molecular triangles and squares held together by Pd/Pt(II)-pyridine interactions.⁵³ In a similar system the relative stability of the square and triangle complexes was explored by using force field methods.⁵⁴ Concentration and temperature dependent studies on the dynamic equilibrium of a supramolecular dimeric rhomboid and trimeric hexagon provided the thermodynamic parameters.⁵⁵

The less labile Pt-acetylene interaction and the limited conformational flexibility of bridging BINOL ligands was facilitating a rare one-pot self-assembly of molecular polygons ranging from triangle to octagon assemblies (with 1.4 to 4.3 nm cavity).⁵⁶

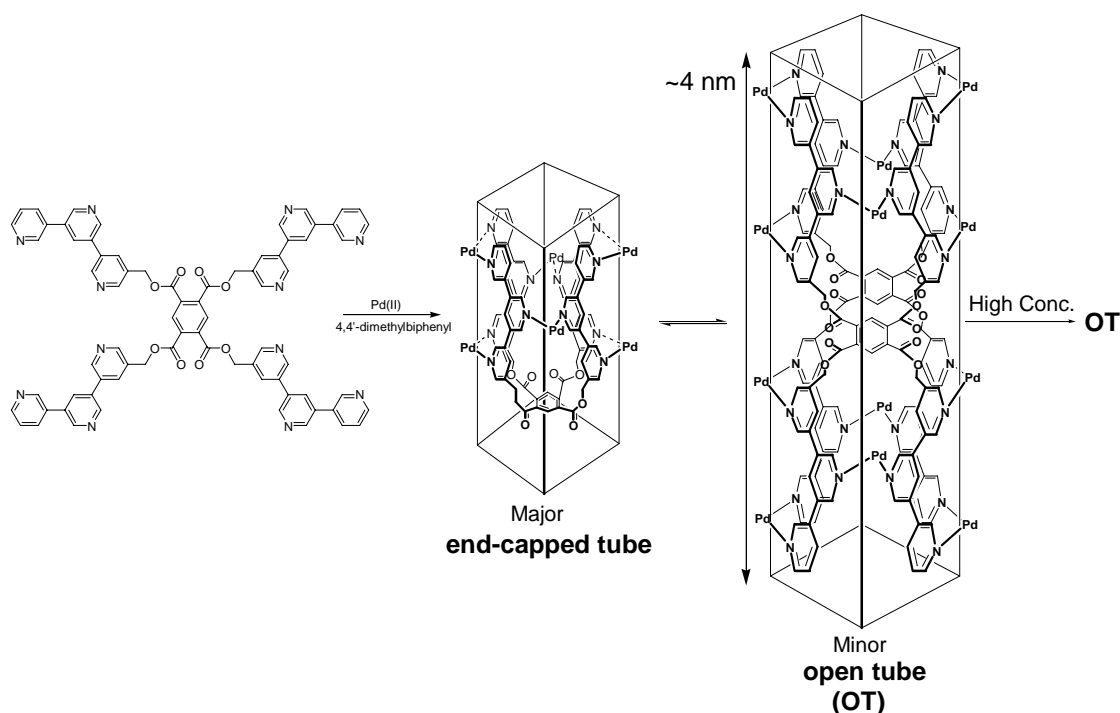
2.4.2.2. 3D Nanoscale Architectures (Polyhedra)

The expansion of metal-ligand self-assembly strategies into the third dimension leads to eye-catching 3D nanoscopic architectures. The first nanoscale cage was elaborated by Fujita *et al.* through metal directed self assembly of two tritopic ligands with three metal corners.⁵⁷ Interestingly, these molecular cages only formed in presence of a suitable guest (induced-fit recognition).⁵⁸ The same tritopic ligand, when reacted with Pd(NO₃)₂, produced a molecular sphere M₆L₈ of octahedral geometry.⁵⁹ The utility of rigid tritopic bridging ligands in constructing nanoscale 3D structures exhibiting dimensions of 2-4 nm was also impressively demonstrated by Stang *et al.*⁶⁰ Likewise, tetratopic bridging ligands have been explored to construct nanocages.⁶¹ For example, Shinkai *et al.* described the construction of homooxacalix[3]arene-based dimeric cages showing reversible inclusion of C₆₀.⁶²

Induced-fit recognition was also a key motif in the construction of nanotubes with disodium-4,4'-biphenyldicarboxylate as a rod like guest.⁶³ In absence of any template or guest molecule only uncharacterized products were formed. Several nanotubes were reported using tape-shaped oligo(3,5-pyridine) ligands and end-capped Pd(II) complexes.^{63a,b} The length of these nanotubes can be controlled by simply varying the number of pyridine nuclei in the back bone of the ligand.

Fujita *et al.* recently demonstrated the self-assembly process of a dodecapyridine ligand where two discrete assemblies, an end-capped tube and an open tube arrangement, are interconverted

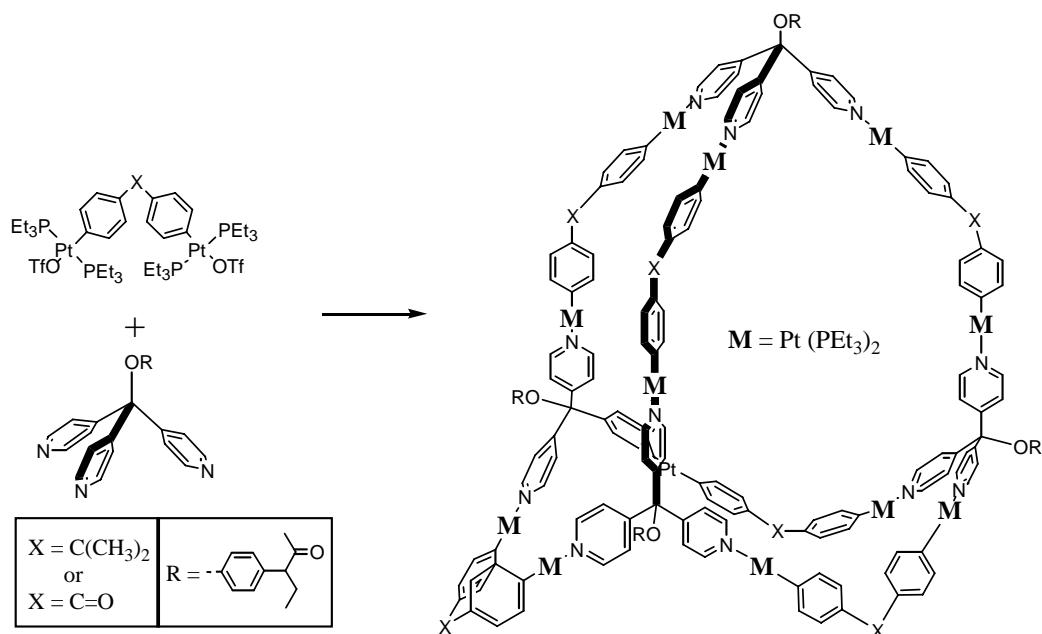
into each other on a relatively flat potential energy surface (Scheme 2-8).⁶⁴ The conversion of the major to the minor component in presence of sodium biphenylcarboxylate is slowly promoted only at high concentrations and much more strongly by removing the minor complex through crystallisation. A similar strategy has been explored to construct quantitatively hetero-metallic nanoscale catenanes.⁶⁵



Scheme 2-8 A dodecapyridine ligand forming an end-capped tube and an open tube arrangement in presence of Pd(II).

Stang *et al.* prepared a family of nanoscale 3D arrays *via* non-covalent interactions using rigid tritopic bridging ligands and rectangular corner units.⁶⁶ The highly symmetrical cage compounds are described as face-directed, self-assembled truncated tetrahedra with T_d symmetry. A nanoscale adamantanoid framework was constructed using an angle-directed, coordination driven approach⁶⁷ by combining six angular ditopic units with four angular tritopic units (Scheme 2-9). A family of nanoscopic prisms of approximate size 1-4 nm has also been reported by using a similar approach.⁶⁸

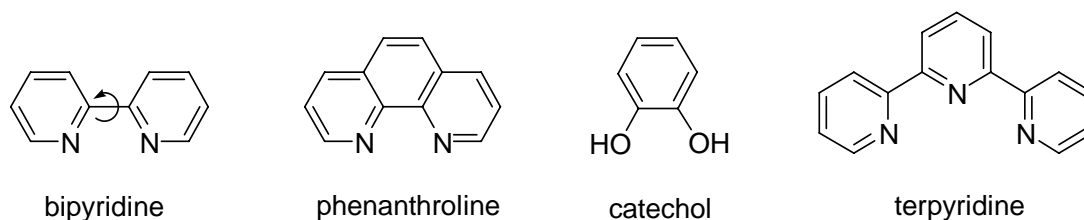
Later work by the same group elaborated a fascinating self-assembled dodecahedra with outer dimensions of ca. 5 and 8 nm from 50 predesigned components via 60 metal-ligand bonds.⁶⁹ The resultant assembly was characterised by pulse gradient spin-echo (PGSE) NMR techniques⁷⁰ and ESI MS.



Scheme 2-9 A nanoscale adamantanoid framework by Stang.

2.4.3 Nanoscale Self-Assemblies Built from Bidentate and Tridentate Ligands

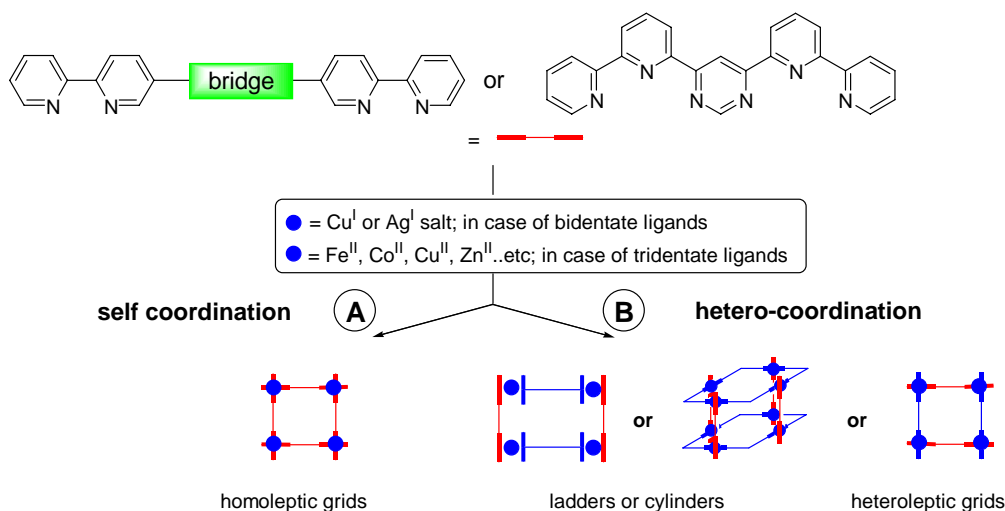
2,2'-Bipyridines, [1,10]phenanthrolines, catechols and terpyridines are among the most commonly used chelating ligands for metallo-supramolecular architectures (Scheme 2-10). As a ligand phenanthroline is structurally very similar to bipyridine, but its higher rigidity leads to a better directionality in coordination processes. Similarly, catechols are rigid bidentate ligands with a high directionality as are terpyridines despite their conformational flexibility.



Scheme 2-10

Multimetallic nanoscale arrays utilizing bi- or terpyridines have been prepared by means of two different approaches (Scheme 2-11). In approach **A**, a bi- or terpyridine type ligand self-assembles in presence of metal ions with itself to homoleptic nanoscopic arrays, such as grids or circular helicates depending on the rigidity of the bridge. On the other side, in approach **B** a

bi- or terpyridine type ligand is combined with another ligand furnishing heteroleptic motifs, such as ladders, cylinders or grids.



Scheme 2-11

A variety of supramolecular structural motifs was created using these ligands as the chelating group, such as racks,⁷¹ ladders,⁷² grids,⁷³ circular helicates,⁷⁴ and cylinders.⁷⁵ In this article ladders, grids, and circular helicates of nanoscale dimensions will be discussed.

2.4.3.1. 2D Assemblies (Homo and Heteroleptic aggregation)

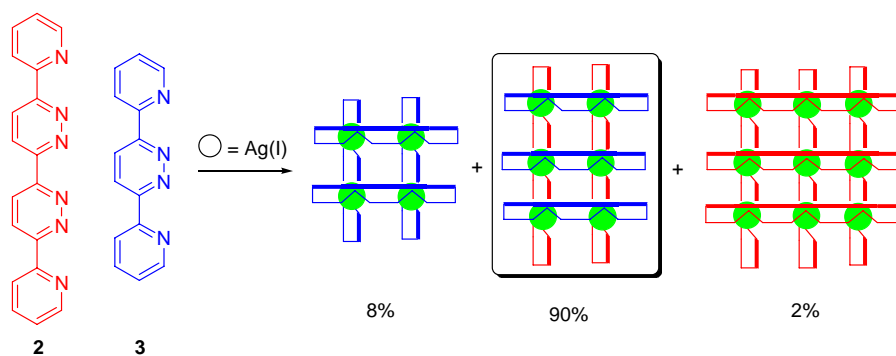
Homoleptic aggregates. The metal directed self-assembly of rigid and linear oligobipyridines can be used for the programmed formation of nanoscale grids. J.-M. Lehn, the leading pioneer in this area, has reported numerous examples of homoleptic nanoscale grids ranging from ~2-5 nm in size.^{73a-m} While the smaller grids had been prepared by simply mixing oligopyridines with metal ions, such as Cu⁺ or Ag⁺ salts, later investigations to construct higher order nanoscale grids, such as a [5x5] grid, resulted in a mixture of equilibrating [4x5] grid and a quadruple helicate.⁷⁶ Both structures could be solved by X-ray structure analysis. A similar equilibrium, now involving a double helical, a triangular and a square structure was detected in solution for another, but much shorter bis(bipyridine) ligand.^{73d} A mechanistic investigation of such self-assembly processes clearly proposes a stepwise construction of these multicomponent architectures.⁷⁷

Another level of complexity addresses the controlled introduction of a given metal ion at specific sites resulting in a heterometallic [2x2] grid of about 2 nm size.⁷⁸ A multi-grid array was built both by metal ion coordination and hydrogen bonding.⁷⁹

A few nanogrid structures based on terpyridine-type ligands have also been reported,^{73k} e.g. a chiral self-assembled [2x2] grid with predetermined configuration by Zelewsky *et al.*,⁸⁰ a rigid tetra-cobalt(III) [2x2] grid by Glass *et al.*,⁸¹ and a related iron(II) box by Constable *et al.*⁸²

Nanoscale hexagons, such as terpyridine-Ru^{II} and Fe^{II} macrocycles, were constructed by stepwise self-assembly procedures.⁸³ The resulting macrocycles are expected to have ~4 nm along the diagonal.

Heteroleptic aggregates. A higher level of structural complexity can be obtained when heteroleptic *vs.* homoleptic interactions can be controlled in dynamic complexes, and not only in kinetically inert systems (e.g. ruthenium complexes). An interesting example solely attributed to recognition motifs^{73c} of hetero-recognition *vs.* homo-recognition could be illustrated in the reaction of **2** with **3** in presence of silver ions.

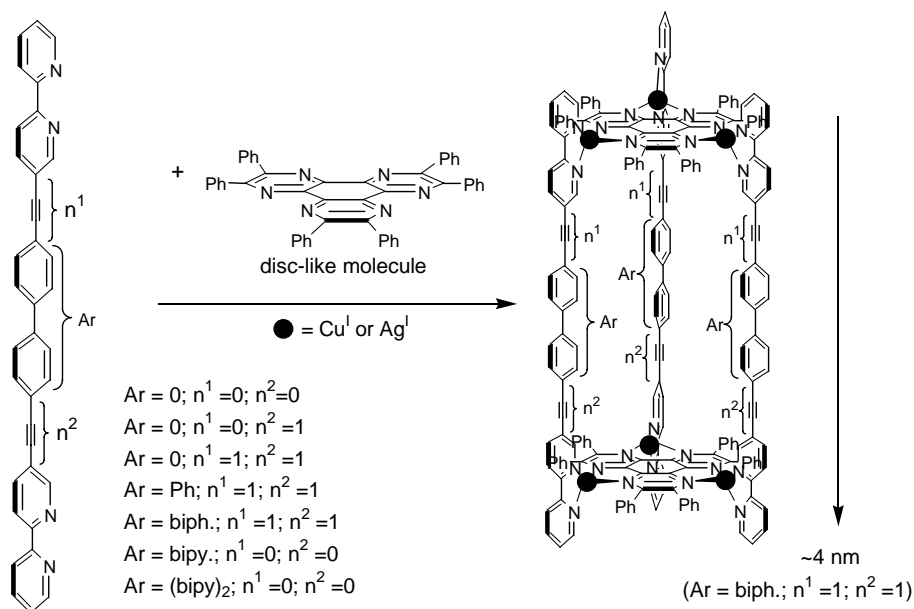


Scheme 2-12 An interesting case of hetero *vs.* homo recognition in the formation of grids.^{73c}

2.4.3.2. 3D (Heteroleptic) assemblies

Tubes and cylinders. Several examples of three dimensional architectures using bidentate ligands have been reported. As outlined above these motifs are heteroleptic in nature. The approach by Lehn *et al.* to nanoscale heteroleptic cylinders makes use of rigid linear polytopic ligands, disc-like molecules and appropriate metal ions. Along this strategy several

nanocylinders ranging from ~2-4 nm in length were prepared. Again, the selective heteroleptic over homoleptic complexation is ascribed to recognition motifs and maximum site occupancy.



Scheme 2-13 Preparation of nanoscale cylinders.

While the first generation of cylindrical architectures was based on bipyridines and tetrahedrally coordinating metal ions, the concept was later extended to terpyridines and octahedrally coordinating metal ions by Lehn *et al.* A family of nanoscale cylinders was prepared by multicomponent hetero-self-assembly. As above, the process was explained by maximum site occupancy and cooperativity rules.

Cyclophanes and ring-in-ring structures. While cyclophanes are well known from ditopic monodentate ligands very few reports are available on cyclophanes using the bidentate ligands bipyridine and phenanthroline. Lehn *et al.* conceived the construction of a metallo-cyclophane by a thermodynamic self-assembly process.⁸⁴ Also, a helical metallocyclophane has been reported.⁸⁵ A small series of nanoscale ring-in-ring structures was also constructed along those lines by Schmittel *et al.*⁸⁶ and later by Siegel *et al.*⁸⁷

Other structures. Saalfrank and others⁸⁸ have developed a predictive design strategy resulting in the synthesis of various high-symmetry coordination clusters. Structural motifs including helicates,^{88b,89} mesocates, tetrahedra, cylinders, and octahedra have been reported.⁹⁰ On the

basis of a bis(pyrazolyl-pyridine) ligand, Ward *et al.* developed a way to a self-assembled molecular cube $Zn_8L_{12}^{16+}$ with S_6 symmetry.⁹¹ By simultaneously fulfilling the symmetry requirements of both the ligand and metal centres, discrete high-symmetry clusters were generated under thermodynamic control. However, most of these structures fall well below the 2 nm scale. Analogously, Powell *et al.* have utilised the specific interaction of metals with small organic species (oxyhydroxy compounds) to create nanoscale aggregates,⁶ such as a huge polyiron cluster, in which a mineral core (metal cluster) is trapped within an organic shell, showing a lot of structural similarities with the protein ferritin.

Helical architectures have received special attention because of their structural similarity with double-stranded DNA. Several circular helicates have been reported by Lehn and others utilising bipyridine and other bidentate ligands⁹² as chelating group.

2.5 Functional Devices

The directed and programmed construction of nanoscale assemblies furnishes new opportunities and tremendous potential for the territory of supramolecular catalysis, molecular electronics, sensor design and optics. At the present time, however, the design of functional working models is still in the fledgling stages and it lags much behind the progress made in structural engineering. In the following, we would like to sketch some recent advances in the ensuing areas: supramolecular catalysis, photoactive assemblies, molecular recognition and switches, and electroactive assemblies. Despite some recent progress, in terms of interdependence and emergence nature and its masterfully designed functional systems outclass any known artificial systems by far.

2.5.1 Supramolecular Catalysis

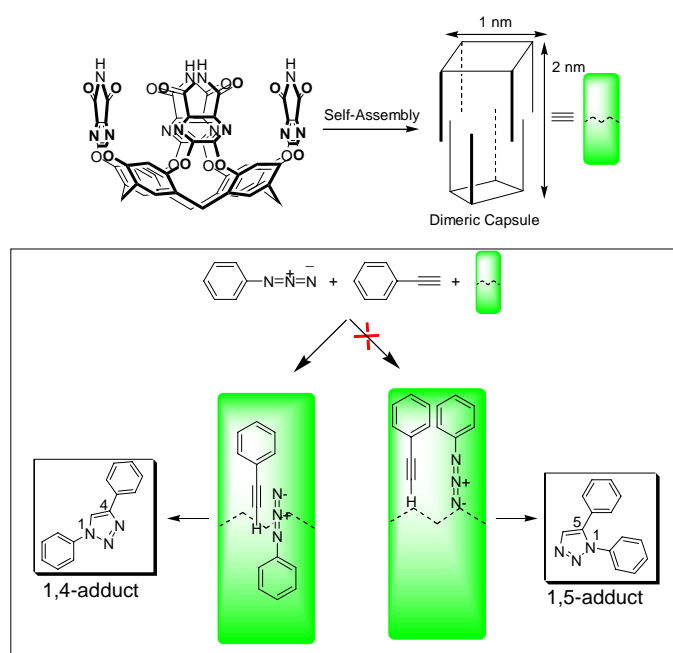
True supramolecular catalysis has to amalgamate peculiarities and vantage grounds of supramolecular architectures and those of catalysis in order to generate a surplus value. Obviously, there is ample room for fascinating combinations of both areas that is only limited by our imagination: *e.g.* the nanoscale assembly can serve as a container to select molecules by size and shape, it can place reactants in adequate distance and geometry, it can use allosteric control over catalysis etc. The art and the beauty of these systems is evident from

the fine interplay of weak bonding interactions and transition state control needed for the catalytic process.

Rebek *et al.*⁹³ have demonstrated the utility of hydrogen bonded cage assemblies. When they were set up to reversibly encapsulate two guest molecules then chemical transformations proceeded faster than in homogeneous solution.^{93a,b,94,95} As outlined below the substrate size is crucial for recognition by the cage assembly.

Rebek *et al.* have shown a spectacular example of a 1,3-dipolar cycloaddition furnishing a triazole (Scheme 2-14) was established in a reversibly formed, self-assembled dimeric capsule.⁹⁶ This example allowed the direct observation of a Michaelis complex (unsymmetrically loaded complex). In absence of the dimeric capsule phenylacetylene and phenylazide reacted very slowly ($4.3 \times 10^{-9} \text{ M}^{-1} \text{ s}^{-1}$) at millimolar concentrations. In contrast, in presence of the dimeric capsule the 1,3-dipolar cycloaddition takes place smoothly. Only the 1,4-isomer is formed and this compound is liberated by the addition of DMF. The analysis indicated that for formation of the 1,4-adduct the two substrates assumed a space saving side-by-side arrangement whereas the cavity space is insufficient for the 1,5-adduct. As a drawback, the system did not solve the turnover problem.

By the same group a remarkable case of autocatalysis, used to amplify amide bond formation, was noticed in presence of dimeric capsules.⁹⁷



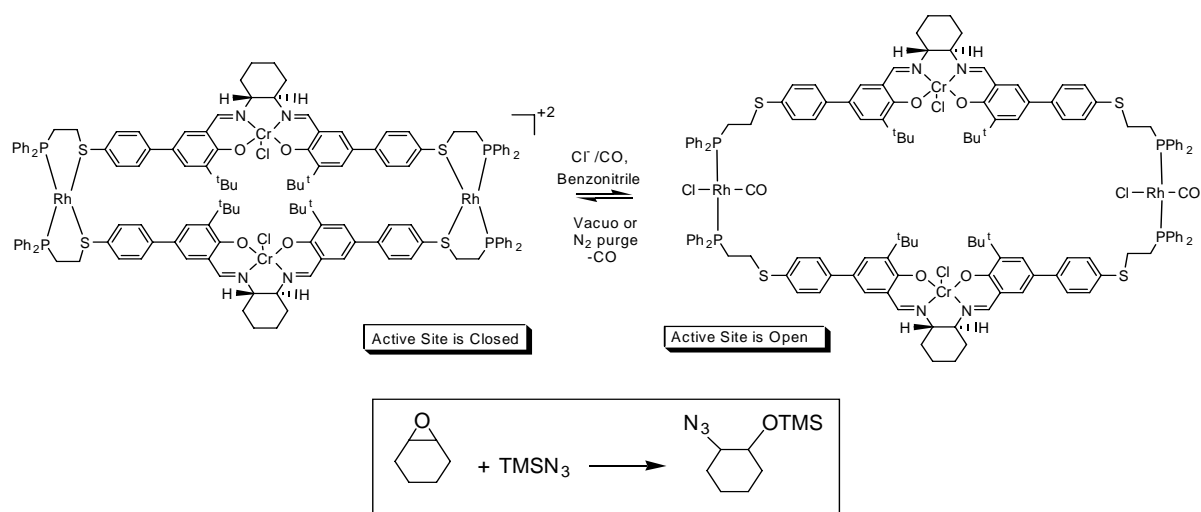
Scheme 2-14 A capsule-accelerated 1,3-dipolar cycloaddition.

Fujita *et al.*⁹⁸ have shown that a nanocage complex can act as a reverse phase-transfer catalyst for the Wacker oxidation of olefins by free $[\text{Pd}(\text{en})(\text{NO}_3)_2]$ (10%) in aqueous media.

Few other reports are also available where supramolecular assemblies were used for the catalytic purposes⁹⁹ or cavity directed synthesis.¹⁰⁰

Lin *et al.* reported on a family of Pt^{II} polygons composed of chiral ligands such as 1,1'-bi-2-naphthol (BINOL) and their utility in enantioselective catalytic diethylzinc additions to aromatic aldehydes. A later report by the same group described the assembly of a chiral cyclophane and its utility in asymmetric catalysis.¹⁰¹ Analogous chiral molecular rhenium squares proved useful for enantioselective sensing due to luminescence quenching by chiral amino alcohols.⁴⁹ To mimick cytochrome P450 Hupp *et al.* encapsulated a manganese porphyrin into a metallosupramolecular square.^{102,103}

The ring opening of epoxides using Cr(III) and Co(III)-based salen catalysts is well known.¹⁰⁴ Oligomeric versions of the Cr(III) catalysts show activities significantly greater than those of monomeric analogues.¹⁰⁵ Recently, Mirkin *et al.* reported on a supramolecular catalyst designed for allosteric control which exhibits a significant increase in the rate and selectivity of the ring opening of cyclohexene oxide.¹⁰⁶ They built heteronuclear rectangles containing catalytically active Cr(III) salen sites and Rh-thioether complexes for allosteric control. As depicted in Scheme 2-15 the weak thioether-Rh bond could be selectively cleaved by the addition of CO and chloride. As a consequence, a $\text{Rh}(\text{CO})(\text{Cl})$ complex formed and the structure opened the way that the catalytically active Cr(III) became accessible. Upon purging with nitrogen or in high vacuum the opened structure experienced loss of CO and Cl^- leading to a closed structure. Hence, the Rh(I) centres act as switches for the catalytic activity of the nanoscale capsule. For the closed structure the ring opening of cyclohexane epoxide by TMSN_3 resulted in product formation with 68% ee, whereas a Cr(III)-salen monomeric analogue only provided 12% ee. This was additionally accompanied by a 20-fold increase in rate as compared to that observed for the monomeric analogue. The rate of formation of 1-azido-2-(trimethylsiloxy)-cyclohexane was doubled in presence of CO and Cl^- as compared to the closed structure.



Scheme 2-15 Allosteric control in a heteronuclear rectangle catalyst for cyclohexene oxide opening.

There are currently many more efforts to apply supramolecular concepts in the field of catalysis that show wonderfully the encouraging prospects of this field. Reek *et al.* have prepared bidentate ligands *via* the assembly of bis-Zn^{II} porphyrin and functionalised pyridine ligands for rhodium complexes designed for the hydroformylation of 1-octene and styrene.¹⁰⁷ Later this idea was extended to a hexaporphyrin assembly.¹⁰⁸

A porphyrin-cyclodextrin 1:2 complex proved to be a supramolecular sensitizer in water providing photooxygenation with high turnover numbers, *e.g.* for phenol degradation. High yield oxidations were obtained for L-methionine methyl ester and uracil.¹⁰⁹

In the realm of smaller supramolecular aggregates (< 2nm) Fujita *et al.* have shown the utility of cadmium-bipyridine squares for heterogeneous catalysis¹¹⁰ in the cyanosilylation of aldehydes. The catalytic activity depended very much on the size of the aldehydes. Süß-Fink *et al.* designed a supramolecular cluster (< 2nm) that proved to be the mildest and the most efficient catalyst for the hydrogenation of benzene.¹¹¹

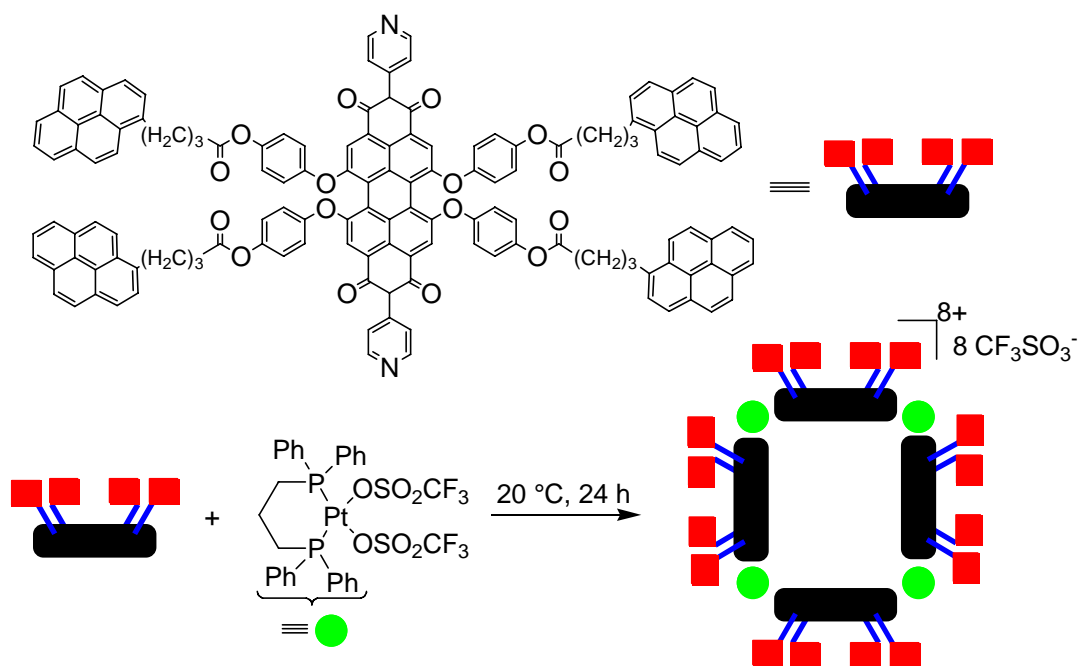
Supramolecular assistance to covalent synthesis is often explored to construct ring systems such as catenanes, knots and macrocycles. A nanoscale macrocycle was constructed using a shape-persistent tricationic platinum template.¹¹²

2.5.2 Photoactive Assemblies

The rich structural variety of supramolecular assemblies and photoactive groups can amalgamate profitably for a melange of purposes: light-harvesting systems, electron or energy transfer in nanostructured systems, photochemical devices etc..

In photosynthesis the energy is collected by light-harvesting antennae systems, from which it is funnelled to the photosynthetic reaction center. This ingenious arrangement of nature has attracted the ample attention of biomimetic chemists due to the effective energy conversion. The structure known from the bacterial photosynthetic system revealed that the reaction center is surrounded by many antennae pigments in cyclic arrangements to collect and transmit light energy efficiently.¹¹³ Subsequently, several discrete photoactive assemblies were reported, quite often containing a porphyrin core to mimic the natural systems. Still, the construction of giant artificial photoactive aggregates using self-assembly techniques is a challenging task. It is interesting to note that almost all of the photoactive assemblies studied so far rely on metallosupramolecular building principles, in particular using Pd/Pt and Re interactions.

Homoleptic devices. Würthner *et al.* incorporated 4 perylene bisimide chromophores into nanoscale Pd and Pt squares. Since the perylene fluorescence was not quenched by the metal ion coordination these systems were able to show fluorescence quantum yields near 100%.^{53b,c} Later the self-assembly of an analogous nanosize scaffold with sixteen additional dyes (pyrenes) was demonstrated to result in efficient energy transfer from the outer antenna pyrenes to the inner perylene chromophore (Scheme 2-16).^{53d} Some other reports have also utilized Pt^{II} metal corners to harvest photoactive devices.¹¹⁴

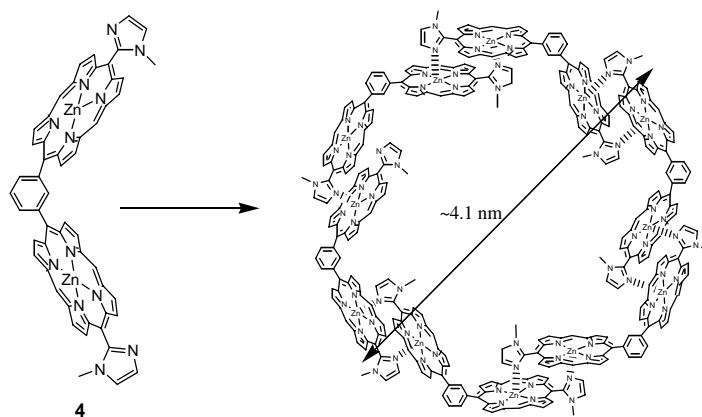


Scheme 2-16 A nanoscale metallosupramolecular square with 16 appended pyrenes.^{53d}

A recent report by Lin *et al.* described chiral nanoscale Pt^{II} molecular squares exhibiting dual luminescence which is of potential use as chiral sensory material.¹¹⁵

Recently, Lehn *et al.* reported about a [2x2] metallogrid that exhibits reversible changes in the optical properties triggered by multiple protonation and deprotonation steps.¹¹⁶ The colour of the solution changed from pale yellow at low pH to orange and finally deep-violet above neutral pH. This process was found to be reversible.

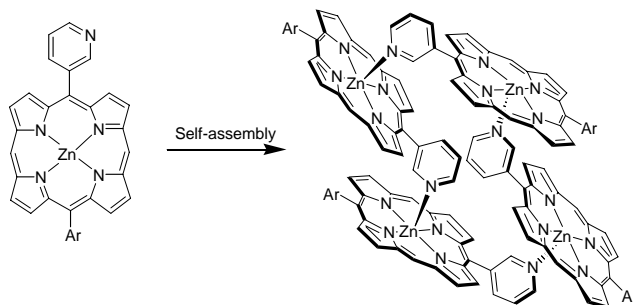
An ingenious hexameric circular assembly was recently reported by Takahashi and Kobuke (Scheme 2-17).¹¹⁷ Starting from the *meta*-gable bis-zinc porphyrin **4** the self-assembly furnished a dodecaporphyrin barrel structure with a diameter of 4.1 nm. The fluorescence quantum yield of the suprastructure relative to that of the monomeric bisporphyrin was 0.51.



Scheme 2-17 A highly fluorescent dodecaporphyrin barrel structure.

Kuroda *et al.* demonstrated the construction of multiporphyrin arrays (nonameric and heptadecameric porphyrins) using a different templating strategy. The fluorescence of the central porphyrin is increased by 77 times to that of the free porphyrin.¹¹⁸ Several photoactive self-assembled squares were reported by Hupp *et al.* using rhenium metal corners.^{39a} A recent example by the same group showed the utility of these devices to construct chemoresponsive photonic lattices capable of functioning as chemical sensors.¹¹⁹ A smaller porphyrin dimer was constructed using rhenium metal corners and the ligand remained fluorescent even after coordination.¹²⁰ A similar size assembly was prepared by Lu *et al.* from 18 components showing on-off switching of emission by presence/absence of aqueous solvent.^{61b}

Aida, Tsuda *et al.* have reported about a 3-pyridyl substituted zinc porphyrin which exhibits supramolecular thermochromism.¹²¹ The compound (shown in Scheme 2-18) displayed a stepwise colour change from green to yellow to red on heating from 0 to 50 to 100 °C in toluene. The vivid colour change is most likely brought about by a thermal self-assembly process to a cyclic tetramer via the axial coordination of the pyridyl group to the zinc porphyrin.

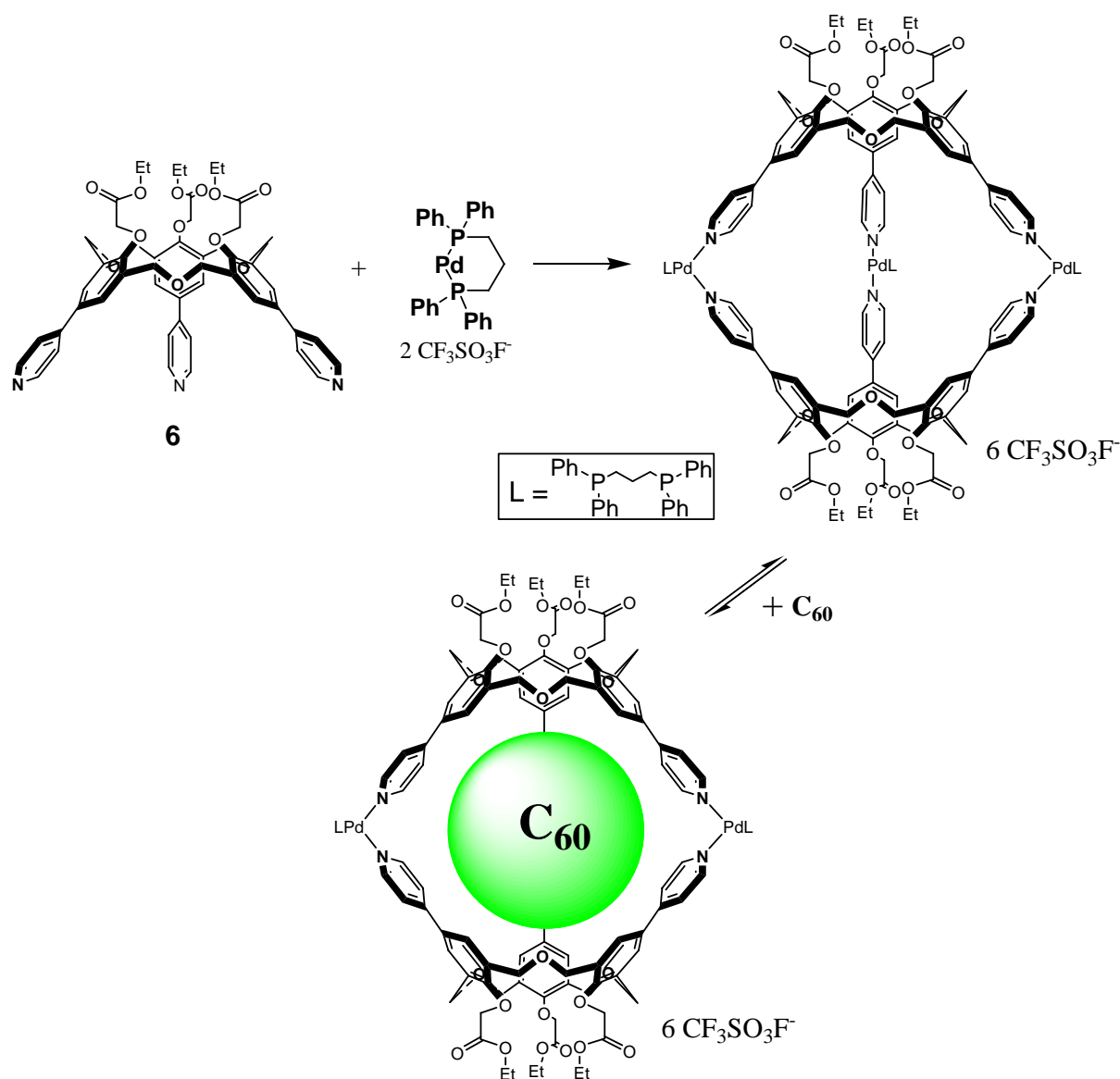


Scheme 2-18. A 3-pyridyl substituted zinc porphyrin tetramer exhibiting supramolecular thermochromism.

2.5.3 Molecular Recognition

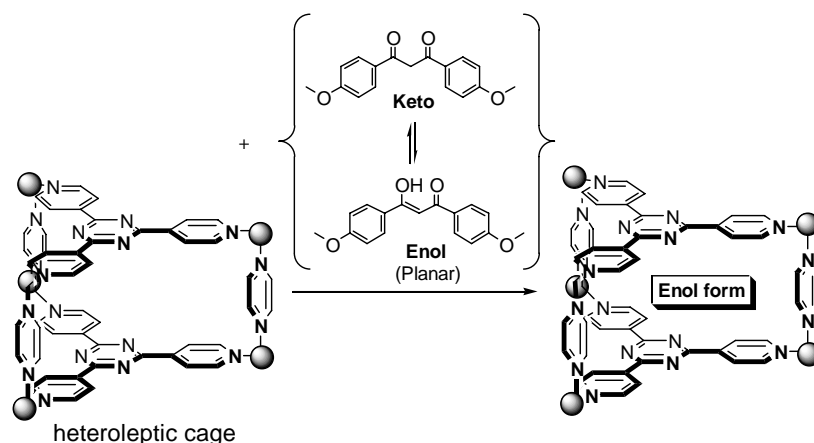
Polygons and polyhedra derived from self-assembly processes often provide a defined cavity which is of good use for molecular recognition or sensing. In some cases, the guest inclusion plays a major role in driving the equilibrium to a unique entity (Induced-fit recognition). Several factors must be taken into account to tune the host-guest interactions. (i) Shape and size of the both host and guest; (ii) complementary binding sites and interactions; (iii) medium (solvent). The early seminal investigations about binding of alkali cations by cryptates, cryptophanes and carcerands paved the way for our understanding of molecular recognition phenomena in supramolecular assemblies. Due to space restriction, supramolecular structures with small guest molecules will not be covered, although there are several spectacular examples known. Herein, we will discuss recent progress of host-guest chemistry of nanoscale supramolecular assemblies with a focus on the complexation of larger molecules and of more than one guest.

Metallosupramolecular systems. Metallosupramolecular nanoscale systems were frequently analysed for their potential to accommodate larger guests. In a striking example Shinkai *et al.* showed that a metallo-supramolecular capsule can be used to purify C₆₀ very effectively following conceptually a purification method for C₆₀ and C₇₀ that used calixarenes as capsules or sieves (Scheme 2-20).¹²² Shinkai constructed a Pd^{II} capsule using pyridine-tethered-calixarenes **6**. With smaller guest molecules such as DMF, adamantane, anthracene, pyrene, and others no guest inclusion complexes were found, due to the large windows present in the capsule. However, ¹³C-enriched [60] fullerene could be enclathrated efficiently while ligand **6** itself did not exhibit enclathration of C₆₀. The enclathration could be monitored by ¹³C and ¹H NMR.



Scheme 2-19 A metallo-supramolecular capsule entrapping C_{60} .

In a recent report by Fujita *et al.* a prism-like Pt^{II} -cage was used to control the equilibrium between planar enol and nonplanar keto tautomers (Scheme 2-21).¹²³ In acetonitrile these exist in a 85:15 ratio that can never be separated due to fast tautomerization. In contrast, in presence of the heteroleptic cage molecule, the β -diketone only existed as enol due to the selective inclusion of the planar enol form.



Scheme 2-20 Selective inclusion of a planar enol form derived from a β -diketone.

Metallo-supramolecular assemblies can also be used to stabilize labile species. The reactive, water sensitive $[\text{Me}_2\text{C}(\text{OH})\text{PEt}_3]^+$ ion was entrapped by Raymond *et al.* in a small metallo-supramolecular capsule,¹²⁴ so that it can survive for a few hours in D_2O . Fujita *et al.*¹²⁵ have shown that a molecular capsule can stabilize cyclic trimers of siloxanes considerably. The labile trimers were effectively trapped during self-assembly of the capsules from which they can no longer escape due a small portal size. These clathrate structures were isolated and proved to be very stable even in acidic aqueous solutions ($\text{pH} < 1$). The same capsule was used to stabilize the tennis-ball shaped noncovalent dimers of *cis*-azobenzenes,¹²⁶ that were selectively enclathrated from a mixture of *cis* and *trans* azobenzene. The enclathrated hydrophobic *cis*-azobenzene dimer stability has increased considerably and has not changed to *trans*-isomer even after exposing to visible light for a few weeks.

Fujita *et al.* have shown the electrochemically driven clathration/declathration of ferrocene in a Pd^{II} capsule.¹²⁷ Because neutral ferrocene enclathrates efficiently into the cage assembly but not the ferrocenium, the encapsulated neutral molecule can be moved in and out by tuning the charge of the guest molecule.

A cationic tetrahedral host with 24 positive charges can even provide shelter for a cationic guest.¹²⁸ The host accommodated the tetraalkylammonium cation together with four BF_4^- ions thus creating a small sphere of inversed polarity. Competition experiments with two differently sized guest molecules (NEt_4^+ vs. NBu_4^+) indicated that the smaller guest forming first a kinetically preferred complex is slowly exchanged by the larger guest to furnish the thermodynamic product. Similar guest exchange processes had been reported earlier.¹²⁹

Because of the high kinetic stability of Pt(II)-cage towards acidic and basic conditions ($-11 < \text{pH} < 1$), it was explored as a pH-responsive host-guest system. Indeed, while dimethylaniline was enclathrated efficiently it was liberated upon protonation due to the repulsions between the generated ammonium ion and the Pt-cations.¹³⁰ Several other systems were equally reported that exhibit a distinct response to the pH.¹³¹

Bosnich *et al.* have reported the assembly of nanoscale heteroleptic trigonal prisms and their host-guest chemistry.¹³² Remarkably, 1:6 and 1:7 host-guest complexes with 9-methylanthracene formed, while another one of the prisms furnished a 1:2 host-guest complex with a very large tritopic tri-anthracene guest. Clearly, the development of such multi-site hosts may eventually lead to the construction of molecular switches and motors which rely on guests moving between the multiple sites of a molecular host.

A dynamic metallo-supramolecular receptor library was generated by Fujita *et al.*^{58c} in which all the receptors were in equilibrium from which the appropriate one was selected by an optimal guest. The dynamic library was generated from the Pd(II) complexes of two different ligands. Large (spherical) or small (flat) guests stabilized the homoleptic cages $M_3(L1)_2 + M_3(L2)_2$, whereas medium sized guests induced the heteroleptic receptor $M_3(L1)(L2)$.

Molecular sensors have been developed, where the binding of the guest could be detected through luminescence.¹³³

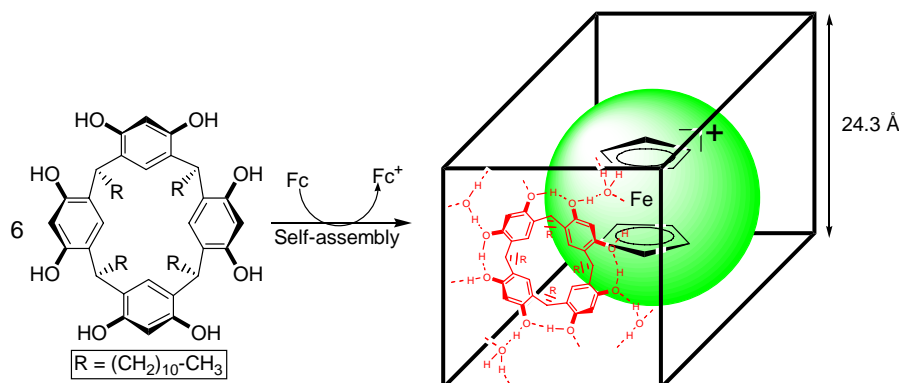
Hydrogen bonded aggregates. But in the field of molecular recognition also hydrogen bonded aggregates play an important role. Rebek *et al.* reported about a dimeric capsule that is able to encapsulate cryptates inside its cavity. Hence, the resulting systems are complexes within complexes and represent a second sphere of supramolecular chemistry.^{94a} A similar system was set up by Raymond *et al.* by incorporating an alkali ion – crown ether into a metallosupramolecular cluster.^{95b}

A self-assembled dimeric capsule was described to accommodate two different molecules (benzene and *p*-xylene).¹³⁴ Such a hetero-guest inclusion reflects how optimal occupancy of the capsule can be reached: two benzene molecules are too small and two *p*-xylene molecules are too crowded for the capsule. This leads to a new form of isomerism, coined as *social isomerism*, that arises from the orientation of two different molecules in the container, *e.g.* in

a cylindrical capsule. The orientation of one guest depends critically on the presence and nature of the second guest molecule.

In a separate study,¹³⁵ Atwood *et al.* have reported the self-assembly of calix[4]arenes to yield trimeric nanoscale structures which can very efficiently entrap highly volatile gases such as methane and freon under relatively extreme conditions of temperature and pressure.

In apolar solvents six calix[4]resorcinarenes undergo self-assembly by means of 60 hydrogen bonds leading to a chiral spherical molecular capsule.¹³⁶ Kaifer *et al.* have shown the efficient formation of a robust molecular capsule of six calix[4]resorcinarenes (inner volume $\sim 1375 \text{ \AA}^3$) around an electrochemically generated ferrocenium ion, which behaves as the nucleus of the assembly (Scheme 2-22).¹³⁷ This encapsulation process is driven by cation- π interactions with the inner surface of the hydrogen bonded calix[4]resorcinarene capsule. Similar results were obtained with cobaltocenium ion. The encapsulation of ferrocenium or cobaltocenium ions slows down their electrochemical reduction requiring an overpotential of 500 mV.



Scheme 2-21 Six calix[4]resorcinarenes forming a hydrogen bonded capsule.

Encapsulation can be used to induce a conformational preference as demonstrated by Rebek *et al.*¹³⁸ When a dimeric capsule incarcerated longer *n*-alkanes the $C_{10}H_{22}$ was still extended while the $C_{14}H_{30}$ ended coiled up in a helical conformation.

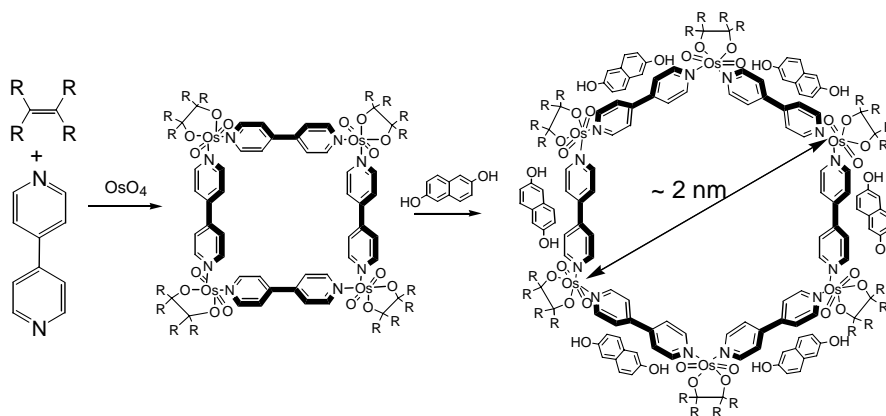
2.5.4 Switching the Molecular Shape of Assemblies

The development of switchable nanoscale assemblies is of great importance to develop molecular level sensors and devices. In seminal contributions, Stoddart,¹³⁹ Sauvage¹⁴⁰ and

others have engineered topologically linked systems which exhibit systematic molecular motions upon photochemical, electrochemical or chemical enticement. While the whole field is still at its infancy the number of examples coming from metallocsupramolecular aggregates seems to outnumber the ones from hydrogen bonded assemblies. This is readily understandable since the stronger driving force per binding contact in metallocsupramolecular structures needs a smaller number of binding sites thus allowing for higher structural flexibility.

Metallocsupramolecular structures. A recent report by Lehn *et al.* demonstrated a spectacular metal mediated interconversion of single helices to a multi-metallic nanoscale grid structure.^{73m} Similar results were found by Shinoya *et al.*, in which the self-assembly structure depends on the amount of metal ion concentration.¹⁴¹

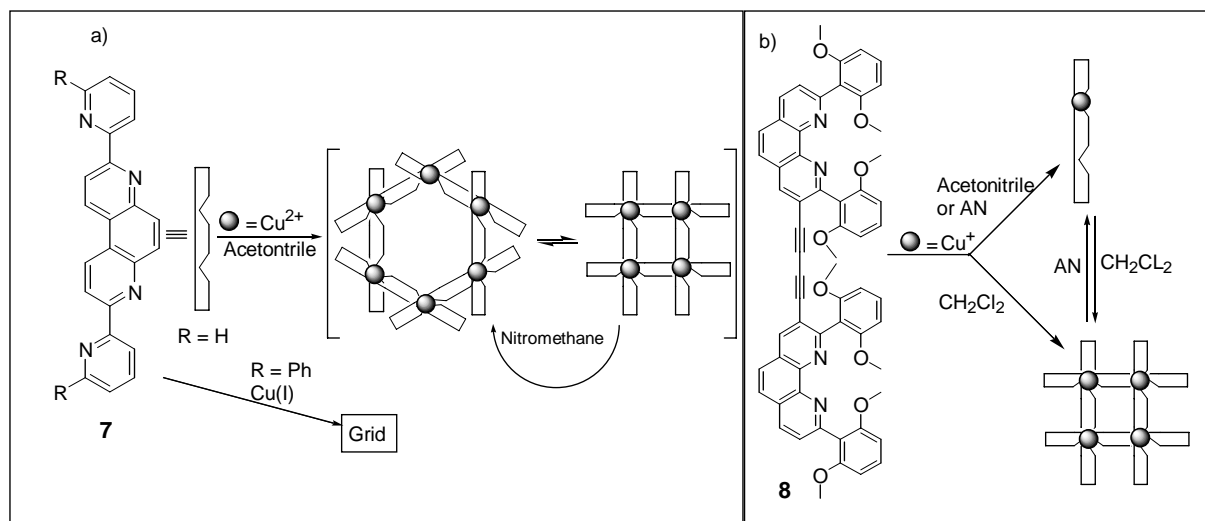
Hexanuclear hexagons were formed after spontaneous reorganisation of osmate ester-based molecular squares in the presence of a naphthalene-2,6-diol as a guest as described by Jeong *et al.* (Scheme 2-23).¹⁴² A solid state structure illustrated the guest's role in driving the tetragon to a hexagon motif. The guest molecule is not filling the void but ends up bound to each side of the cyclic osmate ester by two hydrogen bonds as well as by face-to-face aromatic stacking forces. These observations (guest induced organisation or induced fit organisation) are very much similar to the earlier reports by Fujita *et al.*⁶³



Scheme 2-22 Hexanuclear hexagons formed after spontaneous reorganisation of molecular squares.

Solvent coordination can also play a major role in governing these multicomponent self-assembly processes (Scheme 2-24).¹⁴³ The 1:1 stoichiometric reaction between Cu(II) and **7** in acetonitrile afforded an equilibrating mixture of a tetranuclear grid and a hexameric cyclo-

phane. However, when acetonitrile was replaced by nitromethane only the hexameric arrangement could be observed. Similar results were obtained when **8** was reacted with Cu(I) salt in 1:1 ratio.¹⁴⁴ In acetonitrile the reaction mixture was dominated by an open structure whereas in methylene chloride it self-assembled quantitatively to a tetrameric grid.

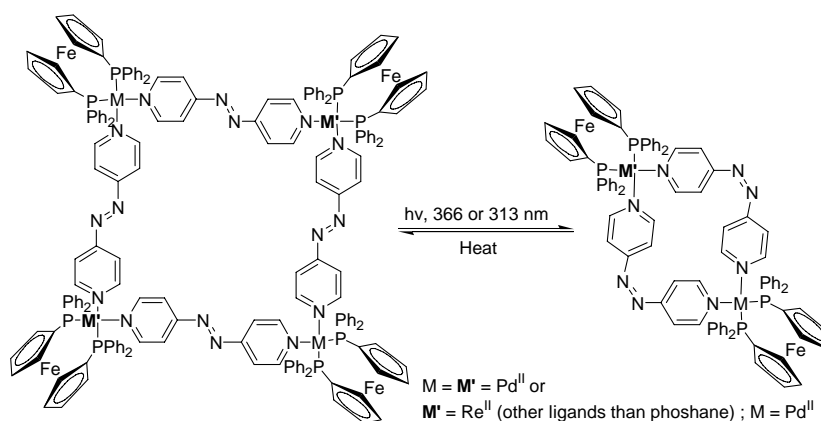


Scheme 2-23 Switching the supramolecular architecture by solvent effects.^{143,144}

An intramolecular coordination behaviour was set up in a similar molecule bringing together three different binding subunits.^{74d} Reaction of the polytopic ligand with Cu(II) or Zn(II) ions generated double helical structures at the expense of grid systems.

An interesting conversion of a triple-helicate and a tetrahedral cluster by means of host-guest interactions has been reported by Raymond *et al.*¹⁴⁵

Lees *et al.* described a series of self-assembled molecular squares containing a photoisomerizable azobenzene unit (Scheme 2-25).¹⁴⁶ The photophysical and photochemical properties of the squares were investigated, and all of them showed a lack of luminescence at rt. However, on irradiation the Pd(II) and Pd(II)-Re(I) tetranuclear squares could be converted to dinuclear squares which returned thermally to the tetranuclear squares.



Scheme 2-24 Molecular squares containing a photoisomerizable azobenzene unit.

Hydrogen bonded structures. In a recent example by Reinhoudt *et al.*,¹⁴⁷ the symmetry of a self-assembled rosette was demonstrated to change in presence of a self-assembled guest molecule.

Supramolecular polymers are interesting examples of self-assembling materials, in which monomeric units are held together by reversible secondary forces — hydrogen bonds, metal–ligand interactions, van der Waals attractions, *etc.*¹⁴⁸ When two calix[4]arene tetraureas were covalently linked at their lower rims, hydrogen bonding yielded a polymeric chain of capsules.¹⁴⁹ In continuation of their earlier work, Rudkevich *et al.* applied reversible carbamate linkages and hydrogen bonding to link calix[4]arene tetraurea dimers.¹⁵⁰ Thereby, a novel supramolecular polymer is constructed through chemical fixation of CO₂ and hydrogen bonding.

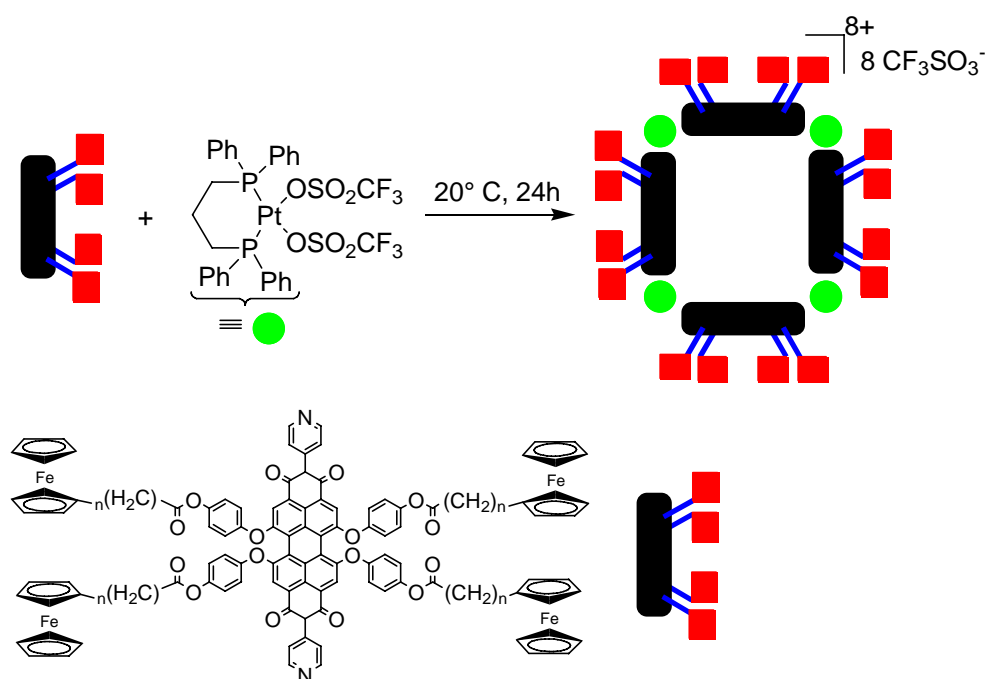
2.5.5 Electroactive and Magnetic Assemblies

The search for high information storage devices has stimulated the search for self-assembled electroactive and magnetic structures having multistable behaviour that can be precisely controlled by external stimuli. Though many of the supramolecular architectures discussed above incorporate several metal centers with distinct stable redox stages, often their electrochemistry and their magnetic properties in paramagnetic redox stages are not thoroughly investigated.

One approach is to study the oxidation/reduction behavior of the coordinating metal centers in metallocupramolecular assemblies. Lehn *et al.* reported on a unique Co^{II} grid assembly possessing exceptional electrochemical properties, in which the metal centers undergo ten well resolved, reversible reduction steps involving eleven electrons.¹⁵¹ A later report by the same group extended these studies to several other grid architectures varying transition metal centers and ligands.¹⁵² A reversible multielectron redox behaviour was also found in Pt^{IV} and rhenium molecular squares by Kaim, Stang *et al.*¹⁵⁴

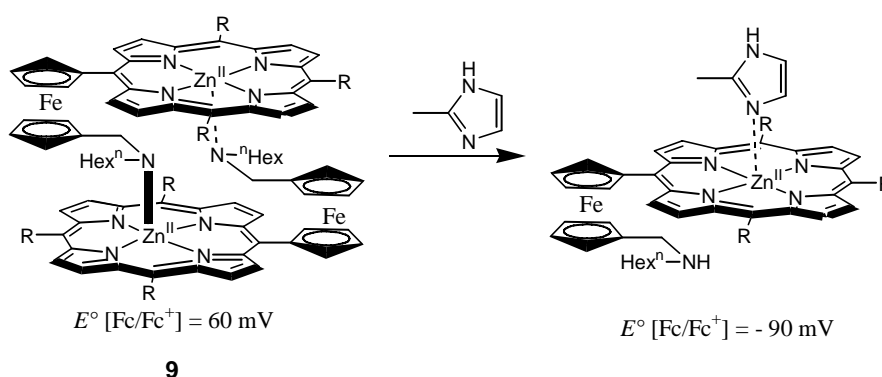
Another approach relies on incorporating known reversible redox systems into the metal ligand sphere, such as the ferrocenephosphanes, as described by Stang¹⁵⁵ and Lees for several molecular squares.

A large number of ferrocenes could be assembled about a supramolecular square using the bridging ligand for attaching the electroactive units.¹⁵⁶ Würthner *et al.* compared the electrochemical properties of these assemblies and the monomeric analogues. The redox response of ferrocene was greatly influenced by the nano environment of the squares. Upon oxidation of all ferrocene units, decomposition of the assembly was observed (Scheme 2-26).



Scheme 2-25 Electroactive (ferrocene based) supramolecular square.

Bucher *et al.* reported on a self-assembled, ferrocene substituted porphyrin, which can sense electrochemically neutral molecules *via* a "tail on-tail off" process.¹⁵⁷ A nitrogen tail was introduced at the ferrocene moiety in order to facilitate the "tail on-tail off" process. The ferrocene substituted porphyrin underwent self-assembly to furnish a dimeric structure **9**. Addition of neutral molecules, such as pyridine, imidazole or 2-methylimidazole, triggered the cleavage of the dimeric structure and thereby shifted the potential of the ferrocene moiety (Scheme 2-27).



Scheme 2-26 Electroactive sensor for neutral coordinating molecules.

Sensing interfaces have been constructed by Willner *et al.* through the non-covalent crosslinking of 12 nm Au colloids with Pd^{II} molecular squares.¹⁵⁸ The molecular squares act as a π -receptors for the complexation of π -donor substrates, such as dialkoxybenzene derivatives. Binding of *p*-hydroquinone increased its local concentration at the electrode surface thus allowing for its electrochemical sensing by the three-dimensional conductive Au-array. The electrochemical response could be increased by augmenting the number of layers.

In a similar study, Hupp *et al.* have analysed the size selective transport of guests through nanocrystalline and/or amorphous thin films made from supramolecular Re-squares by deposition.¹⁵⁹ A main advantage of these systems is the absence of counter ions inside the cavity, making them suitable for membranelike permeation processes. Electrochemical transport experiments with $[\text{Ru}(\text{NH}_3)_6]^{3+}$ ($d \sim 5.5 \text{ \AA}$) and $[\text{Co}(\text{phen})_3]^{2+}$ revealed that the material is exceptionally porous for small molecules and that large molecules were blocked.

A Fe^{II} molecular [2x2] grid exhibits a spin-crossover that is triggered by temperature, pressure and light.¹⁶⁰ The four iron atoms in the assembly can be present in either high-spin(HS) or

low-spin(LS) state. The availability of three distinct magnetic levels (3HS/1LS, 2HS/2LS and 1HS/3LS) in this assembly makes this system a "multiply switchable multilevel device" which is driven by three different triggers (temperature, pressure and light).

2.6 Conclusions

Over the last years, metal coordination and hydrogen bond driven self-assembly has produced an impressive variety of startling supramolecular architectures. While a truly biomimetic approach would typically employ a balanced mixture of weak interactions (hydrogen bonding, π - π interactions, etc.), stronger non-covalent interactions (such as the metal ligand coordinative bond) have equally proven their high utility in the preparation of nanoscale assemblies. The time has come now to install functional elements to nanoscale aggregates in order to build nanoscale devices that exhibit non-linearity, interdependence and emergence, *i.e.* typical characteristics of higher complexity systems. Needless to say these artificial systems in their size and functional complexity are still lagging far behind biological molecules/entities.

In view of these developments, my aim was to develop multicomponent metallo-supramolecular strategies and study their properties. The obtained results will be presented in the following chapters (chapter 3-7).

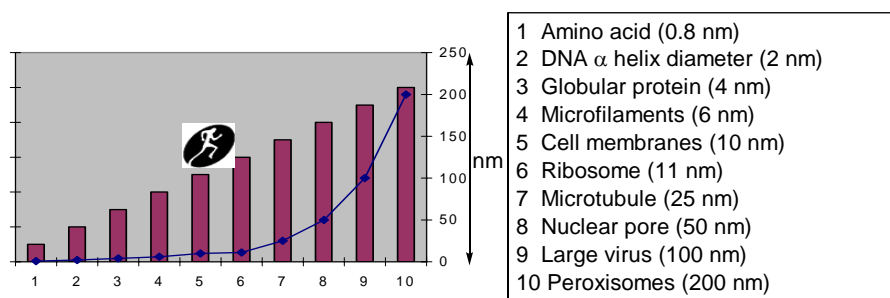


Figure 2-2 Size of selected biological molecules/entities.

Acknowledgements The authors are indebted to the Deutsche Forschungsgemeinschaft and the Fonds der Chemischen Industrie for continued support. This review is dedicated to Prof. Dr. Christoph Rüchardt (Universität Freiburg) on the occasion of his 75th birthday.

2.7 References

- ¹ Parts of this chapter were published in M. Schmittel, V. Kalsni, *Top. Curr. Chem.* **2005**, *245*, 1-53.
- ² J.-M. Lehn, *Supramolecular Chemistry*; VCH Publishers: New York, **1995**.
- ³ S. Gianni, N. R. Guydosh, F. Khan, T. D. Caldas, U. Mayor, G. W. N. White, M. L. DeMarco, V. Daggett, A. R. Fersht, *Proc. Natl. Acad. Sci. U.S.A.*, **2003**, *100*, 13286-13291.
- ⁴ see for example; (a) G. Schmid, R. Pugin, J.-Malm, J.-O. Bovin, *Eur. J. Inorg. Chem.* **1998**, 813-818; (b) A. Müller, C. Serain, *Acc. Chem. Res.* **2000**, *33*, 2-10; (c) J.-C. P. Gabriel, K. Boubekour, S. Uriel, P. Batail, *Chem. Rev.* **2001**, *101*, 2037-2066; (d) H. D. Selby, B. K. Roland, Z. Zheng, *Acc. Chem. Res.* **2003**, *36*, 933-944 and ref's therein.
- ⁵ (a) R. W. Saalfrank, B. Demleitner, H. Glaser, H. Maid, S. Reihls, W. Bauer, M. Maluenga, F. Hampel, M. Teichert, H. Krautscheid, *Eur. J. Inorg. Chem.* **2003**, *6*, 822-829; (b) H. Glaser, R. Puchta, N. J. R. V. E. Hommes, D. Leusser, A. Murso, D. Stalke, W. Bauer, R. W. Saalfrank, *Helv. Chim. Acta.* **2002**, *85*, 3828-3841; (c) R. W. Saalfrank, U. Reimann, M. Göritz, F. Hampel, A. Scheurer, F. W. Heinemann, M. Büschel, J. Daub, V. Schünemann, A. X. Trautwein, *Chem. Eur. J.* **2002**, *8*, 3614-3619; (d) R. W. Saalfrank, B. Demleitner, H. Glaser, H. Maid, D. Bathelt, F. Hampel, W. Bauer, M. Teichert, *Chem. Eur. J.* **2002**, *8*, 2679-2683; (e) R. W. Saalfrank, H. Maid, N. Mooren, F. Hampel, *Angew. Chem. Int. Ed. Engl.* **2002**, *41*, 304-307; (f) R. W. Saalfrank, H. Glaser, B. Demleitner, F. Hampel, M. M. Chowdhry, V. Schünemann, A. X. Trautwein, G. B. M. Vaughan, R. Yeh, A. V. Davis, K. N. Raymond, *Chem. Eur. J.* **2002**, *8*, 493-497; (g) O. Waldmann, R. Koch, S. Schromm, J. Schüle, P. Müller, I. Bernt, R. W. Saalfrank, F. Hampel, E. Baltes, *Inorg. Chem.* **2001**, *40*, 2986-2995; (h) R. W. Saalfrank, I. Bernt, F. Hampel, *Chem. Eur. J.* **2001**, *7*, 2770-2774; (i) R. W. Saalfrank, I. Bernt, M. M. Chowdhry, F. Hampel, G. B. M. Vaughan, *Chem. Eur. J.* **2001**, *7*, 2765-2769 and ref's therein.
- ⁶ A. Mandel, W. Schmitt, T. G. Womack, R. Bhalla, R. K. Henderson, S. L. Heath, A. K. Powell, *Coord. Chem. Rev.* **1999**, *190-192*, 1067-1083 and ref's therein.
- ⁷ L. J. Prins, D. N. Reinhoudt, P. Timmerman, *Angew. Chem. Int. Ed. Engl.* **2001**, *40*, 2383-2426.
- ⁸ (a) H. Fenniri, B.-L. Deng, A. E. Ribbe, K. Hallenga, J. Jacob, O. Thiyagarajan, *Proc. Natl. Acad. Sci. U.S.A.*, **2002**, *99*, 6487-6492; (b) H. Fenniri, M. Packiarajan, K. L. Vidale, D. M. Sherman, K. Hallenga, K. V. Wood, J. G. Stowell, *J. Am. Chem. Soc.* **2001**, *123*, 3854-3855; (c) H. Fenniri, B.-L. Deng, A. E. Ribbe, *J. Am. Chem. Soc.* **2002**, *124*, 11064-11072.
- ⁹ For reviews see; (a) J. Rebek, Jr., *Acc. Chem. Res.* **1999**, *32*, 278-286; (b) J. Rebek, Jr., *Chem. Soc. Rev.* **1996**, 255; (c) M. M. Conn, J. Rebek, Jr., *Chem. Rev.* **1997**, *97*, 1647-1668; (d) V. Bohmer, M. O. Vysotsky, *Aust. J. Chem.* **2001**, *54*, 671-677; (e) D. A. Rudkevich, *Bull. Chem. Soc. Jpn.* **2002**, *75*, 393-413; (f) L. R. MacGillivray, J. L. Atwood, in *Advances in Supramolecular Chemistry*; Gokel, G. W., Ed.; JAI Press: Greenwich, **2000**, 157.
- ¹⁰ (a) V. Berl, I. Huc, R. G. Khoury, M. J. Krische, J.-M. Lehn, *Nature* **2000**, *407*, 720-723; (b) V. Berl, I. Huc, R. G. Khoury, J.-M. Lehn, *Chem. Eur. J.* **2001**, *7*, 2810-2820; (c) V. Berl, I. Huc, R. G. Khoury, J.-M. Lehn, *Chem. Eur. J.* **2001**, *7*, 2798-2809; (d) M. Suarez, J.-M. Lehn, S. C. Zimmerman, A. Skoulios, B. Heinrich, *J. Am. Chem. Soc.* **1998**, *120*, 9526-9532; (e) C. M. Drain, K. C. Russell, J.-M. Lehn, *Chem. Commun.* **1996**, 337-338.
- ¹¹ J. L. Sessler, D. Magda, H. Furuta, *J. Org. Chem.* **1992**, *57*, 818-826.
- ¹² J. L. Sessler, R. Wang, *J. Am. Chem. Soc.* **1996**, *118*, 9808-9809; J. L. Sessler, R. Wang, *Angew. Chem. Int. Ed. Engl.* **1998**, *37*, 1726-1729.
- ¹³ A. Ranganathan, V. R. Pedireddi, C. N. R. Rao, *J. Am. Chem. Soc.* **1999**, *121*, 1752-1753; J.-M. Lehn, M. Mascal, A. Decian, J. Fischer, *J. Chem. Soc. Chem. Commun.* **1990**, 479-481; J. A. Zerkowski, C. T. Seto, D. A. Wierda, G. M. Whitesides, *J. Am. Chem. Soc.* **1990**, *112*, 9025-9026; C. T. Seto, G. M. Whitesides, *J. Am. Chem. Soc.* **1990**, *112*, 6409-6411; J. A. Zerkowski, J. P. Mathias, G. M. Whitesides, *J. Am. Chem. Soc.* **1994**, *116*, 4305-4315.
- ¹⁴ P. Lipkowski, A. Bielejewska, H. Kooijman, A. L. Spek, P. Timmerman, D. N. Reinhoudt, *Chem. Commun.* **1999**, 1311-1312.
- ¹⁵ (a) J. A. Zerkowski, C. T. Seto, G. M. Whitesides, *J. Am. Chem. Soc.* **1992**, *114*, 5473-5475; (b) J. P. Mathias, E. E. Simanek, J. A. Zerkowski, C. T. Seto, G. M. Whitesides, *J. Am. Chem. Soc.* **1994**, *116*, 4316-4325.
- ¹⁶ (a) M. Mammen, E. E. Simanek, G. M. Whitesides, *J. Am. Chem. Soc.* **1996**, *118*, 12614-12623; (b) C. T. Seto, G. M. Whitesides, *J. Am. Chem. Soc.* **1993**, *115*, 905-916; (c) C. T. Seto, G. M. Whitesides, *J. Am. Chem. Soc.* **1993**, *115*, 1330-1340.
- ¹⁷ L. Isaacs, D. N. Chin, N. Bowden, Y. Xia, G. M. Whitesides, *Perspectives in Supramolecular Chemistry*, Vol. 4 (Ed.: D. N. Reinhoudt), Wiley, **1999**.
- ¹⁸ (a) J. P. Mathias, C. T. Seto, E. E. Simanek, G. M. Whitesides, *J. Am. Chem. Soc.* **1994**, *116*, 1725-1736; (b) C. T. Seto, G. M. Whitesides, *J. Am. Chem. Soc.* **1991**, *113*, 712-713.
- ¹⁹ R. H. Vreekamp, J. P. M. Van Duynhoven, M. Hubert, W. Verboom, D. N. Reinhoudt, *Angew. Chem. Int. Ed. Engl.* **1996**, *35*, 1215-1218.
- ²⁰ (a) H. A. Klok, K. A. Jolliffe, C. L. Schauer, L. J. Prins, J. P. Spatz, M. Möller, P. Timmerman, D. N. Reinhoudt, *J. Am. Chem. Soc.* **1999**, *121*, 7154-7155; (b) H. Schönherr, V. Paraschiv, S. Zapotoczny, M. Crego-

- Calama, P. Timmerman, C. W. Frank, G. J. Vancso, D. N. Reinhoudt, *Proc. Natl. Acad. Sci. U.S.A.*, **2002**, *99*, 5024-5027; (c) J. J. Garcia-Lopez, S. Zapotocznny, P. Timmerman, F. C. J. M. Van Veggel, G. J. Vansco, M. Crego-Calama, D. N. Reinhoudt, *Chem. Commun.* **2003**, 352-353.
- ²¹ K. A. Jolliffe, P. Timmerman, D. N. Reinhoudt, *Angew. Chem. Int. Ed. Engl.* **1999**, *38*, 933-937.
- ²² (a) R. Kramer, J.-M. Lehn, A. Marquis-Rigault, *Proc. Natl. Acad. Sci. U.S.A.*, **1993**, *90*, 5394-5398; (b) D. L. Caulder, K. N. Raymond, *Angew. Chem. Int. Ed. Engl.* **1997**, *36*, 1440-1442; (c) M. Albrecht, O. Blau, E. Wegelius, K. Rissanen, *New. J. Chem.* **1997**, *23*, 667-668; (d) M. Albrecht, O. Blau, R. Fröhlich, *Proc. Natl. Acad. Sci. U.S.A.*, **2002**, *99*, 4867-4872.
- ²³ L. J. Prins, E. E. Neuteboom, V. Paraschiv, M. Crego-Calama, P. Timmerman, D. N. Reinhoudt, *J. Org. Chem.* **2002**, *67*, 4808-4820.
- ²⁴ V. Paraschiv, M. Crego-Calama, R. H. Fokkens, C. J. Padberg, P. Timmerman, D. N. Reinhoudt, *J. Org. Chem.* **2001**, *66*, 8297-8301.
- ²⁵ D. Porath, A. Bezryadin, S. De Vries, C. Dekker, *Nature (London)* **2000**, *403*, 635-638.
- ²⁶ (a) D. J. Cram, *Science* **1983**, *219*, 1177-1183; (b) D. J. Cram, S. Karbach, Y. H. Kim, L. Baczynskyj, G. W. Kallemeyn, *J. Am. Chem. Soc.* **1985**, *107*, 2575-2576; (c) J. Conceill, L. Lacombe, A. Collet, *J. Am. Chem. Soc.* **1985**, *107*, 6993-6996; (d) D. J. Cram, M. E. Tanner, C. B. Knobler, *J. Am. Chem. Soc.* **1991**, *113*, 7717-7727; (e) P. Timmerman, W. Verboom, F. C. J. M. Van Veggel, W. P. Wan Hoorn, D. N. Reinhoudt, *Angew. Chem. Int. Ed. Engl.* **1994**, *33*, 1292-1295.
- ²⁷ (a) J. Rebek, Jr., *Pure. Appl. Chem.* **1996**, *68*, 1261-1266; (b) J. De Mendoza, *Chem. Eur. J.* **1998**, *4*, 1373-1377; (c) F. Hof. J. Rebek, Jr., *Proc. Natl. Acad. Sci. U.S.A.*, **2002**, *99*, 4775-4777.
- ²⁸ (a) K. D. Shimizu, J. Rebek, Jr., *Proc. Natl. Acad. Sci. U.S.A.*, **1995**, *92*, 12403-12407; (b) B. C. Hamann, K. D. Shimizu, J. Rebek, Jr., *Angew. Chem. Int. Ed. Engl.* **1996**, *35*, 1326-1329.
- ²⁹ R. P. Bonar-Law, J. K. M. Sanders, *Tetrahedron Lett.* **1993**, *34*, 1677.
- ³⁰ S. B. Lee, J.-I. Hong, *Tetrahedron Lett.* **1996**, *37*, 8501.
- ³¹ (a) S. Zhao, J. H. T. Luong, *J. Chem. Soc. Chem. Commun.* **1994**, 2307-2308; (b) S. Zhao, J. H. T. Luong, *J. Chem. Soc. Chem. Commun.* **1995**, 663-664.
- ³² (a) R. Wyler, J. De Mendoza, J. Rebek, Jr., *Angew. Chem. Int. Ed. Engl.* **1993**, *32*, 1699-1701; (b) T. Martin, U. Obst, J. Rebek, Jr., *Science* **1998**, *281*, 1842-1845; (c) B. M. O'Leary, R. M. Grotzfeld, J. Rebek, Jr., *J. Am. Chem. Soc.* **1997**, *119*, 11701-11702.
- ³³ (a) I. Higler, L. Grave, E. Breuning, W. Verboom, F. de Jong, T. M. Fyles, D. N. Reinhoudt, *Eur. J. Org. Chem.* **2000**, 1727-1734; (b) R. Vreekamp, W. Verboom, D. N. Reinhoudt, *J. Org. Chem.* **1996**, *61*, 4282-4288; (c) F. Corbellini, R. Fiammengo, P. Timmerman, M. Crego-Calama, K. Versluis, A. J. R. Heck, I. Luyten, D. N. Reinhoudt, *J. Am. Chem. Soc.* **2002**, *124*, 6569-6575.
- ³⁴ (a) R. K. Castellano, J. Rebek, Jr., *J. Am. Chem. Soc.* **1998**, *120*, 3657-3663; (b) R. K. Castellano, S. L. Craig, C. Nuckolls, J. Rebek, Jr., *J. Am. Chem. Soc.* **2000**, *122*, 7876-7882.
- ³⁵ (a) A. Shivanyuk, E. F. Paulus, V. Böhmer, *Angew. Chem. Int. Ed. Engl.* **1999**, *38*, 2906-2909; (b) K. Koh, K. Araki, S. Shinkai, *Tetrahedron Lett.* **1994**, *35*, 8255-8258; (c) M. O. Vysotsky, I. Thondorf, V. Böhmer, *Angew. Chem. Int. Ed. Engl.* **2000**, *39*, 1264-1267.
- ³⁶ K. Kobayashi, K. Ishii, S. Sakamoto, T. Shirasaka, K. Yamaguchi, *J. Am. Chem. Soc.* **2003**, *125*, 10615-10624.
- ³⁷ a) S. Leininger, B. Olenyuk, P. J. Stang, *Chem. Rev.* **2000**, *100*, 853-907; b) S. R. Seidel, P. J. Stang, *Acc. Chem. Res.* **2002**, *35*, 972-983.
- ³⁸ (a) M. Fujita, K. Ogura, *Coord. Chem. Rev.* **1996**, *148*, 249-264; (b) M. Fujita, *Chem. Soc. Rev.* **1998**, *27*, 417-425; (c) M. Fujita, *Acc. Chem. Res.* **1999**, *32*, 53-61.
- ³⁹ (a) R. V. Slone, K. D. Benkstein, S. Belanger, J. T. Hupp, I. A. Guzei, A. L. Rheingold, *Coord. Chem. Rev.* **1998**, *171*, 221-243; (b) M. H. Keefe, K. D. Benkstein, J. T. Hupp, *Coord. Chem. Rev.* **2000**, *205*, 201-228.
- ⁴⁰ (a) M. Fujita, J. Yazaki, K. Ogura, *J. Am. Chem. Soc.* **1990**, *112*, 5645-5647; (b) M. Fujita, J. Yazaki, K. Ogura, *Tetrahedron Lett.* **1991**, *32*, 5589-5592; (c) M. Fujita, J. Yazaki, K. Ogura, *Chem. Lett.* **1991**, 1031-1032; (d) M. Fujita, O. Sasaki, T. Mitsuhashi, T. Fujita, J. Yazaki, K. Yamaguchi, K. Ogura, *Chem. Commun.* **1996**, 1535-1536.
- ⁴¹ S. B. Lee, S. Hwang, D. S. Chung, H. Yun, J. I. Hong, *Tetrahedron Lett.* **1998**, *39*, 873-876.
- ⁴² C. A. Schalley, T. Müller, P. Linnartz, M. Witt, M. Schäfer, A. Lützen, *Chem. Eur. J.* **2003**, *8*, 3538-3551.
- ⁴³ P. J. Stang, D. H. Cao, *J. Am. Chem. Soc.* **1994**, *116*, 4981-4982.
- ⁴⁴ P. J. Stang, B. Olenyuk, *Acc. Chem. Res.* **1997**, *30*, 502-518.
- ⁴⁵ (a) J. Manna, J. A. Whiteford, P. J. Stang, D. C. Muddiman, R. D. Smith, *J. Am. Chem. Soc.* **1996**, *118*, 8731-8732; (b) J. Manna, J. A. Whiteford, C. Kuehl, P. J. Stang, *Organometallics* **1997**, *16*, 1897-1905; (c) P. J. Stang, N. E. Persky, J. Manna, *J. Am. Chem. Soc.* **1997**, *119*, 4777-4778.
- ⁴⁶ S.-S. Sun, A. J. Lees, *Inorg. Chem.* **2001**, *40*, 3154-3160.
- ⁴⁷ (a) C. M. Drain, J.-M. Lehn, *J. Chem. Soc. Chem. Commun.* **1994**, 2313-2315; J. Fan, J. A. Whiteford, B. Olenyuk, M. D. Levin, P. J. Stang, E. B. Fleischer, *J. Am. Chem. Soc.* **1999**, *121*, 2741-2752; (b) E. Iengo, E. Zangrando, E. Alessio, *Eur. J. Inorg. Chem.* **2003**, *13*, 2371-2384 and ref's therein; (c) K. Fukushima, K.

- Funatsu, A. Ichimura, Y. Sasaki, M. Suzuki, T. Fujihara, K. Tsuge, T. Imamura, *Inorg. Chem.* **2003**, *42*, 3187-3193.
- ⁴⁸ G. Li, Y. Song, H. Hou, L. Li, Y. Fan, Y. Zhu, X. Meng, L. Mi, *Inorg. Chem.* **2003**, *42*, 913-920 and ref's therein.
- ⁴⁹ S. J. Lee, W. Lin, *J. Am. Chem. Soc.* **2002**, *124*, 4554-4555.
- ⁵⁰ (a) S. J. Lee, A. Hu, W. Lin, *J. Am. Chem. Soc.* **2002**, *124*, 12948-12949; (b) J. Hua, W. Lin, *Org. Lett.* **2004**, ASAP.
- ⁵¹ C. J. Kuehl, S. D. Huang, P. J. Stang, *J. Am. Chem. Soc.* **2001**, *123*, 9634-9641.
- ⁵² K. M. Park, S.-Y. Kim, J. Heo, D. Whang, S. Sakamoto, K. Yamaguchi, K. Kim, *J. Am. Chem. Soc.* **2002**, *124*, 2140-2147 and ref's therein.
- ⁵³ (a) A. Sautter, D. Schmid, G. Jung, F. Würthner, *J. Am. Chem. Soc.* **2001**, *123*, 5424-5430; (b) F. Würthner, A. Sautter, *Chem. Commun.* **2000**, 445-446; (c) F. Würthner, A. Sautter, D. Schmid, P. J. A. Weber, *Chem. Eur. J.* **2001**, *7*, 894-902; (d) F. Würthner, A. Sautter, *Org. Biomol. Chem.* **2003**, *1*, 240-243.
- ⁵⁴ M. Ferrer, M. Mounir, O. Rossell, E. Ruiz, M. A. Maestro, *Inorg. Chem.* **2003**, *42*, 5890-5899.
- ⁵⁵ T. Yamamoto, A. M. Arif, P. J. Stang, *J. Am. Chem. Soc.* **2003**, *125*, 12309-12317.
- ⁵⁶ H. Jiang, W. Lin, *J. Am. Chem. Soc.* **2003**, *125*, 8084-8085.
- ⁵⁷ M. Fujita, S.-Y. Yu, T. Kusukawa, H. Funaki, K. Ogura, K. Yamaguchi, *Angew. Chem. Int. Ed. Engl.* **1998**, *37*, 2082-2085.
- ⁵⁸ (a) M. Fujita, S. Nagao, K. Ogura, *J. Am. Chem. Soc.* **1995**, *117*, 1649-1650; (b) S. Hiroaka, M. Fujita, *J. Am. Chem. Soc.* **1999**, *121*, 10239-10240; (c) S. Hiraoka, Y. Kubota, M. Fujita, *Chem. Commun.* **2000**, 1509-1510.
- ⁵⁹ D. K. Chand, K. Biradha, M. Fujita, S. Sakamoto, K. Yamaguchi, *Chem. Commun.* **2002**, 2486-2487.
- ⁶⁰ (a) C. J. Kuehl, Y. K. Kryshenko, U. Radhakrishnan, S. R. Seidel, S. D. Huang, P. J. Stang, *Proc. Natl. Acad. Sci. USA.*, **2002**, *99*, 4932-4936; (b) C. M. Hartshorn, P. J. Steel, *Chem. Commun.* **1997**, 541-542; (c) C. J. Kuehl, T. Yamamoto, S. R. Seidel, P. J. Stang, *Org. Lett.* **2002**, *6*, 913-915.
- ⁶¹ (a) L. Pirondini, F. Bertolini, B. Cantadori, F. Ugozzoli, C. Massera, E. Dalcanale, *Proc. Natl. Acad. Sci. U.S.A.*, **2002**, *99*, 4911-4915; (b) B. Manimaran, P. Thanasekaran, T. Rajendran, R. T. Liao, Y. H. Liu, G. H. Lee, S. M. Peng, S. Rajagopal, K. L. Lu, *Inorg. Chem.* **2003**, *42*, 4795-4797 and ref's therein.
- ⁶² A. Ikeda, M. Yoshimura, H. Udzu, C. Fukuhara, S. Shinkai, *J. Am. Chem. Soc.* **1999**, *121*, 4296-4297.
- ⁶³ (a) M. Aoyagi, K. Biradha, M. Fujita, *J. Am. Chem. Soc.* **1999**, *121*, 7457-7458; (b) M. Aoyagi, S. Tashiro, M. Tominaga, K. Biradha, M. Fujita, *Chem. Commun.* **2002**, 2036-2037; (c) M. Tominaga, S. Tashiro, M. Aoyagi, M. Fujita, *Chem. Commun.* **2002**, 2038-2039.
- ⁶⁴ S. Tashiro, M. Tominaga, T. Kusukawa, M. Kawano, S. Sakamoto, K. Yamaguchi, M. Fujita, *Angew. Chem. Int. Ed. Engl.* **2003**, *42*, 3267-3270.
- ⁶⁵ (a) A. Hori, H. Kataoka, T. Okano, S. Sakamoto, K. Yamaguchi, M. Fujita, *Chem. Commun.* **2003**, 182-183; (b) C. Dietrich-Buchecker, B. Colasson, M. Fujita, A. Hori, N. Geum, S. Sakamoto, K. Yamaguchi, J.-P. Sauvage, *J. Am. Chem. Soc.* **2003**, *125*, 5717-5725.
- ⁶⁶ S. Leininger, J. Fan, M. Schmitz, P. J. Stang, *Proc. Natl. Acad. Sci. U.S.A.*, **2000**, *97*, 1380-1384.
- ⁶⁷ M. Schweiger, S. R. Seidel, M. Schmitz, P. J. Stang, *Org. Lett.* **2000**, *2*, 1255-1257.
- ⁶⁸ Y. K. Kryshenko, S. R. Seidel, D. C. Muddiman, A. I. Nepomuceno, P. J. Stang, *J. Am. Chem. Soc.* **2003**, *125*, 9647-9652.
- ⁶⁹ B. Olenyuk, M. D. Levin, J. A. Whiteford, J. E. Shield, P. J. Stang, *J. Am. Chem. Soc.* **1999**, *121*, 10434-10435.
- ⁷⁰ (a) E. O. Stejskal, J. E. Tanner, *J. Chem. Phys.* **1965**, *42*, 288; (b) J. Tanner, *J. Chem. Phys.* **1970**, *52*, 2523-2526; (c) O. Mayzel, Y. Cohen, *J. Chem. Soc. Chem. Commun.* **1994**, 1901-1902.
- ⁷¹ G. S. Hanan, C. R. Arana, J.-M. Lehn, G. Baum, D. Fenske, *Chem. Eur. J.* **1996**, *10*, 1292-1302.
- ⁷² G. S. Hanan, J.-M. Lehn, *Chem. Commun.* **1996**, 2019-2020.
- ⁷³ **Bidentate based grids**; (a) P. N. W. Baxter, J.-M. Lehn, J. Fischer, M. T. Youinou, *Angew. Chem. Int. Ed. Engl.* **1994**, *33*, 2284-2287; (b) P. N. W. Baxter, J.-M. Lehn, B. O. Kneisel, D. Fenske, *Chem. Commun.* **1997**, 2231-2232; (c) P. N. W. Baxter, J.-M. Lehn, B. O. Kneisel, D. Fenske, *Angew. Chem., Int. Ed. Engl.* **1997**, *36*, 1978-1981; (d) P. N. W. Baxter, J.-M. Lehn, K. Rissanen, *Chem. Commun.* **1997**, 1323-1324; (e) I. Weissbuch, P. N. W. Baxter, I. Kuzmenko, H. Cohen, S. Cohen, K. Kjaer, P. B. Howes, J. Nielsen, J.-M. Lehn, L. Leiserowitz, M. Lahav, *Chem. Eur. J.* **2000**, *6*, 725-734; **Tridentate based grids**; (f) G. S. Hanan, D. Volkmer, U. S. Schubert, J.-M. Lehn, G. Baum, D. Fenske, *Angew. Chem. Int. Ed. Engl.* **1997**, *36*, 1842-1844; (g) J. Rojo, J.-M. Lehn, G. Baum, D. Fenske, O. Waldmann, P. Müller, *Eur. J. Inorg. Chem.* **1999**, 517-522; (h) O. Waldmann, J. Hassmann, P. Müller, D. Volkmer, U. S. Schubert, J.-M. Lehn, *Phys. Rev. B Cond. Matter* **1998**, *58*, 3277-3285; (i) Weissbuch, P. N. W. Baxter, S. Cohen, H. Cohen, K. Kjaer, P. B. Howes, J. A. Nielsen, G. S. Hanan, U. S. Schubert, J.-M. Lehn, L. Leiserowitz, M. Lahav, *J. Am. Chem. Soc.* **1998**, *120*, 4850-4860; (j) A. M. Garcia, F. J. Romero-Salguero, D. M. Bassani, J.-M. Lehn, G. Baum, D. Fenske, *Chem. Eur. J.* **1999**, *6*, 1803-1808; (k) H. Nierengarten, E. Leize, E. Breuning, A. Garcia, F. Romero-Salguero, J. Rojo, J.-M. Lehn, A. Van Dorsselaer, *J. Mass. Spectrum.* **2002**, *37*, 56-62; (l) J. R. Nitschke, J.-M. Lehn, *Proc. Natl. Acad. Sci. U.S.A.*, **2003**, *100*, 11970-11974; (m) M. Barboiu, G. Vaughan, R. Graff, J.-M. Lehn, *J. Am. Chem. Soc.* **2003**,

125, 10257-10265 and refs therein.; (n) M. T. Youinou, N. Rahmouni, J. Fischer, J. A. Osborn, *Angew. Chem. Int. Ed. Engl.* **1992**, *31*, 733-735.

⁷⁴ (a) D. P. Funeriu, J.-M. Lehn, G. Baum, D. Fenske, *Chem. Eur. J.* **1997**, *3*, 99-104; (b) D. P. Funeriu, J.-M. Lehn, K. M. Fromm, D. Fenske, *Chem. Eur. J.* **2000**, *6*, 2103-2111; (c) J.-M. Lehn, *Chem. Eur. J.* **2000**, *6*, 2097-2102; (d) D. P. Funeriu, K. Rissanen, J.-M. Lehn, *Proc. Natl. Acad. Sci. U.S.A.*, **2001**, *98*, 10546-10551.

⁷⁵ A. M. Garcia, D. M. Bassani, J. M. Lehn, G. Baum, D. Fenske, *Chem. Eur. J.* **1999**, *5*, 1234-1238; P. N. W. Baxter, J.-M. Lehn, O. B. Kneisel, G. Baum, D. Fenske, *Chem. Eur. J.* **1999**, *5*, 113-120; P. N. W. Baxter, J.-M. Lehn, G. Baum, D. Fenske, *Chem. Eur. J.* **1999**, *5*, 102-112; A. Marquis Rigault, A. D. Gervais, P. N. W. Baxter, A. Van Dorsselaer, J.-M. Lehn, *Inorg. Chem.* **1996**, *35*, 2307-2310; P. N. W. Baxter, J.-M. Lehn, A. De Cian, J. Fischer, *Angew. Chem. Int. Ed. Engl.* **1993**, *32*, 69-72; J.-M. Lehn, *Supramolecular Chemistry*; VCH Publishers: Weinheim, Germany, **1995**; p 155.

⁷⁶ P. N. W. Baxter, J.-M. Lehn, G. Baum, D. Fenske, *Chem. Eur. J.* **2000**, *6*, 4510-4517.

⁷⁷ A. Marquis, J.-P. Kintzinger, R. Graff, P. N. W. Baxter, J.-M. Lehn, *Angew. Chem. Int. Ed. Engl.* **2002**, *41*, 2760-2764.

⁷⁸ D. M. Bassani, J.-M. Lehn, K. Fromm, D. Fenske, *Angew. Chem. Int. Ed. Engl.* **1998**, *37*, 2364-2367.

⁷⁹ E. Breuning, U. Ziener, J.-M. Lehn, E. Wegelius, K. Rissanen, *Eur. J. Inorg. Chem.* **2001**, 1515-1521.

⁸⁰ T. Bark, M. Düggeli, H. Stoeckli-Evans, A. von Zelewsky, *Angew. Chem. Int. Ed. Engl.* **2001**, *15*, 2848-2851.

⁸¹ J. P. Plante, P. D. Jones, D. R. Powell, T. E. Glass, *Chem. Commun.* **2003**, 336-337.

⁸² E. C. Constable, E. Schofield, *Chem. Commun.* **1998**, 403-404.

⁸³ G. R. Newkome, T. J. Cho, C. N. Moorefield, R. Cush, P. S. Russo, L. A. Godinez, M. J. Saunders, P. Mohapatra, *Chem. Eur. J.* **2002**, *8*, 2946-2954.

⁸⁴ E. Leize, A. Van Dorsselaer, R. Krämer, J.-M. Lehn, *J. Chem. Soc. Chem. Commun.* **1993**, 990-993.

⁸⁵ T. Bark, T. Weyhermüller, F. Heirtzler, *Chem. Commun.* **1998**, 1475-1476.

⁸⁶ M. Schmittel, A. Ganz, D. Fenske, *Org. Lett.* **2002**, *14*, 2289-2292.

⁸⁷ J. C. Loren, M. Yoshizawa, R. F. Haldimann, A. Linden, J. S. Siegel, *Angew. Chem. Int. Ed. Engl.* **2003**, *42*, 5702-5705.

⁸⁸ (a) E. J. Enemark, T. D. P. Stack, *Angew. Chem. Int. Ed. Engl.* **1998**, *37*, 932-935; (b) M. Albrecht, *Chem. Soc. Rev.* **1998**, *27*, 281-287.

⁸⁹ M. Albrecht, *Chem. Rev.* **2001**, *101*, 3457-3498.

⁹⁰ D. L. Caulder, K. N. Raymond, *Acc. Chem. Res.* **1999**, *32*, 975-982.

⁹¹ Z. R. Bell, L. P. Harding, M. D. Ward, *Chem. Commun.* **2003**, 2432-2433.

⁹² (a) P. De Wolf, S. L. Heath, J. A. Thomas, *Chem. Commun.* **2002**, 2540-2541; (b) C. Bonnefous, N. Bellec, R. P. Thummel, *Chem. Commun.* **1999**, 1243-1244; (c) J. R. Hall, S. J. Loeb, G. K. H. Shimizu, G. P. A. Yap, *Angew. Chem. Int. Ed. Engl.* **1998**, *37*, 121-123.

⁹³ (a) J. Kang, J. Rebek, Jr., *Nature* **1997**, *385*, 50-52; (b) J. Kang, G. Hilmersson, J. Santamaria, J. Rebek, Jr., *J. Am. Chem. Soc.* **1998**, *120*, 3650-3656; (c) J. Kang, J. Santamaría, G. Hilmersson, J. Rebek, Jr., *J. Am. Chem. Soc.* **1998**, *120*, 7389-7390.

⁹⁴ (a) Lützen, A. R. Renslo, C. A. Schalley, B. M. O'Leary, J. Rebek, Jr., *J. Am. Chem. Soc.* **1999**, *121*, 7455-7456; (b) A. Shivanyuk, J. Rebek, Jr., *J. Am. Chem. Soc.* **2002**, *124*, 12074-12075; (c) P. Ballester, A. Shivanyuk, A. Rafai Far, J. Rebek, Jr., *J. Am. Chem. Soc.* **2002**, *124*, 14014-14016; (d) S. L. Craig, S. Lin, J. Chen, J. Rebek, Jr., *J. Am. Chem. Soc.* **2002**, *124*, 8780-8781; (e) O. Hayashida, A. Shivanyuk, J. Rebek, Jr., *Angew. Chem. Int. Ed. Engl.* **2002**, 3423-3426; (f) D. W. Johnson, F. Hof, P. M. Iovine, C. Nuckolls, J. Rebek, Jr., *Angew. Chem. Int. Ed. Engl.* **2002**, *20*, 3793-3796.

⁹⁵ (a) T. Kusukawa, M. Fujita, *J. Am. Chem. Soc.* **2002**, *124*, 13576-13582; (b) T. N. Parac, M. Scherer, K. Raymond, *Angew. Chem. Int. Ed. Engl.* **2000**, *39*, 1239-1242; (c) T. Kusukawa, M. Fujita, *Angew. Chem. Int. Ed. Engl.* **1998**, *37*, 3142-3144; (d) R. Ziessel, L. Charbonniere, M. Cesario, T. Prange, H. Nierengarten, *Angew. Chem. Int. Ed. Engl.* **2002**, *6*, 975-979.

⁹⁶ J. Chen, J. Rebek, Jr., *Org. Lett.* **2002**, *3*, 327-329.

⁹⁷ J. Chen, S. L. Craig, J. Rebek, Jr., *Nature* **2002**, *415*, 385-386.

⁹⁸ H. Ito, T. Kusukawa, M. Fujita, *Chem. Lett.* **2000**, 598-599.

⁹⁹ (a) C. J. Walter, H. L. Anderson, J. K. M. Sanders, *J. Chem. Soc. Chem. Commun.* **1993**, 458-460; (b) D. H. Leung, D. Fiedler, R. G. Bergman, K. N. Raymond, *Angew. Chem. Int. Ed.* **2004**, *43*, 963-933.

¹⁰⁰ (a) M. Yoshizawa, T. Kusukawa, M. Fujita, S. Sakamoto and K. Yamaguchi, *J. Am. Chem. Soc.* **2001**, *123*, 10454-10459; (b) M. Yoshizawa, Y. Takeyama, T. Kusukawa and M. Fujita, *Angew. Chem. Int. Ed.* **2002**, *41*, 1347-1349.

¹⁰¹ H. Jiang, A. Hu, W. Lin, *Chem. Commun.* **2003**, 96-97.

¹⁰² M. L. Merlau, M. D. P. Mejia, S. T. Nguyen, J. T. Hupp, *Angew. Chem. Int. Ed. Engl.* **2001**, *22*, 4239-4242.

¹⁰³ The dynamic equilibrium between bound and unbound porphyrin catalyst could account for the observed eventual destruction of all of the catalyst after three hours.

¹⁰⁴ Jacobsen, E. N, *Acc. Chem. Res.* **2000**, *33*, 421-431.

- ¹⁰⁵ (a) R. G. Konsler, J. Karl, E. N. Jacobson, *J. Am. Chem. Soc.* **1998**, *120*, 10780-10781; (b) J. M. Ready, E. N. Jacobson, *J. Am. Chem. Soc.* **2001**, *123*, 2687-2688; (c) J. M. Ready, E. N. Jacobsen, *Angew. Chem. Int. Ed. Engl.* **2002**, *41*, 1374-1377.
- ¹⁰⁶ N. C. Gianneschi, P. A. Bertin, S. T. Nguyen, C. A. Mirkin, L. N. Zakharov, A. L. Rheingold, *J. Am. Chem. Soc.* **2003**, *125*, 10508-10509.
- ¹⁰⁷ V. F. Slagt, P. W. N. M. Van Leeuwen, J. N. H. Reek, *Chem. Commun.* **2003**, 2474-2475.
- ¹⁰⁸ V. F. Slagt, P. W. N. M. Van Leeuwen, J. N. H. Reek, *Angew. Chem. Int. Ed. Engl.* **2003**, *42*, 5619-5623.
- ¹⁰⁹ M. Bonchio, T. Carofiglio, M. Carraro, R. Fornasier, U. Tonellato, *Org. Lett.* **2002**, *26*, 4635-4637.
- ¹¹⁰ M. Fujita, Y. J. Kwon, S. Washizu, K. Ogura, *J. Am. Chem. Soc.* **1994**, *116*, 1151-1152.
- ¹¹¹ G. Süß-Fink, M. Faure, T. R. Ward, *Angew. Chem. Int. Ed. Engl.* **2002**, *41*, 99-101.
- ¹¹² A. V. Chuchuryukin, H. P. Dijkstra, B. M. J. M. Suijkerbuijk, R. J. M. K. Gebbink, G. P. M. V. Klink, A. M. Mills, A. L. Spek, G. V. Koten, *Angew. Chem. Int. Ed. Engl.* **2003**, *42*, 228-230.
- ¹¹³ H. Ogoshi, T. Mizutani, T. Hayashi, Y. Kuroda, *The Porphyrin Handbook*, **2000**, Academic press: San Diego.
- ¹¹⁴ C. K. Hui, B. W. K. Chu, N. Y. Zhu, V. W. W. Yam, *Inorg. Chem.* **2002**, *41*, 6178-6180.
- ¹¹⁵ S. J. Lee, C. R. Luman, F. N. Castellano, W. Lin, *Chem. Commun.* **2003**, 2124-2125.
- ¹¹⁶ M. Ruben, J.-M. Lehn, G. Vaughan, *Chem. Commun.* **2003**, 1338-1339.
- ¹¹⁷ R. Takahashi, Y. Kobuke, *J. Am. Chem. Soc.* **2003**, *125*, 2372-2373.
- ¹¹⁸ (a) Y. Kuroda, K. Sugou, K. Sasaki, *J. Am. Chem. Soc.* **2000**, *122*, 7833-7834; (b) K. Sugou, K. Sasaki, K. Kitajima, T. Iwaki, Y. Kuroda, *J. Am. Chem. Soc.* **2002**, *124*, 1182-1183.
- ¹¹⁹ G. A. Mines, B. C. Tzeng, K. J. Stevenson, J. Li, J. T. Hupp, *Angew. Chem. Int. Ed. Engl.* **2002**, *41*, 154-157.
- ¹²⁰ K. E. Splan, M. H. Keefe, A. M. Assari, K. A. Walters, J. T. Hupp, *Inorg. Chem.* **2002**, *41*, 619-621.
- ¹²¹ A. Tsuda, S. Sakamoto, K. Yamaguchi, T. Aida, *J. Am. Chem. Soc.* **2003**, *125*, 15722-15723.
- ¹²² J. L. Atwood, G. A. Koutsantonis, C. L. Raston, *Nature* **1994**, *368*, 229-231.
- ¹²³ K. Kumazawa, K. Biradha, T. Kusukawa, T. Okano, M. Fujita, *Angew. Chem. Int. Ed. Engl.* **2003**, *42*, 3909-3913.
- ¹²⁴ M. Ziegler, J. L. Brumaghim, K. N. Raymond, *Angew. Chem. Int. Ed. Engl.* **2000**, *39*, 4119-4121.
- ¹²⁵ M. Yoshizawa, T. Kusukawa, M. Fujita, K. Yamaguchi, *J. Am. Chem. Soc.* **2000**, *122*, 6311-6312.
- ¹²⁶ T. Kusukawa, M. Fujita, *J. Am. Chem. Soc.* **1999**, *121*, 1397-1398.
- ¹²⁷ W.-Y. Sun, T. Kusukawa, M. Fujita, *J. Am. Chem. Soc.* **2002**, *124*, 11570-11571.
- ¹²⁸ J.-P. Bourgeois, M. Fujita, M. Kawano, S. Sakamoto, K. Yamaguchi, *J. Am. Chem. Soc.* **2003**, *125*, 9260-9261.
- ¹²⁹ D. L. Claulder, R. E. Powers, T. N. Parac, K. N. Raymond, *Angew. Chem. Int. Ed. Engl.* **1998**, *37*, 1840-1843.
- ¹³⁰ F. Ibukuro, T. Kusukawa, M. Fujita, *J. Am. Chem. Soc.* **1998**, *120*, 8561-8562.
- ¹³¹ (a) N. Matsumoto, Y. Motoda, T. Matsuo, T. Nakashima, N. Re, F. Dahan, J.-P. Tuchagues, *Inorg. Chem.* **1999**, *38*, 1165-1173 and ref's therein; (b) M. Du, X.-H. Bu, J. Ribas, C. Diaz, *Chem. Commun.* **2002**, 2550-2551.
- ¹³² J. D. Crowley, A. J. Goshe, B. Bosnich, *Chem. Commun.* **2003**, 2824-2825.
- ¹³³ B. J. Holliday, J. R. Farrell, C. A. Mirkin, K.-C. Lam, A. L. Rheingold, *J. Am. Chem. Soc.* **1999**, *121*, 6316-6317.
- ¹³⁴ T. Heinz, D. M. Rudkevich, J. Rebek, Jr., *Nature* **1998**, *394*, 764-766.
- ¹³⁵ J. L. Atwood, L. J. Barbour, A. Jerga, *Science* **2002**, *296*, 2367-2369.
- ¹³⁶ L. R. MacGillivray, J. L. Atwood, *Nature* **1997**, *389*, 469-472.
- ¹³⁷ I. E. Philip, A. E. Kaifer, *J. Am. Chem. Soc.* **2002**, *124*, 12678-12679.
- ¹³⁸ A. Scarso, L. Trembleau, J. Rebek, Jr., *Angew. Chem. Int. Ed. Engl.* **2003**, *42*, 5499-5502.
- ¹³⁹ V. Balzani, A. Credi, F. M. Raymo, J. F. Stoddart, *Angew. Chem. Int. Ed. Engl.* **2000**, *39*, 3349-3391.
- ¹⁴⁰ (a) J. P. Collin, C. Dietrich-Buchecker, P. Gavina, M. C. Jimenez-Molero, J. P. Sauvage, *Acc. Chem. Res.* **2001**, *34*, 477-487; (b) M. J. Blanco, M. C. Jimenez, J. C. Chambron, V. Heitz, M. Linke, J. P. Sauvage, *Chem. Soc. Rev.* **1999**, 293-305.
- ¹⁴¹ S. Hiraoka, T. Yi, M. Shiro, M. Shionoya, *J. Am. Chem. Soc.* **2002**, *124*, 14510-14511.
- ¹⁴² Y. L. Cho, H. Uh, S.-Y. Chang, H.-Y. Chang, M.-G. Choi, I. Shin, K.-S. Jeong, *J. Am. Chem. Soc.* **2001**, *123*, 1258-1259 and ref. therein.
- ¹⁴³ P. N. W. Baxter, R. G. Khoury, J.-M. Lehn, G. Baum, D. Fenske, *Chem. Eur. J.* **2000**, *22*, 4140-4148.
- ¹⁴⁴ M. Schmittel, V. Kalsani, unpublished results.
- ¹⁴⁵ M. Scherer, D. L. Caulder, D. W. Johnson, K. R. Raymond, *Angew. Chem. Int. Ed. Engl.* **1999**, *38*, 1588-1592.
- ¹⁴⁶ S.-S. Sun, J. A. Anspach, A. J. Lees, *Inorg. Chem.* **2002**, *41*, 1862-1869.
- ¹⁴⁷ J. M. C. A. Kerckhoffs, F. W. B. van Leeuwen, A. L. Spek, H. Kooijman, M. Crego-Calama, D. N. Reinhoudt, *Angew. Chem. Int. Ed. Engl.* **2003**, *42*, 5717-5722.
- ¹⁴⁸ L. Brunsveld, B. J. B. Folmer, E. W. Meijer and R. P. Sijbesma, *Chem. Rev.* **2001**, *101*, 4071-4097.
- ¹⁴⁹ R. K. Castellano, D. M. Rudkevich and J. Rebek, Jr., *Proc. Natl. Acad. Sci. U.S.A.*, 1997, **94**, 7132-7137.
- ¹⁵⁰ H. Xu, E. M. Hampe, D. M. Rudkevich, *Chem. Commun.* **2003**, 2828-2829.
- ¹⁵¹ M. Ruben, E. Breuning, J.-P. Gisselbrecht, J.-M. Lehn, *Angew. Chem. Int. Ed. Engl.* **2000**, *39*, 4139-4142.

- ¹⁵² M. Ruben, E. Breuning, M. Barboiu, J.-P. Gisselbrecht, J.-M. Lehn, *Chem. Eur. J.* **2003**, *9*, 291-299.
- ¹⁵³ W. Kaim, B. Schwederski, A. Dogan, J. Fiedler, C. J. Kuehl, P. J. Stang, *Inorg. Chem.* **2002**, *41*, 4025-4028.
- ¹⁵⁴ H. Hartmann, S. Berger, R. Winter, J. Fiedler, W. Kaim, *Inorg. Chem.* **2000**, *39*, 4977-4980.
- ¹⁵⁵ P. J. Stang, B. Olenyuk, J. Fan, A. M. Arif, *Organometallics*, **1996**, *15*, 904-908.
- ¹⁵⁶ C.-C. You, F. Würthner, *J. Am. Chem. Soc.* **2003**, *125*, 9716-9725.
- ¹⁵⁷ C. Bucher, C. H. Devillers, J.-C. Moutet, G. Royal, E. Saint-Aman, *Chem. Commun.* **2003**, 888-889.
- ¹⁵⁸ M. Lahav, R. Gabai, A. N. Shipway, I. Willner, *Chem. Commun.* **1999**, 1937-1938.
- ¹⁵⁹ S. Bélanger, J. T. Hupp, C. L. Stern, R. V. Slone, D. F. Watson, T. G. Carrell, *J. Am. Chem. Soc.* **1999**, *121*, 557-563.
- ¹⁶⁰ (a) E. Breuning, M. Ruben, J.-M. Lehn, F. Renz, Y. Garcia, V. Ksenofontov, P. Gülich, E. Wegelius, K. Rissanen, *Angew. Chem. Int. Ed. Engl.* **2000**, *39*, 2504-2507; (b) D. M. Bassani, J.-M. Lehn, S. Serroni, F. Puntoriero, S. Campagna, *Chem. Eur. J.* **2003**, *9*, 4422-4429.

CHAPTER 3

3. Homo and Heteroleptic Aggregation.....	43
3.1 Introduction	43
3.2 State of Knowledge.....	43
3.3 Motivation	45
3.3.1 Interplay of Steric and Electronic Effects in Homo and Heteroleptic aggregation.....	45
3.3.2 Solvent Induced Interconversion of Supramolecular Entities.....	45
3.3.3 Studies Towards The First Kinetically Stable Copper(I)-bisamine Complex.....	46
3.4 Results and Discussion	46
3.4.1 The Hetphen Approach (Supp 3-1)	46
3.4.1.1 Methylaryl Groups as Steric Stoppers.....	46
3.4.1.2 Methoxyaryl Groups as Steric Stoppers	48
3.4.1.3 Steric and Electronic Bias of Copper(I) and 1f Complexation	49
3.4.1.4 Thermodynamic Stability of Homoleptic and Heteroleptic Complexes from UV- vis Titrations.....	51
3.4.1.5 Formation of a Heteroleptic Spiral assembly	52
3.4.2 Solvent Induced Interconversion of a Grid and Rack Assembly (chapter 2, p. 24)	53
3.4.3 Kinetically Inert Bisphenanthroline Copper Complex (Supp 3-2).....	55
3.5 Summary	57

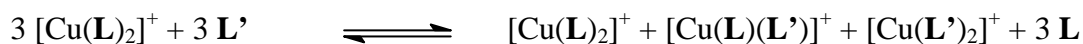
3. Homo and Heteroleptic Aggregation

3.1 Introduction

As discussed in the first and second chapter enormous progress has been made in engineering homoligand supramolecular architectures.¹ Despite this progress, the ability to control assemblies comprised of compositionally different building blocks at will is still very limited. Therefore, investigations into the development of multicomponent supramolecular toolkits is very much warranted. In the present chapter the mechanistic aspects of the HETPHEN (**h**eteroleptic **bisphen**anthroline copper complex, originally developed by Andrea Ganz)^{6a} approach and the selective formation of heteroleptic aggregates over homoleptic ones will be detailed (Supp 3-1). Finally, this approach was used to yield a spiral motif, highlighting the potential of this concept at the supramolecular level (Supp 3-1). A solvent dependent supramolecular system is presented (see chapter 2, p.24). This chapter also includes studies extended towards kinetically inert bisphenanthroline copper complex (Supp 3-2).

3.2 State of Knowledge

As shown in Scheme 3-1, the main problem in building mixed bisphenanthroline copper(I) compounds² is the rapid ligand exchange present in these complexes.³



Scheme 3-1. ligand exchange experiment.

Initial investigations (by Andrea Ganz) of a mixture of phenanthrolines **1a** and **2b** with copper(I) under thermodynamic control, did not lead to a statistical mixture of all three possible complexes. Only the complexes $[\text{Cu}(\mathbf{1a})_2]^+$ and $[\text{Cu}(\mathbf{1a})(\mathbf{2b})]^+$ were formed in a ratio of 2:1, indicating the role of π - π interactions (Figure 3-1).⁴

various possible combinations			
nr. of π - π interactions between biphenyl units (1a) & second phenanthroline 1a or 2b	4	2	0

Figure 3-1. Role of intermolecular (π - π) interactions on homo and heteroleptic composition.

From the above results the following conclusions were drawn. (i) 2,9-arene groups in phenanthrolines stabilize bisphenanthroline copper(I) complexes. (ii) copper(I) complexes with the highest possible number of π - π -stacking interactions are favoured thermodynamically. (iii) bishomoleptic complexes of 4,7-disubstituted ligands do not play a role in the coordination equilibria as long as 2,9-diarylsusbstituted ligands are present.

The qualitative picture of the rapid exchange of phenanthroline ligands (Figure 3-2),⁵ suggests a low barrier I for formation of $[\text{Cu}(\mathbf{1a})_2]^+$. Because the desired bisheteroleptic complex $[\text{Cu}(\mathbf{1a})(\mathbf{2b})]^+$ is not the thermodynamically preferred species in the rapid coordination equilibrium, it was reasoned that increase of the barrier $\text{I} \rightarrow \text{II}$ should reduce the relevant species in solution to a heteroleptic composition $[\text{Cu}(\mathbf{1a})(\mathbf{2b})]^+$.

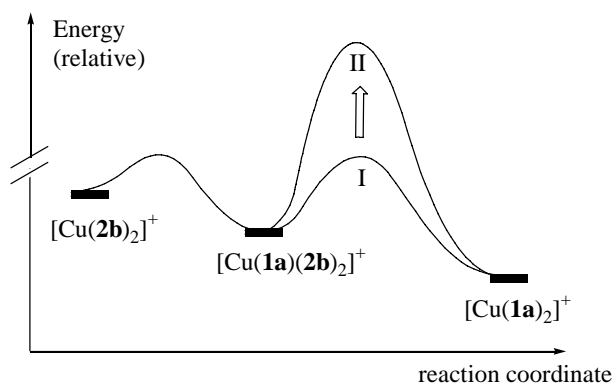


Figure 3-2. Qualitative reaction coordinate for homo and heteroleptic copper(I) phenanthroline complexes. Increase of the barrier from $\text{I} \rightarrow \text{II}$ should reduce the number of relevant species in solution.

The role of steric and electronic effects was probed to increase the barrier as high as II in Figure 3-2 and prevent the formation of $[\text{Cu}(\mathbf{2})_2]^+$. An evaluation of both steric and electronic effects originating from the 2,9-steric stoppers led to the identification of three building blocks which can be explored to give heteroleptic complexes, selectively (Figure 3-3). These building blocks were originally developed by Andrea Ganz and Christoph Michel.⁶

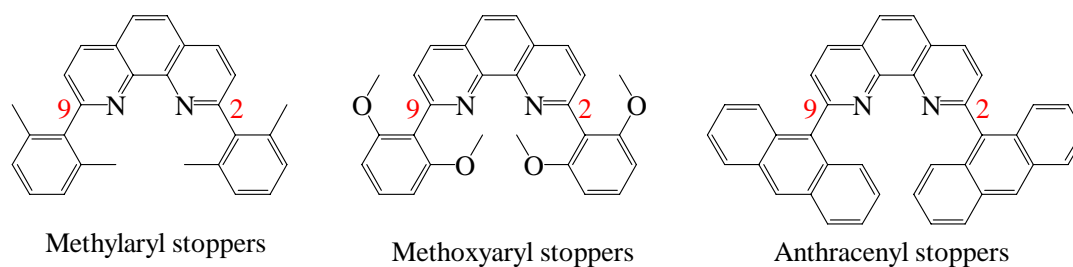


Figure 3-3. HETPHEN building blocks developed by Andrea Ganz and Christoph Michel.

3.3 Motivation

3.3.1 Interplay of Steric and Electronic Effects in Homo and Heteroleptic aggregation

Although the concept to build heteroleptic copper(I) bisphenanthroline complexes (HETPPHEN approach) was developed a while ago, more insight into the mechanistic aspects of the HETPHEN approach was necessary to understand the coordination bias between homo and heteroleptic combinations and apply these principles at the supramolecular level.

Investigations into the selective formation of heteroleptic aggregates over homoleptic ones are of great value for the development of novel supramolecular toolkits. The goal was to study the interplay of steric and electronic factors governing the HETPHEN principles, in solution by ^1H NMR and UV-vis titrations. Finally, the aim was to apply these principles at the supramolecular level to make the HETPHEN approach as a valuable entry into the field of supramolecular chemistry.

3.3.2 Solvent Induced Interconversion of Supramolecular Entities

The effect of solvent on supramolecular entities is well known in hydrogen bond aggregates. However, very few reports are available addressing the solvent role in metal mediated supramolecular aggregates. Since, the coordination behaviour of methoxyaryl building blocks

(**1f**, **1g** and **1h**) was found to be very much solvent dependent it was of very interest to see the the same effect at the supramolecular level.

3.3.3 Studies Towards The First Kinetically Stable Copper(I)-bisamine Complex

Recently, there is also growing interest for the photophysical properties of copper(I)bisimine complexes due to their promising excited state life times which could be comparable to Ru(II)-bisimine complexes. However, in terms of excited state life times copper(I) complexes fall well behind Ru(II)-complexes. Leading pioneers in this area of research, McMillin and Armaroli postulated that the more shielding at the copper(I) center, the higher excited state life times.

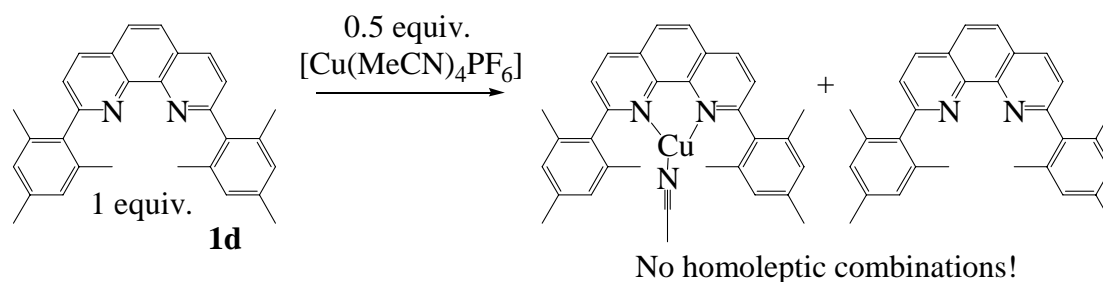
The goal was to prepare a kinetically stable copper(I)bisphenanthroline complex with highest shielding at the copper(I) center and study the effect of shielding and kinetic inertness on the excited state life times.

3.4 Results and Discussion

3.4.1 The Hetphen Approach (Supp 3-1)

3.4.1.1 Methylaryl Groups as Steric Stoppers

The mixture of 1: 0.5-1 equiv. of ligand **1d** and $[\text{Cu}(\text{MeCN})_4]^+$, respectively, in CD_2Cl_2 at room temperature produced only $[\text{Cu}(\mathbf{1d})(\text{MeCN})]^+$ and **1d** (Scheme 3-1). The homoleptic complex $[\text{Cu}(\mathbf{1d})_2]^+$ could not be prepared even under vigorous conditions (heated to reflux in chloroform, DMSO or in tetrachloroethane).^{6a} Since, model calculations proposed that the complex $[\text{Cu}(\mathbf{1d})_2]^+$ should be stable due to the absence of substantial steric hindrance the formation of the bishomoleptic complex $[\text{Cu}(\mathbf{1d})_2]^+$ is most likely kinetically impeded.



Scheme 3-1. Coordination behaviour of **1d** with copper(I) salt.

However, when a 2,9-unsubstituted phenanthroline (*i.e.* **2,3**) was reacted with $[\text{Cu}(\mathbf{1d})(\text{MeCN})]^+$, the mixed complex $[\text{Cu}(\mathbf{1d})(\mathbf{2,3})]^+$ formed exclusively and most importantly in quantitative yield. One complex, $[\text{Cu}(\mathbf{1d})(\mathbf{3b})]^+$, could also be characterized in the solid state (Figure 3- 4).

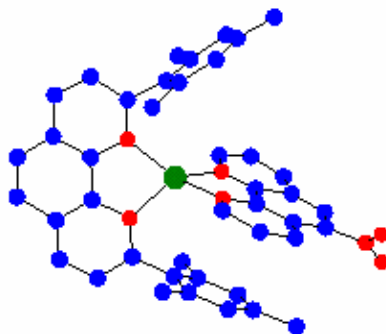
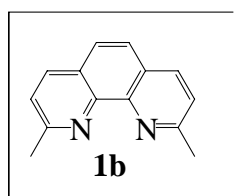
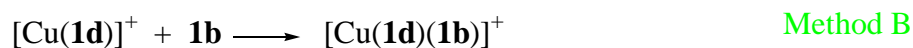
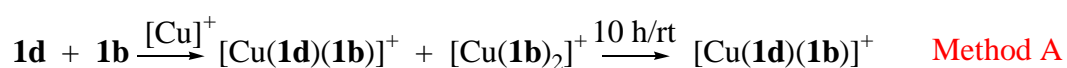


Figure 3- 4. Single crystal structure of $[\text{Cu}(\mathbf{1d})(\mathbf{3b})]^+$ (coop. with Prof. M. U. Schmidt, University of Frankfurt).

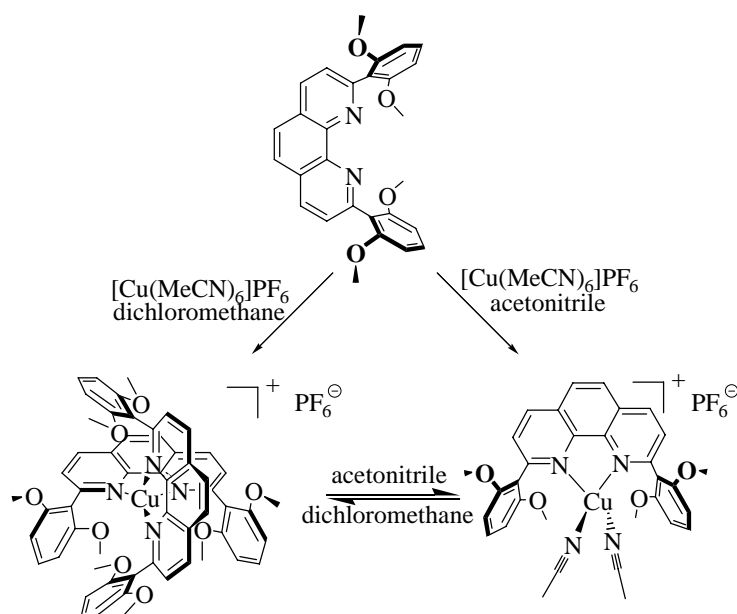
An unexpectedly slow equilibration was observed with $[\text{Cu}(\mathbf{1d})(\mathbf{1b})]^+$ (Scheme 3-2). Both $[\text{Cu}(\mathbf{1b})_2]^+$ and $[\text{Cu}(\mathbf{1d})(\mathbf{1b})]^+$ were resulted when copper(I) salt was reacted with **1d** and **1b** (1:1:1 equiv., respectively) (method A). Since **1b** can also form a strong $[\text{Cu}(\mathbf{1b})_2]^+$, this process runs in competition with $[\text{Cu}(\mathbf{1d})(\mathbf{1b})]^+$. However, after standing at room temperature for 10 h (likewise for 7 d), quantitative formation of the heteroleptic complex resulted. In contrast, when **1b** was added to the methylene chloride solution containing $[\text{Cu}(\mathbf{1d})]^+$ (method B) the heteroleptic complex was afforded instantaneously. Due to this reason we have carried out all the spectrophotometric titrations by method B.



Scheme 3-2. The role of sequential additions in the coordination properties of bisimine ligands.

3.4.1.2 Methoxyaryl Groups as Steric Stoppers

Interesting results were obtained in case of methoxyaryl group stoppers, because the homo and heteroleptic bias was found to be very much solvent dependent. As shown in Scheme 3-3, the methoxy aryl groups in **1f** are not sufficiently bulky to prevent formation of the bishomoleptic complexes $[\text{Cu}(\mathbf{1f})_2]^+$ on steric grounds. However, in presence of less hindered coordination ligands (MeCN or 2,9-unsubstituted phenanthroline) **1f** and Cu(I) salt produced heteroleptic aggregates, selectively.



Scheme 3- 3. The coordination equilibrium of **1f** with copper(I) in different solvents.

Structures of $[\text{Cu}(\mathbf{1f})(1,10\text{-phenanthroline})]^+$ and $[\text{Cu}(\mathbf{1f})(\text{MeCN})_2]^+$ could be characterized in the solid state (Figure 3- 5, Supp 3-1, Supp 7-2 and Supp 7-3).

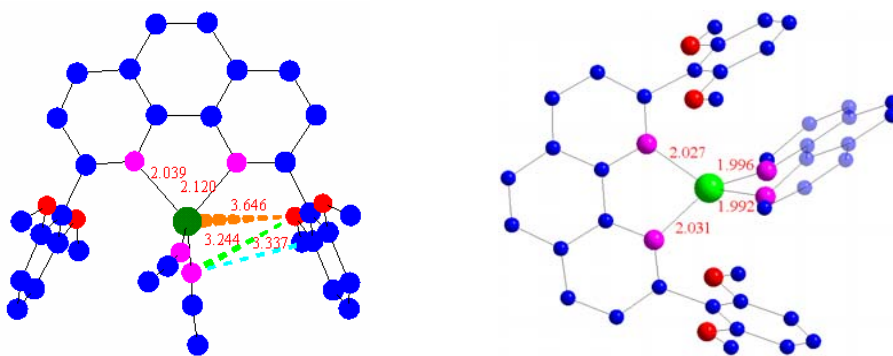
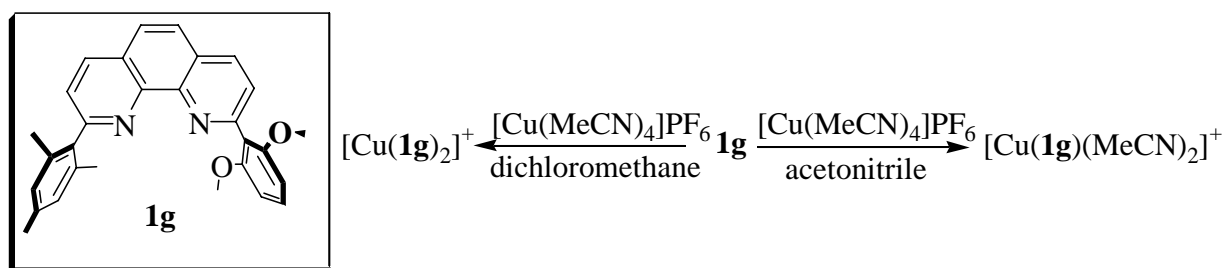


Figure 3- 5. Solid state structure of $[\text{Cu}(\mathbf{1f})(\text{MeCN})_2]^+$ (left) and $[\text{Cu}(\mathbf{1f})(\text{phen})]^+$ (right). Dotted lines showing the intramolecular interactions (coop. with M. Schlosser, Prof. H.-J. Deiseroth, University of Siegen).

3.4.1.3 Steric and Electronic Bias of Copper(I) and **1f** Complexation

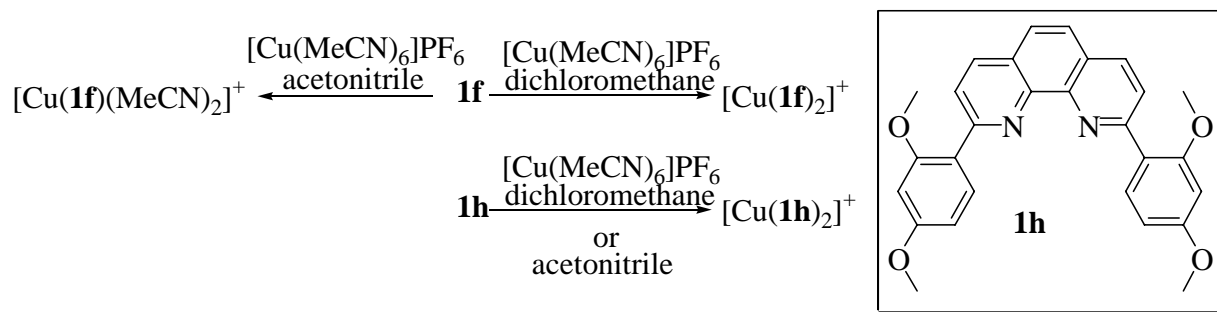
To further understand the interplay of steric and electronic effects in **1d** and **1f**, ligand **1g** sharing both the steric and electronic motifs of **1d** and **1f**, was designed. **1g** showed similar coordination properties with copper(I) as **1f** (Scheme 3- 4) as addition of even small amounts of acetonitrile reverted this complex back to $[\text{Cu}(\mathbf{1g})(\text{MeCN})_2]\text{PF}_6$, indicating a strong coordination of acetonitrile to the copper(I) center.



Scheme 3- 4. Coordination behaviour of ligand **1g** with copper(I) in both dichloromethane and acetonitrile.

The effect of various solvents on the coordination properties of $[\text{Cu}(\mathbf{1f})_2]^+$ was investigated. Interestingly, only solvents with $\text{C}\equiv\text{N}$ have interfered with the homoleptic $[\text{Cu}(\mathbf{1f})_2]\text{PF}_6$ complex to give $[\text{Cu}(\mathbf{1f})(\text{S})_2]\text{PF}_6$ (S = solvent). These observations highlighted the role of $\text{C}\equiv\text{N}$ in stabilizing the $[\text{Cu}(\mathbf{1f})(\text{S})_2]\text{PF}_6$. This fact was also evident from the solid state structure of $[\text{Cu}(\mathbf{1f})(\text{MeCN})_2]$, where strong π - π interactions were detected in between $\text{C}\equiv\text{N}$ and the 2,9-aryl stoppers (3.3 Å).

In order to further check the role of electronic and steric factors, the behaviour of compound **1h** was investigated. Ligands **1h** and **1f** exhibit roughly the same donor properties but they differ markedly in their steric shielding at the phenanthroline binding site. Reaction of **1h** with $[\text{Cu}(\text{MeCN})_4]^+$ in both acetonitrile and methylene chloride resulted in the clean formation of the homoleptic complex $[\text{Cu}(\mathbf{1h})_2]^+$ (Scheme 3- 5), indicating that it is not the methoxy donor groups in **1f** that account for the different behaviour as compared to **1d**.



Scheme 3- 5. Coordination properties of **1f** and **1h** with Cu(I) salt in dichloromethane and acetonitrile.

Apart from the solution state characterization the structure of $[\text{Cu}(\text{1h})_2]^+$ could also be solved by single crystal analysis (Figure 3-6). The dominating role of sterics is very clear from the solid state structure. As shown in Figure 3-6, the ortho-methoxy groups are pointing away (shown with arrows) from the copper(I) center to release the strain in $[\text{Cu}(\text{1h})_2]^+$. Therefore, this complex does not dissociate in coordinating solvents such as acetonitrile or benzonitrile. However, due to the absence of such a strain release (pointing away two artho-methoxy groups from copper(I) center) in $[\text{Cu}(\text{1f})_2]^+$ leads to more strained complex thus, dissociating in presence of coordinating solvents such as acetonitrile.

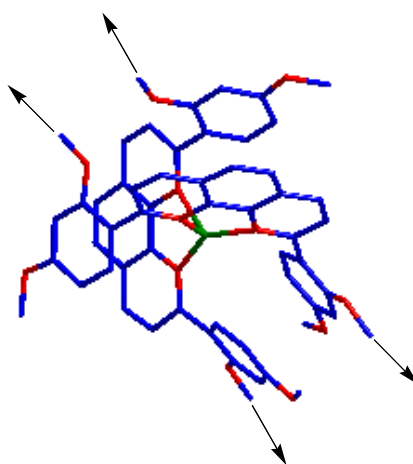


Figure 3-6. Single crystal structure of $[\text{Cu}(\text{1h})_2]^+$ (coop. with Prof. M. U. Schmidt, University of Frankfurt).

3.4.1.4 Thermodynamic Stability of Homoleptic and Heteroleptic Complexes from UV-vis Titrations

Further insight was gained into the complexation equilibria using spectrophotometric titrations (using dichloromethane). The constants were measured for the following equilibria (equations 1 and 2) and results are listed in Table 3-1.



Table 3-1. Equilibrium constants $\log \beta_{111} = \log K_{\text{CuL}}^{\text{Cu}} + \log K_{\text{CuLL}'}^{\text{CuL}}$ for a series of homoleptic and heteroleptic copper bisphenanthroline complexes.

complex	$\log K_{\text{CuL}}^{\text{Cu}}$	$\log K_{\text{CuLL}'}^{\text{CuL}}$	$\log \beta_{111}$ or $\log \beta_{21}$	Literature
$[\text{Cu}(\mathbf{1b})_2]^+$	5.52 ^a	4.58 ^a	10.10 ^a ($\log \beta_{21}$)	11.7 ^b , 9.9 ^c , 10.9 ^{sd}
$[\text{Cu}(\mathbf{3a})_2]^+$	5.30 ^a	4.10 ^a	9.40 ^a ($\log \beta_{21}$)	15.82 ^{9e} , 9.7 ^{7f} , 10.6 ^{7g}
$[\text{Cu}(\mathbf{1d})]^+$	5.10 ^a	-	-	-
$[\text{Cu}(\mathbf{1d})(\mathbf{1a})]^+$	5.10 ^a (for $[\text{Cu}(\mathbf{1d})]^+$)	4.75 ^a	9.85 ^a	-
$[\text{Cu}(\mathbf{1d})(\mathbf{1b})]^+$	5.10 ^a (for $[\text{Cu}(\mathbf{1d})]^+$)	4.60 ^a	9.70 ^a	-
$[\text{Cu}(\mathbf{1d})(\mathbf{2a})]^+$	5.10 ^a (for $[\text{Cu}(\mathbf{1d})]^+$)	4.82 ^a	9.92 ^a	-
$[\text{Cu}(\mathbf{1d})(\mathbf{2b})]^+$	5.10 ^a (for $[\text{Cu}(\mathbf{1d})]^+$)	4.73 ^a	9.83 ^a	-
$[\text{Cu}(\mathbf{1d})(\mathbf{2e})]^+$	5.10 ^a (for $[\text{Cu}(\mathbf{1d})]^+$)	4.63 ^a	9.73 ^a	-
$[\text{Cu}(\mathbf{1d})(\mathbf{3a})]^+$	5.10 ^a (for $[\text{Cu}(\mathbf{1d})]^+$)	4.37 ^a	9.47 ^a	-
$[\text{Cu}(\mathbf{1d})(\mathbf{3b})]^+$	5.10 ^a (for $[\text{Cu}(\mathbf{1d})]^+$)	4.80 ^a	9.90 ^a	-
$[\text{Cu}(\mathbf{1f})]^+$	5.45 ^a	-	-	-
$[\text{Cu}(\mathbf{1f})(\mathbf{3b})]^+$	5.45 ^a (for $[\text{Cu}(\mathbf{1f})]^+$)	4.93 ^a	10.38 ^a	-
$[\text{Cu}(\mathbf{1f})(\mathbf{2a})]^+$	5.45 ^a (for $[\text{Cu}(\mathbf{1f})]^+$)	4.69 ^a	10.14 ^a	-
$[\text{Cu}(\mathbf{1f})(\mathbf{3a})]^+$	5.45 ^a (for $[\text{Cu}(\mathbf{1f})]^+$)	4.82 ^a	10.27 ^a	-
$[\text{Cu}(\mathbf{1f})_2]^+$	5.45 ^a (for $[\text{Cu}(\mathbf{1f})]^+$)	4.55 ^a	10.00 ^a	-
$[\text{Cu}(\mathbf{1g})(\mathbf{3a})]^+$	5.26 ^a (for $[\text{Cu}(\mathbf{1g})]^+$)	4.35 ^a	9.61 ^a	-
$[\text{Cu}(\mathbf{1g})_2]^+$	5.26 ^a	4.20 ^a	9.46 ^a	-
$[\text{Cu}(\mathbf{1h})_2]^+$	5.96 ^a	5.34 ^a	11.30 ^a	-

^a Present work, methylene chloride; $T = 25$ °C; spectrophotometry

^b CH₃CN/DCM/H₂O 80/15/5 (v/v); $T = 25$ °C; (*n*-C₄H₉)₄NCF₃SO₃; spectrophotometry.

^c CH₃CN; $T = 25$ °C; (C₂H₅)₄NClO₄; potentiometry; ref. 7

^d CH₃CN; $T = 25$ °C; spectrophotometry; ref. 8

^e H₂O; $T = 25$ °C; K₂SO₄; potentiometry

^f CH₃CN; $T = 25$ °C; (C₂H₅)₄NClO₄; potentiometry

^g CH₃CN; $T = 25$ °C; (C₂H₅)₄NClO₄; spectrophotometry

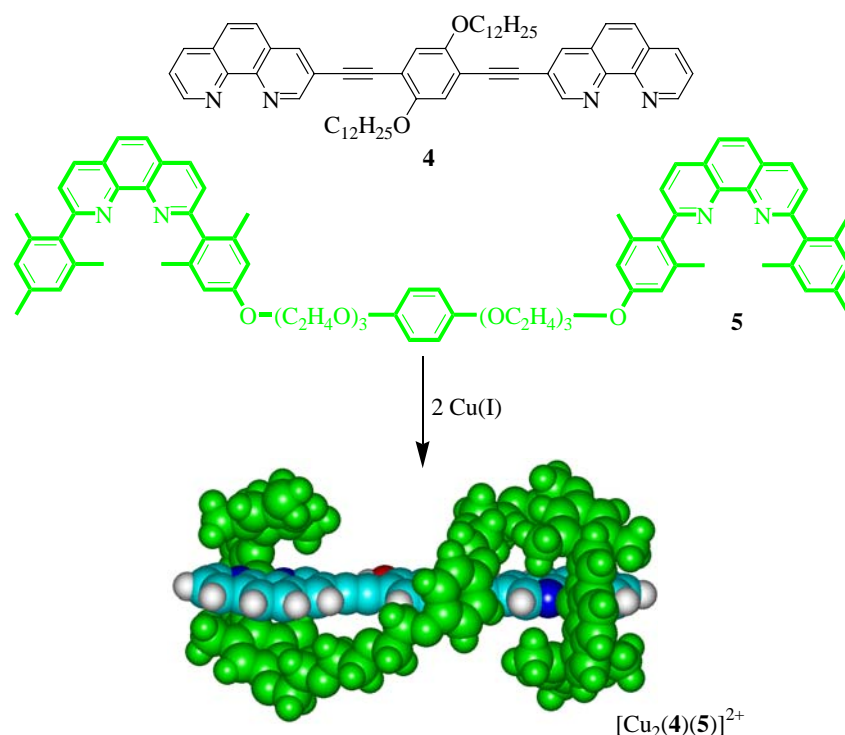
As shown in Table 3-1, there is a higher binding constants for $[\text{Cu}(\mathbf{1b})_2]^+$ than for $[\text{Cu}(\mathbf{3a})_2]^+$, which was readily rationalised by the higher basicity of the nitrogen donor centers in **1b** ($pK_a = 5.35$) than in **3a** ($pK_a = 4.53$)⁹ due to the inductive effect of the methyl groups. Higher binding constants obtained for $[\text{Cu}(\mathbf{1d})(\mathbf{3a})]^+$ and $[\text{Cu}(\mathbf{1f})(\mathbf{3a})]^+$ (heteroleptic complexes) over $[\text{Cu}(\mathbf{3a})_2]^+$ (homoleptic complexes) thus, heteroleptic complexes are preferred over

homoleptic ones. However, due to the interplay of sterics and electronics the data could not be solely explained by electronic factors. **1f** and **1h** share similar electronic effects, they differ distinctly in the steric effects. The higher value obtained for $[\text{Cu}(\mathbf{1h})_2]^+$ ($\log K = 11.3$) than $[\text{Cu}(\mathbf{1f})_2]^+$ ($\log K = 10.0$), highlighting the role of sterics over electronics in this particular case.

Due to the presence of electron donating groups (OMe) in **1f,1g** and **1h** the binding constants are higher than heteroleptic complexes with **1d**. A detailed discussion of these results, including relative stability constants obtained by PM3 calculations and NMR experiments is presented in Supp 3-2.

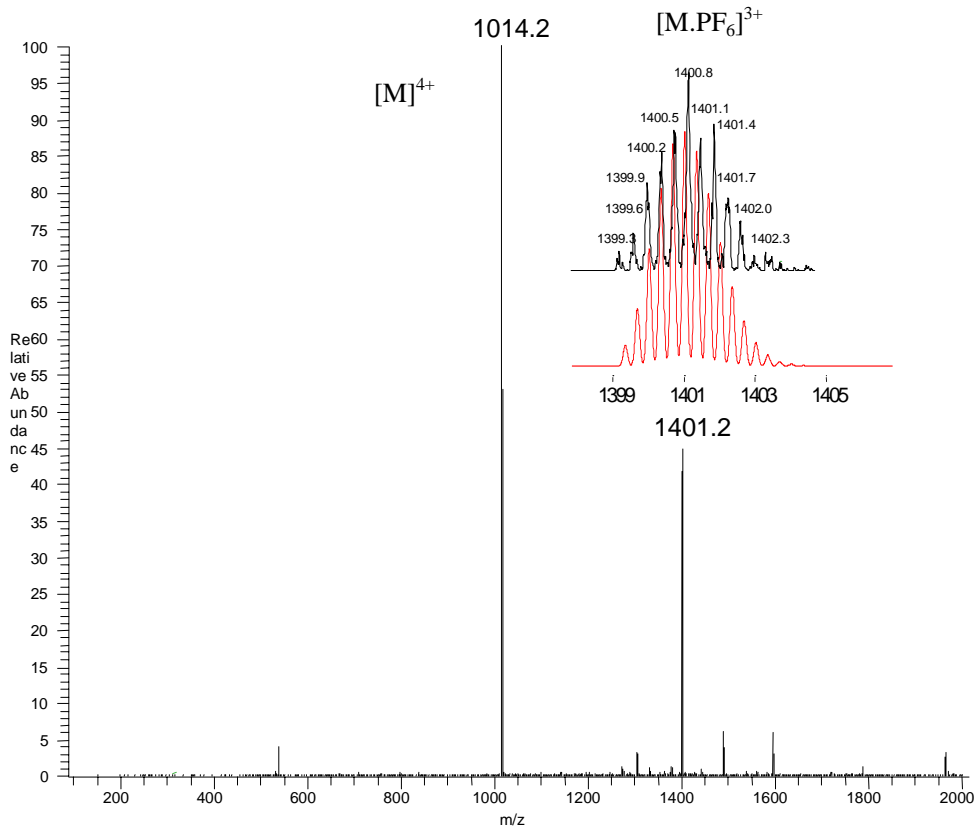
3.4.1.5 Formation of a Heteroleptic Spiral assembly

In order to investigate the potential of the HETPHEN approach at the supramolecular level, a spiral assembly was conceived. As can be seen in Scheme 3-6, a spiral assembly could be obtained by simply reacting ligands **4**¹⁰ and **5**.¹¹



Scheme 3-6. Self-assembly of a supramolecular spiral assembly. $[\text{Cu}_2(\mathbf{4})(\mathbf{5})]^{2+}$ is represented as Hyperchem minimized structure.

a)



b)

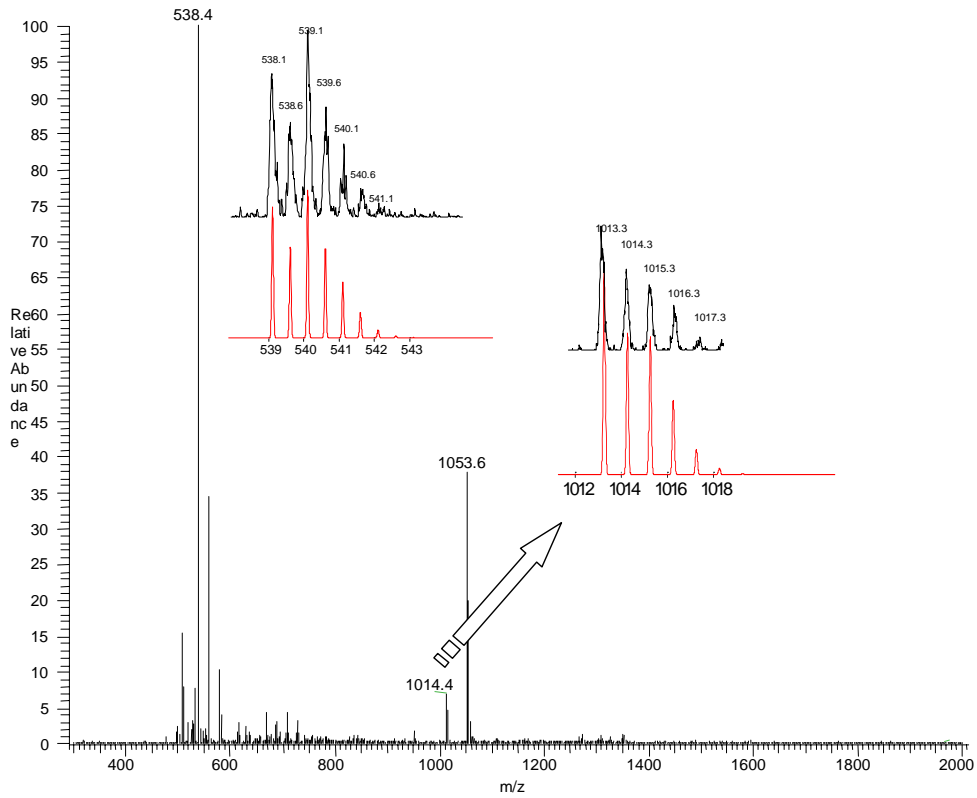
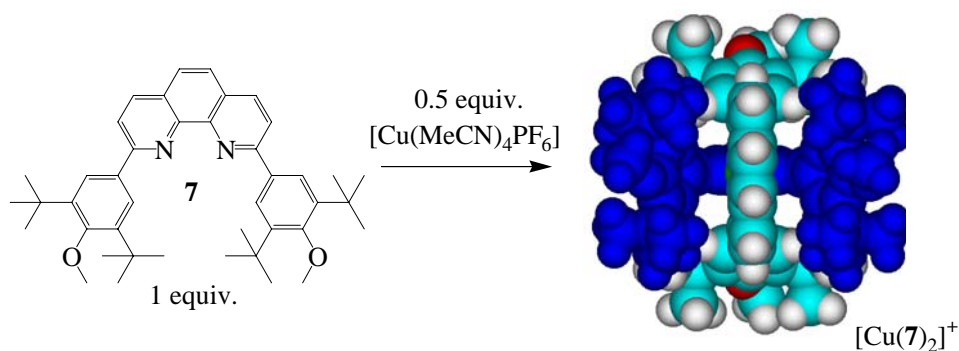


Figure 3-7. a) ESI MS in methylene chloride. b) ESI MS in acetonitrile.

3.4.3 Kinetically Inert Bisphenanthroline Copper Complex (Supp 3-2)

Our interest further extended into designing the first kinetically inert bisphenanthroline copper complex. Due to the increasing attention towards bisphenanthroline copper complex photochemistry,¹⁴ it was postulated that the highest shielding around the copper(I) center would lead to highest excited state life times (Supp 3-2). Therefore, using model calculations we designed a simple phenanthroline ligand bearing steric stoppers at 3 and 5 positions of the aryls (Scheme 3- 8). As shown by the minimised structure (Cu-N_{dist} are kept at 2 Å),¹⁵ the *tert*-butyl groups lock the complex [Cu(7)₂] and lead to a very efficient shielding around copper(I) center.



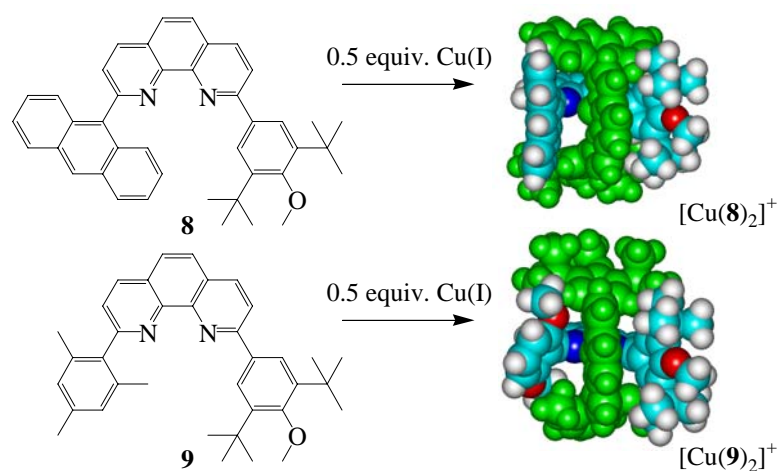
Scheme 3- 8. Formation of [Cu(7)₂]⁺.

As seen by ¹H NMR, the formation of [Cu(7)₂] is very slow (5 d at rt), due to the strain built up by the steric stoppers in the Ts (transition state). Its kinetic inertness towards other weakly coordinating solvents (MeCN or PhCN) and other ligands (2,9-unsubstituted [1,10]phenanthrolines) was probed. In all cases, the homoleptic complex [Cu(7)₂]⁺ was not affected by other ligands and no mixed combinations could be detected. The situation remained the same even at elevated temperatures. Interestingly, sequential addition experiments provided different set of homo and heteroleptic compositions (Supp 3-2). All these observations point to the slow kinetics of [Cu(7)₂]⁺.

The photophysical properties of [Cu(7)₂]⁺ were explored in collaboration with Prof. Armaroli. It was found that unlike any other reported bisphenanthroline copper complex, the emission intensity is not affected by the presence of a Lewis base such as acetone (at 298K), suggesting an efficient shielding of the phenanthroline units from quencher molecules. The emission

spectra of $[\text{Cu}(\mathbf{7})_2]^+$ in four solvents of different polarity and nucleophilic character (DCM, DMF, MeOH, and THF, see Supp 3-2) showed a relatively low decrease of the emission intensity. This behaviour is rather uncommon for copper complexes, whose MLCT band is normally switched off in nucleophilic solvents. These observations point to an extraordinary shielding of the metal center of $[\text{Cu}(\mathbf{7})_2]^+$.

In order to further probe the steric and electronic effects of **7**, ligands **8** and **9** are prepared. However, **8** and **9** form homoleptic complexes instantaneously upon mixing with copper(I) salt (1: 0.5 equiv., respectively). Interestingly, also these homoleptic complexes did not exchange ligands upon the addition of [1,10]phenanthroline (0.5-10 equiv./heat/2 d), indicating kinetic inertness of these complexes. Energy minimised structures propose high shielding around the copper(I) center (Scheme 3- 9). The photophysical properties of these complexes are under investigation.



Scheme 3- 9. Coordination behaviour of ligands **8** and **9** and their homoleptic complexes. Structures of $[\text{Cu}(\mathbf{8})_2]^+$ and $[\text{Cu}(\mathbf{9})_2]^+$ are represented as Hyperchem models.

Interestingly, all three building blocks (**7**, **8** and **9**) could potentially be used to prepare heteroleptic complexes, provided the sequence of addition is controlled (see for details: Supp 3-2). In conclusion, kinetically inert bisphenanthroline copper complexes were realised with promising photophysical characteristics.

3.5 Summary

The ^1H NMR and UV-vis investigations (binding constants) of the coordination properties of ligands **1d-g** led to deeper understanding about the bias present between homo and heteroleptic combinations. Two scenarios were found in this series of ligands investigated

1). In case of ligands **1d,e** (arylmethyl steric stoppers) due to the sterically bulky *ortho*-methyl groups a high kinetic barrier prevents the formation of the homoleptic combination $[\text{Cu}(\mathbf{1d}$ or $\mathbf{1e})_2]^+$. As a consequence the principle of maximum occupancy drives the coordination equilibrium towards the heteroleptic complex (log K 9.4-9.9).

2). Whereas, in case of ligands **1f,g,i** (arylmethoxy steric stoppers) the situation is completely different and $[\text{Cu}(\mathbf{1f,g,i})_2]^+$ becomes the only product in nitrile-free solvents. However, in presence of a second phenanthroline the heteroleptic complex is thermochemically preferred due to the fact that $[\text{Cu}(\mathbf{1f,g,i})_2]^+$ are sterically destabilized. Exploration of these principles led to the construction several supramolecular structures such as spiral and homoleptic grid assembly, making this approach as a valuable entry into the field of supramolecular chemistry.

The deeper insight into these simple complexes paved the way to design the first kinetically stable copper(I)-bisphenanthroline complex $[\text{Cu}(\mathbf{7})_2]^+$. The photophysical properties of this complex were very promising and makes it possible to design better efficient photoactive copper(I) based complexes. Studies in this direction are under investigation, in collaboration with Prof. N. Armaroli.

-
- (1) M. Schmittel, V. Kalsani, Functional, Discrete, Nanoscale Supramolecular Assemblies, *Top. Curr. Chem.* **2005**, 245, 1-53.
 - (2) Copper complexes of phenanthroline/bipyridine with other ligands are rather well studied: a) H. Sigel, P. R. Huber, R. Griesser, B. Prijs, Ternary complexes in solution. XV. Mixed-ligand copper(II) complexes with 2,2'-bipyridyl or 1,10-phenanthroline and pyrocatecholate or derivatives thereof, *Inorg. Chem.* **1973**, 12, 1198-1200. b) H. Sigel, Ternary Cu^{2+} Complexes-Stability, Structure, and Reactivity, *Angew. Chem. Int. Ed. Engl.* **1975**, 14, 394-402. (c) M. Bastian, H. Sigel, Extent of Intermolecular Aromatic-Ring Stacking in Ternary Cu^{2+} Complexes Formed by 2,2'-Bipyridyl or 1,10-Phenanthroline and Flavin Mononucleotide (FMN(2-)), *Inorg. Chem.* **1997**, 36, 1619-1624. (d) C. P. Da Costa, B. Song, F. Gregan, H. Sigel, Intramolecular chelate formation involving the carbonyl oxygen of acetyl phosphate or acetylphosphonate in mixed ligand copper(II) complexes containing also 2,2'-bipyridine or 1,10-phenanthroline. A decreased solvent polarity favours the metal ion-carbonyl oxygen recognition, *Dalton Trans.* **2000**, 899-904.
 - (3) a) H. L. Hodges, M. A. de Araujo, Kinetic investigation of the equilibrium between mono- and bis(1,10-phenanthroline)copper(I) in aqueous and sodium dodecyl sulfate solution, *Inorg. Chem.* **1982**, 21, 3236-3239. b) M. I. Pilo, G. Manca, M. A. Zoroddu, Electrochemical Properties of Copper-Complexes with Unsubstituted and Substituted 1,10-Ortho-Phenanthrolines in N,N-Dimethylformamide Solvent, *Inorg. Chim. Acta* **1991**, 180, 225-230. c) Y. Lei, F. C. Anson, Dynamics of the Coordination Equilibria in

- Solutions Containing Copper(II), Copper(I), and 2,9-Dimethyl-1,10-phenanthroline and Their Effect on the Reduction of O₂ by Cu(I), *Inorg. Chem.* **1995**, *34*, 1083-1089. d) E. Riesgo, Y.-Z. Hu, F. Bouvier, R. P. Thummel, Evaluation of Diimine Ligand Exchange on Cu(I), *Inorg. Chem.* **2001**, *40*, 2541-2546. e) V. Desvergues-Breuil, V. Hebbe, C. Dietrich-Buchecker, J. P. Sauvage, J. Lacour, NMR Evaluation of the Configurational Stability of Cu(I) Complexes, *Inorg. Chem.* **2003**, *42*, 255-257.
- (4) π - π stacking has also been identified in [Cu(phen)(ArCH₂COO)]⁺ complexes: R. Malini-Balakrishnan, K. H. Scheller, U. K. Haering, R. Tribolet, H. Sigel, Ternary complexes in solution. 45. Intramolecular aromatic-ring stacking interactions in dependence on the ligand structure, geometry of the coordination sphere of the metal ion, and solvent composition, *Inorg. Chem.* **1985**, *24*, 2067-2076.
- (5) NMR Experiments at low temperature demonstrate that ligand exchange is rapid at temperatures above -20 °C.
- (6) a) M. Schmittel, A. Ganz, Stable Mixed Phenanthroline Copper(i) Complexes. Key Building Blocks for Supramolecular Coordination Chemistry, *Chem. Commun.* **1997**, 999-1000. b) M. Schmittel, C. Michel, S.-X. Liu, D. Schildbach, D. Fenske, New Sterically Encumbered 2,9-Diarylphenanthrolines for the Selective Formation of Heteroleptic Bis(phenanthroline)copper(I) Complexes, *Eur. J. Inorg. Chem.* **2001**, 1155-1166.
- (7) P. Leupin, Ph.D. Thesis, Université de Fribourg, Switzerland **1980**.
- (8) C. E. Atkins, S. E. Park, J. A. Blaszak, D. R. McMillin, A two-level approach to deconvoluting absorbance data involving multiple species. Applications to copper systems, *Inorg. Chem.* **1984**, *23*, 569-572.
- (9) B. R. James, R. J. P. Williams, *J. Chem. Soc.* **1961**, 2007.
- (10) See Supp 4-2
- (11) See Supp 5-2
- (12) M. Schmittel, C. Michel, A. Wiegrefe, V. Kalsani, Synthesis of soluble, linear bisphenanthrolines for the construction of heteroleptic NanoGrids and nanoboxes, *Synthesis*, **2001**, 1561-1567.
- (13) a) P. N. W. Baxter, R. G. Khoury, J.-M. Lehn, G. Baum, D. Fenske, Adaptive Self-Assembly: Environment-Induced Formation and Reversible Switching of Polynuclear Metallocyclophanes, *Chem. Eur. J.* **2000**, *6*, 4140-4148. b) S. J. Park, D. M. Shin, S. Sakamoto, K. Yamaguchi, Y. K. Chung, M. S. Lah, J.-I. Hong, Dynamic Equilibrium between a Supramolecular Capsule and Bowl Generated by Inter- and Intramolecular Metal Clipping, *Chem. Eur. J.* **2004**, *11*, 235-241.
- (14) N. Armaroli, Photoactive Mono- and Polynuclear Cu(i) Phenanthrolines. A Viable Alternative to Ru(ii) Polypyridines?, *Chem. Soc. Rev.* **2001**, 113-124.
- (15) ~ 2 Å Cu-N_{dist.} is found in solid state (for example see crystal structure of [Cu(**1f**)₂]⁺; Supp 3-1.

Supp 3-1

* Author to whom correspondence should be addressed: *Prof. Dr. Michael Schmittel*, Tel. Int. + 49 271 740 4356; FAX Int. + 49 271 740 3270; e-mail: schmittel@chemie.uni-siegen.de

The HETPHEN approach - Selective Formation of HETeroleptic Cu(I) BisPHENanthroline Complexes: Interplay of π - π Interactions, Solvent Association, and Steric Hindrance.

Michael Schmittel,^{*,‡} Andrea Ganz,[†] Marc Schlosser,[§] Hans-Jörg Deiseroth,[§] Shi Xia Liu,[‡]
Venkateshwarlu Kalsani [‡]

[‡] *Center of Micro and Nanochemistry and Engineering, Organische Chemie I, Universität Siegen, Adolf-Reichwein-Str., D-57068 Siegen, Germany.*

[†] *Institut für Organische Chemie der Universität Würzburg, Am Hubland, D-97074 Würzburg, Germany,*

[§] *Center of Micro and Nanochemistry and Engineering, Anorganische Chemie I, Universität Siegen, Adolf-Reichwein-Str., D-57068 Siegen, Germany.*

Received.....

(Abstract)

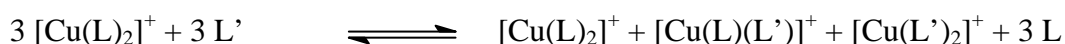
The effects of 2,9-aryl substituents in phenanthrolines on the selective formation of heteroleptic Cu(I) bisphenanthroline complexes provide detailed insight into the multifaceted interplay of π - π interactions, steric hindrance, and solvent association that turn out to be the key features of the HETPHEN concept (heteroleptic bisphenanthroline complex formation). Several new Cu(I) bisphenanthroline complexes were prepared and characterized (including by X-ray diffraction). Absolute and relative complex stability constants were determined by UV-vis titration and equilibration experiments monitored by ¹H NMR. The log β_{111} values demonstrate that the heteroleptic complexes are more stable than the parent [Cu(phen)₂]⁺. One-electron oxidation potentials of the heteroleptic Cu⁺ complexes suggest that the Cu²⁺ species are kinetically and thermodynamically stabilized due to the shielding aryl groups.

Due to the sterically bulky *ortho*-methyl groups in ligands **1d,e** a high kinetic barrier prevents formation of the homoleptic combination $[\text{Cu}(\mathbf{1d} \text{ or } \mathbf{1e})_2]^+$. As a consequence the principle of maximum occupancy drives the coordination equilibrium towards the heteroleptic complex ($\log K > 9.4-9.9$). In contrast, *ortho*-methoxy groups in **1f,g,i** can not prevent the formation of $[\text{Cu}(\mathbf{1f,g,i})_2]^+$, at least in nitrile-free solvents. Due to the fact that $[\text{Cu}(\mathbf{1f,g,i})_2]^+$ are sterically destabilized, however, a heteroleptic complex with a second phenanthroline will be thermochemically preferred. PM3 calculations on isodesmic reactions shed further insight into the thermochemistry of the coordination equilibria.

Introduction

In search for new nanostructured materials, concepts of supramolecular chemistry¹ are proving increasingly important because only a skillful application of weak interactions allows to construct nanostructures² from small building blocks in a highly modular, convergent and versatile fashion. In this context, coordination chemistry has adopted a unique standing because the concise spatial arrangement of building blocks can readily be predicted and varied.

Today it is textbook^{1,3} knowledge that topological instructions engraved into bisimine ligands (phenanthroline or bipyridine) and metal ions (*e.g.* copper(I)) could be used to prepare mesmerizing structures such as catenanes, rotaxanes, molecular knots, lattices, double or three-stranded helices, etc.. Despite these highlights, our capability to fabricate highly diverse dynamic assemblies of metal bisphenanthrolines/bisbipyridines by combining compositionally different building blocks is still rather restricted.^{4,5} The main problem is the well-known rapid ligand exchange of these substitution labile tetrahedral metal complexes⁶ leading to a mixture of all possible coordination compounds (*e.g.* for copper(I)):⁷

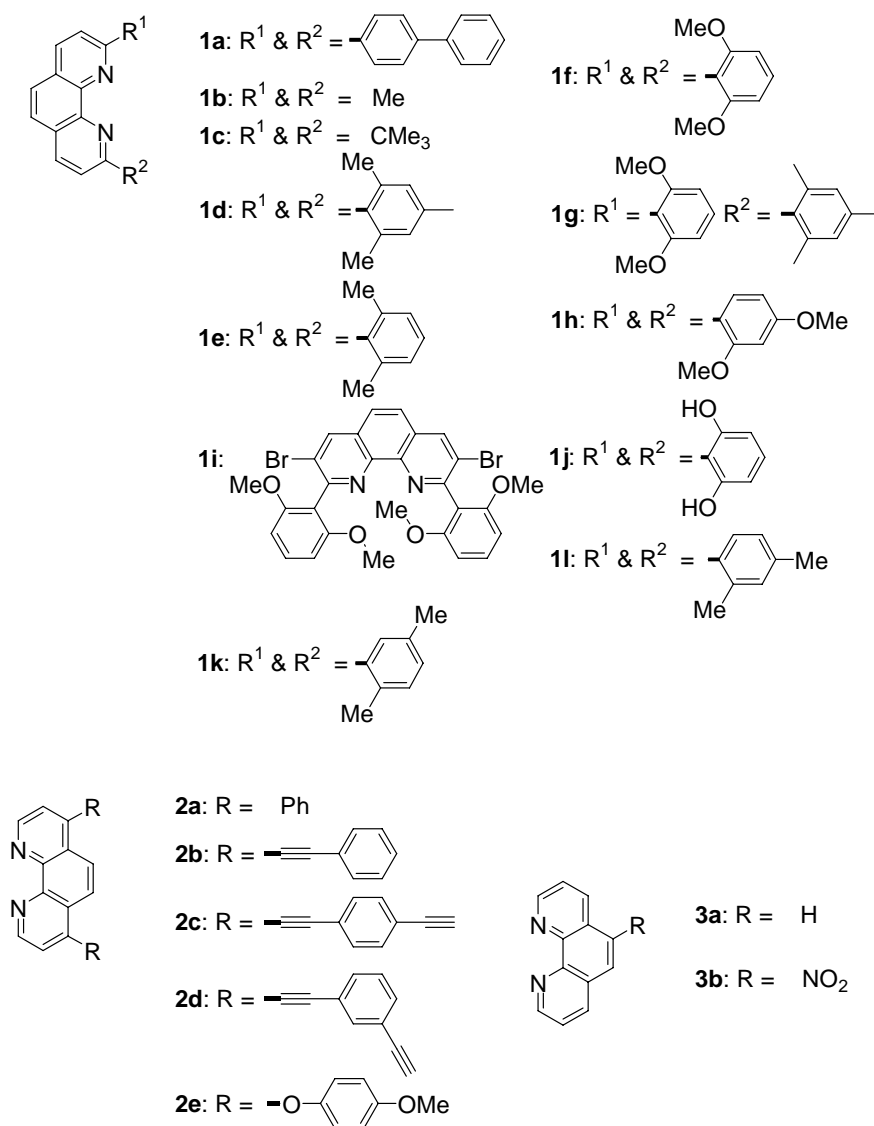


Several years ago we communicated a quantitative approach to heteroleptic bisphenanthroline copper(I),⁸ silver(I) and zinc(II) complexes⁹ using bulky 2,9-diarylphenanthrolines which we called the HETPHEN (heteroleptic bisphenanthroline complex formation) concept. It proved to be a *conditio sine qua non* for the distinct formation of supramolecular nanobox,¹⁰ heteroleptic grid,¹¹ ring-in-ring¹² and rack¹³ structures. The concept was later exploited by *Karpishin*,¹⁴ who modified it for the preparation of $[\text{Cu}(\mathbf{1b})(\mathbf{1c})]^+$ (*cf.* scheme 1) with 2,9-di-*tert*-butylphenanthroline as the bulky ligand.¹⁵ However, since his approach was based mostly on maximum site occupancy thereby not providing a thermochemical bias for the heteroleptic complex, the homoleptic complex $[\text{Cu}(\mathbf{1b})_2]^+$ formed as well. Herein, we present for the first time a detailed mechanistic study on the HETPHEN approach. The results explain the efficiency and the high yields in the formation of heteroleptic copper(I)bisphenanthroline complexes¹⁶ using ligands with either (i) *ortho*-dialkyl substituted or (ii) *ortho*-dialkoxy substituted arene groups. Moreover, a supramolecular application of the approach will be given. Our approach elegantly

complements the one selected by *Sauvage*¹⁷ and *Swager*,¹⁸ who chose to stabilize heteroleptic bisphenanthroline copper(I) complexes through geometric constraints, *i.e.* in oligomeric ligands or in cyclic ring systems with endotopic coordination sites to prevent formation of homoleptic complexes. An alternative approach utilizing the different energies of heteroleptic diastereomeric complexes, has been described recently, but has not proven its generality.¹⁹

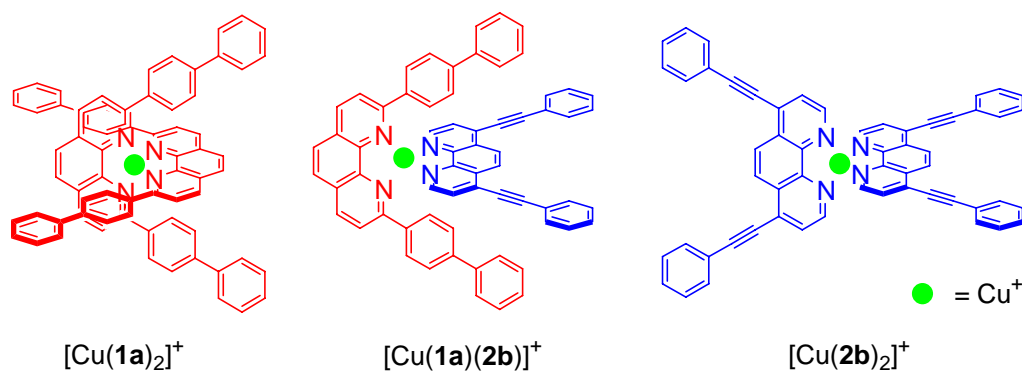
Results

The synthesis of the phenanthroline ligands used in the present study (scheme 1) is described elsewhere except for **1g** and **1h**.^{16,20} Ligands **1** are typified by substituents in 2- and 9-position, mostly aryl groups, whereas ligands **2** carry substituents in 4- and 7-positions.



Scheme 1: Phenanthroline ligands used in the present study.

When the coordination equilibria using phenanthrolines **1a** and **2b** with copper(I) was investigated under thermodynamic control, we did not obtain a statistical mixture of all three possible complexes, but only $[\text{Cu}(\mathbf{1a})_2]^+$ and $[\text{Cu}(\mathbf{1a})(\mathbf{2b})]^+$ in a ratio of 2:1. Signals for the homoleptic complex $[\text{Cu}(\mathbf{2b})_2]^+$ were not detected. The large thermodynamic bias for $[\text{Cu}(\mathbf{1a})_2]^+$ and $[\text{Cu}(\mathbf{1a})(\mathbf{2b})]^+$ was suggested to originate from π - π interactions²¹ between the electron-rich biphenyl units of **1a** and the electron-deficient second phenanthroline (either **1a** or **2b**). Such a motif is present four times in the homoleptic complex $[\text{Cu}(\mathbf{1a})_2]^+$, twice in the bisheteroleptic complex $[\text{Cu}(\mathbf{1a})(\mathbf{2b})]^+$, but not at all in $[\text{Cu}(\mathbf{2b})_2]^+$.



As a consequence of the results above, it was concluded that (i) 2,9-arene groups in phenanthrolines stabilize bisphenanthroline copper(I) complexes.^{45a} (ii) copper(I) complexes with the highest possible number of π - π -stacking interactions are favored thermodynamically. (iii) bishomoleptic complexes of 4,7-disubstituted ligands do not play a role in the coordination equilibria as long as 2,9-diarylsubstituted ligands are present. The rapid exchange of phenanthroline ligands,²² as depicted in a qualitative picture (Fig. 1), suggests a low barrier I for formation of $[\text{Cu}(\mathbf{1a})_2]^+$. Because the desired bisheteroleptic complex $[\text{Cu}(\mathbf{1a})(\mathbf{2b})]^+$ is not the thermodynamically preferred species in the rapid equilibrium, we reasoned that increase of the barrier I \rightarrow II should reduce the number of relevant species in solution.

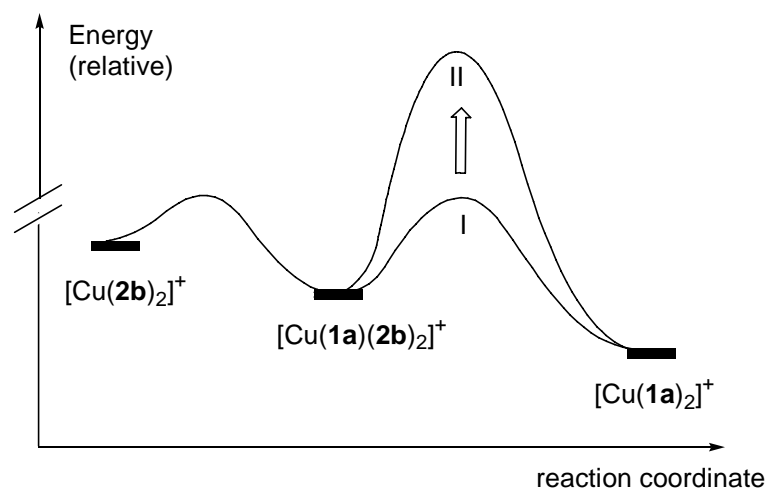


Figure 1 Qualitative reaction coordinate for the equilibrium of homo and heteroleptic copper(I) phenanthroline complexes. Increase of the barrier from I \rightarrow II should reduce the number of relevant species in solution.

How can we raise the barrier as high as II in Figure 1? We decided to test whether formation of $[\text{Cu}(\mathbf{1})_2]^+$ can be prevented on steric grounds. First we need to keep 2,9-aryl groups at the phenanthroline **1** as otherwise the thermodynamic ranking between $[\text{Cu}(\mathbf{1})_2]^+$, $[\text{Cu}(\mathbf{1})(\mathbf{2})]^+$, and $[\text{Cu}(\mathbf{2})_2]^+$ would alter. Second, we need to implement steric stopper groups at the 2,9-aryl groups to prevent formation of $[\text{Cu}(\mathbf{1})_2]^+$. In the following we will detail two concepts along the above considerations.

Methylaryl Groups as Steric Stoppers. In order to examine how 2,9-(2,6-dimethylphenyl) groups at the phenanthroline influence the coordination equilibria the behavior of ligand **1d,e** with copper(I) ions was investigated. It has already been demonstrated by *Thompson*²³ and *Zacharias*²⁴ that bulky substituents may bring about remarkable effects due to the steric shielding.

After mixing 1:0.5-1 amounts of **1d** and $[\text{Cu}(\text{MeCN})_4]\text{BF}_4$, respectively, in CD_2Cl_2 at room temperature a yellow solution was obtained. The ^1H NMR spectrum showed the expected downfield shift of the phenanthroline signals, indicating coordination of **1d** to the positively charged copper(I) ion. The electrospray mass spectroscopy (ESI MS) analysis displayed only molecular ions at m/z 520.4 and m/z 417.9 corresponding to $[\text{Cu}(\mathbf{1d})(\text{MeCN})]^+$ and $[\mathbf{1d}+\text{H}]^+$, respectively. Even in the presence of an excess of **1d** no additional signals were obtained in the NMR as well as in the ESI MS spectrum, except for those of the excess free ligand. The stability constant for $[\text{Cu}(\mathbf{1d})]^+$ was determined to $\log K_{11} = 5.10$.

When a mixture of an excess of **1d** and $[\text{Cu}(\text{MeCN})_4]\text{BF}_4$ was heated to reflux in

chloroform, DMSO or in tetrachloroethane, only the complex with a 1:1 copper to ligand stoichiometry $[\text{Cu}(\mathbf{1d})]^+$ along with the free ligand could be detected by NMR as well as ESI MS. However, when we added a less hindered phenanthroline (*i.e.* **2,3**) to the yellow solution containing $[\text{Cu}(\mathbf{1d})(\text{MeCN})]^+$, the mixed complex $[\text{Cu}(\mathbf{1d})(\mathbf{2,3})]^+$ was formed exclusively and most importantly in quantitative yield. Its formation was visibly indicated by the immediate occurrence of a red color upon addition of the second ligand. Analytical samples were obtained by recrystallization. As expected, analogous heteroleptic complexes can be prepared with **1e** as the sterically hindered ligand.

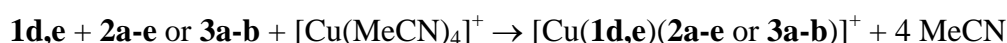


Table 1. Characteristic ^1H NMR shifts of sterically hindered ligands **1c-g** in mixed-ligand copper(I) complexes and their oxidation potentials. Oxidation potentials are measured in dichloromethane and are referenced to the ferrocene/ferrocenium couple.

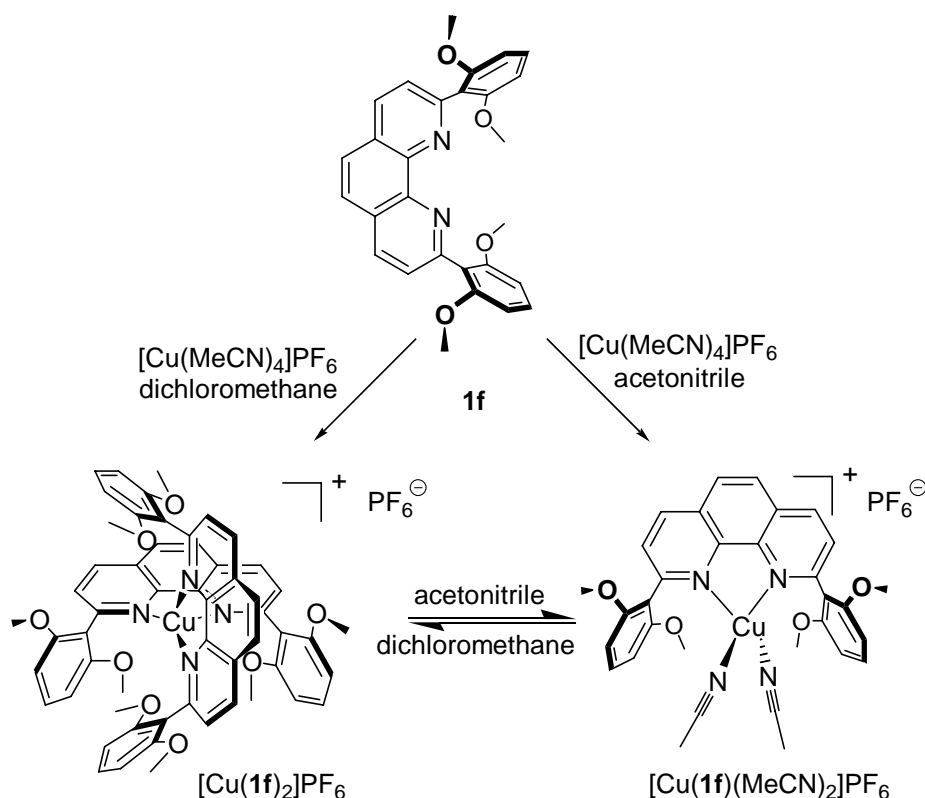
complex or ligand	$E_{1/2}$ (V)	ΔE_p (V)	4-,7-H	5-,6-H	3-,8-H	arene-H	Me-groups
free ligand 1c ^a			8.11	7.68	7.69	--	1.58
$[\text{Cu}(\mathbf{1c})(\mathbf{2b})]\text{BF}_4^a$			8.60	8.09	8.00	--	1.33
free ligand 1d ^a			8.28	7.86	7.57	6.93	2.31, 2.13
$[\text{Cu}(\mathbf{1d})(\text{MeCN})_2]\text{PF}_6$			8.64	8.11	7.85	6.99	1.89, 1.70
$[\text{Cu}(\mathbf{1d})(\mathbf{1b})]\text{BF}_4^a$	+0.47	90 mV	8.68	8.21	8.12	6.10	1.79, 1.60
$[\text{Cu}(\mathbf{1d})(\mathbf{2b})]\text{BF}_4^a$	+ 0.30	70mV	8.73	8.26	7.79	6.08	1.72, 1.75
$[\text{Cu}(\mathbf{1d})(\mathbf{2c})]\text{BF}_4^a$	$E_{pa} =$ +0.66 V		8.74	8.24	7.77	6.07	1.70, 1.74
$[\text{Cu}(\mathbf{1d})(\mathbf{2d})]\text{BF}_4^b$	+0.41	90 mV	9.03	8.47	8.07	6.19	1.74, 1.88
$[\text{Cu}(\mathbf{1d})(\mathbf{2e})]\text{BF}_4^a$	+0.21	90 mV	8.28	8.18	7.58	6.16	1.86, 1.70
$[\text{Cu}(\mathbf{1d})(\mathbf{3a})]\text{BF}_4^a$	+0.31	100 mV	8.67	8.20	7.79	5.97	1.73, 1.61
$[\text{Cu}(\mathbf{1d})(\mathbf{3b})]\text{BF}_4^a$	+0.36	90 mV	8.61	8.13	7.72	5.93	1.61, 1.56
free ligand 1e ^c			8.30	7.88	7.59	7.00-7.20	2.15
$[\text{Cu}(\mathbf{1e})(\mathbf{2b})]\text{BF}_4^c$	+0.36	60 mV	8.72	8.24	7.86	6.30	1.79
free ligand 1f ^a			8.24	7.81	7.64	7.30, 6.66	3.72
$[\text{Cu}(\mathbf{1f})(\text{MeCN})_2]\text{PF}_6$			8.57	7.88	7.45	6.79, 5.89	3.42
$[\text{Cu}(\mathbf{1f})(\mathbf{1b})]\text{BF}_4$	+0.17	70 mV	8.61	8.16	7.55	6.46, 5.68	3.21
$[\text{Cu}(\mathbf{1f})(\mathbf{2b})]\text{BF}_4^c$	+0.04	70 mV	8.60	8.16	7.82	6.50, 5.75	3.30
$[\text{Cu}(\mathbf{1f})(\mathbf{3a})]\text{BF}_4^a$	+0.03	90 mV	8.44	8.00	7.63	6.25, 5.50	3.09
free ligand 1i ^c			8.52	7.79	--	7.39, 6.66	3.70
$[\text{Cu}(\mathbf{1i})(\mathbf{2a})]\text{PF}_6^c$			8.83	8.08	--	6.52, 5.72	3.33
free ligand 1g ^c			8.31	7.87	7.56	6.96, 6.70	3.70
$[\text{Cu}(\mathbf{1g})(\text{MeCN})_2]\text{PF}_6^c$			8.62	8.09	7.80	6.96, 6.72	3.60
$[\text{Cu}(\mathbf{1g})_2]\text{PF}_6^c$			8.36	7.99	7.36	6.35, 5.76	3.32
$[\text{Cu}(\mathbf{1g})(\mathbf{3a})]\text{PF}_6^c$			8.49	8.17	7.73	6.50, 5.79	3.33
free ligand 1h			8.21	8.21	7.74	8.39, 6.76, 6.59	3.90
$[\text{Cu}(\mathbf{1h})_2]\text{PF}_6^c$			8.36	7.90	7.86	7.25, 5.85, 5.42	3.46

^a measured in CDCl_3 ; ^b in d_6 -acetone; ^c in CD_2Cl_2 ;

The formation of the heteroleptic complexes is supported by characteristic ^1H NMR spectra. Signals for free ligands as well as for homoleptic complexes were not detected. While in $[\text{Cu}(\mathbf{1d,e})(\text{MeCN})]^+$ the binding of **1d,e** to the positively charged metal ion results in

downfield shifts for all protons at the phenanthroline core, the arene groups experience a strong upfield shift in the heteroleptic complex $[\text{Cu}(\mathbf{1})(\mathbf{2} \text{ or } \mathbf{3})]^+$. Apparently, the pseudo-tetrahedral coordination (see X-ray structures below) of the two phenanthrolines leads to a geometry in which the arene substituents of ligands **1e,f** (in general valid for **1a,d-h**) are situated below and above the aromatic plane of the second phenanthroline ligand **2** or **3**. Hence, the upfield shift is caused by the shielding of the arene protons by phenanthroline **2** or **3**. *Vice versa*, the 4,7-disubstituted phenanthrolines experience some shielding from the arene groups of ligands **1a,d-h**. NMR data for several heteroleptic complexes are compiled in table 1. The composition of all new complexes was confirmed additionally by elemental analysis and by ESI MS analysis.

Methoxyaryl Groups as Steric Stoppers. In order to test for other substituents at the 2,9-aryl groups that would work as steric stoppers we turned our attention to 2,6-dimethoxyphenyl substituted ligands, such as **1f** or **1i**. Mixing one equivalent of ligands **1f,i** with half an equivalent of copper(I) salt in acetonitrile afforded a yellow solution showing conspicuous downfield shifts at the phenanthroline ligand and a molecular ion corresponding to $[\text{Cu}(\mathbf{1f,i})(\text{MeCN})_2]^+$ along with the signals corresponding to excess of free ligand **1f** or **1i** (**1f,1i-H⁺**, in case of ESI MS).²⁵ The same experiment in dichloromethane, however, led after a few seconds to a red solution indicative of a bishomoleptic phenanthroline complex. Indeed, the isolated products were identified as $[\text{Cu}(\mathbf{1f})_2]^+$ and $[\text{Cu}(\mathbf{1i})_2]^+$, respectively by the distinct ¹H NMR upfield shifts of signals at the arene substituents, which were markedly different from those of the monosubstituted species (table 1). In acetonitrile, however, $[\text{Cu}(\mathbf{1f})(\text{MeCN})_2]^+$ did not react to $[\text{Cu}(\mathbf{1f})_2]^+$ even after heating the solution to reflux for several days. Only when the solvent was evaporated rigorously and the residue was taken up in a weakly coordinating solvent such as dichloromethane the characteristic red color of the bishomoleptic complex immediately emerged.



Scheme 2: The coordination equilibrium of **1f** with copper(I) in acetonitrile and dichloromethane.

It is evident from the above observations (scheme 2) that the methoxy aryl groups in **1f** and **1i** are not sufficiently bulky to prevent formation of the bishomoleptic complexes $[\text{Cu}(\mathbf{1f})_2]^+$ or $[\text{Cu}(\mathbf{1i})_2]^+$ on steric grounds. The situation in acetonitrile, however, encouraged us to examine the coordination behavior of $[\text{Cu}(\mathbf{1f})]^+$ and $[\text{Cu}(\mathbf{1i})_2]^+$ in the presence of unhindered ligands. Mixing equimolar amounts of **1f** (or **1i**), $[\text{Cu}(\text{MeCN})_4]^+$ and ligand **2** (or **3**) in acetonitrile afforded immediately a red solution containing exclusively the heteroleptic complexes (table 1). Elemental analysis and again ESI MS analysis confirmed the composition of the products.

Two crystal structures provide additional insight. Crystals of $[\text{Cu}(\mathbf{1f})(\text{MeCN})_2]\text{PF}_6$ were obtained by the slow evaporation of acetonitrile.²⁶ The solid state structure clearly showed a pseudotetrahedral coordination sphere at the copper(I) center with the phenanthroline **1f** as a chelate ligand ($d_{\text{Cu-N}} = 2.06$ and 2.08 Å) and two additional acetonitrile ligands ($d_{\text{Cu-N}} = 1.95$ and 1.97 Å) (Table 2). Both aryl residues exhibit an almost orthogonal angle with the phenanthroline, as also seen in a copper(II) complex with **1f**,²⁷ which does not allow for strong interaction of the methoxy oxygens and copper ($d_{\text{O-Cu}} = 3.64$ Å). While there are potentially some π - π interactions existing between the $\text{C}\equiv\text{N}$ and the aryl groups ($d = 3.33$

Å), no stabilizing motifs can be recognized in between methoxy oxygens and the metal center. On an intermolecular level it is interesting to note that there are strong CH- π and π - π interactions between two neighbouring complexes.

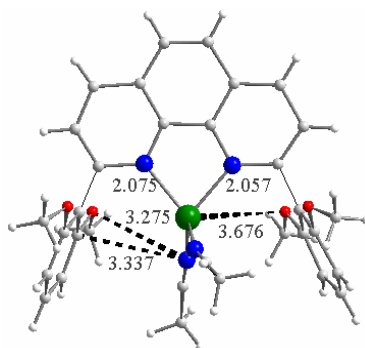


Figure 2: Solid state ball and stick representation of $[\text{Cu}(\mathbf{1f})(\text{MeCN})_2]^+$ with the dotted lines showing some intramolecular distances.

Suitable dark red crystals of $[\text{Cu}(\mathbf{1f})(\mathbf{3a})]\text{PF}_6$ were obtained by slow diffusion of toluene into a dichloromethane solution containing the heteroleptic complex.²⁸ It became evident from the solid state structure of $[\text{Cu}(\mathbf{1f})(\mathbf{3a})]\text{PF}_6$ that the parent phenanthroline ligand is strongly bent towards one of the aryl groups. The Cu atom has a distorted tetrahedral coordination. The N-Cu-N angles reach from $82.0(1)^\circ$ to $126.9(2)^\circ$. The Cu-N distances range from $1.992(1)$ to $2.031(1)$ Å (Table 2). Both aromatic systems are almost coplanar showing an average distance of 3.4 Å which is indicative of π - π interactions. There is no strong interaction of the methoxy oxygens and copper ($d_{\text{O}-\text{Cu}} = 4.0$ Å). The crystal packing showed an intermolecular π - π interactions (3.3 Å) between phenanthroline ($\mathbf{3a}$) groups leading to solid state dimerization (Figure 3b).

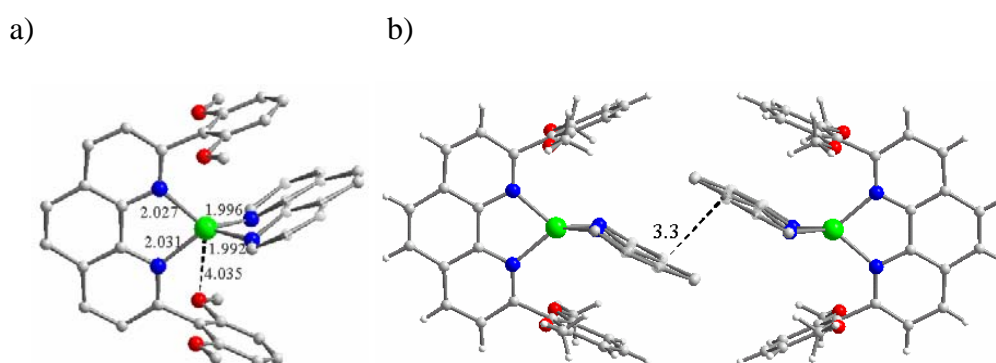


Figure 3: a) Solid state structure ball and stick representation of $[\text{Cu}(\mathbf{1f})(\mathbf{3a})]\text{PF}_6$ showing the Cu-N distances. Hydrogen atoms and counter ions are omitted for clarity. b) Intermolecular packing.

Table 2. Selected bond lengths (Å) and angles (deg) for $[\text{Cu}(\mathbf{1f})(\mathbf{3a})]^+$ and $[\text{Cu}(\mathbf{1f})(\text{MeCN})_2]^+$.

[Cu(1f)(3a) ⁺]						
bond		length / Å	angle / deg			angle / deg
Cu1	N4	1.992(1)	N4	Cu1	N3	84.28(2)
Cu1	N3	1.996(1)	N4	Cu1	N1	121.23(2)
Cu1	N1	2.027(1)	N3	Cu1	N1	126.24(2)
Cu1	N2	2.031(1)	N4	Cu1	N2	126.97(2)
			N3	Cu1	N2	121.79(1)
			N1	Cu1	N2	82.04(1)
[Cu(1f)(MeCN) ₂] ⁺						
bond		length / Å	angle / deg			angle / deg
Cu1	N1	1.946(1)	N1	Cu1	N3	110.29(1)
Cu1	N3	1.966(3)	N1	Cu1	N2	121.59(1)
Cu1	N2	2.057(2)	N3	Cu1	N2	106.30(1)
Cu1	N4	2.075(3)	N1	Cu1	N4	120.65(1)
			N3	Cu1	N4	114.88(1)
			N2	Cu1	N4	79.67(1)

Other phenanthrolines. To further understand the interplay of sterics and electronics we decided to examine the coordination properties of phenanthroline **1g** sharing both the steric and electronic motifs of **1d** and **1f**. When we reacted 0.5 or 1 equivalent of [Cu(MeCN)₄]⁺ and **1g** in acetonitrile only a yellow colored solution resulted that by ¹H-NMR and ESI MS contained solely [Cu(**1g**)(MeCN)₂]PF₆. When acetonitrile was removed *in vacuo* and replaced by dichloromethane a dark red colour solution formed immediately. Analysis by ¹H-NMR and ESI MS now indicated the formation of [Cu(**1g**)₂]PF₆. Addition of even small amounts of acetonitrile reverted this complex back to [Cu(**1g**)(MeCN)₂]PF₆, indicating coordination of acetonitrile to the copper(I) center. Hence, **1g** showed similar coordination properties with copper(I) as **1f** and **1i**. In order to elucidate the coordination effects of other solvents for this interconversion we investigated the effect of various solvents on **1f** with copper(I) as a prototype reaction (Table 3).

Table 3. Complexes formed from **1f** with Cu(I) salt in various solvents.

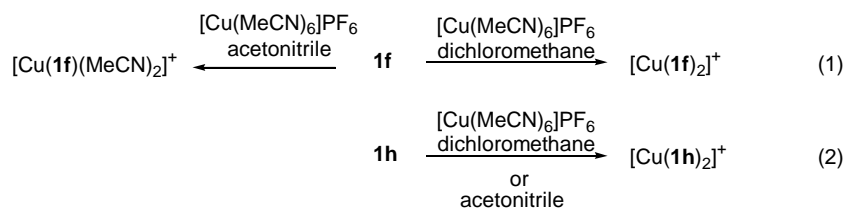
solvent (S)	[Cu(1f)(S) ₂]PF ₆	[Cu(1f) ₂]PF ₆
dichloromethane	no	yes
acetone	no	yes
pyridine	no	yes
dimethylformamide	no	yes
nitromethane	no	yes
acetonitrile	yes	no
benzonitrile	yes	no

Interestingly, even pyridine (Table 3), a relatively strong coordinating ligand, had no effect on [Cu(**1f**)₂]PF₆ complex whereas acetonitrile and benzonitrile led to formation of [Cu(**1f**)(S)₂]⁺. These observations highlight the role of nitriles in coordination equilibria with copper(I) and **1f**, **1g** and **1i**.

Furthermore, we checked whether the sterically less shielded **1f** or **1g** can form a heteroleptic complex with the bulky ligand **1d**. Reacting **1f** or **1g** with **1d** and copper(I) salt in acetonitrile resulted in a yellow colored solution whose analysis by ¹H NMR and ESI MS revealed the presence of [Cu(**1f**)(MeCN) or (**1g**)(MeCN)]PF₆ and [Cu(**1d**)(MeCN)]PF₆ and unreacted ligands. The same reaction mixture in dichloromethane afforded both homo and heteroleptic complexes. The formation of [Cu(**1d**)(**1f,g**)]PF₆ in dichloromethane and its dissociation in acetonitrile indicates that these complexes, although stable, are sterically destabilized, since two MeCN ligands can thermochemically override complexation with **1f** or **1g**.

When heteroleptic bisphenanthroline complexes [Cu(**1f,g**)(**2** or **3**)]PF₆, prepared in MeCN, were dissolved in CD₂Cl₂ the bishomoleptic complexes [Cu(**1f**)₂]⁺ or [Cu(**1g**)₂]⁺ could not be detected. Hence, even though steric blockage does not seem to apply in the case of **1f** and **1g**, the concept of preparing selectively bisheteroleptic complexes is still successful.

Finally, the behaviour of compound **1h** was investigated. Ligands **1h** and **1g** exhibit roughly the same donor properties but they differ markedly in the steric shielding of the phenanthroline binding site. Reaction of **1h** with [Cu(MeCN)₄]⁺ in both acetonitrile and dichloromethane resulted in the clean formation of the homoleptic complex [Cu(**1h**)₂]⁺ (Scheme 3). This indicates that it is not the (OMe) donor groups in **1f** that account for the different behaviour as compared to **1d**. This observation is in agreement with the solid state structure of [Cu(**1f**)(MeCN)₂] where no interaction of the (OMe) donor groups with the metal center could be detected.



Scheme 3: Coordination properties of **1f** and **1h** with Cu(I) salt in dichloromethane and acetonitrile.

When **1h** was reacted with **3a** a mixture resulted containing both $[\text{Cu}(\mathbf{1h})_2]^+$ and $[\text{Cu}(\mathbf{1h})(\mathbf{3a})]^+$. As analyzed by ^1H NMR and ESI MS the homoleptic complex was the major component. Apparently, the high σ -basicity of ligand **1h** is having a larger effect than steric repulsions. The observed binding constant ($\log \beta_{21} = 11.30$) for $[\text{Cu}(\mathbf{1h})_2]^+$ is in line with this interpretation.

Electrochemical Properties. Redox potentials of the Cu(I/II) couple were measured for a series of heteroleptic (Table 1) and homoleptic complexes in solution (Table 4) and compared to $\text{p}K_a$ values of the ligands. All potentials were referenced to the ferrocene/ferrocenium couple.

Table 4. Oxidation potentials (vs. Fc/Fc^+) for the Cu(I/II) couple of various homoleptic complexes and $\text{p}K_a$ ²⁹ values of the ligands.

Complex	$E_{1/2}^{\text{ox}}$ (V vs. Fc^+)	ΔE (mV)	$\text{p}K_a$ of ligand
$[\text{Cu}(\mathbf{1a})_2]^+$	+0.40	70	<4.14
$[\text{Cu}(\mathbf{1b})_2]^+$	+0.43	120	6.17
$[\text{Cu}(\mathbf{1f})_2]^+$	-0.10	80	6.96
$[\text{Cu}(\mathbf{2b})_2]^+$	-0.05	150	4.74
$[\text{Cu}(\mathbf{2e})_2]^+$	-0.17	150	5.34

Thermodynamic stability from UV-vis titrations. Recently, phenanthroline copper complexes had been studied by Albrecht-Gary in pure acetonitrile and mixture of solvents including water.³⁰ We chose dichloromethane as solvent due to solubility reasons and in order to unambiguously generate heteroleptic complexes with **1f**. No inert electrolyte was used since the influence of the ionic strength on the stability of homoleptic copper(I) phenanthroline complexes had been demonstrated to be negligible. The constants were measured for the following equilibria:



Slow equilibration was observed with $[\text{Cu}(\mathbf{1d})(\mathbf{1b})]^+$. When copper(I) salt was added

to the mixture of ligands (method A) signals for both the heteroleptic and the $[\text{Cu}(\mathbf{1b})_2]^+$ complex emerged. $\mathbf{1b}$ can form a very strong $[\text{Cu}(\mathbf{1b})_2]^+$; thus this process runs in competition to heteroleptic complex formation. After standing at room temperature for 10 h (likewise for ref. 6d), however, quantitative formation of the heteroleptic complex resulted. In contrast, when $\mathbf{1b}$ was added to the dichloromethane solution containing $[\text{Cu}(\mathbf{1d})]^+$ (method B) the heteroleptic complex was afforded instantaneously. Therefore, we carried out all spectrophotometric titrations by method B. The equilibrium constants $\log \beta_{111}$ for $[\text{Cu}(\mathbf{1b})_2]^+$ and $[\text{Cu}(\mathbf{3a})_2]^+$ are in agreement with those described in the literature. In dichloromethane there is a higher binding constant for $[\text{Cu}(\mathbf{1b})_2]^+$ than for $[\text{Cu}(\mathbf{3a})_2]^+$, which is readily rationalized by the higher basicity of the nitrogen donor centers in $\mathbf{1b}$ ($\text{p}K_{\text{a}} = 5.35$) than in $\mathbf{3a}$ ($\text{p}K_{\text{a}} = 4.53$)^{29c} due to the inductive effect of the methyl groups.

Table 5. Equilibrium constants $\log \beta_{111} = \log K_{\text{CuL}}^{\text{Cu}} + \log K_{\text{CuLL}'}^{\text{CuL}}$ for a series of homoleptic and heteroleptic copper bisphenanthroline complexes.

complex	$\log K_{\text{CuL}}^{\text{Cu}}$	$\log K_{\text{CuLL}'}^{\text{CuL}}$	$\log \beta_{111}$ or $\log \beta_{21}$	Literature
$[\text{Cu}(\mathbf{1b})_2]^+$	5.52 ^a	4.58 ^a	10.10 ^a ($\log \beta_{21}$)	11.7 ^{30b} , 9.9 ^{31c} , 10.9 ^{32d}
$[\text{Cu}(\mathbf{3a})_2]^+$	5.01 ^a	4.31 ^a	9.32 ^a ($\log \beta_{21}$)	15.82 ^{29ce} , 9.7 ^{31f} , 10.6 ^{31g}
$[\text{Cu}(\mathbf{1d})]^+$	5.10 ^a	-	-	-
$[\text{Cu}(\mathbf{1d})(\mathbf{1a})]^+$	5.10 ^a (for $[\text{Cu}(\mathbf{1d})]^+$)	4.75 ^a	9.85 ^a	-
$[\text{Cu}(\mathbf{1d})(\mathbf{1b})]^+$	5.10 ^a (for $[\text{Cu}(\mathbf{1d})]^+$)	4.60 ^a	9.70 ^a	-
$[\text{Cu}(\mathbf{1d})(\mathbf{2a})]^+$	5.10 ^a (for $[\text{Cu}(\mathbf{1d})]^+$)	4.82 ^a	9.92 ^a	-
$[\text{Cu}(\mathbf{1d})(\mathbf{2b})]^+$	5.10 ^a (for $[\text{Cu}(\mathbf{1d})]^+$)	4.73 ^a	9.83 ^a	-
$[\text{Cu}(\mathbf{1d})(\mathbf{2e})]^+$	5.10 ^a (for $[\text{Cu}(\mathbf{1d})]^+$)	4.63 ^a	9.73 ^a	-
$[\text{Cu}(\mathbf{1d})(\mathbf{3a})]^+$	5.10 ^a (for $[\text{Cu}(\mathbf{1d})]^+$)	4.37 ^a	9.47 ^a	-
$[\text{Cu}(\mathbf{1d})(\mathbf{3b})]^+$	5.10 ^a (for $[\text{Cu}(\mathbf{1d})]^+$)	4.80 ^a	9.90 ^a	-
$[\text{Cu}(\mathbf{1f})]^+$	5.45 ^a	-	-	-
$[\text{Cu}(\mathbf{1f})(\mathbf{3b})]^+$	5.45 ^a (for $[\text{Cu}(\mathbf{1f})]^+$)	4.93 ^a	10.38 ^a	-
$[\text{Cu}(\mathbf{1f})(\mathbf{2a})]^+$	5.45 ^a (for $[\text{Cu}(\mathbf{1f})]^+$)	4.69 ^a	10.14 ^a	-
$[\text{Cu}(\mathbf{1f})(\mathbf{3a})]^+$	5.45 ^a (for $[\text{Cu}(\mathbf{1f})]^+$)	4.82 ^a	10.27 ^a	-
$[\text{Cu}(\mathbf{1f})_2]^+$	5.45 ^a (for $[\text{Cu}(\mathbf{1f})]^+$)	4.55 ^a	10.00 ^a	-
$[\text{Cu}(\mathbf{1g})(\mathbf{3a})]^+$	5.26 ^a (for $[\text{Cu}(\mathbf{1g})]^+$)	4.35 ^a	9.61 ^a	-
$[\text{Cu}(\mathbf{1g})_2]^+$	5.26 ^a	4.20 ^a	9.46 ^a	-
$[\text{Cu}(\mathbf{1h})_2]^+$	5.96 ^a	5.34 ^a	11.30 ^a	-

^a Present work, dichloromethane; $T = 25$ °C; spectrophotometry

^b $\text{CH}_3\text{CN}/\text{DCM}/\text{H}_2\text{O}$ 80/15/5 (v/v); $T = 25$ °C; $(n\text{-C}_4\text{H}_9)_4\text{NCF}_3\text{SO}_3$; spectrophotometry; ref. 30

^c CH_3CN ; $T = 25$ °C; $(\text{C}_2\text{H}_5)_4\text{NClO}_4$; potentiometry; ref. 31

^d CH_3CN ; $T = 25$ °C; spectrophotometry; ref. 32

^e H_2O ; $T = 25$ °C; K_2SO_4 ; potentiometry

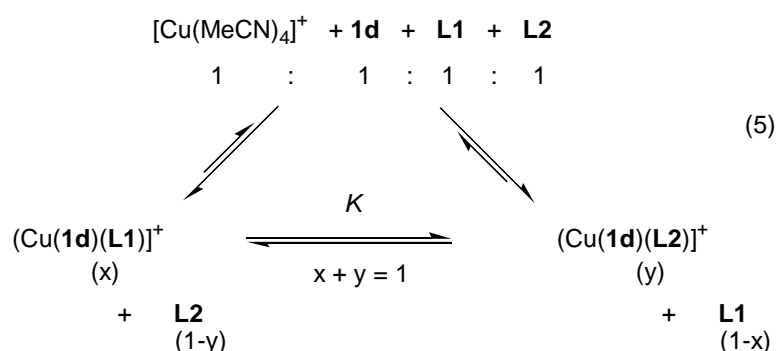
^f CH_3CN ; $T = 25$ °C; $(\text{C}_2\text{H}_5)_4\text{NClO}_4$; potentiometry

^g CH_3CN ; $T = 25$ °C; $(\text{C}_2\text{H}_5)_4\text{NClO}_4$; spectrophotometry

Unfortunately, equilibrium constants obtained for the various heteroleptic complexes $[\text{Cu}(\mathbf{1d})(\text{L})]^+$ are very close, precluding a differentiating evaluation of electronic and steric influences of L. Hence, we designed a simple ligand exchange competition for further insight.

Relative stabilities of $[\text{Cu}(\mathbf{1d})(\text{L})]^+$ from competitive ligand exchange studies. As

the supramolecular self-assembly processes are usually conducted in chloroform or dichloromethane the experiments on the relative thermodynamic stability of the new heteroleptic complexes were studied in deuterated chloroform using ^1H NMR analysis. The relative stability of the heteroleptic copper phenanthroline complexes with **1d** were determined from competition experiments after thermodynamic equilibration. The analysis can be facilitated based on our previous findings, as (i) in presence of an excess of ligands the coordination equilibrium is shifted so much towards the bisphenanthroline complexes that monocoordinated $\text{Cu}^+\bullet\text{L}$ species do not play a role; and (ii) the bishomoleptic $[\text{Cu}(\mathbf{1d})_2]^+$ can not be formed due to steric hindrance. Thus, in a mixture of equimolar amounts of **1d**, $[\text{Cu}(\text{MeCN})_4]^+$, and of two unhindered ligands **L1** and **L2** (both selected from **2a-e,3**) the following equilibrium can be assumed.



Relative binding constants (K) and ΔG -values are calculated according to the following equation (6).

$$\Delta G = -RT \ln K$$

$$K = \frac{[\text{Cu}(\mathbf{1d})(\mathbf{L2})][(\mathbf{L1})]}{[\text{Cu}(\mathbf{1d})(\mathbf{L1})][(\mathbf{L2})]} = \frac{[\text{Cu}(\mathbf{1d})(\mathbf{L2})]^2}{[\text{Cu}(\mathbf{1d})(\mathbf{L1})]^2} \quad (6)$$

Table 6. Results of the equilibration investigations in CDCl_3 according to equation (5) using **1d**, **L1** and **L2** in 1:1:1 molar ratio. Average product ratios were obtained from three independent ^1H -NMR experiments at 298 K by integration of characteristic signals. K and ΔG were determined according to equation 6.

L1	L2	$[\text{Cu}(\mathbf{1d})(\mathbf{L1})]^+ : [\text{Cu}(\mathbf{1d})(\mathbf{L2})]^+{}^a$	ΔG (kcal mol $^{-1}$) b
2b	2e	2.11 : 1.00	-0.88
2b	3a	1.18 : 1.00	-0.20
1b	3a	1.65 : 1.00	-0.59
2b	3b	3.58 : 1.00	-1.51

a Other complexes were not found or were less than 10%. b Only approximative driving forces could be determined due to the fact that minor traces of other complexes were also present in the mixture but not taken into account.

The ratio of $[\text{Cu}(\mathbf{1d})(\mathbf{L1})]^+ : [\text{Cu}(\mathbf{1d})(\mathbf{L2})]^+$ was received from ^1H NMR integration data (Table 6). Similarly, the relative stability of the complexes $[\text{Cu}(\mathbf{1d})(\text{L})]^+$ in comparison to $[\text{Cu}(\mathbf{1f})(\text{L})]^+$ was investigated using analogous ligand competition experiments. In the latter set of experiments the heteroleptic complex $[\text{Cu}(\mathbf{1d})(\mathbf{1f})]^+$ can be detected in small amounts as long as there is no other ligand present. Fortunately, this species doesn't complicate the analysis, because upon addition of another phenanthroline, $[\text{Cu}(\mathbf{1d})(\mathbf{1f})]^+$ disappeared. A ratio of $[\text{Cu}(\mathbf{1d})(\mathbf{3a})]^+ : [\text{Cu}(\mathbf{1f})(\mathbf{3a})]^+ = 1:1.80$ was found. Hence, the equilibrium is shifted to $[\text{Cu}(\mathbf{1f})(\mathbf{3a})]^+$, in full agreement with the numbers from the UV-vis titration.

Table 7. Results of the equilibration investigations in CDCl_3 starting from $\mathbf{1d}$, $\mathbf{L1}$ and $\mathbf{L2}$. Average product ratios were obtained from three independent ^1H -NMR experiments at 298 K by integration of characteristic signals. K and ΔG were determined according to equation 6.

L1	L2	Product ratio ^a	$\Delta G / \text{kcal mol}^{-1}$ ^b
1a	-	$[\text{Cu}(\mathbf{1a})(\mathbf{1d})]^+ : [\text{Cu}(\mathbf{1a})_2]^+$ 1.00 : 5.71	+2.1
1a	3b	$[\text{Cu}(\mathbf{1d})(\mathbf{3b})]^+ : [\text{Cu}(\mathbf{1a})_2]^+$ 1.00 : 1.01	+0.01
1f	3a	$[\text{Cu}(\mathbf{1d})(\mathbf{3a})]^+ : [\text{Cu}(\mathbf{1f})(\mathbf{3a})]^+$ 1 : 1.80	+0.70

^a Other complexes were not found or were less than 10%. ^b Only approximative driving forces could be determined due to the fact that minor traces of other complexes were also present in the mixture but not taken into account.

Relative stabilities of complexes from PM3 calculations. Due to the difficult separation of steric and electronic contributions in the complex stability and the inaccessibility of complex $[\text{Cu}(\mathbf{1d})_2]^+$, we carried out PM3 calculations for further insight.³³ Possible deviations in the heats of formation caused by the parametrization of the copper(I) ion should only lead to small mistakes in data from isodesmic reactions due to error cancelation.

Table 8. Heat of formation of ligands and homoleptic and heteroleptic complexes as calculated using PM3.

ligand	$\Delta H_f / \text{kcal mol}^{-1}$	homoleptic complex	$\Delta H_f / \text{kcal mol}^{-1}$	heteroleptic complex	$\Delta H_f / \text{kcal mol}^{-1}$
1d	73.3	$[\text{Cu}(\mathbf{1d})_2]^+$	161.1	$[\text{Cu}(\mathbf{1d})(\mathbf{3a})]^+$	142.1
1e	91.9	$[\text{Cu}(\mathbf{1e})_2]^+$	202.7	$[\text{Cu}(\mathbf{1e})(\mathbf{3a})]^+$	161.3
1f	-19.5	$[\text{Cu}(\mathbf{1f})_2]^+$	-29.5	$[\text{Cu}(\mathbf{1f})(\mathbf{3a})]^+$	45.5
				$[\text{Cu}(\mathbf{1f})(\mathbf{1j})]^+$	-64.0
1g	27.1	$[\text{Cu}(\mathbf{1g})_2]^+$	68.7	$[\text{Cu}(\mathbf{1g})(\mathbf{3a})]^+$	93.6
1h	-24.9	$[\text{Cu}(\mathbf{1h})_2]^+$	-53.6	$[\text{Cu}(\mathbf{1h})(\mathbf{3a})]^+$	42.1
				$[\text{Cu}(\mathbf{1h})(\mathbf{1f})]^+$	-45.8
				$[\text{Cu}(\mathbf{1h})(\mathbf{1j})]^+$	-74.6
1i	1.2	$[\text{Cu}(\mathbf{1i})_2]^+$	23.5	$[\text{Cu}(\mathbf{1i})(\mathbf{3a})]^+$	68.6
1j	-54.5	$[\text{Cu}(\mathbf{1j})_2]^+$	-97.4	$[\text{Cu}(\mathbf{1j})(\mathbf{3a})]^+$	18.1
1k	88.5	$[\text{Cu}(\mathbf{1k})_2]^+$	173.5	$[\text{Cu}(\mathbf{1k})(\mathbf{3a})]^+$	157.9
1l	88.6	$[(\text{Cu } \mathbf{1l})_2]^+$	172.7	$[\text{Cu}(\mathbf{1l})(\mathbf{3a})]^+$	158.0
3a	71.6	$[\text{Cu}(\mathbf{3a})_2]^+$	144.0		

An evaluation of ΔH_f of ligands using Benson's strainless heat of formation increments indicated that hardly any strain energy is stored in **1d** ($E_s = 1.3 \text{ kcal mol}^{-1}$), **1e** ($E_s = 3.5 \text{ kcal mol}^{-1}$), or **1k** ($E_s = 0.91 \text{ kcal mol}^{-1}$) vs. **3a**. Hence, significant strain energies will only arise in the copper complexes.

Discussion

The present investigation interrogates how strain³⁴ and stress³⁵ in interplay with electronic effects, such as π - π stacking, can be used for the defined preparation of heteroleptic copper(I) bisphenanthroline complexes. The first of the two closely related strategies relies on the use of sterically shielded 2,9-bis(2,6-dimethylphenyl) substituted phenanthrolines **1d,e**, the second one on the use of 2,9-bis(2,6-dimethoxyphenyl) substituted phenanthrolines **1f,i**. While originally we assumed that steric control exerted by the aryl substituents in 2,9-position is a common motif to both sets of ligands, the above results allow to conclude that the coordination features of the two phenanthrolines are quite different.

Homoleptic Bisphenanthroline Complexes with 1d-g. The homoleptic $[\text{Cu}(\mathbf{1d})_2]^+$ could not be prepared neither after heating the phenanthroline **1d** and Cu^+ at reflux in tetrachloroethane nor at any other conditions. Since PM3 model calculation indicated that the complex is thermodynamically possible (Table 8, Figure 4) its resistance to form can only be attributed to a high kinetic barrier of at least 170 kJ mol^{-1} . Indeed, model studies indicate that on the way to coordinate a second **1d** to complex $[\text{Cu}(\mathbf{1d})]^+$ an unavoidable penetration of the *ortho* methyl groups has to take place at a copper-nitrogen distance of about $4.0 - 4.3 \text{ \AA}$.

Analogously, $[\text{Cu}(\mathbf{1e})_2]^+$ could not be prepared.

On the contrary, the steric bulk exerted by four *ortho* OMe groups does not suffice to prevent formation of a bishomoleptic complex, since $[\text{Cu}(\mathbf{1f})_2]^+$ could unambiguously be identified in dichloromethane. We have thus to conclude that the barrier for formation of $[\text{Cu}(\mathbf{1f})_2]^+$ must be much lower than for $[\text{Cu}(\mathbf{1d})_2]^+$. For this reaction to occur a simple bond rotation about the C–O bond allows the dimethoxyphenyl groups to readily pass by each other, contrary to the situation with $[\text{Cu}(\mathbf{1d})_2]^+$.³⁶

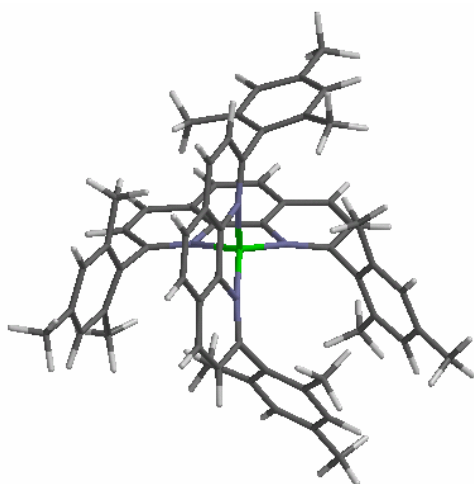


Figure 4. The PM3 minimized structure of $[\text{Cu}(\mathbf{1d})_2]^+$.

In acetonitrile, however, the monophenanthroline complex $[\text{Cu}(\mathbf{1f})(\text{MeCN})_2]^+$ whose structure has been identified by ^1H and ^{13}C NMR, ESI and more convincingly by its crystal structure (*vide supra*) proves to be stable and doesn't react with excess of $\mathbf{1f}$ to form $[\text{Cu}(\mathbf{1f})_2]^+$. This behavior can easily be rationalized on thermodynamic grounds. The monophenanthroline complex $\mathbf{1f}$ is stabilized by two additional Cu--NCMe bonds, by interactions between C \equiv N and the oxygen atom of the methoxy aryl group (3.3 Å) and strong π - π interactions between C \equiv N and the aryl group (3.33 Å).³⁷ Only when acetonitrile was removed rigorously and replaced by a noncoordinating solvent such as dichloromethane, the homoleptic complex $[\text{Cu}(\mathbf{1f})_2]^+$ was afforded exclusively. Obviously, without the stabilizing interaction with one or two MeCN ligands, $[\text{Cu}(\mathbf{1f})]^+$ will react to $[\text{Cu}(\mathbf{1f})_2]^+$. It is also interesting to note that only ligands RC \equiv N (acetonitrile and benzonitrile) stabilize $[\text{Cu}(\mathbf{1f})]^+$.

A picture of the PM3 calculated $[\text{Cu}(\mathbf{1f})_2]^+$ (Figure 5a,b) reveals that this complex is highly strained despite its formation. Therefore, this complex readily dissociates in presence

of less hindered phenanthrolines and various nitriles. This phenomenon of reduced stability of the complex due to sterically impeding substituents is well known: *e.g.*, 2,9-neopentyl-substituted phenanthrolines afford only poorly stable complexes.³⁸

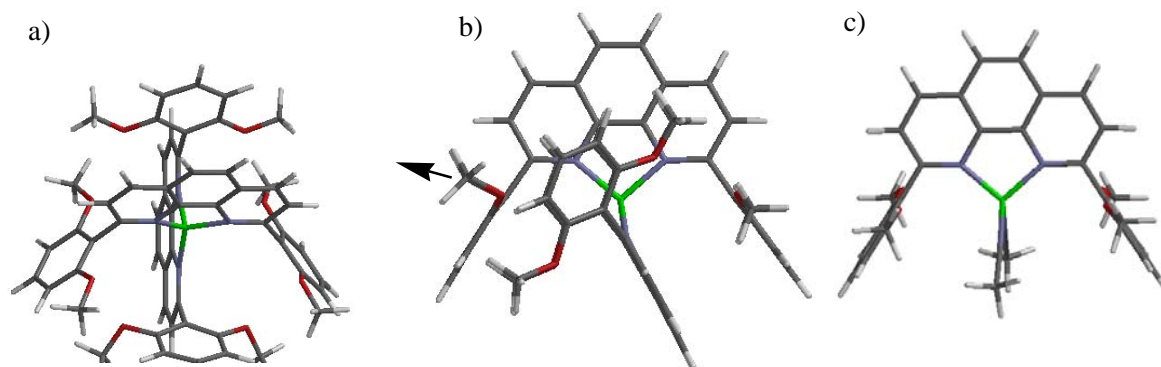
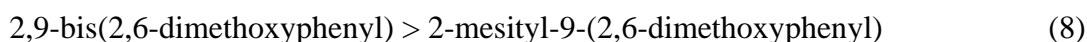
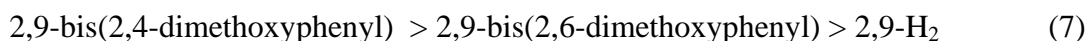
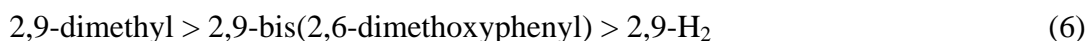


Figure 5. PM3 calculated structures of a,b) $[\text{Cu}(\mathbf{1f})_2]^+$, c) $[\text{Cu}(\mathbf{1f})(\text{MeCN})_2]^+$.

A similar behavior as with **1f** was observed with ligand **1g**, i.e. formation of $[\text{Cu}(\mathbf{1g})]^+$ in acetonitrile and of $[\text{Cu}(\mathbf{1f})_2]^+$ in dichloromethane. This indicates that presence of one single dimethoxyaryl group suffices to bring about this interesting behaviour.

Thermodynamic stability of homoleptic and heteroleptic complexes. The present investigation provides insight into the thermodynamic stability through experimental data and PM3 calculations. Due to the interplay of electronic and steric effect the equilibrium constants of the homoleptic complexes are not easily rationalized. Usually, for simple bisphenanthroline complexes with little steric bulk there is a linear correlation between $\text{p}K_a$ and the $\log \beta_{21}$ values: the higher the basicity the stronger the complexes. This is indeed also found for the formation constants $\log K^{\text{Cu}}_{\text{CuL}}$ (**1h** > **1f** > **1g** > **1d** > **3a**) of the monophenanthroline CuL complexes. In contrast, the equilibrium constants $\log \beta_{21}$ of the homoleptic bisphenanthroline complexes are not dominated solely by electronic effects, but also by steric effects:

Trends for $\log \beta_{21}$ with varying 2,9-substituents:



According to equations 6 and 7 donor substituents only lead to higher stability in the complexes when there is no strain built up in the coordination process. In a first approximation, we would expect 2,9-bis(2,4-dimethoxyphenyl) and 2,9-bis(2,6-dimethoxyphenyl) substituents to exert similar effects on the σ basicity of the phenanthroline ligand, but they differ in their $\Delta \log \beta_{21}$ by 1.30 pointing to significant strain in $[\text{Cu}(\mathbf{1f})_2]^+$ in comparison to $[\text{Cu}(\mathbf{1h})_2]^+$. Likewise, Albrecht-Gary *et al.* ascribed the lower coordination power of *p*-anisyl compared to methyl (as substituent in 2,9-positions of phenanthrolines) partly to steric effects.

Since there is no experimental thermodynamic data available for $[\text{Cu}(\mathbf{1d})_2]^+$, we have used an isodesmic reaction (see equation 10) using the PM3 calculated heats of formation to evaluate qualitatively the relative stability of the homolepic complexes of ligands **1d**, **1f** and **1g**. In order to test whether the two different aryl groups in **1g** are contributing independently to the heat of formation, we assessed the isodesmic reaction (9). Indeed, the thermoneutrality of equation (9) shows that the presence of both mesityl and 2,6-dimethoxyphenyl groups in **1g** is not leading to special electronic and steric interactions. This should allow to relate the thermochemical stability of $[\text{Cu}(\mathbf{1d})_2]^+$ to that of $[\text{Cu}(\mathbf{1f})_2]^+$ and $[\text{Cu}(\mathbf{1g})_2]^+$, with the advantage that for the latter two we have determined experimentally the equilibrium constants. Quite surprisingly, the equilibrium in (10) lies on the left side, with $[\text{Cu}(\mathbf{1d})_2]^+$ and $[\text{Cu}(\mathbf{1f})_2]^+$ being more stable than two complexes $[\text{Cu}(\mathbf{1g})_2]^+$. In terms of equilibrium constants this suggests that $\log \beta_{21}([\text{Cu}(\mathbf{1d})_2]^+) + \log \beta_{21}([\text{Cu}(\mathbf{1f})_2]^+) > 2 \log \beta_{21}([\text{Cu}(\mathbf{1g})_2]^+)$ placing $\log \beta_{21}([\text{Cu}(\mathbf{1d})_2]^+) > 8.9$. In conclusion, this finding suggests again that the formation of $[\text{Cu}(\mathbf{1d})_2]^+$ is not precluded on thermodynamic grounds but is precluded by a high kinetic barrier.

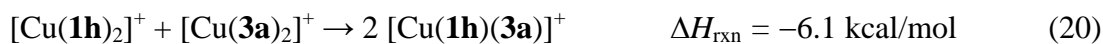
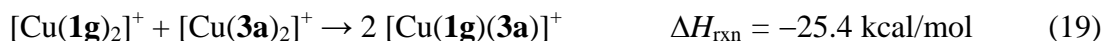
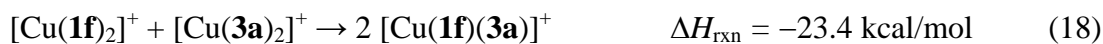
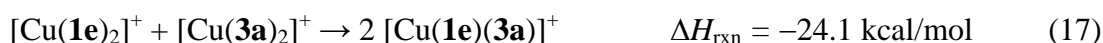
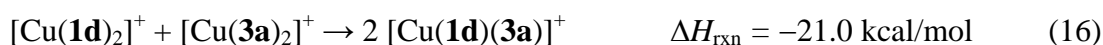


To evaluate the electronic effect of 2,9-diarylphenanthrolines in the coordination equilibrium we operated with the approximation that in the formation of $[\text{Cu}(\mathbf{1})(\mathbf{3a})]^+$ there is little steric interaction between **1** and **3a**. If this accepted, then the ΔH_{rxn} of the following reactions express the donor qualities of the ligands **1** exempted of steric factors.



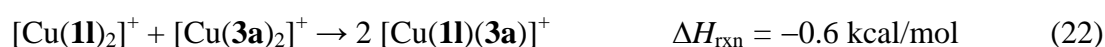
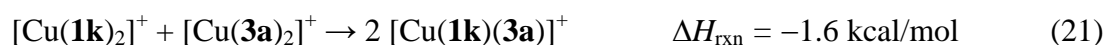
According to eqs. (11)-(15) the ranking of the donor qualities is $\mathbf{1f} > \mathbf{1g,h} > \mathbf{1d,e}$. While the order $\mathbf{1f} > \mathbf{1g} > \mathbf{1d,e}$ is expected, it is surprising to find the donor qualities of $\mathbf{1h}$ to be smaller than those of $\mathbf{1f}$, since this is contrary to our experimental $K_{\text{CuL}}^{\text{Cu}}$ in Table 5. However, $K_{\text{CuL}}^{\text{Cu}}$ may be influenced by entropic terms and by solvation contributions that are not accounted for by the calculations.

While in principle it is not possible to separate steric and electronic effects perfectly, we assume for an evaluation of steric effects in the bishomoleptic complexes, that donor contributions simply behave in an additive manner, so that they should formally cancel in the following isodesmic equations. Also we assume the heteroleptic complex and $[\text{Cu}(\mathbf{3a})_2]^+$ to be strainfree (or almost strainfree).

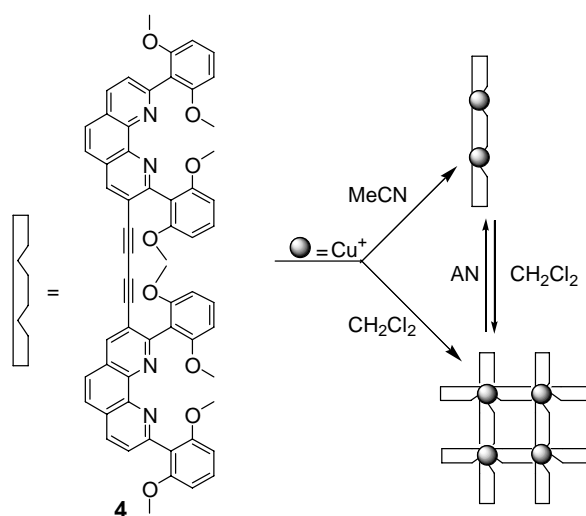


In all equations (eqs. 15-20) the heteroleptic combination is clearly favored thermochemically, a situation that has been experimentally verified for eqs. 16-19. For reaction 20, the experimental observation shows the homoleptic complexes to be favored. Hence, we have to remember that the term ΔH_{rxn} does not contain solvation and entropic factors. Such factors

must raise $\Delta G_{\text{rxn}} > 0$ for eq. 20. Nevertheless, the ΔH_{rxn} in eqs. 16-19 advocate that the steric strain generated in the formation of $[\text{Cu}(\mathbf{1})_2]^+$ is roughly the same for **1d-g**. As $[\text{Cu}(\mathbf{1f,g})_2]^+$ and even $[\text{Cu}(\mathbf{1d})(\mathbf{1g})]^+$ are known to form, this data again support our hypothesis that $[\text{Cu}(\mathbf{1d,e})_2]^+$ is thermochemically possible, but does not form on kinetic grounds. In no way, the calculated reaction enthalpies are biased due to an intrinsic electronic stabilization of the heteroleptic complexes, since for the related complexes $[\text{Cu}(\mathbf{1k})_2]^+$ and $[\text{Cu}(\mathbf{1l})_2]^+$ the conversion to the heteroleptic complexes is almost thermoneutral.



In reality, the situation is certainly more difficult as other complexes, such as $[\text{Cu}(\mathbf{1})]^+$ and $[\text{Cu}(\mathbf{1})(\text{S})]^+$ may also contribute to the thermodynamics. We have seen these species to become thermodynamically competitive for **1f,g,i** and solvents $\text{S} = \text{nitriles}$. Apparently, bishomoleptic complexes from copper(I) and **1f,g,i** are strained so much, that in presence of unshielded coordinating nitriles the formation of $[\text{Cu}(\mathbf{1})(\text{nitrile})]^+$ is favored. This is a property which is of interest in the context of adaptive self assembly processes.³⁹ *Kalsani* used this property when bisphenanthroline **4** was reacted with Cu(I) salt in 1:1 ratio.⁴⁰ In acetonitrile, the reaction mixture was dominated by an open structure $[\text{Cu}(\mathbf{4})(\text{MeCN})_n]^+$ whereas in dichloromethane it self-assembled quantitatively to a tetrameric grid.⁴¹



In summary, we learn that the heteroleptic copper(I) complexes of **1d-g,i** with **2,3** form since they have a thermodynamic advantage over the two homoleptic complexes. This

driving force arises from a thermodynamic destabilization of the homoleptic complex due to a steric interaction of the two bulky phenanthrolines. A kinetic inhibition of the formation of the homoleptic complexes, such as in $[\text{Cu}(\mathbf{1d},\mathbf{e})_2]^+$ is helpful, but not a *conditio sine qua non*. When formation of the homoleptic complex is possible, such as in $[\text{Cu}(\mathbf{1f},\mathbf{g},\mathbf{i})_2]^+$, we still see with all ligands **2** and **3** a clean formation of heteroleptic complexes $[\text{Cu}(\mathbf{1f},\mathbf{g},\mathbf{i})(\mathbf{2} \text{ or } \mathbf{3})]^+$, as long as latter ones are little strained. Is there no thermodynamic advantage of the heteroleptic complex, as with **1h** and for combinations bringing together two sterically shielded ligands (such as $[\text{Cu}(\mathbf{1f},\mathbf{g},\mathbf{i})(\mathbf{1f},\mathbf{g},\mathbf{i})]^+$), then both homo- and heteroleptic combinations arise in dichloromethane, acetone, DMF, pyridine and nitromethane.

Relative stabilities of heteroleptic complexes. The small changes in the experimental values of $\log \beta_{111}$ (from UV-vis titration, Table 5) for heteroleptic complexes $[\text{Cu}(\mathbf{1d},\mathbf{f},\mathbf{g})(\text{L})]^+$ don't allow for a reliable analysis of the effects of the second substituent L. This was the reason we undertook equilibration experiments that were monitored by ^1H NMR (see Tables 6,7). While the relative stabilities of the various heteroleptic complexes are afflicted with some imprecision due to spurious amounts of complexes that had to be neglected in the calculation of ΔG , we feel that these data nevertheless allow to discuss semiquantitatively the effect of substituents at the phenanthroline ligands on the thermodynamic stability of heteroleptic complexes. The results in Table 6,7 and Figure 7 indicate a strong dependence of the stability on the electronic nature of the second ligand. The most stable product is complex $[\text{Cu}(\mathbf{1f})(\mathbf{2b})]^+$. It is more stable than $[\text{Cu}(\mathbf{1d})(\mathbf{2b})]^+$ by $0.7 \text{ kcal mol}^{-1}$, in line with data from the UV-vis titration indicating that complexes with ligand **1f** (either monophenanthroline $[\text{Cu}(\mathbf{1d},\mathbf{f})]^+$ or heteroleptic complexes $[\text{Cu}(\mathbf{1d},\mathbf{f})(\text{L})]^+$) are more stable in general than those with **1d**. Equally, **1f** has a higher $\text{p}K_a$ ($\text{p}K_a = 6.94$) than **1e** ($\text{p}K_a = 5.09$)⁴². The latter value should be comparable to that of **1d**.

In general, electron rich ligands form stronger metal-ligand bonds than electron poor ones,⁴³ because stability constants of copper(I) phenanthroline complexes are higher the more basic the ligands.^{30,44} Along this line, the high stability of complexes of **1d** with ligand **1b** and the instability of that with ligand **3b** can be explained. However, this simple picture of σ -donation does not explain the trend observed within the series $[\text{Cu}(\mathbf{1d})(\text{L})]^+$. A counter-acting influence must play a role as complexes with the electron neutral ligands **2b** or **3a** are more stable than those with the electron-donating ligand **2e**. Therefore, intramolecular interactions have to be discussed.

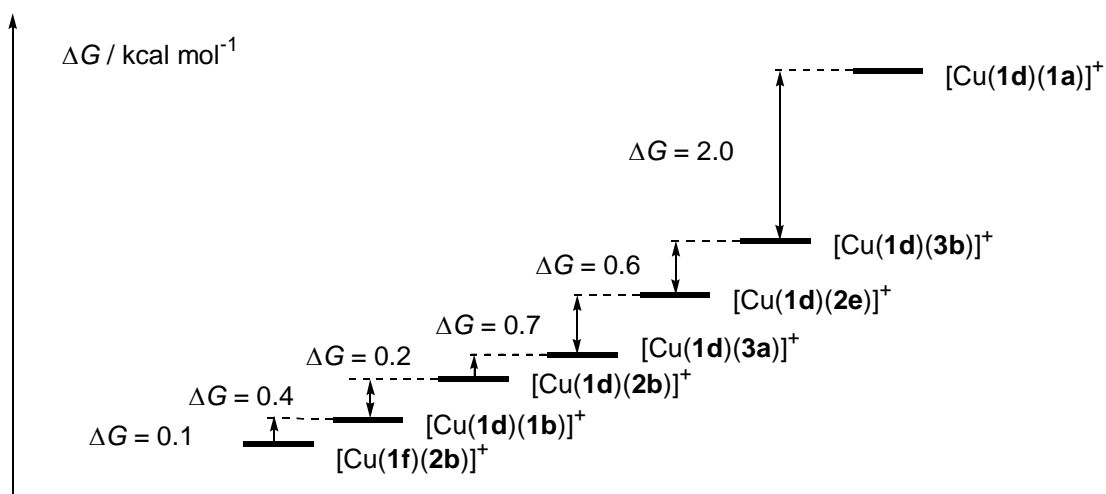


Figure 6. Relative stability of heteroleptic complexes from equilibration experiments in CDCl_3 .

Since σ -donor property considerations fail to explain the stability order of complexes $[\text{Cu}(\mathbf{1d})(\text{L})]^+$ with $\text{L} = \mathbf{3a}$, $\mathbf{2e}$ and $\mathbf{3b}$ and since steric strain elements should be comparable in this small series, we need to discuss π - π -interactions as additional stabilizing motif.^{30,45} Indeed, complexes $[\text{Cu}(\mathbf{1d-g})(\text{L})]^+$ are characterized by conspicuous π - π -stacking of the 2,9-aryl groups of $\mathbf{1d-g}$ with the phenanthroline moiety of L as demonstrated by the shielding effects in the ^1H NMR. Moreover, according to our present (see Figure 3) and recent literature X-Ray data, one arene substituent of $\mathbf{1}$ and the phenanthroline moiety of the second ligand arrange almost parallel to each other at a distance of 3-4 Å so that such an interaction must be quite prominent.⁴⁶ π - π stacking interactions have been analyzed by Hunter and Sanders, who predicted the interaction energy based on competing electrostatic and van-der-Waals forces.⁴⁷ If the aromatic system is polarised by a substituent or a heteroatom, stacking interactions will be affected. For example, an electron donating substituent (*e.g.* OMe, NMe_2) should increase the electron density associated with the ring, therefore augmenting the π -electron repulsion. An electron withdrawing substituent (*e.g.* NO_2) should have the opposite effect. We therefore argue that the increased π -electron repulsion term in $[\text{Cu}(\mathbf{1d})(\mathbf{2e})]^+$ as compared to that in $[\text{Cu}(\mathbf{1d})(\mathbf{3a})]^+$ apparently offsets the higher σ -basicity of $\mathbf{2e}$ with regard to that of $\mathbf{3a}$. The π -electron repulsion must operate between the 4,7-substituents and the 2,9-aryl groups, as the above argument does not strike in complexes without 2,9-aryl groups; *e.g.* $\mathbf{1b}$ is likewise an electron rich phenanthroline ligand but it forms more stable complexes than $\mathbf{3a}$.

A big surprise is the low stability of $[\text{Cu}(\mathbf{1d})(\mathbf{1a})]^+$ that can not be explained solely on electronic effects. Due to the presence of the two biphenyl substituents in $\mathbf{1a}$ and the 2,9-mesityl groups in $\mathbf{1d}$, there must be a sizeable steric strain in the complex.

Oxidation properties of the complexes. Cu(I) as a d^{10} system is known to prefer a tetrahedral coordination. Due to stabilization by π -stacking in our heteroleptic Cu(I) complexes a distorted pseudotetrahedral geometry is found. Hence, oxidation of Cu(I) to Cu(II), the latter adopting usually a six-coordinate tetragonal (distorted octahedral) geometry, will go along with some structural reorganisation.⁴⁸

The comparison of ligands of similar pK_a indicates that oxidation potentials of the homoleptic complexes $[\text{Cu}(\mathbf{1})_2]^+$ are intrinsically higher than those of $[\text{Cu}(\mathbf{2})_2]^+$. While oxidation potentials of $[\text{Cu}(\mathbf{2})_2]^+$ follow the basicity of the ligands, such a correlation is not found for complexes $[\text{Cu}(\mathbf{1})_2]^+$. Apparently, the oxidation potential of the complex is additionally influenced by steric strain. Since Rorabacher *et al.*⁴⁹ have emphasized that for a large variety of ligands the Cu(I) complexes exhibit similar stabilities and that the formal potentials of the Cu(II/I) couple correlate with the stabilities of the Cu(II) complexes, the data in Table 4 may also point to different stabilities of the Cu(II) complexes. The large peak separations ΔE_p of $[\text{Cu}(\mathbf{2})_2]^+$ may point to a more pronounced reorganization in the oxidation process as compared to $[\text{Cu}(\mathbf{1})_2]^+$ oxidations.

For the heteroleptic complexes it appears that steric encapsulation of the Cu(I/II) redox center by one 2,9-diaryl phenanthroline increased the kinetic stability of the copper(II) redox state as with few exceptions, the heteroleptic complexes exhibit fully reversible oxidation waves at all scan rates (Table 1 and 4). Nevertheless, peak separation ($\Delta E_p = 70 - 100$ mV) is a little bit increased with regard to the theoretical value indicative of major reorganization processes of the ligands about the copper.

At first glance, the irreversible oxidation of $[\text{Cu}(\mathbf{1d})(\mathbf{2c})]^+$ is unexpected. From studies on terminal acetylenes linked to triarylamine redox centers, however, we know that oxidation at the redox center leads to deprotonation at the acetylene, a reaction motif that should equally be operative in $[\text{Cu}(\mathbf{1d})(\mathbf{2c})]^+$. Indeed, for this system broad oxidation waves presumably due to polymerization and strong deposition on the electrode were observed.

A dependence of the oxidation potential on the basicity of ligands $\mathbf{1}$ can be observed within a small comparable series of heteroleptic complexes. For example, complexes with ligand $\mathbf{1f}$ ($pK_a = 6.96$) generally display a lower oxidation potential (by 0.3 V) than

complexes containing ligand **1d** ($pK_a = 5.11$). Within complexes of type $[\text{Cu}(\mathbf{1d})(\mathbf{2} \text{ or } \mathbf{3})]^+$ this trend can be observed as well.

Conclusions. Our concept to prepare heteroleptic copper(I) bisphenanthroline complexes along the HETPHEN concept is based on the use of sterically bulky aryl groups in 2,9-position of one of the phenanthroline ligands. The present investigation sheds light on the *modus operandi* of the different ligands **1d-g**. For ligands **1d,e** one factor is decisive: due to the sterically bulky *ortho*-methyl groups a high kinetic barrier that could not be determined prevents formation of the homoleptic combination $[\text{Cu}(\mathbf{1d} \text{ or } \mathbf{1e})_2]^+$. As a consequence the principle of maximum occupancy drives the coordination equilibrium towards the heteroleptic complex ($\log K$ 9.4-9.9). For ligands **1f,g,i** the situation is completely different: the *ortho*-methoxy groups can not prevent the formation of $[\text{Cu}(\mathbf{1f,g,i})_2]^+$ and the bishomoleptic complex becomes the main product in nitrile-free solvents. However, in presence of a second phenanthroline the heteroleptic complex is thermochemically preferred due to the fact that $[\text{Cu}(\mathbf{1f,g,i})_2]^+$ are sterically destabilized.

Ligands designed along the HETPHEN protocol are most helpful for the construction of heteroleptic supramolecular structures. This has been shown in recent reports about nanoscaffolds, such as nanogrids, nanoracks and nanoboxes.¹⁰⁻¹³

Acknowledgements. We are indebted to the Deutsche Forschungsgemeinschaft for generous support of this research and the Fonds der Chemischen Industrie. Also we would like to thank the Humboldt Stiftung for support of Shi-Xia Liu. V. K. thanks Annie Marquis-Rigault, Université Louis Pasteur, Strasbourg, France, for help with the fitting programs.

Experimental Section

Materials and General Procedures. The following chemicals were prepared according to literature procedures: $[\text{Cu}(\text{MeCN})_4]\text{BF}_4$, $[\text{Cu}(\text{MeCN})_4]\text{PF}_6$.⁵⁰ The synthesis of the phenanthroline ligands employed in these studies has been described earlier,^{20,16} except **1g**, **1i** (synthesis is described in this paper). All other chemicals were commercially available and used without further purification. The solvents were distilled before use and dried with appropriate desiccants (CH_2Cl_2 from P_2O_5 , MeCN from P_2O_5 and NaH, DMSO from calcium sulfate under reduced pressure). ^1H NMR spectra were recorded on either Bruker AC 200

(200 MHz) or Bruker AC 250 (250 MHz) spectrometers (using the deuterated solvent as the lock and residual solvent as the internal reference). IR spectra were recorded on a Perkin-Elmer (1605 FT-IR). Microanalyses were carried out with a Carlo Erba Elemental Analyzer 1106. Melting points were determined by using a Mettler FP5.0 and are uncorrected. Electrospray mass spectra (ESI MS) were recorded on a TSQ 7000 Triple-Quadrupole-Tandem-Mass spectrometer (Finnigan MAT) with Finnigan ESI-Interface. Data recording and evaluation was carried out using the ICIS 8.1 software package (Finnigan MAT). Electrochemical measurements were performed with a Princeton Applied Research Model 362 potentiostat with a Philips model PM 8271 XYt-recorder.

Synthesis of 1g: A solution of 1-bromo-2,6-dimethoxybenzene (0.629 g, 3.16 mmol) in dry diethylether (10 ml) was treated dropwise with 2.5 M *n*-butyllithium (1.39 ml, 3.47 mmol) at 0 °C and stirred for 6 h at room temperature. After the addition of 2-(2,6-dimethoxy-phenyl)-9-(2,4,6-trimethyl-phenyl)-[1,10]phenanthroline (0.500 g, 1.58 mmol) the resulting purple solution was stirred for 48 h at room temperature. After hydrolysis with aqueous NH₄Cl (20 ml) and separation of the phases, the aqueous layer was extracted with dichloromethane three times (3 x 10 ml). The combined organic layers were dried over MgSO₄ and the solvents were removed to give a bright yellow oil. The resulting mixture was purified by column chromatography (SiO₂, CH₂Cl₂, *R*_f = 0.35) to provide a white solid. Yield: 310 mg (45%), mp. 256 °C. ¹H NMR (CD₂Cl₂, 200 MHz): δ 8.30 (d, *J* = 8.1 Hz, 2H, phen), 7.87 (s, 2H, phen), 7.56 (dd, *J* = 8.3 Hz, *J* = 4.4 Hz, 2H, phen), 7.36 (t, *J* = 8.3 Hz, 1H, phenyl), 6.96 (s, 2H, phenyl); 6.69 (d, *J* = 8.3 Hz, 2H, phenyl), 3.70 (s, 6H, methoxy), 2.34 (s, 3H, benzyl), 2.03 (s, 6H, benzyl); ¹³C NMR (CD₂Cl₂, 50 MHz): δ 160.1, 158.2, 155.2, 138.3 (2C), 137.3, 136.1, 135.7, 135.5 (2C), 129.7, 128.2, 128.0 (2C), 127.6, 127.2, 126.2, 125.8, 124.3, 104.3 (arom), 69.8 (methoxy), 20.8, 20.1 (aliph.); ESI MS: calcd. for C₂₉H₂₇N₂O₂ [M-H⁺]: *m/z* 435.5, found: *m/z* (%) 435.4 (100); IR (KBr): ν 3439, 2965, 2917, 2835, 1736, 1585, 1470, 1246, 1103, 858, 735, 631; Anal. Calcd. for C₂₉H₂₆N₂O₂·H₂O: C, 76.97; H, 6.24; N, 6.19. Found: C, 77.16; H, 5.96; N, 6.61.

Synthesis of 1h: Analogous procedure was applied as in case of **1g** synthesis. Compound **1i** was synthesized in two steps starting from phenanthroline. Yield: 89% and 72%. ¹H NMR (CD₂Cl₂, 200 MHz): δ 8.38 (d, *J* = 8.62 Hz, 2H, phen), 8.21 (dd, *J* = 8.3 Hz, *J* = 4.3 Hz, 4H, phen), 7.74 (s, 2H, phenyl), 6.76 (d, *J* = 2.46 Hz, 2H, phenyl), 6.59 (d, *J* = 2.46 Hz, 2H, phenyl); 3.90 (s, 12H, methoxy); ¹³C NMR (CD₂Cl₂, 50 MHz): δ 162.0, 159.1, 156.2, 146.5, 135.6, 133.7, 127.5, 125.9, 124.8, 123.1, (arom), 56.17, 55.90 (methoxy); ESI MS: calcd. for

$C_{28}H_{24}N_2O_4$ [$M-H^+$]: m/z 453.5, found: m/z (%) 454.2 (100); IR (KBr): ν 3358, 2996, 2935, 1612, 1581, 1488, 1463, 1414, 1279, 1207, 1159, 1134, 1028, 937, 857, 828, 794, 748, 635; Anal. Calcd. for $C_{28}H_{24}N_2O_4 \cdot H_2O$: C, 71.47; H, 5.57; N, 5.95. Found: C, 71.76; H, 5.56; N, 6.0.

General procedure for symmetrical copper(I) complexes: To two equivalent of sterically unhindered 2,9-disubstituted phenanthroline (**2b** or **1a** or **1f** or **1g** or **1h**) in dry dichloromethane (1 μ mol/ml) was added under an inert atmosphere one equivalent of a $[Cu(MeCN)_4]BF_4$. The resulting red solution was stirred for 5 min. at room temperature, then the solvent was removed *in vacuo* and characterized without any further purification. Analytical samples were obtained by recrystallization.

[Cu(2b)₂]BF₄: M.p. > 300 °C; ¹H NMR (CD_3SOCD_3 , 200 MHz): δ 9.00 (d, J = 4.8 Hz, 4H, phen), 8.64 (s, 4H, phen), 8.05 (d, J = 4.8 Hz, 4H, phen), 7.79 (m, 8H, phenyl), 7.52 (m, 12H, phenyl); ¹³C NMR (CD_3SOCD_3 , 50 MHz): δ 149.0, 143.2, 132.3, 130.6, 129.6, 129.2, 128.5, 127.8, 125.6, 120.9 (arom), 101.4, 84.6 (ethynyl); ESI MS: calcd. for $[CuC_{56}H_{32}N_4]^+$ [M^+]: m/z 824.4, found: m/z (%) 824.1 (100); IR (KBr): ν 3051, 2195, 1616, 1588, 1556, 1508, 1442, 1422, 1282, 1233, 1035, 844, 754, 729, 688; Anal. Calcd. for $C_{56}H_{32}N_4CuBF_4$: C, 73.81; H, 3.54; N, 6.15. Found: C, 73.61; H, 3.69; N, 6.18.

[Cu(1a)₂]BF₄: M.p. > 300 °C; ¹H NMR (CD_3COCD_3 , 200 MHz): δ 8.67 (d, J = 8.4 Hz, 4H, phen), 8.13 (d, J = 8.4 Hz, 4H, phen), 8.06 (s, 4H, phen), 7.77 (d, J = 8.2 Hz, 8H, phenyl), 7.43 (m, 12H, phenyl), 7.23 (m, 8H, phenyl), 6.90 (d, J = 8.2 Hz, 8H, phenyl); ¹³C NMR (CD_3COCD_3 , 50 MHz): δ 156.9, 153.0, 144.1, 142.1, 140.1, 138.5, 138.2, 129.3, 129.1, 128.3, 127.3, 127.1, 126.1, 125.1 (arom); ESI MS: calcd. for $[CuC_{72}H_{48}N_4]^+$ [M^+]: m/z 1032.7, found: m/z (%) 1031.1 (100); IR (KBr): ν 3029, 1649, 1605, 1583, 1484, 1357, 1053, 870, 840, 766, 748, 697; Anal. Calcd. for $C_{72}H_{48}N_4CuBF_4$: C, 77.25; H, 4.32; N, 5.00. Found: C, 77.28; H, 4.42; N, 4.71.

[Cu(1f)₂]PF₆: M.p. > 300 °C; ¹H NMR ($CDCl_3$, 200 MHz): δ 8.24 (d, J = 8.3 Hz, 4H, phen), 7.89 (s, 4H, phen), 7.44 (d, J = 8.3 Hz, 4H, phen), 6.80 (t, J = 8.4 Hz, 4H, phenyl), 5.87 (d, J = 8.4 Hz, 8H, phenyl), 3.03 (s, 24H, methoxy); ¹³C NMR (CD_3COCD_3 , 50 MHz): δ 157.5, 145.0, 143.5, 141.9, 135.9, 130.8, 129.4, 128.3, 127.1, 103.2 (arom), 54.4 (methoxy); ESI MS: calcd. for $[C_{56}H_{48}N_4O_8Cu]^+$ [M^+]: m/z 967.3, found: m/z (%) 967.6 (100); IR (KBr): ν 2935, 2835, 1623, 1598, 1508, 1470, 1430, 1349, 1290, 1252, 1149, 1110, 1020, 840, 778,

733, 659. Anal. Calcd. for $C_{56}H_{48}N_4O_8CuPF_6 \cdot 4H_2O$: C, 56.73; H, 4.76; N, 4.73. Found: C, 56.50; H, 4.35; N, 5.15.

[Cu(1g)₂]PF₆: M.p. > 300 °C; ¹H NMR (CD₂Cl₂, 200 MHz): δ 8.33 (dd, *J* = 8.9 Hz, *J* = 3.9 Hz, 4H, phen), 7.99 (s, 4H, phen), 7.56 (dd, *J* = 8.3 Hz, 2H, phen), 7.36 (t, *J* = 8.3 Hz, 2H, phen), 6.90 (t, *J* = 8.3 Hz, 2H, phenyl), 6.46 (s, 2H, phenyl), 6.30 (s, 2H, phenyl), 6.09 (d, *J* = 8.3 Hz, 2H, phenyl), 5.76 (d, *J* = 8.3 Hz, 2H, phenyl), 3.32 (s, 12H, methoxy), 2.64 (s, 6H, benzyl), 2.19 (s, 6H, benzyl), 1.49 (s, 6H, benzyl); ¹³C NMR (CD₂Cl₂, 50 MHz): δ 160.0 (2C), 158.4 (2C), 155.5, 143.4, 143.2 (2C), 138.8, 137.6 (2C), 136.0 (2C), 131.5 (2C), 128.3 (2C), 127.0, 127.0, 104.3 (arom), 55.9 (methoxy), 20.6, 19.6 (aliph); ESI MS: calcd. for [C₅₈H₅₂N₄O₄Cu⁺] [M⁺]: *m/z* 932.6, found: *m/z* (%) 933.2 (100); IR (KBr): ν 3462, 2923, 1588, 1474, 1252, 1110, 1023, 840, 784, 735, 557. Anal. Calcd. for $C_{58}H_{52}N_4O_6CuPF_6 \cdot 3H_2O$: C, 61.56; H, 5.17; N, 4.95. Found: C, 61.76; H, 4.61; N, 4.75.

[Cu(1g)(MeCN)₂]PF₆: M.p. > 300 °C; ¹H NMR (CD₂Cl₂, 200 MHz): δ 8.62 (dd, *J* = 8.9 Hz, *J* = 3.9 Hz, 1H, phen), 8.37 (dd, *J* = 8.9 Hz, *J* = 3.9 Hz, 2H, phen), 8.09 (s, 1H, phen), 7.92 (s, 1H, phen), 7.81 (dd, *J* = 2.2 Hz, *J* = 2.2 Hz, 1H, phen), 7.57 (s, 1H, phenyl), 7.38 (m, 1H, phenyl), 6.95 (d, *J* = 8.8 Hz, 1H, phenyl), 6.72 (t, *J* = 8.3 Hz, 2H, phenyl), 3.60 (s, 6H, MeCN), 2.28 (s, 3H), 1.90 (s, 6H), ESI MS: calcd. for [C₂₉H₂₆N₂O₂Cu⁺] [M⁺]: *m/z* 498.0, found: *m/z* (%) 497.2 (100); IR (KBr): ν 3446, 2917, 1587, 1473, 1431, 1252, 1110, 839, 784, 734, 557.

[Cu(1d)(MeCN)₂]PF₆: M.p. > 300 °C; ¹H NMR (CD₃CN, 200 MHz): δ 8.67 (d, *J* = 8.3 Hz, 2H, phen), 8.12 (s, 2H, phen), 7.80 (d, *J* = 8.3 Hz, 2H, phen), 6.98 (s, 4H, phenyl), 2.31 (s, 6H, benzyl), 2.16 (s, 12H, benzyl), 1.91 (s, 3H, MeCN), ESI MS: calcd for [C₃₂H₃₁N₃Cu⁺] [M⁺]: *m/z* 520.2, found: *m/z* (%) 520.3 (100).

[Cu(1h)₂]PF₆: M.p. > 300 °C; ¹H NMR (CD₂Cl₂, 200 MHz): δ 8.34 (d, *J* = 8.36 Hz, 4H, phen), 7.88 (d, *J* = 8.36 Hz, 4H, phen), 7.25 (d, *J* = 8.36 Hz, 4H, phen), 5.85 (s, 4H, phenyl), 5.43 (s, 8H, phenyl), 3.46 (s, 12H, methoxy); ¹³C NMR (CD₃SOCD₃, 50 MHz): δ 161.5, 157.3, 155.0, 143.9, 135.6, 130.8, 127.8, 126.2, 121.1, 103.2 (arom), 55.31 (methoxy); ESI MS: calcd. for [C₅₆H₄₈N₄O₈Cu⁺] [M⁺]: *m/z* 968.5, found: *m/z* (%) 967.3 (100); IR (KBr): ν 3446, 2917, 1587, 1473, 1431, 1252, 1110, 839, 784, 734, 557; Anal. Calcd. for $C_{56}H_{32}N_4CuBF_4$: C, 73.81; H, 3.54; N, 6.15. Found: C, 73.61; H, 3.69; N, 6.18.

General procedure for the synthesis of mixed ligand copper(I) complexes: To one equivalent of $[\text{Cu}(\text{MeCN})_4]\text{BF}_4$ or $[\text{Cu}(\text{MeCN})_4]\text{PF}_6$ in dry dichloromethane (1 $\mu\text{mol}/\text{ml}$) was added under an inert atmosphere one equivalent of a sterically hindered 2,9-disubstituted phenanthroline (**1d** or **1e** or **1f** or **1g**). The resulting yellowish solution was stirred for 5 min. at room temperature, then one equivalent of a 2,9-unsubstituted phenanthroline (**1b** or **2a-e** or **3a-b**) was added and a deep red solution immediately formed. After 30 min the solvent was removed *in vacuo* and characterized with any further purification. Analytical samples were obtained by recrystallization.

[Cu(1d)(1b)]PF₆: ¹H NMR (CDCl_3 , 250 MHz): δ 8.70 (d, $J = 8.1$ Hz, 2H, phen), 8.28 (d, $J = 8.3$ Hz, 2H, phen), 8.23 (s, 2H, phen), 7.80 (s, 2H, phen), 7.78 (d, $J = 8.1$ Hz, 2H, phen), 7.54 (d, $J = 8.3$ Hz, 2H, phen), 6.11 (s, 4H, phenyl), 2.20 (s, 6H, methyl), 1.78 (s, 6H, benzyl), 1.60 (s, 12H, benzyl); ¹³C NMR (CDCl_3 , 50 MHz): δ 159.4, 156.7, 143.7, 142.5, 137.7, 137.5, 136.7, 136.5, 134.4, 128.5, 128.1, 127.3, 127.2, 127.1, 125.5, 125.0 (arom), 26.2, 20.6, 19.8 (aliph); ESI MS: calcd. for $[\text{CuC}_{44}\text{H}_{40}\text{N}_2]^+$ [M^+]: m/z 688.4, found: m/z (%) 687.2 (100); IR (KBr): ν 2918, 1612, 1509, 1480, 1439, 1377, 1358, 1031, 840, 729; Anal. Calcd. for $\text{C}_{44}\text{H}_{40}\text{N}_4\text{CuPF}_6 \cdot \text{H}_2\text{O}$: C, 62.08; H, 4.97; N, 6.58. Found: C, 61.99; H, 4.75; N, 7.00.

[Cu(1d)(2a)]PF₆: M.p. > 300 °C; ¹H NMR (CDCl_3 , 250 MHz): δ 8.67 (d, $J = 8.2$ Hz, 2H, phen), 8.46 (m, 4H, phen), 8.20 (s, 2H, phen), 7.87 (s, 2H, phen), 7.79 (d, $J = 8.2$ Hz, 2H, phen), 7.74 (m, 10H, phenyl), 5.97 (s, 4H, phenyl), 1.70 (s, 12H, benzyl), 1.61 (s, 6H, benzyl); ¹³C NMR (CDCl_3 , 50 MHz): δ 158.9, 147.5 (2C), 143.8, 137.6, 137.3 (2C), 136.9 (2C), 136.2 (2C), 134.4, 128.6, 128.4, 127.8, 127.0, 126.7, 126.4, 124.7, 123.4 (arom), 20.4, 19.9 (aliph); ESI MS: calcd. for $[\text{CuC}_{54}\text{H}_{44}\text{N}_4]^+$ [M^+]: m/z 812.5, found: m/z (%) 812.3 (100); IR (KBr): ν 2919, 1610, 1584, 1509, 1480, 1423, 1380, 1142, 840, 726; Anal. Calcd. for $\text{C}_{42}\text{H}_{36}\text{N}_4\text{CuPF}_6 \cdot 1.5\text{H}_2\text{O}$: C, 60.61; H, 4.72; N, 6.73. Found: C, 60.73; H, 4.53; N, 6.64.

[Cu(1d)(2b)]BF₄: M.p. > 300 °C; ¹H NMR (CDCl_3 , 200 MHz): δ 8.73 (d, $J = 8.3$ Hz, 2H, phen), 8.51 (d, $J = 5.1$ Hz, 2H, phen), 8.44 (s, 2H, phen), 8.26 (s, 2H, phen), 7.89 (d, $J = 5.1$ Hz, 2H, phen), 7.79 (d, $J = 8.3$ Hz, 2H, phen), 7.75 (m, 4H, phenyl), 7.51 (m, 6H, phenyl), 6.08 (s, 4H, phenyl), 1.75 (s, 12H, benzyl), 1.72 (s, 6H, benzyl); ¹³C NMR (CDCl_3 , 50 MHz): δ 158.9, 147.0, 143.8, 143.0, 137.7, 137.6, 136.9, 134.5, 132.1, 130.2, 128.9, 128.8, 128.4, 128.0, 127.0, 126.8, 126.4, 124.9, 121.3, 102.0 (arom), 84.2 (ethynyl), 20.6, 20.0 (aliph); ESI MS: calcd. for $[\text{CuC}_{58}\text{H}_{44}\text{N}_4]^+$ [M^+]: m/z 860.5, found: m/z (%) 859.4 (100); IR (KBr): ν 3050, 2962, 2919, 2209, 1616, 1587, 1559, 1508, 1478, 1442, 1421, 1261, 1054, 846, 802, 758, 690;

Anal. Calcd. for $C_{58}H_{44}N_4CuBF_4 \cdot 3H_2O$: C, 69.57; H, 5.03; N, 5.60. Found: C, 69.22; H, 5.18; N, 5.47.

[Cu(1d)(2c)]BF₄: M.p. 164-165 °C; ¹H NMR (CD₂Cl₂, 200 MHz): δ 8.71 (d, *J* = 8.2 Hz, 2H, phen), 8.47 (d, *J* = 5.2 Hz, 2H, phen), 8.46 (s, 2H, phen), 8.23 (s, 2H, phen), 7.87 (d, *J* = 5.2 Hz, 2H, phen), 7.85 (d, *J* = 8.2 Hz, 2H, phen), 7.75 (d, *J* = 8.4 Hz, 4H, phenyl), 7.62 (d, *J* = 8.4 Hz, 4H, phenyl), 6.08 (s, 4H, phenyl), 3.37 (s, 2H, ethynyl), 2.12 (s, 12H, benzyl), 2.02 (s, 6H, benzyl); ¹³C NMR (CDCl₃, 63 MHz): δ 158.9, 147.1, 143.8, 142.9, 137.7, 136.9, 134.6, 132.4, 132.0, 129.7, 128.6, 128.4, 128.1, 127.2, 127.0, 126.5, 124.9, 124.0, 121.7, 101.1 (arom), 89.7, 85.8, 82.7, 80.2 (ethynyl), 20.6, 20.0 (aliph); ESI MS: calcd. for [CuC₆₂H₄₄N₄]⁺ [M⁺]: *m/z* 908.6, found: *m/z* (%) 908.9 (100); IR (KBr): ν 3040, 2919, 2202, 2094, 1617, 1508, 1384, 1031, 847, 804; Anal. Calcd. for $C_{62}H_{44}N_4CuBF_4 \cdot 4H_2O$: C, 69.76; H, 4.91; N, 5.25. Found: C, 69.74; H, 4.52; N, 5.50.

[Cu(1d)(2d)]BF₄: M.p. > 300 °C; ¹H NMR (CD₃COCD₃, 200 MHz): δ 9.03 (d, *J* = 8.3 Hz, 2H, phen), 8.97 (d, *J* = 4.8 Hz, 2H, phen), 8.76 (s, 2H, phen), 8.47 (s, 2H, phen), 8.18 (d, *J* = 4.8 Hz, 2H, phen), 8.07 (d, *J* = 8.3 Hz, 2H, phen), 8.05 (m, 2H, phenyl), 7.93 (m, 2H, phenyl), 7.64 (m, 4H, phenyl), 6.19 (s, 4H, phenyl), 3.86 (s, 2H, ethynyl), 1.88 (s, 12H, benzyl), 1.74 (s, 6H, benzyl); ¹³C NMR (CDCl₃, 50 MHz): δ 159.1, 146.8, 143.8, 143.0, 137.6, 136.9, 135.3, 134.8, 134.4, 133.4, 132.6, 129.8, 129.0, 128.5, 128.0, 127.0, 126.5, 125.0, 122.9, 121.7, 107.0, 100.7 (arom), 85.3, 84.8, 82.2, 78.6 (ethynyl), 20.8, 20.1 (aliph); ESI MS: calcd. for [CuC₆₂H₄₄N₄]⁺ [M⁺]: *m/z* 908.6, found: *m/z* (%) 908.2 (100); IR (KBr): ν 2916, 2205, 1617, 1591, 1553, 1508, 1477, 1422, 1376, 1057, 848, 798, 685; Anal. Calcd. for $C_{62}H_{44}N_4CuBF_4 \cdot 2H_2O$: C, 72.20; H, 4.69; N, 5.43. Found: C, 71.94; H, 4.59; N, 5.52.

[Cu(1d)(2e)]PF₆: ¹H NMR (CD₂Cl₂, 200 MHz): δ 8.72 (d, *J* = 8.1 Hz, 3H, phen), 8.41 (s, 2H, phen), 8.23 (s, 2H, phen), 7.89 (d, *J* = 8.4 Hz, 3H, phen), 7.70 (s, 2H, phen), 7.16 (d, *J* = 8.4 Hz, 2H, phenyl), 6.71 (d, *J* = 8.6 Hz, 4H, phenyl), 6.08 (s, 4H, phenyl), 2.32 (s, 6H, methoxy), 1.79 (s, 12H, benzyl), 1.62 (s, 6H, benzyl); ¹³C NMR (CD₂Cl₂, 50 MHz): δ 159.1, 156.2, 151.2 (2C), 138.0, 137.7, 135.0, 133.3, 132.4 (2C), 130.7, 128.2 (2C), 127.1, 127.0, 126.7 (2C), 123.4, 121.2, 115.4 (arom), 80.7 (methoxy), 31.7, 30.3, 29.3 (aliph); ESI MS: calcd. for [CuC₅₆H₄₈N₄O₄]⁺ [M⁺]: *m/z* 904.5, found: *m/z* (%) 904.3 (100).

[Cu(1d)(3a)]PF₆: ¹H NMR (CDCl₃, 250 MHz): δ 8.67 (d, *J* = 8.2 Hz, 2H, phen), 8.46 (m, 4H, phen), 8.20 (s, 2H, phen), 7.87 (s, 2H, phen), 7.79 (d, *J* = 8.2 Hz, 2H, phen), 7.74 (m, 2H, phen), 5.97 (s, 4H, phenyl), 1.70 (m, 12H, benzyl), 1.61 (s, 6H, benzyl); ¹³C NMR (CDCl₃, 50

MHz): δ 158.9, 147.5, 143.8, 137.6, 137.3, 136.9, 136.2, 134.4, 128.6, 128.4, 127.8, 127.0, 126.7, 126.4, 124.7 (arom), 20.4, 19.9 (aliph); ESI MS: calcd. for $[\text{CuC}_{42}\text{H}_{36}\text{N}_4]^+$ $[\text{M}^+]$: m/z 660.3, found: m/z (%) 659.2 (100); IR (KBr): ν 2919, 1610, 1584, 1509, 1480, 1423, 1380, 1142, 840, 726; Anal. Calcd. for $\text{C}_{42}\text{H}_{36}\text{N}_4\text{CuPF}_6 \cdot 1.5\text{H}_2\text{O}$: C, 60.61; H, 4.72; N, 6.73. Found: C, 60.73; H, 4.53; N, 6.64.

[Cu(1d)(3b)]PF₆: M.p. > 300 °C; ¹H NMR (CDCl₃, 200 MHz): δ 9.01 (m, 1H, phen), 8.71 (s, 1H, phen), 8.61 (d, J = 8.2 Hz, 2H, phen), 8.55 (m, 3H, phen), 8.13 (s, 2H, phen), 7.84 (m, 2H, phen), 7.72 (d, J = 8.2 Hz, 2H, phen), 5.93 (s, 4H, phenyl), 1.61 (s, 12H, phen), 1.56 (s, 6H, phen); ¹³C NMR (CD₃COCD₃, 50 MHz): δ 161.5, 154.0, 152.3, 146.8, 146.6, 146.5, 145.5, 141.2, 140.4, 140.1, 139.8, 137.3, 135.5, 130.6, 129.5, 129.4, 129.2, 129.0, 128.9, 128.6, 128.2, 123.7 (arom), 22.2, 21.9 (aliph); ESI MS: calcd. for $[\text{CuC}_{42}\text{H}_{35}\text{N}_5\text{O}_2]^+$ $[\text{M}^+]$: m/z 705.3, found: m/z (%) 704.1 (100); IR (KBr): ν 2918, 1618, 1583, 1534, 1509, 1480, 1448, 1419, 1354, 1148, 841, 732; Anal. Calcd. for $\text{C}_{42}\text{H}_{35}\text{O}_2\text{N}_5\text{CuPF}_6 \cdot \text{H}_2\text{O}$: C, 58.10; H, 4.30; N, 8.07. Found: C, 58.24; H, 4.49; N, 7.82.

[Cu(1e)(2b)]BF₄: ¹H NMR (CD₂Cl₂, 200 MHz): δ 8.72 (d, J = 8.2 Hz, 2H, phen), 8.46 (d, J = 5.0 Hz, 2H, phen), 8.45 (s, 2H, phen), 8.24 (s, 2H, phen), 7.86 (d, J = 8.2 Hz, 2H, phen), 7.84 (d, J = 5.0 Hz, 2H, phen), 7.78 (m, 4H, phenyl), 7.52 (m, 6H, phenyl), 6.30 (m, 6H, phenyl), 1.79 (s, 12H, benzyl); ¹³C NMR (CD₂Cl₂, 63 MHz): δ 159.1, 147.1, 144.2, 143.2, 139.9, 137.9, 134.9, 132.4, 130.6, 130.4, 129.1, 128.9, 128.3, 128.0, 127.2, 127.0, 126.6, 125.5, 121.7, 102.0, 92.6, 84.4, 20.1; ESI MS: calcd. for $[\text{CuC}_{56}\text{H}_{40}\text{N}_4]^+$ $[\text{M}^+]$: m/z 832.5, found: m/z (%) 832.1 (100); IR (KBr): ν 3064, 2966, 2907, 2211, 1618, 1588, 1560, 1508, 1422, 1382, 1057, 864, 759, 691; Anal. Calcd. for $\text{C}_{56}\text{H}_{40}\text{N}_4\text{CuBF}_4$: C, 73.17; H, 4.39; N, 6.09. Found: C, 72.76; H, 4.49; N, 5.93.

[Cu(1f)(2a)]PF₆: M.p. > 300 °C; ¹H NMR (d₆-acetone, 200 MHz): δ 8.84 (d, J = 8.3 Hz, 2H, phen), 8.65 (dd, ³ J = 2.7 Hz, ⁴ J = 1.2 Hz, 2H, phen), 8.63 (m, 2H, phen), 8.36 (s, 2H, phen), 8.07 (s, 2H, phen), 7.94 (m, 2H, phen), 7.92 (d, J = 8.3 Hz, 2H, phen), 6.45 (t, J = 8.4 Hz, 2H, phenyl), 5.79 (d, J = 8.4 Hz, 4H, phenyl), 3.30 (s, 12H, benzyl); ¹³C NMR (CDCl₃, 50 MHz): δ 157.7, 154.7, 148.2, 144.4, 143.7, 136.7, 136.5, 130.2, 129.2, 128.3, 127.1, 127.0, 124.8, 123.2, 118.2, 102.9 (arom), 55.8 (aliph); ESI MS: calcd. for $[\text{CuC}_{52}\text{H}_{40}\text{N}_4\text{O}_4]^+$ $[\text{M}^+]$: m/z 848.4, found: m/z (%) 847.2 (100); IR (KBr): ν 2943, 2839, 1599, 1587, 1474, 1433, 1254, 1110, 838, 724; Anal. Calcd. for $\text{C}_{40}\text{H}_{32}\text{N}_4\text{O}_4\text{CuPF}_6 \cdot \text{H}_2\text{O}$: C, 55.92; H, 3.99; N, 6.52. Found: C, 56.04; H, 4.17; N, 6.36.

[Cu(1f)(2b)]BF₄: M.p. > 300 °C; ¹H NMR (CD₂Cl₂, 200 MHz): δ 8.60 (d, *J* = 8.2 Hz, 2H, phen), 8.47 (d, *J* = 5.1 Hz, 2H, phen), 8.47 (s, 2H, phen), 8.16 (s, 4H, phen), 7.82 (d, *J* = 8.2 Hz, 2H, phen), 7.78 (m, 6H, phenyl), 7.52 (m, 6H, phenyl), 6.50 (t, *J* = 8.4 Hz, 2H, phenyl), 5.75 (d, *J* = 8.4 Hz, 4H, phenyl), 3.30 (s, 12H, methoxy); ¹³C NMR (CDCl₃, 63 MHz): δ 157.4, 154.4, 147.1, 144.0, 143.3, 136.5, 135.4, 132.3, 130.4, 130.0, 129.3, 129.1, 128.7, 127.9, 126.8, 126.7, 125.2, 121.7, 117.9, 102.7 (arom), 84.5, 76.1 (ethynyl), 55.5 (methoxy); ESI MS: calcd. for [CuC₅₆H₄₀N₄O₄]⁺ [M⁺]: *m/z* 896.5, found: *m/z* (%) 895.9 (100); IR (KBr): ν 3020, 2935, 2836, 2210, 1588, 1560, 1509, 1473, 1422, 1252, 1112, 1055, 861, 759, 690; Anal. Calcd. for C₅₆H₄₀N₄O₄CuBF₄: C, 68.40; H, 4.10; N, 5.70. Found: C, 68.16; H, 4.07; N, 5.56.

[Cu(1f)(2e)]PF₆: ¹H NMR (CD₂Cl₂, 200 MHz): δ 8.62 (d, *J* = 8.4 Hz, 3H, phen), 8.40 (s, 2H, phen), 8.17 (s, 2H, phen), 7.87 (d, *J* = 8.2 Hz, 3H, phen), 7.72 (s, 2H, phen), 7.20 (d, *J* = 8.4 Hz, 4H, phenyl), 6.60-6.71 (m, 6H, phenyl), 5.86 (d, *J* = 8.4, 4H, phenyl), 3.28 (s, 12H, methoxy), 2.33 (s, 12H, methoxy); ¹³C NMR (CD₂Cl₂, 50 MHz): δ 157.2, 155.6, 155.4, 153.5, 150.7, 143.5, 135.9, 132.7, 131.3, 130.2, 129.4, 127.7, 127.5, 126.2, 122.9, 120.6, 117.8, 114.8, 103.7, 102.3 (arom), 55.6, 55.2 (methoxy), 31.06, 29.6 (aliph); ESI MS: calcd. for [CuC₅₄H₄₄N₄O₈]⁺ [M⁺]: *m/z* 940.5, found: *m/z* (%) 939.6 (100).

[Cu(1f)(1b)]BF₄: M.p. > 300 °C; ¹H NMR (CD₂Cl₂, 200 MHz): δ 8.61 (d, *J* = 8.3 Hz, 2H, phen), 8.27 (d, *J* = 8.3 Hz, 2H, phen), 8.16 (s, 2H, phen), 7.82 (d, *J* = 8.3 Hz, 2H, phen), 7.79 (s, 2H, phen), 7.55 (d, *J* = 8.3 Hz, 2H, phen), 6.46 (t, *J* = 8.4 Hz, 2H, phenyl), 5.68 (d, *J* = 8.4 Hz, 4H, phenyl), 3.21 (s, 12H, methoxy), 2.29 (s, 6H, methyl); ¹³C NMR (CD₂Cl₂, 50 MHz): δ 157.4, 154.7, 148.2, 144.2, 142.8, 136.5, 130.1, 129.0, 128.4, 128.3, 127.0, 125.6, 124.8, 117.9, 107.8, 102.7 (arom), 55.3 (methoxy), 25.0 (aliph); ESI MS: calcd. for [CuC₄₂H₃₆N₄O₄]⁺ [M⁺]: *m/z* 724.3, found: *m/z* (%) 723.8 (100); IR (KBr): ν 2951, 2850, 1588, 1508, 1474, 1431, 1252, 1109, 1080, 871; Anal. Calcd. for C₄₂H₃₆N₄O₄CuBF₄*2H₂O: C, 55.72; H, 4.45; N, 6.19. Found: C, 56.02; H, 4.02; N, 6.04.

[Cu(1f)(3a)]PF₆: ¹H NMR (CD₃COCD₃, 200 MHz): δ 8.84 (d, *J* = 8.3 Hz, 2H, phen), 8.65 (dd, ³*J* = 2.7 Hz, ⁴*J* = 1.2 Hz, 2H, phen), 8.63 (m, 2H, phen), 8.36 (s, 2H, phen), 8.07 (s, 2H, phen), 7.94 (m, 2H, phen), 7.92 (d, *J* = 8.3 Hz, 2H, phen), 6.45 (t, *J* = 8.4 Hz, 2H, phenyl), 5.79 (d, *J* = 8.4 Hz, 4H, phenyl), 3.30 (s, 12H, methoxy); ¹³C NMR (CDCl₃, 50 MHz): δ 157.7, 154.7, 148.2, 144.4 (2C), 143.7, 136.7, 136.5, 130.2, 129.2, 128.3, 127.1, 127.0, 124.8, 118.2, 102.9 (arom), 55.8 (methoxy); ESI MS: calcd. for [CuC₄₀H₃₂N₄O₄]⁺ [M⁺]: *m/z* 696.2,

found: m/z (%) 695.1 (100); IR (KBr): ν 2943, 2839, 1599, 1587, 1474, 1433, 1254, 1110, 838, 724; Anal. Calcd. for $C_{40}H_{32}N_4O_4CuPF_6 \cdot H_2O$: C, 55.92; H, 3.99; N, 6.52. Found: C, 56.04; H, 4.17; N, 6.36.

[Cu(1c)(2b)]BF₄: ¹H NMR (CDCl₃, 200 MHz): δ 8.62 (s, 2H), 8.60 (d, J = 8.4 Hz, 2H), 8.47 (d, J = 5.1 Hz, 2H), 8.09 (s, 2H), 8.00 (d, J = 8.4 Hz, 2H), 7.94 (d, J = 5.1 Hz, 2H), 7.70 (m, 4H), 7.46 (m, 6H), 1.33 (s, 18H).

[Cu(1g)(3a)]PF₆: M.p. > 300 °C; ¹H NMR (CD₂Cl₂, 200 MHz): δ 8.63 (d, J = 8.3 Hz, 2H, phen), 8.48 (d, J = 4.6 Hz, 2H, phen), 8.42 (d, J = 7.7 Hz 2H, phen), 8.17 (s, 2H, phen), 7.88 (s, 2H, phen), 7.70 (m, 4H, phen), 6.49 (t, J = 8.8 Hz, 1H, phenyl), 5.79 (t, J = 8.6 Hz, 4H, phenyl), 3.33 (s, 6H, methoxy), 1.58 (s, 9H, benzyl); ¹³C NMR (CD₂Cl₂, 50 MHz): δ 158.7, 157.3, 147.6, 143.9, 143.1, 140.7, 137.1, 136.0 (2C), 134.4 (2C), 129.9, 128.6, 127.9, 127.6 (2C), 126.7 (2C), 126.6 (2C), 126.5 (2C), 126.4, 124.2 (2C), 102.5 (arom), 69.7 (methoxy), 20.8 (2C, aliph); ESI MS: calcd. for $C_{41}H_{34}N_4O_2Cu^+$ [M^+]: m/z 678.2, found: m/z (%) 677.2 (100); IR (KBr): ν 3392, 1597, 1509, 1474, 1253, 1109, 840, 726, 557; Anal. Calcd. for $C_{41}H_{34}N_4O_2CuPF_6 \cdot 2H_2O$: C, 57.31; H, 4.46; N, 6.52. Found: C, 57.16; H, 3.79; N, 6.27.

[Cu₂(4)(5)]2PF₆: M.p. > 300 °C; ¹H NMR (CD₂Cl₂, 400 MHz): δ 8.70 (s, 2H, phen), 8.68 (d, J = 3.1 Hz, 2H, phen), 8.41-8.54 (m, 8H, phen), 8.20 (s, 4H, phen), 7.82-7.95 (m, 8H, phen), 7.73 (d, J = 4.5 Hz, 2H, phen), 7.08 (s, 2H, phenyl), 6.81 (s, 2H, phenyl), 6.79 (s, 2H, phenyl), 6.05 (s, 2H, phenyl), 5.99 (s, 2H, phenyl), 5.78 (s, 1H, phenyl), 5.76 (s, 1H, phenyl), 3.97-4.04 (m, 9H, methoxy), 3.49-3.80 (m, 23H, methoxy and aliph), 1.61-1.90 (m, 36H, aliph), 1.16-1.40 (m, 26H, aliph), 0.86 (s, 4H, aliph), 0.66 (t, J = 6.9 Hz, 6H, aliph); ¹³C NMR (CD₂Cl₂, 100 MHz): δ 159.4, 159.1, 158.1, 154.1, 153.3, 149.5, 148.3, 144.2, 143.1, 141.8, 138.0, 137.7, 136.8, 135.0, 134.7, 133.0, 129.4, 128.2, 127.4, 126.5, 125.1, 121.7, 116.9, 115.5, 112.4, 111.7 (arom), 90.9 (ethynyl), 71.6, 71.3, 70.9, 70.1, 69.6, 68.3, 67.1 (methoxy), 31.6, 30.0, 29.3, 25.8 (2C), 22.7 (2C), 20.6, 20.4, 20.1 (2C), 14.2, 13.9 (2C) (aliph); ESI MS: calcd. for $[Cu_2C_{134}H_{144}N_8O_{10}]^{2+}$ [M^{2+}]: m/z 1076.8, found: m/z (%) 1076.6 (100); Anal. Calcd. for $Cu_2C_{134}H_{144}N_8O_{10}2PF_6 \cdot 3CH_2Cl_2$: C, 60.98; H, 5.60; N, 4.15. Found: C, 61.33; H, 5.14; N, 4.60.

Oxidation of a mixed ligand complex

To $[Cu(1d)(2b)]PF_6$ (5.00 mg, 5.12 μ mol) in dry dichloromethane (2 ml) was added under vigorous stirring a solution of 3.2 mg (5.12 μ mol) of tris(*p*-tolyl)aminium

hexachloroantimonate in dichloromethane (5 ml) under an inert atmosphere. After 30 min the color of the solution changed to a light brown. The reaction mixture was subsequently hydrolysed with sat. NaHCO₃ solution (10 ml). The organic layer was separated and analyzed by ESI MS.

Spectrophotometric titrations

Equilibrium constants were calculated by using dichloromethane as the solvent. In case of heteroleptic complexes, copper(I) tetrakisacetonitrile hexafluorophosphate and sterically shielded ligands (**1d**, **1i**) were titrated with aliquot amounts of a stock solution of unshielded ligands (**1a**, **1b**, **2a**, **2b**, **2e**, **3a**, and **3b**). And in case of homoleptic complexes the ligands (**1b** and **3a**) were titrated with aliquot amounts of copper(I) tetrakisacetonitrile hexafluorophosphate solution. All stock solutions were prepared by careful weighing using analytical balance. Absorption spectra were recorded at 25.0-(0.1) °C. Since the formation kinetics are instantaneous as evidenced by proton NMR and ESI-MS analysis and the visible colour change, the solutions were immediately analysed by the spectroscopy, this would also prevent the concentration changes. The wavelengths ranging from 240nm to 600nm were taken in to account. Each time two equivalents of titrant has been added in 20 number of titration's. These entire multiwavelength data sets comprising absorbances measured in one nanometer steps were decomposed in their principal components by factor analysis, and subsequently the formation constants including their standard deviation were calculated by using SPECFIT program⁵¹ and are presented in Table-3.

Since the equilibrium constants calculated were not seem to be very much dependent on the solvent and usually the phenanthrolines are more soluble in dichloromethane than in acetonitrile, dichloromethane has been chosen as a solvent. A typical set of absorption spectra in case of homoleptic complex and heteroleptic complex are depicted in figure **1a** and figure **1b** respectively. Since there is no formation of homoleptic complex with the sterically shielded ligands as evidenced by ESI-MS, proton NMR and absence of MLCT absorption band at around 460-500nm (characteristic for the copper(I) phenanthroline complexes), sterically shielded ligands and copper(I) salts were titrated with the unshielded ligand. The analysis of the data set by the SPECFIT programme indicated the presence of two chemically sensible species in solution, one of them can be readily assigned to free ligand and the second one can be assigned to 1:1 species as evidenced by proton NMR and ESI-MS analysis. From this independent titration the equilibrium constant for the 1:1 species was calculated (Table-3) and this value then used for later calculations of heteroleptic complexes of **1d**. The binding

constants were calculated in two independent titration's and the results obtained are very much the same in both the titration's.

- (1) (a) Lehn, J.-M. *Supramolecular Chemistry*, VCH, Weinheim, **1995**. (b) Holliday, B.; Mirkin, C. A. *Angew. Chem. Int. Ed.* **2001**, *40*, 2022–2043. (c) Prins, L. J.; Reinhoudt, D. N.; Timmerman, P. *Angew. Chem. Int. Ed.* **2001**, *40*, 2383–2426. (d) Seidel, S. R.; Stang, P. J. *Acc. Chem. Res.* **2002**, *35*, 972–983. (e) Wuerthner, F.; You, C. C.; Saha-Moeller, C. R. *Chem. Soc. Rev.* **2004**, 133–146. (f) Schmittel, M.; Kalsani, V. *Topics in Current Chemistry*, **2005**, *245*, 1–53. (g) Fujita, M.; Tominaga, M.; Hori, A.; Therrien, B. *Acc. Chem. Res.* **2005**, **ASAP**.
- (2) (a) Nitschke, J. R.; Lehn, J.-M. *Proc. Natl. Acad. Sci. USA* **2003**, *100*, 11970–11974. (b) Tominaga, M.; Suzuki, K.; Kawano, M.; Kusakawa, T.; Ozeki, T.; Sakamoto, S.; Yamaguchi, K.; Fujita, M. *Angew. Chem. Int. Ed.* **2004**, *43*, 5621–5625. (c) Chichak, K. S.; Cantrill, S. J.; Pease, A. R.; Chiu, S.-H.; Cave, G. W. V.; Atwood, J. L.; Stoddart, J. F. *Science* **2004**, *304*, 1308–1312.
- (3) (a) von Zelewsky, A. *Stereochemistry of Coordination Compounds*, Wiley, Chichester **1995**. (b) Sauvage, J.-P.; Dietrich-Buchecker, C.; Eds. *Molecular Catenanes, Rotaxanes and Knots*, Wiley-VCH, Weinheim **1999**.
- (4) Heteroleptic complex formation of bisimine ligands is well known for ruthenium(II) complexes, but these complexes are kinetically inert: (a) MacDonnell, F. M.; Kim, M. J.; Bodige, S. *Coord. Chem. Rev.* **1999**, *186*, 535–549. (b) MacDonnell, F. M.; Ali, M. D. M.; Kim, M. J. *Comm. Inorg. Chem.* **2000**, *22*, 203–225.
- (5) Copper complexes of phenanthroline/bipyridine with other ligands are rather well studied: (a) Sigel, H.; Huber, P. R.; Griesser, R.; Prijs, B. *Inorg. Chem.* **1973**, *12*, 1198–1200; (b) Sigel, H. *Angew. Chem. Int. Ed. Engl.* **1975**, *14*, 394–402. (c) Bastian, M.; Sigel, H. *Inorg. Chem.* **1997**, *36*, 1619–1624. (d) Da Costa, C. P.; Song, B.; Gregan, F.; Sigel, H. *Dalton Trans.* **2000**, 899–904.
- (6) (a) Hodges, H. L.; de Araujo, M. A. *Inorg. Chem.* **1982**, *21*, 3236–3239. (b) Pilo, M. I.; Manca, G.; Zoroddu, M. A. *Inorg. Chim. Acta* **1991**, *180*, 225–230. (c) Lei, Y.; Anson, F. C. *Inorg. Chem.* **1995**, *34*, 1083–1089. (d) Riesgo, E.; Hu, Y.-Z.; Bouvier, F.; Thummel, R. P. *Inorg. Chem.* **2001**, *40*, 2541–2546. (e) Desvergues-Breuil, V.; Hebbe, V.; Dietrich-Buchecker, C.; Sauvage, J. P.; Lacour, J. *Inorg. Chem.* **2003**, *42*, 255–257.
- (7) Colton, R.; James, B. D.; Potter, I. D.; Traeger, J. C. *Inorg. Chem.* **1993**, *32*, 2626–2629.
- (8) Schmittel, M.; Ganz, A. *J. Chem. Soc., Chem. Commun.* **1997**, 999–1000.
- (9) Schmittel, M.; Ganz, A.; Fenske, D.; Herderich, M. *J. Chem. Soc., Dalton Trans.* **2000**, 353–359.
- (10) Schmittel, M.; Ammon, H.; Kalsani, V.; Wiegrefe, A.; Michel, C. *Chem. Comm.* **2002**, 2566–2567.
- (11) Schmittel, M.; Kalsani, V.; Fenske, D.; Wiegrefe, A.; *Chem. Commun.* **2004**, 490–491.
- (12) Schmittel, M.; Ganz, A.; Fenske, D. *Org. Lett.* **2002**, *4*, 2289–2292.
- (13) Kalsani, V.; Bodenstedt, H.; Fenske, D.; Schmittel, M. *Eur. J. Inorg. Chem.* **2005**, **in press**.
- (14) Miller, M. T.; Gantzel, P. K.; Karpishin, T. B. *Inorg. Chem.* **1999**, *38*, 3414–3422.
- (15) Miller, M. T.; Gantzel, P. K.; Karpishin, T. B. *J. Am. Chem. Soc.* **1999**, *121*, 4292–4293.
- (16) (a) Schmittel, M.; Lüning, U.; Meder, M.; Ganz, A.; Michel, C.; Herderich, M. *Heterocycl. Comm.* **1997**, *3*, 493–498. (b) Schmittel, M.; Liu, S.-X.; Michel, C. *Org. Lett.* **2000**, *25*, 3959–3962.
- (17) Dietrich-Buchecker, C. O.; Sauvage, J. P.; Kintzinger, J. P. *Tetrahedron Lett.* **1983**, *24*, 5095–5098.
- (18) Zhu, S. S.; Carroll, P. J.; Swager, T. M. *J. Am. Chem. Soc.* **1996**, *118*, 8713–8714.
- (19) Takacs, J. M.; Hrvatin, P. M.; Atkins, J. M.; Sahadeva Reddy, D.; Clark, J. L. *New. J. Chem.* **2005**, 263–265.
- (20) Schmittel, M.; Ganz, A. *Synlett* **1997**, 710–712.
- (21) π - π stacking has also been identified in $[\text{Cu}(\text{phen})(\text{ArCH}_2\text{COO})]^+$ complexes: Malini-Balakrishnan, R.; Scheller, K. H.; Haering, U. K.; Tribolet, R.; Sigel, H. *Inorg. Chem.* **1985**, *24*, 2067–2076.

- (22) NMR Experiments at low temperature demonstrate that ligand exchange is rapid at temperatures above $-20\text{ }^{\circ}\text{C}$.
- (23) Trofimenko, S.; Calabrese, J.C.; Thompson, J. S. *Inorg. Chem.* **1987**, *26*, 1507–1514.
- (24) (a) Masood, Md. A.; Zacharias, P. S. *J. Chem. Soc. Dalton Trans.* **1991**, 111–114. (b) Masood, Md. A.; Jagannathan, R.; Zacharias, P. S. *J. Chem. Soc. Dalton Trans.* **1991**, 2553–2557. (c) Masood, Md. A.; Zacharias, P. S. *Polyhedron* **1991**, *10*, 811–818. (d) Masood, Md.A.; Hodgson, D.J.; Zacharias, P.S. *Inorg. Chim. Acta* **1994**, *221*, 99–108.
- (25) Lüning *et al.* were not able to identify the 1:1 complex in acetonitrile: Lüning, U.; Müller, M; Gelbert, M; Peters, K, von Schnering, H. G.; Keller, M. *Chem. Ber.* **1994**, *127*, 2297–2306.
- (26) Crystal data for $[\text{Cu}(\mathbf{1f})(\text{CH}_3\text{CN})_2\text{PF}_6]$: $\text{CuC}_{32}\text{H}_{30}\text{N}_4\text{O}_4\cdot\text{PF}_6$, triclinic, space group $P\bar{1}$, $a = 11.497(2)\text{ \AA}$, $b = 12.177(2)\text{ \AA}$, $c = 13.345(3)\text{ \AA}$, $\alpha = 112.41(3)^{\circ}$, $\beta = 103.93(3)^{\circ}$, $\gamma = 97.64(3)^{\circ}$, $V = 1623.0(5)\text{ \AA}^3$, $Z = 2$, $D_{\text{calcd}} = 1.521\text{ Mg/m}^3$, $T = 173(2)\text{ K}$, $\lambda(\text{Mo K}\alpha) = 0.71069\text{ \AA}$, 8912 reflexions measured, 4539 unique ($R_{\text{int}} = 0.0916$) which were used in all calculations. Final R indices [$I > 2\sigma(I)$] $R1 = 0.0555$, $wR2 = 0.1284$, R indices (all data) $R1 = 0.1238$, $wR2 = 0.1501$, $\text{GOF} = 0.843$. CCDC reference number **xxxx**. See also supp. information.
- (27) Gelbert, M.; Körber, C.; Friedrich, O.; Fahrenkrug, F.; Keller, M.; Lüning, U. *Supramol. Chem.* **2002**, *14*, 199–210.
- (28) Crystal data for $[\text{Cu}(\mathbf{1f})_2\text{PF}_6]$: $\text{CuC}_{40}\text{H}_{32}\text{N}_4\text{O}_4\cdot\text{PF}_6$, triclinic, space group $P\bar{1}$, $a = 24.156(5)\text{ \AA}$, $b = 14.352(3)\text{ \AA}$, $c = 21.352(4)\text{ \AA}$, $\alpha = 90.00(0)^{\circ}$, $\beta = 90.00(0)^{\circ}$, $\gamma = 90.00(0)^{\circ}$, $V = 7402(3)\text{ \AA}^3$, $Z = 8$, $D_{\text{calcd}} = 1.438\text{ Mg/m}^3$, $T = 153(2)\text{ K}$, $\lambda(\text{Mo K}\alpha) = 0.71073\text{ \AA}$, 4236 reflexions measured, 2547 unique ($R_{\text{int}} = 0.0751$) which were used in all calculations. Final R indices [$I > 2\sigma(I)$] $R1 = 0.0717$, $wR2 = 0.2037$, R indices (all data) $R1 = 0.1093$, $wR2 = 0.2251$, $\text{GOF} = 1.001$. CCDC reference number **xxxx**. See also supp. information.
- (29) (a) Yandell, J. K. in "Copper Coordination Chemistry: Biochemical and Inorganic Perspectives", Karlin, K. D.; Zubieta, J.; Eds., Adenine Press, New York, **1983**, 157. (b) Sanna, G.; Pilo, M. L.; Zoroddu, M. A.; Seeber, R.; Mosca, S. *Inorg. Chim. Acta* **1993**, *208*, 153–158. (c) James, B. R.; Williams, R. J. P. *J. Chem. Soc.* **1961**, 2007–2019.
- (30) Meyer, M.; Albrecht-Gary, A. M.; Dietrich-Buchecker, C. O.; Sauvage, J. P. *Inorg. Chem.* **1999**, *38*, 2279–2287.
- (31) Leupin, P. Ph.D. Thesis, Universität de Fribourg, Switzerland **1980**.
- (32) Atkins, C. E.; Park, S. E.; Blaszak, J. A.; McMillin, D. R. *Inorg. Chem.* **1984**, *23*, 569–572.
- (33) Stewart, J. J. P. *J. Comput. Chem.* **1989**, *10*, 209–220.
- (34) Riesgo, E. C.; Hu Y.Z.; Bouvier, F. Thummel, R. P.; Scaltrito D. V., Meyer, G. J. *Inorg. Chem.* **2001**, *40*, 3413–3422.
- (35) Comba, P.; *Coord. Chem. Rev.* **1999**, *182*, 343–371.
- (36) $[\text{Cu}(\mathbf{1d})_2]^+$ does not form even when all the acetonitrile has been removed.
- (37) In the solid state, the two acetonitrile molecules are even more stabilized by interacting with two more acetonitriles of an another molecule.
- (38) Eggleston M. K.; Fanwick, P. E, A; Pallenberg, J.; McMillin, D. R.; *Inorg. Chem.* **1997**, *36*, 4007–4010.
- (39) Lehn, J.-M. *Chem. Eur. J.* **2000**, *22*, 4140–4148.
- (40) V. Kalsani, PhD thesis, Universität Siegen, **2005**.
- (41) Due to the insoluble nature of **4**, this interconversion could only be performed by ESI MS and UV-vis spectroscopy.
- (42) Müller, M.; PhD thesis, Universität Freiburg, **1991**.
- (43) Brisbin, D. A.; McBryde, W. A. E. *Can. J. Chem.* **1963**, *41*, 1135–1141.
- (44) (a) McBryde, W. A. E. *Critical Review of Equilibrium Data for Proton and Metal Complexes of 1,10-Phenanthroline, 2,2'-Bipyridyl and Related Compounds: Critical Evaluation of Equilibrium Constants in Solution*, Pergamon Press, Oxford, **1978**. (b) Zamudio, W.; Baraona, R.; Campos, M. *Vib. Spectros.* **1997**, *13*, 159-161.

- (45) (a) Dietrich-Buchecker, C. O.; Sauvage, J. P.; Kern, J. M. *J. Am. Chem. Soc.* **1989**, *111*, 7791–7800. (b) Pallenberg, A. J.; Koenig, K. S.; Barnhart, D. M. *Inorg. Chem.* **1995**, *34*, 2833–2840.
- (46) Boekelheide, V. *Pure Appl. Chem.* **1975**, *44*, 751–765.
- (47) Hunter, C. A.; Sanders, J. K. M. *J. Am. Chem. Soc.* **1990**, *112*, 5525–5534.
- (48) Rorabacher, D. B. *Chem. Rev.* **2004**, *104*, 651–697.
- (49) Ambundo, E. A.; Deydier, M.-V.; Grall, A. J.; Aguera-Vega, N.; Dressel, L. T.; Cooper, T. H.; Heeg, M. J.; Ochrymowycz, L. A.; Rorabacher, D. B. *Inorg. Chem.* **1999**, *38*, 4233–4242.
- (50) Meerwein, H.; Hederich, V.; Wunderlich, K. *Arch. Pharm.* **1958**, *291*, 541–545.
- (51) (a) Gampp, H.; Maeder, M.; Meyer, C. J.; Zuberbühler, A. D. *Talanta* **1985**, *32*, 95–101. (b) Rossoti, F. J. C.; Rossoti, H. S.; Whewell, R. J. *J. Inorg. Nucl. Chem.* **1971**, *33*, 2051–2065. (c) Gampp, H.; Maeder, M.; Meyer, C. J.; Zuberbühler, A. D. *Talanta* **1985**, *32*, 257–264. (d) Gampp, H.; Maeder, M.; Meyer, C. J.; Zuberbühler, A. D. *Talanta* **1986**, *33*, 943–951.

Supp 3-2

Towards a kinetically stable bis-phenanthroline copper complex

Introduction:

Phenanthroline based building blocks have found application in many fields such as supramolecular engineering,¹ photoactive materials,² metal nanoparticle formation³ and liquid crystalline materials.⁴ For years, bidentate ligands, including phenanthroline and bipyridine building blocks, have been the celebrating building blocks to construct the most popular photoactive family of $[\text{Ru}(\text{bpy})_3]^{2+}$ complexes. However, in recent years, Cu(I)-phenanthrolines, which are cheaper and easily accessible and mostly in quantitative yields, have emerged as promising competitors for Ru^{2+} based complexes.⁵

The Cu(I)-bisphenanthroline complexes exhibit metal-to-ligand-charge-transfer (MLCT) absorption bands in the visible region and, they may exhibit MLCT luminescence in non-coordinating solvents. However, in terms of excited state life times these complexes proved to be far behind their Ru^{2+} counter parts. According to McMillin and Armaroli's theory (Fig. 1), the metal ion is converted to Cu(II) when it is excited and thereby resulting a larger coordination number (V) than in the ground state (IV). The new coordination site is assumed to be occupied by the counterion or a solvent molecule, giving rise to a 5-coordinated excited complex (exciplex). The exciplex formation leads to a non-radiative deactivations to the ground state and the excited state lifetime shortened. This hypothesis demands more shielding at the Cu(I) center in order to have higher excited state life times.

Armaroli's hypothesis:

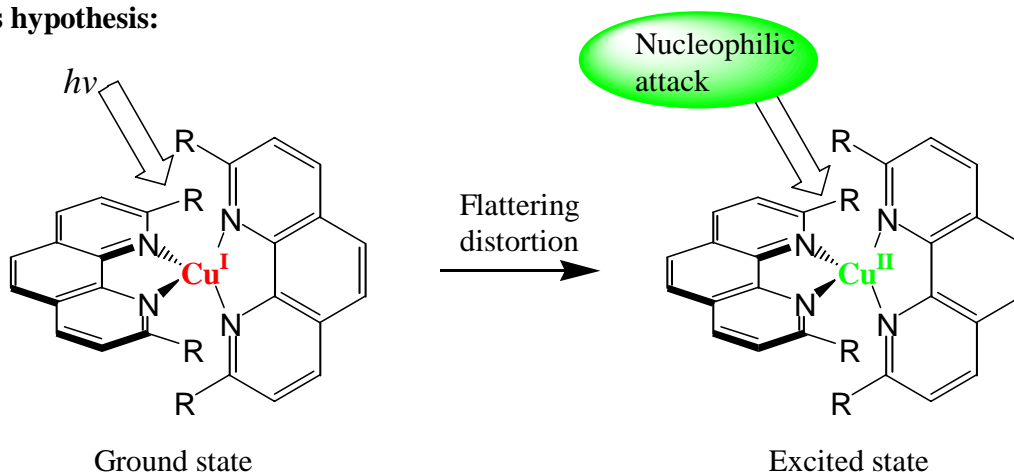


Figure 1. Light excitation of Cu(I)-bisphenanthroline complexes leading to flattering distortion and subsequently attacked by either solvent or counterion or other molecules.

The major difference in between Ru^{2+} (octahedral) and Cu^+ -bis-phenanthroline complexes (tetrahedral) is the nature of the chemical bond present in them. In case of Ru^{2+} the metal coordination bond is kinetic in nature whereas, with Cu^+ complexes it is dynamic in nature and the role of kinetic lability on the photophysical properties is not known (Fig. 2). In the following, design of the first kinetically inert copper(I)-bisphenanthroline complex and its photophysical properties will be discussed.

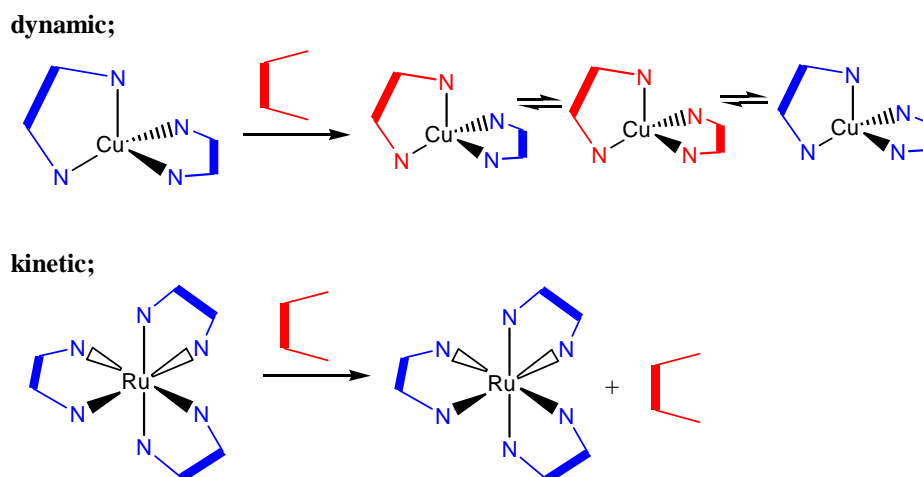
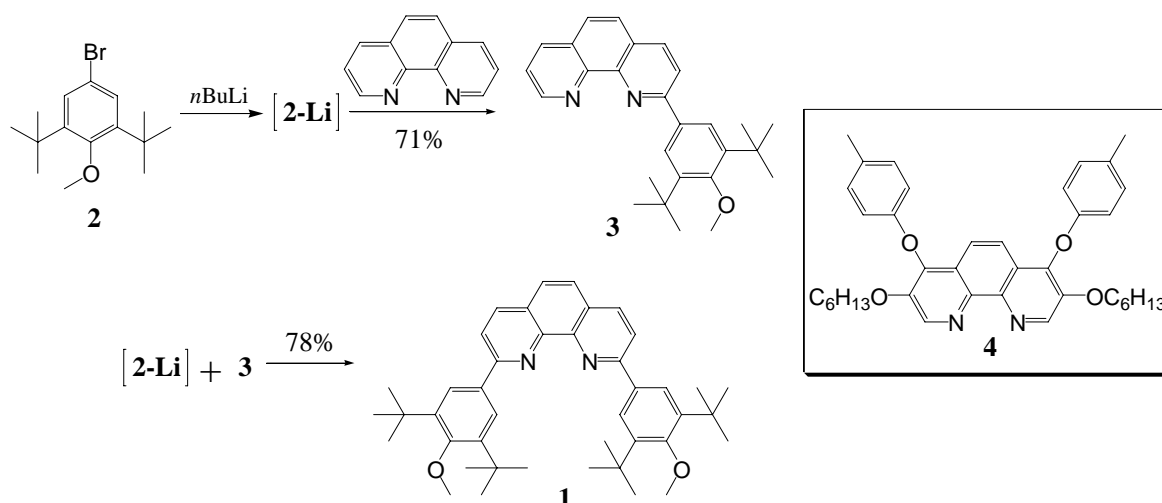


Figure 2. Cartoon representation of probing the nature of bond present in Ru(II) and Cu(I)-polypyridyl complexes.

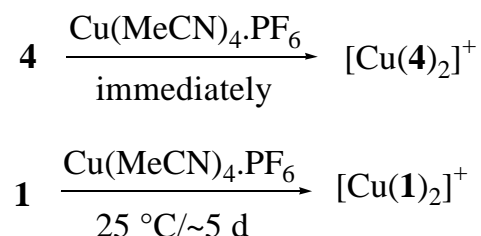
Results and Discussion:

Compound **1** and **4** are synthesised according to the known procedures (scheme 1),⁶ in a stepwise sequential addition of aromatic groups at 2 and 9 positions of the phenanthroline. The aryllithium derivative of **2** was obtained by the treatment of **2** (2 eq.) with *n*-BuLi (2.1 eq.) and followed by the addition of the parent phenanthroline (1 eq.), hydrolysis and rearomatisation with active MnO_2 resulting **3** in 71% yield. Following the similar procedure described above compound **1** is prepared from **3** and **2**. Compound **4** synthesis was described in ref 7.⁷



Scheme 1. Synthesis of compound **1** and **4**.

The copper(I) complexes $[\text{Cu}(\mathbf{1})_2]^+$ and $[\text{Cu}(\mathbf{4})_2]^+$ were obtained quantitatively by the treatment of ligands **1** and **4** with $\text{Cu}(\text{MeCN})_4\text{PF}_6$ (1:0.5 equiv. respectively) in CH_2Cl_2 at ambient temperature (Scheme 2). It is interesting to note that the formation of $[\text{Cu}(\mathbf{1})_2]^+$ was sluggish ($\sim 25^\circ\text{C}/5\text{ d}$) whereas, $[\text{Cu}(\mathbf{4})_2]^+$ is obtained immediately. It can also be added that the complex $[\text{Cu}(\mathbf{1})_2]^+$ is violet in colour whereas $[\text{Cu}(\mathbf{4})_2]^+$ is dark red, normally observed colour for bis-phenanthroline copper complexes. These early observations point a different stability and ground state properties for the $[\text{Cu}(\mathbf{1})_2]^+$ complex, with respect to other homoleptic bisphenanthroline copper complexes.



Scheme 2. Synthesis of copper(I) complexes, $[\text{Cu}(\mathbf{4})_2]^+$ and $[\text{Cu}(\mathbf{1})_2]^+$, respectively.

The structure of $[\text{Cu}(\mathbf{1})_2]^+$ was confirmed by $^1\text{H-NMR}$, $^{13}\text{C-NMR}$, ESI MS and elemental analysis. In particular, the $^1\text{H-NMR}$ spectrum of $[\text{Cu}(\mathbf{1})_2]^+$ shows sharp and single set of signals which are characteristic features of the presence of single species (Fig. 3). The spectral pattern is typical to other bis-phenanthroline complexes.⁸ The proton NMR revealed upfield shift of 0.64 ppm (from δ 8.12 to 7.48 ppm) for the phenyl protons due to the increased electron density around phenyl protons. Also methoxy and *t*-butyl protons experienced significant upfield shift (from δ 3.76 to 3.20 and 1.55 to 0.90 ppm, respectively) indicating highly shielded environment for 2,9-aryl groups. These assignments are further

confirmed by COSY. ^{13}C NMR showed single set of 13 expected signals for $[\text{Cu}(\mathbf{1})_2]^+$, which are different from $\mathbf{1}$, further supporting the proposed composition (Fig. 4).

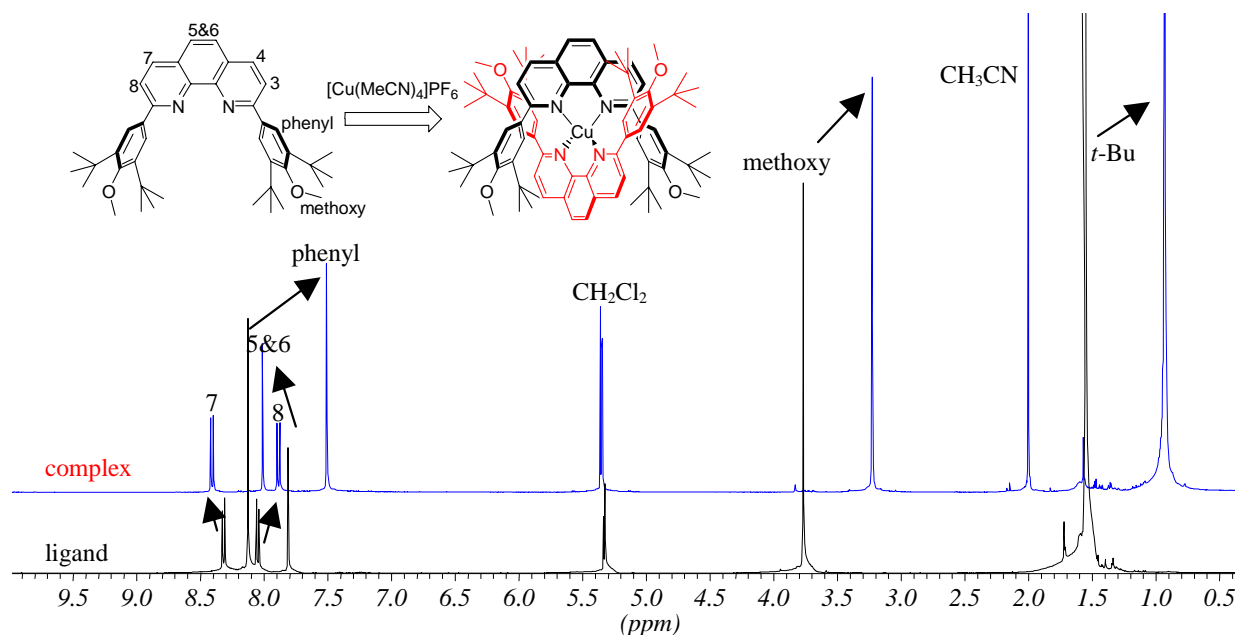


Figure 3. ^1H NMR spectral changes upon homoleptic complex $[\text{Cu}(\mathbf{1})_2]^+$ formation.

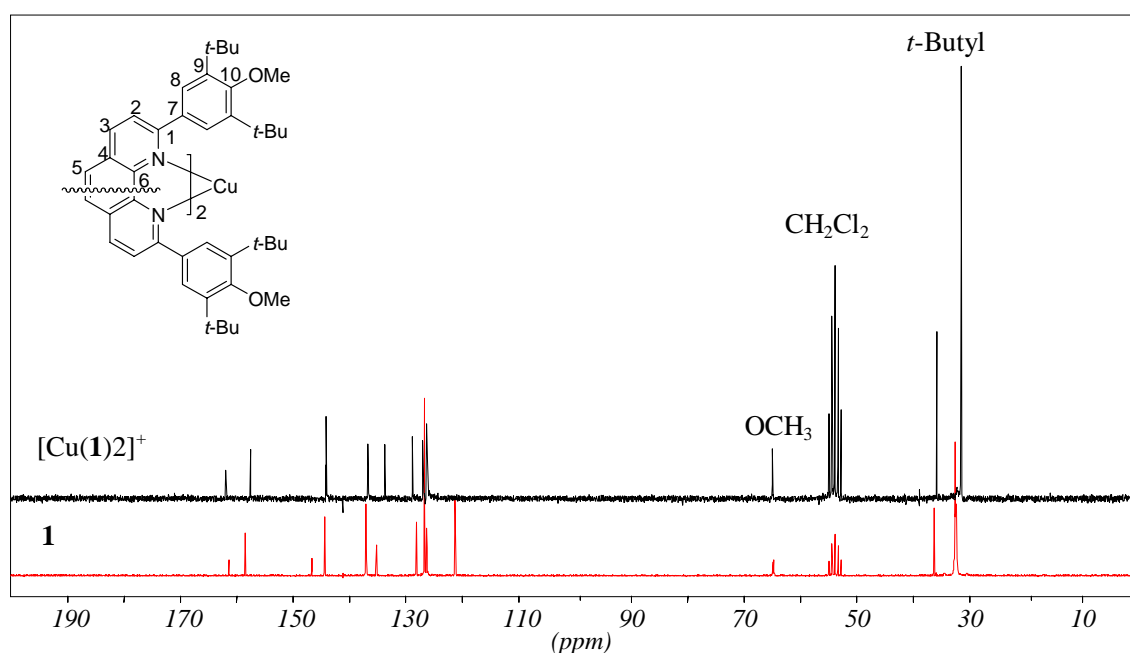


Figure 4. ^{13}C NMR spectral changes upon homoleptic complex $[\text{Cu}(\mathbf{1})_2]^+$ formation.

The ESI-MS (electrospray Ionization Mass Spectrometry) provided more conclusive picture of the composition and exhibiting a singly charged signal at m/z 1296.1 which was assigned to $[\text{Cu}(\mathbf{1})_2]^+$ after the loss of the counter ion hexafluorophosphate (Fig. 5). No other signals could be detected up to 4000 Da. It is noteworthy to mention that under ESI MS conditions normal bisphenanthroline copper complexes fragment to a large extent (>30 %) however, complex $[\text{Cu}(\mathbf{1})_2]^+$ does not show any significant fragmentation (<5%) indicating its

higher stability over other complexes. Further, elemental analysis is in accordance with the proposed composition.

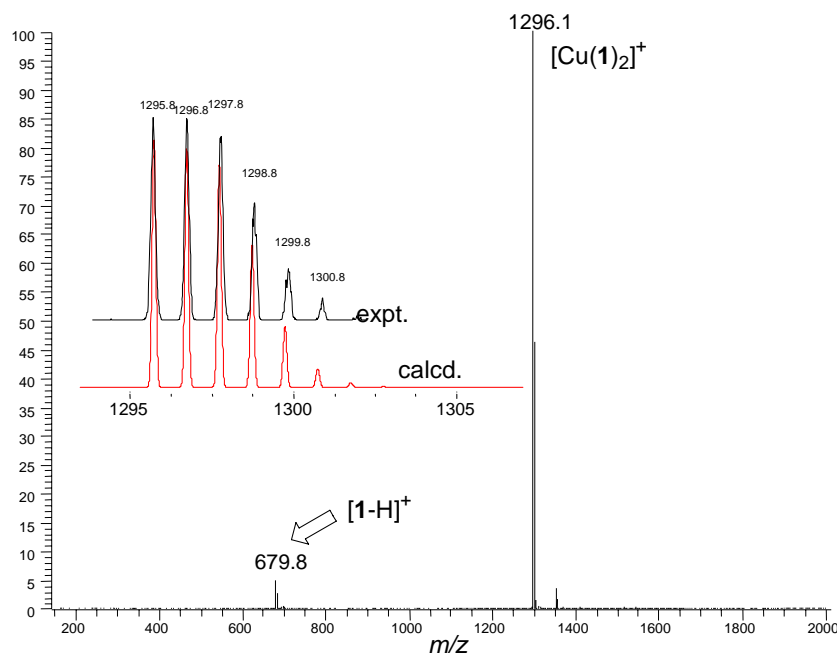
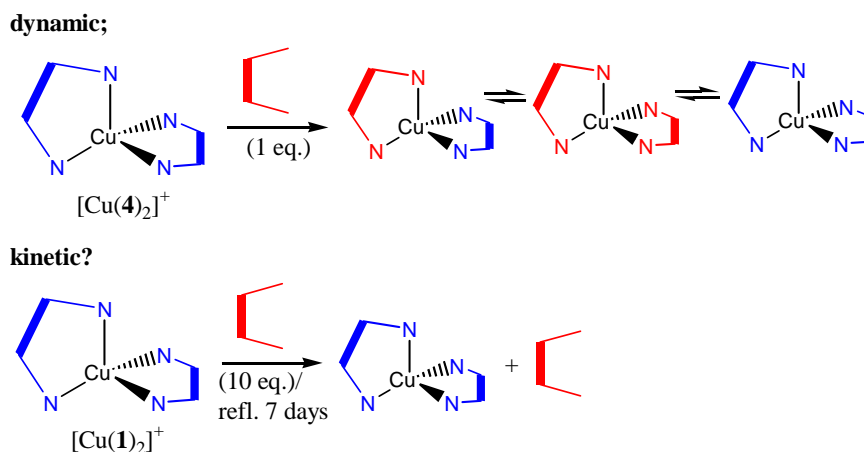


Figure 5: ESI MS of $[\text{Cu}(\mathbf{1})_2]^+$ and its isotopic distribution (dark: experimental, red: calculated).

The nature of the bonding present in $[\text{Cu}(\mathbf{1})_2]^+$ and $[\text{Cu}(\mathbf{4})_2]^+$ was probed by mixing with parent 1,10-phenanthroline (**phen**, 1:0.5-10 equiv., respectively). In complex $[\text{Cu}(\mathbf{4})_2]^+$, similar to other homoleptic complexes,⁹ ligand exchange could be noticed instantaneously (by ^1H NMR and ESI MS) by the addition of [1,10]phenanthroline (0.5-1.0 equiv), giving additional signals corresponding to heteroleptic $[\text{Cu}(\mathbf{4})_2(\text{phen})]^+$ and homoleptic $[\text{Cu}(\text{phen})_2]^+$ complexes. Interestingly, as detected by ESI MS,¹⁰ $[\text{Cu}(\mathbf{4})(\text{phen})_2]^+$ found to be the major species indicating the role of cooperativity.

However, in $[\text{Cu}(\mathbf{1})_2]^+$, as shown by ESI MS and ^1H NMR no heteroleptic aggregate can be detected at rt (over a period of 15 d/rt). This situation has not changed even after refluxing the reaction mixture for one week in methylene chloride or acetonitrile, indicating the kinetic inertness of the $[\text{Cu}(\mathbf{1})_2]^+$ (Scheme 3).



Scheme 3. Ligand exchange experiment.

As shown in Figure 5, ^1H NMR spectrum of a mixture of **phen** (0.5 equiv) and $[\text{Cu}(\mathbf{1})_2]^+$ (1 equiv) showed only signals corresponding to free **phen** and $[\text{Cu}(\mathbf{1})_2]^+$. No heteroleptic complex $[\text{Cu}(\mathbf{1})(\mathbf{phen})]$ could be detected, as seen by the absence of signal at δ 7.27 ppm (Fig. 6, indicated with the downward arrow). Even the presence of an excess of **phen** (10 equiv.) no additional signals could be detected, except for those of the excess of **phen**. This composition remained same after 15 d at rt and even refluxing the solution for one week has not produced any signals corresponding to heteroleptic complex. ESI MS results are in agreement with the NMR observations, no signals can be detected for heteroleptic complex.

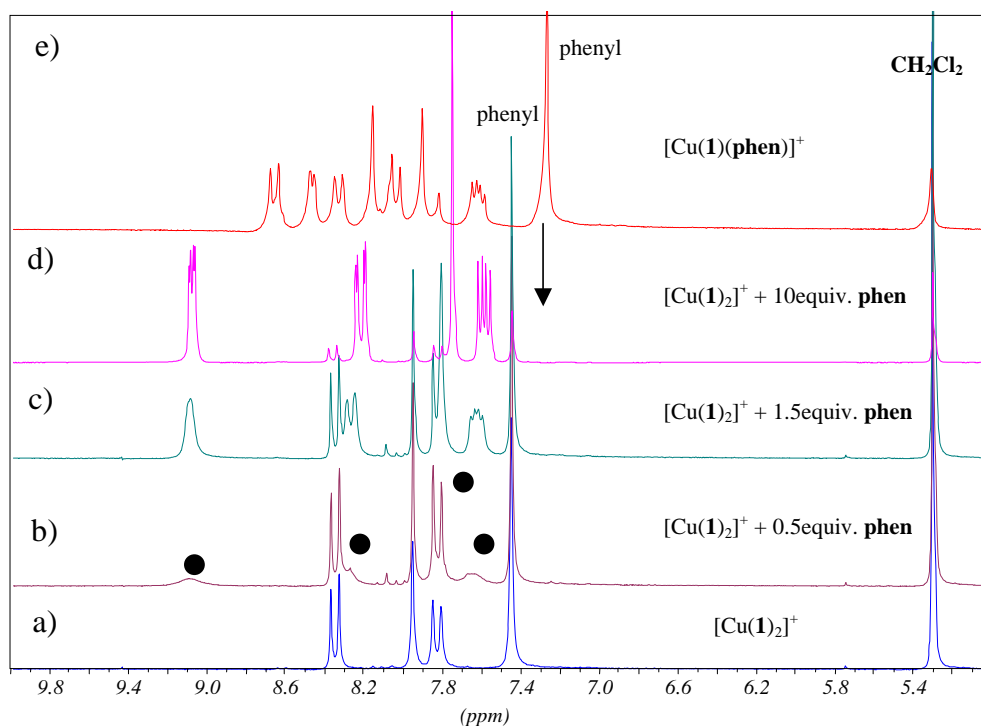


Figure 6. ^1H NMR of ligand exchange experiment; solvent: dichloromethane; temp: 298 K; selected aromatic region of, a) $[\text{Cu}(\mathbf{1})_2]^+$, b) $[\text{Cu}(\mathbf{1})_2]^+$ and 0.5 equiv. of **phen**, c) $[\text{Cu}(\mathbf{1})_2]^+$ and 1.5 equiv. of **phen**, d) $[\text{Cu}(\mathbf{1})_2]^+$ and 10 equiv. of **phen**, e) $[\text{Cu}(\mathbf{1})_2(\mathbf{phen})]^+$. Filled circles indicating the signals for free **phen**.

However, as shown in table 1, different results are obtained when a sequential addition experiments were performed. In experiment-4, as shown by ESI MS and ^1H NMR both homo and heteroleptic aggregates are observed. The homoleptic complex presence increased with increasing the temperature over a period of seven days. In experiment-2 and -3, only heteroleptic complex is observed (the reaction mixture is monitored over a period of 7 d/rt). These experiments indicate that once the $[\text{Cu}(\mathbf{1})_2]^+$ complex is formed it is kinetically locked due to the large steric stoppers added at 2,9-positions of the phenanthroline. To the best of our knowledge it is the first bisphenanthroline copper complex which do not exchange with 2,9-unsubstituted external ligands indicating kinetic inertness of this unique complex.

Experiment number	Sequential addition	Observed species
1	$[\text{Cu}(\mathbf{1})_2]^+ + \mathbf{phen}$ (0.5-10 equiv)	$[\text{Cu}(\mathbf{1})_2]^+$ and \mathbf{phen}
2	$[\text{Cu}(\mathbf{Phen})_2]^+ + \mathbf{1}$ (0.25–1.0 equiv.)	$[\text{Cu}(\mathbf{1})(\mathbf{phen})]^+$
3	$\mathbf{1} + \mathbf{phen} + \text{Cu(I)}$	$[\text{Cu}(\mathbf{1})(\mathbf{phen})]^+$
4	$[\text{Cu}(\mathbf{Phen})]^+ + \mathbf{1}$ (0.25-1 equiv.)	$[\text{Cu}(\mathbf{1})(\mathbf{phen})]^+$ and $[\text{Cu}(\mathbf{1})_2]^+$ $[\text{Cu}(\mathbf{1})_2]^+$ intensity got increased with the time (10 to 60% over a period of 18h, as seen by ESI MS)

Table 1.

Further information about the structure was obtained by an energy minimised structure by force field calculations.¹¹ The interlocked nature of this complex is well evident from the minimised structure. As shown in Figure 7, large steric stoppers (*tert*-butyl groups) lock the complex $[\text{Cu}(\mathbf{1})_2]^+$ in participating any association/dissociation processes with other 2,9-unsubstituted phenanthrolines.

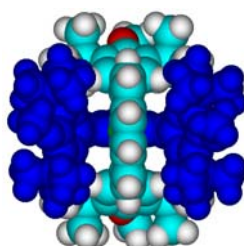


Figure 7. Space filling model of $[\text{Cu}(\mathbf{1})_2]^+$ optimised with MM⁺ force field simulations.

Absorption and Emission Properties of $[\text{Cu}(\mathbf{1})_2]^+$:

The photophysical properties of $[\text{Cu}(\mathbf{1})_2]^+$ were explored in collaboration with Prof. Armaroli. Absorption (DCM at 298 K) and emission spectra (DCM 298 K, 77K, polystyrene matrix and solid state) were recorded for $\mathbf{1}$ and $[\text{Cu}(\mathbf{1})_2]^+$ complex. Lifetime decays and emission quantum yield were also obtained. (See Table 2).

As shown in Figure 8, $\mathbf{1}$ emits at 550 nm when excited at 316 nm (in dichloromethane at 298 K) and two emission bands are detected for $[\text{Cu}(\mathbf{1})_2]^+$ when excited at 550 nm (MLCT band).

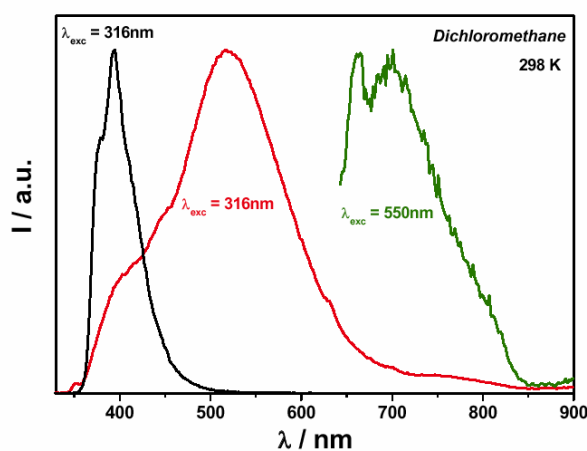


Figure 8. Emission spectra of $\mathbf{1}$ (dark), $\mathbf{1}$ protonated form (red) and $[\text{Cu}(\mathbf{1})_2]^+$ (olive).

For $[\text{Cu}(\mathbf{1})_2]^+$, at 298 K in dichloromethane solution, an “anomalous” *green* (max at ca. 550 nm) emission band was detected. In order to understand its origin, a titration of the free ligand ($\mathbf{1}$) with CF_3COOH (Fig. 9) was performed. The change of the absorption spectrum and the strong increase of the *green* emission band confirmed the hypothesis that the protonated phenanthroline was most likely responsible for the observed emission. A very low concentration of H^+ (as typically found in DCM) is able to originate the “undesired” signal.

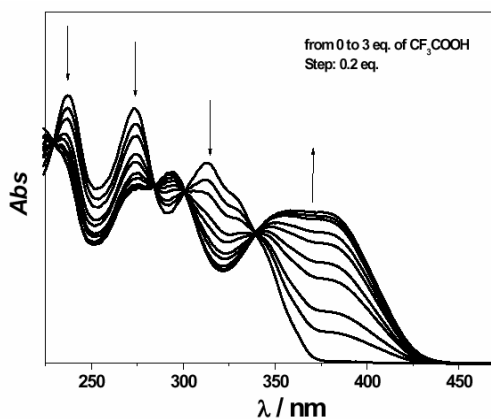


Figure 9.

Interestingly, unlike to any reported bisphenanthroline copper complex, the emission intensity is not effected by the presence of a Lewis base such as acetone (at 298K), suggesting an efficient shielding of the phenanthroline units from quencher molecules. Comparison between emission spectra of $[\text{Cu}(\mathbf{1})_2]^+$ obtained in four solvents of different polarity and nucleophilic character (DCM, DMF, MeOH, and THF, see Fig. 10) showed a relatively low decrease of the emission intensity. This behaviour is rather uncommon for copper complexes, whose MLCT band is normally switched off in nucleophilic solvents. Thus, the present coordination environment is extraordinarily efficient for shielding the metal center from external contacts. Notably, the MLCT emission yield and lifetimes are also insensitive to the presence of oxygen; this is also unprecedented for Cu(I)-phenanthrolines. However, very low excited state life times (87 ns, in dichloromethane at 298 K) detected for this unique complex.

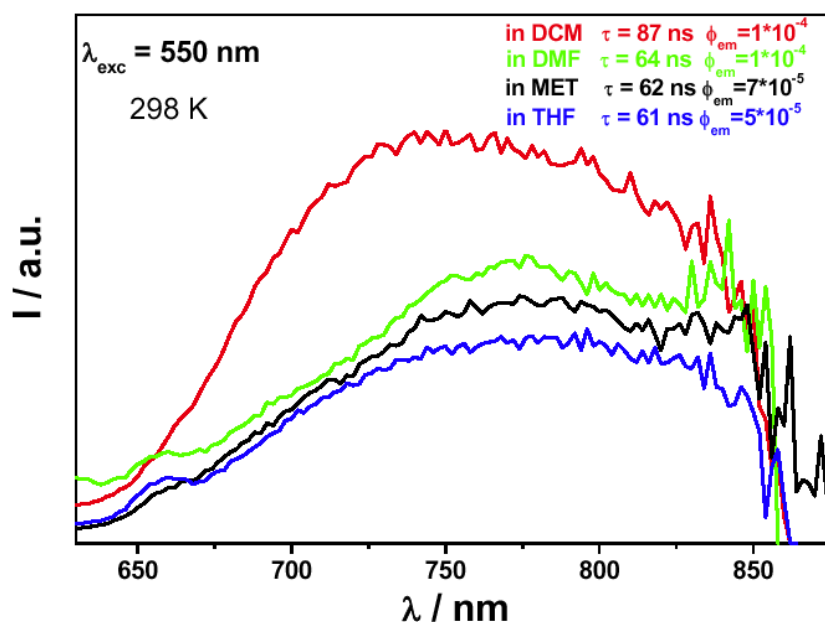
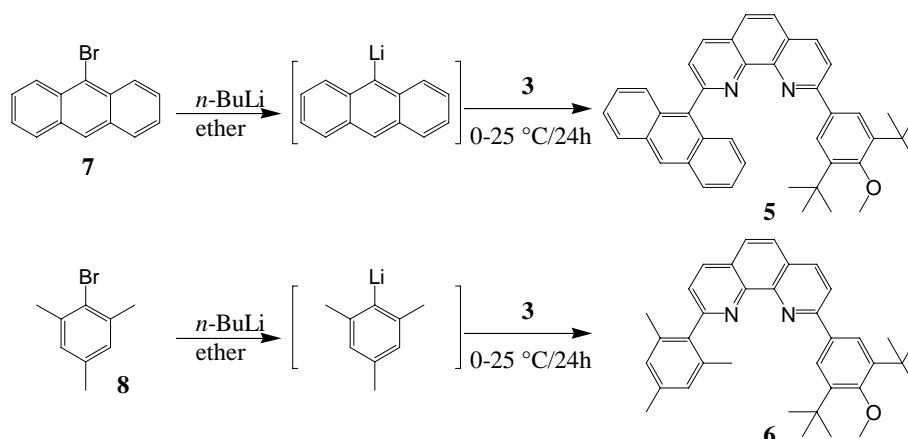


Figure 10.

In conclusion, although the Cu(I) is highest protected in $[\text{Cu}(\mathbf{1})_2]^+$ it emits intrinsically weak (even in solid state), indicating the role of other parameters which govern the excited state life times.

In order to probe the role of sterics and electronic effects originating from 2,9-steric stoppers further, ligands **5** and **6**, sharing the steric stoppers discussed in 3C-SC-1 and 3C-SC-2 were designed. Ligands **5** and **6** were prepared along the strategy outlined for **1**, starting from **3** (Scheme 4). Upon the addition of copper(I) salt to methylene chloride solution of **5** or **6** (0.5: 1 eq. respectively, at rt) resulting dark red solution, immediately, characteristic of bisphenanthroline copper complex formation.¹² NMR, ESI MS and elemental analysis is in accordance with the proposed composition (see experimental section). The photophysical

studies of these two ligands (**5** and **6**) and their copper(I) complexes is under progress (in collaboration with Prof. Armaroli).



Scheme 4. Synthesis of ligands **5** and **6**.

Although, the formation of $[\text{Cu}(\mathbf{5})_2]^+$ and $[\text{Cu}(\mathbf{6})_2]^+$ was immediate, their minimised structures indicate, similar to $[\text{Cu}(\mathbf{1})_2]^+$, high shielding around copper(I) center (Fig. 11). Indeed, when an ligand exchange experiment was performed as with $[\text{Cu}(\mathbf{1})_2]^+$, no ligand exchange could be detected (2 d/rt). Therefore, photophysical studies of these two ligands (**5** and **6**) and their complexes is also of interest to further elucidate the interplay of steric and electronic factors on the emission properties of copper(I) complexes (work is under progress, in collaboration with Prof. Armaroli).

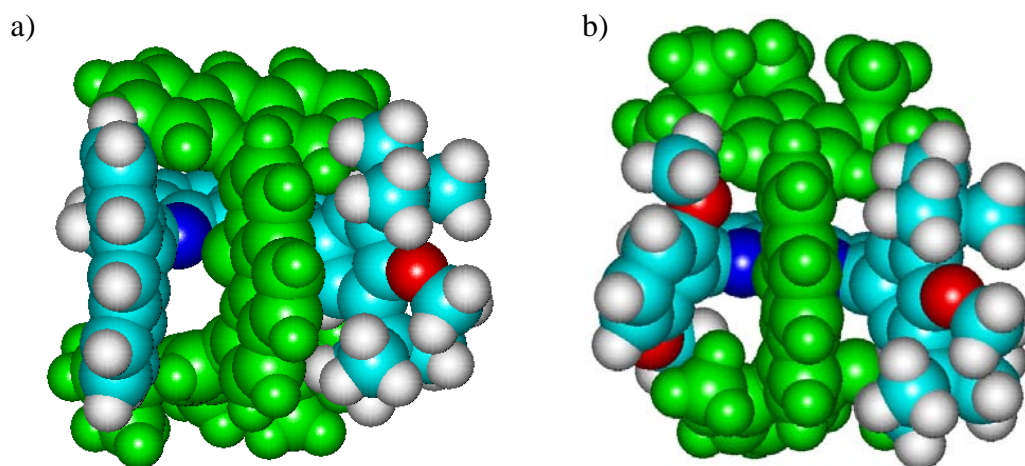
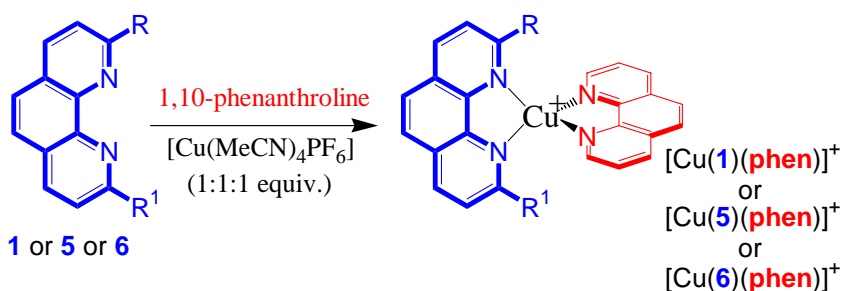


Figure 11. Space filling model of a) $[\text{Cu}(\mathbf{5})_2]^+$ and b) $[\text{Cu}(\mathbf{6})_2]^+$, optimised with MM^+ force field simulations.

Heteroleptic complexes:

The ability of **1**, **5** and **6** as potential HETPHEN building blocks was investigated by reacting them with parent 1,10-phenanthroline and $[\text{Cu}(\text{MeCN})_4\text{PF}_6]$ (1:1:1 equiv.

respectively) in methylene chloride. As shown by ^1H NMR and ESI MS heteroleptic complexes were formed, exclusively (Scheme 5). Therefore, similar to other HETPHEN building blocks these building blocks (**1**, **5** and **6**) can also be explored to generate multicomponent supramolecular aggregates. In particular, building block **1** is very interesting because of the kinetic inertness observed for its copper complex $[\text{Cu}(\mathbf{1})_2]^+$, indicating its potential to envisage kinetically stable supramolecular structures.



Scheme 5.

In conclusion, A first kinetically inert copper bisphenanthroline complex $[\text{Cu}(\mathbf{1})_2]^+$ was prepared. The emission properties of $[\text{Cu}(\mathbf{1})_2]^+$ were not effected by the medium, indicating the amount of shielding around copper(I) center. Further studies are in progress to design photoactive copper complexes with high excited state life times.

Experimental:

Starting materials, [1,10]phenanthroline (**phen**), **7**, **8** and *n*-BuLi were purchased from Aldrich or Merck, and used as received. **2** was prepared by known procedures. ^1H NMR and ^{13}C NMR were measured on a Bruker AC 400 (400 MHz) unless specified otherwise. ESI MS spectra were measured on a LCQ Deca Thermo Quest instrument. Typically, each time 25 scans were accumulated for one spectrum. All the complexes were characterized by ^1H -, ^{13}C -, ESI MS, IR and elemental analysis.

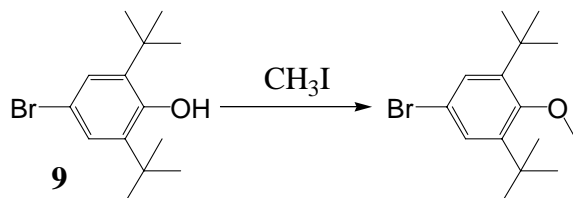
General procedure for the aryl additions at 2 and 9-positions of the [1,10]phenanthroline:

In a typical procedure, a 2.5 M solution of *n*-butyllithium in hexane (2.1 eq.) was slowly added to a solution of bromoarene (2 eq.) in diethyl ether at 0 °C. The solution was allowed to stir for 4h at rt and a suspension of **2** or **3** (1 eq.) in diethylether was added to it. The solution immediately turned dark violet. The mixture was stirred for 24 h at room temperature. Prolonged reaction times lead to the formation of unwanted products. These additions are very sensitive to moisture. Best yields are obtained by monitoring the reaction using ESI MS. After the reaction is completed aq.NH₄Cl was added and the layers were

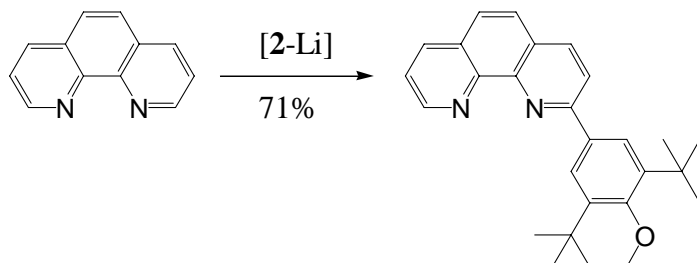
separated. The aqueous layer was extracted 3-4 times with dichloromethane. The combined organic extracts were stirred with activated MnO_2 (20 eq.) for 12 h. The mixture was then filtered over celite, dried with MgSO_4 and evaporated. The resulting solid was separated by column chromatography (SiO_2 , initially passed by hexane and later by dichloromethane). The products were eluted as white to pale yellow solids.

General Procedure for the copper complex formation:

Homoleptic complexes were prepared by reacting **1** or **5** or **6** with $[\text{Cu}(\text{MeCN})_4]\text{PF}_6$ (1:0.5 equiv. respectively) in dichloromethane. The resulting dark red solutions were analysed without any further purification by ESI MS, ^1H NMR, ^{13}C NMR, and elemental analysis.

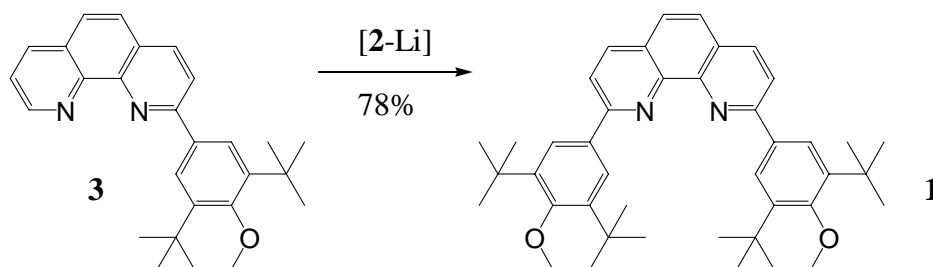


5-bromo-1,3-di-*tert*-butyl-2-methoxy-benzene (**2**): To a acetone solution (1000 ml) of 4-bromo-2,6-di-*tert*-butylphenol (**9**, 25 g, 87 mmol) and methyl iodide (124 g, 870 mmol), K_2CO_3 (138 g) was added and the resulting mixture was refluxed for 24h. The solvent was removed and the reaction is quenched with H_2O (500 ml), and extracted with dichloromethane (500 ml). The organic phase was separated and dried over magnesium sulfate. After concentration of the filtrate the crude product was purified by column chromatography with *n*-hexane to give methylated product **3** as a colourless liquid (38 %). ^1H NMR (CDCl_3 , 200 MHz): δ 7.35 (s, 2H, arom), 3.69 (s, 3H, methoxy), 1.43 (s, 18H, *t*-Bu); ^{13}C NMR (CD_2Cl_2 , 100 MHz): δ 159.1, 147.2, 130.1, 126.9 (arom), 64.0 (methoxy), 37.5, 33.3 (aliph.).

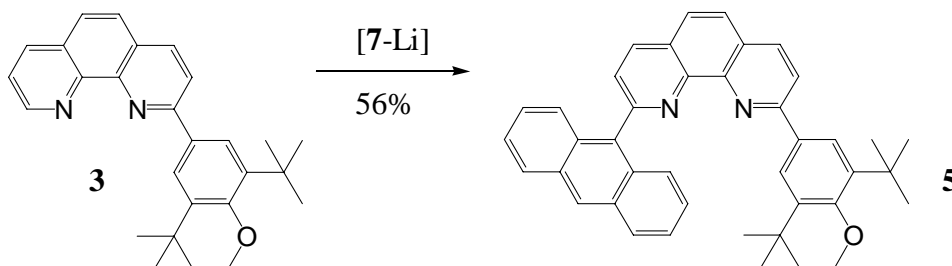


2-(3,5-Di-*tert*-butyl-4-methoxy-phenyl)-[1-10]phenanthroline (**4**): 71%; M.p. 156 °C; ^1H NMR (CDCl_3 , 400 MHz): δ 9.24 (dd, $J = 4.3, 1.8$ Hz, 1H, phen), 8.33 (d, $J = 8.3$ Hz, 1H, phen), 8.29 (dd, $J = 8.1, 1.8$ Hz, 1H, phen), 8.21 (s, 2H, phenyl), 8.11 (d, $J = 8.3$ Hz, 1H, phen), 7.84 (d, $J = 8.6$ Hz, 1H, phen), 7.79 (d, $J = 8.6$ Hz, 1H, phen), 7.67 (dd, $J = 8.1, 4.3$ Hz,

1H, phen), 3.82 (s, 3H, methoxy), 1.61 (s, 18H, aliph.); ^{13}C NMR (CDCl_3 , 100 MHz): δ 162.0, 159.9, 151.2, 151.1, 147.0, 144.9, 137.6, 136.9, 135.7, 129.9, 128.1, 127.6, 127.3, 126.9, 123.8, 122.2 (arom), 65.5 (methoxy), 36.9, 33.1 (alkyl); IR (KBr): ν 3395, 2959, 1618, 1589, 1547, 1508, 1489, 1445, 1409, 1362, 1226, 1117, 1009, 779, 746, 717, 627; ESI MS: m/z (%): 399.4 (100) $[\text{M}+\text{H}]^+$; Anal. Calcd. for $\text{C}_{27}\text{H}_{30}\text{N}_2\text{O}$: C, 81.37; H, 7.59; N, 7.03. Found: C, 81.08; H, 7.86; N, 6.82.

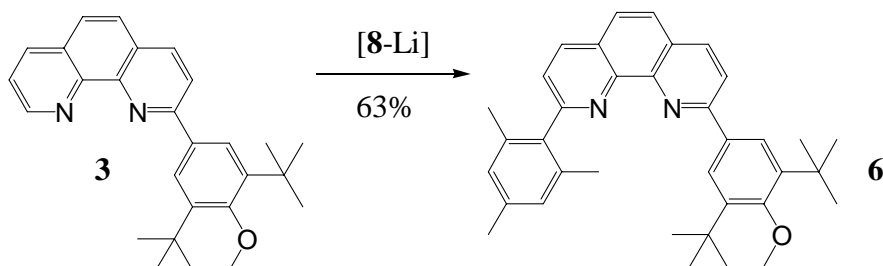


2,9-Bis-(3,5-di-*tert*-butyl-4-methoxyphenyl)-[1,10]phenanthroline (**1**): 78%; M.p. > 230 °C; ^1H NMR (CD_2Cl_2 , 400 MHz): δ 8.31 (d, 2H, $J = 8.3$ Hz, phen), 8.12 (s, 4H, phenyl), 8.04 (d, 2H, $J = 8.3$ Hz, phen), 7.81 (s, 2H, phen), 3.77 (s, 6H, methoxy), 1.55 (s, 36, *t*-Bu); ^{13}C NMR (CD_2Cl_2 , 50 MHz): δ 161.0, 158.1, 146.3, 144.0, 136.7, 134.8, 127.7, 126.3, 125.9, 120.9 (arom.), 64.4 (methoxy), 35.9, 32.0 (aliph.); IR (KBr): ν 3387, 2960, 2867, 1623, 1607, 1590, 1498, 1466, 1408, 1392, 1359, 1313, 1259, 1225, 1115, 1006, 889, 854, 804, 738, 648; ESI MS: m/z (%): 1296.1 $[\text{M}+\text{H}]^+$; Anal. Calcd. for $\text{C}_{42}\text{H}_{52}\text{N}_2\text{O}_2$: C, 81.78; H, 8.50; N, 4.54. Found: C, 81.71; H, 8.89; N, 4.42.

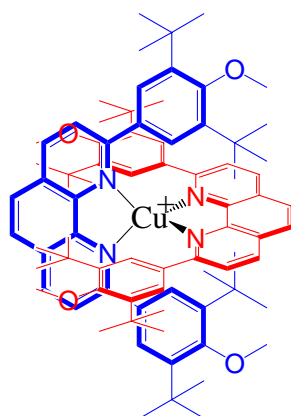


2-Anthracen-9-yl-9-(3,5-di-*tert*-butyl-4-methoxyphenyl)-[1,10]phenanthroline (**5**): M.p. 166 °C; ^1H NMR (CD_2Cl_2 , 400 MHz): δ 8.54 (s, 1H, phen), 8.39 (d, $J = 8.1$ Hz, 1H, phen), 8.26 (d, $J = 8.3$ Hz, 1H, phen), 8.03 (d, $J = 8.6$ Hz, 2H, phen), 7.96 (d, $J = 8.4$ Hz, 1H, phen), 7.91 (s, 2H, phenyl), 7.80-7.85 (m, 5H, anthracene), 7.39-7.42 (m, 2H, anthracene), 7.26-7.31 (m, 2H, anthracene), 3.54 (s, 3H, methoxy), 1.24 (s, 18H, *t*-Bu); ^{13}C NMR (CD_2Cl_2 , 50 MHz) : 161.0, 157.8, 146.5, 146.2, 143.8, 136.5, 135.9, 135.7, 134.1, 131.5, 130.3, 128.4, 127.8 (2C), 127.7, 127.4, 126.7, 126.6, 126.3, 126.1, 125.8, 125.7, 125.1, 120.4 (arom.), 64.3 (methoxy), 35.7, 31.7 (aliph.); IR (KBr): ν 3425, 3048, 2955, 2867, 1618, 1603, 1584, 1493, 1444, 1406,

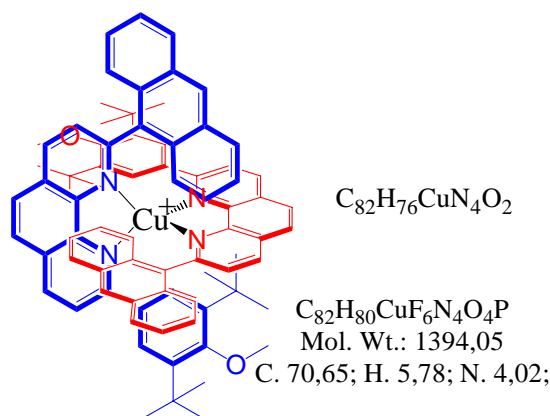
1337, 1313, 1224, 1195, 115, 1009, 886, 862, 846, 788, 732, 639, 618; ESI MS: m/z (%): 575.1 (100) $[M+H]^+$; Anal. Calcd. for $C_{41}H_{38}N_2O$: C, 85.68; H, 6.66; N, 4.87. Found: C, 85.27; H, 6.64; N, 4.67.



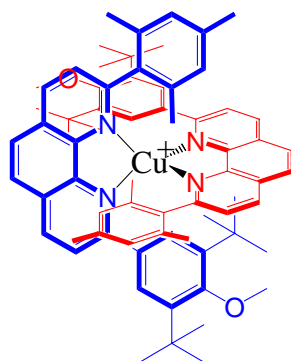
2-(3,5-Di-*tert*-butyl-4-methoxyphenyl)-9-(2,4,6-trimethylphenyl)-[1,10]phenanthroline (**6**): 63%; M.p. 182 °C; 1H NMR ($CDCl_3$, 400 MHz): δ 8.30 (d, $J = 8.0$ Hz, 1H, phen), 8.28 (d, $J = 8.0$ Hz, 1H, phen), 8.15 (s, 2H, phenyl), 8.04 (d, $J = 8.4$ Hz, 1H, phen), 7.83 (m, 2H, phen), 7.63 (d, $J = 8.0$ Hz, 1H, phen), 7.01 (s, 2H, phenyl), 3.75 (s, 3H, methoxy), 2.39 (s, 3H, benzyl), 2.32 (s, 6H, benzyl), 1.54 (s, 18H, *t*-Bu); ^{13}C NMR (CD_2Cl_2 , 50 MHz): δ 161.5, 160.0, 158.5, 146.7, 146.3, 144.3, 138.3, 137.8, 136.9, 136.8, 135.8, 134.9, 129.0, 127.6, 127.4, 126.9, 126.4, 126.1, 125.6, 120.8, 64.9, 36.4, 32.5, 21.6, 21.4; IR (KBr): ν 3417, 2960, 2916, 2867, 1620, 1587, 1540, 1495, 1479, 1410, 1394, 1356, 1313, 1223, 1115, 1099, 1007, 887, 859, 751, 729, 631, 583; ESI MS: m/z (%): 517.5 (100) $[M+H]^+$; Anal. Calcd. for $C_{36}H_{40}N_2O$: C, 83.68; H, 7.80; N, 5.42. Found: C, 83.22; H, 8.24; N, 5.15.



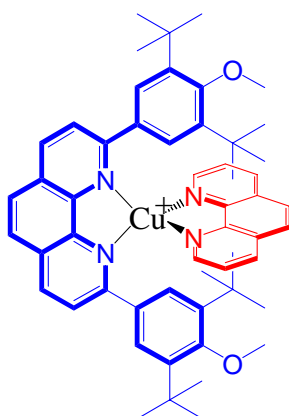
$[Cu(1)_2]^+$: 1H NMR (CD_2Cl_2 , 400 MHz): δ 8.38 (d, $J = 8.5$ Hz, 4H, phen), 7.98 (s, 4H, phen), 7.85 (d, $J = 8.5$ Hz, 4H, phen), 7.48 (s, 8H, phenyl), 3.20 (s, 12H, methoxy), 0.90 (s, 72H, *t*-Bu); ^{13}C NMR (CD_2Cl_2 , 100 MHz): 161.9, 157.6, 144.1, 144.0, 136.7, 133.6, 128.8, 126.9, 126.3, 126.1 (arom.), 63.6 (methoxy), 35.3, 31.7 (aliph.); IR (KBr): ν 3393, 2961, 1582, 1504, 1451, 1409, 1391, 1349, 1314, 1113, 1004, 862, 841, 753, 557, 526; ESI MS: m/z (%): 1296.1 (100) $(M-PF_6)^+$; Anal. Calcd. for $CuC_{84}H_{104}Br_2N_4O_4 \cdot PF_6$: C, 69.95; H, 7.27; N, 3.88. Found: C, 69.76; H, 7.58; N, 3.69.



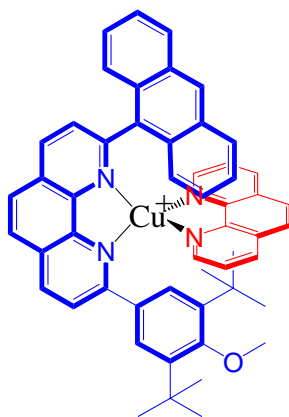
$[Cu(5)_2]^+$: 1H NMR (CD_2Cl_2 , 400 MHz): δ 8.29 (d, $J = 8.5$ Hz, 2H, phen), 8.18 (d, $J = 8.6$ Hz, 2H, phen), 7.98 (s, 2H, anthracene), 7.85 (d, $J = 8.8$ Hz, 2H, phen), 7.69-7.73 (m, 6H, anthracene), 7.60 (d, $J = 8.1$ Hz, 2H, phen), 7.48 (s, 4H, phenyl), 7.34 (d, $J = 8.6$ Hz, 2H, phen), 7.22-7.28 (m, 4H, anthracene), 6.98-7.02 (m, 4H, anthracene), 6.89 (d, $J = 8.6$ Hz, 2H, phen), 6.53-6.58 (m, 2H, anthracene), 3.29 (s, 6H, methoxy), 0.78 (s, 36H, *t*-Bu); ^{13}C NMR (CD_2Cl_2 , 100 MHz) : 161.3, 157.2, 156.4, 144.6, 143.2, 142.6 (2C), 137.8, 137.0, 132.1, 131.4, 129.7, 129.2, 128.9, 128.1, 128.0, 127.8, 127.1, 126.8, 126.1, 125.9, 125.6, 125.1, 124.3 (arom.), 64.7 (methoxy), 35.4, 31.5 (*t*-Bu); IR (KBr): ν 3392, 2952, 1624, 1583, 1544, 1504, 1446, 1409, 1359, 1342, 1316, 1222, 1113, 1009, 841, 790, 736, 625, 557; ESI MS: m/z (%): 1210.3 (100) $[M-PF_6]^+$; Anal. Calcd. for $CuC_{82}H_{80}N_4O_4 \cdot PF_6 \cdot 2H_2O$: C, 70.65; H, 5.78; N, 4.02. Found: C, 70.52; H, 5.65; N, 3.94.



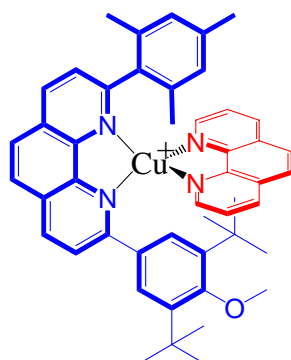
$[Cu(6)_2]^+$: 1H NMR (CD_2Cl_2 , 200 MHz): δ 8.54 (d, $J = 8.3$ Hz, 2H, phen), 8.50 (d, $J = 8.3$ Hz, 2H, phen), 8.15 (d, $J = 8.3$ Hz, 2H, phen), 8.05-8.12 (m, 6H, phen), 7.47 (s, 2H, phenyl), 7.44 (s, 2H, phenyl), 6.29 (s, 2H, MesH), 5.74 (s, 2H, MesH), 3.41 (s, 6H, methoxy), 2.12 (s, 6H, benzyl), 2.09 (s, 12, benzyl), 0.99 (s, 36H, *t*-Bu); ESI MS: m/z (%): 1095.7(100) $[M-PF_6]^+$; Anal. Calcd. for $CuC_{72}H_{80}N_4O_2 \cdot PF_6 \cdot 2H_2O$: C, 67.67; H, 6.63; N, 4.38. Found: C, 67.62; H, 6.49; N, 4.33.



[Cu(**1**)(phen)]⁺: ¹H NMR (CD₂Cl₂, 200 MHz): δ 8.66 (d, *J* = 8.1 Hz, 2H, phen), 8.47 (d, *J* = 4.3 Hz, 2H, **phen**), 8.34 (d, *J* = 8.1 Hz, 2H, phen), 8.16 (s, 2H, phen), 8.04 (d, *J* = 8.4 Hz, 2H, **phen**), 7.91 (s, 2H, **phen**), 7.63 (dd, *J* = 8.1, 4.3 Hz, 2H, **phen**), 7.27 (s, 4H, phenyl), 2.98 (s, 6H, methoxy), 0.82 (s, 32H, *t*-Bu); ¹³C NMR (CD₂Cl₂, 50 MHz): δ 160.2, 158.9, 148.1, 143.9, 143.5, 142.9, 137.0, 136.1, 134.8, 129.4, 128.0, 126.4, 126.3, 126.1, 125.9, 125.1 (arom.), 64.1 (methoxy), 35.1, 31.0 (aliph.); IR (KBr): ν 3404, 2922, 1586, 1508, 1459, 1408, 1356, 1224, 1115, 1006, 838, 726, 557; ESI MS: *m/z* (%): 859.5 (100) [M-PF₆]⁺; Anal. Calcd. for [CuC₅₄H₆₀O₂.PF₆]: C, 64.50; H, 6.01; N, 5.57. Found: C, 64.44; H, 6.77; N, 4.93.



[Cu(**5**)(phen)]⁺: ¹H NMR (CD₂Cl₂, 200 MHz): δ 8.78 (q, *J* = 8.1 Hz, 2H, phen), 8.28 (s, 2H, phen), 8.15 (d, *J* = 8.1 Hz, 1H, phen), 8.04 (t, *J* = 8.3 Hz, 3H, phen), 7.86 (s, 2H, anthracene), 7.73 (s, 2H, anthracene), 7.52 (s, 2H, phenyl), 7.36 (s, 4H, phen), 7.20 (d, *J* = 7.6 Hz, 2H, phen), 6.98-7.04 (m, 5H, anthracene), 2.64 (s, 3H, methoxy), 0.71 (s, 18H, *t*-Bu); ¹³C NMR (CD₂Cl₂, 100 MHz) : 160.8, 159.7, 159.6 (2C), 147.3, 144.7, 144.0, 143.9, 143.6, 142.2, 137.5, 135.7, 135.5, 133.6, 133.3, 130.1, 129.4, 128.9, 128.7, 128.5, 128.1, 127.9, 126.8, 126.6, 126.4, 126.3 (2C), 124.8, 120.7, 117.0 (arom.), 64.2 (methoxy), 35.3, 31.2 (aliph.); IR (KBr): ν 3417, 2961, 2909, 1654, 1619, 1508, 1424, 1409, 1224, 1009, 839, 737, 725, 625, 558; ESI MS: *m/z* (%): 817.5 (100) [M-PF₆]⁺.



[Cu(**6**)(phen)]⁺: ¹H NMR (CD₂Cl₂, 200 MHz): δ 8.64 (d, *J* = 8.4 Hz, 2H, phen), 8.46 (m, 3H), 8.17 (m, 4H), 7.92 (s, 2H, phen), 7.70 (m, 3H), 7.45 (s, 2H, phenyl), 5.71 (s, 2H, MesH), 2.80 (s, 3H, methoxy), 1.65 (s, 3H, benzyl), 1.57 (s, 6H, benzyl), 0.83 (s, 18H, *t*-Bu); ¹³C NMR (CD₂Cl₂, 50 MHz): δ 160.6, 159.5, 158.5, 149.1, 147.9, 146.9, 144.1, 143.7, 143.4, 143.1, 140.8, 139.0, 137.3, 136.5, 136.1, 135.4, 134.4, 133.9, 129.0, 128.0, 126.8, 126.5, 125.8, 124.9, 117.6, 116.7 (arom.), 63.4 (methoxy), 35.1, 31.0 (3C) (aliph.); IR (KBr): ν 3423, 2965, 1618, 1583, 1509, 1459, 1411, 1223, 1111, 1003, 840, 729, 557, 541; ESI MS: *m/z* (%): 759.4 (100) [M-PF₆]⁺.

- (1) M. Schmittel, V. Kalsani, *Topics in Current Chemistry*, **2004**, 245, 1-54.
- (2) a) P. F. H. Schwab, M. D. Levin, J. Michl, *Chem. Rev.* **1999**, 99, 1863-1933. b) A. Harriman, R. Ziessel, *Coord. Chem. Rev.* **1998**, 171, 331-339.
- (3) M. Schmittel, V. Kalsani, L. Kienle, *Chem. Commun.* **2004**, 1534-1535.
- (4) R. Ziessel, G. Pickaert, F. Camerel, B. Donnio, D. Guillon, M. Cesario, T. Prangè, *J. Am. Chem. Soc.* **2004**, 126, 12403-12413.
- (5) N. Armaroli, *Chem. Soc. Rev.* **2001**, 30, 113-124.
- (6) M. Schmittel, C. Michel, A. Wiegrefe, V. Kalsani, *Synthesis*, **2001**, 1561 – 1567.
- (7) M. Schmittel, H. Ammon. *Eur. J. Org. Chem.* **1999**, 785-792.
- (8) a) M. Schmittel, A. Ganz, *Chem. Commun.* **1997**, 99-100; b) M. Schmittel, U. Lüning, M. Meder, A. Ganz, C. Michel, M. Herderich, *Heterocycl. Commun.* **1997**, 3, 493-498.
- (9) a) R. Colton, B. D. James, I. D. Potter, J. C. Traeger, *Inorg. Chem.* **1993**, 32, 2626–2629. b) V. Kalsani, H. Bodenstedt, D. Fenske, M. Schmittel, *Eur. J. Inorg. Chem.* **2005**, in press.
- (10) ¹H NMR signals could not be quantified due to signal overlap.
- (11) HyperchemTM 6.02 Release for Windows by Hypercube, Inc. 2000. MM+ force field.
- (12) V. Kalsani, H. Ammon, F. Jäckel, J. P. Rabe, M. Schmittel, *Chem. Eur. J.* **2004**, 10, 5481-5492.

CHAPTER 4

4. Synthesis, Structures and Surface Patterning of Oligophenanthrolines. Versatile Precursors to Heteroleptic/Heterometallic Supramolecular Rack and Grids.....	115
4.1 Introduction and Objective	115
4.2 Synthesis of Bisphenanthrolines (Supp 4-1 and Supp 4-2).....	116
4.2.1 Introduction	116
4.2.2 Covalent Approach.....	117
4.2.2 Non-Covalent Approach; Synthesis of Pt-linked Bisphenanthrolines	123
4.3 Self-Assembly of Hetero or Homometallic/Heteroleptic Racks and Grids (Supp 4-3, Supp 4-4 and Supp 4-5).....	124
4.3.1 Racks (Supp 4-3).....	124
4.3.2 Grids (Supp 4-4).....	128
4.3.3 Racks to Grid motifs (Supp 4-5)	130
4.3.4 Nature of the Grid Motifs: Kinetic or Dynamic?	130
4.4 Conclusions	131

4. Synthesis, Structures and Surface Patterning of Oligophenanthrolines. Versatile Precursors to Heteroleptic/Heterometallic Supramolecular Rack and Grids.

4.1 Introduction and Objective

As discussed earlier (chapter 1), the coordination driven approach and hydrogen bonding have enabled the fabrication of fascinating molecular structures.¹ The coordination driven approach has become famous due to the coordination of transition metal cations to polypyridine fragments incorporated into oligomeric strands leading to sparkling motifs. Several polypyridyl ligands have been tailored in this purpose, that they organise in the presence of suitable metal cations. Among the polypyridyl ligands explored, oligo-2,2'-bipyridines,² oligo-1,10-phenanthrolines and oligo-terpyridines³ are the most commonly used ligands due to the rigidity along their axis. This allows them to assemble with a predictable geometry and coordination towards various metal ions (chart 4-1).

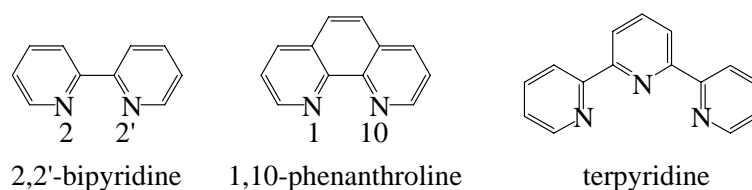


Chart 4-1.

Racks and grids are among the most celebrated structures in the field of metallo-supramolecular chemistry because of their interesting perspectives for the creation of molecular-level wires and potential hosts (Figure 4-1a, also see chapter 2). Several racks (heteroligand) and grids (homoligand) were reported on the basis of phenanthroline/bipyridine/terpyridine subunits by using self-recognition and positive cooperativity principles. Later studies by Lehn *et al.*, had revealed a remarkable example of heteroligand grid aggregation (Figure 4-1b).⁴ However, this unique motif did not formed quantitatively in solution. Later studies by Cohen⁵ and Schmittel proved that the chosen approach is not a general one and requested further control in order to drive multi-component aggregation. Due to our early success with the HETPHEN⁶ approach, it was of interest to explore its potential to prepare multi-component supramolecular motifs. In the following, several multi-component racks and grids, built using the HETPHEN principle, will be presented.

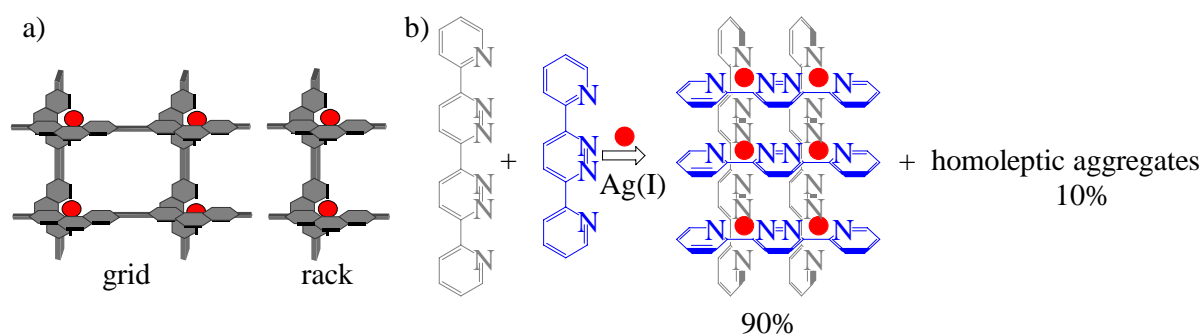


Figure 4-1. a) Cartoon representation of heteroleptic grid and rack motifs. b) A multi-component grid assembly by Lehn.

Recently, there is also a growing interest for surface chemistry of organic/inorganic materials.⁷ Organic molecules possessing chelating groups, such as pyridine, bipyridine,⁸ phenanthroline or terpyridine,⁹ are of great interest, due to their potential use in preparing metallo-supramolecular aggregates on surfaces. Since these aggregates possess metal ions at defined positions, the resulting surfaces could be loaded with highly ordered metal ions (Figure 4-2). In this respect, few of the building blocks (**9a** and **9c**) were studied at solid-liquid interfaces.

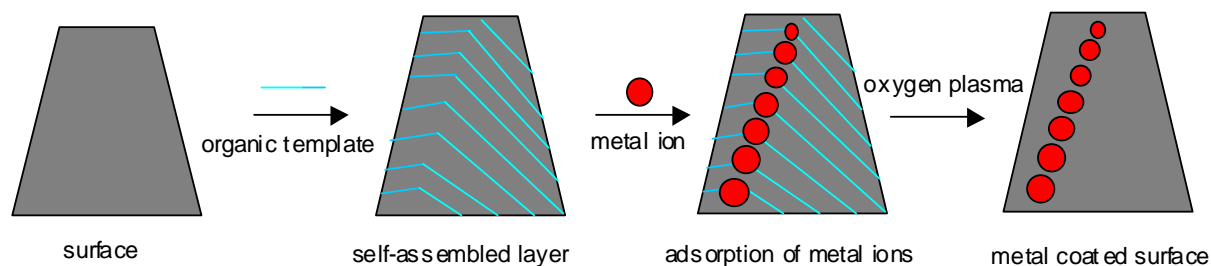


Figure 4-2. Self-assembled organic templates for highly ordered metal coated surfaces.

4.2 Synthesis of Bisphenanthrolines (Supp 4-1 and Supp 4-2)

4.2.1 Introduction

The design of a new series of bisphenanthrolines was dictated by virtue of their steric shielding (alkyl-aryl and anthracene, Figure 4-3) and their ability to give exclusively multi-component heteroleptic racks and grids (Figure 4-1). Along these lines, we prepared several photoactive bisphenanthrolines and probed their ability to form heteroleptic aggregates (Figure 4-3). The synthesis is based either on a covalent or a coordinative (with *trans*-Pt(PEt)₂Cl₂) strategy.¹⁰ Four of the bisphenanthrolines (**7b**, **7f**, **9a** and **9b**) were characterized in the solid state. Appropriate combinations of these building blocks with appropriate metal

cations (Cu(I) or Ag(I)) provided a series of unique multi-component rack and grid aggregates.¹¹ Mechanistic investigations provided crucial information about the possible intermediates formed during the self-assembly processes.

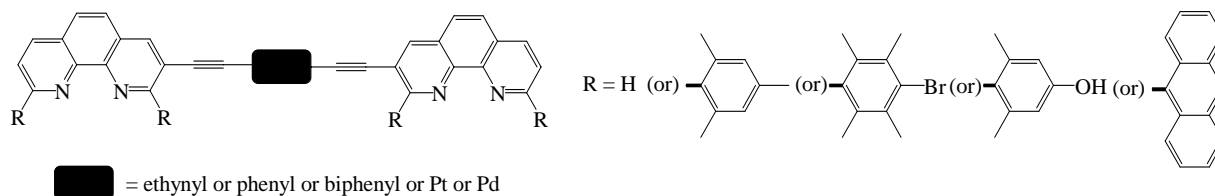


Figure 4-3. Steric stoppers loaded and unloaded bisphenanthrolines.

The idea of having phenolic and bromoduryl groups was to install functionalities that could be varied at a final stage of the synthesis. These functionalised ligands are expected to form circular structures (grid or box or cylinder motifs) when they are reacted according to the HETPHEN concept (Figure 4-4).

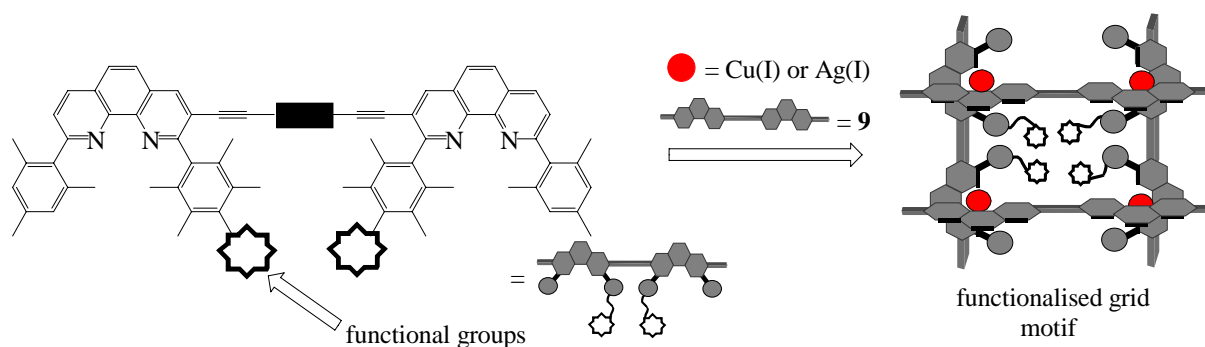
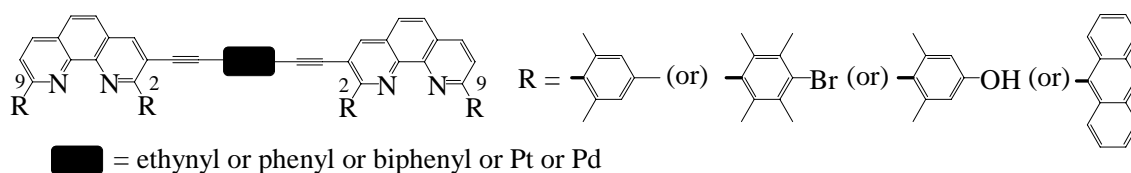


Figure 4-4. Towards functionalised nanogrids.

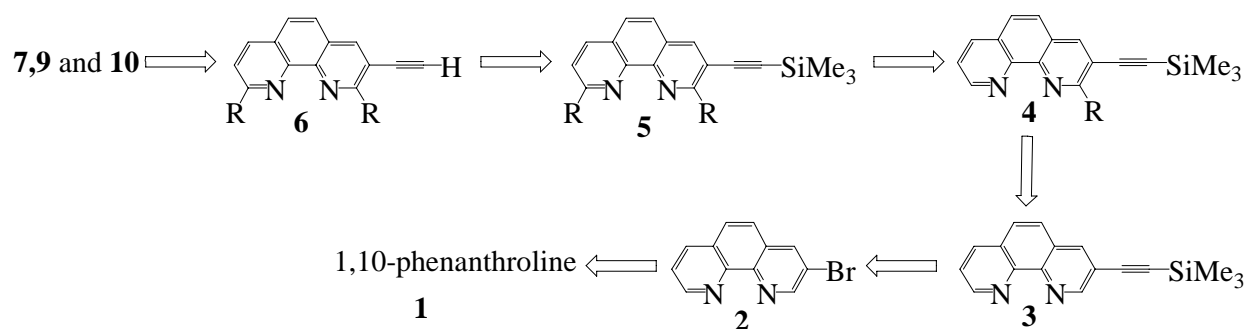
4.2.2 Covalent Approach

4.2.2.1 Synthesis of Sterically Loaded (2,9-substituted) Bisphenanthrolines



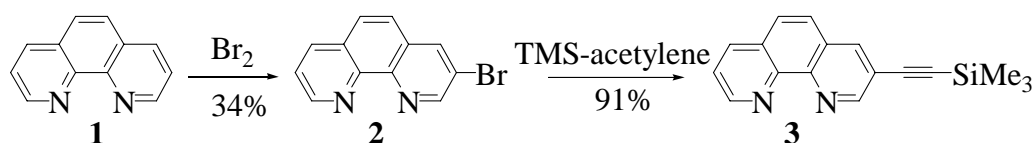
2,9-loaded bis-phenanthroline

The retrosynthetic analysis of various bisphenanthrolines is depicted in Scheme 4-1. Butadiyne, 1,4-diethynylbenzene (covalent) and Pt/Pd-centers (coordinative) were chosen as rigid linear spacers between the phenanthrolines



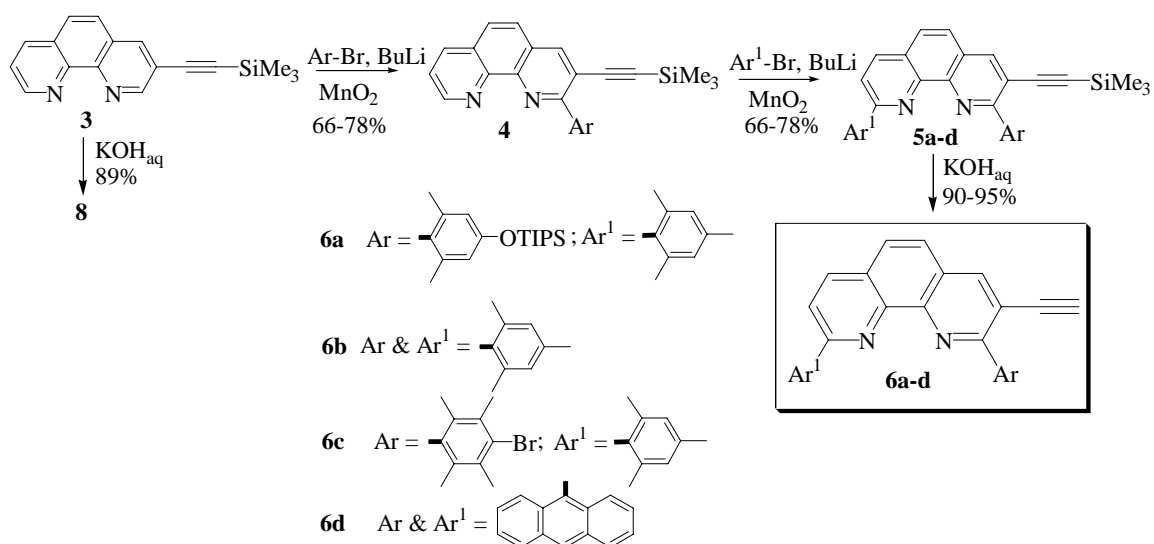
Scheme 4-1. Synthetic strategy for bisphenanthrolines **7**, **9** and **10**.

According to the strategy outlined above, 3-bromophenanthroline **2** was prepared starting from 1,10-phenanthroline **1** (Scheme 4-2).¹² The bromo group was then replaced by trimethylsilylacetylene which could be used to direct the regioselective substitution at position 2 of the 1,10-phenanthroline. Later it could be removed to prepare bisphenanthrolines **7**, **9** and **10**.



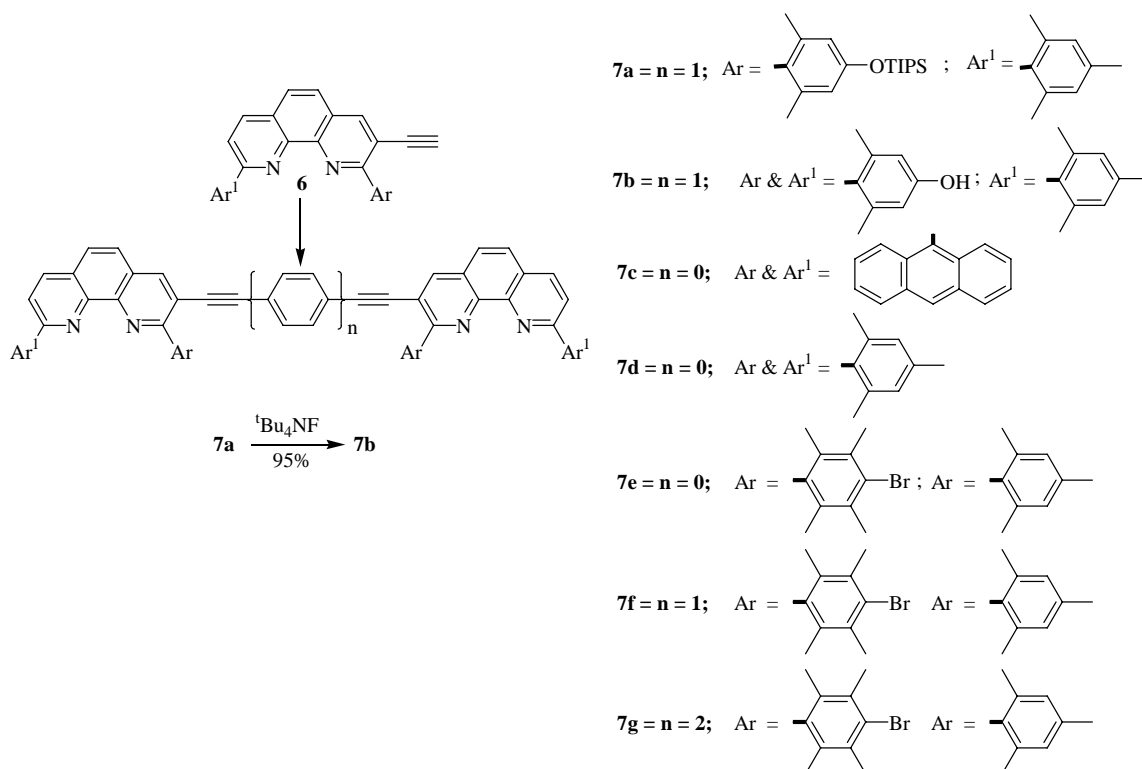
Scheme 4-2. Synthesis of 3-trimethylsilylethynyl-1,10-phenanthroline (**3**).

The predesigned steric stoppers were added in 2- and 9-position by nucleophilic substitution according to Sauvage (Scheme 4-3).¹³ The addition products were isolated and oxidized with activated manganese dioxide to afford the monosubstituted phenanthrolines **5a-d**. The deprotection of **5** with aqueous KOH provided the useful precursors **6a-d** for the bisphenanthrolines **7**, **9** and **10**. (See the attached Supp 4-1 and Supp 4-2 for detailed description of the experiments and yields; Scheme 4-4).



Scheme 4-3. Synthesis of ethynyl phenanthroline building blocks **6a-d**.

Pd/Cu-catalyzed Sonogashira coupling of **6a** or **6c** with 1,4-diiodobenzene afforded the corresponding bisphenanthrolines **7a** or **7f** (see Supp 4-1), in good yields (89 and 62%). Ligand **7g** is obtained when **6c** was reacted with 4,4'-diiodobiphenyl using Sonogashira coupling conditions. For best yields, the reaction was conveniently monitored by ESI-MS spectroscopy. Even under stringently dry conditions, homocoupled phenanthrolines were found in traces. Isolation of the pure bisphenanthrolines was readily achieved by column chromatography and subsequent recrystallisation from cyclohexane. Ligands **7c** or **7d** or **7e** were obtained under homocoupling conditions from **6d** or **6b** or **6c** (see the experimental section). **7b** was obtained by the TIPS-deprotection of **7a** using ${}^t\text{Bu}_4\text{NF}$. All of these bisphenanthrolines were characterized by ${}^1\text{H}$ -, ${}^{13}\text{C}$ -NMR, ESI MS, UV/vis and elemental analysis. In addition, **7b** and **7f** were characterized by single crystal structure analysis.



Scheme 4-4. Synthesis of bisphenanthrolines **7a-7g**.

The stick and space filling representation of **7b** is depicted in Figure 4-5. A thorough literature survey indicated that **7b** is the first single crystal structure of this series of bisphenanthrolines. Surprisingly, this molecule has a cisoid conformation in the solid state which may be driven by weak intermolecular hydrogen bonding (see Supp 4-2). In contrast, **7f** has a transoid conformation in the solid state, as expected (Figure 4-6). The absorption and emission properties of the sterically loaded bisphenanthrolines **7** will be discussed in Supp 4-2.

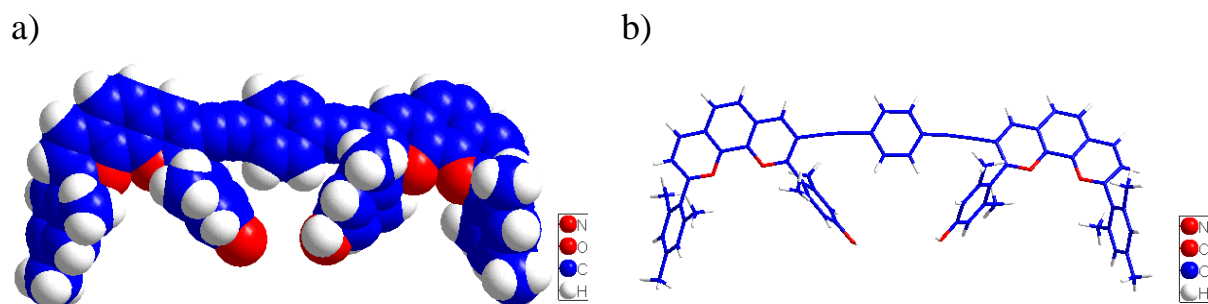


Figure 4-5. Single crystal structure of **7b**: a) space filling representation b) stick representation (in cooperation with Prof. D. Fenske, University of Karlsruhe, Germany).

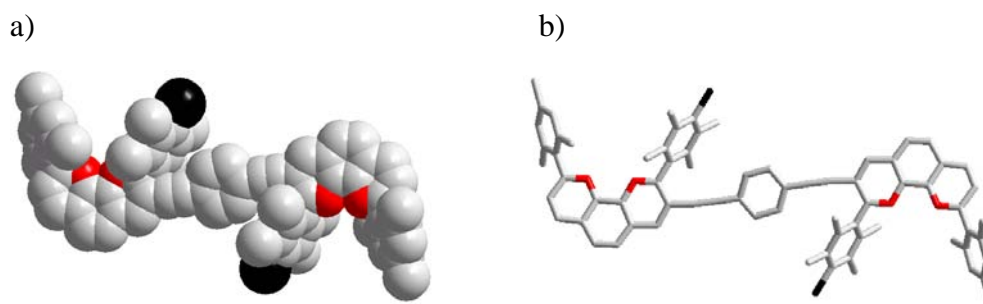
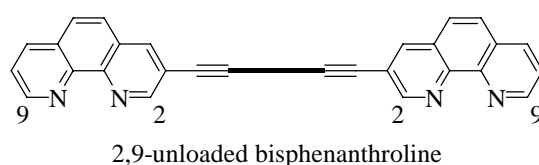
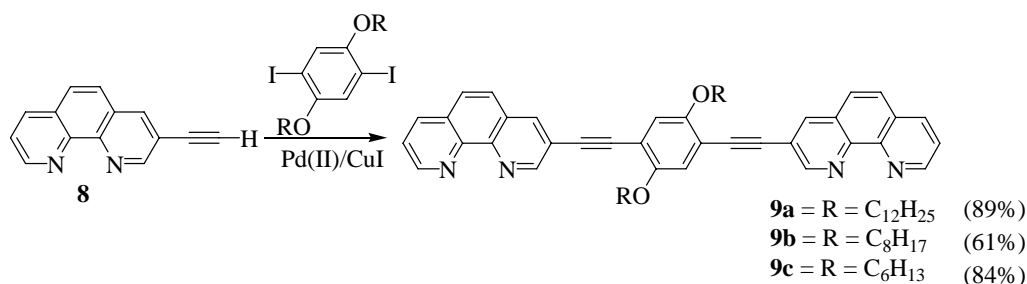


Figure 4-6. Single crystal structure of **7f**: a) space filling representation b) stick representation (in cooperation with Dr. J. W. Bats, Johann Goethe-University, Frankfurt am Main, Germany). Hydrogen atoms were omitted for clarity.

4.2.2 Synthesis of Sterically Unloaded (2,9-unsubstituted) Bisphenanthrolines and Their Self-Assembly at Solid-Liquid Interfaces



Ligands **9a-c** (Scheme 4-5) were synthesized using similar conditions as mentioned above (see experimental section for full details; manuscript 2). Similar ligands were reported by Grummt *et al.*,¹⁴ and others¹⁵ including **9a**; however, their self-assembly behavior has not been explored.



Scheme 4-5. Synthesis of 2,9-unsubstituted bisphenanthrolines, **9a-c**.

Ligand **9a** was characterized by a single crystal structure analysis which showed the presence of intermolecular π - π interactions and alignment of the alkyl chains. This behaviour is in accordance with the self-assembly pattern observed at the solid-liquid interface (Figure 4-7a). Similar to **7b**, this molecule was also detected in a cisoid conformation. In contrast, **9b** has a transoid conformation in the solid state (Figure 4-7b), and intermolecular interactions between dichloromethane (solvent) and **9b** were detected (see Supp 4-2). From the solid state structure analysis of **7b**, **7f**, **9a** and **9b**, their nanoscopic nature has become evident (~3 nm of length along their axis), which may be the reason why it had been difficult to obtain suitable single crystals for this series of bisphenanthrolines.

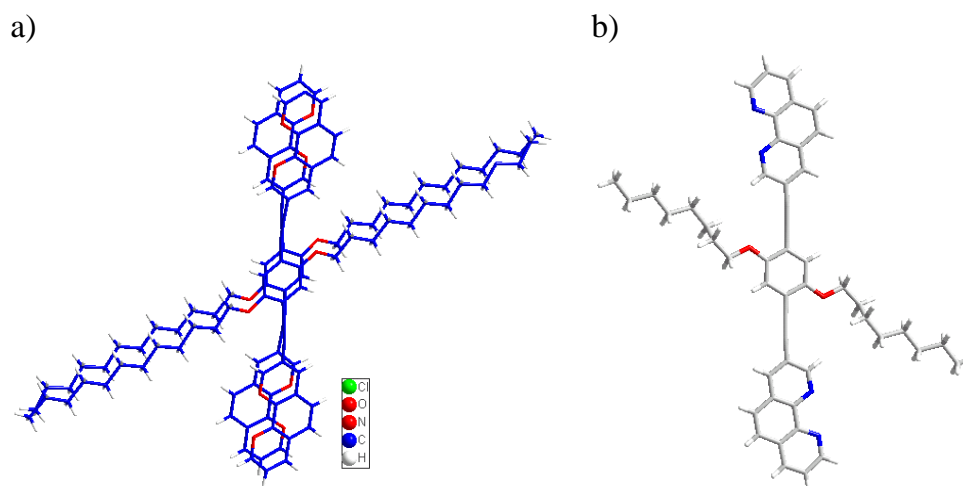


Figure 4-7. a) Single crystal structure of **9a**: Solid state dimers due to intermolecular π - π stackings (~ 3.5 Å) (in cooperation with Prof. D. Fenske, University of Karlsruhe, Germany). b) Single crystal structure of **9b** (in cooperation with Dr. J. W. Bats, Johann Wolfgang Goethe-University, Frankfurt an Main, Germany).

Surface Imaging (in cooperation with Prof. J. P. Rabe, University of Berlin, Berlin): We studied the formation of highly ordered monolayers of the bisphenanthrolines **9a** and **9c** at the solid/liquid interface. Interestingly, two distinct patterns were observed for this small series of ligands. As Figure 4-8 shows, **9a** is arranged in a head-to-head packing (Figure 4-10; *type-b*) whereas, **9c** is arranged in an interpenetrating packing (Figure 4-10; *type-a*).

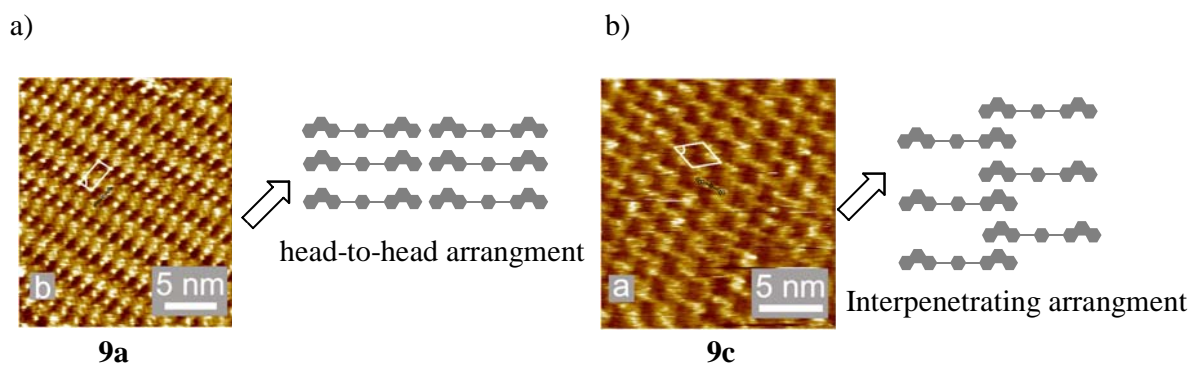


Figure 4-8. Self-assembly of **9a** and **9c** at solid-liquid interfaces (in cooperation with Prof. J. P. Rabe, University of Berlin, Berlin).

The length of the alkyl chains of bisphenanthrolines **9a** and **9c** determines the morphology of their self-assembled monolayers on HOPG. Bisphenanthrolines having less than C_6 alkyl chain prefer the *type-a* pattern, whereas these with longer C_{12} -chain prefer *type-b* pattern (Figure 4-9). In case of C_{12} alkyl chain the solid/liquid pattern (*type-b*) is in good agreement with its solid state structure. Modelling studies proposed that in case of alkyl chain $<C_6$ containing bisphenanthrolines, there is a space limitation for *type-b* pattern. Whereas, in case of $>C_6$ there is enough space for the insertion of other phenanthroline building blocks leading

to *type-a* pattern. This alkyl chain length effect on the monolayer morphology of the supramolecular synthons **9a** and **9c** represents a generalised example of structural effects previously observed in alkanolic acid and derivatives of anthracene monolayers formed on HOPG (see Supp 4-2).¹⁶

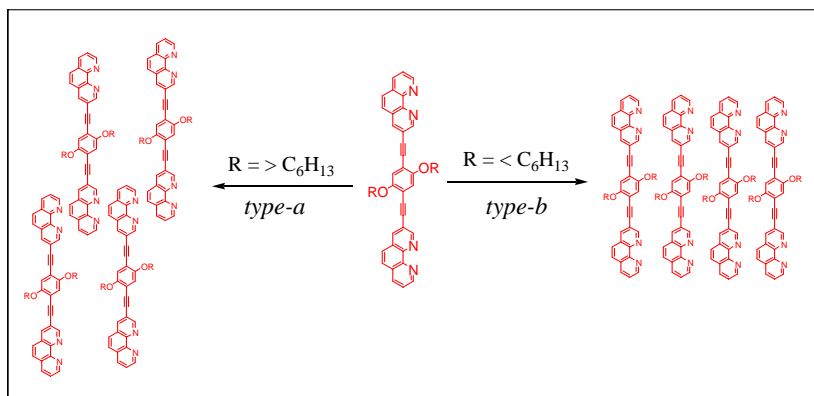
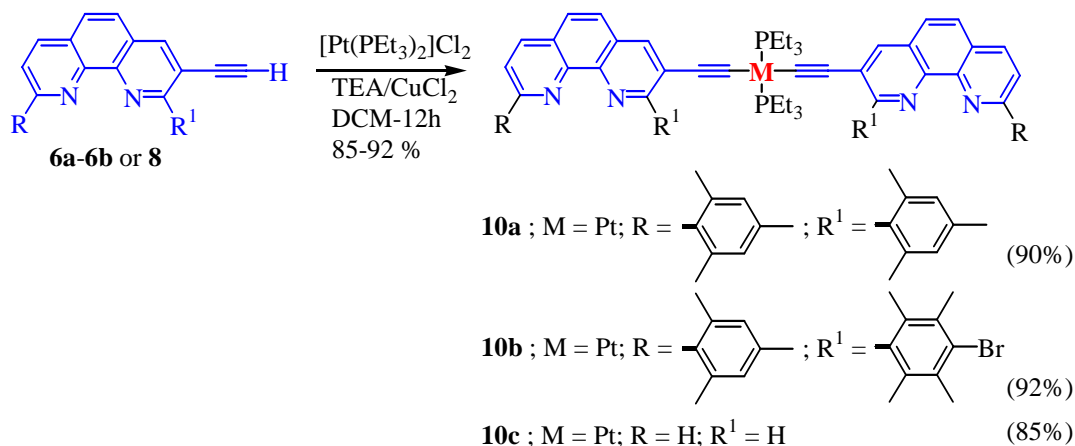


Figure 4-9. Generalised representation of bisphenanthrolines **9a** and **9c** and their solid/liquid pattern.

4.2.2 Non-Covalent Approach; Synthesis of Pt-linked Bisphenanthrolines



Scheme 4-6. Pt-linked bisphenanthrolines **10a-c** synthesis.

A small series of Pt-linked bisphenanthrolines **10a-c** were prepared according to Lin *et al.*¹⁷ Ligands **10** are better soluble than bisphenanthrolines **7** and **9** in chlorinated solvents. The bisphenanthrolines **10** were isolated either by simply precipitation in dichloromethane/hexane (9:1) or by a filter column (eluent: hexane/EA/DCM: 7/2/1). This strategy (Scheme 4-6) has two main advantages over a covalent approach (Sonagashira coupling reaction) which was used for **7** and **9**:

- 1) The ligands obtained by this strategy are relatively more soluble than bisphenanthrolines **7** and **9**.

2) Chromatographic separation was not required.

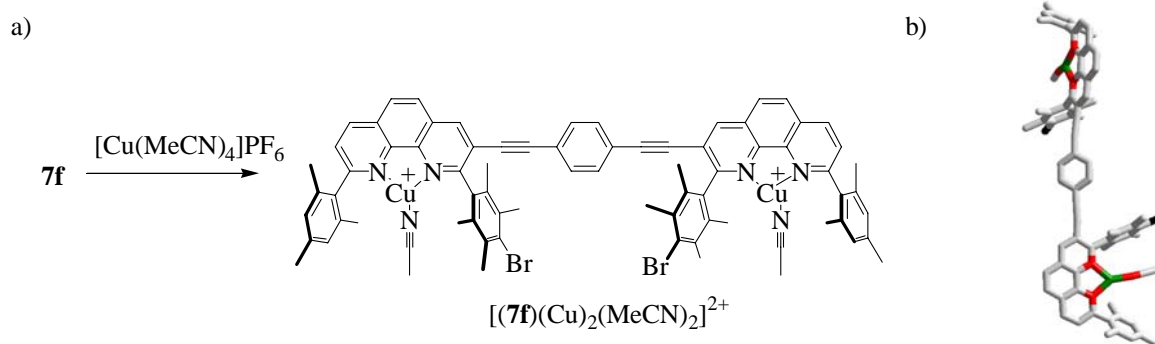
All the complexes were characterised by ^1H NMR, ^{13}C NMR, ^{31}P NMR, ESI MS and elemental analysis. Full details regarding the synthesis and characterization of these compounds are presented in the Supp 4-2.

4.3 Self-Assembly of Hetero or Homometallic/Heteroleptic Racks and Grids (Supp 4-3, Supp 4-4 and Supp 4-5)

Using the HETPHEN approach, a series of racks and grids were engineered which are truly heteroleptic/homometallic (*unlike* ligands/*like* metal ions) or heteroleptic/heterometallic (*unlike* ligands/*unlike* metal ions) in nature.¹⁸ The present racks represent the first dynamic multi-component racks motifs.

4.3.1 Racks (Supp 4-3)

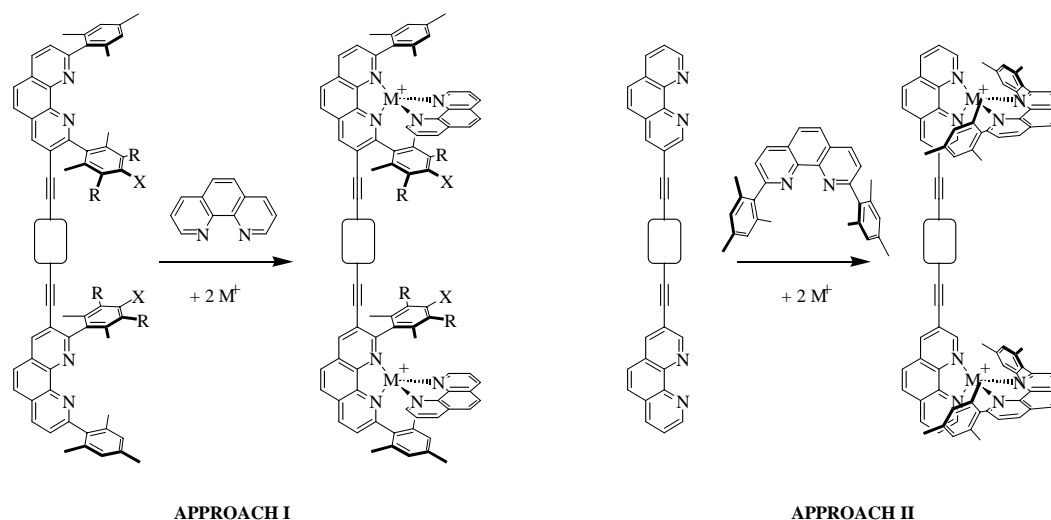
The need for the HETPHEN approach in the formation of dynamic rack assemblies becomes evident when bisphenanthroline **9a** was reacted with **1** in presence of $[\text{Cu}(\text{MeCN})_4]\text{PF}_6$. The desired rack was obtained only as a minor component, as evidenced by ESI-MS and ^1H NMR. In contrast to earlier reports by Lehn *et al.*, we realised that cooperativity and maximum site occupancy can not be used solely to build dynamic heteroleptic aggregates. The combination of **7f** and Cu(I) salt (1:2 equiv.) provided a molecular receptor which could be isolated and characterised in solution. In addition, it was possible to obtain a solid state structure for this unique intermediate (Scheme 4-7b).



Scheme 4-7. a) Synthesis of the molecular receptor $[(\mathbf{7f})(\text{MeCN})_2(\text{Cu})_2]^{2+}$ and b) its single crystal structure (in cooperation with Prof. D. Fenske, University of Karlsruhe, Germany).

Racks were generated in two different approaches highlighting the HETPHEN strategy as a general case (Scheme 4-8). Both approaches use one ligand loaded with steric stoppers and the other without. In approach I, the linear bisphenanthroline is loaded with sterically bulky

aryl groups at the 2,9-positions of each phenanthroline site. In contrast, **approach II** makes use of monophenanthrolines that are equipped with the steric stoppers, while the linear bisphenanthroline is devoid of them.



Scheme 4-8. Two possible approaches for heteroleptic/homometallic rack aggregation.

Using the approaches outlined above, a series of rack structures was generated and characterised by $^1\text{H-NMR}$, $^{13}\text{C-NMR}$, ESI-MS, and elemental analysis (see Supp 4-3 for more detailed information). In addition to the solution state characterisation, it was possible to obtain single crystal structure data for two of these nanoscale racks (Figure 4-10). **R1** is constructed using approach A, whereas **R2** is constructed using approach B.

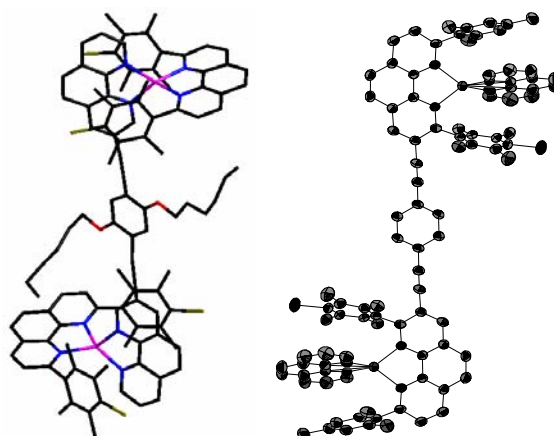
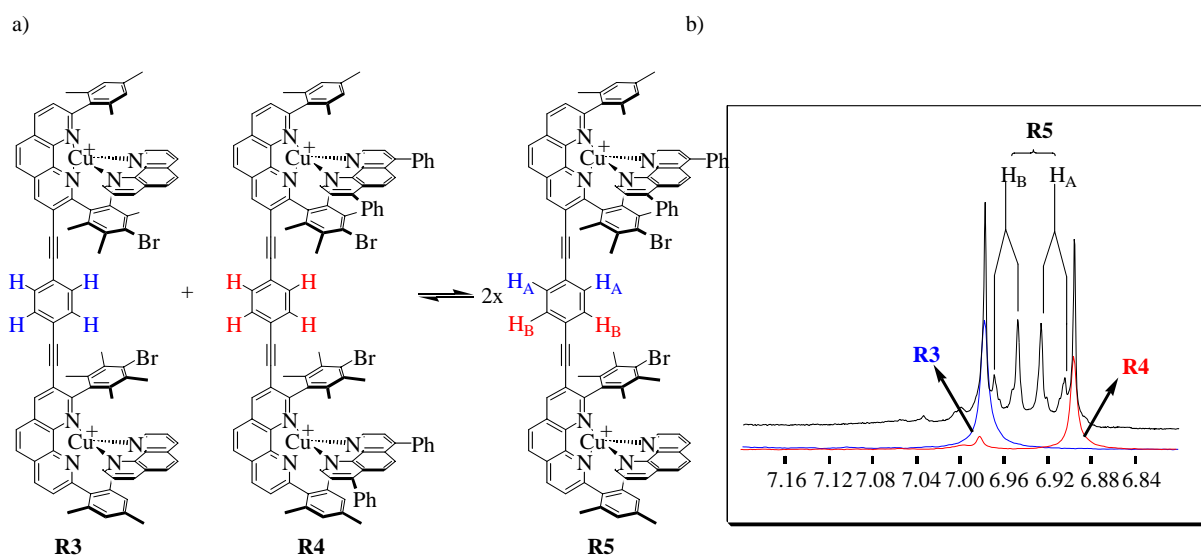


Figure 10. Crystal structures of racks; **R1** and **R2** (in cooperation with Prof. D. Fenske, University of Karlsruhe, Germany).

The dynamic nature of the racks was interrogated by an exchange experiment (Scheme 4-9). Two racks **R3** and **R4**, which are different by their molecular weights, were mixed and the resulting solution was studied by ESI MS and $^1\text{H NMR}$. As indicated by ESI MS, the mixed

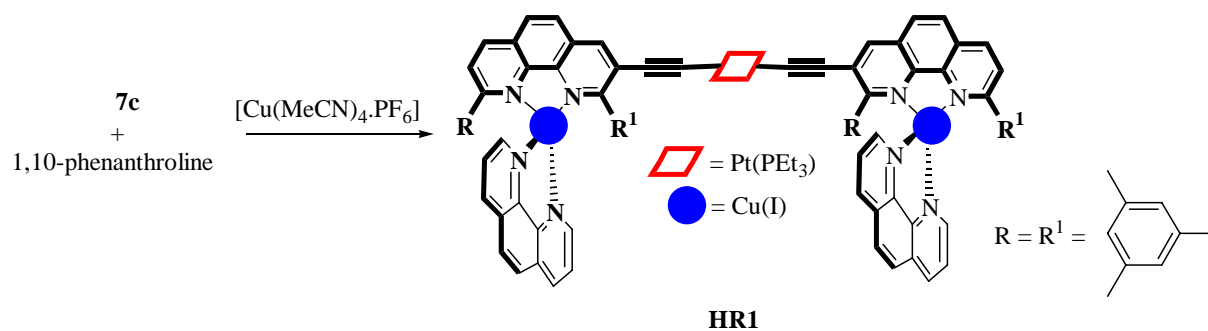
rack **R5** is obtained along with the added racks **R3** and **R4**, giving direct evidence for their dynamic nature.

The ^1H NMR investigations of rack **R3** and **R4** showed singlets for all bridge phenyl protons because of their homotopic nature (scheme 4-9b, blue and red). Interestingly, when **R3** and **R4** were reacted a new set of signals was observed for the bridge protons of **R5**, along with signals corresponding to **R3** and **R4**. In **R5**, the bridge phenyl protons become constitutionally heterotopic; therefore, it appeared as a pair of doublets. The fast formation of **R5** indicates the dynamic nature of these aggregates (scheme 4-9b, dark).



Scheme 4-9. a) Ligand exchange equilibrium in solution after mixing **R3** and **R4**. b) Selected region of the ^1H NMR showing signals corresponding to bridge phenyl protons for **R3** (blue), **R4** (red) and **R3-R4-R5** (dark).

Along the same token a heteroleptic/heterometallic rack motif was prepared when **10a** and **1** were reacted in presence of Cu(I) salt (Scheme 4-10). The resulting heterometallic structures were characterised by ^1H -NMR, ^{13}C -NMR, ^{31}P -NMR, ESI-MS, and elemental analysis. ^{31}P NMR showed a single set of signals centred at 13.3 (with its Pt-satellites) and -143.2 (with its F-satellites) corresponding to P-Pt and PF_6 , respectively. In addition, it was possible to obtain a single crystal structure for this unique assembly (Figure 4-11, Supp 4-5). This is the first example of a heterometallic/heteroleptic rack series, demonstrating the versatility of the HETPHEN approach in designing novel compounds.



Scheme 4-10. Self-assembly of heterometallic rack motif, **HR1**.

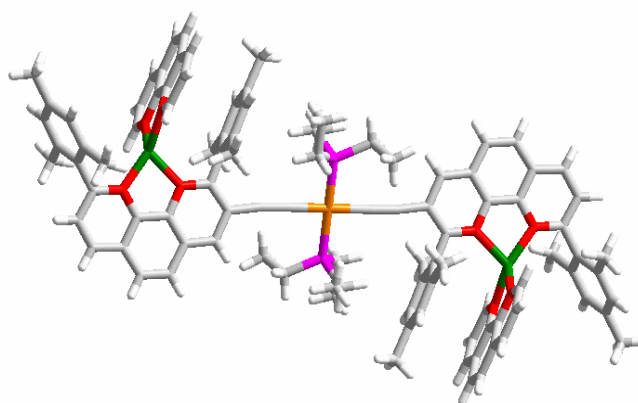
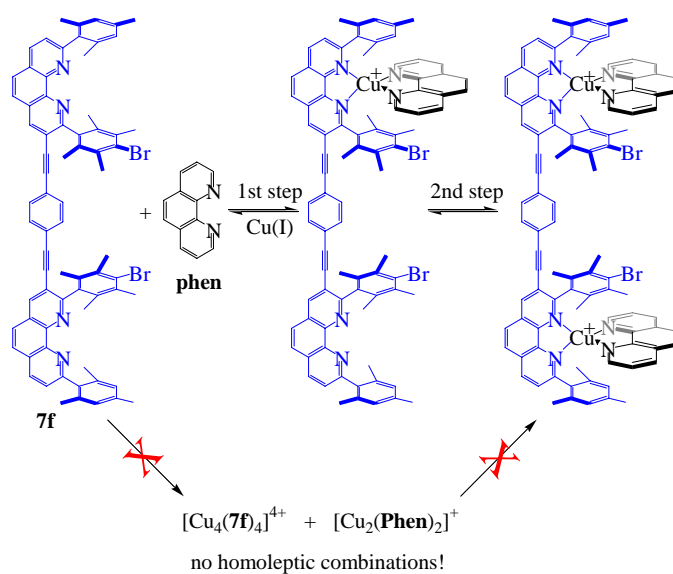


Figure 4-11. Single crystal structure of **HR1**; stick representation (in cooperation with Prof. J. W. Bats, Johann Wolfgang Goethe-University, Frankfurt am Main, Germany).

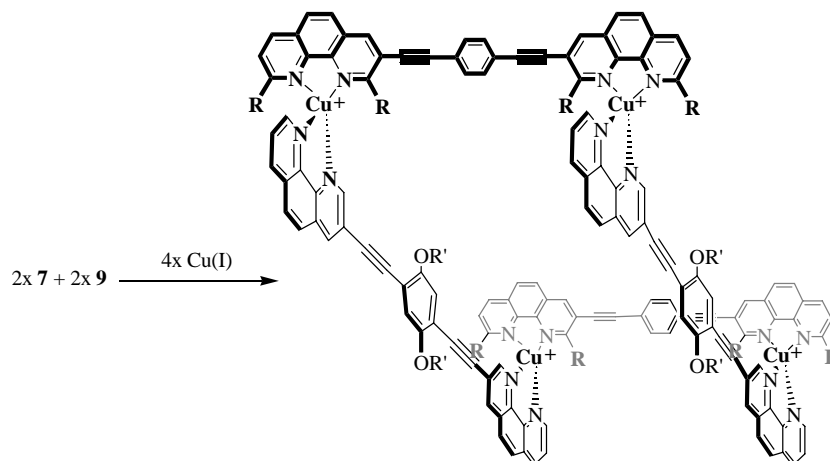
1H NMR, ESI MS and UV/vis titrations provided interesting mechanistic insight into these unique dynamic rack structures proposing a two step self-assembly path (scheme 4-11).



Scheme 4-11. Self-assembly mechanism for rack aggregation.

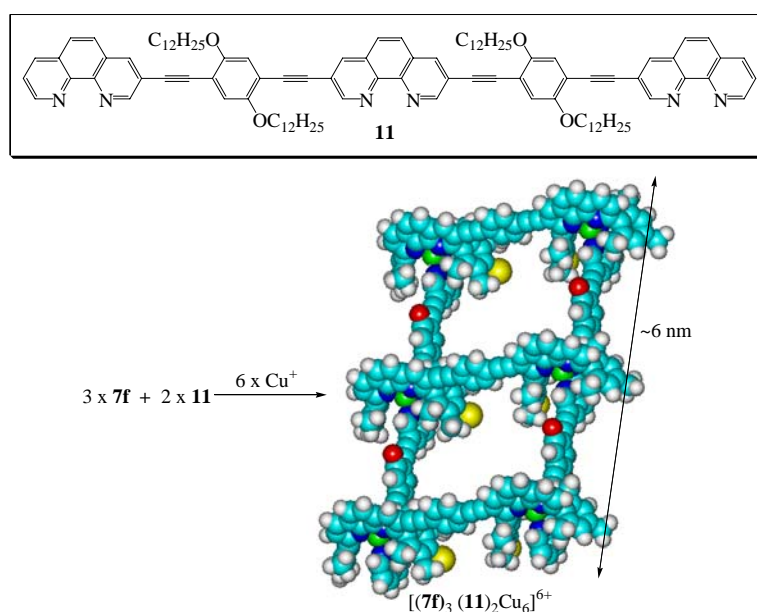
4.3.2 Grids (Supp 4-4)

Rewardingly, a series of multi-component grids could be generated, quantitatively using the HETPHEN principles (Scheme 4-12), for the first time. These structures were characterized by ^1H NMR, COSY, ESI-MS and the elemental analysis (Supp 4-4). These grids represent the large void containing aggregates, indicative of their potential for host-guest chemistry.



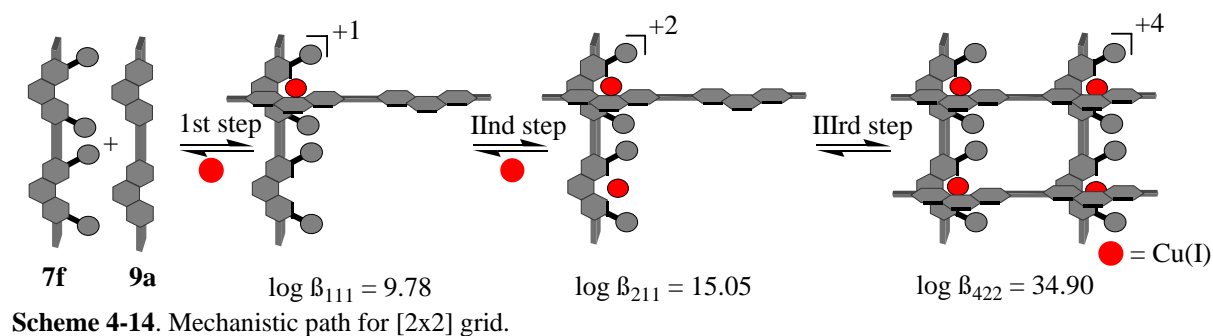
Scheme 4-12. Self-assembly of multi-component [2x2] grids.

This approach could also be applied to the self-assembly of a [2x3] grid (Scheme 4-13). However, we noted a sluggish reaction over two days until finally the [2x3] grids had formed. Ligand **11** was obtained from Kishore¹⁹ (Supp 4-4). This series of [2x3] grids represent the largest grid structures known to date!

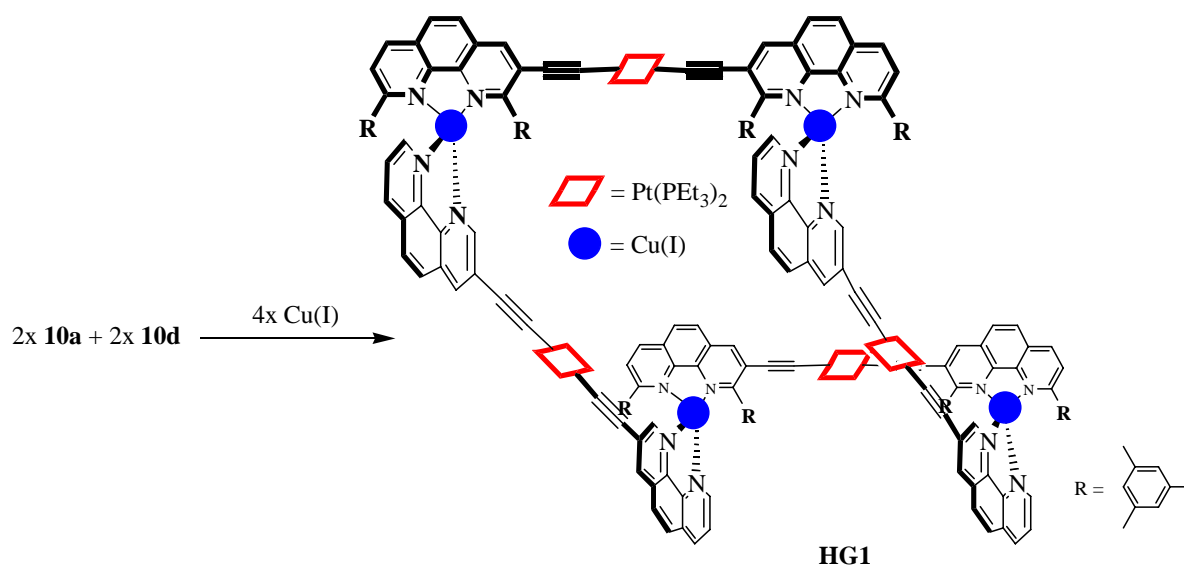


Scheme 4-13. Self-assembly of a multi-component [2x3] grid, represented as Hyperchem model (alkoxy chains were omitted for clarity).

To understand their formation, we carried out mechanistic investigation using ESI MS (qualitative analysis) and UV/vis (quantitative analysis). Both titrations indicated a three step process on the way to the grid (Scheme 4-14), providing complexation constants for two intermediate complexes and the final grid (Supp 4-4).



A unique heterometallic/heteroleptic grid **HG1** resulted when **10a**, **10d** and Cu(I) (1:1:2 eq.) salts were reacted in dichloromethane solution (Scheme 4-15) (Supp 4-5).



ESI MS analysis of **HG1** showed signals formed by the successive loss of counter ions. The isotopic distribution of the 3+ and 4+ charged species are in excellent agreement with the calculated ones (Figure 4-12).

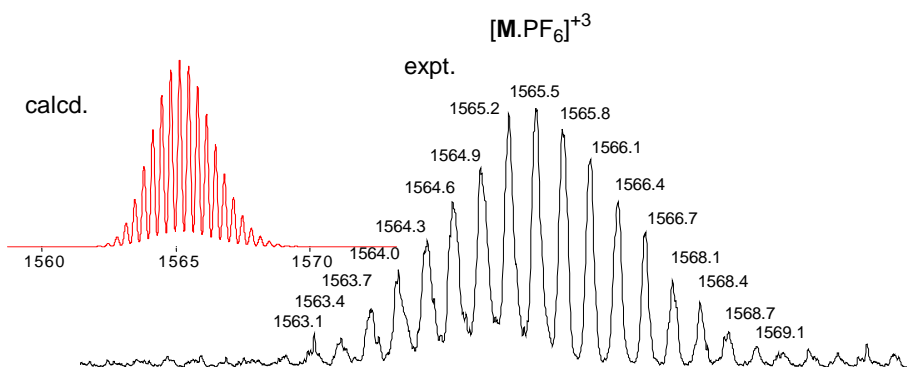
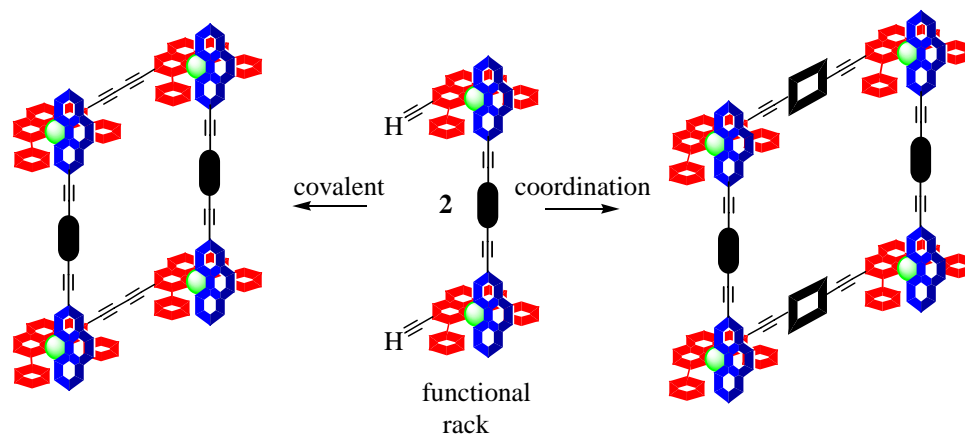


Figure 4-12. Experimentally obtained isotopic distribution (dark) for $[\text{HG1.PF}_6]^{+3}$ species along with its calculated one (red).

4.3.3 Racks to Grid motifs (Supp 4-5)

After having success with the self-assembly of racks and grids using the divergent approach, a convergent approach was outlined for grids (Scheme 4-16). The rack assemblies were self-assembled (that by their very nature must be heteroleptic) some of which were equipped with alkyne termini for further functionalization. The latter feature suggested to use the racks as versatile precursors^{18f} for supramolecular nanostructures. Using this approach we outlined two strategies, a covalent and a coordination route, to fabricate heteroleptic grids directly from the supramolecular racks (see Supp 4-5 for more details). Such a convergent strategy should facilitate the access to grid like motifs.

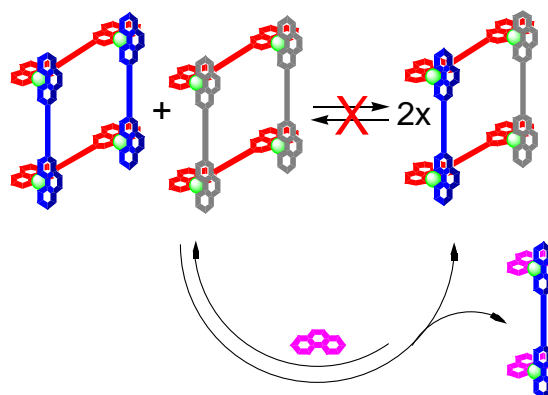


Scheme 4-16. A convergent approach for heteroleptic grid motifs.

4.3.4 Nature of the Grid Motifs: Kinetic or Dynamic?

When two grids were reacted together no mixed motifs could be detected, even at elevated temperatures. This observation remained consistent with prolonged time (7days), indicating that these structures may be kinetically locked or they are the thermodynamically most stable complexes. Interestingly, when a simple phenanthroline was added to the mixture, a mixed

species could be detected immediately. This indicates that the grids do not mix due to a high kinetic barrier (Scheme 4-17).



Scheme 4-17. Kinetic unlocking of multi-component grids.

4.4 Conclusions

In summary, a family of rigid linear bisphenanthrolines with or without bulky groups at the bisimine site has been synthesized. As a key step, the coupling of diiodo (covalent) and Pt/Pd chemistry (non-covalent) was used. Four of these nanoscale bisphenanthrolines (**7b**, **7f**, **9a** and **9b**) were characterized in solid state. The ability of these ligands to form multi-component/multi-metallic rack and grid motifs was probed. A small family of bisphenanthrolines could be imaged on surface. Future perspectives will be to explore studies of these higher aggregates with functionalised ligands, their surface chemistry and their photophysical studies.

- (1) M. Schmittel, V. Kalsani, Functional, Discrete, Nanoscale Supramolecular Assemblies, *Top. Curr. Chem.*, **2005**, 245, 1-53.
- (2) M. Ruben, J. Rojo, F. J. Romero-Salguero, L. H. Uppadine, J.-M. Lehn, Grid-Type Metal Ion Architectures: Functional Metallosupramolecular Arrays, *Angew. Chem. Int. Ed.* **2004**, 43, 3644-3662.
- (3) H. Hofmeier, U. S. Schubert, Recent developments in the supramolecular chemistry of terpyridine metal complexes, *Chem. Soc. Rev.* **2004**, 373-399.
- (4) P. N. W. Baxter, J.-M. Lehn, G. Baum, D. Fenske, Multicomponent Self-Assembly: Preferential Generation of a Rectangular [2 × 3]G Grid by Mixed-Ligand Recognition, *Angew. Chem. Int. Ed. Engl.* **1997**, 36, 1978-1981.
- (5) M. Greenwald, D. Wessely, E. Katz, I. Willner, Y. Cohen, From Homoleptic to Heteroleptic Double Stranded Copper(I) Helicates: The Role of Self-Recognition in Self-Assembly Processes, *J. Org. Chem.* **2000**, 65, 1050-1058.
- (6) a) M. Schmittel, A. Ganz, Stable Mixed Phenanthroline Copper(i) Complexes. Key Building Blocks for Supramolecular Coordination Chemistry, *Chem. Commun.* **1997**, 99-100. b) M. Schmittel, U. Luning, M. Meder, A. Ganz, C. Michel, M. Herderich, Synthesis of Sterically Encumbered 2,9-Diaryl Substituted Phenanthrolines. Key Building Blocks for the Preparation of Mixed (Bis-Heteroleptic) Phenanthroline Copper(I) Complexes (I), *Heterocycl. Commun.* **1997**, 3, 493-498.
- (7) S. De Feyter and F. C. De Schryver, Two-dimensional supramolecular self-assembly probed by scanning tunneling microscopy, *Chem. Soc. Rev.* **2003**, 139-150.

- (8) M. M. Abdel-Mottaleb, N. Schuurmans, S. De Feyter, J. Va Esch, B. L. Feringa, F. C. De Schryver, Submolecular Visualisation of Palladium Acetate Complexation with a Bipyridine Derivative at a Graphite Surface, *Chem. Commun.*, **2002**, 1894-1895.
- (9) D. Wouters, S. Höppener, R. Lunkwitz, L. Chi, H. Fuchs, U. S. Schubert, Highly Ordered Self-Assembled Architectures of Modified Terpyridines on Highly Ordered Pyrolytic Graphite Imaged by Scanning Tunneling Microscopy, *Adv. Funct. Mater.* **2003**, *13*, 277-280.
- (10) R. Ziessel, M. Hissler, A. El-ghayoury, Multifunctional transition metal complexes: Information transfer at the molecular level, *Coord. Chem. Rev.* **1998**, *178-180*, 1251-1298.
- (11) A. Petitjean, N. Kyritsakas, J.-M. Lehn, Programmed Single Step Self-Assembly of a [2 x 2] Grid Architecture Built on Metallic Centers of Different Coordination Geometries, *Chem. Commun.*, **2004**, 1168-1169.
- (12) M. Schmittel, A. Wiegrefe, C. Michel, V. Kalsani, Synthesis of Soluble, Linear Bisphenanthrolines for the Construction of Heteroleptic NanoGrids and NanoBoxes, *Synthesis* **2001**, 1561-1567.
- (13) C. O. Dietrich-Buchecker, P. A. Marnot, J. P. Sauvage, Direct Synthesis of Disubstituted Aromatic Polyimine Chelates, *Tetrahedron Lett.* **1982**, *23*, 5291-5294.
- (14) E. Birckner, U.-W. Grummt, A. H. Göller, T. Pautzsch, D. A. M. Egbe, M. Al-Higari, and E. Klemm, Photophysics of Arylene and Heteroaryleneethynylenes, *J. Phys. Chem. A*, **2001**, *105*, 10307-10315.
- (15) V. Grosshenny, F. M. Romero, R. Ziessel, Construction of Preorganized Polytopic Ligands via Palladium-Promoted Cross-Coupling Reactions, *J. Org. Chem.* **1997**, *62*, 1491-1500.
- (16) Y. Wei, K. Kannappan, G. W. Flynn, M. B. Zimmt, Scanning Tunneling Microscopy of Prochiral Anthracene Derivatives on Graphite: Chain Length Effects on Monolayer Morphology, *J. Am. Chem. Soc.* **2004**, *126*, 5318-5322 and ref's therein.
- (17) H. Jiang and W. Lin, Expeditious Assembly of Mesoscopic Metallocycles, *J. Am. Chem. Soc.*, **2004**, *126*, 7426 and ref's therein.
- (18) a) H. Sleiman, P. Baxter, J.-M. Lehn, K. Rissanen, Self-assembly of rigid-rack multimetallic complexes of rotaxane-type, *J. Chem. Soc. Chem. Commun.* **1995**, 715-716. b) G. S. Hanan, C. R. Arana, J.-M. Lehn, G. Baum, D. Fenske, Photonic Molecular Devices: Reversibly Photoswitchable Fluorophores for Nondestructive Readout for Optical Memory, *Angew. Chem. Int. Ed. Engl.* **1995**, *10*, 1119-1122. c) G. S. Hanan, C. R. Arana, J.-M. Lehn, G. Baum, Coordination Arrays: Synthesis and Characterisation of Rack-Type Dinuclear Complexes, D. Fenske, *Chem. Eur. J.* **1996**, *10*, 1292-1302. d) H. Sleiman, P. N. W. Baxter, J.-M. Lehn, K. Airola, K. Rissanen, Multicomponent Self-Assembly: Generation of Rigid-Rack Multimetallic Pseudorotaxanes, *Inorg. Chem.* **1997**, *36*, 4734-4742. e) D. Brown, R. Zong, R. P. Thummel, Ru^{II} Complexes of Bis(1,10-phenanthrolin-2-yl)diazines, *Eur. J. Inorg. Chem.* **2004**, 3269-3272. f) M. Benaglia, F. Ponzini, C. R. Woods, J. S. Siegel, Synthesis of Oligopyridines and Their Metal Complexes as Precursors to Topological Stereoisomers, *Org. Lett.* **2001**, *3*, 967-969. g) P. Ceroni, A. Credi, V. Balzani, S. Campagna, G. S. Hanan, C. R. Arana, J.-M. Lehn, Absorption and Emission Properties of Di- and Trinuclear Ruthenium(II) Rack-Type Complexes, *Eur. J. Inorg. Chem.* **1999**, 1409-1414.
- (19) Thanks to Kishore for donating some of his ligand, **11**.

Supp 4-1

Synthesis **2001**, 1561-1567.

Reproduced by permission of *Thieme Chemistry*

Synthesis of Soluble, linear Bisphenanthrolines for the Construction of Heteroleptic Nanogrids and Nanoboxes

Michael Schmittel,* Christoph Michel, Andreas Wiegrefe, Venkateshwarlu Kalsani

FB 8 - OC1 (Chemie und Biologie), Universität Siegen, Adolf-Reichwein-Strasse, D-57068 Siegen, Germany.

Tel. (+49)-271-4356, Fax (+49) 271-3270, e-mail schmittel@chemie.uni-siegen.de

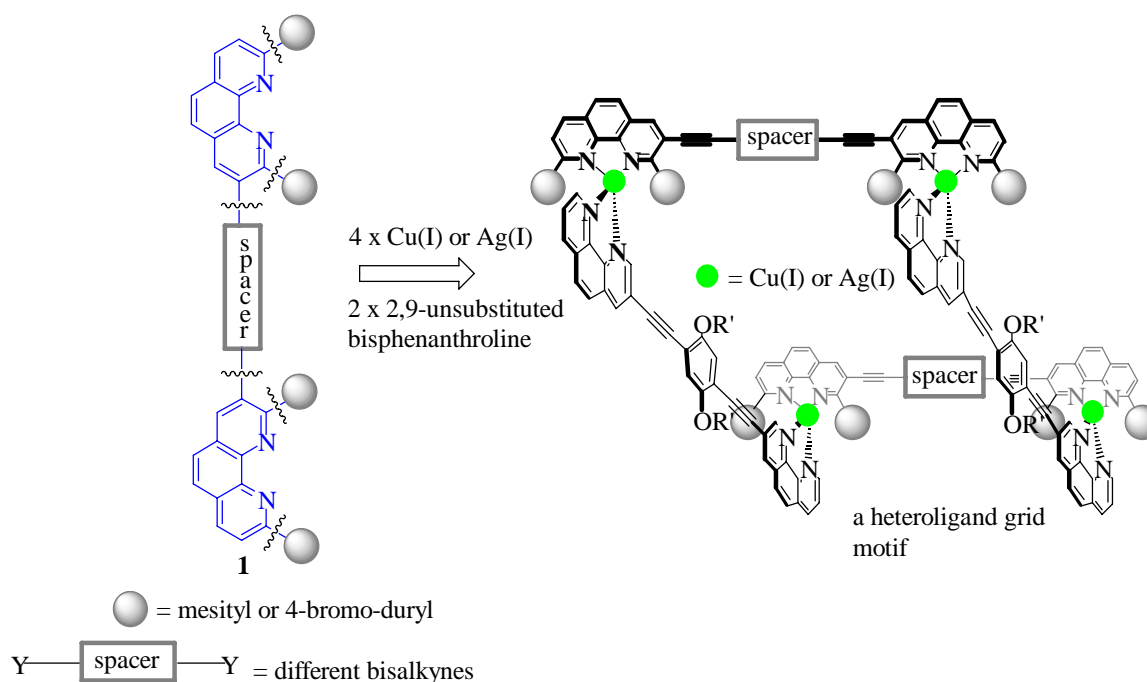
ABSTRACT: The preparation of several novel and soluble bisphenanthrolines that are important building blocks for various supramolecular structures based on heteroleptic copper(I) complexes is described.

Key words: palladium, cross-coupling, nucleophilic substitution, phenanthrolines

Currently, there is enormous interest in the design and synthesis of polydentate ligands capable of self-assembly processes.¹ Among the polydentate ligands, oligo-2,2'-bipyridines² and oligophenanthrolines³ have assumed a particular standing because in presence of numerous metal cations they form strong complexes with a predictable spatial arrangement, an advantage used extensively for the preparation of various supramolecular architectures, for example ladders, grids, rotaxanes, helicates and others.^{1,2}

Multiion nanometer-sized lattice or grid structures may open interesting perspectives for the creation of molecular-level devices.⁴ As the leading pioneer in this field, Lehn *et al.* have elaborated numerous one ligand [n x n] grids (n = 2,3,4,5) on the basis of bipyridine subunits.⁵ Defects in [5 x 5] grids caused by one lacking ligand have recently led to a single example of a [4 x 5] grid, while filling of interstitial spaces in [2 x 2] grids driven by π,π -stacking have formally resulted in [3 x 3] bisbipyridine grids.⁶

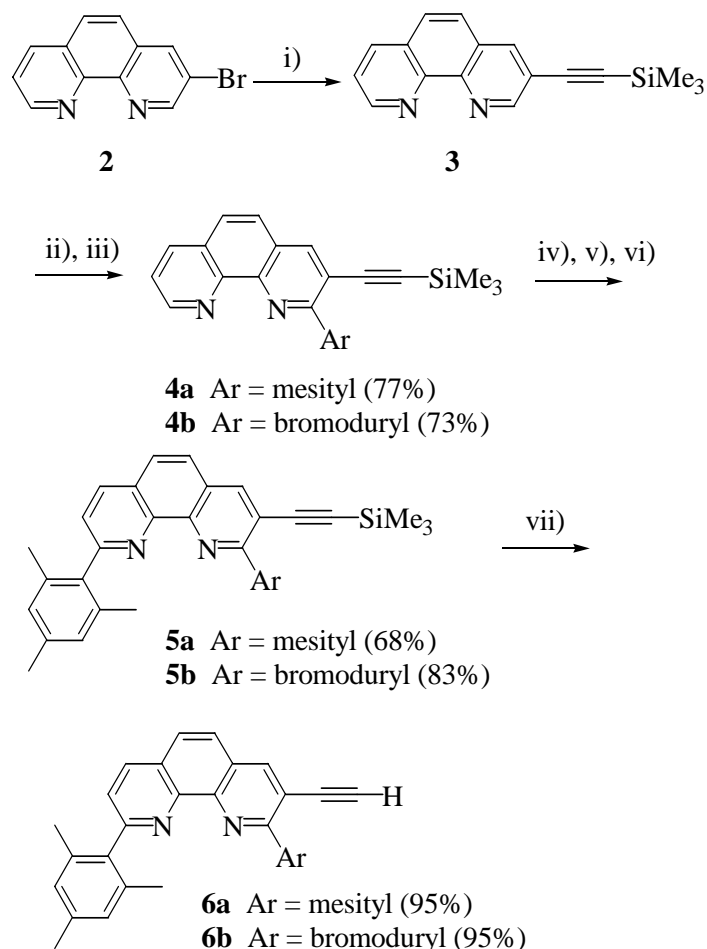
While all latter examples were based on homoleptic complexes (= one ligand systems), a spectacular example of an $[n_A \times m_B]$ grid (ligand A with n binding sites + ligand B with m binding sites), *i.e.* a $[2 \times 3]$ grid,⁷ has been described recently. Its thermodynamically controlled formation, however, was accompanied by small amounts of the $[2 \times 2]$ and $[3 \times 3]$ grids. Hence, we now propose to develop a general and quantitative route to heteroleptic $[n_A \times m_B]$ grids (Scheme 1) by making use of our concept for the clean formation of heteroleptic copper(I)⁸ and silver(I)⁹ bisphenanthroline complexes. The viability of our concept has already been demonstrated for simple and nanosize structures.¹⁰ As our concept critically depends on a fine balance of steric shielding and of π -stacking interactions^{8,9} the preparation of a series of linear bisphenanthrolines, characterized by bulky *ortho*-aryl substituents at the bisimine binding sites, is warranted.



Scheme 1

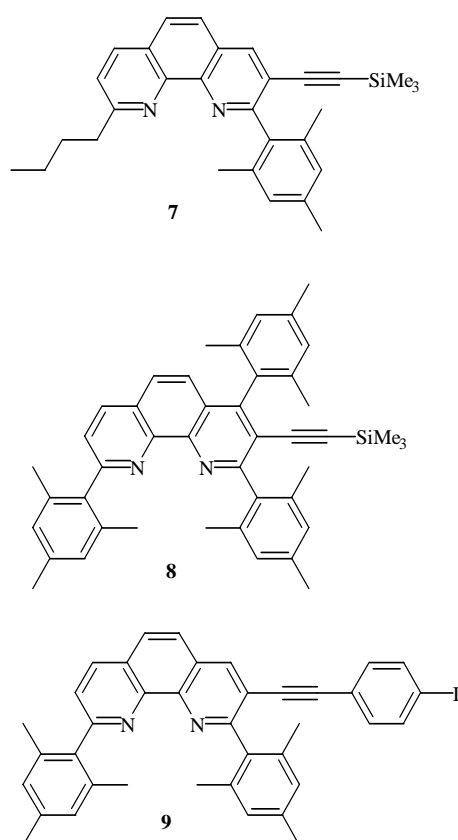
For systematic studies of the coordination chemistry we first chose to synthesize a small series of bisphenanthroline ligands **1** bearing sterically encumbered groups. The mesityl or duryl groups not only serve to control the heteroleptic complex formation but should also help to raise the solubility which is a notorious problem for longer linear polytopic bisimines. As rigid linear spacers between the phenanthroline we chose to test butadiyne, 1,4-diethynylbenzene and diethynylbiphenyl.

The starting point of our synthetic strategy is 3-bromophenanthroline (**1**)¹¹ that, following a protocol of Sonogashira,¹² was coupled with trimethylsilylacetylene in presence of $[\text{PdCl}_2(\text{PPh}_3)_2]$ and CuI to provide **3** in 92% yield (Scheme 2). The arene groups were now added in 2- and 9-position by nucleophilic substitution according to Sauvage.¹³ After some optimization we realized that the stepwise addition of both aryl groups was superior to the one-pot procedure. Interestingly, upon addition of 1.5 equivalent of the aryl lithium compound (prepared by halogen-metal exchange after analysis by GC) to **2** a highly regioselective addition in 2-position occurred. Only in one case the 9-addition product was detected in traces. The addition products were isolated (in the mesityl case as bright yellow crystals) and oxidized with activated manganese dioxide to afford the monosubstituted phenanthrolines **4a-b**.



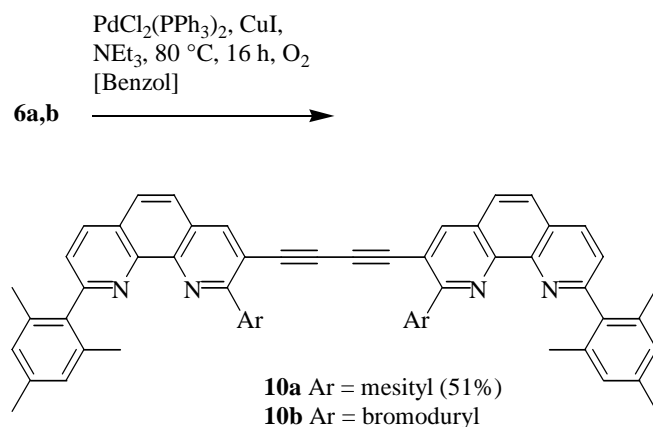
Scheme 2: i) $\text{HC}\equiv\text{C}(\text{TMS})$, $[\text{PdCl}_2(\text{PPh}_3)_2]$, CuI, benzene, NEt_3 , 80-90 °C, 1 d. ii) ArBr, *n*-BuLi, Et_2O , RT. iii) H_2O , MnO_2 , CH_2Cl_2 , 20 h. iv) MesBr, *n*-BuLi, Et_2O , RT. v) H_2O . vi) MnO_2 . vii) KOH (aq).

In the second substitution step a mesityl group was introduced in 9-position following the same protocol as mentioned above. Again the halogen-metal exchange had to be controlled carefully. In one case, the butylsubstituted phenanthroline **7** (9%) was furnished when we used an excess of *n*-butyllithium. On the other side, when a large excess of mesityllithium was used double substitution steps takes place resulting in the formation of phenanthroline **8**. To the best of our knowledge that is known only in one case (Scheme 3).¹⁴ A similar reactivity from is known from pyridine only in some cases.¹⁵

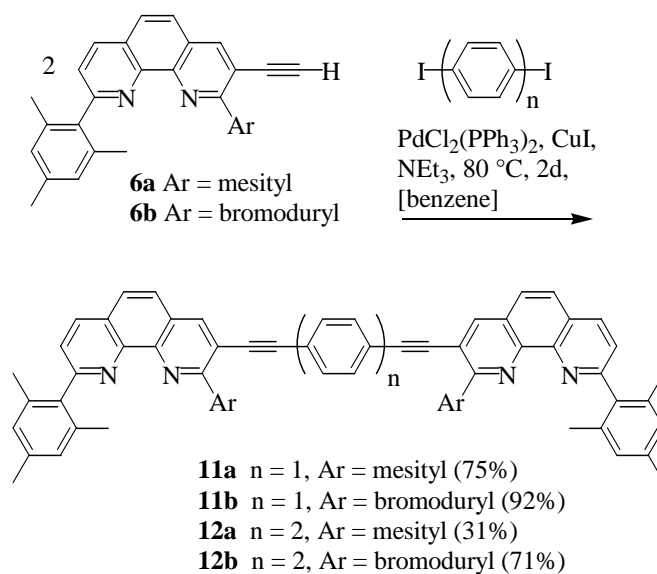


Scheme 3

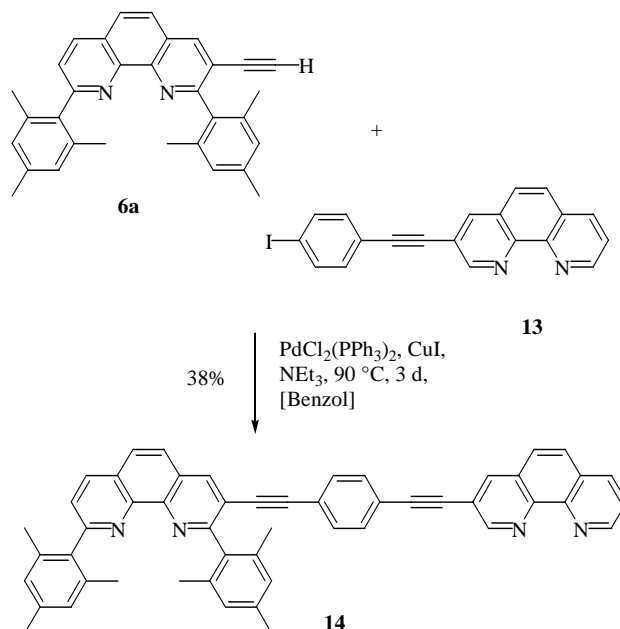
After deprotection of **5** with aqueous KOH we obtained the free acetylene **6** constituting a useful precursor for the bisphenanthrolines. The bisphenanthrolines **10-12** were obtained along two different methods. Various attempts to synthesize the desired bisphenanthroline **10** using Hay oxidation conditions¹⁶ failed, while coupling of **6a** under Pd-catalyzed¹⁷ conditions readily afforded **10** in 51% yield (Scheme 4). The product could be purified by column chromatography.


Scheme 4

Pd/Cu-catalyzed Sonogashira coupling^{12,18} of **6a-b** with 1,4-diiodobenzene and 4,4'-diiodobiphenyl, respectively afforded the corresponding bisphenanthrolines **11a,b** and **12a,b** in yields from 31% - 92% (Scheme 5). For best yields, the reaction is conveniently monitored by ESI-MS spectroscopy. As a side product linear phenanthrolines **10a** or **10b** were found in traces. Coupling at room temperature under the same conditions led to the monophenanthroline **9** in very low yield. Alternatively, attempts to synthesize **11b** through the coupling of **6a** with 4,4'-dibromobiphenyl under Pd-catalysis failed resulting in recovering only the starting material. Isolation of the pure bisphenanthrolines was readily achieved by column chromatography and subsequent recrystallization from cyclohexane.


Scheme 5. Synthesis of rigid bisphenanthrolines **11a-b** and **12a-12b**.

As a reference we also synthesized the unsymmetrical bisphenanthroline **14** that combines a steric encumbered phenanthroline with an unhindered one. It can be prepared by Sonogashira coupling by the reaction of **6a** with the phenanthroline **13** (Scheme 6).¹⁹



Scheme 6. Synthesis of unsymmetrical bisphenanthroline **14**.

Conclusions

In summary, a method for the convergent preparation of different substituted bisphenanthrolines has been developed. As a key step the coupling of various diiodo compounds with substituted ethynylphenanthrolines was used. The ability of the obtained ligands to form supramolecular coordination compounds is now under investigation in our laboratories and has led to the preparation of nanoboxes.²⁰ The resulting complexes may perform useful light- and/or redox-induced functions- as well as studies of electron transfer.²¹ Especially bipyridyls and phenanthrolines motifs are very useful in ligands because of their good coordinating behaviour towards different metals.²² They have also several applications as tuneable fluorophores²³ are molecular machines and photoactive wires^{24,25}. They have been demonstrated to be useful building blocks in metallocsupramolecular chemistry.²⁶ To prepare heteroleptic bisphenanthroline copper(I) complexes it is necessary to steric demanding groups in position to the nitrogen atoms.

Experimental

All reagents were commercially available and used without further purification. The solvents were dried with appropriate desiccants and distilled before use (CH_2Cl_2 from P_2O_5 , MeCN from P_2O_5 and NaH, DMSO from calcium sulfate under reduced pressure). - ^1H NMR spectra were recorded on either Bruker AC 200 (200 MHz) or Bruker AC 250 (250 MHz) spectrometers (using the deuterated solvent as the lock and residual solvent as the internal reference). - IR spectra were recorded on a Perkin-Elmer (1605 FT-IR). - Microanalyses were carried out with a Carlo Erba Elemental Analyzer 1106. - Electrospray mass spectra (ES-MS) were recorded using a ThermoQuest LCQ Deca Finnigan. TLC was done on SiO_2 (silica gel 60 F₂₅₄, Merck). The degree of lithiation can readily be monitored by GC, while progress of substitution at phenanthroline is best controlled by ESI-MS.

2-(2,4,6-Trimethylphenyl)-3-(trimethylsilanylethynyl)-[1,10]phenanthroline (**4a**):

A solution of 1-bromo-2,4,6-trimethylbenzene (3.69 g, 18.5 mmol) in dry diethylether (45 ml) was treated dropwise with 2.5 M *n*-butyllithium (12.4 ml, 31.0 mmol, solution in hexane) and stirred for 14 h at 0 °C. After addition of 3-trimethylsilanylethynyl-[1,10]phenanthroline (1.80 g, 6.52 mmol) the resulting purple solution was stirred for 22 h at room temperature. After hydrolysis with aqueous NH_4Cl (50 ml) and separation of the phases, the aqueous layer was extracted with dichloromethane three times (3 x 30 ml). The combined organic layers were dried over MgSO_4 and the solvents were removed to give a bright yellow oil. After adding pentane (20 ml) yellow crystals of 2-(2,4,6-trimethylphenyl)-3-(trimethylsilanylethynyl)-1,2-dihydro-[1,10]phenanthroline precipitated (1.99 g, 77%);

2-(2,4,6-Trimethylphenyl)-3-(trimethylsilanylethynyl)-1,2-dihydro-[1,10]phenanthroline:

mp. 188-190 °C; ^1H NMR (CDCl_3 , 250 MHz): δ = 0.02 (s, 9 H, 3'-H), 2.27 (s, 3 H, 8''-H), 2.31 (br s*, 6 H, 7''-, 9''-H), 5.88 (s, 1 H, N-H), 6.53 (d, J = 2.1 Hz, 1 H, 2-H), 6.71 (d, J = 2.1 Hz, 1 H, 4-H), 6.8 - 6.9 (br s*, 2 H, 3''-H, 5''-H), 6.84 (d, J = 8.3 Hz, 1 H, 6-H), 7.01 (d, J = 8.3 Hz, 1 H, 5-H), 7.24 (dd, J_1 = 8.0 Hz, J_2 = 4.3 Hz, 1 H, 8-H), 7.92 (dd, J_1 = 8.0 Hz, J_2 = 1.8 Hz, 1 H, 7-H), 9.15 (dd, J_1 = 4.3 Hz, J_2 = 1.8 Hz, 1 H, 9-H) *coalescence; IR (KBr): $\tilde{\nu}$ = 3395 (N-H), 2954 (C-H), 2137 ($\text{C}\equiv\text{C}$), 1598 ($\text{C}=\text{C}$), 1558, 1513, 1481, 1387, 1248, 1108, 1001, 920, 846 (Mes-H), 791, 758 (Ph-H), 682 cm^{-1} . Anal. Calcd for $\text{C}_{26}\text{H}_{28}\text{N}_2\text{Si}$: C, 78.74; H, 7.12; N, 7.06. Found: C, 78.51; H, 6.98; N, 6.73.

Activated manganese dioxide (5.00 g, 5.75 mmol) was added in two portions to a solution of 2-(2,4,6-trimethylphenyl)-3-(trimethylsilanylethynyl)-1,2-dihydro-[1,10]phenanthroline (3.08 g, 7.77 mmol) in CH₂Cl₂ (50 ml) and stirred for 2 h at room temperature. After drying over MgSO₄ the solvent was removed and the resulting solid was purified by column chromatography (SiO₂, CHCl₃, *R_f* = 0.35) to provide a white solid. Yield: 2.76 g (90%). Mp. 276 °C; ¹H NMR (CDCl₃, 250 MHz): δ = 0.02 (s, 9 H, 3'-H), 2.00 (s, 6 H, 7''-, 9''-H), 2.31 (s, 3 H, 8''-H), 6.87 (s, 2 H, 3''-H, 5''-H), 7.60 (dd, *J*₁ = 8.0 Hz, *J*₂ = 4.2 Hz, 1 H, 8-H), 7.76 (d, *J* = 8.5 Hz, 1 H, 6-H), 7.80 (d, *J* = 8.5 Hz, 1 H, 5-H), 8.23 (dd, *J*₁ = 8.0 Hz, *J*₂ = 1.5 Hz, 1 H, 7-H), 8.37 (s, 1 H, 4-H), 9.20 (dd, *J*₁ = 4.2 Hz, *J*₂ = 1.5 Hz, 1 H, 9-H); ¹³C NMR (CDCl₃, 53 MHz): δ = -0.6 (C-3'), 19.9 (C-7'', -9''), 21.1 (C-8''), 101.0 (C-1'), 101.9 (C-2'), 120.1 (C-3), 123.0 (C-8), 125.9 (C-3''), 126.5 (C-4a), 126.8 (C-6a), 127.7 (C-5), 129.2 (C-6), 135.7 (C-4''), 135.9 (C-7), 137.0 (C-2''), 137.1 (C-1''), 138.6 (C-4), 144.9 (C-10a), 146.1 (C-1a), 150.6 (C-9), 163.3 (C-2); IR (KBr): $\tilde{\nu}$ = 2956, 2918, 2845, 2156 (C≡C), 1614, 1584, 1547, 1467, 1396, 1299, 1249, 1179, 1156, 1104, 996, 846, 696, 636 cm⁻¹; Anal. Calcd for C₂₆H₂₆N₂Si: C, 79.14; H, 6.64; N, 7.10. Found: C, 78.80; H, 6.76; N, 6.89.

2-(4-Bromo-2,3,5,6-tetramethylphenyl)-3-(trimethylsilanylethynyl)-[1,10]phenanthroline (4b) :

1,4-Dibromo-2,3,5,6-tetramethylbenzene²⁷ (17.5 g, 60.0 mmol) was dissolved in ether (100 ml) before adding 2.5 M *n*-butyllithium (24.0 ml, 60.0 mmol, solution in hexane) dropwise over 30 minutes at 0 °C. 3 hours later the lithiation was completed (according to GC) and phenanthroline **3** (8.50 g, 30.7 mmol) was added slowly under nitrogen atmosphere over 15 minutes. The solution turned to a dark violet color, and was now stirred for 24 hours at room temperature while following the reaction by electrospray ionisation mass spectroscopy (ESI-MS). After neutralisation with saturated NH₄Cl solution (250 ml) and extraction with dichloromethane (3 x 100 ml), the organic layer was dried over magnesium sulfate. The concentrated reaction mixture (volume: 50 ml) was subsequently oxidised with MnO₂ (15.6 g, 180 mmol) for 12 hours and filtered through a pad of celite. After concentration of the filtrate the crude product was purified by column chromatography using first dichloromethane and then ether to afford a light yellow solid, which on washing with cyclohexane furnished a white solid. Yield: 10.9 g (22.4 mmol), 73 %, Mp.: 238 °C; ¹H-NMR (200 MHz, CDCl₃) δ = -

0.0016 (s, 9 H, 3'-H), 1.95 (s, 6 H, 2''H, 6''H), 2.43 (s, 6H, 3''H, 5''H), 7.60 (dd, $J_1 = 8.0$ Hz, $J_2 = 4.3$ Hz, 1 H, 8-H), 7.77 (d, $J = 8.8$ Hz, 1 H, 6-H), 7.80 (d, $J = 8.8$ Hz, 1 H, 5-H), 8.23 (dd, $J_1 = 8.0$ Hz, $J_2 = 1.8$ Hz, 1 H, 7-H), 8.38 (s, 1 H, 4-H), 9.19 (dd, $J_1 = 4.3$ Hz, $J_2 = 1.8$ Hz, 1 H, 9-H); ^{13}C -NMR (CDCl_3 , 200 MHz): $\delta = -0.6$ (C-3'), 19.5 (C-7'', C-10''), 20.9 (C-8'', C-9''), 101.0 (C-1'), 101.9 (C-2'), 120.1 (C-3), 123.0 (C-8), 125.9 (C-3''), 126.7 (C-4a), 126.8 (C-6a), 127.7 (C-5), 129.4 (C-6), 136.1 (C-4''), 135.9 (C-7), 137.2 (C-2''), 137.3 (C-1''), 138.4 (C-4), 144.9 (C-10a), 146.0 (C-1a), 150.6 (C-9), 163.8 (C-2); IR (KBr): $\tilde{\nu} = 3037, 2956, 2154 \text{ cm}^{-1}$ (C \equiv C), 1585 (C=C), 1550, 1490, 1469, 1391, 1248, 1187, 863, 843, 759, 695, 637 cm^{-1} ; MS(ESI) m/z (%): 488.5 (100) $[\text{M} + \text{H}]^+$; Anal. Calcd. for: $\text{C}_{27}\text{H}_{27}\text{N}_2\text{SiBr}$: C 66.52, H 5.58, N 5.75. Found: C 66.63, H 5.59, N 5.79.

9-Butyl-2-(2,4,6-trimethylphenyl)-3-(trimethylsilanylethynyl)-[1,10]phenanthroline (7):

Obtained as side product in the preparation of **5a**. $R_f = 0.45$ (trichloromethane) Yield: 280 mg (9%); mp. 188-190 °C; ^1H NMR (CDCl_3 , 250 MHz): $\delta = 0.04$ (s, 9 H, 3'-H), 0.94 (t, $J = 7.3$ Hz, 3 H, -CH $_3$), 1.43 (m, 2 H, -CH $_2$), 1.81 (m, 2 H, -CH $_2$), 1.89 (s, 6 H, 7'', 9''-H), 2.34 (s, 3 H, 8''-H), 3.13 (t, $J = 8.0$ Hz, 2 H, Ar-CH $_2$), 6.92 (s, 2 H, 3''-H, 5''-H), 7.49 (d, $J = 8.3$ Hz, 1 H, 8-H), 7.69 (d, $J = 8.6$ Hz, 1 H, 5-H), 7.76 (d, $J = 8.6$ Hz, 1 H, 6-H), 8.13 (d, $J = 8.3$ Hz, 1 H, 7-H), 8.35 (s, 1 H, 4-H); ^{13}C NMR (CDCl_3 , 53 MHz): $\delta = 0.6$ (Si-CH $_3$), 14.0, 20.0, 21.1, 22.6, 32.3, 38.9, 100.6 (C \equiv C), 102.2 (C \equiv C), 119.7, 123.0, 124.8, 126.6, 126.8, 127.3, 127.5, 127.9, 136.0, 136.1, 136.9, 138.8, 144.6, 145.6, 162.3, 163.7; IR (KBr): $\tilde{\nu} = 2947, 2866, 2155$ (C \equiv C), 1616, 1584, 1541, 1463, 1394, 1366, 1249, 912, 864, 845, 758, 641 cm^{-1} ; Anal. Calcd for $\text{C}_{30}\text{H}_{34}\text{N}_2\text{Si} \cdot 0.5 \text{ H}_2\text{O}$: C, 78.38; H, 7.67; N, 6.09. Found: C, 78.62; H, 7.36; N, 6.06.

2,9-Bis-(2,4,6-trimethylphenyl)-3-trimethylsilanylethynyl-[1,10]phenanthroline (5a):

A 2.5 M solution of *n*-butyllithium in pentane (12.40 ml, 31.1 mmol) was slowly added to a solution of 1-bromo-2,4,6-trimethylbenzene (3.69 g, 18.6 mmol) in dry diethylether (100 ml) at 0 °C. The solution was allowed to stir for 7 h at 0 °C (GC control). After addition of 2-(2,4,6-trimethylphenyl)-3-trimethylsilanylethynyl-[1,10]phenanthroline (1.82 g, 5.62 mmol) the solution assumed first a yellow and then a dark violet color. The mixture was stirred for 24 h at room temperature. After addition of aqueous NH_4Cl (50 ml) the layers were separated and the aqueous layer was extracted three times with dichloromethane (3 x 30 ml). The combined organic extract was stirred with 5 g of activated MnO_2 for 3 h. The mixture was

dried with MgSO_4 and filtered. After evaporation of the filtrate the resulting brown oil was purified by column chromatography (SiO_2 , trichloromethane, $R_f = 0.51$) yielding a colorless solid. Yield: 68%. Mp. 276 °C; ^1H NMR (CDCl_3 , 250 MHz): $\delta = 0.04$ (s, 9 H, 3'-H), 2.05 (s, 6 H, 7''-, 9''-H), 2.11 (s, 6 H, 7'''-, 9'''-H), 2.29 (s, 3 H, 8''-H), 2.30 (s, 3 H, 8'''-H), 6.86 (s, 2 H, 3''-H, 5''-H), 6.92 (s, 2 H, 3'''-H, 5'''-H), 7.56 (d, $J = 8.2$ Hz, 1 H, 8-H), 7.78 (d, $J = 8.9$ Hz, 1 H, 6-H), 7.85 (d, $J = 8.9$ Hz, 1 H, 5-H), 8.26 (d, $J = 8.2$ Hz, 1 H, 7-H), 8.39 (s, 1 H, 4-H); ^{13}C NMR (CDCl_3 , 63 MHz): $\delta = -0.6$ (C-3'), 20.0 (C-7'', -9''), 20.5 (C-7''', -9'''), 21.1 (C-8''), 21.2 (C-8'''), 100.7 (C-1'), 102.2 (C-2'), 119.9 (C-3), 125.1 (C-8), 125.6 (C-3''), 126.3 (C-3'''), 126.8 (C-4a), 127.5 (C-6a), 127.8 (C-5), 128.5 (C-6), 135.8 (C-4'''), 136.0 (C-4''), 136.1 (C-2''), 136.8 (C-2'''), 137.1 (C-1'''), 137.5 (C-1''), 137.9 (C-7), 138.8 (C-4), 144.8 (C-10a), 145.9 (C-1a), 160.4 (C-9), 162.6 (C-2); IR (KBr): $\tilde{\nu} = 2956, 2918, 2845, 2156$ ($\text{C}\equiv\text{C}$), 1614, 1584, 1547, 1467, 1396, 1299, 1249, 1179, 1156, 1104, 996, 846, 696, 636 cm^{-1} ; Anal. Calcd for $\text{C}_{35}\text{H}_{36}\text{N}_2\text{Si}$: C, 81.98; H, 7.08; N, 5.46. Found: C, 81.88; H, 7.35; N, 5.16.

2-(4-Bromo-2,3,5,6-tetramethylphenyl)-3-(trimethylsilylethynyl)-9-(2,4,6-trimethylphenyl)-[1,10]phenanthroline (5b) :

2.5 M *n*-Butyllithium (8.00 ml, 20.0 mmol, solution in hexane) was added slowly at 0 °C to a solution of dry ether (25 ml) containing bromomesitylene (3.90 g, 3.00 ml, 20.0 mmol). This mixture was stirred for 3 hours at room temperature while lithiation was monitored by GC. To this solution compound **4b** (5.00 g, 10.2 mmol) was added over a period of 15 minutes and the resulting violet color solution was stirred for 24 hours at room temperature. The reaction was monitored by ESI and neutralised with saturated NH_4Cl , extracted with dichloromethane. The organic layer was concentrated to 50 ml volume and oxidised with MnO_2 (5.20 g, 60.0 mmol) for 16 hours. The reaction mixture was now filtered through a pad of celite and the solvent was removed under reduced pressure. The crude product obtained was purified by column chromatography using 5% of ethylacetate in hexane affording a light brown solid which on washing with cyclohexane furnished a white solid. Yield: 5.20 g (8.50 mmol), 83 %, Mp.: 243-245 °C; ^1H -NMR (200 MHz, CDCl_3) $\delta = -0.01$ (s, 9 H, 3'-H), 1.96 (s, 6 H, 2''H, 6''H), 2.09 (s, 6 H, 2'''H, 6'''H), 2.30 (s, 3 H, 4'''H), 2.42 (s, 6 H, 3''H, 5''H), 6.90 (s, 2 H, 5'''H, 3'''H) 7.54 (dd, $J = 8.0$ Hz, $J = 4.3$ Hz, 1 H, 8-H), 7.81 (dd, $J = 9.8, 2.1$ Hz, 2 H, 5-H, 6-H), 8.24 (d, $J = 8.0$ Hz, 1 H, 7-H), 8.39 (s, 1 H, 4-H); ^{13}C -NMR (CDCl_3 , 200 MHz): $\delta = -0.5$ (C-3'), 20.0 (C-7'', C-10''), 20.4 (C-7''', C-9'''), 20.9 (C-8'', C-9''), 21.2 (C-8'''), 100.9 (C-1'), 102.0

(C-2'), 119.2 (C-3), 125.0 (C-8), 125.6 (C-3''), 126.0 (C-3'''), 126.8 (C-4a), 127.2 (C-6a), 127.6 (C-5), 128.3 (C-6), 134.9 (C-4'''), 135.2 (C-4'') 135.4 (C-2''), 136.0 (C-2'''), 137.0 (C-1'''), 137.5 (C-1''), 137.8 (C-7), 138.4 (C-4), 144.2 (C-10a), 145.7 (C-1a), 160.0 (C-9), 162.1 (C-2); IR (KBr): $\tilde{\nu}$ = 2953, 29517, 2144 cm^{-1} (C=C), 1618, 1580, 1537, 1506 1461, 1418, 1357, 1248, 1196, 1146, 1103, 1016, 988, 897, 864, 848, 759, 698, 640, 581 cm^{-1} ; MS(ESI) m/z (%): 606.6 (100) $[\text{M} + \text{H}]^+$; Anal. Calcd. For: $\text{C}_{36}\text{H}_{37}\text{N}_2\text{SiBr}$: C 71.39, H 6.16, N 4.63. Found: C 71.40, H 6.15, N 4.65.

2,9-Bis-(2,4,6-trimethylphenyl)-3-ethynyl-[1,10]phenanthroline (6a):

2,9-Bis-(2,4,6-trimethylphenyl)-3-trimethylsilylanylethynyl-10-phenanthroline (**5a**) (170 mg, 330 μmol) was dissolved in THF (10 ml) before aqueous KOH (1 N, 10 ml) was added. After stirring for 2 h the solution was diluted with aqueous NH_4Cl (20 ml) and extracted with CH_2Cl_2 (3 x 5 ml). The combined organic phases were dried over MgSO_4 . The solvents were removed yielding a colorless solid. Mp. 248 $^\circ\text{C}$; yield 138 mg (95%); ^1H NMR (CDCl_3 , 200 MHz): δ = 2.08 (s, 6 H, 7''-, 9''-H), 2.13 (s, 6 H, 7'''-, 9'''-H), 2.31 (s, 6 H, 8''-, 8'''-H), 3.13 (s, 1 H, 3'-H), 6.90 (s, 2 H, 3''-H, 5''-H), 6.92 (s, 2 H, 3'''-H, 5'''-H), 7.58 (d, J = 8.3 Hz, 1 H, 8-H), 7.80 (d, J = 8.8 Hz, 1 H, 5-H), 7.87 (d, J = 8.8 Hz, 1 H, 6-H), 8.28 (d, J = 8.3 Hz, 1 H, 7-H), 8.48 (s, 1 H, 4-H); ^{13}C NMR (CDCl_3 , 53 MHz): δ = 20.0 (C-7'', 9''), 20.5 (C-7''', -9'''), 21.1 (C-8''), 21.2 (C-8'''), 80.8 (C-2'), 82.2 (C-1'), 118.7 (C-3), 125.3 (C-8), 125.4 (C-3''), 126.5 (C-3'''), 127.0 (C-4a), 127.6 (C-6a), 128.0 (C-5), 128.5 (C-6), 135.8 (C-4'''), 136.1 (C-4''), 136.6 (C-2''), 136.7 (C-2'''), 137.4 (C-1''), 137.5 (C-1'''), 137.9 (C-4), 140.3 (C-7), 145.2 (C-10a), 145.8 (C-1a), 160.4 (C-9), 161.8 (C-2); IR (KBr): $\tilde{\nu}$ = 3274 ($\equiv\text{C-H}$), 2955, 2915, 2849, 2091 ($\text{C}\equiv\text{C}$), 1615, 1582, 1536, 1458, 1105, 848, 637, 614 cm^{-1} ; Anal. Calcd for $\text{C}_{32}\text{H}_{28}\text{N}_2 \cdot 0.25\text{H}_2\text{O}$: C, 86.35; H, 6.45; N, 6.43. Found: C, 86.18; H, 6.38; N, 6.27.

2-(4-Bromo-2,3,5,6-tetramethylphenyl)-9-(2,4,6-trimethylphenyl)-3-ethynyl-[1,10]phenanthroline (6b):

2-(4-Bromo-2,3,5,6-tetramethylphenyl)-3-(trimethylsilylanylethynyl)-9-(2,4,6-trimethylphenyl)-1,10-phenanthroline (**5b**) (2.50 g, 4.10 mmol) was dissolved in a mixture of methanol (120 ml) and THF (100 ml). A solution of KOH (150 ml, 1 N) was added slowly, stirred for 12 hours at room temperature while the reaction was monitored by ESI. Afterwards the solution was neutralised with saturated NH_4Cl and extracted with dichloromethane (200

ml). The combined organic layers were dried over magnesium sulfate. After evaporation of the solvent a yellow solid was provided that was purified by column chromatography using 5% ethylacetate in hexane as the eluent. The resultant light yellow solid afforded upon washing with cyclohexane a white solid. Yield: 2.10 g (3.90 mmol), 95%, Mp.: 227-235 °C; $^1\text{H-NMR}$ (200 MHz, CDCl_3) δ = 1.98 (s, 6 H, 2''H, 6''H), 2.11 (s, 6 H, 2'''H, 6'''H), 2.30 (s, 3 H, 4'''H), 2.42 (s, 6 H, 3''H, 5''H), 3.11 (s, 1 H, 7''H), 6.91 (s, 2 H, 3'''H, 5'''H) 7.55 (d, J = 8.0 Hz, 1 H, 8-H), 7.78 (dd, J = 9.8, 2.1 Hz, 2H, 5-H, 6-H), 8.26 (d, J = 8.0 Hz, 1 H, 7-H), 8.48 (s, 1 H, 4-H); $^{13}\text{C-NMR}$ (CDCl_3 , 200 MHz): δ = 19.8 (C-7'', C-10''), 20.2 (C-7''', C-9'''), 20.7 (C-8'', C-9''), 21.0 (C-8'''), 82.4 (C-2'), 85.7 (C-1'), 119.4 (C-3), 124.7 (C-8), 125.0 (C-3''), 126.1 (C-3'''), 126.7 (C-4a), 127.1 (C-6a), 127.7 (C-5), 128.3 (C-6), 134.8 (C-4'''), 135.2 (C-4'') 135.4 (C-2''), 136.2 (C-2'''), 136.9 (C-1''), 137.2 (C-1'''), 137.8 (C-4), 138.4 (C-7), 144.4 (C-10a), 145.7 (C-1a), 160.4 (C-9), 162.4 (C-2); IR (KBr): $\tilde{\nu}$ = 3271($\equiv\text{C-H}$), 3000, 2923, 2850 cm^{-1} (C=C), 1615, 1579, 1537, 1504, 1488, 1460, 1450 1416, 1383, 1358 1288, 1186, 1146, 1102, 1014, 983, 931, 896, 849, 761, 674, 639, 582 cm^{-1} ; MS(ESI) m/z (%): 533.5 (100) [$\text{M} + \text{H}$] $^+$; Anal. Calcd. For: $\text{C}_{33}\text{H}_{29}\text{N}_2\text{Br}$: C 74.29, H 5.48, N 5.25. Found: C 74.40, H 5.75, N 5.65.

1,4-Bis-[3-(2,9-di(2,4,6-trimethylphenyl)-[1,10]phenanthrolinyl)]butadiyne (10a):

2,9-Bis-(2,4,6-trimethylphenyl)-3-ethynyl-[1,10]phenanthroline (**6a**) (73.0 mg, 166 μmol), CuI (16.0 mg, 84.2 μmol) and $[\text{PdCl}_2(\text{PPh}_3)_2]$ (22.0 mg, 34.0 μmol) were stirred in dry benzene (20 ml) and NEt_3 (5 ml) under Ar for 16 h at 80 °C. After removal of the solvents the remaining solid was dissolved in CH_2Cl_2 and washed with aqueous KCN (2%, 20 ml). The residue was purified by column chromatography (SiO_2 , CH_2Cl_2 , R_f = 0.23) to furnish a white crystalline product. Mp. 279 °C; yield: 37.0 mg (51%); $^1\text{H NMR}$ (CDCl_3 , 250 MHz): δ = 2.03 (s, 12 H, 7''-, 9''-H), 2.10 (s, 12 H, 7'''-, 9'''-H), 2.30 (s, 6 H, 8''-H), 2.34 (s, 6 H, 8'''-H), 6.92 (s, 8 H, 3''-, 5''-, 3'''-, 5'''-H), 7.58 (d, J = 8.3 Hz, 2 H, 8-H), 7.79 (d, J = 8.8 Hz, 2 H, 5-H), 7.87 (d, J = 8.8 Hz, 2 H, 6-H), 8.27 (d, J = 8.3 Hz, 2 H, 7-H), 8.45 (s, 2 H, 4-H); $^{13}\text{C NMR}$ (CDCl_3 , 53 MHz): δ = 20.0 (C-7'', -9''), 20.5 (C-7''', -9'''), 21.1 (C-8''), 21.2 (C-8'''), 87.0 (C-1'), 94.9 (C-2'), 120.0 (C-3), 125.1 (C-8), 125.7 (C-3''), 126.8 (C-3'''), 128.0 (C-4a), 128.3 (C-6a), 128.5 (C-5), 131.6 (C-6), 135.8 (C-4'''), 136.1 (C-4''), 136.2 (C-2''), 136.8 (C-2'''), 137.3 (C-1''), 137.5 (C-1'''), 137.8 (C-4), 138.4 (C-7), 144.7 (C-10a), 145.9 (C-1a), 160.5 (C-9), 162.0 (C-2); IR (KBr): $\tilde{\nu}$ = 3024, 2918, 1854, 2210 (C \equiv C), 1614, 1578, 1535, 1457, 1392, 1292, 1156, 1107, 1030, 913, 886, 847, 774, 719, 613 cm^{-1} ; MS (ESI) m/z (%): 880.4 (100) [$\text{M} +$

$\text{H}]^+$, 440.2 (40) $[\text{M}/2 + \text{H}]^+$; Anal. Calcd for $\text{C}_{64}\text{H}_{54}\text{N}_4 \cdot \text{H}_2\text{O}$: C, 85.68; H, 6.29; N, 6.24. Found: C, 85.42; H, 6.31; N, 6.00.

1,4-Bis-[3-(2,9-di(2,4,6-trimethylphenyl)-[1,10]phenanthrolinyl)ethynyl]benzene (11a):

2,9-Bis-(2,4,6-trimethylphenyl)-3-ethynyl-[1,10]phenanthroline (**6a**) (149 mg, 338 μmol), 1,4-diiodobenzene (55.8 mg, 169 μmol), CuI (25 mg, 132 μmol) and $[\text{PdCl}_2(\text{PPh}_3)_2]$ (11.8 mg, 16.9 μmol) were stirred in dry benzene (5 ml) and NEt_3 (5 ml) under Ar for 3 d at 80 °C. The solvents were removed and the residue was dissolved in CH_2Cl_2 (30 ml). The resulting solution was washed with aqueous KCN (2%, 10 ml). The organic phase was dried over MgSO_4 and after removal of the solvent the residue was purified by column chromatography (SiO_2 , CHCl_3 , $R_f = 0.20$) and recrystallized from cyclohexane to yield a yellow solid. Yield: 80 mg (75%). Mp. 280 °C; ^1H NMR (CDCl_3 , 250 MHz): $\delta = 2.07$ (s, 12 H, 7"-, 9"-H), 2.11 (s, 12 H, 7'''-, 9'''-H), 2.31 (s, 6 H, 8"-H), 2.35 (s, 6 H, 8'''-H), 6.93 (s, 8 H, 3"-, 5"-, 3'''-, 5'''-H), 7.03 (s, 4 H, 4'-Ph-H), 7.58 (d, $J = 8.3$ Hz, 2 H, 8-H), 7.83 (d, $J = 8.8$ Hz, 2 H, 5-H), 7.88 (d, $J = 8.8$ Hz, 2 H, 6-H), 8.29 (d, $J = 8.3$ Hz, 2 H, 7-H), 8.46 (s, 2 H, 4-H); ^{13}C NMR (CDCl_3 , 53 MHz): $\delta = 20.0$ (C-7", -9"), 20.5 (C-7'''-, -9'''-), 21.1 (C-8"), 21.2 (C-8'''), 89.1 (C-2'), 94.6 (C-1'), 119.7 (C-3), 122.8 (C-3'), 125.1 (C-8), 125.6 (C-3'''), 126.8 (C-3'''), 126.9 (C-4a), 127.5 (C-6a), 127.9 (C-5), 128.5 (C-6), 131.4 (C-4'), 135.9 (C-2''), 136.1 (C-2'''), 136.2 (C-4''), 136.8 (C-1''), 137.3 (C-4), 137.6 (C-7), 137.8 (C-4'''), 138.4 (C-1'''), 144.8 (C-10a), 145.8 (C-1a), 160.5 (C-9), 162.0 (C-2); IR (KBr): $\tilde{\nu} = 2923, 2854, 2207$ ($\text{C}\equiv\text{C}$), 1698, 1613, 1580, 15363, 1503, 1457, 1400, 1293, 1144, 1106, 1065, 1031, 991, 913, 846, 774, 637 cm^{-1} ; MS (ESI) m/z (%): 955.8 (100) $[\text{M} + \text{H}]^+$, 478.5 (20) $[\text{M}/2 + \text{H}]^+$; MS (CI) (70 - 100 eV): m/z (%) = 955 (100) $[\text{M}^+]$, 427 (5) $[\text{M}]$, 279 (16), 143 (12), 114 (21), 93 (9), 85 (6); Anal. Calcd for $\text{C}_{70}\text{H}_{58}\text{N}_4 \cdot 1.5\text{H}_2\text{O}$: C, 85.59; H, 6.26; N, 5.70. Found: C, 85.47; H, 6.26; N, 5.59.

1,4-Bis-[3-(2-(4-bromo-2,3,5,6-tetramethylphenyl)-9-(2,4,6-trimethylphenyl)-[1,10]phenanthroline)-ethynyl]-benzene (11b):

2-(4-Bromo-2,3,5,6-tetramethylphenyl)-3-(ethynyl)-9-(2,4,6-trimethylphenyl)-1,10-phenanthroline (**6b**) (300 mg, 0.56 mmol), diiodobenzene (92.7 mg, 0.28 mmol), $[\text{Pd}(\text{PPh}_3)_2\text{Cl}_2]$ (9.70 mg, 0.03 mmol), and CuI (41.0 mg, 0.22 mmol) were dissolved in benzene (10 ml) and triethylamine (10 ml) under nitrogen. This reaction mixture was refluxed at 90 °C for 24 hours and monitored by ESI. It was diluted with dichloromethane (60 ml) and

washed two times with aqueous KCN solution (400 mg in 10 ml water) and finally with water. The organic layer was dried over MgSO₄. Solvent evaporation yielded a light brown solid, which was purified by column chromatography (5% ethylacetate in hexane) to give the linear ligand as a light yellow solid. Upon washing with cyclohexane a white solid was furnished. Yield: 299 mg (0.26 mmol), 92%, Mp.: 285 °C; ¹H-NMR (200 MHz, CDCl₃) δ = 2.01 (s, 12 H, 2''H,6''H), 2.11 (s, 12 H, 2'''H, 6'''H), 2.3 (s, 6 H, 4'''H), 2.46 (s, 12 H, 3'''H, 5'''H), 6.93 (s, 4 H, 5'H, 3'H), 6.98 (s, 4H, 4'-Ph-H) 7.56 (d, *J* = 8.0 Hz, 2 H, 8-H), 7.81 (dd, *J* = 9.8, 2.1 Hz, 4 H, 5-H, 6-H), 8.28 (d, *J* = 8.0 Hz, 2 H, 7-H), 8.47 (s, 2 H, 4-H); ¹³C-NMR (CDCl₃, 200 MHz): δ = 20.5 (C-7'', C-10''), 20.9 (C-7''', C-9'''), 21.0 (C-8'',C-9''), 21.1 (C-8'''), 89.0 (C-2'), 95.0 (C-1'), 119.7 (C-3), 122.7 (C-3'), 125.2 (C-8), 125.6 (C-3''), 126.8 (C-3'''), 127.1 (C-4a), 127.6 (C-6a), 128.4 (C-5), 128.5 (C-6), 129.2 (C-4'), 131.3 (C-2''), 133.5 (C-2'''), 133.6 (C-4''), 134.5 (C-1''), 136.0 (C-4), 137.5 (C-7), 137.8 (C-4'''), 138.9 (C-1'''), 144.7 (C-10a), 145.8 (C-1a), 160.6 (C-9), 162.4 (C-2); IR (KBr): $\tilde{\nu}$ = 3437 (≡C-H), 2949, 2857 cm⁻¹ (C≡C), 2209, 1614, 1584, 1532, 1504, 1458, 1416, 1383, 1261, 1162, 1141, 1100, 1016, 986,848, 771, 720, 639, 583, 544 cm⁻¹; MS(ESI) *m/z* (%): 1142.1 (100) [M + H]⁺; Anal. Calcd. for: C₇₂H₆₀N₄Br₂: C 75.79, H 5.30, N 4.91. Found: C 76.02, H 5.12, N 4.75.

4,4'-Bis-[3-(2,9-di(2,4,6-trimethylphenyl)-[1,10]phenanthrolinyl)ethynyl]-biphenyl (12a): 2,9-Bis(2,4,6-trimethylphenyl)-3-ethynyl-[1,10]phenanthroline (150 mg, 340 μmol), 4,4'-diiodobiphenyl (60 mg, 150 μmol), CuI (20.0 mg, 105 μmol), and [PdCl₂(PPh₃)₂] (23.8 mg, 34.0 μmol) in dry benzene (10 ml) and NEt₃ (2 ml) were stirred for 2 d at 85 °C. Work-up was analogous to that for **11a** (*R_f* = 0.17) and provided a yellow solid. Mp. 293 °C; yield: 87 mg (31%); ¹H NMR (CDCl₃, 250 MHz): δ = 2.10 (s, 12 H, 7''-, 9''-H), 2.12 (s, 12 H, 7'''-, 9'''-H), 2.31 (s, 6 H, 8''-H), 2.35 (s, 6 H, 8'''-H), 6.93 (bs, 8 H, 3''-, 5''-, 3'''-, 5'''-H), 7.22 (d, *J* = 8.5 Hz, 4 H, Ar-H), 7.48 (d, *J* = 8.5 Hz, 4 H, Ar-H), 7.58 (d, *J* = 8.2 Hz, 2 H, 8-H), 7.83 (d, *J* = 9.0 Hz, 2 H, 5-H), 7.89 (d, *J* = 9.0 Hz, 2 H, 6-H), 8.29 (d, *J* = 8.2 Hz, 2 H, 7-H), 8.48 (s, 2 H, 4-H); ¹³C NMR (CDCl₃, 53 MHz): δ = 20.1 (C-7'', -9''), 20.5 (C-7''', -9'''), 21.1 (C-8''), 21.2 (C-8'''), 88.1 (C-2'), 94.7 (C-1'), 120.0 (C-3), 122.2 (C-3'), 125.1 (C-8), 125.7 (C-3''), 126.7 (C-3'''), 126.8 (C-4a), 127.5 (C-6a), 127.6 (C-5') 128.0 (C-5), 128.5 (C-6), 132.1 (C-4'), 135.9 (C-2''), 136.1 (C-2'''), 136.2 (C-4''), 136.9 (C-1''), 137.3 (C-4), 137.6 (C-7), 137.9 (C-4'''), 138.4 (C-1'''), 140.2 (C-6'), 144.9 (C-10a), 145.9 (C-1a), 156.7 (C-9), 160.5 (C-2); IR (KBr): $\tilde{\nu}$ = 2919, 2860, 2202 (C≡C), 1611, 1456, 1378, 1269, 1109, 1067, 1025, 848, 820 cm⁻¹; MS (ESI)

m/z (%): 1031.3 (100) $[M + H]^+$, 515.6 (40) $[M/2 + H]^+$; Anal. Calcd for $C_{76}H_{62}N_4 \cdot 1CH_2Cl_2$: C, 82.85; H, 5.78; N, 5.02. Found: C, 82.45; H, 5.42; N, 5.11.

4,4'-Bis-[3-(2-(4-bromo-2,3,5,6-tetramethylphenyl)-9-(2,4,6-trimethylphenyl)-[1,10]phenanthrolinyl)-ethynyl]-biphenyl (12b):

Phenanthroline **6b** (300 mg, 0.56 mmol), diiodobiphenyl (114 mg, 0.28 mmol), $[Pd(Ph_3P)_2Cl_2]$ (19.7 mg, 0.03 mmol), and CuI (41.0 mg, 0.22 mmol) were dissolved in dry benzene (10 ml) and dry triethylamine (10 ml). This mixture was refluxed at 90 °C for 28 hours while monitoring the reaction by ESI. After cooling to room temperature it was diluted with dichloromethane (60 ml) and washed with aqueous KCN solution (400 mg in 10 ml water) and finally with water. The organic layer was dried over $MgSO_4$ and solvent evaporation yielded a light orange colour solid. Purification by column chromatography (20% ethylacetate in hexane) and washing with cyclohexane afforded the linear ligand **12b** as a yellow solid. Yield: 243 mg (0.20 mmol), 71 %, Mp.: 296 °C; 1H -NMR (200 MHz, $CDCl_3$) δ = 2.04 (s, 12 H, 2''H, 6''H), 2.12 (s, 12 H, 2'''H, 6'''H), 2.31 (s, 6 H, 4''''H), 2.46 (s, 12 H, 3'', 5''H), 6.92 (s, 4 H, 3'''H, 5'''H), 7.13 (d, J = 8.7 Hz, 4 H, 2', 6'), 7.49 (d, J = 8.7 Hz, 4 H, 3', 5'), 7.57 (d, J = 8.0 Hz, 2 H, 8-H), 7.82 (dd, J = 9.8 Hz, 4 H, 5-H, 6-H), 8.29 (d, J = 8.0 Hz, 2 H, 7-H), 8.49 (s, 2 H, 4-H); ^{13}C -NMR ($CDCl_3$, 200 MHz): δ = 20.5 (C-7'', C-10''), 20.9 (C-7''', C-9'''), 21.0 (C-8'', C-9''), 21.1 (C-8'''), 89.0 (C-2'), 95.0 (C-1'), 119.7 (C-3), 122.7 (C-3'), 125.2 (C-8), 125.6 (C-3''), 126.8 (C-3'''), 127.1 (C-4a), 127.5 (C-6a), 128.0 (C-5') 128.4 (C-5), 128.7 (C-6), 129.1 (C-4'), 131.9 (C-2''), 133.5 (C-2'''), 133.5 (C-4''), 134.5 (C-1''), 135.9 (C-4), 137.5 (C-7), 137.9 (C-4'''), 138.9 (C-1'''), 140.4 (C-6'), 144.7 (C-10a), 145.7 (C-1a), 160.5 (C-9), 162.4 (C-2); IR (KBr): $\tilde{\nu}$ = 3434 ($\equiv C-H$), 2920, 2855 cm^{-1} , 2207 ($C\equiv C$), 1719, 1613, 1583, 1534, 1493, 1458, 1417, 1382, 1292, 1161, 1141, 1004, 985, 912, 849, 822, 771, 755, 720, 689, 540 cm^{-1} ; MS(ESI) m/z (%): 1217.2 (100) $[M + H]^+$; Anal. Calcd. for: $C_{78}H_{64}Br_2N_4$: C 76.97, H 5.30, N 4.60. Found: C 77.24, H 5.65, N 4.48.

3-(4-[1,10]Phenanthrolin-3yl-ethynyl-phenylethynyl)-2,9-bis-(2,4,6-trimethylphenyl)-[1,10]phenanthroline (14):

2,9-Bis-(2,4,6-trimethylphenyl)-3-ethynyl-[1,10]phenanthroline (**6a**) (106 mg, 240 μ mol), 3-(4-iodo-phenylethynyl)-[1,10]phenanthroline (**13**) (98.0 mg, 240 μ mol), CuI (20.0 mg, 105 μ mol), and $[PdCl_2(PPh_3)_2]$ (10.0 mg, 12.0 μ mol) in dry benzene (10 ml) and dry NEt_3 (10 ml)

were stirred under Ar for 3 d at 85 °C. Work-up was analogous to that for **11a** ($R_f = 0.21$) providing a yellow solid. Yield: 66.0 mg (38%). Mp. > 300 °C; ^1H NMR (CDCl_3 , 250 MHz): $\delta = 2.09$ (s, 6 H, 7'''-, 9'''-H), 2.10 (s, 6 H, 7''''-, 9''''-H), 2.28 (s, 3 H, 8'''-H), 2.33 (s, 3 H, 8''''-H), 6.90 (s, 2 H, 3'''-H), 6.92 (s, 2 H, 3''''-H), 7.17 (d, $J = 8.6$ Hz, 2 H, 4'-H), 7.52 (d, $J = 8.6$ Hz, 2 H, 5'-H), 7.52 (d, $J = 8.3$ Hz, 1 H, 8''-H), 7.65 (dd, $J = 8.0$ Hz, $J = 4.4$ Hz, 1 H, 8-H), 7.77 (d, $J = 8.4$ Hz, 2 H, 6-, 6''-H), 7.84 (d, $J = 8.4$ Hz, 2 H, 5-, 5''-H), 8.26 (dd, $J = 8.0$ Hz, $J = 1.8$ Hz, 1 H, 7-H), 8.29 (d, $J = 8.3$ Hz, 1 H, 7''-H), 8.38 (d, $J = 1.9$ Hz, 1 H, 4-H), 8.48 (s, 1 H, 4''-H), 9.21 (dd, $J = 4.4$ Hz, $J = 1.8$ Hz, 1 H, 9-H), 9.26 (d, $J = 1.9$ Hz, 1 H, 2-H); ^{13}C NMR (CDCl_3 , 53 MHz): $\delta = 20.0$ (C-7''', -9'''), 20.5 (C-7'''', -9''''), 21.0 (C-8'''), 21.1 (C-8''''), 87.7 (C-2'), 88.3 (C-7'), 94.4 (C-1'), 95.0 (C-8'), 119.2 (C-3), 119.6 (C-3''), 122.4 (C-3'), 123.2 (C-8''), 125.1 (C-8), 125.6 (C-3'''), 125.9 (C-6'), 126.8 (C-4a), 126.9 (C-3''''), 127.3 (C-4a''), 127.4 (C-6a), 127.6 (C-6a''), 127.9 (C-5''), 128.3 (C-5), 128.5 (C-6''), 128.9 (C-6), 131.5 (C-4'), 131.9 (C-5'), 135.8 (C-2'''), 135.9 (C-2''''), 136.2 (C-4'''), 136.8 (C-1'''), 137.2 (C-4''), 137.4 (C-7''), 137.6 (C-4), 137.8 (C-7), 138.0 (C-4''''), 138.5 (C-1''''), 144.8 (C-10a''), 144.9 (C-1a''), 145.8 (C-10a), 145.9 (C-1a), 150.5 (C-9), 151.9 (C-2) 160.4 (C-9''), 161.9 (C-2''); IR (KBr): $\tilde{\nu} = 3205$ (s, C-H), 2202 (w, C \equiv C), 1590 (m, C=C), 1477 (s, C=C), 1415 (s), 1261 (m), 1095 (m), 1053 (m), 1202 (s), 940 (m), 818 (s, Ar-H), 729 (s, Ar-H) cm^{-1} ; MS (ESI): m/z (%): 719.4 (100) $[\text{M} + \text{H}]^+$, 360.3 (20) $[\text{M}/2 + \text{H}]^+$.

ACKNOWLEDGEMENT

We are grateful to the DFG and the Fonds der Chemischen Industrie for generous financial support.

REFERENCES

- (1) Swiegers, G. F.; Malefeste, T. J. *Chem. Rev.* **2000**, *100*, 3483-3537
- (2) a) Constable, E. C. *Pure Appl. Chem.* **1996**, *68*, 253-260.
b) Kaes, C.; Katz, A.; Hosseini, M. W. *Chem. Rev.* **2000**, *100*, 3553-3590.
- (3) a) Blanco, M. J.; Jimenez, M. C.; Chambron, J. C.; Heitz, V.; Linke, M.; Sauvage, J.-P. *Chem. Soc. Rev.* **1999**, *28*, 293-305.
b) Sauvage, J.-P. *Acc. Chem. Res.* **1998**, *31*, 611-619.
- (4) Baxter, P. N. W.; Lehn, J.-M.; Baum, G.; Fenske, D. *Chem. Eur. J.* **2000**, *6*, 4510-4517.
- (5) Garcia, A. M.; Romero-Saluelo, F. J.; Bassani, D. M.; Lehn, J.-M.; Baum, G.; Fenske, D. *Chem. Eur. J.* **1999**, *5*, 1803-1807.
- (6) Toyota, S.; Woods, C. R.; Benaglia, M.; Haldimann, R.; Wärnmark, K.; Hardcastle, K.; Siegel, J. S. *Angew. Chem.* **2001**, *111*, 773-776; *Angew. Chem. Int. Ed.* **2001**, *40*, 751-754.
- (7) Baxter, P. N. W.; Lehn, J.-M.; Kneisel, B. O.; Fenske, D. *Angew. Chem.* **1997**, *109*, 2067-2070; *Angew. Chem. Int. Ed.* **1997**, *36*, 1978-1981.
- (8) a) Schmittel, M.; Ganz, A. *Chem. Commun.* **1997**, 999-1000.

- b) Schmittel, M.; Lüning, U.; Meder, M.; Ganz, A.; Michel, C.; Herderich, M. *Heterocycl. Commun.* **1997**, *3*, 493-498.
- (9) Schmittel, M.; Ganz, A.; Fenske, D.; Herderich, M. *J. Chem. Soc., Dalton Trans.* **2000**, 353-359.
- (10) Schmittel, M.; Michel, C.; Ganz, A.; Herderich, M. *J. Prakt. Chem.* **1999**, *341*, 228-236.
- (11) Tzalis, D.; Tor, Y.; Failla, S.; Siegel, J. S. *Tetrahedron Lett.* **1995**, *36*, 3489-3492.
- (12) Sonogashira, K.; Tohda, Y.; Hagihara, N. *Tetrahedron Lett.* **1975**, 4467-4470.
- (13) Dietrich-Buchecker, C. O.; Marnot, P. A.; Sauvage, J. P. *Tetrahedron Lett.* **1982**, *23*, 5291-5294.
- (14) Schmittel, M.; Michel, C.; Liu, S.-X.; Schildbach, D.; Fenske, D. *Eur. J. Inorg. Chem.* **2001**, in press.
- (15) Comins, D. L.; Abdullah, A. H. *J. Org. Chem.* **1982**, *47*, 4315-4319.
- (16) Hay, A. S. *J. Org. Chem.* **1962**, *27*, 3320-3321.
- (17) Heck, R. F. *Palladium Reagents in Organic Synthesis*, Academic Press London, **1985**.
- (18) Meijere, A. de; Meyer, F. E. *Angew. Chem.* **1994**, *106*, 2473-2506; *Angew. Chem. Int. Ed.* **1994**, *33*, 2379-2411.
- (19) Michel, C.; Habibi, D.; Schmittel, M. *Molecules*, **2001**, submitted.
- (20) Schmittel, M.; Michel, C.; Wiegrefe, A.; Kalsani, V. unpublished results.
- (21) Balzani, V.; Juris, A.; Venturi, M.; Campagna, S.; Serroni, S. *Chem. Rev.* **1996**, *96*, 759-833.
- (22) Sammes, P. G.; Yahsioglu, G. *Chem. Soc. Rev.* **1994**, *23*, 327-334.
- (23) Joshi, H. S.; Jamshidi, R.; Tor, Y. *Angew. Chem.* **1999**, *111*, 2887-2891.
- (24) Barigelletti, F.; Flamigni, L. *Chem. Soc. Rev.* **2000**, *29*, 1-12.
- (25) Schlicke, B.; Belser, P.; De Cola, L.; Sabbioni, W.; Balzani, V. *J. Am. Chem. Soc.* **1999**, *121*, 4207-4214.
- (26) a) Schmittel, M.; Ganz, A. *Chem. Commun.*, **1997**, 999-1000.
b) Schmittel, M.; Ganz, A. *Synlett*, **1997**, 710-711.
- (27) Jannasch, P.; Fittig, R. *Zeit. Chem.*, **1870**, 162-163.

Supp 4-2

Rigid Bisphenanthrolines: Their Synthesis, Structure and Self-Assembly at the Solid-Liquid Interface and in Solution

Michael Schmittel,^{a*} Venkateshwarlu Kalsani,^a Dieter Fenske,^b Frank Jäckel,^c Jürgen P. Rabe,^c Jan W. Bats^d

^a Center of Micro and Nanochemistry and Engineering, Organische Chemie I, Universität Siegen, Adolf-Reichwein-Str., D-57068 Siegen, Germany, Fax: (+49) 271 740 3270.

^b Institut für Anorganische Chemie, Universität Karlsruhe, Engesserstr. 3045, D-76128 Karlsruhe, Germany.

^c Humboldt University Berlin, Department of Physics, Newtonstraße 15, D-12489 Berlin (Germany).

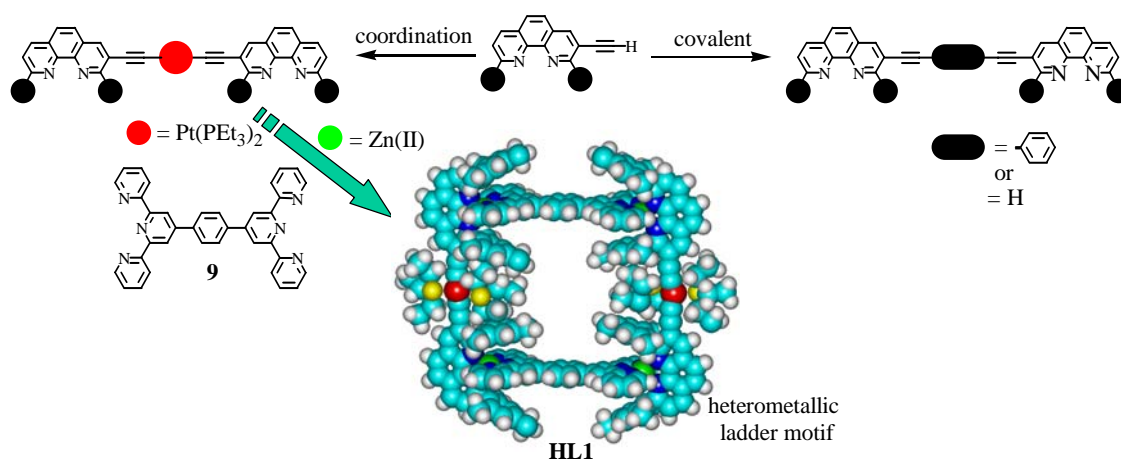
^d Institute für Organische Chemie und Chemische Biologie, Johann Wolfgang Goethe-Universität, Marie-Curie-Strasse 11, D 60439 Frankfurt am Main, Germany.

schmittel@chemie.uni-siegen.de

bisphenanthrolines, their structures, and their self-assembly at the solid-liquid interface and in solution

Abstract

Several rigid linear bisphenanthrolines with or without bulky groups at the bisimine sites were synthesized either through covalent coupling or by coordination chemistry. For three representatives, the solid state structures was elucidated. Due to their rigidity their potential was explored for multicomponent/multimetallic supramolecular ladder aggregates and for self-assembled monolayers by scanning tunnelling microscopy (STM).



Introduction

The fabrication of sparkling symmetric and aesthetic architectures by self-assembly strategies has blossomed during the past decade.^{1,2} Aside of hydrogen bonding, the coordination driven approach has assumed a particular standing in the preparation of complex aggregates.¹⁻² This approach relies on the coordination of transition metal cations to multisite ligands, such as polypyridines incorporated into oligomeric strands, that served for the preparation of helicates.

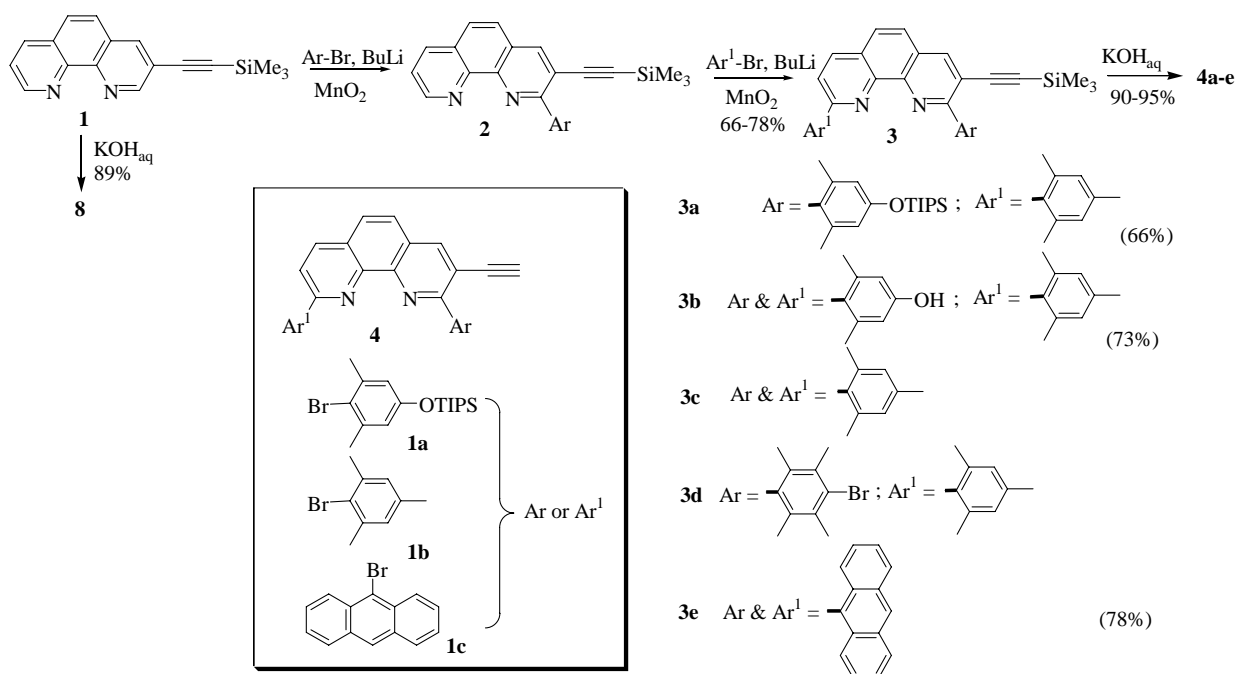
Amid the rigid multisite ligands, oligo-2,2'-bipyridines, oligo-1,10-phenanthrolines and oligo-terpyridines are the most commonly used systems due to the stiffness along their axis allowing them to assemble with a predictable geometry and coordination towards various metal ions.^{3,4} While there are numerous grids²¹ amongst the known supramolecular (dynamic) motifs, racks^{4d} and ladders⁵ have received much less coverage due to the problems with their inherent heteroleptic construction, that can not be solved by using simply self-recognition and positive cooperativity principles. Recently, Schmittel *et al.* have proposed two general strategies to engineer heteroligand metallo-supramolecular structures, that is the HETPHEN⁶ (**h**eteroleptic **p**henanthroline complexes) and the HETTAP⁷ (**h**eteroleptic **t**erpyridine **a**nd **p**henanthroline) concept. Ligands designed along those concepts will lead to exclusive heteroleptic dynamic aggregation in solution when combined with the appropriate metal ions. Several oligo-phenanthrolines have already been prepared earlier⁸ and used in the self-assembly of nanoscale structures, such as heteroleptic grids, racks, ring-in-ring structures, nanobasket, nanobox and nanoladder motifs.^{4b-d,7}

In the following, we present the synthesis of several new nanoscale rigid bisphenanthrolines, their structures, and their self-assembly at the solid-liquid interface and in solution. As both the HETPHEN and HETTAP concept^{6,7} critically depend on the proper fine tuning of steric hindrance and π,π -interactions, the linear bisphenanthrolines⁹ must be equipped with bulky substituents at the bisimine binding sites.

We have recently reported about phenanthroline building blocks with alkylaryl groups as steric stoppers, that serve as a blueprint for the ligands of the present study. Herein, we will use anthracenyl¹⁰ and new alkylaryl groups as steric stoppers, that should equally prevent any homoleptic complex formation in presence of various metal ions. But while earlier we used exclusively a covalent route, we will here additionally investigate a coordinative (with *trans*-Pt(PEt)₂Cl₂) roadmap for the preparation of ligands **5-7**.

Synthesis and properties of sterically encumbered bisphenanthrolines **5,6**

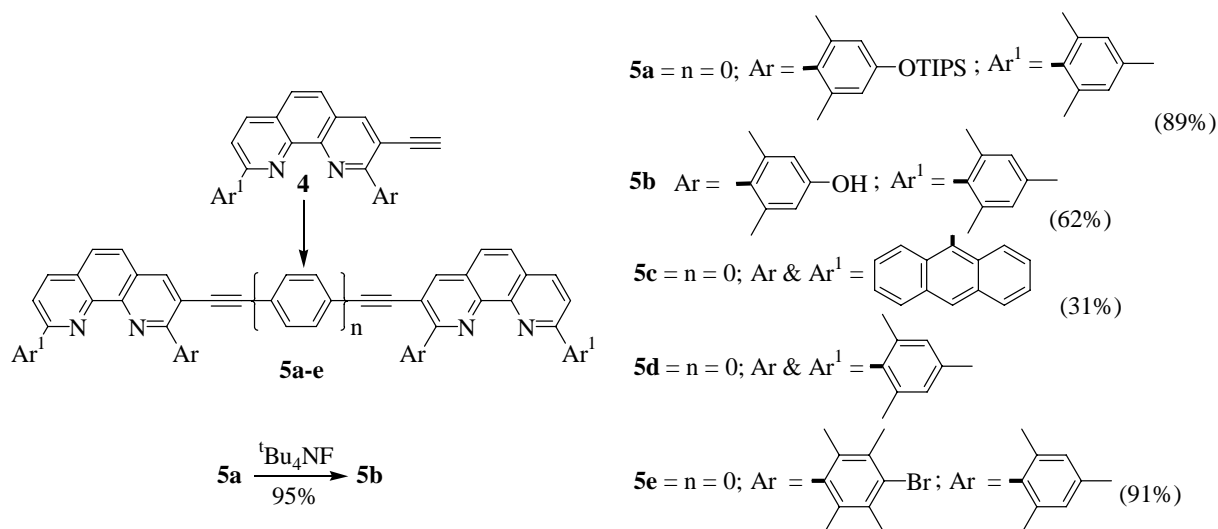
The steric stoppers were added to **1** in 2- and 9-position by a stepwise nucleophilic substitution protocol developed by Sauvage (Scheme 1).¹¹ The addition products were isolated and oxidized with activated manganese dioxide to afford finally the disubstituted phenanthrolines **3a-e**.¹² Deprotection of **3a-e** with aqueous KOH afforded the useful precursors **4a-e** for the bisphenanthrolines **5, 6** and **7**.



Scheme 1. Synthesis of ethynyl phenanthrolines as building blocks (**4a-4e**).

Similar to the procedure in a previous report, Pd/Cu-catalyzed Sonogashira coupling¹³ of **4a** or **4b** with 1,4-diiodobenzene afforded the corresponding bisphenanthrolines **5a** or **5b** in good yields (89% and 62%) (Scheme 2). **5b** could also be obtained by the deprotection of **5a** in 95% yield. Isolation of the pure **5a** was readily achieved by column chromatography and subsequent recrystallization from cyclohexane. **5b** was isolated by repeated recrystallization from DMF. Ligands **5c**, **5d**, and **5e** were obtained in coupling reactions from **4c-4e**. For best yields, the reaction was monitored by ESI-MS spectroscopy. Even under stingently dry

conditions, homocoupled phenanthrolines were found in traces. All bisphenanthrolines were characterized by ^1H -, ^{13}C -NMR, ESI MS, UV/vis and elemental analysis.



Scheme 2. Synthesis of bisphenanthrolines **5a-5e**.

Ligand **5b** proved to be insoluble in many solvents (acetone, chlorinated solvents (sparingly soluble), nitromethane, DMSO and acetonitrile), while it was soluble in dimethylformamide (DMF) upon heating. Upon cooling the DMF solution, suitable single crystals of ligand **5b** were furnished for X-ray crystal structure analysis (Figure 1).¹⁴ To the best of our knowledge, **5b** is the first single crystal structure of this series of rigid bisphenanthrolines.

The stick and spacefilling representation of **5b** is depicted in Figure 1. Surprisingly, this molecule exhibited a *cisoid* conformation in the solid state that is most likely driven by weak intermolecular hydrogen bonding (2.8 Å) leading to extended arrays of molecules at the intermolecular level (Figure 1c). From the space filling representation the amount of sterics loaded in this series of ligands becomes obvious. It is this bulk that prevents any homoleptic complex formation even at elevated temperatures.

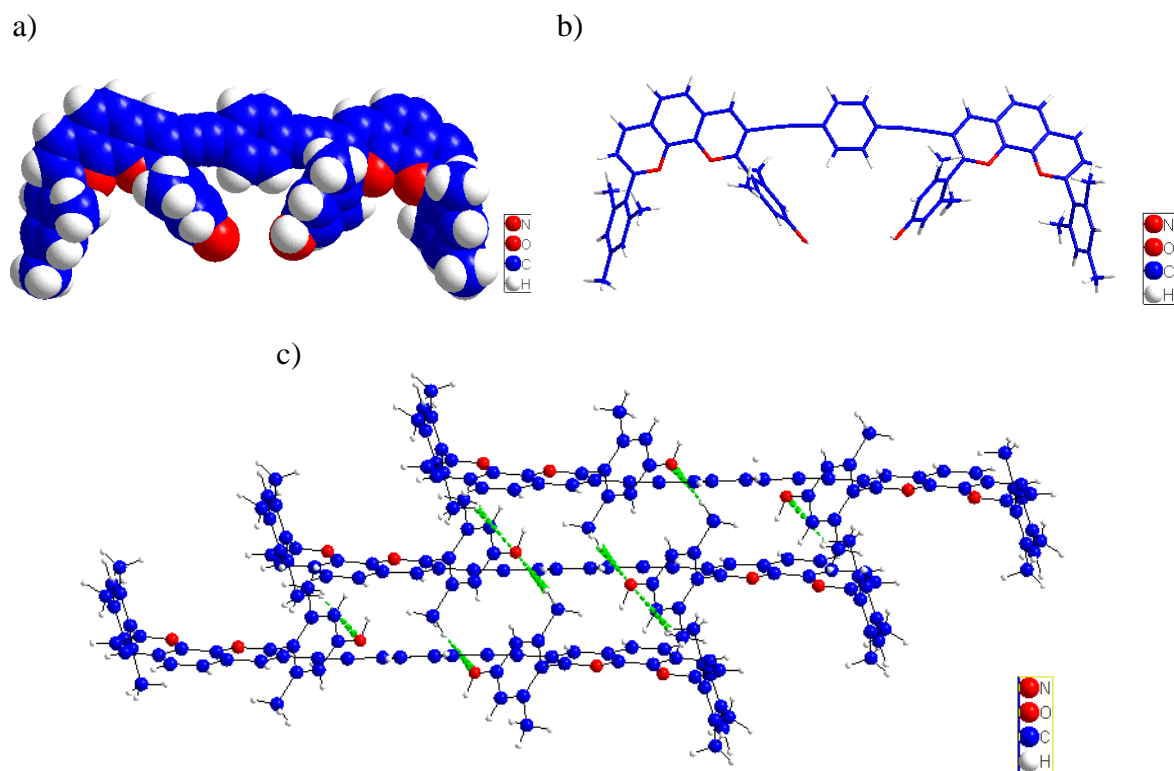


Figure 1. Single crystal structure of **5b**: a) space filling representation b) stick representation c) intermolecular hydrogen bonding (2.8 Å).

The absorption and emission properties of the sterically loaded bisphenanthrolines **5a-e** were investigated in dichloromethane solution at rt (Figure 2). The UV-vis absorption spectra of the bisphenanthrolines displayed well resolved, intense bands at ~230-380 nm. These absorptions were assigned to π - π^* transitions originating from the phenyl and pyridyl rings as well as from the ethynyl fragments. The lowest energy band is shifted progressively toward lower energy with increasing number of conjugated π electrons.¹⁵ For example, ligand **5a** and **5b** with a total of 62 conjugated π electrons exhibited a maximum of absorption at ~380 nm, whereas ligands **5d** and **5e** (with a total of 56 conjugated π electrons) showed the absorption at ~375 nm.

The fluorescence emissions were found not to depend on the excitation wavelength. Similar to the absorption behaviour, the fluorescence bands were shifted progressively toward lower energy upon increasing the number of conjugated π electrons (Figure 2b).

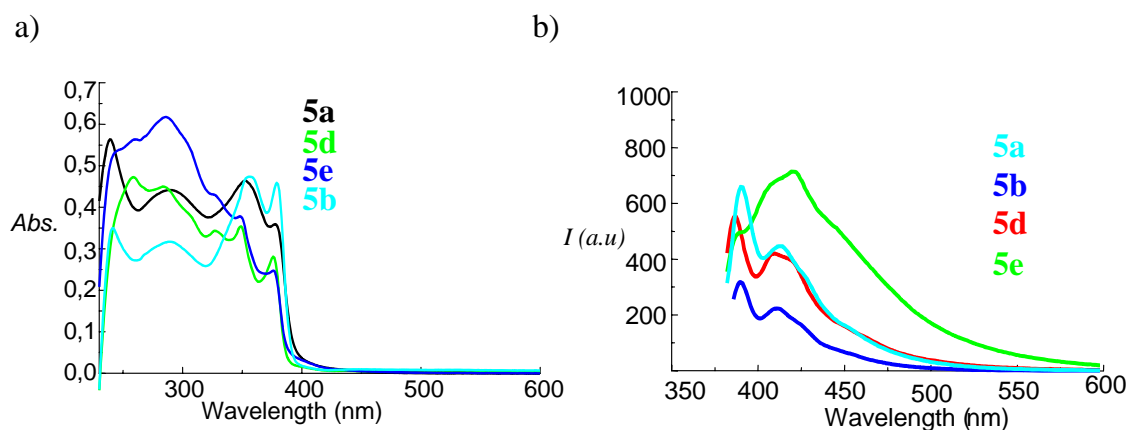
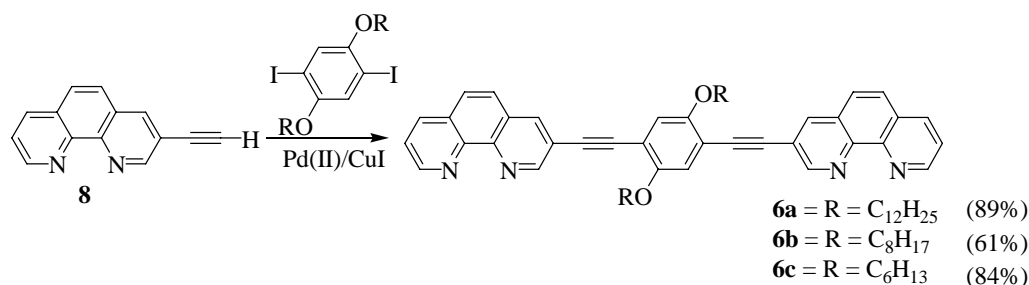


Figure 2. Absorption (a) and emission (b) spectra of bisphenanthrolines (**5a-b,d-e**) in dichloromethane. (1.6×10^{-5} M). (λ_{max} 389 nm).

Synthesis of unshielded bisphenanthrolines **6** and their self-assembly at solid-liquid interfaces

In order to realise heteroligand assemblies in combination with **5a-5e**, access to unshielded bisphenanthrolines is warranted. Grummt and others¹⁶ have reported on the synthesis of several bisphenanthrolines, including **6a**, and their photophysical properties; however, their self-assembly behaviour at the solid-liquid interface and in solution has not been explored. We have recently utilised these ligands to prepare multi-component rack and grid motifs.^{4b,4d} Herein, we present the synthesis of **6a-6c** (Scheme 3), their solid state structures (**6a** and **6b**) and their self-assembly behaviour at the solid-liquid interface (**6a** and **6c**).

Ligands **6a-6c** were synthesized using similar conditions as mentioned above through a Sonogashira coupling reaction.



Scheme 3. Synthesis of 2,9-unsubstituted bisphenanthrolines, **6a-6c**.

Suitable single crystals of **6a**¹⁷ (Figure 3) and **6b**¹⁸ (Figure 4) were obtained by the slow evaporation of a dichloromethane solution. The single crystal structure analysis of **6a**

provided ample information about intermolecular packing due to π - π stacking (~ 3.5 Å) and parallel alignment of the alkyl chains. Similar to **5b**, this molecule also crystallized in a *cisoid* conformation. Ligands **6a** and **5b** exhibited a length of ~ 3 nm along the bisphenanthroline axis which might be the reason why it was difficult to obtain suitable single crystals for this series of compounds. Intermolecular interactions between dichloromethane (solvent) and phenanthroline bisimine site could also be noticed; however, due to the poor crystal quality the role of the solvent was not explored in more detail.

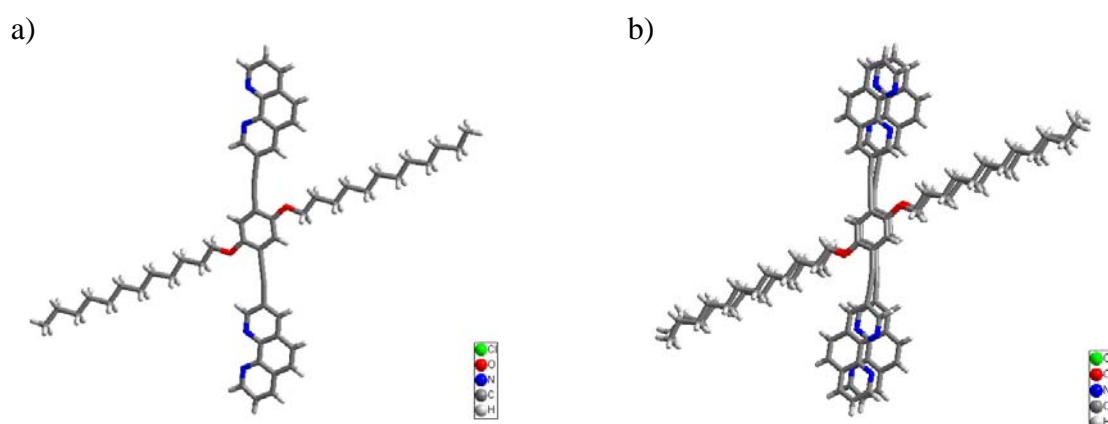


Figure 3. Single crystal structure of **6a**: a) stick representation. b) Solid state dimer due to intermolecular π - π stacking (~ 3.5 Å).

The single crystal structure of **6b** showing a *transoid* arrangement of the two phenanthroline binding sites is shown in Figure 4. The molecule is centrosymmetric with a crystallographic inversion center at the midpoint of the central planar benzene ring. The phenanthroline group is almost planar, with a mean deviation from an ideal plane of 0.021 Å. The asymmetric unit contains dichloromethane as a solute. The dichloromethane donates a weak bifurcated hydrogen bond to the nitrogen atoms N1 and N2 (Figure 4b). A similar bifurcated interaction involving a chloroform molecule was found in a 1,10-phenanthroline-3-ylethynyl compound reported by Lindner *et al.*¹⁹ The solvent is also involved in six intermolecular C-H...Cl interactions with H...Cl distances between 2.93 and 3.14 Å. The crystal packing also shows a number of intermolecular π - π interactions with C...C distances between 3.39 and 3.52 Å and a number of weak intermolecular C-H... π (C) interactions.

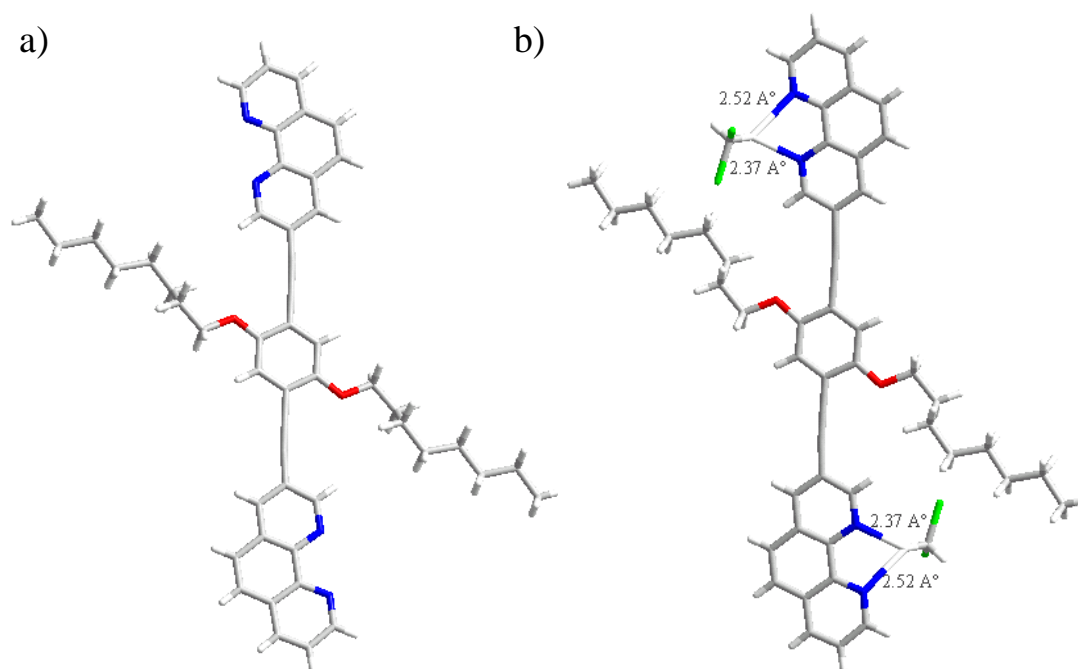


Figure 4. Single crystal structure of **6b**: a) stick representation. b) intermolecular interactions between the solvent (dichloromethane) and **6b** (N...H \sim 2.37-2.52 Å).

Self-assembly at the solid-liquid interface:

Recent years have witnessed the significance of self-assembly of organic compounds in the context of nanomaterials and nanotechnology. In particular, nano-patterning has become one of the hot subject.²⁰ Thanks to scanning tunneling microscopy (STM) a sub-molecular image resolution has been achieved for surface arrangements.²¹ Several groups have investigated the patterning of organic molecules²² and supramolecular aggregates, such as hydrogen bonded assemblies²³ at the solid-liquid interface. Organic molecules possessing coordinating functionalities, such as pyridine,²⁴ bipyridine,²⁵ phenanthroline or terpyridine²⁶ are of particular interest due to their potential use in preparing metallo-supramolecular aggregates. Recently, Schryver and Schubert have reported on the surface patterning of bipyridines and terpyridines. Ordered monolayers of these molecules, which are able to interact with metal ions, could potentially act as templates to generate highly ordered metal surfaces. In the following, we report the formation of highly ordered monolayers of two bisphenanthrolines (**6a** and **6c**) at the solid-liquid interface. Their self-assembly on surfaces is of special interest due to their exciting photophysical properties²⁷ and their potential for the construction of nanoordered metallo-supramolecular aggregates.

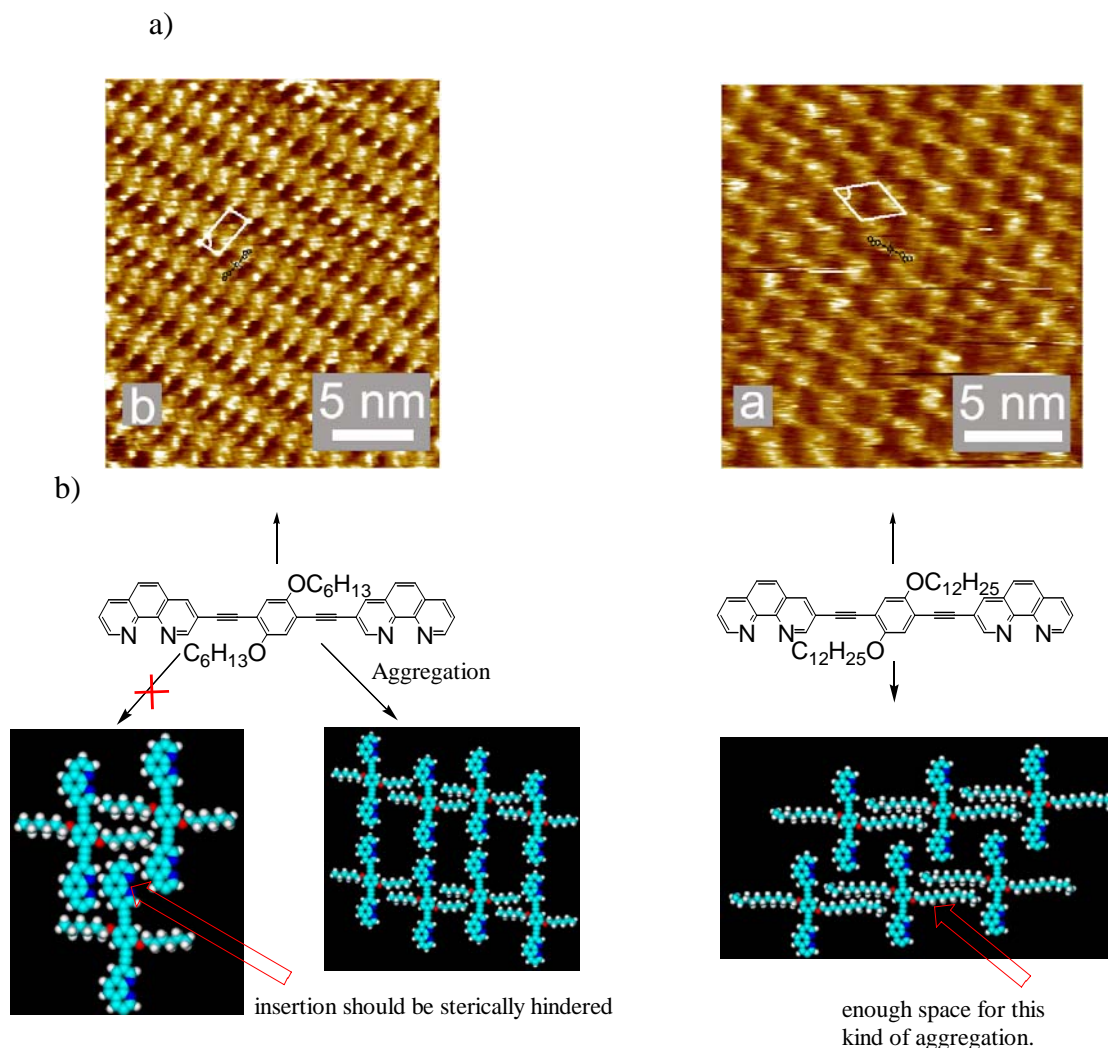
Results and Discussion²⁸

Figure 5. a) Self-assembly of two bisphenanthrolines at the solid-liquid interface. b) Plausible explanation for the two different arrangements.

As shown in Figure 5, the length of the alkyl chains of **6a** and **6c** determines apparently the morphology of their self-assembled monolayers on highly oriented pyrolytic graphite (HOPG). Bisphenanthrolines having shorter alkyl chains than C_6 prefer *type-b* pattern, whereas those with longer C_n chains prefer *type-a* pattern (Figure 6). In case of C_{12} alkyl chain the surface pattern (*type-a*) is in good agreement with its solid state structure intermolecular packing. Modelling studies propose that in case of bisphenanthrolines containing alkyl chains of less than C_6 , there is a space problem for arrangements of *type-b*. In contrast, in case of molecules with $C_n > C_6$ there is enough space for the insertion of other phenanthroline building block. This alkyl chain length effect on the monolayer morphology of the supramolecular synthons **6a** and **6c** represents an further example of structural effects on

the morphology, as it was previously observed in monolayers formed on HOPG of alkanolic acids and derivatives of anthracene.²⁹ Future studies will focus on realising solid-liquid patterning of complex supramolecular aggregates, for example built from **6a**, **6b** and **6c**, and their use as templates for ordering of metal nanoparticles on the surface.

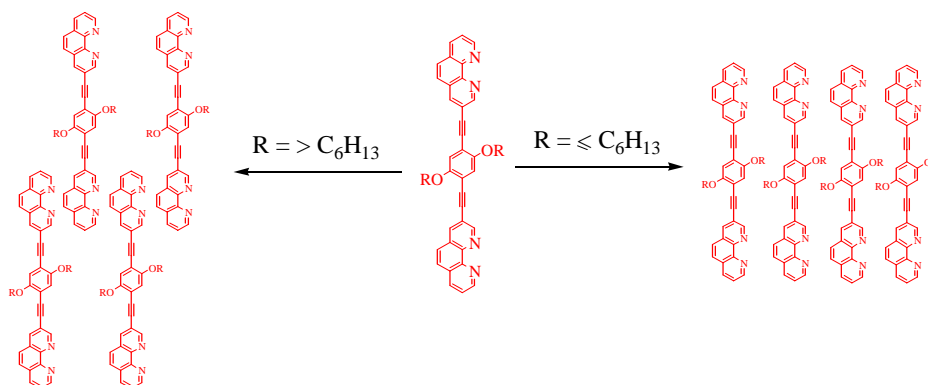
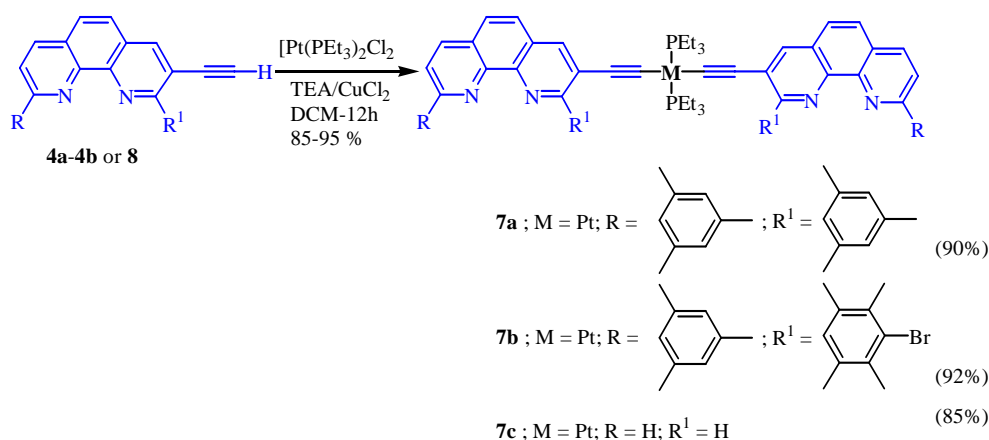


Figure 6. Generalised representation of the ordering of bisphenanthrolines **6a** and **6c** at the solid-liquid interface.

Synthesis of Pt-linked bisphenanthrolines

Ziessel and others have studied extensively the synthesis and photophysical properties of conjugated polypyridyl ligands and complexes.³⁰ Recently, the interest has shifted towards polypyridyl building blocks connected through metal units and their photophysical properties in relation to their all carbon counter parts.³¹ However, these novel ligands have not found ample recognition with respect to supramolecular chemistry and self-assembly, although their use should provide direct access to heterometallic architectures.³² Consequently, we have decided to investigate the synthesis of the Pt-linked bisphenanthrolines **7a-c** and their use in the formation of heterometallic nanoscale ladder motifs.



Scheme 4. Self-assembly of Pt-linked bisphenanthrolines.

The Pt-linked bisphenanthrolines (**7a-c**) were prepared according to a general procedure by Lin *et al.*³³ Ligands **7a-c** were synthesized from **4a-b**, **8** and [*trans*-Pt(PEt)₂Cl₂] (2:1 mol ratio) in presence of an excess of triethylamine as a base and of CuCl₂ (0.01 equiv.) as a catalyst (Scheme 4). It has to be mentioned here that under these conditions no homocoupling product was formed, which was a major problem using Sonogashira coupling conditions.⁸ Also ligands **7** showed a better solubility than the ligands **5** and **6**. Bisphenanthrolines **7** were isolated either by simple precipitation from dichloromethane/hexane (9:1) or after a filter column (eluent: hexane/ethyl acetate/dichloromethane: 7:2:1). All complexes were characterized by ESI-MS, ¹H-, ³¹P-, ¹³C-NMR, IR, UV-Vis and elemental analysis. Ligands **7a-b** were designed according to the HETPHEN concept, *i.e.*, the 2,9-positions of the phenanthroline sites were loaded with steric stoppers in order to prevent homoleptic coordination. In contrast, ligand **7c** does not carry any 2,9-steric stopper; thus it can self-assemble to homoleptic aggregates. In the ¹H NMR spectra, the proton signals assigned to the phenanthroline ligand are shifted up-field for the new complexes **7a-c** compared with those of the precursor ligands **4a-4b** or **8**. The most diagnostic upfield shifts are observed for 4-H_{phen} due to the coordination, which experienced a ~1 ppm shift (δ 9.1 to 8.2 ppm: Figure 7). The neutral Pt complexes were readily characterised by ESI MS.³⁴ The signals obtained from ESI MS were further confirmed by comparing their isotopic distribution with the calculated ones (Figure 8).

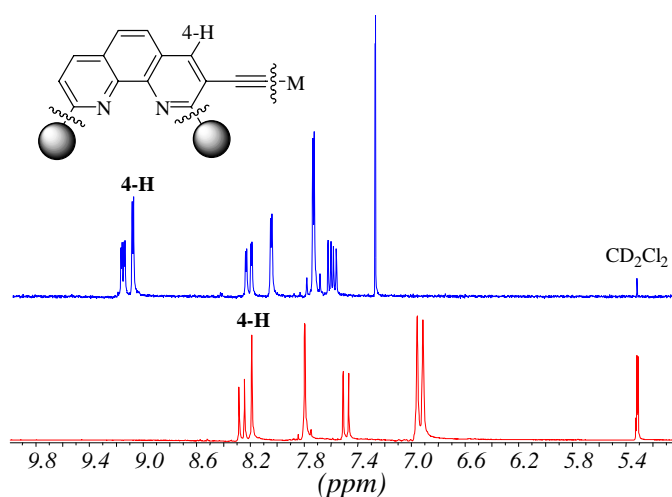


Figure 7. Aromatic region of **7d** (blue) and **7a** (red).

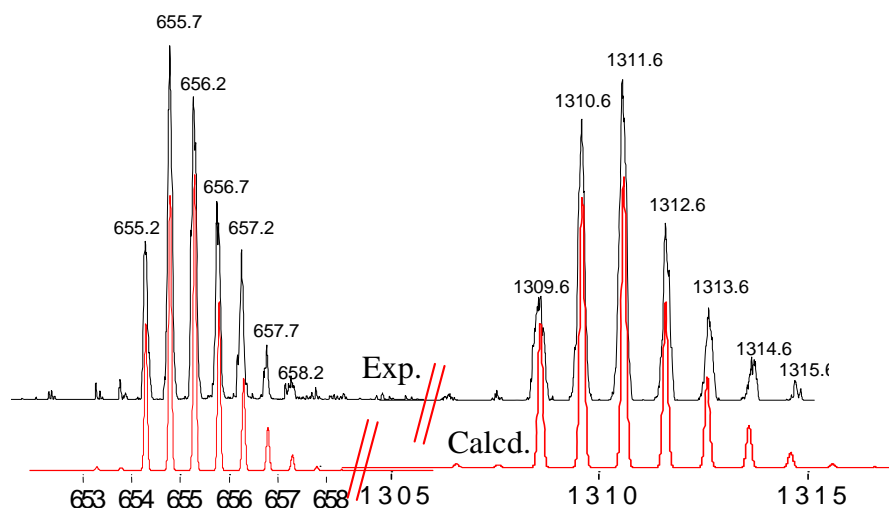


Figure 8. Isotopic distributions of one (right) and two (left) charged species of **7a**.

Absorption and Emission Spectra

The electronic properties of **7a-c** were investigated in dichloromethane at rt. The UV-vis absorption spectra of bisphenanthrolines **7a-c** displayed well resolved and intense bands lying at ~230-380 nm (Figure 9a). These transitions were assigned to π - π^* bands originating from phenyl and pyridyl rings as well as from the ethynylene fragments (Figure 11a, see manuscript 2 for the detailed description). Again, the lowest energy band is very much dependent on the number of conjugated π electrons. Thus, a higher value was observed for **7a** and **7b** (56 conjugated π electrons) than for **7c** (32 conjugated π electrons).

Similar to the trend observed with the wavelength of absorption, the fluorescence emission spectra were also dependent on the number of conjugated π electrons (Figure 9b). Ligand **7c** with a number of 32 conjugated π electrons exhibited the lowest fluorescence emission maximum in comparison to ligands **7a** and **7b** (with a total of 56 number of conjugated π electrons).

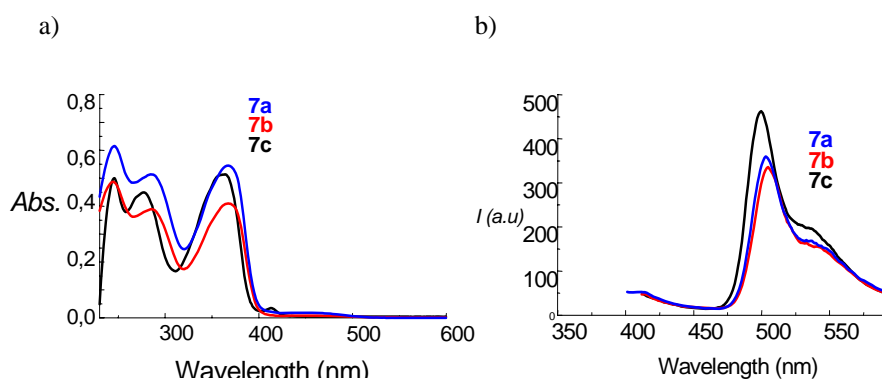
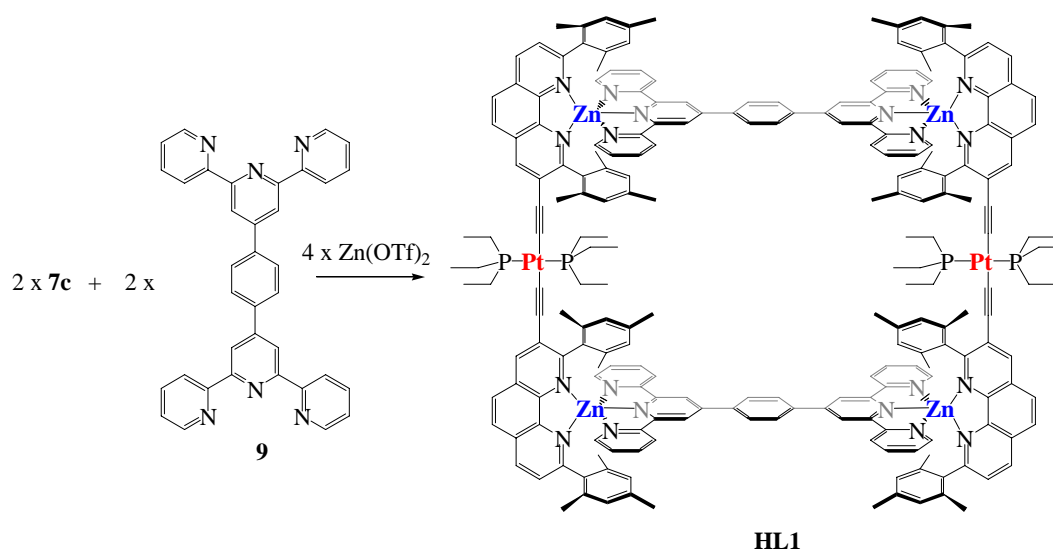


Figure 9. Absorption (a) and emission spectra (b) of Pt-linked bisphenanthrolines (**7a-c**) in dichloromethane at rt (1.6×10^{-5} M).

Stepwise Construction of a Heterometallic/Heteroleptic Ladder, HL1

As discussed earlier, Pt-linked bisphenanthrolines are expected to yield heterometallic nanoscaffolds when reacted according to the HETPHEN or HETTAP (**heteroleptic phenanthroline/heteroleptic terpyridine and phenanthroline**)³⁵ concepts. Recently, there has been a growing interest for discrete heterometallic structures due to their potentially new properties. Due to our success with the HETPHEN and HETTAP principles, it was of interest to explore the utility of ligands **7** in the preparation of discrete heterometallic nanostructures. Herein, we present the synthesis of a heterometallic (comprised of two different sorts of metal ions) and heteroleptic (two different ligands) ladder. Since the present strategy allows for a two step sequential assembly,^{32,36} a controlled incorporation of two different metal centers (Pt/Zn) at specific sites (Scheme 5) of the heteroligand aggregate was readily achieved.



Scheme 5. Self-assembly of heterometallic/heteroleptic nanoladder motif **HL1**.

According to HETTAP concept, the combination of bisphenanthroline **7c** and bisterpyridine **9**³⁷ was expected to yield the novel structure **HL1**. Indeed, **HL1** was formed quantitatively upon complexation of **7c** with **9** in presence of $\text{Zn}(\text{OTf})_2$ (1:1:2). The resulting heterometallic structure was characterised by $^1\text{H-NMR}$, $^{13}\text{C-NMR}$, $^{31}\text{P-NMR}$, ESI-MS, and elemental analysis. The $^1\text{H NMR}$ of **HL1** displayed a single set of sharp signals with characteristic high field shifts for the mesityl protons ($\delta \sim 7.0$ to ~ 6.0 ppm) indicative of the formation of a heteroleptic complex. Likewise, ESI MS showed a single set of signals corresponding to $\text{HL1}^{(8-n)+}$ with $n = 4$ and 5. The isotopic distribution of these signals was in good agreement

with the calculated ones (Figure 10a). In addition, ^{31}P NMR showed a single set of signals centred at 15.6 (with its Pt-satellites; Figure 10b). These assignments are in accordance with our previous report on similar heterometallic motifs.³⁸

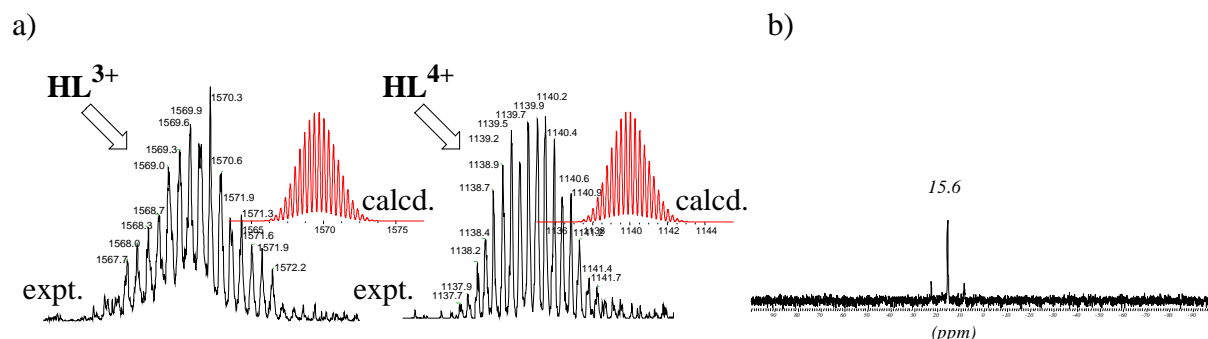


Figure 10. a) Isotopic distributions of 3+ and 4+ charged species (dark: xperimental, red: calculated). b) ^{31}P NMR spectra of **HL1** in dichloromethane (162 MHz).

Because suitable crystals for X-ray structure determination could not be obtained, the dimensions of the nanoladder were assessed from a MM+ force field minimised structure.³⁹ As depicted in Figure 11, the dimensions of **HL1** were 2.8 nm (extension along the bisphenanthroline) and 2.2 nm for the Zn-Zn diagonal.

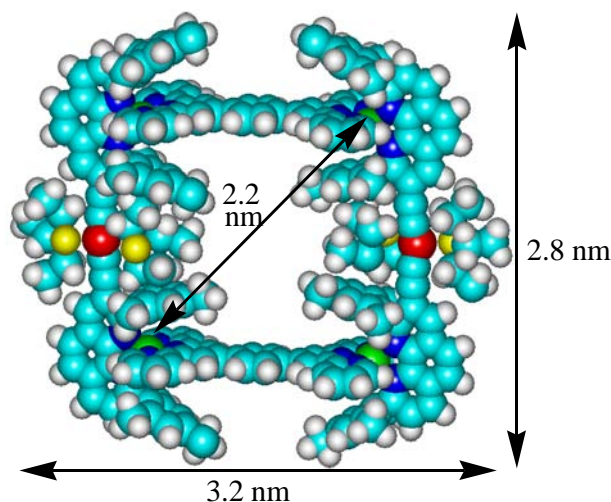


Figure 11. Space filling model of **HL1** optimised with the MM+ force field simulation. Alkoxy chains are omitted for clarity. Key: cyan = C, white = H, blue = N, yellow = P, green = Zn, red = Pt.

Conclusions

Several rigid linear bisphenanthrolines with or without bulky groups at the bisimine sites were synthesized either through covalent coupling or by coordination chemistry. For three representatives the solid state structures was elucidated. Due to their rigidity their

potential was explored for multicomponent/multimetallic supramolecular ladder aggregates and for self-assembled monolayers by scanning tunnelling microscopy (STM). Future studies will focus on surface chemistry of these ligands in presence of an metal cations and their photophysical studies.

Experimental

All reagents were commercially available and used without further purification. The solvents were dried with appropriate desiccants and distilled prior to use (CH_2Cl_2 from P_2O_5 , MeCN from P_2O_5 and NaH, diethylether from Na). ^1H NMR spectra were recorded on Bruker AC 200 (200 MHz) and Bruker AC 400 (400 MHz) spectrometers (using the deuterated solvent as the lock and residual solvent as the internal reference). IR spectra were recorded on a Perkin-Elmer 1605 FT-IR. - Microanalyses were carried out with a Carlo Erba Elemental Analyzer 1106. Electrospray mass spectra (ESI-MS) were recorded using a ThermoQuest LCQ Deca. The degree of lithiation was readily monitored by GC, while progress of the substitution at phenanthroline was best controlled by ESI-MS. **1b**, **1c** and **9** were purchased from Fluka or Aldrich and used as received. **1** and **8** were prepared according to the known procedures. For a complete characterization of **6a** see ref 12.

STM at the solid-liquid-interface⁴⁰ was performed using a home-built beetle-type STM interfaced with a commercial controller (Omicron). STM tips were prepared by mechanically cutting a 0.25 thick Pt/Ir (80%/20%) wire. A drop of an almost saturated solution of the bisphenanthrolines in 1,2,4-trichloro-benzene was applied to the basal plane of freshly cleaved highly oriented pyrolytic graphite (HOPG). The lattice of the underlying substrate could be visualised during measurements by simply changing the tunneling parameters to small tunneling impedance. This allows in-situ *x-y*-calibration of the piezo-scanner and drift-correction of the images recorded.

Molecular modelling was done with the MM+ force field as implemented in Hyperchem 6.02.³⁹

General procedure for the addition of aryl units to the 2 and 9-positions of the phenanthroline building blocks (for preparation of 3a-3e).

In a typical procedure, a 2.5 M solution of n-butyllithium in hexane (8.30×10^{-3} mmol) was slowly added to a solution of bromoarene **1a** or **1b** or **1c** (8.30×10^{-3} mmol) in diethyl ether (20 ml) at 0 °C. The solution was allowed to stir for 4 h at rt, then a suspension of **1** or **2** (4.15×10^{-3}) in diethylether (20 ml) was added at 0 °C during 10 minutes. The solution immediately

turned dark violet. The mixture was stirred for 24 h at room temperature. Prolonged reaction times led to the formation of unwanted products. The additions were very sensitive to moisture. Best yields were obtained by monitoring the reaction using ESI MS. After the reaction had been completed, saturated NH_4Cl (25 ml) was added, and the layers were separated. The aqueous layer was extracted 3-4 times with dichloromethane (4 x 50 ml). The combined organic extracts were stirred with activated MnO_2 (8.31×10^{-2} mmol) for 12 h. The mixture was then filtered through celite, dried over MgSO_4 and evaporated. The resulting solid was separated by column chromatography (SiO_2 , initially hexane, then later dichloromethane). The products were received as white to pale yellow solids.

General procedure for the TMS or TIPS deprotection (for preparation of 4a-4e or 5b):

TMS deprotection: Typically, the 3-trimethylsilanylethynylphenanthroline building block (**4a-e**, 1.95×10^{-1} mmol) was first dissolved in THF/MeOH, then aqueous KOH (1 N, 10 ml) was added. After stirring for 12 h the solution was diluted with aqueous NH_4Cl and extracted with CH_2Cl_2 . The combined organic layers were dried over MgSO_4 and the solvents were removed to yield colorless solid. They were further purified by column chromatography (SiO_2 , dichloromethane) to yield product as white crystalline material.

TIPS deprotection:⁴¹ A solution of THF (12 ml) and H_2O (12 ml) containing **5a** (200 mg, 1.57×10^{-1} mmol) and $(^t\text{Bu})_4\text{NF} \cdot 3\text{H}_2\text{O}$ (248 mg, 7.86×10^{-1} mmol), was stirred for 12 h under argon at room temperature. An aqueous pH 7.0 buffer solution was added until a solid began to precipitate. Then THF and water were evaporated under vacuum. The resulting solid was washed with water several times to afford the phenol **5b** as light yellow solid. Yield, 87%.

General Procedure for Sonagashira coupling reactions (5a-b):

3-Ethynylphenanthroline block (**4X-b**) (1.6×10^{-3} mol), CuI (1.66×10^{-3} mol) and $[\text{PdCl}_2(\text{PPh}_3)_2]$ (1.66×10^{-4} mol) were stirred in dry benzene (15 ml) and NEt_3 (15 ml) under argon for 24 h at 80 °C. The reaction was monitored by ESI MS or TLC. After removal of the solvents, the remaining solid was dissolved in CH_2Cl_2 and washed with aqueous KCN (50 ml, 2% w/v). The residue was purified by column chromatography (SiO_2 , hexane at first and CH_2Cl_2 later) to furnish a white crystalline product.

General Procedure for homocoupling coupling reactions (5c-e):

4c-e (2.27×10^{-2} mmol) were reacted with catalytic amounts of anhydrous CuCl (3.06 g, 30.9 mmol eq)/CuCl₂ (3.06g, 2.27×10^{-3} mmol) and triethylamine (2 ml). The solution was stirred for 24 h under O₂ (the flask containing the reaction mixture was stoppered with a drying tube filled with CaCl₂ so that the mixture was protected against moisture but in contact with the air) while monitoring the reaction by ESI MS.⁴² Thereafter, the solvent was removed, and the remainder was washed with water (4 x 50 ml). After drying over MgSO₄ the solvent was evaporated. The resulting mixture was separated by column chromatography using dichloromethane/methanol. As ligand **5c** was sparingly soluble in many of the solvents, it was purified by precipitation (dichloromethane) leading to poor yields.

General Procedure for Pt-linked bisphenanthrolines (7a-7c):

Ligand (**4c-d, 8**; 1.87×10^{-1} mmol) was treated with *trans*-[Pt(PEt₃)₂]Cl₂ (9.37×10^{-2} mmol) and triethylamine (TEA, 1 ml) in dichloromethane (75 ml). The reaction was monitored by ESI MS. After 24 h the solvent was removed and the resulting yellow solid was washed with water. The organic layer was separated, dried over MgSO₄, evaporated to dryness and purified by either recrystallisation in a dichloromethane/hexane mixture (8:2) or by column chromatography (SiO₂, dichloromethane). All the obtained ligands were well soluble in chlorinated solvents.

Procedure for the formation of ladder (HL1) motif:

HL1 was prepared by reacting **7c** (5.0 mg, 3.81×10^{-3} mmol) and **9** (2.06 mg, 3.81×10^{-3} mmol) with Zn(OTf)₂ (2.77 mg, 7.63×10^{-3} mmol) (1:1:2 equiv.) in dichloromethane/methanol (8:2). The resulting yellow solution was analysed without any further purification by ESI MS, ¹H NMR, ¹³C NMR, ³¹P NMR, IR and elemental analysis.

1a: Triisopropylchlorosilane (10.0 g, 5.18×10^{-2} mol) was added to a degassed solution of 3,5-dimethyl-4-bromophenol (6.90 g, 3.2×10^{-2} mol) in dry DMF (160 mL), heated at 50 °C under nitrogen for 18 h. The solvent was removed under high vacuum and the residue was taken up in ether (200 mL). The resulting solution was washed three times with water, dried over MgSO₄ and evaporated to dryness. The crude product was purified by column chromatography on silica gel (eluent: hexane) giving pure **1a** (11.0 g, 3.08×10^{-2} mol; 90% yield) as a colourless liquid. ¹H NMR (CDCl₃, 200 MHz): δ 6.62 (s, 2H, arom.), 2.35 (s, 6H, benzyl), 1.12 (m, 21H, TIPS); ¹³C NMR (CD₂Cl₂, 50 MHz): 120.7, 120.6, 120.5, 119.4

(arom), 24.9, 18.8, 13.6 (aliph); IR: $\tilde{\nu}$ 2945, 2867, 1582, 1466, 1412, 1327, 1247, 1174, 1055, 1032, 1019, 883, 862, 805, 686.

2-(2,6-Dimethyl-4-triisopropylsilyloxy-phenyl)-3-trimethylsilylethynyl-

[1,10]phenanthroline (**2a**): ^1H NMR (CDCl_3 , 200 MHz): δ 9.21 (d, $J = 4.5$ Hz, 1H), 8.39 (s, 1H), 8.23 (d, $J = 8.1$ Hz, 1H), 7.77 (s, 2H), 7.59 (dd, $J = 8.1, 4.5$ Hz, 1H), 6.60 (s, 2H), 2.01 (s, 6H), 1.16 (m, 21H, TIPS), 0.06 (s, 9H, TMS); ^{13}C NMR (CDCl_3 , 50 MHz): 163.8, 156.4, 151.6, 147.1, 145.8, 140.0, 139.9, 138.3, 136.8, 130.1, 127.8, 127.4, 126.8, 123.9, 121.3, 118.9 (arom.), 102.8 (2C, ethynyl), 21.2, 19.1, 13.8, 0.49; IR (KBr): ν 2945, 2868, 2152, 1601, 1466, 1397, 1319, 1249, 1160, 1047, 996, 858, 843, 812, 686, 608; ESI MS: calcd. for $[\text{C}_{34}\text{H}_{44}\text{N}_2\text{OSi}_2\text{-H}]^+$: m/z 553.9, found: m/z 553.6; Anal. Calcd. for $\text{C}_{34}\text{H}_{44}\text{N}_2\text{OSi}_2$: C, 73.86; H, 8.02; N, 5.07. Found: C, 73.75; H, 7.94; N, 4.95.

2-Anthracen-9-yl-3-trimethylsilylethynyl-[1,10]phenanthroline (**2e**): ^1H NMR (CD_2Cl_2 , 200 MHz): δ 9.07 (d, $J = 4.5$ Hz, 1H), 8.64 (s, 1H, anthracene), 8.57 (s, 1H), 8.31 (d, $J = 8.4$ Hz, 1H), 8.11-8.16 (m, 2H, anthracene), 7.95 (s, 2H), 7.63 (dd, $J = 8.4, 4.5$ Hz, 1H), 7.46-7.53 (m, 4H, anthracene), 7.29-7.38 (m, 2H, anthracene), 0.54 (s, 9H, TMS); ^{13}C NMR (CD_2Cl_2 , 50 MHz): 160.4, 150.7, 139.0, 138.9, 136.0, 131.4, 130.2, 129.4, 128.5, 127.7, 127.6, 127.5 (2C), 126.0, 125.9, 125.7, 125.6, 125.1, 123.3, 121.4 (arom.), 88.2, 77.2 (ethynyl), -1.4; ESI MS: calcd. for $[\text{C}_{31}\text{H}_{24}\text{N}_2\text{Si-H}]^+$: m/z 453.6, found: m/z 453.4; Anal. Calcd. for $\text{C}_{31}\text{H}_{24}\text{N}_2\text{Si}$: C, 82.26; H, 5.34; N, 6.19. Found: C, 82.30; H, 5.43; N, 6.17.

2-(2,6-Dimethyl-4-triisopropylsilyloxy-phenyl)-9-(2,4,6-trimethyl-phenyl)-3-

trimethylsilylethynyl-[1,10]phenanthroline (**3a**): Yield: 66%. ^1H NMR (CDCl_3 , 200 MHz): δ 8.39 (s, 1H), 8.25 (d, $J = 8.3$ Hz, 1H), 7.81 (s, 2H), 7.56 (d, $J = 8.3$ Hz, 1H), 6.92 (s, 2H), 6.57 (s, 2H), 2.30 (s, 3H), 2.12 (s, 6H), 2.03 (s, 6H), 1.21 (m, 21H, TIPS), 0.09 (s, 9H, TMS); ^{13}C NMR (CD_2Cl_2 , 100 MHz): 145.3, 144.9, 142.9, 139.0, 138.1, 137.3, 136.1, 135.7, 132.8, 128.3, 128.2, 128.1, 127.6, 126.8, 126.6, 125.5, 124.7, 119.9, 118.1, 115.6 (arom.), 98.9, 94.2 (ethynyl), 20.1, 19.6, 17.9 (2C), 12.8, -1.0 (aliph.); IR (KBr): ν 3442, 2943, 2865, 2152 (ν $\text{C}\equiv\text{C}$), 1602, 1459, 1393, 1321, 1249, 1162, 1048, 996, 858, 846, 810, 686, 641; ESI MS: calcd. for $[\text{C}_{43}\text{H}_{54}\text{N}_2\text{OSi}_2\text{-H}]^+$: m/z 672.1, found: m/z 671.8; Anal. Calcd. for $\text{C}_{43}\text{H}_{54}\text{N}_2\text{OSi}_2$: C, 76.96; H, 8.11; N, 4.17. Found: C, 76.65; H, 8.30; N, 4.01.

2,9-Di-anthracen-9-yl-3-trimethylsilylethynyl-[1,10]phenanthroline (**3e**): Yield: 78%. ^1H NMR (CD_2Cl_2 , 400 MHz): δ 8.62 (s, 1H, phenanthroline), 8.44-8.49 (m, 2H, anthracene), 8.35 (d, 1H, $J = 8.3$ Hz, phenanthroline), 8.04 (s, 2H, phenanthroline), 7.95-7.97 (m, 4H, anthracene), 7.66-7.78 (m, 4H, anthracene), 7.65 (d, $J = 8.3$ Hz, 1H, phenanthroline), 7.22-

7.61 (m, 8H, anthracene), -0.41 (s, 9H, TMS); ^{13}C NMR (CD_2Cl_2 , 100 MHz): 161.1, 159.4, 146.7 (2C), 145.4, 139.5 (2C), 136.4 (2C), 135.7 (2C), 134.5, 133.8, 131.7 (2C), 130.9, 128.7, 128.6 (2C), 128.1, 127.9 (2C), 126.8 (2C), 126.0, 125.6, 125.3, 122.1 (arom.), 102.7 80.9 (ethynyl), -0.67; ESI MS: calcd. for $[\text{C}_{45}\text{H}_{32}\text{N}_2\text{Si-H}]^+$: m/z 629.8, found: m/z (%) 629.6 (100); Anal. Calcd. for $\text{C}_{45}\text{H}_{32}\text{N}_2\text{Si}$: C, 85.95; H, 5.13; N, 4.45. Found: C, 85.63; H, 5.07; N, 4.83.

4a: Yield: 89%. ^1H NMR (CDCl_3 , 200 MHz): δ 8.45 (s, 1H), 8.26 (d, $J = 8.1$ Hz, 1H), 7.83 (broad s, 2H), 7.57 (d, $J = 8.1$ Hz, 1H), 6.92 (s, 2H), 6.61 (s, 2H), 3.06 (s, 1H), 2.31 (s, 3H), 2.13 (s, 6H), 2.05 (s, 6H), 1.24 (m, 21H, TIPS); ^{13}C NMR (CDCl_3 , 50 MHz): 162.8, 161.4, 156.4, 146.9, 146.2, 141.3, 141.2, 138.8, 138.5, 137.2, 133.7, 129.5, 129.4, 128.5, 127.9, 127.5, 126.4, 126.3, 120.1, 119.6 (arom.), 83.1, 81.7 (ethynyl), 24.8, 21.5, 19.0 (2C), 13.7 (aliph.); IR (KBr): ν 3412, 2924, 2866, 2110 ($\text{C}\equiv\text{C}$), 1603, 1460, 1395, 1319, 1159, 1046, 884, 849, 810, 686, 639; ESI MS: calcd. for $[\text{C}_{40}\text{H}_{46}\text{N}_2\text{OSi-H}]^+$: m/z 599.9, found: m/z 599.7; Anal. Calcd. for $\text{C}_{40}\text{H}_{46}\text{N}_2\text{OSi}$: C, 80.22; H, 7.74; N, 4.68. Found: C, 79.89; H, 7.69; N, 4.55.

5a: Yield: 89%. ^1H NMR (CD_2Cl_2 , 200 MHz): δ 8.52 (s, 2H), 8.34 (d, $J = 8.1$ Hz, 2H), 7.89 (s, 4H), 7.56 (d, $J = 8.1$ Hz, 2H), 7.13 (s, 4H, phenyl spacer), 6.93 (s, 4H), 6.67 (s, 4H), 2.30 (s, 6H), 2.01 (br. s, 24H), 1.10 (m, 42H, TIPS); ^{13}C NMR (CD_2Cl_2 , 50 MHz): 161.5, 160.6, 155.5, 137.6, 137.5, 136.4, 136.2, 135.7, 131.4, 131.3, 131.1, 128.2, 128.0, 127.9, 127.7, 127.0, 126.9, 125.6, 125.0, 122.9, 119.9, 118.4 (arom.), 94.1, 88.7 (ethynyl), 20.2, 17.7 (3C), 12.7; IR (KBr): ν 3407, 3044, 2944, 2865, 1720 ($\text{C}\equiv\text{C}$), 1602, 1537, 1504, 1458, 1395, 1320, 1165, 1047, 992, 917, 885, 847, 809, 685, 637; ESI MS: calcd. for $[\text{C}_{86}\text{H}_{94}\text{N}_4\text{O}_2\text{Si}_2\text{-H}]^+$: m/z 1271.7, found: m/z (%) 1272.0 (70); ESI MS: calcd. for $[\text{C}_{86}\text{H}_{94}\text{N}_4\text{O}_2\text{Si}_2\text{-2H}]^{+2}$: m/z 637.0, found: m/z (%) 637.4 (100); Anal. Calcd. for $\text{C}_{86}\text{H}_{94}\text{N}_4\text{O}_2\text{Si}_2 \cdot 3/4\text{CH}_2\text{Cl}_2$: C, 78.01; H, 7.21; N, 4.20. Found: C, 78.26; H, 7.64; N, 3.97.

5b: ^1H NMR ($\text{D}_7\text{-DMF}$, 200 MHz): δ 9.52 (s, 2H, -OH), 8.86 (s, 2H), 8.64 (d, $J = 8.1$ Hz, 2H), 8.16 (s, 4H), 7.76 (d, $J = 8.1$ Hz, 2H), 7.28 (s, 4H, phenyl spacer), 6.97 (s, 4H), 6.68 (s, 4H), 2.31 (s, 6H), 2.03 (s, 12H), 2.01 (s, 12H); ^{13}C NMR ($\text{d}_7\text{-DMF}$, 50 MHz): 163.1, 162.5 (2C), 161.9, 161.8, 160.7, 157.9, 145.4, 138.8 (2C), 137.7, 137.6, 137.1, 135.9, 132.6, 131.9, 128.4, 127.5 (2C), 123.3, 119.9, 114.5 (arom.), 89.9 (2C, ethynyl), 20.1, 18.1, 13.5; IR (KBr): ν 3284, 2919, 2854, 2210 ($\text{C}\equiv\text{C}$), 1612, 1503, 1456, 1397, 1315, 1157, 1030, 909, 848, 775, 638; ESI MS: calcd. for $[\text{C}_{68}\text{H}_{54}\text{N}_4\text{O}_2\text{-H}]^+$: m/z 960.2, found: m/z (%) 959.9 (100); ESI MS: calcd. for $[\text{C}_{68}\text{H}_{54}\text{N}_4\text{O}_2\text{-2H}]^{+2}$: m/z 480.6, found: m/z (%) 480.9 (70%); Anal. Calcd. for $\text{C}_{68}\text{H}_{54}\text{N}_4\text{O}_2 \cdot 1/4\text{CH}_2\text{Cl}_2$: C, 83.61; H, 5.60; N, 5.71. Found: C, 83.96; H, 5.71; N, 5.81. See also single crystal structure.

5c: Yield: 31%. ^1H NMR (CD_2Cl_2 /trifluoroacetic acid (0.3/0.01 ml, respectively), 200 MHz): δ 8.89 (d, $J = 8.3$ Hz, 2H), 8.35 (s, 2H), 8.21 (d, $J = 8.3$ Hz, 2H, phenanthroline), 8.05 (s, 4H), 7.90-7.94 (m, 6H, anthracene), 7.51-7.60 (m, 8H, anthracene), 6.88-6.99 (m, 12H, anthracene), 6.72-6.81 (m, 8H, anthracene), 6.60-6.64 (m, 2H, anthracene); ESI MS: calcd. for $[\text{C}_{84}\text{H}_{46}\text{N}_4\text{-H}]^+$: m/z 1112.3, found: m/z (%) 1111.7 (100); ESI MS: calcd. for $[\text{C}_{84}\text{H}_{46}\text{N}_4\text{-2H}]^{2+}$: m/z 556.6, found: m/z (%) 557.5 (72). Anal. Calcd. for $\text{C}_{90}\text{H}_{50}\text{N}_4$: C, 91.04; H, 4.24; N, 4.72. Found: C, 91.10; H, 4.01; N, 4.90.

6a: Yield: 89%. ^1H NMR (CD_2Cl_2 , 200 MHz): δ 9.26 (br. s, 2H), 9.16 (d, $J = 4.2$ Hz, 2H), 8.35 (s, 2H), 8.23 (d, $J = 8.5$ Hz, 2H), 7.78 (d, $J = 8.6$ Hz, 2H), 7.76 (d, $J = 8.6$ Hz, 2H), 7.67-7.58 (m, 2H), 7.10 (s, 2H, phenyl), 4.07 (t, $J = 7.1$ Hz, 4H, $-\text{OCH}_2-$), 1.85 (q, $J = 7.1$ Hz, 4H, aliph.), 1.15-1.09 (m, 36H, aliph.), 0.79 (t, $J = 6.4$ Hz, 6H, $-\text{CH}_3$); ESI MS: calcd. for $[\text{C}_{58}\text{H}_{66}\text{N}_4\text{O}_2\text{-H}]^+$: m/z 852.2, found: m/z (%) 851.7 (100); ESI MS: calcd. for $[\text{C}_{58}\text{H}_{66}\text{N}_4\text{O}_2\text{-2H}]^{2+}$: m/z 426.6, found: m/z (%) 426.6 (25); Anal. Calcd. for $\text{C}_{58}\text{H}_{66}\text{N}_4\text{O}_2$: C, 81.84; H, 7.82; N, 6.58. Found: C, 81.40; H, 7.91; N, 6.70. See also single crystal structure.

6b: Yield: 61%. ^1H NMR (CD_2Cl_2 , 200 MHz): δ 9.23 (br. s, 2H), 9.13 (d, $J = 4.5$ Hz, 2H), 8.36 (s, 2H), 8.26 (d, $J = 8.1$ Hz, 2H), 7.82 (d, $J = 8.3$ Hz, 2H), 7.80 (d, $J = 8.3$ Hz, 4H), 7.64 (dd, $J = 8.1$ Hz, $J = 4.5$ Hz, 2H), 7.15 (s, 2H, phenyl), 4.10 (t, $J = 6.4$ Hz, 4H, $-\text{OCH}_2-$), 1.98-1.84 (m, 4H, aliph.), 1.66-1.56 (m, 4H, aliph.), 1.52-1.26 (m, 16H, aliph.), 0.82 (t, $J = 6.9$ Hz, 6H, $-\text{CH}_3$); ^{13}C NMR (CD_2Cl_2 , 50 MHz): 153.9, 151.7, 150.5, 146.0, 144.9, 137.8 (2C), 135.9, 129.1, 127.9, 126.1, 123.2, 119.5, 116.9, 113.7 (arom.), 92.0, 90.1 (ethynyl), 69.7 (CH₂-O), 31.9, 29.4 (2C), 26.1, 22.7 (2C), 13.9 (aliph.); IR (KBr): ν 3027, 2921, 2851, 2204 ($\text{C}\equiv\text{C}$), 1589, 1552, 1505, 1467, 1411, 1383, 1277, 1218, 1123, 1097, 1062, 970, 908, 833, 734, 694; ESI MS: calcd. for $[\text{C}_{50}\text{H}_{50}\text{N}_4\text{O}_2\text{-H}]^+$: m/z 739.9, found: m/z (%) 739.6 (100); Anal. Calcd. for $\text{C}_{50}\text{H}_{50}\text{N}_4\text{O}_2$: C, 81.27; H, 6.82; N, 7.58. Found: C, 81.29; H, 6.90; N, 7.32. See also single crystal structure.

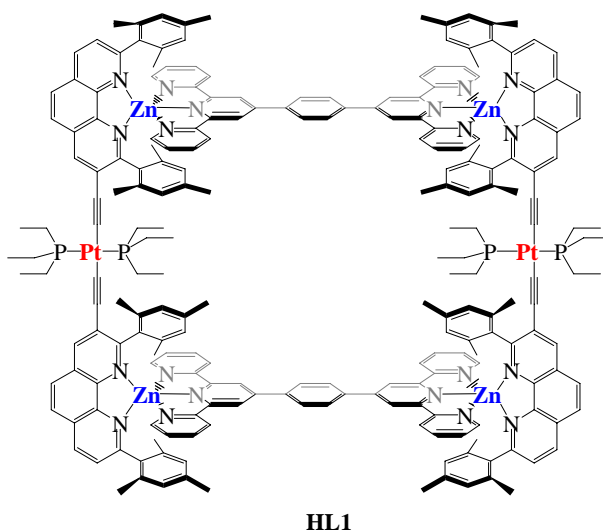
6c: Yield: 84%. ^1H NMR (CD_2Cl_2 , 200 MHz): δ 9.20 (s, 2H), 9.11 (d, $J = 4.5$ Hz, 2H), 8.35 (s, 2H), 8.23 (d, $J = 8.4$ Hz, 2H), 7.77 (d, $J = 8.4$ Hz, 2H), 7.75 (d, $J = 8.4$ Hz, 2H), 7.61 (dd, $J = 8.4$ Hz, $J = 4.5$ Hz, 2H), 7.13 (s, 2H, phenyl), 4.09 (t, $J = 6.4$ Hz, 4H, $-\text{OCH}_2-$), 1.97-1.64 (m, 4H, aliph), 1.60-1.32 (m, 12H, aliph.), 0.82 (t, $J = 6.9$ Hz, 6H, $-\text{CH}_3$); ^{13}C NMR (CD_2Cl_2 , 100 MHz): 151.9, 148.7, 144.1, 142.8, 136.1, 134.1, 130.2, 127.0, 125.8, 124.1, 121.3 (2C), 117.8, 114.9, 111.9 (arom.), 90.2, 88.4 (ethynyl), 54.1 (CH₂-O), 29.9, 27.8, 27.5, 24.2, 20.7; ESI MS: calcd. for $[\text{C}_{46}\text{H}_{42}\text{N}_4\text{O}_2\text{-H}]^+$: m/z 683.3, found: m/z (%) 683.1 (100); Anal. Calcd. for $\text{C}_{46}\text{H}_{42}\text{N}_4\text{O}_2$: C, 80.91; H, 6.20; N, 8.20. Found: C, 80.54; H, 6.32; N, 8.12.

Pt-linked bisphenanthrolines:

7a: ^1H NMR (CD_2Cl_2 , 200 MHz): δ 8.26 (d, $J = 8.1$ Hz, 2H, phenanthroline), 8.19 (s, 2H, phenanthroline), 7.80 (s, 4H, phenanthroline), 7.48 (d, $J = 8.1$ Hz, 2H, phenanthroline), 6.95 (s, 4H, phenyl), 6.91 (s, 4H, phenyl), 2.33 (s, 12H, benzyl), 2.01 (s, 24H, benzyl), 1.74-1.81 (m, 12H, aliph.), 0.95-1.10 (m, 18H, aliph.); ^{13}C NMR (CD_2Cl_2 , 50 MHz): 161.3, 160.1, 146.4, 142.7, 138.6, 138.3, 137.5 (2C), 137.2, 136.5, 135.5(t, 2C), 128.1(d, 2C), 127.8, 127.5, 126.8, 126.1, 125.6, 124.9, 123.8 (arom.), 116.5(t), 106.3 (ethynyl), 20.9(d), 19.9(m, 2C), 15.7(t, 2C), 7.9(t) (aliph.); $^{31}\text{P}\{^1\text{H}\}$ NMR (CD_2Cl_2 , 162 MHz): 12.59; IR (KBr): $\tilde{\nu}$ 3408, 2962, 2917, 2874, 2093 ($\text{C}\equiv\text{C}$), 1613, 1573, 1455, 1409, 1389, 1185, 1156, 1105, 1034, 902, 887, 849, 768, 735, 639, 617, 541; ESI MS: calcd. for $[\text{C}_{76}\text{H}_{84}\text{P}_2\text{N}_4\text{Pt-H}]^+$: $m/z(\%)$ 1310.5, found: m/z 1310.7(100), $[\text{C}_{76}\text{H}_{84}\text{N}_4\text{P}_2\text{Pt-2H}]^{+2}$: m/z 655.3, found: $m/z(\%)$ 655.6(25); Anal. Calcd. for $\text{C}_{76}\text{H}_{84}\text{N}_4\text{P}_2\text{Pt}\cdot\text{H}_2\text{O}$: C, 68.71; H, 6.52; N, 4.22. Found: C, 68.32; H, 6.47; N, 4.01.

7b: ^1H NMR (CD_2Cl_2 , 200 MHz): δ 8.22 (d, $J = 8.4$ Hz, 2H, phenanthroline), 8.14 (s, 2H, phenanthroline), 7.72 (s, 4H, phenanthroline), 7.49 (d, $J = 8.1$ Hz, 2H, phenanthroline), 6.91 (s, 2H, phenyl), 2.38 (s, 6H, benzyl), 2.17 (s, 12H, benzyl), 2.07 (s, 12H, benzyl), 1.95 (s, 12H, benzyl), 1.69-1.75 (m, 12H, aliph), 0.94-1.12 (m, 18H, aliph); ^{13}C NMR (CD_2Cl_2 , 100 MHz): 146.7, 143.1, 141.4, 141.0, 138.6, 137.7, 136.3, 136.2, 134.3 (2C), 133.7 (t), 128.9, 128.6, 127.9, 127.2, 126.7, 1260.0, 125.3, 124.3 (arom.), 117.3, 106.6 (ethynyl), 21.2, 20.4, 18.8, 16.2 (t), 8.3; $^{31}\text{P}\{^1\text{H}\}$ NMR (CD_2Cl_2 , 162 MHz): 10.42; IR (KBr): $\tilde{\nu}$ 3414, 2963, 2921, 2091 ($\text{C}\equiv\text{C}$), 1613, 1576, 1457, 1413, 1381, 1354, 1186, 1143, 1034, 986, 903, 847, 768, 733, 640; ESI MS: calcd. for $[\text{C}_{78}\text{H}_{87}\text{Br}_2\text{N}_4\text{P}_2\text{Pt-H}]^+$: m/z 1497.4, found: $m/z(\%)$ 1497.6(100), $[\text{C}_{78}\text{H}_{87}\text{Br}_2\text{N}_4\text{P}_2\text{Pt-2H}]^{+2}$: m/z 748.6, found: $m/z(\%)$ 749.8(5); Anal. Calcd. for $\text{C}_{78}\text{H}_{86}\text{Br}_2\text{N}_4\text{P}_2\text{Pt}\cdot\text{CH}_2\text{Cl}_2$: C, 60.00; H, 5.61; N, 3.54. Found: C, 59.60; H, 5.66; N, 3.38.

7c: ^1H NMR (CD_2Cl_2 , 200 MHz): δ 9.13 (d, $J = 7.8$ Hz, 2H, phenanthroline), 9.07 (d, $J = 8.2$ Hz, 2H, phenanthroline), 7.83 (d, $J = 7.9$ Hz, 2H, phenanthroline), 8.21 (dd, $J = 8.2$ Hz, 2H, phenanthroline), 8.04 (d, $J = 8.3$ Hz, 2H, phenanthroline), 7.72 (dd, $J = 8.8$ Hz, 2H, phenanthroline), 7.58 (d, $J = 4.4$ Hz, 2H, phenanthroline), 2.18-2.31 (m, 12H, aliph), 1.21-1.37 (m, 18H, aliph); ^{13}C NMR (CD_2Cl_2 , 100 MHz): 155.3, 152.6, 148.6, 145.0, 138.3, 130.7, 130.6, 128.9, 128.6, 127.2, 124.8, 18.8(t), 10.7; $^{31}\text{P}\{^1\text{H}\}$ NMR (CD_2Cl_2 , 162 MHz): 10.56; IR (KBr): $\tilde{\nu}$ 3432, 2962, 2932, 2874, 2094 ($\text{C}\equiv\text{C}$), 1585, 1499, 1455, 1417, 1225, 1178, 1099, 1037, 898, 832, 771, 733, 527; ESI MS: calcd. for $[\text{C}_{40}\text{H}_{44}\text{P}_2\text{N}_4\text{Pt-H}]^+$: m/z 838.9, found: m/z 839.3; Anal. Calcd. for $\text{C}_{40}\text{H}_{44}\text{N}_4\text{P}_2\text{Pt}\cdot 2\text{CH}_2\text{Cl}_2$: C, 50.62; H, 4.80; N, 5.56. Found: C, 51.02; H, 5.44; N, 5.51.



HL1: ^1H NMR (CD_2Cl_2 , 200 MHz): δ 8.99-9.03 (m, 12H, phenanthroline and terpyridine), 8.94 (d, $J = 8.1$ Hz, 4H, phenanthroline), 8.71 (s, 8H, phenyl), 8.52 (s, 8H, terpyridine), 8.39 (dd, $J = 9.1$ Hz, $J = 4.2$ Hz, 8H, phenanthroline), 8.33 (dt, $J = 6.1$ Hz, $J = 1.7$ Hz, 8H, terpyridine), 8.02 (d, $J = 8.3$ Hz, 4H, phenanthroline), 7.68 (d, $J = 4.9$ Hz, 8H, terpyridine), 7.52 (dt, $J = 5.4$ Hz, $J = 1.9$ Hz, 8H, terpyridine), 6.20 (s, 8H, phenyl), 6.09 (s, 8H, phenyl), 1.90 (s, 12H, benzyl), 1.73 (s, 12H, benzyl), 1.49-1.51 (m, 24H, aliph), 1.05 (s, 24H, benzyl), 1.13 (s, 24H, benzyl), 0.67-0.86 (m, 36H, aliph); ^{13}C NMR (CD_2Cl_2 , 50 MHz): 160.9, 155.4, 151.1, 148.5 (2C), 147.8 (2C), 146.8, 142.7, 141.3, 140.7, 139.7, 137.5, 135.2, 135.0, 134.8, 134.5, 134.0, 129.6, 129.3, 129.2, 128.5, 127.9, 127.4, 127.3, 127.2, 127.1, 120.2, 117.4, 102.6 (arom.), 77.2, 91.8 (ethynyl), 20.3, 19.1, 19.0, 18.5, 18.4, 7.4 (aliph.); $^{31}\text{P}\{^1\text{H}\}$ NMR (CD_2Cl_2 , 162 MHz): 15.67; ESI MS: calcd. for $[\text{C}_{224}\text{H}_{216}\text{N}_{20}\text{P}_4\text{Pt}_2\text{Zn}_4*4\text{OTf}]^{+4}$: m/z 1140.0, found: m/z (%) 1140.0(100), calcd. for $[\text{C}_{224}\text{H}_{216}\text{N}_{20}\text{P}_4\text{Pt}_2\text{Zn}_4*5\text{OTf}]^{+3}$: m/z 1569.7, found: m/z (%) 1568.8(55); Anal. Calcd. for $\text{C}_{224}\text{H}_{216}\text{N}_{20}\text{P}_4\text{Pt}_2\text{Zn}_4*8\text{OTf}*4\text{H}_2\text{O}$: C, 53.29; H, 4.32; N, 5.36. Found: C, 53.55; H, 4.12; N, 5.25.

- (1) M. Schmittel, V. Kalsani, *Top. Curr. Chem.* **2005**, *245*, 1-53.
- (2) (a) S. J. Cantrill, K. S. Chichak, A. J. Peters, J. F. Stoddart, *Acc. Chem. Res.* **2005**, *38*, 1-9. (b) N. W. Ockwig, O. Delgado-Friedrichs, M. O'Keeffe, and O. M. Yaghi, *Acc. Chem. Res.* **2005**, *38*, 176-182. (c) A. S. Borovik, *Acc. Chem. Res.* **2005**, 54-61. (d) P. J. Steel, *Acc. Chem. Res.* **2005**, ASAP. (e) S.-I. Nishikiori, H. Yoshikawa, Y. Sano, and T. Iwamoto, *Acc. Chem. Res.* **2005**, ASAP. (f) M. Fujita, M. Tominaga, A. Hori, and B. Therrien, *Acc. Chem. Res.* **2005**, ASAP. (g) M. W. Hosseini, *Acc. Chem. Res.* **2005**, ASAP. (h) D. Fiedler, D. H. Leung, R. G. Bergman, and K. N. Raymond, *Acc. Chem. Res.* **2005**, ASAP. (i) J. Rebek, Jr., *Angew. Chem. Int. Ed.* **2005**, ASAP. (j) L. J. Prins, D. N. Reinhoudt, P. Timmerman, *Angew. Chem. Int. Ed.* **2001**, *40*, 2382-2426. (k) B. J. Holliday, C. A. Mirkin, *Angew. Chem. Int. Ed.* **2001**, *40*, 2022-2043. (l) M. Ruben, J. Rojo, F. J. Romero-Salguero, L. H. Uppadine, J.-M. Lehn, *Angew. Chem. Int. Ed.* **2004**, *43*, 3644-3662. (m) O. Lukin, F. Vögtle, *Angew. Chem. Int. Ed.* **2005**, *44*, 1456-1477.
- (3) G. F. Swiegers, T. J. Malefetse, *Chem. Rev.* **2000**, *100*, 3483-3538.
- (4) (a) R. Ziessel, L. Charbonnière, M. Cesario, T. Prangé and H. Nierengarten, *Angew. Chem. Int. Ed.*

- 2002**, *41*, 975-979. (b) M. Schmittel, V. Kalsani, D. Fenske, A. Wiegrefe, *Chem. Commun.*, **2003**, 490-491. (c) V. Kalsani, H. Ammon, F. Jäckel, J. P. Rabe, M. Schmittel, *Chem. Eur. J.* **2004**, *10*, 5481-5492. (d) V. Kalsani, H. Bodenstedt, M. Schmittel, D. Fenske, *Eur. J. Inorg. Chem.* **2005**, in press. (e) J.-P. Sauvage, *Chem. Commun.* **2005**, 1507-1510 and ref's therein. (f) B. J. Holliday, T. Swager, *Chem. Commun.* **2005**, 23-36. (g) E. C. Glazer, D. Magde, Y. Tor, *J. Am. Chem. Soc.* **2005**, ASAP. (g) H. Hofmeier, U. S. Schubert, *Chem. Soc. Rev.* **2004**, *33*, 373-399.
- (5) (a) P. N. W. Baxter, G. S. Hanan, J.-M. Lehn, *Chem. Commun.* **1996**, 2019-2020. (b) M. Schmittel, H. Ammon, V. Kalsani, A. Wiegrefe, C. Michel, *Chem. Commun.* **2002**, 2566-2567.
 - (6) a) M. Schmittel, A. Ganz, *Chem. Commun.* **1997**, 999-1000. b) M. Schmittel, U. Lüning, M. Meder, A. Ganz, C. Michel, M. Herderich, *Heterocycl. Commun.* **1997**, *3*, 493-498.
 - (7) M. Schmittel, V. Kalsani, J. W. Bats, **2005**, manuscript in preparation.
 - (8) M. Schmittel, C. Michel, A. Wiegrefe, V. Kalsani, *Synthesis* **2001**, 1561-1567.
 - (9) Related, but unsubstituted bisphenanthrolines were originally reported as ruthenium complexes, D. Tzalis, Y. Tor, *Chem. Commun.* **1996**, 1043-1044.
 - (10) M. Schmittel, C. Michel, S.-X. Liu, D. Schildbach, D. Fenske, *Eur. J. Inorg. Chem.* **2001**, 1155-1166.
 - (11) Dietrich-Buchecker, C. O.; Marnot, P. A.; Sauvage, J. P. *Tetrahedron Lett.* **1982**, *23*, 5291-5294.
 - (12) The synthesis of **3c** and **3d** has been reported earlier.
 - (13) Meijere, A. de; Meyer, F. E. *Angew. Chem.* **1994**, *106*, 2473-2506; *Angew. Chem. Int. Ed.* **1994**, *33*, 2379-2411.
 - (14) Crystal data for **5b**: C₆₈H₅₄N₄O₂*4DMF (DMF = dimethylformamide), *M* = 1251.54, Triclinic, space group *P*-1, *a* = 32.113(6) Å, *b* = 15.049(3) Å and *c* = 14.506(3) Å, *V* = 6996 (2) Å³, *T* = 443 (2) K, *Z* = 4, *D*_c = 1.188 g/cm³, λ(Mo Kα) = 0.71073 Å, 8207 reflexions measured, 5570 unique (*R*_{int} = 0.0509) which were used in all calculations. *R*₁ = 0.0781 (*I* > 2 σ (*I*)) and *wR*₂ = 0.1679, GOF = 1.075. CCDC reference number **xxxx**. See also supp. information.
 - (15) A. Khatyr, R. Ziessel, *J. Org. Chem.* **2000**, *65*, 7814-7828.
 - (16) (a) U.-W. Grummt, E. Birckner, M. Al-Higari, D. A. M. Egbe, E. Klemm, E. *Journal of Fluorescence*, **2001**, *11*, 41-51. (b) M. Al-Higari, E. Birckner, B. Heise, E. Klemm, *J. Poly. Sci. Part A: Polymer Chemistry*, **1999**, *37*, 4442-4448.
 - (17) Crystal data for **6a**: Suitable single crystals were obtained by the slow of evaporation of dichloromethane solution containing **6a**. Solvent could be located partially. C₆₀H₇₀N₄O₂*nCH₂Cl₂, *M* = 1016.97, Triclinic, space group *P*-1, *a* = 11.973(2) Å, *b* = 13.924(3) Å and *c* = 18.606(4) Å, *V* = 2872 (10) Å³, *T* = 193 (2) K, *Z* = 2, *D*_c = 1.176 g/cm³, λ(Mo Kα) = 0.71073 Å, 12600 reflexions measured, 8519 unique (*R*_{int} = 0.0310) which were used in all calculations. *R*₁ = 0.1138 (*I* > 2 σ (*I*)) and *wR*₂ = 0.3082, GOF = 1.041. CCDC reference number **xxxx**. See also supp. information.
 - (18) Crystal data for **6b**: Suitable single crystals were obtained by the slow of evaporation of dichloromethane solution containing **6b**. C₅₀H₅₀N₄O₂*2CH₂Cl₂, *M* = 908.79, Triclinic, space group *P*-1, *a* = 10.866(16) Å, *b* = 10.987(2) Å and *c* = 12.019(2) Å, *V* = 1173 (4) Å³, *T* = 155 (2) K, *Z* = 1, *D*_c = 1.286 g/cm³, λ(Mo Kα) = 0.71073 Å, 20884 reflexions measured, 7645 unique (*R*_{int} = 0.0428) which were used in all calculations. *R*₁ = 0.0458 (*I* > 2 σ (*I*)) and *wR*₂ = 0.1167, GOF = 1.028; max/min residual density 0.587/-0.337 e Å⁻³. CCDC reference number **xxxx**. See also supp. information.
 - (19) E. Lindner, R. Zong, M. Ströbele, K. Eichele, *Z. Anorg. Allg. Chem.* **2003**, *629*, 587-588.
 - (20) (a) C. M. Drain, F. Nifiatis, A. Vasenko, J. D. Batteas, *Angew. Chem. Int. Ed. Engl.* **1998**, *37*, 2344-2347. (b) R. Takahashi, Y. Kobuke, *J. Am. Chem. Soc.* **2003**, *125*, 2372-2373. (c) S. De Feyter, F. C. De Schryver, *Chem. Soc. Rev.* **2003**, *32*, 139-150. (d) A. Semenov, J. P. Spatz, M. Möller, J.-M. Lehn, B. Sell, D. Schubert, C. H. Weidl, U. S. Schubert, *Angew. Chem. Int. Ed. Engl.* **1999**, *38*, 2547-2550. (e) U. Ziener, J.-M. Lehn, A. Mourran, M. Möller, *Chem. Eur. J.* **2002**, *8*, 951-957. (f) M. Tominaga, K. Suzuki, M. Kawano, T. Kusakawa, T. Ozeki, S. Sakamoto, K. Yamaguchi, M. Fujita, *Angew. Chem. Int. Ed.* **2004**, *43*, 5621-5625.
 - (21) G. Bining, H. Rohrer, G. Gerber, and E. Weibel, *Phys. Rev. Lett.*, **1982**, *49*, 57-61.
 - (22) S. De Feyter, A. Gesquiere, M. M. Abdel-Mottaleb, P. C. M. Grim, M. Sieffert, C. Meiners, S. Valiyavetil, K. Müllen, and F. C. De Schryver, *Acc. Chem. Res.* **2000**, *33*, 520-531.
 - (23) J. V. Barth, J. Weckesser, C. Cai, P. Günter, L. Bürgi, O. Jeandupeaux, K. Kern, *Angew. Chem. Int. Ed.* **2000**, *39*, 1230-1234.
 - (24) N. Lin, S. Stepanow, F. Vidal, J. V. Barth, K. Kern, *Chem. Commun.* **2005**, ASAP.
 - (25) M. M. Abdel-Mottaleb, N. Schuurmans, S. De Feyter, J. Va Esch, B. L. Feringa, F. C. De Schryver, *Chem. Commun.* **2002**, 1894-1895.
 - (26) D. Wouters, S. Höppener, R. Lunkwitz, L. Chi, H. Fuchs, U. S. Schubert, *Adv. Funt. Mater.* **2003**, *13*, 277-280.
 - (27) (a) S. Goeb, A. De Nicola, R. Ziessel, *J. Org. Chem.* **2005**, *70*, 1518-1529 and ref's therein.

- (b) T. Yamamoto, K. Anzai, T. Iijima, H. Fukumoto, *Macromolecules*, **2004**, *37*, 3064-3067.
- (28) Studies are in progress in cooperation with Prof. J. P. Rabe., Humboldt University Berlin, Berlin.
- (29) Y. Wei, K. Kannappan, G. W. Flynn, M. B. Zimmt, *J. Am. Chem. Soc.* **2004**, *126*, 5318-5322 and ref's therein.
- (30) R. Ziessel, M. Hissler, A. El-Ghayoury, A. Harriman, *Coord. Chem. Rev.* **1998**, *178-180*, 1251-1298.
- (31) M. Hissler, A. Harriman, A. Khatyr, R. Ziessel, *Chem. Eur. J.* **1999**, *5*, 3366-3381.
- (32) (a) D. M. Bassani, J.-M. Lehn, K. Fromm, D. Fenske, *Angew. Chem. Int. Ed.* **1998**, *37*, 2364-2367. (b) G. R. Newkome, T. J. Cho, C. N. Moorefield, P. P. Mohapatra, L. A. Godínez, *Chem. Eur. J.* **2004**, *10*, 1493-1500. (c) A. Petitjean, N. Kyritsakas, J.-M. Lehn, *Chem. Commun.* **2004**, 1168-1169. (d) A. H. Eisenberg, M. V. Ovchinnikov, C. A. Mirkin, *J. Am. Chem. Soc.* **2003**, *125*, 2836-2837. (e) M. Schmittel, V. Kalsani, J. W. Bats, *Inorg. Chem.* **2005**, in press.
- (33) H. Jiang, W. Lin, *J. Am. Chem. Soc.* **2004**, *126*, 7426-7427 and ref's therein.
- (34) During ESI MS characterisation acid addition lead to the decomplexation of the ligands **7a-c**; however, they could be charged by the ESI MS source due to the presence of some acid left over from the previous measurements.
- (35) See chapter 6 for more discussion of HETTAP approach.
- (36) (a) L. H. Uppadine, J.-M. Lehn, *Angew. Chem. Int. Ed.* **2004**, *43*, 240-243. (b) G. N. Newkome, T. J. Cho, C. N. Moorefield, R. Cush, P. S. Russo, L. A. Godínez, M. J. Saunders, P. Mohapatra, *Chem. Eur. J.* **2002**, *8*, 2946-2954. (c) S.-S. Sun, A. S. Silva, I. M. Brinn, A. J. Lees, *Inorg. Chem.* **2000**, *39*, 1344-1345. (d) S.-S. Sun, A. J. Lees, *Inorg. Chem.* **2001**, *40*, 3154-3160.
- (37) Terpyridine building block, **9** was purchased from Aldrich and used as recieved.
- (38) M. Schmittel, V. Kalsani, J. W. Bats, *Inorg. Chem.* **2005**, in press.
- (39) Hyperchem[®] 6.02 Release for Windows by Hypercube, Inc. **2000**. MM+ force field.
- (40) J. P. Rabe, S. Buchholz, *Science* **1991**, *253*, 424-427.
- (41) J.-M. Kern, J.-P. Sauvage, J.-L. Weidmann, N. Armaroli, L. Flamigni, P. Ceroni, and V. Balzani, *Inorg. Chem.* **1997**, *36*, 5329-5338
- (42) R. F. Carina, C. D. Dietrich-Buchecker, J.-P. Sauvage, *J. Am. Chem. Soc.* **1996**, *118*, 9110-9116.

Supp 4-3

Eur. J. Inorg. Chem. **2005**, in press.

Reproduced by permission of *Wiley-VCH Verlag GmbH & Co KG*

Supramolecular Copper Phenanthroline Racks: Structures, Mechanistic Insight and Dynamic Nature

Venkateshwarlu Kalsani,^[a] Heinrich Bodenstedt,^[a] Dieter Fenske,^[b] Michael Schmittel*^[a]

^[a] *Center of Micro and Nanochemistry and Engineering, Organische Chemie I, Universität Siegen, Adolf-Reichwein-Str., D-57068 Siegen, Germany, Fax: (+49) 271 740 3270*

^[b] *Institut für Anorganische Chemie, Universität Karlsruhe, Engesserstr. 3045, D-76128 Karlsruhe, Germany*

Received (will be filled in by the editorial staff)

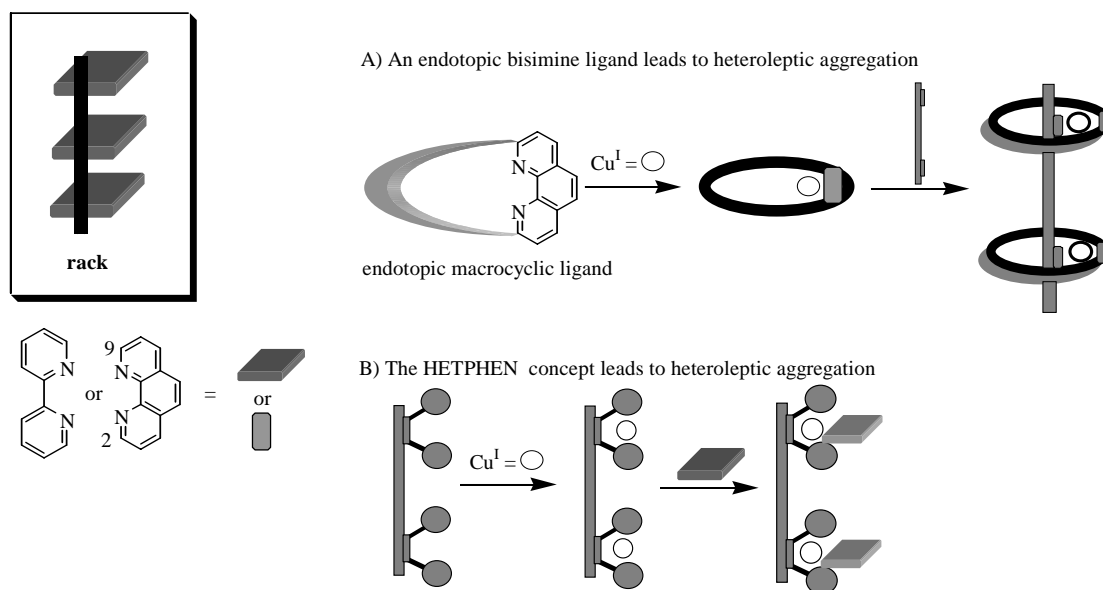
Key words: rack, HETPHEN, self-assembly, phenanthroline, dynamics.

Abstract: Herein, we describe the preparation of several dynamic multicomponent supramolecular racks based on copper phenanthroline complexes using the HETPHEN concept (heteroleptic bisphenanthroline complexes). This approach employs bulky aryl substituents at the bisimine coordination sites to control the coordination equilibrium. The racks were characterised by spectroscopic methods, both in solution (¹H NMR, ESI-MS, UV-vis, vapour pressure osmometry) and in the solid state (X-Ray). Ligand exchange studies established the reversible nature of the aggregates, the details of which are vital for the development of higher level multicomponent structures. In this regard, the present rack assemblies contrast to the large multitude of known rack motifs that are almost exclusively built using kinetically inert coordination building blocks.

Introduction

Metallo-rack structures have a high standing in the burgeoning field of supramolecular chemistry due to their spatially well-defined linear array of metal ions that is attractive for many purposes, such as photoactive and electroactive nanowires.^[1] Therefore, facile and quantitative access to rack aggregates is the goal of current research efforts.^[1] Racks, however, by their very nature are multi-component structures that are most conveniently assembled under kinetic control, *cf.* using kinetically stable ruthenium coordination complexes,^[1b,c,e-g] even at the price of moderate yields. Preparation of rack structures under thermodynamic control is much more a challenge since in a dynamic multitopic aggregation scenario the requested heteroleptic combinations have to compete with homoleptic ones.^[1d] Rewardingly, dynamic aggregation should allow for self-repair thus securing the most stable complex in very high yields if sufficient thermodynamic bias is installed.^[2] Once the proof of principle is established one is set up to construe dynamic aggregates at surfaces that should be very useful for sensory purposes.^[3]

At present, only one strategy is known to construct *dynamic* multicomponent rack structures (Scheme 1; strategy A).^[4] Accordingly, ring constraints are utilised to prevent the formation of the homoleptic combination of one of the ligands, *e. g.* of an endotopic macrocyclic ligand. In combination with another rigid ligand the arrested ligand can combine to a heteroleptic rack-pseudorotaxane motif following the maximum site occupancy principle.^[1d] A much easier way to *dynamic* multicomponent racks, however, should emerge from the HETPHEN^[5] approach (strategy B). We have recently utilised the HETPHEN concept to establish heteroleptic bisphenanthroline copper complexes as building blocks for large nanostructures.^[6] In our approach, heteroleptic aggregation is driven by steric and electronic factors which do not require an endotopic macrocycle. Instead, steric stoppers are required at the 2,9-positions of one of the bisimine coordination sites to prevent any homoleptic combination with itself. Therefore, in combination with another bisimine ligand only hetero combinations will result. This opens a much more facile way to heteroleptic dynamic aggregation than in previous reports.^[7]

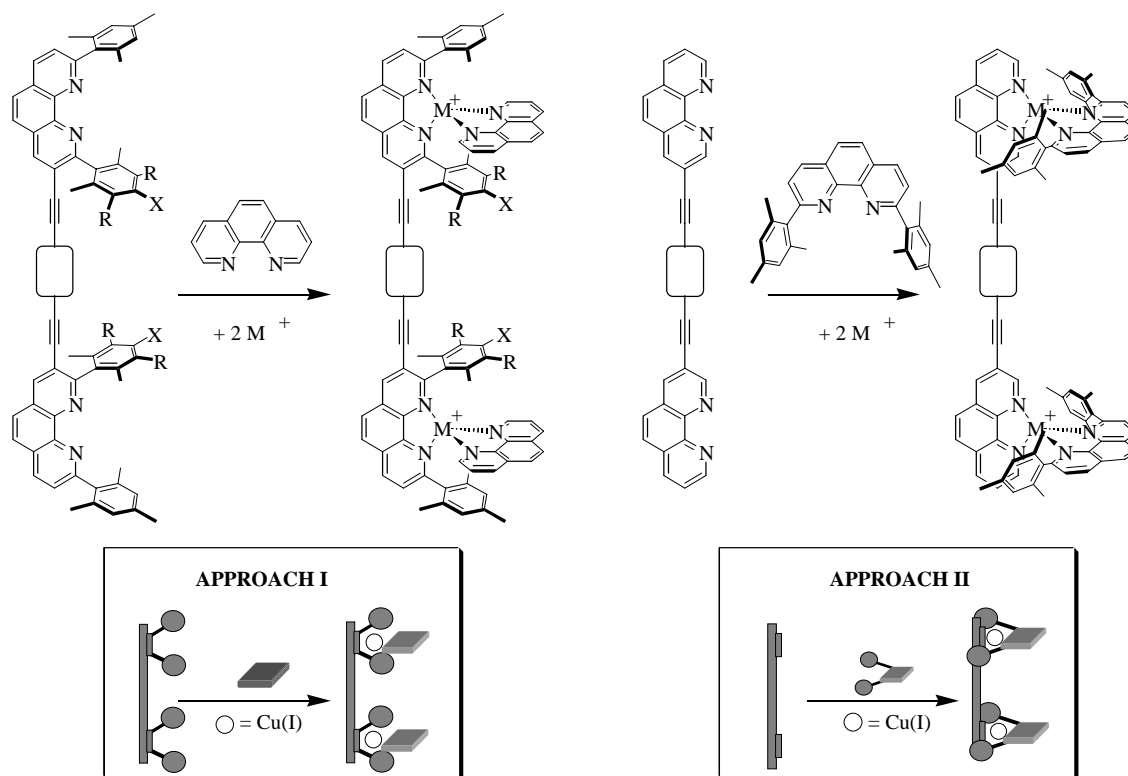


Scheme 1. Strategies to prepare dynamic rack-type motifs.^[1d]

We have recently disclosed some preliminary results on dynamic rack structures in the context of our work on supramolecular nanogrids.^[8] Herein, we now detail the potential of the HETPHEN^[9] concept as a general strategy for the construction of multicomponent dynamic racks, provide structural insight into products and intermediates, and interrogate the dynamic nature of these unique assemblies.

Results and Discussion

Following the HETPHEN concept two approaches can be explored to prepare dynamic rack-type aggregates (Scheme 2). In both approaches one set of the ligand has to be instructed with the steric stoppers. In approach I, the linear bisphenanthroline is loaded with sterically bulky aryl groups at the 2,9-positions of each phenanthroline site. In contrast, approach II makes use of monophenanthrolines that are equipped with the steric stoppers, while the linear bisphenanthroline is devoid of them.



Scheme 2. Two different approaches for constructing dynamic multitopic *rack*-type motifs along the HETPHEN concept (in the bottom: a pictorial cartoon representation of the two approaches).

The linear bisphenanthrolines **1a**,^[10] **1b**^[10] and **2**,^[11] as well as the monophenanthrolines **3a**, **3b**,^[13] **4a**,^[6c] **4b**^[12] and **4c**^[13] were chosen for this study (Chart 1). Assembly of **1,2** with **3,4** in presence of metal ions of tetrahedral coordination geometry, such as copper(I) or silver(I) ions, is expected to yield the desired dynamic multicomponent racks.

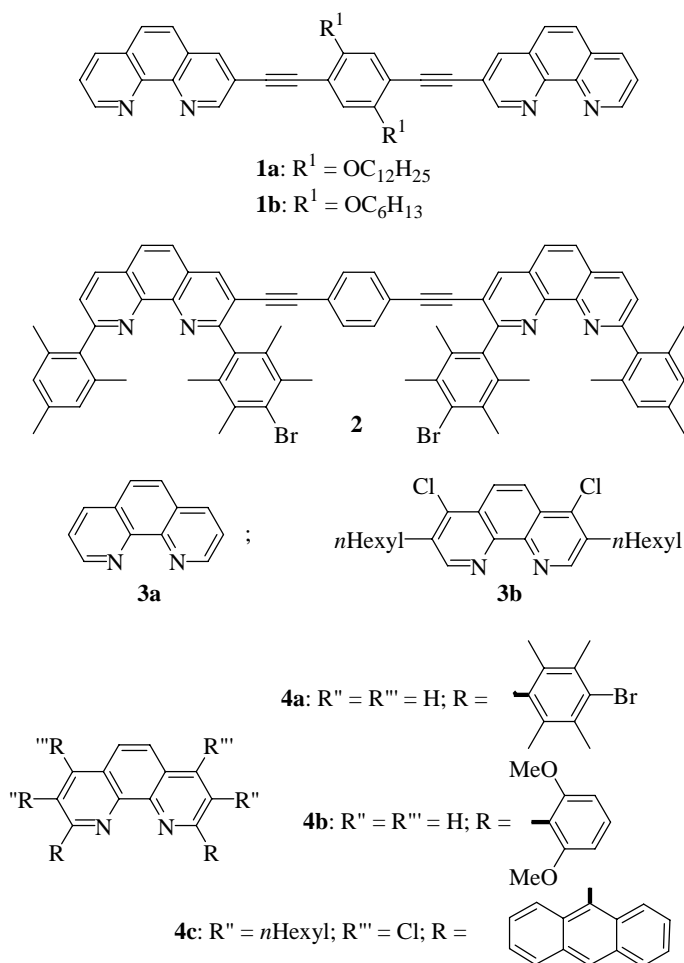
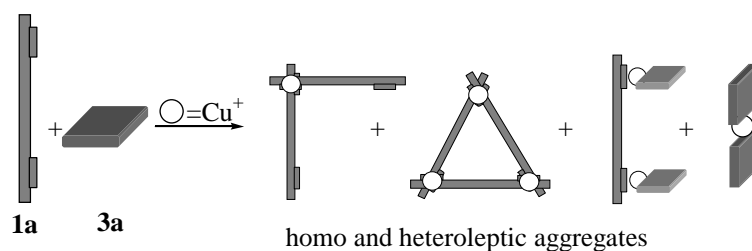


Chart 1.

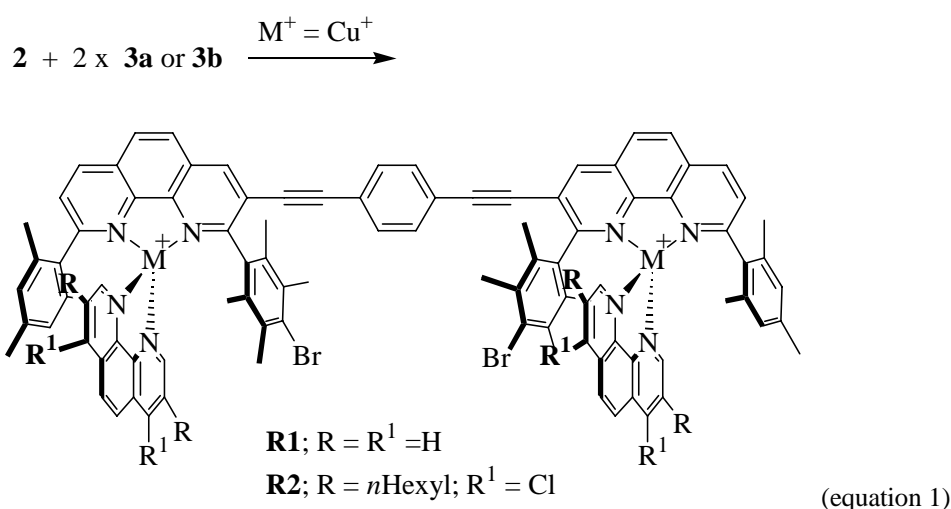
To illustrate the need for control in the formation of dynamic rack assemblies using a coordination approach bisphenanthroline **1a** was reacted with **3a** in presence of $[Cu(MeCN)_4]PF_6$. The desired rack was obtained only as a minor component as evidenced by ESI-MS and 1H NMR. Rather, a complex mixture formed showing signals corresponding to the triangular-grid and signals corresponding to the homoleptic complex of **3a** as depicted in scheme 3. 1H NMR showed various sets of signals which arise from the resulting different aggregates. It is clear from the above experiment that cooperativity can not be used solely to build dynamic heteroleptic aggregates.



Scheme 3. Cartoon representation of the self-assembly of linear bisphenanthrolines and monophenanthrolines that are not instructed along the HETPHEN concept.

Approach I

As discussed above, approach I uses a bisphenanthroline bearing steric stoppers (as in ligand **2**) in combination with any phenanthroline with no steric stoppers at 2,9-positions (*i.e.* **3a-3b**). The combination of these two building blocks and Cu(I) salt should result in heteroleptic racks.^[8] Indeed, upon addition of [Cu(MeCN)₄]PF₆ to a dichloromethane solution of **2** and **3** the rack structures **R1,R2** were exclusively furnished as demonstrated by ¹H-NMR, ¹³C-NMR, ESI-MS, and elemental analysis.



Mechanistic Tests on Formation of [Cu₂(2**)]²⁺.** Rack **R1** [Cu₂(**2**)(**3a**)₂]²⁺ was selected as a model system and its formation systematically investigated using a variety of spectroscopic techniques (by ¹H NMR, ESI-MS and spectrophotometric titrations). Treatment of ligand **2** with 2 equiv. of [Cu(MeCN)₄]PF₆ resulted in a yellow solution, the analysis of which by UV-vis (absence of a MLCT band at 430-550 nm of a [Cu(phenanthroline)₂]⁺ complex), ESI-MS and ¹H NMR suggested the formation of [Cu₂(**2**)(MeCN)₂]²⁺ as the sole species. As expected, ligand **2** acts as a **HETPHEN** ligand that is not able to self-assemble to a homoleptic grid.

Progressive addition of [Cu(MeCN)₄]PF₆ to **2** (in dichloromethane) provided valuable information about the intermediates as they could be readily detected by ESI-MS, ¹H NMR, and UV-vis spectroscopy. In the ¹H NMR spectrum, for example, the mesityl protons Mes-H can be used as a diagnostic marker to assign the composition of the intermediate species present in the equilibrium. Addition of Cu(I) salt to **2** in dichloromethane resulted in two new sets of signals, one of which built up at the initial stage of the titration and disappeared as the titration proceeded. The first set of signals, formed during addition of the first eq. of Cu(I) salt, was assigned to [Cu(**2**)(MeCN)]⁺. After addition of 2 eqs. of Cu(I) salt a single set of signals resulted which could be readily assigned to [Cu₂(**2**)(MeCN)₂]²⁺. Importantly, during

the whole process no signals were detectable at 5-6 ppm, which is considered to be a characteristic range for mesityl protons of a $[\text{Cu}(\text{phenanthroline})_2]^+$ complex.^[9] ESI-MS titration results further supported the above assignments.

The UV-vis titration revealed the absence of a band at ~500 nm, indicating that formation of a $[\text{Cu}(\text{phenanthroline})_2]^+$ complex with its characteristic MLCT had not occurred. These results indicate that in line with the behaviour of monophenanthroline analogs^[9] ligand **2** has been successfully instructed not to assemble with itself.

Most convincingly the structure of $[\text{Cu}_2(\mathbf{2})(\text{MeCN})_2]^{2+}$ was supported by a single crystal structure analysis (Figure 1). It is worthwhile to note that, though the present system is a simple one, the solid state characterisation of such an intermediate in a coordination equilibrium is quite unique. $[\text{Cu}_2(\mathbf{2})(\text{MeCN})_2]^{2+}$ has neither a *syn* or *anti* conformation with regard to the two phenanthroline binding sites. Instead, the two sites comprise a dihedral angle of ~122 deg. Each copper(I) center is coordinated to one phenanthroline and a single acetonitrile molecule. The average $\text{Cu}-\text{N}_{\text{phen}}$ bond distance is 204 ± 3 pm, while the $\text{Cu}-\text{N}_{\text{MeCN}}$ distance is much shorter with 186 pm (Table 1). In conclusion, the solid state structure along with the ^1H NMR, ESI-MS and UV-vis studies proves unequivocally that the HETPHEN concept allows to control the coordination equilibrium of specially designed phenanthroline ligands and to prevent formation of any bishomoleptic complex formation.

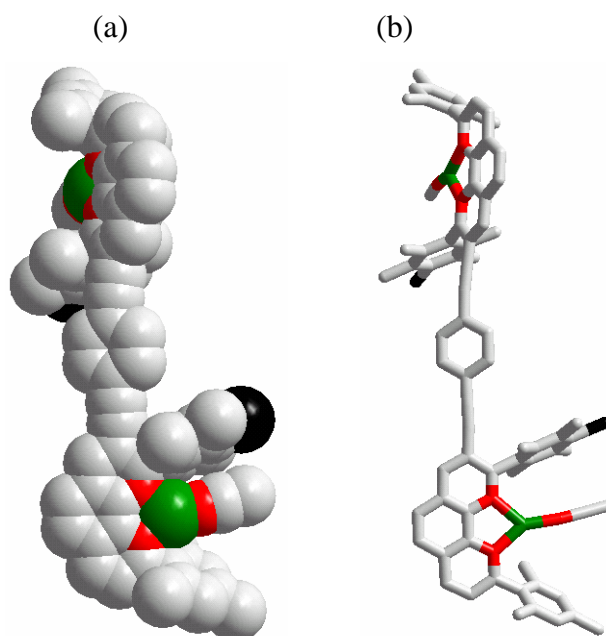


Figure 1. a) Space filling and b) stick representation of the crystal structure of $[\text{Cu}_2(\mathbf{2})(\text{MeCN})_2]^{2+}$.

Table 1. Selected Bond Lengths (Å) and Angles (deg) for $[\text{Cu}_2(\mathbf{2})(\text{MeCN})_2]^{2+}$.

bond		length (Å)	angle			angle (deg)
N1	CU1	2.016(17)	N1	CU1	N5	146.14(1)
N2	CU1	2.050(9)	N2	CU1	N5	130.10(1)
N5	CU1	1.856(18)	N2	CU1	N1	82.91(2)
N3	CU2	2.071(7)	N3	CU2	N6	131.88(1)
N4	CU2	2.017(21)	N4	CU2	N6	142.61(2)
N6	CU2	1.861(20)	N3	CU2	N4	82.54(2)

Mechanistic Tests on Formation of $[\text{Cu}_2(\mathbf{2})(\mathbf{3a})_2]^{2+}$. Upon addition of a second phenanthroline, such as **3a** or **3b**, to the intermediate $[\text{Cu}_2(\mathbf{2})(\text{MeCN})_2]^{2+}$ in dichloromethane, the racks **R1** or **R2** were afforded in basically quantitative yield as evidenced by $^1\text{H-NMR}$ and ESI-MS. For example, in case of **R1** ESI-MS showed the presence of one single species at $m/z = 814.5$ which corresponds to **R1** $^{2+}$. Equally, the $^1\text{H-NMR}$ illustrated the presence of a single symmetric species (Figure 2). The distinct high field shifts for the mesitylene protons (6.76 to 5.89 ppm) of **2** clearly indicated the formation of a bisheteroleptic complex.

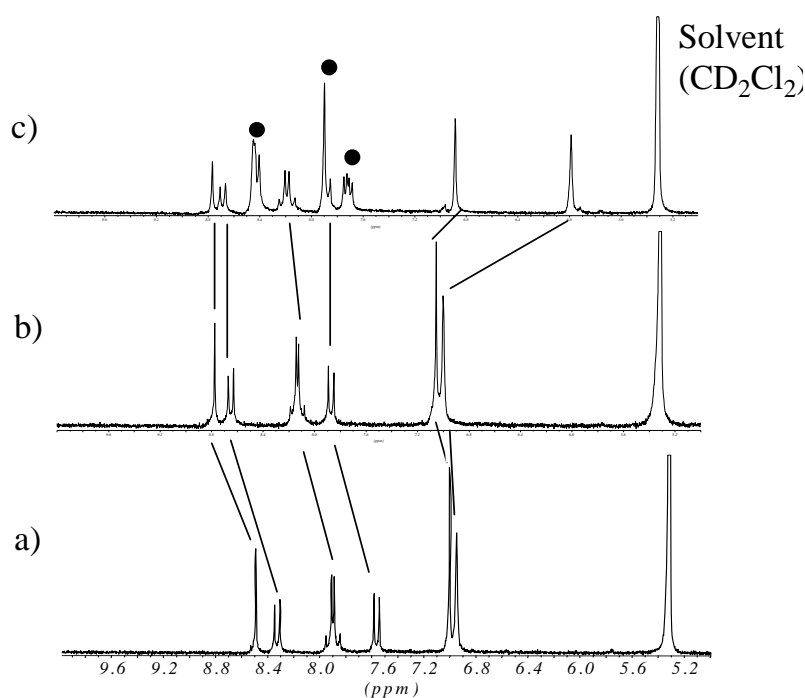


Figure 2. ^1H NMR changes in the aromatic region of **2** upon complexation with **3a**. a) free **2**; b) $[\text{Cu}_2(\mathbf{2})(\text{MeCN})_2]^{2+}$; c) $[\text{Cu}_2(\mathbf{2})(\mathbf{3a})_2]^{2+}$. Signals in figure **c** being marked by filled spheres belong to phenanthroline (**3a**) protons.

For further understanding, a titration was performed, in which **3a** was added to a dichloromethane solution of $[\text{Cu}_2(\mathbf{2})(\text{MeCN})_2]^{2+}$ leading to pronounced changes in the ^1H NMR spectra. With the titration proceeding, two different sets of signals evolved for the mesityl protons that were readily assigned to $[\text{Cu}(\mathbf{2})(\mathbf{3a})]^+$ and $[\text{Cu}_2(\mathbf{2})(\mathbf{3a})_2]^{2+}$ using parallel ESI-MS results. While ESI-MS and ^1H NMR titrations proposed a qualitative picture of the mechanism of the self-assembly process, a UV-vis titration was undertaken to determine the binding constants. It was performed by titrating **2** (1.2×10^{-6} M) and **3a** (2.4×10^{-6} M) with aliquot amounts of Cu(I) solution in 20 additions (total 4 eq. of Cu^+). Figure 3 displays the UV-vis changes upon Cu(I) salt addition showing the emerging MLCT transition at ~ 490 nm that is responsible for the red color. As shown in Scheme 4 a two step pathway seems most reasonable for the rack assembly process: it starts out with the formation of $[\text{Cu}(\mathbf{2})(\mathbf{3a})]^+$ taking up one more ligand **3a** and Cu(I) to furnish the $[\text{Cu}_2(\mathbf{2})(\mathbf{3a})_2]^{2+}$ complex. The structure of $[\text{Cu}_2(\mathbf{2})(\mathbf{3a})_2]^{2+}$ was confirmed by its single crystal analysis.^[81] Upon fitting this model with UV-vis data using the SPECFIT program^[14] binding constants could readily be extracted for complexes $[\text{Cu}(\mathbf{2})(\mathbf{3a})]^+$ ($\log K_{111} = 11.6$) and $[\text{Cu}_2(\mathbf{2})(\mathbf{3a})_2]^{2+}$ ($\log \beta_{212} = 23.1$). Models that did not fit were rejected.

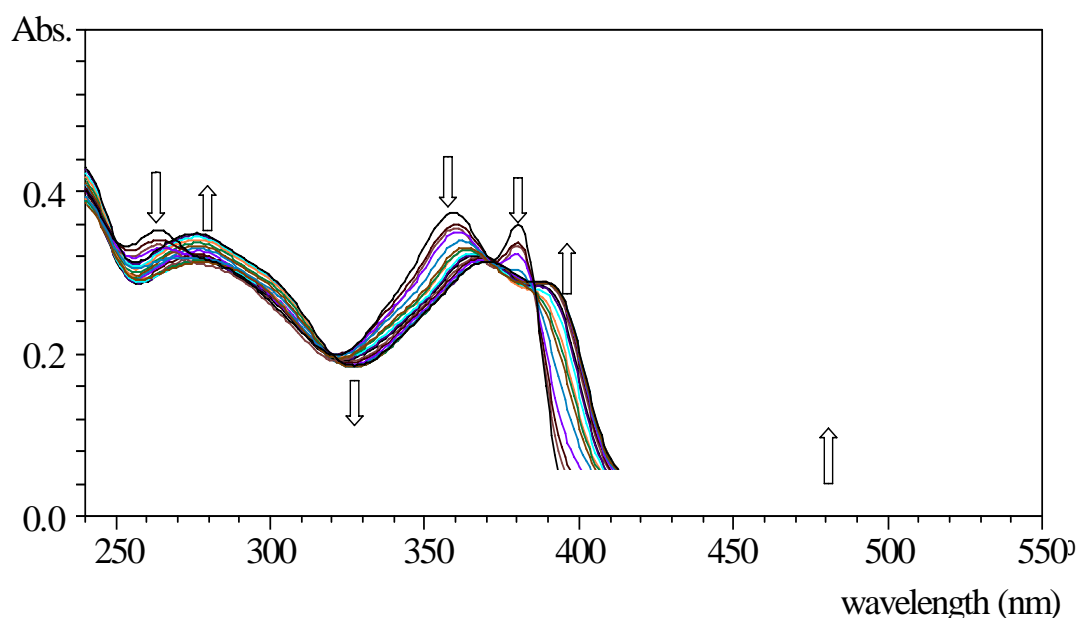
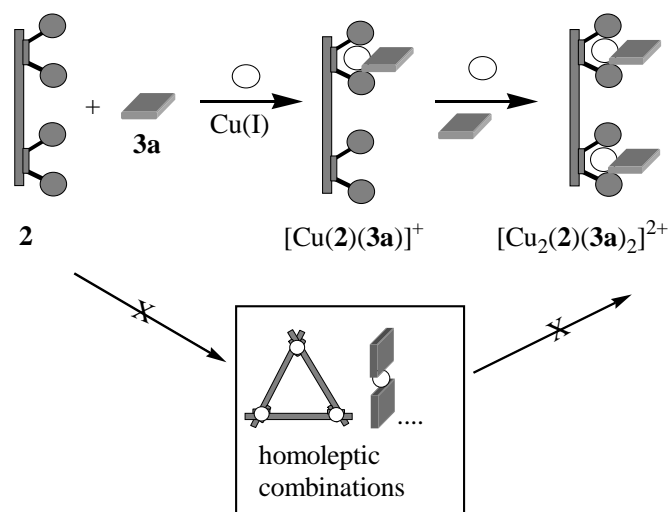


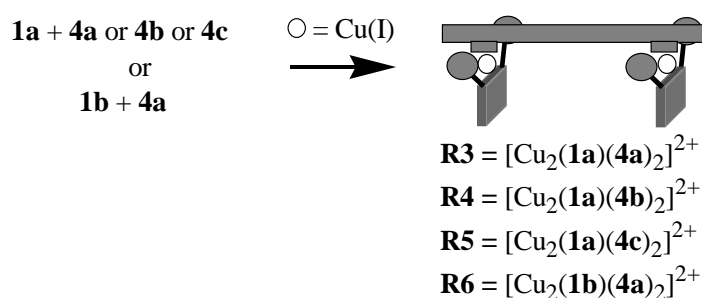
Figure 3. Spectrophotometric titration of **2** and 1,10-phenanthroline (**3a**) by aliquot amounts of Cu(I) salt in 20 additions. Solvent: dichloromethane. $T = 25(1) \text{ }^\circ\text{C}$; $[\mathbf{2}] = 1.20 \times 10^{-6}$ M and $[\mathbf{3a}] = 2.40 \times 10^{-6}$ M.



Scheme 4. Self-assembly path for **R1**.

Approach II

As suggested above, rack-motifs should also be accessible by approach II. **4a-c** were designed according to the HETPHEN strategy, *i.e.* the 2,9-positions of all monophenanthrolines were loaded with steric stoppers while bisphenanthroline **1a** and **1b** were devoid of this element. Notably, racks **R3-R5** were readily afforded upon reacting **1a** with **4a-c** in presence of $[\text{Cu}(\text{MeCN})_4]\text{PF}_6$ (Scheme 5). Similarly, **R6** was obtained by reacting **1b**, **4a** and Cu(I) salt in dichloromethane (1:2:2 eqs.). All spectral data was consistent with the proposed composition (see experimental section).



Scheme 5.

Mechanistic tests. Apart from conventional characterisation techniques (^1H NMR, ESI-MS, UV-vis, and elemental analysis), vapour pressure osmometry (VPO) was applied to characterise **R3** as one of the aggregates. VPO is a very useful method to analyse self assembled systems even if they are dynamic;^[15] unfortunately, this technique has not been utilised frequently. For **R3** VPO provided a molar mass of 2417 Da, which is in excellent

agreement (-2%) with the mass obtained from ESI-MS (2473). The characterisation of even larger dynamic structures by VPO is currently under investigation in our laboratory.

The structure of **R6** was solved by single crystal X-ray analysis. The stick representation of the solid state structure of **R6** is depicted in Figure 4. Unlike a previous structure^[8] this rack has some deviation from perfect transoid conformation. Each copper(I) centre exhibits a pseudotetrahedral coordination geometry (N1–Cu1–N4; 108.4°, N2–Cu1–N3; 125.0°, N5–Cu2–N8; 123.1°, N6–Cu2–N7, 120.1°) and finds itself encapsulated by two bromoduryl rings of the bisphenanthroline (Table 2). The duryl groups of **4a** and the phenanthroline plane of the second ligand **1b** are oriented face-to-face separated by 3.5 Å, suggesting π -stacking.

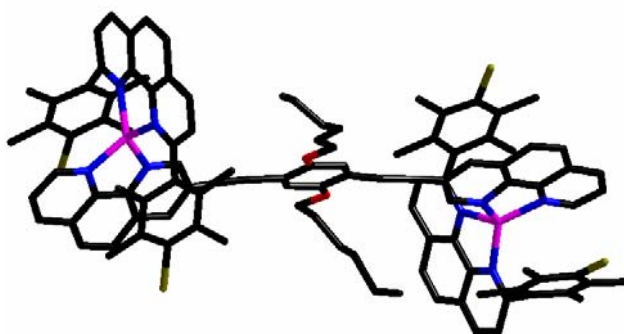


Figure 4. Single crystal structure of **R6**; stick representation.

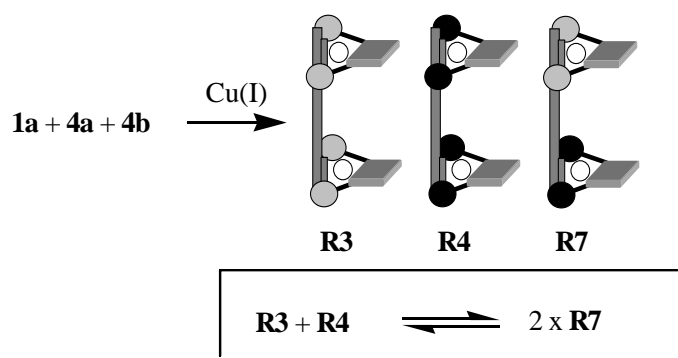
Table 2. Selected bond lengths (Å) and angles (deg) for **R6**.

bond		length (Å)	angle		angle (in degrees)	
Cu1	N4	1.998	N4	Cu1	N2	131.9(4)
Cu1	N3	2.038	N4	Cu1	N3	81.5(4)
Cu1	N2	2.063	N2	Cu1	N3	125.0(4)
Cu1	N1	2.092	N4	Cu1	N1	108.0(4)
			N2	Cu1	N1	81.0(5)
			N3	Cu1	N1	135.0(4)
Cu2	N8	2.062	N7	Cu2	N8	80.0(5)
Cu2	N7	2.006	N7	Cu2	N6	119.5(4)
Cu2	N5	2.029	N8	Cu2	N6	127.5(4)
Cu2	N6	2.069	N7	Cu2	N5	129.0(4)
			N8	Cu2	N5	123.0(4)
			N6	Cu2	N5	82.5(4)

Dynamic Nature of Rack Motifs

The dynamic nature of the rack motifs was tested by an exchange experiment.^[16] Specifically, we monitored the ligand exchange between **R3** and **R4** by using ESI-MS, with ligand **1a** being common in both **R3** and **R4** (Scheme 6). ¹H NMR experiments on the **R3** + **R4** \rightleftharpoons **R7** equilibration could not be performed due to signal overlap. However, the present example was studied by ESI-MS furnishing sensible insight into the dynamics of such aggregates. Such investigations are very informative when NMR application is limited.

R3 and **R4** in dry dichloromethane were reacted in a 1:1 stoichiometric ratio. The ligand exchange process was observed readily (within ~5 min) by ESI-MS exhibiting signals corresponding to a mixture of the three racks **R3**, **R4** and **R7** in a %ratio of 55, 55 and 100, respectively. This ratio did not change after longer times, indicating that equilibrium had been established at rt within less than 5 min (Figure 5). Analogous results were obtained when the racks were generated in one pot by reacting **1a**, **4a** and **4b** in presence of Cu(I) salt. Isotopic distributions of **R3**, **R4** and **R7** were in excellent agreement with the calculated ones.



Scheme 6. Cartoon representation of ligand exchange equilibrium in solution after mixing **R3** and **R4**.

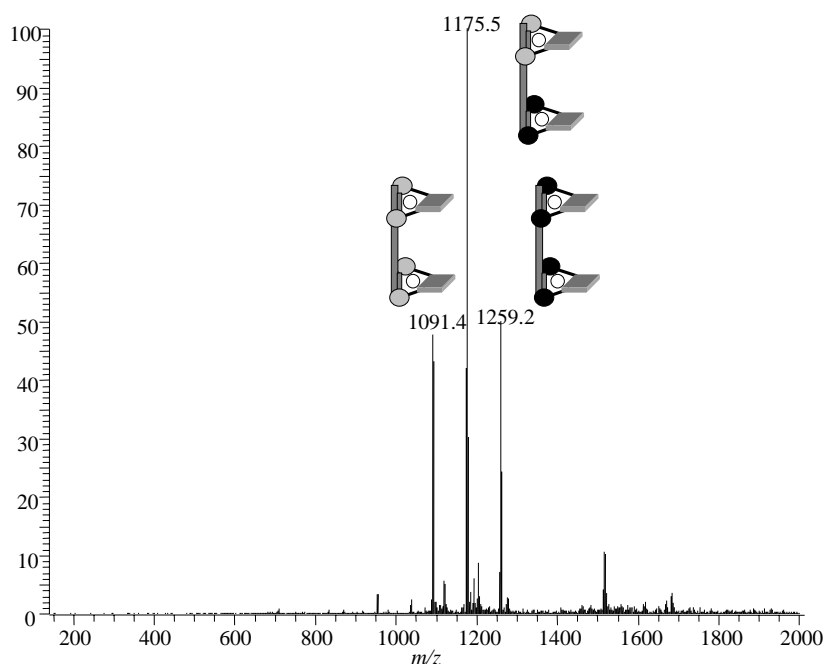
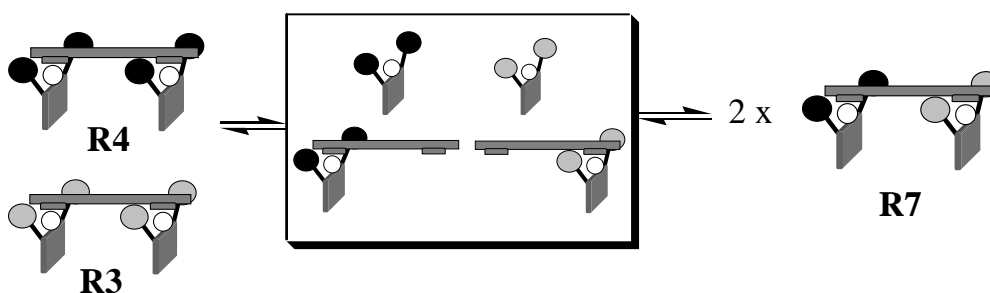


Figure 5: ESI-MS of the reaction mixture obtained when **1a**, **4a**, **4b** are reacted with Cu(I) salt in dichloromethane.

The composition was further confirmed by collisional fragmentation experiments. At higher voltages and temperature the ESI-MS is dominated by $[\text{Cu}(\mathbf{4a} \text{ or } \mathbf{4b})(\mathbf{1a})]^+$ and $[\text{Cu}(\mathbf{4a} \text{ or } \mathbf{4b})]^+$ as fragments. It is interesting to note that a similar behaviour was observed for all rack structures, *i.e.* it is always the sterically loaded ligand that is bound to the metal ion in fragmentation processes. Presumably due to cation- π interactions between Cu^+ and 2,9-aryl groups complexes $[\text{Cu}(\mathbf{4a} \text{ or } \mathbf{4b})]^+$ are more stable than other combinations. These findings were corroborated through collisional fragmentation experiments of **R3**, **R4** and **R7**. For example, fragmentation of **R4** produced signals corresponding to the $[\text{Cu}(\mathbf{4b})(\mathbf{1a})]^+$ and $[\text{Cu}(\mathbf{4b})]^+$ species. If we translate these ESI-MS results onto the equilibration process in solution then it is reasonable to assume that in the dynamic ligand exchange any dissociation occurs with the metal ions attached to the sterically shielded HETPHEN ligands (Scheme 7).



Scheme 7. Mechanism of the dynamic ligand exchange in the interconversion of racks.

Conclusion. In summary, the HETPHEN concept proves its value for the clean preparation of racks **R1-R6** from various bisphenanthrolines and monophenanthrolines in presence of Cu^+ . X-ray and solution spectroscopic data, including ESI-MS, UV-vis titrations and vapour pressure osmometry, disclose a clear picture of the self-assembly pathway and the products. Accordingly, ligands shielded along the HETPHEN concept (**2** and **4**) bind strongly to the copper ions but are instructed not to undergo self-association to homoleptic complexes. In combination with unshielded ligands **1** and **3** racks **R1-R6** are formed in a stepwise manner. Racks **R1-R6** are dynamic in nature as demonstrated in exchange processes at room temperature. Since Cu(I)-based bisphenanthroline complexes are potential photoactive devices,^[17] the present results should open an easy venue to diverse functional aggregates. Studies are in progress to install multi-functionalities into these rack motifs and to study their properties as a function of the dynamic behaviour.

Experimental

Ligands, **1a**,^[11] **1b**,^[11] **2**,^[11] **3b**,^[13] **4a**,^[6c] **4b**^[12] and **4c**^[13] were prepared according to known procedures. ^1H NMR and ^{13}C NMR were measured on a Bruker AC 200 (200 MHz) or Bruker AC 400 (400 MHz). All ^1H NMR measurements were carried at room temperature in $[\text{D}_2]$ -dichloromethane. ESI-MS spectra were measured on a LCQ Deca Thermo Quest. Typically, each time 25 scans were accumulated for one spectrum. UV-vis spectra were recorded on a Tidas II spectrophotometer using dichloromethane as the solvent.

Spectrophotometric titrations: Equilibrium constants of the complexes were determined in dichloromethane. Ligands **2** and **3a** were titrated with aliquot amounts of a stock solution of copper(I) tetrakisacetonitrile hexafluorophosphate. All stock solutions were prepared by careful weighing on a μg analytical balance. Absorption spectra were recorded at $25.0 \pm (0.1)$ °C. Since the formation is instantaneous as evidenced by proton NMR, ESI-MS analysis and visible colour changes, the solutions were immediately analysed spectroscopically to avoid problems with the volatile solvent. The wavelength region from 240 nm to 600 nm was taken into account. Two equivalents (total) of metal salt in dichloromethane solution were added in 20 portions. The entire data sets comprising absorbances measured with one nanometer resolution were decomposed in their principal components by factor analysis. Subsequently, formation constants and their standard deviations were calculated by using the SPECFIT^[14] program. Binding constants were determined from two independent titrations.

Vapor-Pressure Osmometry: The instrument (EuroOsmo 7000) was operated at 27 °C using dry dichloromethane as solvent. It was calibrated using tetrabutylammonium hexafluorophosphate as standard.

General procedure for the preparation of racks R1-R6:

Racks **R1-6** were prepared by mixing **1** (or **2**) and **3** (or **4**) with [Cu(MeCN)₄]PF₆ (1:2:2 equiv. respectively) in dichloromethane. The resulting dark red compound was analysed without any further purification by ESI-MS, ¹H NMR, COSY, ¹³C NMR, IR and elemental analysis.

[Cu₂(**2**)(**3a**)₂](PF₆)₂ (**R1**): M.p. > 300 °C; ¹H NMR (CD₂Cl₂, 400 MHz): δ 8.81 (s, 2H, phen), 8.73 (d, *J* = 8.1 Hz, 2H, phen), 8.40-8.50 (m, 8H, phen), 8.23 (dd, 4H, *J* = 8.1 Hz, *J* = 4.0 Hz, phen), 7.94 (s, 4H, phen), 7.92 (d, *J* = 8.1 Hz, 2H, phen), 7.75 (m, 4H, phen), 6.93 (s, 4H, phenyl), 6.03 (s, 4H, mes), 1.81 (s, 12H, CH₃), 1.59 (s, 12H, CH₃), 1.57 (s, 18H, CH₃); ¹³C NMR (CD₂Cl₂, 100 MHz): δ 161.3, 159.9, 148.1, 144.3, 143.2, 142.9, 139.9, 139.1, 138.2, 138.1, 136.9, 135.0, 134.1, 133.6, 132.5, 131.9, 129.2, 129.1, 128.7, 128.1, 127.9, 127.6, 127.3, 125.1, 122.9, 122.5, 117.5, 117.1 (arom.); 96.7, 87.7 (ethynyl); 20.6, 20.3 (2C), 18.5 (aliph.); IR (KBr): ν 3411, 3057, 2919, 2209 (ν C≡C), 1718, 1655, 1636, 1509, 1438, 1381, 1083, 856, 729, 550; ESI-MS: calcd. for C₉₆H₇₆N₈Br₂Cu₂²⁺ [M²⁺]: *m/z* 814.3, found: *m/z* 814.5; Anal. Calcd. for C₉₆H₇₆N₈Br₂Cu₂*2PF₆*2H₂O (1954.54): C, 58.99; H, 4.13; N, 5.73. Found: C, 58.95; H, 4.01; N, 5.84.

[Cu₂(**2**)(**3b**)₂](PF₆)₂ (**R2**): M.p. > 300 °C; ¹H NMR (CD₂Cl₂, 200 MHz): δ 8.78 (s, 2H, phen), 8.74 (d, 2H, *J* = 8.4 Hz, phen), 8.20-8.36 (m, 10H, phen), 7.91 (d, 2H, *J* = 7.9 Hz, phen), 7.53 (s, 2H, phen), 6.84 (s, 4H, phenyl), 6.15 (s, 4H, mes), 2.91-3.01 (m, 8H, hexyl), 1.83 (s, 12H, benzyl), 1.56 –1.65(m, 30H, benzyl), 1.33 (s, 32H, aliph.), 0.86 (s, 12H, aliph.); ¹³C NMR (CD₂Cl₂, 100 MHz): δ 161.0, 159.9, 149.2, 144.1, 142.7, 142.3, 142.1, 140.5, 139.7, 138.6, 138.4, 138.1, 138.0, 137.7, 134.9, 133.4, 132.3, 131.8, 129.9, 129.1, 128.8, 128.1, 127.6, 127.3, 126.8, 124.4, 122.8, 122.5 (arom.); 96.7, 87.5 (ethynyl); 32.1, 31.8, 30.0, 29.4, 22.9, 20.6, 20.3, 20.1, 18.4, 14.2 (aliph.); IR (KBr): ν 3439, 2926, 2857, 2212 (ν C≡C), 1617, 1571, 1492, 1459, 1421, 1371, 1084, 842, 727, 635, 558; ESI-MS: calcd. for C₁₂₀H₁₂₀N₈Cl₂Br₂Cu₂²⁺ [M²⁺]: *m/z* 1051.5, found: *m/z* 1052.3; Anal. Calcd. for C₁₂₀H₁₂₄N₈Cl₄O₂Br₂Cu₂*2PF₆*2H₂O (2428.96): C, 59.34; H, 5.15; N, 4.61. Found: C, 59.13; H, 4.95; N, 4.51.

[Cu₂(**1a**)(**4a**)₂](PF₆)₂ (**R3**): M.p. > 300 °C; ¹H NMR (CD₂Cl₂, 200 MHz): δ 8.51 (d, *J* = 8.6 Hz, 4H, phen), 8.43 (m, 8H, phen), 7.99 (s, 4H, phen), 7.91 (m, 8H, phen), 7.75 (dd, *J* = 8.9

Hz, $J = 4.9$ Hz, 2H, phen), 7.06 (s, 2H, phenyl), 4.01 (t, $J = 5.5$ Hz, 4H, -OCH₂-), 1.70 (m, 40H, benzyl), 1.53 (s, 14H, benzyl and aliph.), 1.17-1.22 (m, 34H, aliph.), 0.86 (t, $J = 5.5$ Hz, 6H, aliph.); ¹³C NMR (CD₂Cl₂, 100 MHz): δ 160.1, 154.2, 149.3, 148.6, 145.1, 143.3, 142.1, 141.7, 138.9, 138.4, 136.3, 134.1, 133.6, 133.1, 130.4, 129.7, 129.1, 127.5, 126.8, 126.4, 123.4, 123.1, 118.5, 113.1 (arom.); 93.5, 91.4 (ethynyl); 33.4, 29.7 (2C), 30.1 (2C), 30.9 (2C), 26.5, 23.4, 21.1 (2C), 20.4, 19.1 (2C), 14.5 (aliph.); IR (KBr): ν 3444, 2852, 2208 (ν C \equiv C), 1618, 1579, 1498, 1459, 1426, 1388, 1221, 1164, 1018, 936, 872, 843, 724, 632, 558; ESI-MS: calcd. for C₁₂₂H₁₂₆N₈O₂Br₄Cu₂²⁺ [M²⁺]: m/z 1091.5, found: m/z 1090.7; Anal. Calcd. for C₁₂₂H₁₂₈N₈O₃Br₄Cu₂*2PF₆*H₂O (2491.01): C, 58.82; H, 5.18; N, 4.50. Found: C, 58.62; H, 5.29; N, 4.34.

[Cu₂(**1a**)(**4b**)₂](PF₆)₂ (**R4**): M.p. > 300 °C; ¹H NMR (CD₂Cl₂, 200 MHz): δ 8.62 (s, 2H, phen), 8.58 (s, 4H, phen), 8.39-8.851 (m, 6H, phen), 8.15 (s, 4H, phen), 7.18-7.96 (m, 8H, phen), 7.70 (dd, $J = 8.9$ Hz, $J = 4.1$ Hz, 2H, phen), 7.01 (s, 2H, phenyl), 6.45 (t, 4H, $J = 8.4$ Hz, phenyl), 5.71 (m, 8H, phenyl), 3.95 (t, $J = 6.7$ Hz, 4H, -OCH₂-), 3.30 (s, 12H, methoxy), 3.26 (s, 12H, methoxy), 1.70-1.77 (m, 4H, aliph.), 1.15-1.40 (m, 36H, aliph.), 0.86 (t, $J = 5.9$ Hz, 6H, aliph.); ¹³C NMR (CD₂Cl₂, 100 MHz): δ 160.4, 159.3, 148.6, 143.5, 141.7, 141.5, 139.9, 139.2, 138.1, 137.9, 137.4, 137.1, 134.3, 132.8, 131.7, 131.2, 128.5, 128.2, 127.5, 127.0, 126.2, 123.8, 122.2, 121.9 (arom.); 96.1, 86.9 (ethynyl); 31.5, 31.3, 29.6, 29.4, 28.8, 22.3, 20.1, 19.7, 19.6, 18.2, 18.0, 17.9, 13.6 (aliph.); IR (KBr): ν 3443, 2924, 2851, 2208 (ν C \equiv C), 1589, 1499, 1433, 1253, 1222, 1112, 1023, 841, 777, 723, 558; ESI-MS: calcd. for C₁₁₄H₁₁₄N₈O₁₀Cu₂²⁺ [M²⁺]: m/z 941.5, found: m/z 941.2; Anal. Calcd. for C₁₁₄H₁₁₈N₈O₁₂Cu₂*2PF₆*2H₂O (2209.22): C, 61.98; H, 5.38; N, 5.07. Found: C, 61.85; H, 4.35; N, 5.04.

[Cu₂(**1a**)(**4c**)₂](PF₆)₂ (**R5**): M.p. > 300 °C; ¹H NMR (CD₂Cl₂, 200 MHz): δ 8.80 (s, 4H, phen), 7.93 (s, 2H, phen), 7.83 (d, 2H, $J = 7.9$ Hz, phen), 7.61 (dd, $J = 8.8$ Hz, $J = 4.1$ Hz, 4H, phen), 6.85-7.22 (m, 40H, phen and anthracene), 6.64 (m, 4H, phen and phenyl), 4.19 (t, $J = 6.4$ Hz, 8H, -OCH₂-), 2.78 (m, 8H, aliph. and benzyl), 1.24-1.63 (m, 50H, benzyl), 0.76-0.93 (m, 24H, aliph.), 0.49 (t, $J = 5.9$ Hz, 12H, aliph.); ¹³C NMR (CD₂Cl₂, 100 MHz): δ 158.4, 158.4, 154.5, 155.2, 149.1, 147.3, 143.7, 143.1, 141.6, 140.9, 140.4, 139.6, 138.4, 136.6, 135.1, 133.5, 130.4, 129.4, 128.3, 127.4, 126.8, 125.9, 125.3, 124.9, 121.3, 117.5, 114.3, 103.9 (arom.); 91.9, 84.5 (ethynyl); 32.4, 32.3 (2C), 31.1 (2C), 30.1 (2C), 29.2 (2C), 26.5, 23.1 (2C), 22.3 (2C), 14.5, 14.3, 13.8 (2C) (aliph.); IR (KBr): ν 3461, 3053, 2923, 2853, 2209 (ν C \equiv C), 1622,

1604, 1545, 1498, 1461, 1366, 1345, 1276, 1220, 1106, 1014, 958, 841, 791, 736, 723, 557, 532; ESI-MS: calcd. for $C_{162}H_{158}Cl_4O_2N_8Cu_2^{2+}$ [M^{2+}]: m/z 1258.9, found: m/z 1257.9; Anal. Calcd. for $C_{162}H_{164}Cl_4N_8O_5Cu_2 \cdot 2PF_6 \cdot 3H_2O$ (2861.92): C, 67.99; H, 5.78; N, 3.92. Found: C, 67.54; H, 5.32; N, 3.85.

$[Cu_2(\mathbf{1b})(\mathbf{4a})_2](PF_6)_2$ (**R6**): M.p. > 300 °C; 1H NMR (CD_2Cl_2 , 400 MHz): δ 8.75 (d, $J = 8.08$, 4H, phen), 8.43-8.52 (m, 8H, phen), 8.25 (s, 4H, phen), 7.91 (m, 8H, phen), 7.75 (q, $J = 4.8$ Hz, 2H, phen), 7.08 (s, 2H, phenyl), 4.02 (t, $J = 6.3$ Hz, 4H, $-OCH_2-$), 2.40 (s, 3H, benzyl), 1.95 (s, 3H, benzyl), 1.77 (s, 16H, aliph.), 1.65 (s, 12H, benzyl), 1.53 (s, 12H, benzyl), 1.45 (s, 6H, benzyl), 1.41 (m, 6H, benzyl), 1.20 (m, 6H, benzyl), 0.71 (t, $J = 7.08$ Hz, 6H, aliph.); ^{13}C NMR (CD_2Cl_2 , 100 MHz): δ 159.1, 154.3, 149.0, 148.1, 144.6, 142.4, 141.2, 140.7, 138.7, 138.1, 135.2, 134.6, 133.1, 132.9, 132.5, 129.7, 128.8, 128.1, 127.1, 126.4, 125.2, 121.5, 116.1, 113.2 (arom.); 92.4, 91.1 (ethynyl); 31.2, 29.4, 25.4, 22.1, 21.6, 20.9, 19.6, 14.1 (aliph.); IR (KBr): ν 3394, 2921, 2301 ($\nu C\equiv C$), 1736, 1618, 1495, 1427, 1426, 1368, 1018, 956, 842, 724, 633, 557; ESI-MS: calcd. for $C_{110}H_{102}N_8O_2Br_4Cu_2^{2+}$ [M^{2+}]: m/z 1007.3, found: m/z 1006.2; X-ray structure see Figure 4.

Crystal Structure Determinations: Crystals were obtained by slow diffusion of toluene into a solution of the complexes in dichloromethane. Due to the poor quality of the crystals the crystal data are not excellent. Solvent molecules are severely disordered. The measurements were carried out with a STOE-IPDS2 diffractometer with graphite-monochromatised Mo- $K\alpha$ radiation. Table 3 summarises the crystal data, data collection, and refinement parameters. All calculations were performed with the SHELXS-97 package.

Table 3. X-ray experimental data for [Cu₂(**2**)(MeCN)₂*2PF₆] and [Cu₂(**1b**)(**4a**)*2PF₆].

Formula	[Cu ₂ (2)(MeCN) ₂ *2PF ₆] Cu ₂ C ₇₆ H ₆₆ Br ₂ F ₁₂ N ₆ P ₂	[Cu ₂ (1b)(4a)*2PF ₆] Cu ₂ C ₁₁₀ H ₁₀₂ Br ₄ F ₁₂ N ₈ O ₂ P ₂
M _w	1640.21	2304.68
Crystal system	monoclinic	triclinic
Space group	P 1 21/c 1 (no. 14)	P -1 (no. 2)
a [Å°]	21.297(4)	13.0625(80)
b [Å°]	22.658(5)	21.250(15)
c [Å°]	17.044(3)	23.75(2)
α [°]	90.00	113.00(3)
β [°]	104.29(3)	95.00(3)
γ [°]	90.00	94.00(3)
V [Å ³]	7970(3)	6006.46(800)
Z	4	2
color	yellow	red
crystal shape	needle	needle
crystal dimensions	0.3X0.15X0.1	0.3X0.15X0.1
D _{calcd} (g cm ⁻³)	1.367	1.274
F000	3656	2656
radiation	MoK\α graphite	MoK\α graphite
device type	IPDS2 STOE	IPDS2 STOE
Reflections collected	44882	43551
R(int)	0.0543	0.1144
Independent reflections	20487	22023
Data/parameters	20487/900	22023/1285
GOF on F ²	1.564	1.234
reflections threshold	>2sigma(I)	>2sigma(I)
expression		
hkl limits (max/min)	-23/29, -26/31, -23/21	-16/16, -26/26, -29/29
Final R indices [I > 2σ(I)]	R ₁ = 0.0919, wR ₂ = 0.2404	R ₁ = 0.1281, wR ₂ = 0.2960
R indices (all data)	R ₁ = 0.1259, wR ₂ = 0.2558	R ₁ = 0.2317, wR ₂ = 0.3352

Acknowledgements. We would like to express our gratitude to the Deutsche Forschungsgemeinschaft (Schm 647/12-1 and 13-1) and the Fonds der Chemischen Industrie for financial support.

[1] [1a] H. Sleiman, P. Baxter, J.-M. Lehn, K. Rissanen, *J. Chem. Soc. Chem. Commun.* **1995**, 715-716. [1b] G. S. Hanan, C. R. Arana, J.-M. Lehn, G. Baum, D. Fenske, *Angew. Chem. Int. Ed. Engl.* **1995**, *10*, 1119-1122. [1c] G. S. Hanan, C. R. Arana, J.-M. Lehn, G. Baum, D. Fenske, *Chem. Eur. J.* **1996**, *10*, 1292-1302. [1d] H. Sleiman, P. N. W. Baxter, J.-M. Lehn, K. Airola, K. Rissanen, *Inorg. Chem.* **1997**, *36*, 4734-4742. [1e] D. Brown, R. Zong, R. P. Thummel, *Eur. J. Inorg. Chem.* **2004**, 3269-3272. [1f] M. Benaglia, F. Ponzini, C. R. Woods, J. S. Siegel, *Org. Lett.* **2001**, *3*, 967-969. [1g] P. Ceroni, A. Credi, V. Balzani, S. Campagna, G. S. Hanan, C. R. Arana, J.-M. Lehn, *Eur. J. Inorg. Chem.* **1999**, 1409-1414.

[2] M. Schmittel, V. Kalsani, *Top. Curr. Chem.* **2004**, *245*, 1 - 53.

- [3] [3a] U. Drechsler, B. Erdogan, V. M. Rotello, *Chem. Eur. J.* **2004**, *10*, 5570-5579. [3b] P. H. Kwan, M. J. MacLachlan, T. M. Swager, *J. Am. Chem. Soc.* **2004**, *126*, 8638-8639.
- [4] [4a] C. O. Dietrich-Buchecker, J. P. Sauvage, J. P. Kintzinger, *Tetrahedron Lett.* **1983**, *24*, 5095-5098. [4b] U. Velten, M. Rehahn, *J. Chem. Soc., Chem. Commun.* **1996**, 2639-2640. [4c] S. S. Zhu, P. J. Carroll, T. M. Swager, *J. Am. Chem. Soc.* **1996**, *118*, 8713-8714.
- [5] The HETPHEN (**heteroleptic bisphenanthroline**) approach is based on steric and electronic effects originating from bulky aryl substituents at the bisimine coordination sites to control the coordination equilibrium both kinetically and thermodynamically.
- [6] [6a] V. Kalsani, H. Ammon, F. Jäckel, J. P. Rabe, M. Schmittel, *Chem. Eur. J.* **2004**, *10*, 5481-5492. [6b] M. Schmittel, V. Kalsani, L. Kienle, *Chem. Commun.* **2004**, 1534-1535. [6c] M. Schmittel, A. Ganz, D. Fenske, *Org. Lett.* **2002**, *4*, 2289-2292. [6d] M. Schmittel, H. Ammon, V. Kalsani, A. Wiegrefe, C. Michel, *Chem. Commun.* **2002**, 2566-2567.
- [7] [7a] A. Marquis-Rigault, A. Dupont-Gervais, P. N. W. Baxter, A. Van Dorsselaer, J.-M. Lehn, *Inorg. Chem.* **1996**, *35*, 2307-2310. [7b] P. N. W. Baxter, J.-M. Lehn, B. O. Kneisel, G. Baum, D. Fenske, *Chem. Eur. J.* **1999**, *5*, 113-120. [7c] A. M. Garcia, D. M. Bassani, J.-M. Lehn, G. Baum, D. Fenske, *Chem. Eur. J.* **1999**, *5*, 1234-1238. [7d] P. N. W. Baxter, J.-M. Lehn, B. O. Kneisel, D. Fenske, *Angew. Chem. Int. Ed.* **1997**, *36*, 1978-1981.
- [8] M. Schmittel, V. Kalsani, D. Fenske, A. Wiegrefe, *Chem. Commun.* **2004**, 490-491.
- [9] [9a] M. Schmittel, A. Ganz, *Chem. Commun.* **1997**, 999-1000. [9b] M. Schmittel, U. Lüning, M. Meder, A. Ganz, C. Michel, M. Herderich, *Heterocycl. Commun.* **1997**, *3*, 493-494.
- [10] M. Schmittel, V. Kalsani, unpublished results.
- [11] M. Schmittel, C. Michel, A. Wiegrefe, V. Kalsani, *Synthesis* **2001**, 1561-1567.
- [12] U. Lüning, M. Müller, *Chem. Ber.* **1990**, *123*, 643-645.
- [13] M. Schmittel, C. Michel, S. X. Liu, D. Schildbach, D. Fenske, *Eur. J. Inorg. Chem.* **2002**, 1155-1166.
- [14] [14a] H. Gampp, M. Maeder, C. J. Meyer, A. D. Zuberbühler, *Talanta* **1985**, *32*, 95-101. [14b] F. J. C. Rossotti, H. S. Rossotti, R. J. Whewell, *J. Inorg. Nucl. Chem.* **1971**, *33*, 2051-2065. [14c] H. Gampp, M. Maeder, C. J. Meyer, A. D. Zuberbühler, *Talanta* **1985**, *32*, 257-264. [14d] H. Gampp, M. Maeder, C. J. Meyer, A. D. Zuberbühler, *Talanta* **1986**, *33*, 943-951.
- [15] I. Higler, L. Grave, E. Breuning, W. Verboom, F. D. Jong, T. M. Fyles, D. N. Reinhoudt, *Eur. J. Org. Chem.* **2000**, 1727-1734.
- [16] [16a] P. N. W. Baxter, *Comprehensive, supramolecular chemistry*, ed. J. L. Atwood, J. E. D. Davies, D. D. MacNicol, F. Vögtle and J.-M. Lehn, Pergamon, Oxford, **1996**, *9*, chapter 5, 165-211. [16b] L. J. Charbonnière, A. F. Williams, U. Frey, A. E. Merbach, P. Kamalaprija, O. Schaad, *J. Am. Chem. Soc.* **1997**, *119*, 2488-2496. [16c] Olenyuk, A. Fechtenkotter, P. J. Stang, *J. Chem. Soc., Dalton. Trans.* **1998**, *11*, 1707-1728. [16d] S. Leininger, B. Olenyuk, P. J. Stang, *Chem. Rev.* **2000**, *100*, 853-907. [16e] C. Addicott, N. Das, P. J. Stang, *Inorg. Chem.* **2004**, *43*, 5335-5338. [16f] F. Würthner, A. Sautter, D. Schmid, P. J. A. Weber, *Chem. Eur. J.* **2001**, *7*, 894-902. [16g] S. Hiraoka, Y. Kubota, M. Fujita, *Chem. Commun.* **2000**, 1509-1510.
- [17] N. Armaroli, *Chem. Soc. Rev.* **2001**, 113-124.

Supp 4-4

Chem. Commun. **2004**, 490-491.

Reproduced by permission of *The Royal Society of Chemistry*

Self-Assembly of Heteroleptic [2x2] and [2x3] Nanogrids

Michael Schmittel,^{*a} Venkateshwarlu Kalsani,^a Dieter Fenske^b and Andreas Wiegrefe^a

^a Center of Micro and Nanochemistry and Engineering, Organische Chemie I, Universität Siegen, Adolf-Reichwein-Str., D-57068 Siegen, Germany, Fax: (+49) 271 740 3270; Tel: (+49) 271 740 4356; E-mail: schmittel@chemie.uni-siegen.de

^b Institut für Anorganische Chemie, Universität Karlsruhe, Engesserstr. 3045, D-76128 Karlsruhe, Germany.

Abstract: Using the HETPHEN concept a general and quantitative approach to the formation of heteroleptic nanogrids is illustrated.

The design and engineering of nanoscale supramolecular devices possessing unique functionalities has become an active field of research.¹ Cylinders,² squares, polyhedra^{1,3} and grids⁴ are among the most targeted assemblies. Seminal work by Lehn *et al.* has shown how to engineer homoleptic and even multimetallic metallosupramolecular grid architectures. Due to the desideratum to explore highly functionalised assemblies, however, a strategy to prepare heteroleptic nanogrids would be quite welcome in order to combine different sets of functionalities. While a first example of a heteroleptic grid⁵ was explored by Lehn *et al.* the chosen approach proved not to be general.

In recent years we have developed the HETPHEN concept^{6,7} and demonstrated its potential for the quantitative formation of nanoscale heteroleptic assemblies, *e.g.* the formation of nanoboxes⁸ and ring-in-ring⁹ structures. Herein, we describe the synthesis of four truly nanoscale metallosupramolecular grids along this concept and their characterisation.

The rigid bis- and trisphenanthroline ligands **1-5** were synthesised utilising sequential Sonogashira coupling protocols that will be published elsewhere (Chart 1). Ligands **1,5** were encoded with the required control features to furnish exclusively heteroleptic assemblies, *i.e.* the 2,9 positions of each phenanthroline unit in **1,5** are shielded with bulky methylaryl groups thus preventing any association to homoleptic complexes. The appropriate combination of

this ligand with metal ions such as Cu(I) is expected to yield heteroleptic grids over homoleptic ones.

As a test case for the necessity to apply the HETPHEN concept we first monitored the self-assembly behaviour of **2** and **3** in the presence of $[\text{Cu}(\text{MeCN})_4]\text{PF}_6$ by ESI. A mixture of the homoleptic [2x2] grids $[\text{Cu}_4(\mathbf{2})_4]^{4+}$ and $[\text{Cu}_4(\mathbf{3})_4]^{4+}$ was formed aside of about equal amounts of the heteroleptic grid $[\text{Cu}_4(\mathbf{2})_2(\mathbf{3})_2]^{4+}$. Interestingly, 3:1 combinations, such as $[\text{Cu}_4(\mathbf{2})_3(\mathbf{3})]^{4+}$ or $[\text{Cu}_4(\mathbf{2})(\mathbf{3})_3]^{4+}$, were not detected. The need of additional control becomes even more evident when ligands **2** and **4** were treated in presence of Cu(I) salt to explore the formation of the [2x3] grid. By ESI no [2x3] or [3x3] grids were observed. As the major product the homoleptic [2x2] grid $[\text{Cu}_4(\mathbf{2})_4]^{4+}$ was afforded along with small mononuclear complexes. Apparently, entropic reasons favor formation of the [2x2] grid over any [2x3] and [3x3] grids. From the above results it is clear that it is not possible to build heteroleptic nanoscale grids just relying on maximum site occupancy and cooperativity motifs.

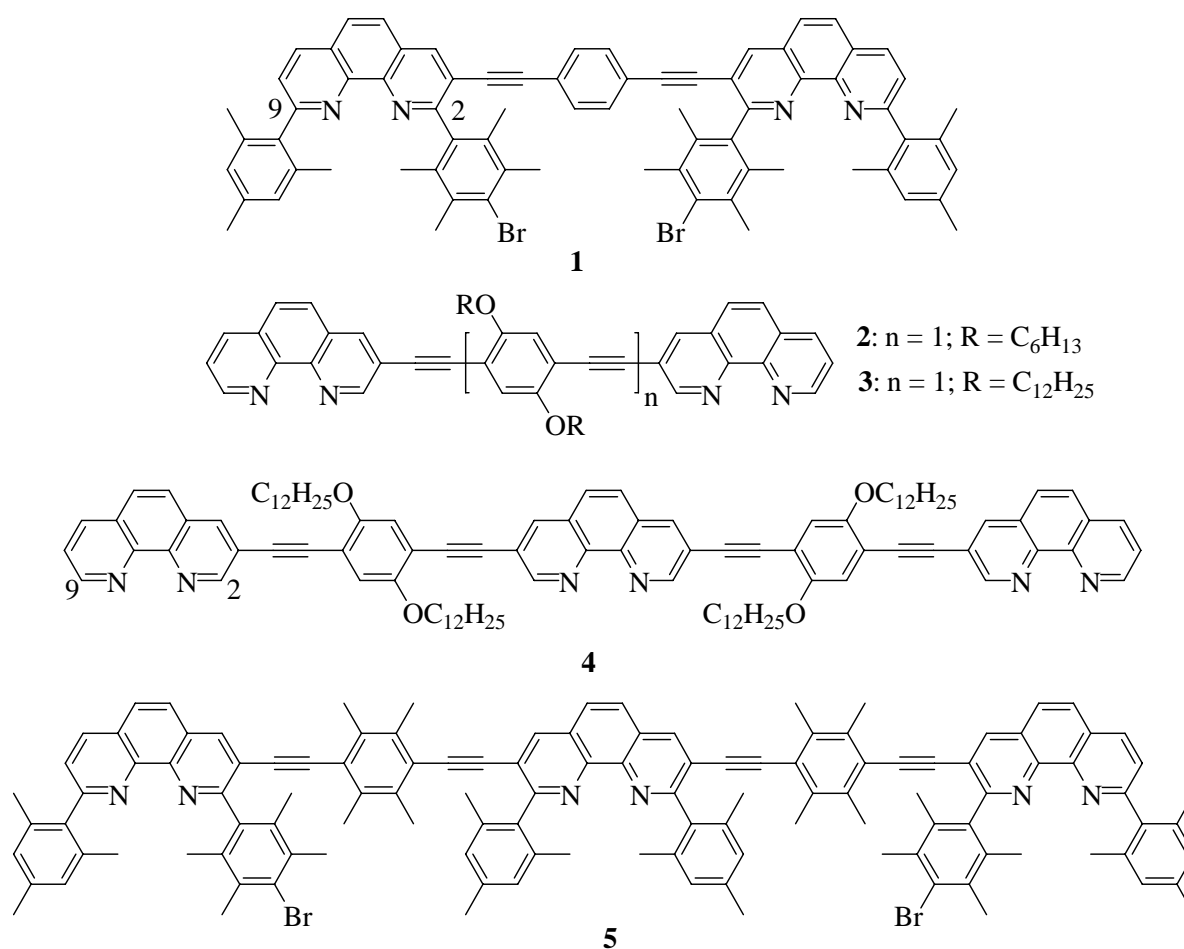


Chart 1. Ligands used to probe the self-assembly of heteroleptic grid motifs.

In contrast, treatment of HETPHEN ligand **1** with 1-2 equiv. of Cu(I) salt resulted in a yellow solution the analysis of which by UV/vis, ESI MS and ^1H NMR indicated $[(\text{Cu})_2(\mathbf{1})]^{2+}$ as the only species. Obviously, formation of any homoleptic complex of **1** is prevented. Addition of two equiv. of the parent phenanthroline (**6**) led to a red solution which by ESI, ^1H -NMR and UV-vis analysis only contained the bisheteroleptic complex $[\text{Cu}_2(\mathbf{1})(\mathbf{6})_2]^{2+}$ demonstrating the validity of the HETPHEN concept.^{6,7} The single crystal structure is presented in figure 1. Accordingly, the molecule has a transoid conformation with C_2 symmetry.

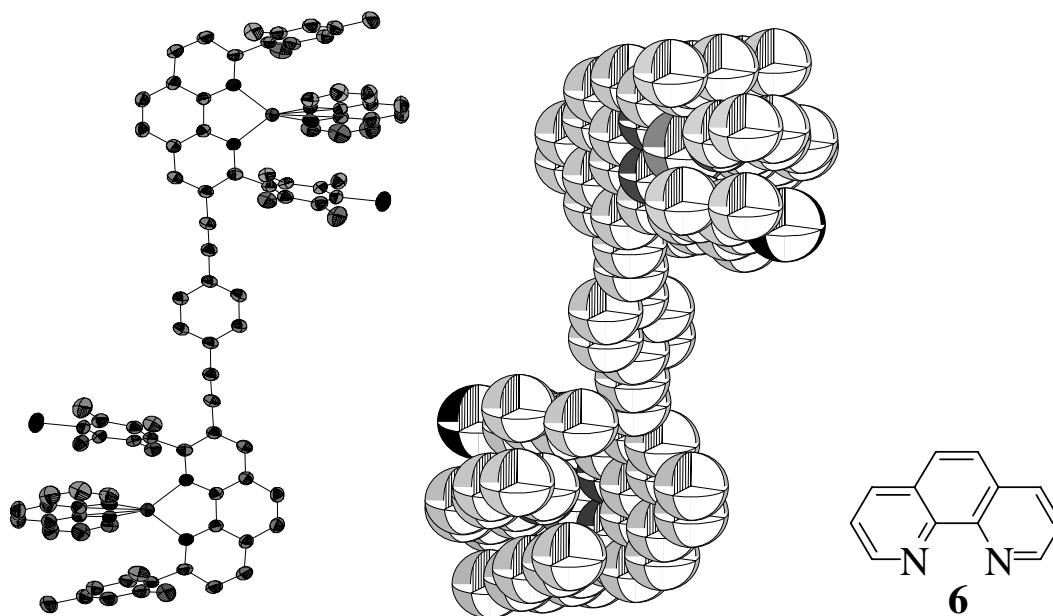
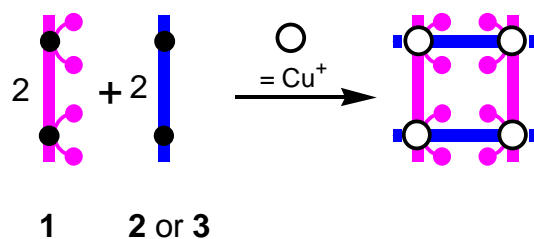


Figure 1. Solid state structure of $[\text{Cu}_2(\mathbf{1})(\mathbf{6})_2]^{2+}$; ball and stick (left) and space filling (middle) representation.

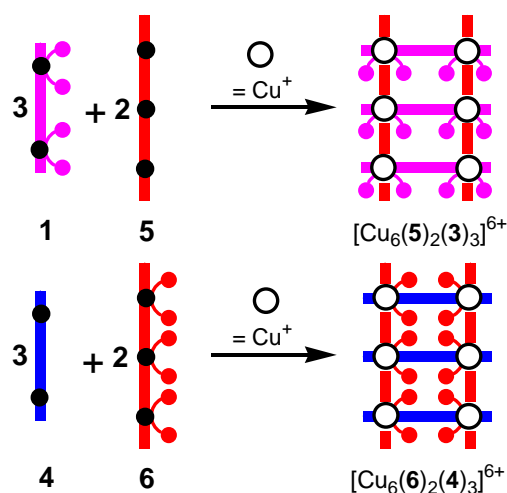
Each copper(I) centre exhibits a pseudotetrahedral coordination geometry (N2-Cu1-N3, 116.1° and N1-Cu-N4, 120.5°) and finds itself encapsulated by two duryl rings of the bisphenanthroline. The duryl groups and the the second ligand (phenanthroline **6**) are oriented face-to-face separated by 3.4 \AA , suggesting π -stacking. As such, compound $[\text{Cu}_2(\mathbf{1})(\mathbf{6})_2]^{2+}$ represents a rigid anti-rack complex.

HETPHEN ligand **1** was now reacted separately with ligands **2** or **3** in presence of $[\text{Cu}(\text{MeCN})_4]\text{PF}_6$ leading to the instant formation of the corresponding [2x2] nanogrids $[\text{Cu}_4(\mathbf{1})_2(\mathbf{2})_2]^{4+}$ and $[\text{Cu}_4(\mathbf{1})_2(\mathbf{3})_2]^{4+}$ as sole products. Each of them displays a sharp and single set of signals in the ^1H NMR, indicating a highly symmetric species. The chemical shifts of the mesityl protons ($\delta \sim 7.0$ in ligand, $\delta \sim 6.0$ ppm in complex) are most diagnostic for heteroleptic complex formation as demonstrated earlier. In summary, the observed ^1H NMR, COSY, ESI-MS and the elemental analysis data are all consistent with the formation of single, highly symmetric heteroleptic assemblies. Though different configurational isomers should be

present in solution, it was not possible to quantify them because of their similar chemical shifts.



To probe the HETPHEN concept for [2x3] grids we reacted **1** with **4** and **3** with **5**. In contrast to the immediate formation of the [2x2] grids we noted a sluggish reaction over two days until finally the [2x3] grids $[\text{Cu}_6(\mathbf{1})_3(\mathbf{4})_2]^{6+}$ and $[\text{Cu}_6(\mathbf{3})_3(\mathbf{5})_2]^{6+}$ had formed. Again, as before the spectroscopic data (^1H NMR, elemental analysis, ESI-MS), in particular isotopic splitting, indicated clean formation of the desired nanogrids.



To obtain more insight into the mechanistic scenario leading to these assemblies, formation of $[\text{Cu}_4(\mathbf{1})_2(\mathbf{3})_2]^{4+}$ was monitored by both ESI MS (qualitative analysis) and UV/vis (quantitative analysis). Two series of titrations were performed. In the first series **1** and **3** were titrated with Cu(I) salt and in the second series **1** and Cu(I) salt were titrated with aliquot amounts of **3**. Both titrations indicated a three step process on the way to the grid (Figure 2) providing complexation constants for two intermediate complexes and the final grid.

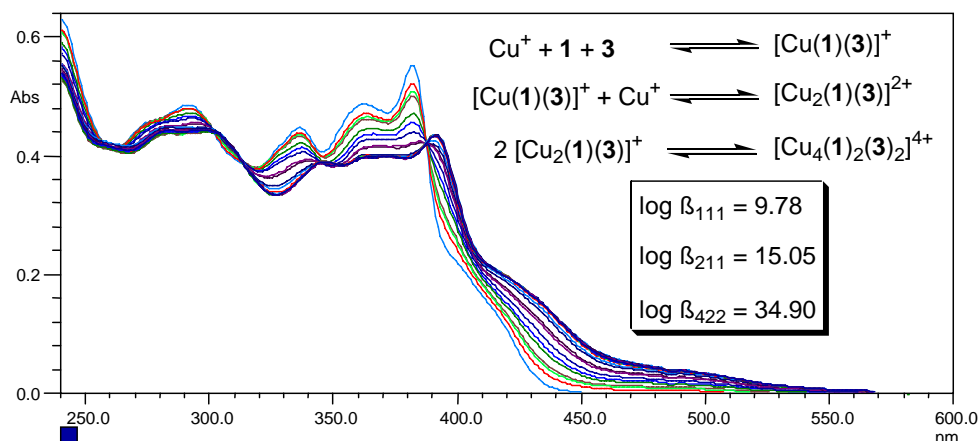


Figure 2. UV-vis titration of **1** and **3** with Cu^+ .

It has to be mentioned that these truly nanoscopic grids do not readily crystallise due to their large voids. Dimensions of the [2x2] grids are 2.9 nm along the edge and 2.5 nm for the Cu-Cu diagonal. The larger [2x3] grids exhibit a length of 6.0 nm and a Cu-Cu diagonal of 5.0 nm.

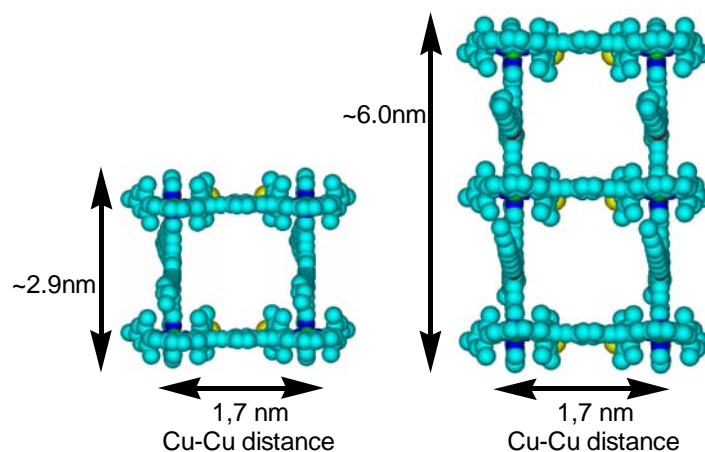


Figure 3. Hyperchem representations of $[\text{Cu}_4(\mathbf{1})_2(\mathbf{3})_2]^{4+}$ (left) and $[\text{Cu}_6(\mathbf{1})_3(\mathbf{4})_2]^{6+}$.

In conclusion, the formation of four heteroleptic nanogrids using the HETPHEN concept has been unambiguously demonstrated. This concept is very powerful in preparing heteroleptic supramolecular architectures, which have been impossible to prepare using simply maximum site occupancy and cooperativity motifs.

Acknowledgements: We are indebted to the Deutsche Forschungsgemeinschaft and the Fonds der Chemischen Industrie for financial support.

Notes:

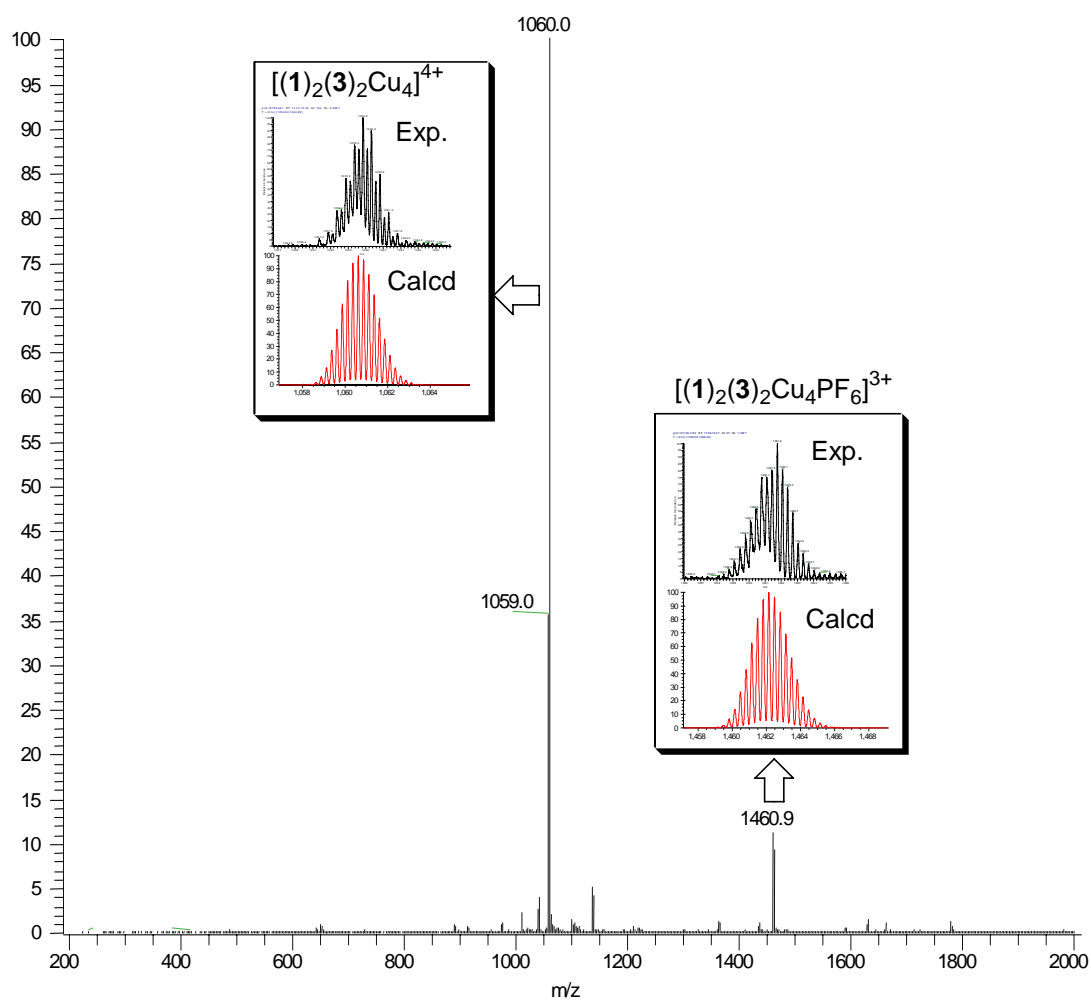
Crystal data for $[\text{Cu}_2(\mathbf{1})(\mathbf{6})_2]^{2+}$. Crystals were obtained by slow diffusion of toluene into methylene chloride solution of the complex. Only poor quality crystals could be obtained due to which the crystal analysis is poor. Solvent (unidentified) molecules are severely disordered. Hydrogen atoms are not included in the refinement. Formula sum $\text{C}_{96}\text{H}_{76}\text{Br}_2\text{Cu}_2\text{F}_{12}\text{N}_8\text{P}_2$, Formula weight 1918.49 (solvent excluded), Crystal system: triclinic, Space group: $P-1$, Unit cell dimensions $a = 10.4460(21) \text{ \AA}$, $b = 14.0790(28) \text{ \AA}$, $c = 16.8010(34) \text{ \AA}$, $\alpha = 84.70(3)^\circ$, $\beta = 80.32(3)^\circ$, $\gamma = 88.63(3)^\circ$, Cell volume: $2425.23(1407) \text{ \AA}^3$, Density, calculated: 1.348 g/cm^3 , Pearson code: aP142, Formula typ: NOPQ4R58, Wyckoff sequence: i^{71}

Supporting Information:

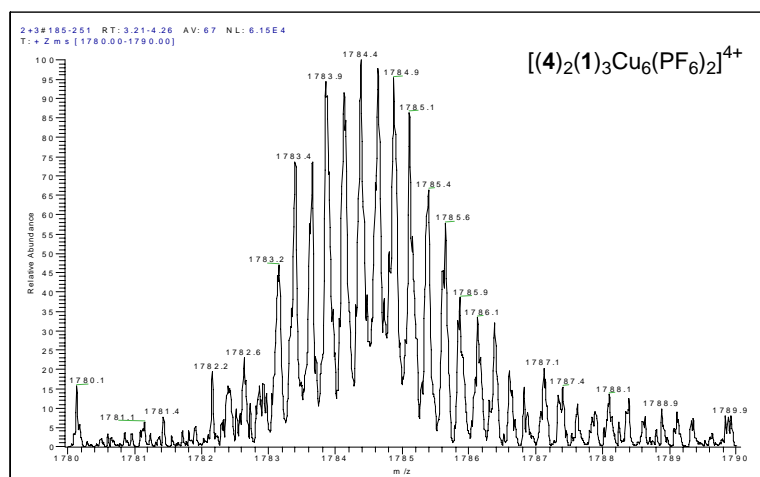
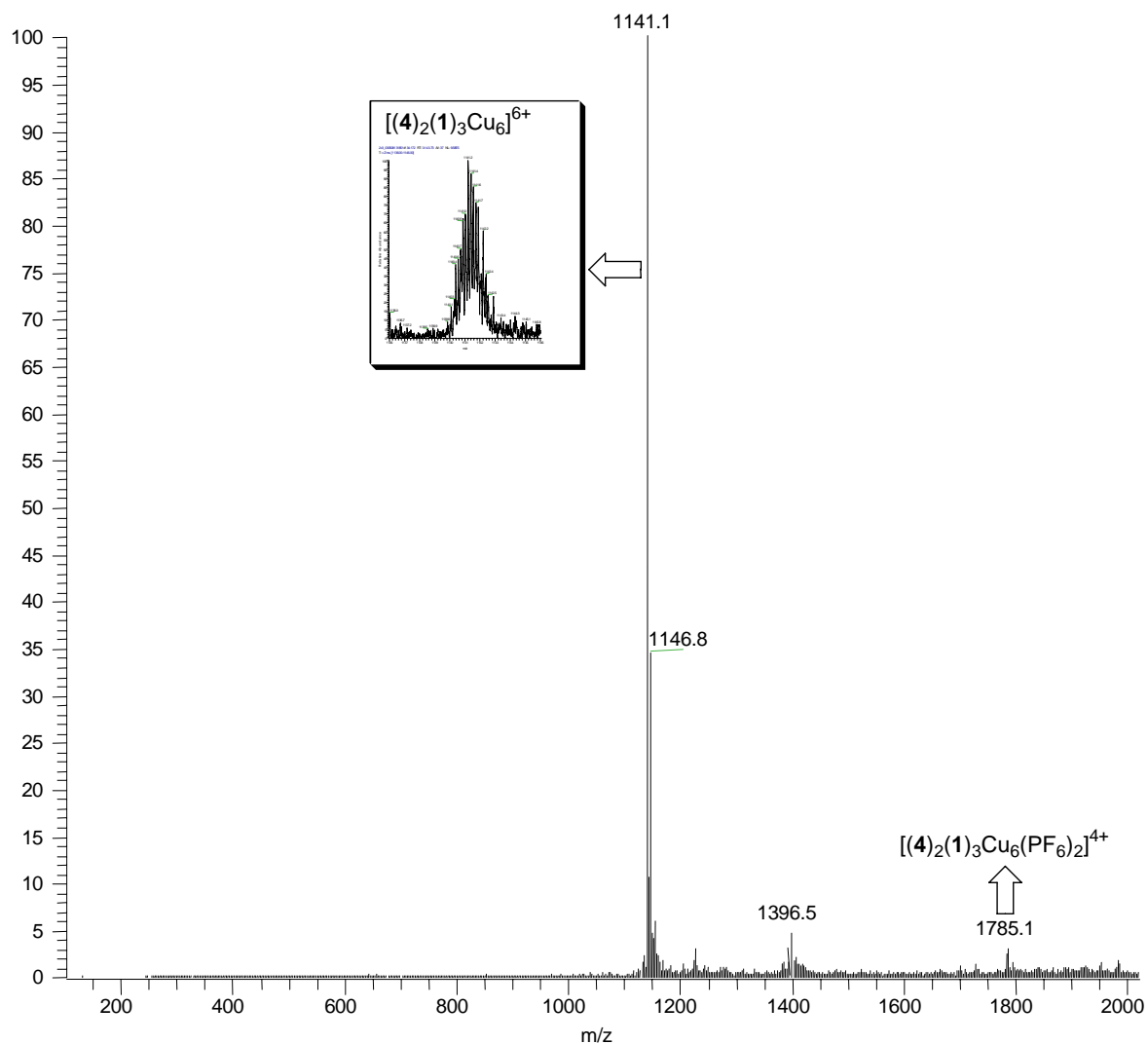
General procedure for preparing copper nanogrids:

[2x2] nanogrids were prepared by mixing **1** and **2** (or **3**) with $[\text{Cu}(\text{MeCN})_4]\text{PF}_6$ (1:1:2 equiv. respectively) in methylene chloride. The resulting dark red solution was analysed by ESI MS, ^1H NMR, COSY, elemental analysis and UV/vis spectroscopy. [2x3] grids were prepared in a similar way by mixing **4** (or **5**) and **1** (or **2**) with Cu(I) salt in 1: 1.5: 3 equiv. respectively.

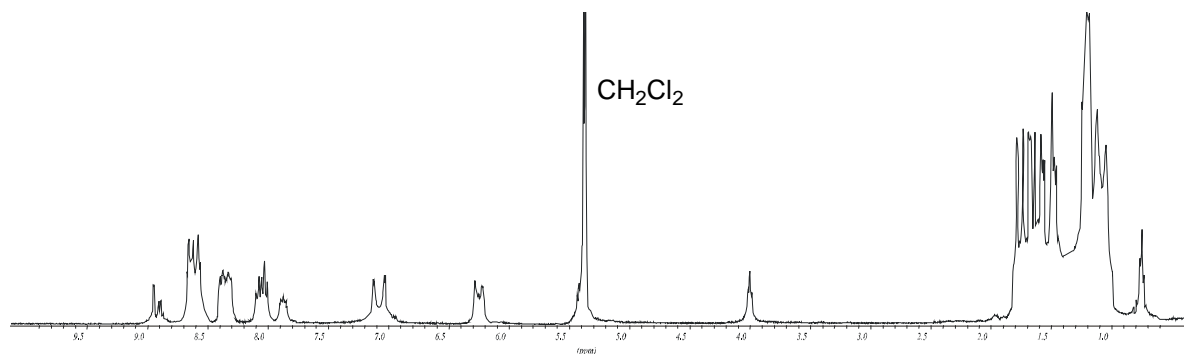
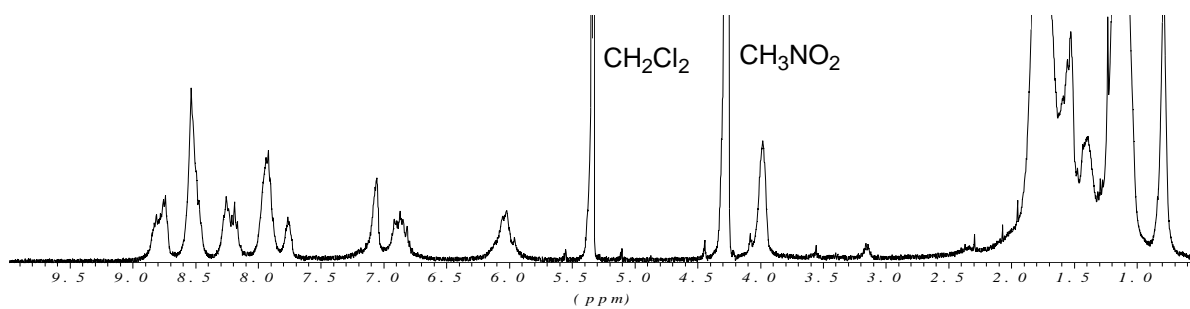
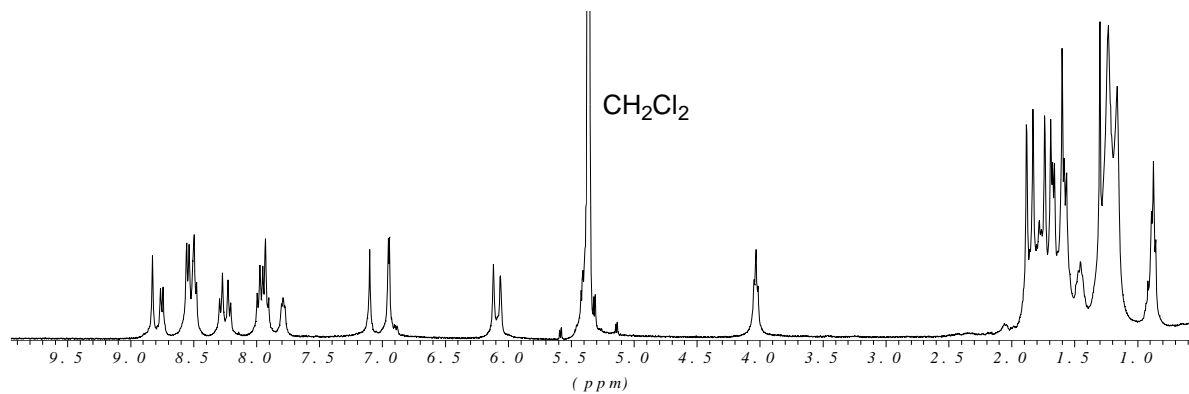
ESI MS of [2x2] Nanogrid



ESI MS of [2x3] Nanogrid

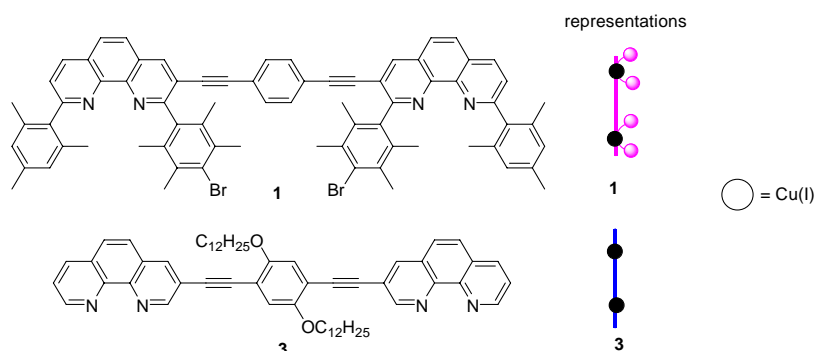


^1H NMR of [2x2] and [2x3] grids



Mechanistic Insight into [2x2] Nanogrid Assembly

ESI MS Titration of $[\text{Cu}_4(\mathbf{1})_2(\mathbf{3})_2]^{+4}$:



a) ESI-MS titration of **1** and **3** with Cu(I) salt in methylene chloride.

Table 1. ESI MS titration data along with proposed formula of observed species.

Titration Nr.	Stoichiometric ratio of 1 , and 3 Cu(I) resp.	Observed m/z	Formula
1	1: 1: 0.2	1141.6 (100%) 707.7 (50%) 912.8 (40%) 1027.7 (30%) 1082.3 (18%) 1629.7 (35%)	$[(\mathbf{1})(\text{H})]^+$ $[(\mathbf{1})(\text{Cu})_2(\text{H}_2\text{O})(\text{AN})_3]^{+2}$ $[(\mathbf{3})(\text{Cu})]^+$ $[(\mathbf{1})(\mathbf{3})(\text{Cu})(\text{H})]^{+2}$ $[(\mathbf{1})(\mathbf{3})(\text{Cu})_2(\text{AN})\text{PF}_6]^+$ $[(\mathbf{1})_2(\mathbf{3})(\text{Cu})_2]^{+2}$
2	1: 1: 0.4	707.7 (20%) 912.8 (25%) 1060.9(45%) 1082.3 (68%) 1629.7 (100%)	$[(\mathbf{1})(\text{Cu})_2(\text{H}_2\text{O})(\text{AN})_3]^{+2}$ $[(\mathbf{1})(\text{Cu})]^+$ $[(\mathbf{1})(\mathbf{3})(\text{Cu})_2]^{+2}$ $[(\mathbf{1})(\mathbf{3})(\text{Cu})_2(\text{AN})\text{PF}_6]^+$ $[(\mathbf{1})_2(\mathbf{3})(\text{Cu})_2]^{+2}$
3	1: 1: 0.6	707.7 (10%) 912.8 (5%) 1060.9(65%) 1082.3 (68%) 1629.7 (100%)	$[(\mathbf{1})(\text{Cu})_2(\text{H}_2\text{O})(\text{AN})_3]^{+2}$ $[(\mathbf{1})(\text{Cu})]^+$ $[(\mathbf{1})(\mathbf{3})(\text{Cu})_2]^{+2}$ $[(\mathbf{1})(\mathbf{3})(\text{Cu})_2(\text{AN})\text{PF}_6]^+$ $[(\mathbf{1})_2(\mathbf{3})(\text{Cu})_2]^{+2}$
4	1: 1: 0.8	707.7 (5%) 1060.9(100%) 1629.7 (60%)	$[(\mathbf{1})(\text{Cu})_2(\text{H}_2\text{O})(\text{AN})_3]^{+2}$ $[(\mathbf{1})(\mathbf{3})(\text{Cu})_2]^{+2}$ $[(\mathbf{1})_2(\mathbf{3})(\text{Cu})_2]^{+2}$
5	1: 1: 1.0	1060.9(100%) 1461.4 (20%) 1629.7 (60%)	$[(\mathbf{1})(\mathbf{3})(\text{Cu})_2]^{+2}$ and $[(\mathbf{1})_2(\mathbf{3})_2(\text{Cu})_4]^{+4}$ $[(\mathbf{1})_2(\mathbf{3})_2(\text{Cu})_4\text{PF}_6]^{+3}$ $[(\mathbf{1})_2(\mathbf{3})(\text{Cu})_2]^{+2}$
6	1: 1: 1.2	1060.9(100%) 1461.4 (20%)	$[(\mathbf{1})(\mathbf{3})(\text{Cu})_2]^{+2}$ and $[(\mathbf{1})_2(\mathbf{3})_2(\text{Cu})_4]^{+4}$ $[(\mathbf{1})_2(\mathbf{3})_2(\text{Cu})_4\text{PF}_6]^{+3}$
7	1: 1: 1.4	1060.9(100%) 1461.4 (20%)	$[(\mathbf{1})(\mathbf{3})(\text{Cu})_2]^{+2}$ and $[(\mathbf{1})_2(\mathbf{3})_2(\text{Cu})_4]^{+4}$ $[(\mathbf{1})_2(\mathbf{3})_2(\text{Cu})_4\text{PF}_6]^{+3}$
8	1: 1: 2.0	1060.9(100%) 1461.4 (20%)	$[(\mathbf{1})_2(\mathbf{3})_2(\text{Cu})_4]^{+4}$ $[(\mathbf{1})_2(\mathbf{3})_2(\text{Cu})_4\text{PF}_6]^{+3}$
9	1: 1: 4.0	1060.9(100%) 1461.4 (20%)	$[(\mathbf{1})_2(\mathbf{3})_2(\text{Cu})_4]^{+4}$ $[(\mathbf{1})_2(\mathbf{3})_2(\text{Cu})_4\text{PF}_6]^{+3}$

All relevant signals appearing during the titration process could be identified and are listed in Table 1. As data in Table 1 indicate, no homoleptic complexes of **1** were formed during the whole titration process, highlighting the **HETPHEN** concept in preparing the heteroleptic assemblies. The data clearly indicate the stepwise assembly of the nanogrid. Excess (4 eq. with respect to ligands) addition of Cu(I) salt did not affect already formed nanogrid. Fragmentation of the signals further confirmed the assignments. For example, fragmentation of $[(\mathbf{1})_2(\mathbf{3})(\text{Cu})_2]^{+2}$ produced the signal corresponding to $[(\mathbf{1})(\mathbf{3})(\text{Cu})_2]^{+2}$ and both the species were further confirmed by their isotopic distributions (Figure 2).

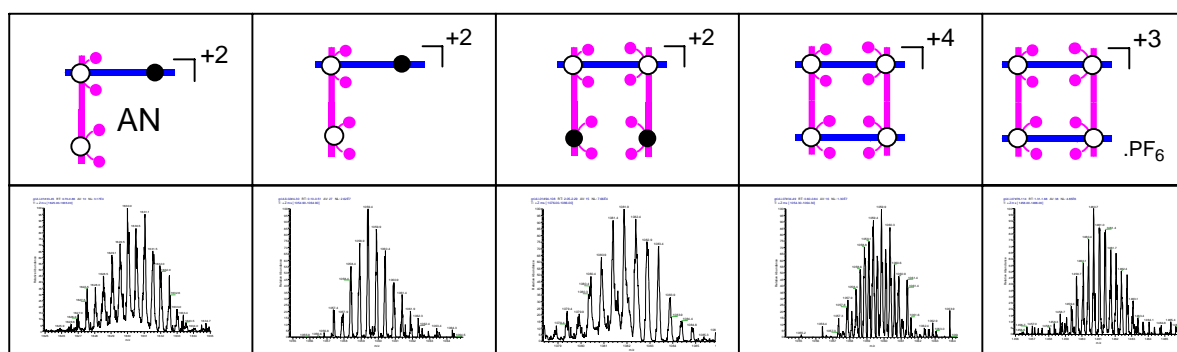


Figure 1. Proposed symbols and their isotopic distributions for the species detected when **1** and **3** were titrated with Cu(I) salt.

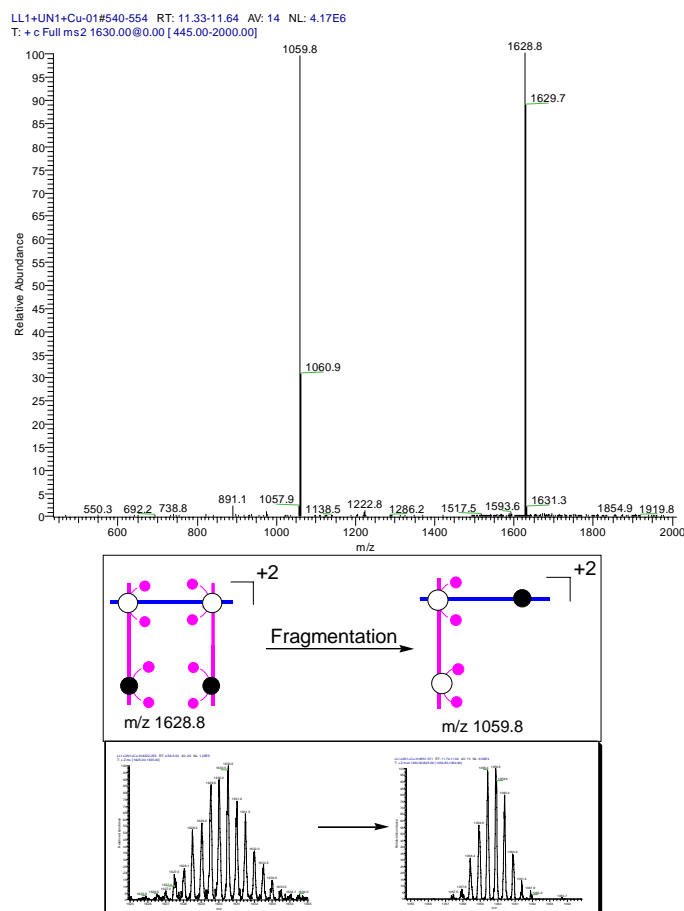


Figure 2. Fragmentation of signal at m/z 1629.

b) ESI-MS titration of 1 and Cu(I) with 3 in methylene chloride.

The second series of experiments was carried out by the titration of **1** and the Cu(I) salt with aliquot amounts of **3** in methylene chloride. As the titration proceeded signals corresponding to the nanobox intensified with the final spectrum only containing signals corresponding to the nanogrid. In contrast to the first titration, excess addition of **3** led to destruction of the nanogrid. Notably, similar intermediates were observed in both the titrations. All the signals are in good agreement with their isotopic splittings.

Table 2. ESI MS titration data along with proposed formula of observed species.

Titration Nr.	Stoichiometric ratio of 1 , Cu(I) and 3 resp.	Observed m/z	Formula
1	1: 1: 0.2	652.4 (40%)	$[(\mathbf{1})(\text{Cu})_2(\text{AN})]^{+2}$
		1059.8 (100%)	$[(\mathbf{1})(\mathbf{3})(\text{Cu})_2]^{+2}$
		1220.8 (90%)	$[(\mathbf{1})(\text{Cu})(\text{H}_2\text{O})]^+$
		1303.0 (55%)	$[(\mathbf{1})(\text{Cu})(\text{AN})_2(\text{H}_2\text{O})]^+$
2	1: 1: 0.4	1059.8 (100%)	$[(\mathbf{1})(\mathbf{3})(\text{Cu})_2]^{+2}$
		1220.8 (90%)	$[(\mathbf{1})(\text{Cu})(\text{H}_2\text{O})]^+$
		1303.0 (55%)	$[(\mathbf{1})(\text{Cu})(\text{AN})_2(\text{H}_2\text{O})]^+$
		1629.8 (8%)	$[(\mathbf{1})_2(\mathbf{3})(\text{Cu})_2]^{+2}$
3	1: 1: 0.6	1059.8 (100%)	$[(\mathbf{1})(\mathbf{3})(\text{Cu})_2]^{+2}$
		1220.8 (10%)	$[(\mathbf{1})(\text{Cu})(\text{H}_2\text{O})]^+$
		1303.0 (15%)	$[(\mathbf{1})(\text{Cu})(\text{AN})_2(\text{H}_2\text{O})]^+$
		1629.8 (5%)	$[(\mathbf{1})_2(\mathbf{3})(\text{Cu})_2]^{+2}$
4	1: 1: 0.8	1059.8 (100%)	$[(\mathbf{1})(\mathbf{3})(\text{Cu})_2]^{+2}$ and $[(\mathbf{1})_2(\mathbf{3})_2(\text{Cu})_4]^{+4}$
		1220.8 (15%)	$[(\mathbf{1})(\text{Cu})(\text{H}_2\text{O})]^+$
		1303.0 (10%)	$[(\mathbf{1})(\text{Cu})(\text{AN})_2(\text{H}_2\text{O})]^+$
		1461.3(10%)	$[(\mathbf{1})_2(\mathbf{3})_2(\text{Cu})_4\text{PF}_6]^{+3}$
		1629.8 (5%)	$[(\mathbf{1})_2(\mathbf{3})(\text{Cu})_2]^{+2}$
		1059.8 (100%)	$[(\mathbf{1})(\mathbf{3})(\text{Cu})_2]^{+2}$ and $[(\mathbf{1})_2(\mathbf{3})_2(\text{Cu})_4]^{+4}$
5	1: 1: 1.0	1220.8 (5%)	$[(\mathbf{1})(\text{Cu})(\text{H}_2\text{O})]^+$
		1303.0 (5%)	$[(\mathbf{1})(\text{Cu})(\text{AN})_2(\text{H}_2\text{O})]^+$
		1461.3(5%)	$[(\mathbf{1})_2(\mathbf{3})_2(\text{Cu})_4\text{PF}_6]^{+3}$
		1629.8 (5%)	$[(\mathbf{1})_2(\mathbf{3})(\text{Cu})_2]^{+2}$
		1059.8 (100%)	$[(\mathbf{1})(\mathbf{3})(\text{Cu})_2]^{+2}$ and $[(\mathbf{1})_2(\mathbf{3})_2(\text{Cu})_4]^{+4}$
		1220.8 (5%)	$[(\mathbf{1})(\text{Cu})(\text{H}_2\text{O})]^+$
6	1: 1: 1.2	1303.0 (5%)	$[(\mathbf{1})(\text{Cu})(\text{AN})_2(\text{H}_2\text{O})]^+$
		1461.3(5%)	$[(\mathbf{1})_2(\mathbf{3})_2(\text{Cu})_4\text{PF}_6]^{+3}$
		1629.8 (5%)	$[(\mathbf{1})_2(\mathbf{3})(\text{Cu})_2]^{+2}$
		1059.8 (100%)	$[(\mathbf{1})(\mathbf{3})(\text{Cu})_2]^{+2}$ and $[(\mathbf{1})_2(\mathbf{3})_2(\text{Cu})_4]^{+4}$
		1220.8 (5%)	$[(\mathbf{1})(\text{Cu})(\text{H}_2\text{O})]^+$
		1303.0 (5%)	$[(\mathbf{1})(\text{Cu})(\text{AN})_2(\text{H}_2\text{O})]^+$
7	1: 1: 1.6	1461.3(15%)	$[(\mathbf{1})_2(\mathbf{3})_2(\text{Cu})_4\text{PF}_6]^{+3}$
		1059.8 (100%)	$[(\mathbf{1})(\mathbf{3})(\text{Cu})_2]^{+2}$ and $[(\mathbf{1})_2(\mathbf{3})_2(\text{Cu})_4]^{+4}$
		1461.3(15%)	$[(\mathbf{1})_2(\mathbf{3})_2(\text{Cu})_4\text{PF}_6]^{+3}$
		1059.8 (100%)	$[(\mathbf{1})(\mathbf{3})(\text{Cu})_2]^{+2}$ and $[(\mathbf{1})_2(\mathbf{3})_2(\text{Cu})_4]^{+4}$
8	1: 1: 1.8	1461.3(15%)	$[(\mathbf{1})_2(\mathbf{3})_2(\text{Cu})_4\text{PF}_6]^{+3}$
		1059.8 (100%)	$[(\mathbf{1})(\mathbf{3})(\text{Cu})_2]^{+2}$ and $[(\mathbf{1})_2(\mathbf{3})_2(\text{Cu})_4]^{+4}$
		1461.3(15%)	$[(\mathbf{1})_2(\mathbf{3})_2(\text{Cu})_4\text{PF}_6]^{+3}$
9	1: 1: 2.0	1059.8 (100%)	$[(\mathbf{1})_2(\mathbf{3})_2(\text{Cu})_4]^{+4}$
		1461.3(15%)	$[(\mathbf{1})_2(\mathbf{3})_2(\text{Cu})_4\text{PF}_6]^{+3}$
		1059.8 (100%)	$[(\mathbf{1})_2(\mathbf{3})_2(\text{Cu})_4]^{+4}$
10	1: 1: 4.0	1059.8 (100%)	$[(\mathbf{1})_2(\mathbf{3})_2(\text{Cu})_4]^{+4}$
		1022.5 (100%)	$[(\mathbf{1})(\mathbf{3})_2(\text{Cu})_3(\text{H}_2\text{O})_2]^{+3}$
		1461.3(10%)	$[(\mathbf{1})_2(\mathbf{3})_2(\text{Cu})_4\text{PF}_6]^{+3}$

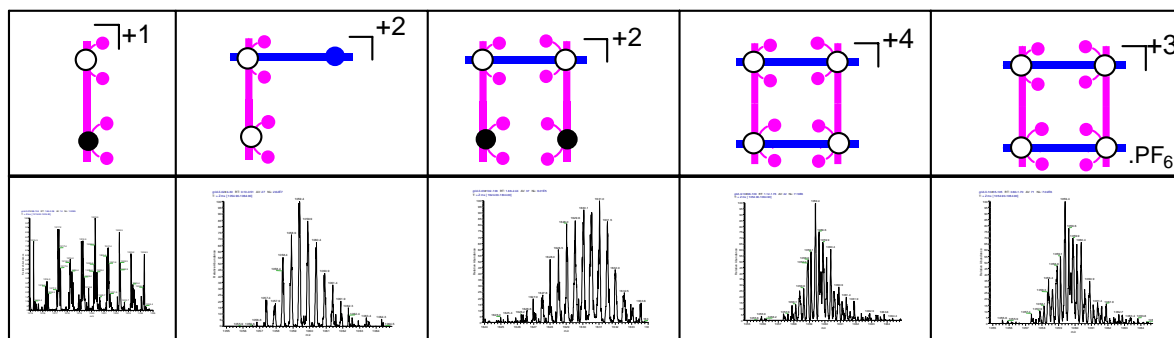
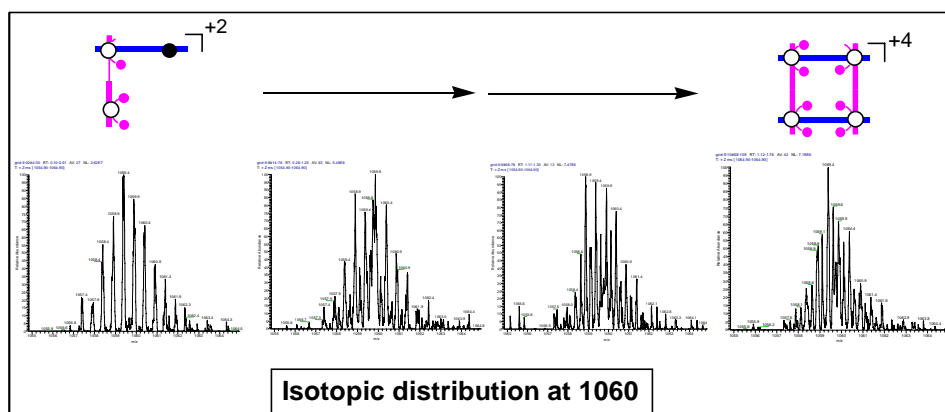


Figure 3. Proposed symbols for the species detected when **1** and Cu(I) salt were titrated with aliquot amounts of **3**.

ESI-MS titrations provide a qualitative picture of possible intermediates on the way to the nanogrid assembly and the observed intermediates are independent of the type of titration. These models (Figure 1 and 3) were then used to calculate the equilibrium constants from analysis of the corresponding spectrophotometric titration curves.

Change of the 2+ charged to 4+ charged species in the titration:



Spectrophotometric Titrations and Thermodynamic Parameters:

Ligand **1** and **3** were titrated with aliquot amounts of Cu(I) salt in methylene chloride at 25 °C. Upon complexation with Cu(I) ions significant shifts were observed in UV/vis spectra. The characteristic MLCT band appeared at ~ 490 nm that is responsible for the red colour of the complexes.¹⁰ Figure 4 displays the UV/vis changes upon Cu(I) salt titration with the solution containing ligand **1** and **3**. Three isosbestic points can be distinguished at 302, 312, and 387 nm. As the titration proceeds, π to π^* bands are shifted bathochromically because of complex formation. Insert in figure 4 indicates that the final complex nanogrid is fully formed at 2 equiv. of Cu(I) salt. Excess addition of the Cu(I) salt did not affect the already formed nanogrid, as demonstrated by ESI MS data. The data obtained from the titration spectra were

used to determine the binding constants (Table-3) of the intermediates and the nanogrid using the program SPECFIT¹¹.

As evidenced by the ESI MS and spectrophotometric titration, a three step formation process was proposed for the formation of the eight-component nanogrid assembly. Step 1 leads to the formation of the heteroleptic $[\text{Cu}(\mathbf{1})(\mathbf{3})]^+$ complex. In the second step, the $[\text{Cu}(\mathbf{1})(\mathbf{3})]^+$ complex takes up one more Cu(I) salt to furnish the $[\text{Cu}_2(\mathbf{1})(\mathbf{3})]^{2+}$ complex, with Cu(I) most likely attached to ligand **1** due to the larger stabilisation of Cu^+ in between two aromatic rings (cation- π interactions). In the final step, two of the $[\text{Cu}_2(\mathbf{1})(\mathbf{3})]^{2+}$ complexes combine together to afford the final nanogrid.

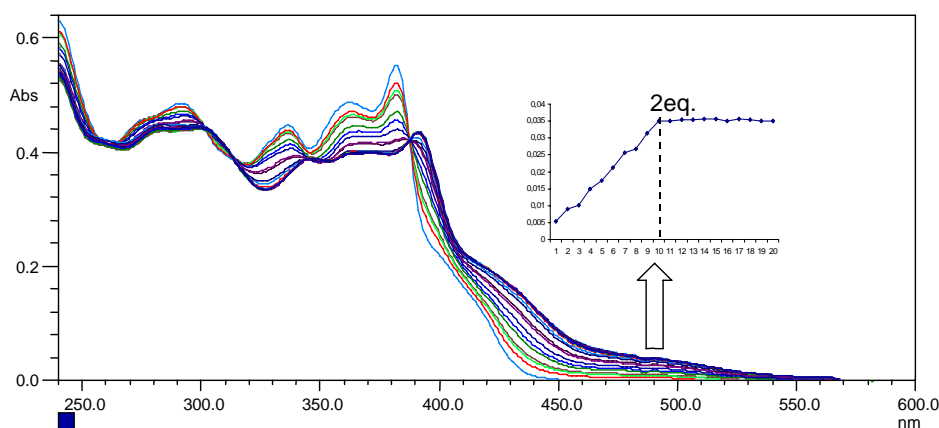


Figure 4. UV/vis spectral changes of **1** and **3** on addition of Cu(I) salt in methylene chloride. The inset shows the plot of absorbances at 497 nm against the molar ratio of Cu(I) salt.

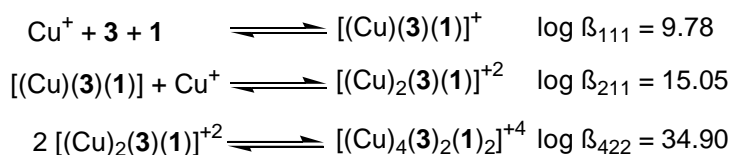
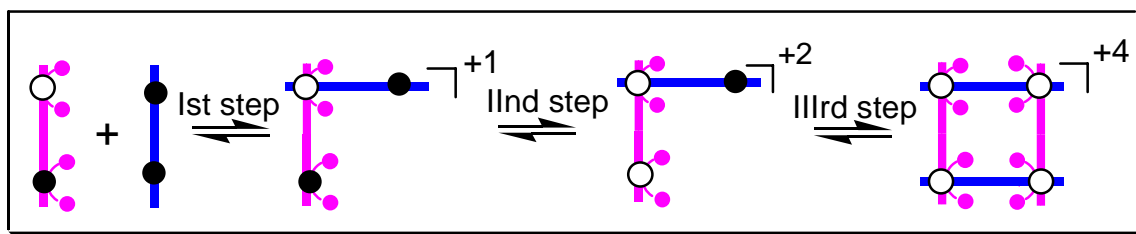


Table 3. Obtained binding constants for different intermediates.

Proposed mechanistic three-step pathway to $[\text{Cu}_4(\mathbf{1})_2(\mathbf{3})_2]^{+4}$ assembly:



- (1) (a) K. E. Drexler, *Nanosystems: Molecular Machinery, Manufacturing and Computation*; Wiley: New York, **1992**. (b) Special issue "Nanostructures": E. A. Chandross, R. D. Miller, *Chem. Rev.* **1999**, *99*, 1644-1990. (c) M. Fujita, D. Oguro, M. Miyazawa, H. Oka, K. Yamaguchi, K. Ogura, *Nature* **1995**, *378*, 469-471. (d) S. Leininger, B. Olenyuk, P. J. Stang, *Chem. Rev.* **2000**, *3*, 853-908. (e) H.-R. Tseng, S. A. Vignon, J. F. Stoddart, *Angew. Chem. Int. Ed.* **2003**, *13*, 1491-1495. (f) V. Balzani, A. Credi, F. M. Raymo, J. F. Stoddart, *Angew. Chem. Int. Ed.* **2000**, *39*, 3348-3391. (g) H. Ito, T. Kusukawa, M.

-
- Fujita, *Chem. Lett.* **2000**, 598-599. (h) S. J. Lee, W. Lin, *J. Am. Chem. Soc.* **2002**, *124*, 4554-4555. (i) M. L. Merlau, M. D. P. Mejia, S. T. Nguyen, J. T. Hupp, *Angew. Chem. Int. Ed.* **2001**, *22*, 4239-4242. (j) R. Takahashi, Y. Kobuke, *J. Am. Chem. Soc.* **2003**, *125*, 2372-2372 and refs therein.
- (2) (a) P. N. W. Baxter, J. M. Lehn, B. O. Kneisel, G. Baum, D. Fenske, *Chem. Eur. J.* **1999**, *5*, 102-112. (b) P. N. W. Baxter, J. M. Lehn, B. O. Kneisel, G. Baum, D. Fenske, *Chem. Eur. J.* **1999**, *5*, 113-120.
- (3) (a) J. Manna, J. A. Whiteford, P. J. Stang, *J. Am. Chem. Soc.* **1996**, *118*, 8731-8732. (b) P. J. Stang, N. E. Persky, J. Manna, *J. Am. Chem. Soc.* **1997**, *119*, 4777-4778. (c) B. Olenyuk, M. D. Levin, J. A. Whiteford, J. E. Shield, P. J. Stang, *J. Am. Chem. Soc.* **1999**, *121*, 10434-10435.
- (4) (a) P. N. W. Baxter, J. M. Lehn, G. Baum, D. Fenske, *Chem. Eur. J.* **2000**, *24*, 4510-4517. (b) E. Breuning, G. S. Hanan, F. J. Romero-Salguero, A. M. Garcia, P. N. W. Baxter, J. M. Lehn, E. Wegelius, K. Rissanen, H. Nierengarten, A. V. Dorsselaer, *Chem. Eur. J.* **2002**, *15*, 3458-3466. (c) U. Ziener, E. Breuning, J. M. Lehn, E. Wegelius, K. Rissanen, G. Baum, D. Fenske, G. Vaughan, *Chem. Eur. J.* **2000**, *6*, 4132-4139. (d) M. Barboiu, G. Vaughan, R. Graff, J. M. Lehn, *J. Am. Chem. Soc.* **2003**, *125*, 10257-10265 and refs therein.
- (5) P. N. W. Baxter, J. M. Lehn, B. O. Kneisel, D. Fenske, *Angew. Chem. Int. Ed.* **1997**, *36*, 1978-1981.
- (6) HETPHEN concept: quantitative approach to heteroleptic bisphenanthroline metal complexes.⁶ This approach utilizes steric and electronic effects originating from bulky aryl substituents at the bisimine coordination sites (as seen in **1** and **5**) to control the coordination equilibrium both kinetically and thermodynamically.
- (7) M. Schmittel, A. Ganz, *Chem. Commun.* **1997**, 99-101. M. Schmittel, U. Lüning, M. Meder, A. Ganz, C. Michel, M. Herderich, *Heterocycl. Commun.* **1997**, *3*, 493-494.
- (8) M. Schmittel, H. Ammon, V. Kalsani, A. Wiegrefe, C. Michel, *Chem. Commun.* **2002**, 2566-2567.
- (9) M. Schmittel, A. Ganz, D. Fenske, *Org. Lett.* **2002**, *14*, 2289-2292.
- (10) E. Müller, C. Piguet, G. Bernardinelli, A. F. Williams, *Inorg. Chem.* **1988**, *27*, 849-855.
- (11) M. Maeder, A. D. Zuberbühler. *Anal. Chem.* **1990**, *62*, 2220-2224.

Supp 4-5

Metal-Driven and Covalent Fabrication of Supramolecular Grids from Racks: A Convergent Approach to Heterometallic and Heteroleptic Nanostructures

Michael Schmittel,*^a Venkateshwarlu Kalsani,^a Jan W. Bats^b

^a Center of Micro and Nanochemistry and Engineering, Organische Chemie I, Universität Siegen, Adolf-Reichwein-Str., D-57068 Siegen, Germany, Fax: (+49) 271 740 3270.

^b Institut für Organische Chemie und Chemische Biologie, Johann Wolfgang Goethe-Universität, Marie-Curie-Strasse 11, D-60439 Frankfurt am Main, Germany.

Abstract. Conversion of dynamic supramolecular racks into supramolecular nanogrids by using either a covalent (with CuCl/O₂) or coordinative (with [*trans*-(PEt₃)₂PtCl₂]) approach to couple terminal alkynes is described. Due to rapid equilibration (as tested by exchange reactions) oligomeric adducts potentially formed in the coupling process will furnish selectively nanogrids through an entropically driven self-repair mechanism. In order to ascertain the assignment, the nanogrids were also fabricated by an independent strategy.

The masterful use of metal coordination chemistry is a *conditio sine qua non* for the preparation of discrete metallosupramolecular aggregates such as cylinders,¹ racks,² nanoscaffolds and grids.³ At present, most of these structures are characterised by bis- or polyhomoleptic coordination motifs, but there is growing interest to prepare heteroleptic aggregates,⁴ for which several strategies have been designed. In this context, we have recently developed the HETPHEN⁵ approach allowing to build heteroleptic bisphenanthroline metal complexes of tetrahedrally coordinated metal ions.⁶ Utilising this methodology several nanoscale supramolecular scaffolds, such as a nanobasket,⁷ ring-in-ring structures,⁸ nanoscaffolds,⁹ nanoracks and nanogrids¹⁰ were afforded, that by their heteroleptic nature are ideally suited for functional applications.¹¹

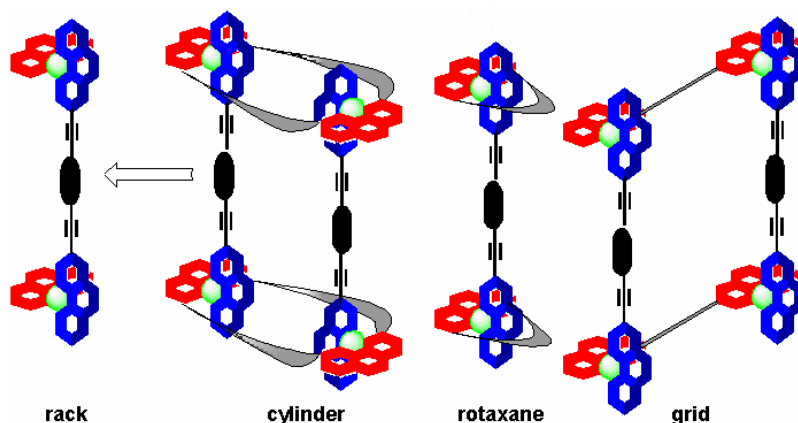


Figure 1. Cartoon representation of a rack as a potential precursor to cylinder, pseudorotaxane/rotaxane, and grid motifs.

We recently reported on dynamic bisphenanthroline copper(I) racks^{10b} that contrast to the large multitude of kinetically stable ruthenium based complexes.^{2,12} Herein, we wish to describe the clean self-assembly of functional rack motifs which are equipped with bromo and alkyne termini. The latter feature suggested to us to use the racks as versatile precursors for supramolecular nanostructures, such as pseudorotaxanes/rotaxanes, cylinders or grid structures (Fig. 1). As a demonstration of the power of this approach we present two strategies, a covalent and a coordinative route, to fabricate heteroleptic grids directly from supramolecular racks.

Ligands **1** and **2** were prepared by known procedures¹³ using sequential Sonogashira coupling reactions (Chart 1). The synthesis of phenanthrolines **3-5** whose 2,9-disubstitution with bulky aryl groups (mesityl=Mes or duryl=Dur) is dictated by the HETPHEN approach, was described elsewhere.^{8,13}

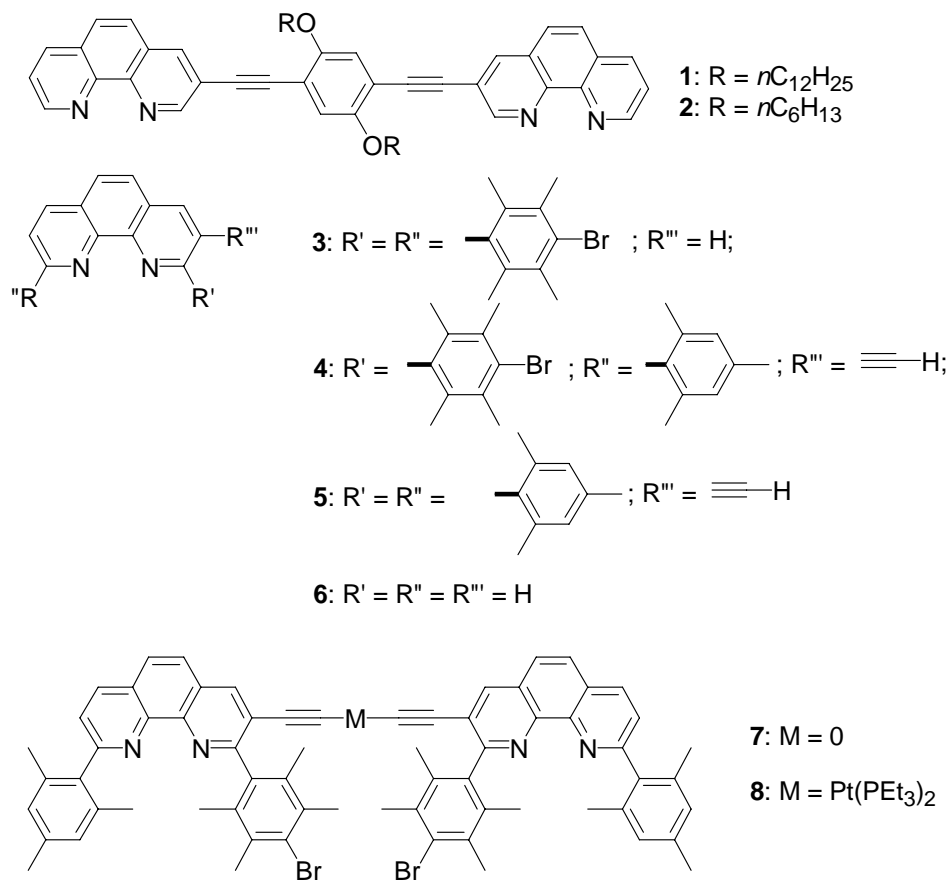
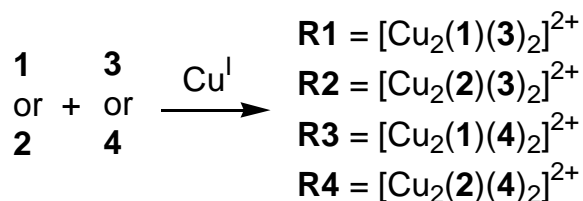


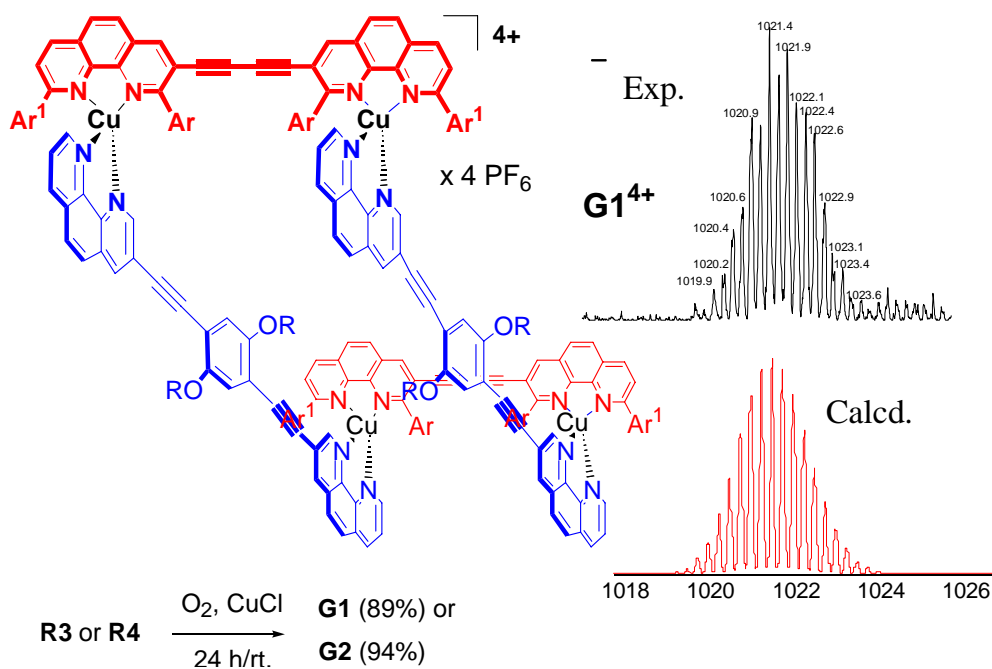
Chart 1. Ligands used for the construction of heteroleptic, functional racks.

The combination of ligand **1** or **2** with **3**^{10b} or **4** in presence of $[\text{Cu}(\text{CH}_3\text{CN})_4]^+$ (1:2:2) produced the racks **R1-R4** in basically quantitative yields. For all racks **R1-R4**, the ESI-MS exhibited a single set of signals formed by the successive loss of counter ions (supp. information). Moreover, characteristic high field shifts in the ¹H NMR for the MesH and DurMe protons of **3** and **4** in **R1-R4** were indicative of heteroleptic bisphenanthroline complex formation.



As emphasised above, racks with functional groups, such as terminal alkynes, may serve as precursors for higher supramolecular aggregates (Fig. 1). In the first try, **R3** and **R4** were reacted under oxidative conditions typical for homocoupling of terminal alkynes (O_2 , CuCl, NEt₃, CH₂Cl₂)¹⁴ to furnish **G1** (89%) and **G2** (94%) in high yield (supp. information). ¹H NMR spectra

confirmed the grid structure showing a single set of signals being characterised by the lack of the acetylene proton at $\delta \sim 3.5$ ppm and the presence of a diagnostic signal for the heteroleptic complex at $\delta \sim 6$ ppm (MesH). Moreover, ESI-MS analysis showed the signals of grids **G1** and **G2** (supp. information and Scheme 1) with a correct isotopic distribution of the 3+ and 4+ charged species. All other data were equally in accordance with those of previously reported nanogrid structures.^{10a}



Scheme 1. Fabrication of grids **G1**, **G2** under oxidative conditions from racks **R3** and **R4**, respectively. ESI-MS signal of **G1**⁴⁺ as inset.

Recently, connecting terminal alkynes through Pt(II)- or Pd(II)-centres by a coordinative approach was utilised by Lin *et al.*¹⁵ for the formation of polygons. As an extension, we decided to probe the self-recognition of Cu(I) ions and phenanthrolines and that of Pt(II) ions and alkynyl ligands in one pot. By mixing **5**, **6** and $[\text{Cu}(\text{CH}_3\text{CN})_4]^+$ (1:1:1, respectively) in dichloromethane at rt and followed by a posttreatment with $[\text{trans}-(\text{PEt}_3)_2\text{PtCl}_2]$ the heterometallic rack **R6** formed exclusively (supp. information), as proven by ¹H NMR, ESI-MS and ³¹P{H}-NMR (δ 13.3 ppm). The structure of **R6** structure was confirmed by single crystal analysis.¹⁶ In Fig. 2 a stick representation of the solid state structure is presented. The molecule is centrosymmetric with the Pt atom at a crystallographic inversion center.¹⁰ The Cu atom has a heavily distorted tetrahedral coordination. The N-Cu-N angles reach from 82.1(2)° to 141.5(2)°. The Cu-N distances range

from 1.989(5) to 2.088(4) Å. The Pt atom exhibits a square-planar coordination and the Pt-P distances of 2.296(2) Å and Pt-C distances of 1.976(6) Å agree with values found in related structures.¹⁷ The crystal packing showed an intermolecular δ - δ interactions (3.4 Å) between phenanthroline groups (see supp. information).

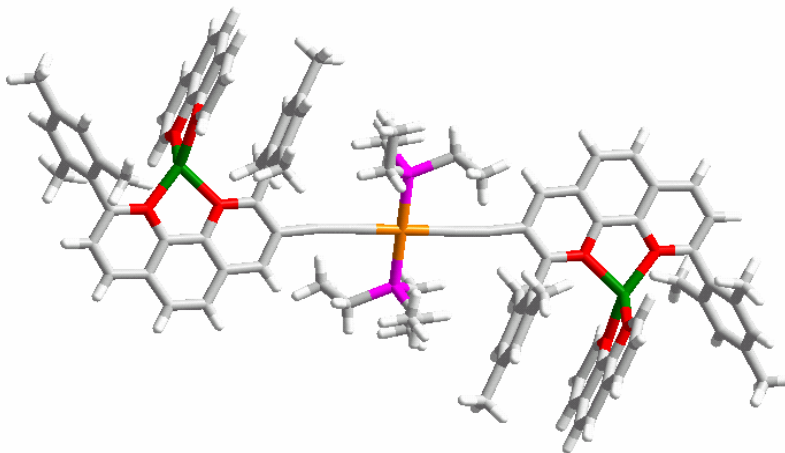
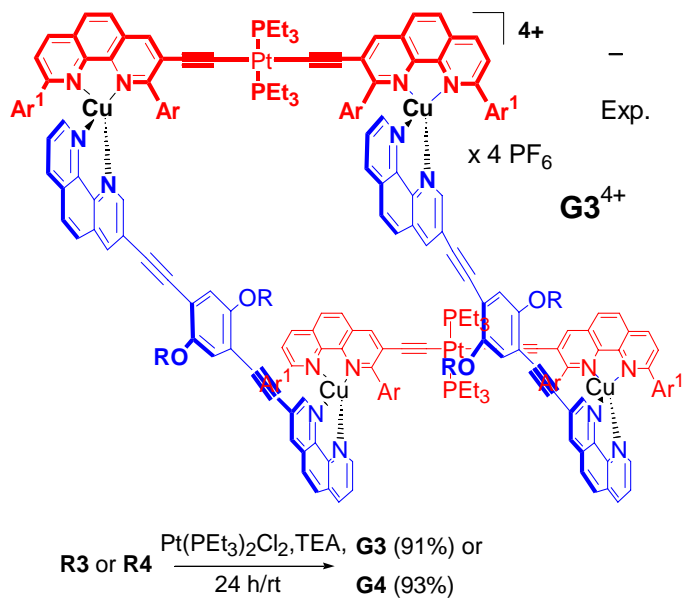


Figure 2. Single crystal structure of **R6**; stick representation.

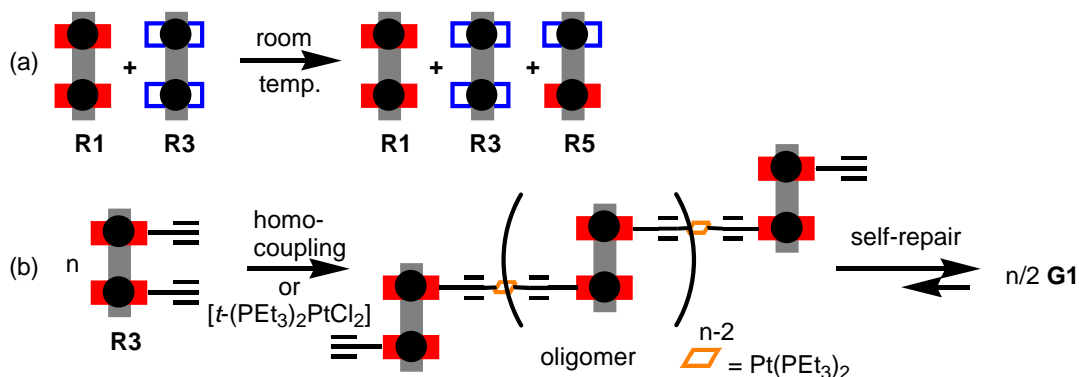
When **R3** or **R4** were reacted with [*trans*-(PEt₃)₂PtCl₂] the heterometallic¹⁸ and heteroleptic grids **G3** and **G4** formed (Scheme 2) as demonstrated by ESI-MS (supp. information). The isotopic distributions of the 3+ and 4+ charged species was in good agreement with the calculated ones. ¹H-, ³¹P{¹H}-NMR, ESI-MS and elemental analysis point to the formation of a single heterometallic grid species. For example, ³¹P{¹H} NMR spectra of **G3** and **G4** exhibited a single peak at δ ~11.6 ppm with a set of Pt^{II} satellites (supp. information).¹⁵

The above results demonstrate that coupling reactions of racks to grids both under covalent or coordinative conditions proceed with high yields (~90%). In contrast to systems of Siegel *et al.*, racks **R1-R4** rapidly equilibrate at room temp. as shown in exchange reactions by ESI-MS (Scheme 3a).¹⁹ This precludes that oligomeric adducts form in any substantial amounts (Scheme 3b); entropically driven self-repair will always lead selectively to grid motifs.



Scheme 2. Fabrication of grids **G3**, **G4** from **R3** and **R4**, respectively, in presence of $[\text{trans}-(\text{PEt}_3)_2\text{PtCl}_2]$. ESI-MS signal of G3^{4+} as inset.

In order to ascertain the above assignment beyond doubt, we prepared the ligands **7** and **8** from **4** through oxidative coupling and coordination with $[\text{trans}-(\text{PEt}_3)_2\text{PtCl}_2]$, respectively.²⁰ In analogy to our recent work on the fabrication of nanogrids, **G1-G4** were prepared independently from combination of **1,2** with **7** and **8**, respectively, in presence of $[\text{Cu}(\text{CH}_3\text{CN})_4]^+$. Full agreement of their spectral data with those of the grids prepared by routes shown in Schemes 1 and 2 was obtained. Alike previous reports¹⁰ the assignments were further confirmed by UV/vis and ESI-MS titrations (supp. information).



Scheme 3. Cartoon representation (a) of the equilibration of racks at room temp., and (b) of the entropically driven repair mechanism that will suppress formation of oligomeric aggregates due to the kinetic lability of the rack assembly.

Since suitable crystals for X-ray structure determination could not be obtained, dimensions of these nanogrids were assessed from calculated, energy minimised structures.²¹ As depicted in Fig. 3, the dimensions of **G1,G2** are 2.9 nm (extension along the bisphenanthroline) and 2.3 nm for the Cu-Cu diagonal.

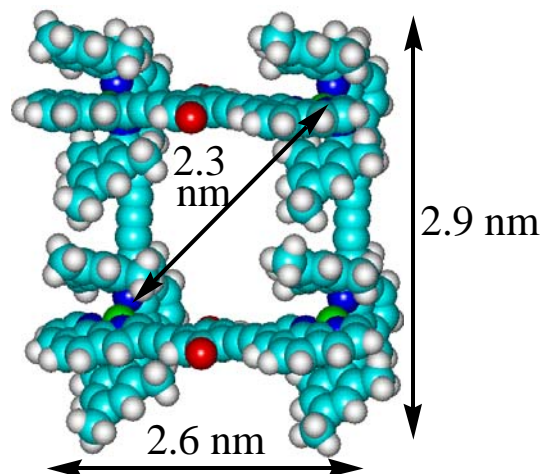


Figure 3. Space filling model of **G1,G2** (both differ only by the alkoxy chain) optimised with the MM⁺ force field simulation. Alkoxy chains are omitted for clarity.

The present results illustrate the potential of functional racks as precursors to supramolecular grids, and possibly for even more complex aggregates such as rotaxanes and cylinders. As some of the grids are both heterometallic and heteroleptic the present approach should be fruitful for the preparation of highly diversified assemblies. Hence, further studies are in progress to fabricate racks into higher aggregates and to study their properties.

Acknowledgment. We are indebted to the Deutsche Forschungsgemeinschaft (Schm 647/12-1) and the Fonds der Chemischen Industrie for financial support.

Supporting Data

Table of contents:

Contents	Page number
Experimental	S2
Procedure for the preparation of racks R1-R4	S1
Experimental data of racks R3-R4 and [Cu(5)(6)]PF ₆	S2
Procedure for the fabrication of grids G1-G2 by homocoupling	S2
Experimental data and ESI MS of G1-G2	S3
Procedure for metal-driven fabrication of G3-G4 and R6	S3-S4
Experimental data, ESI MS, and ³¹ P NMR of R6 and G3-G4	S4-S5
ESI MS titration data of 7, 1 with Cu(I) salt	S6
Isotopic distribution of proposed intermediates	S7
Isotopic distribution changes at m/z :1020, during the titration process	S7
Collisional activation study on G1	S7-S8
ESI MS of reaction mixture when R1 and R2 are reacted in dichloromethane	S8
¹ H NMR of reaction mixture when R7 and R8 are reacted in dichloromethane	S9
Intermolecular π - π stackings of R6 in the solid state	S9

Experimental:

Metal salts, *trans*-[Pt(PEt₃)₂Cl₂] and CuCl (anhydrous) were purchased from Aldrich or Merck, and used as received. ¹H NMR and ¹³C NMR were measured on a Bruker AC 400 (400 MHz) unless specified otherwise. All the ¹H NMR analysis was carried at room temperature in deuterated dichloromethane unless specified otherwise. ESI MS spectra were measured on a LCQ Deca Thermo Quest instrument. Typically, each time 25 scans were accumulated for one spectrum. All the complexes were characterized by ¹H-, ¹³C, ESI MS, IR and elemental analysis.

Procedure for the preparation of racks R1-R4

General procedure:

Functional racks **R1-R4** were prepared by mixing **1** (or **2**) and **3** (or **4**) with $[\text{Cu}(\text{MeCN})_4]\text{PF}_6$ (1:2:2 equiv., respectively) in dichloromethane. The resulting dark red solution was analysed by ESI MS, ^1H NMR, COSY, elemental analysis, without any further purification. For full characterization of **R1** and **R2** see reference 1.²²

R3: M.p. 238-240 °C; ^1H NMR (CD_2Cl_2 , 400 MHz): δ 8.84 (s, 2H, phen), 8.73 (d, $J = 8.4$ Hz, 2H, phen), 8.51 (s, 4H, phen), 8.46 (d, $J = 6.6$ Hz, 4H, phen), 8.22 (dd, $J = 8.8$ Hz, $J = 4.8$ Hz, 4H, phen), 7.94 (m, 6H, phen), 7.90 (t, $J = J = 8.9$ Hz, 2H, phen), 7.08 (s, 2H, phenyl), 6.04 (s, 2H, phenyl), 6.01 (s, 2H, phenyl), 4.02 (t, $J = 6.3$ Hz, 4H, methoxy), 3.2 (s, 2H, ethynyl), 1.65 (m, 76H, benzyl and aliph.), 0.87 (broad s, 12H, aliph.); ^{13}C NMR (CD_2Cl_2 , 100 MHz) : 161.1, 159.2, 154.5, 149.6, 143.4 (2C), 142.1, 141.6 (2C), 149.5 (2C), 138.8, 138.6, 138.1 (2C), 132.1, 136.4, 135.1(2C), 133.3, 131.0, 132.1, 129.9 (2C), 128.8, 128.4, 127.7, 127.0, 126.1, 125.4, 121.5, 117.4, 113.1, 92.4 (arom.), 90.1, 85.5 (ethynyl), 32.1, 30.9 (2C), 30.6 (2C), 30.1, 29.3 (2C), 23.5 (2C), 20.1 (2C), 18.5 (2C), 18.1, 14.2; IR (KBr): ν 3413, 3061, 2921, 2852, 2209 (ν $\text{C}\equiv\text{C}$), 1618, 1499, 1461, 1414, 1381, 1275, 1220, 1014, 912, 842, 723, 634, 557; ESI MS: calcd. for $\text{C}_{124}\text{H}_{124}\text{N}_8\text{O}_2\text{Br}_2\text{Cu}_2^{2+}$ [M^{2+}]: m/z 1022.6, found: m/z 1022.7; Anal. Calcd. for $\text{C}_{124}\text{H}_{124}\text{Br}_2\text{Cu}_2\text{N}_8\text{O}_2 \cdot 2\text{PF}_6 \cdot \text{CH}_2\text{Cl}_2 \cdot \text{H}_2\text{O}$: C, 61.58; H, 5.29; N, 4.60. Found: C, 61.41; H, 5.10; N, 4.68.

R4: M.p. 218-220 °C; ^1H NMR (CD_2Cl_2 , 400 MHz): δ 8.84 (s, 2H, phen), 8.73 (s, 2H, phen), 8.48 (m, 8H, phen), 8.23 (m, 4H, phen), 7.94 (s, 6H, phen), 7.76 (s, 2H, phen), 7.09 (s, 2H, phenyl), 6.02 (s, 4H, phenyl), 4.02 (s, 4H, methoxy), 3.28 (s, 2H, ethynyl), 1.70 (m, 52H, benzyl and aliph.), 0.75 (s, 12H, aliph.); ^{13}C NMR (CD_2Cl_2 , 100 MHz) : 161.0, 159.2, 148.9 (2C), 147.1 (2C), 144.5, 143.2, 141.1 (2C), 140, 138.5 (2C), 137.5 (2C), 136.3, 134.5, 133.2, 132.1, 131.9, 128.1, 127.8, 126.9 (2C), 125.8 (2C), 124.6 (2C), 121.2, 116.6, 113.4 (2C), 91.9 (2C) (arom.), 90.2, 84.6 (ethynyl), 78.4, 69.3, 31.3, 28.9, 25.3, 22.4, 19.8 (2C), 17.8, 13.6; IR (KBr): ν 3285, 3268, 3066, 2921, 2855, 2207 (ν $\text{C}\equiv\text{C}$), 1618, 1578, 1550, 1498, 1466, 1426, 1415, 1381, 1275, 1220, 1147, 1014, 985, 912, 842, 724, 634, 557; ESI MS: calcd. for $[\text{C}_{112}\text{H}_{100}\text{Br}_2\text{N}_8\text{O}_2\text{Cu}_2]^{2+}$

[M²⁺]: m/z 938.4, found: m/z 938.7; Anal. Calcd. for C₁₁₂H₁₀₀Br₂Cu₂N₈O₂.2PF₆.2CH₂Cl₂: C, 58.60; H, 4.49; N, 4.80. Found: C, 58.56; H, 4.10; N, 5.03.

[Cu(**5**)(**6**)]PF₆: M.p. 149-151 °C; ¹H NMR (CD₂Cl₂, 200 MHz): δ 8.82 (s, 1H, phen), 8.69 (d, J = 8.1 Hz, 1H, phen), 8.40-8.48 (m, 4H, phen), 8.19 (d, J = 8.9 Hz, 2H, phen), 7.88 (s, 2H, phen), 7.86 (d, J = 8.1 Hz, 1H, phen), 7.72 (q, J = 4.7 Hz, 2H, phen), 5.96 (s, 2H, MesH), 5.89 (s, 2H, MesH), 3.24 (s, 1H, ethynyl), 1.72 (s, 6H, benzyl), 1.70 (s, 6H, benzyl), 1.5 (s, 6H, benzyl); ¹³C NMR (CD₂Cl₂, 100 MHz): 160.3, 159.1, 147.3, 143.4, 142.7, 140.4, 138.7, 138.2, 137.4, 137.1, 136.8, 135.9, 134.3, 128.3, 128.0, 127.9, 127.7, 127.2, 127.1, 126.7, 126.5, 126.3, 125.7, 124.3, 121.0, 119.3 (arom.), 83.8, 78.6 (ethynyl), 20.0, 19.8, 19.5, 19.0 (aliph.); IR (KBr): ν 3444, 3275, 2919, 2214 (ν C≡C), 1612, 1577, 1545, 1461, 1424, 1377, 1223, 1144, 1030, 993, 841, 774, 727, 635, 620, 558; ESI MS: calcd. for C₄₄H₃₆N₄Cu⁺ [M⁺]: m/z 684.3, found: m/z 683.4; Anal. Calcd. for CuC₄₄H₃₆N₄.PF₆: C, 63.73; H, 4.38; N, 6.76. Found: C, 63.61; H, 4.31; N, 6.80.

Procedure for the fabrication of grids G1-G2 by homocoupling:

General procedure:

R3 or **R4** (1.0 eq.) were reacted with catalytic amounts of anhydrous CuCl (0.1 eq) and triethylamine (2 ml for 5.8x10⁻³ mmol of **R3** or **R4**). The dark red solution was stirred for 24 h and the reaction was monitored by ESI MS.²³ Thereafter, the solvent was removed, and the remainder was washed with water (4 x 50 ml). After drying over MgSO₄ and evaporation of the solvent the grids were received as the main product in ~90% yield (by ESI MS and NMR). The dark red solution was analysed by ESI MS, ¹H NMR, without any further purification. For complete characterization, grids **G1-G2** were made independently by mixing **1** or **2** with **5**.

G1: M.p. > 300 °C; ¹H NMR (CD₂Cl₂, 400 MHz): δ 8.71-8.74 (m, 8H, phen), 8.45 –8.47 (m, 16H, phen), 8.08-8.23 (m, 4H, phen), 7.76-7.90 (m, 20H, phen), 7.05 (s, 4H, phenyl), 5.99 (s, 8H, phenyl), 3.99 (s, 8H, methoxy), 1.20-1.80 (m, 164H, benzyl and aliph.), 0.85 (s, 12H, aliph.); IR (KBr): ν 3288, 2928, 2856, 2207 (ν C≡C), 1719, 1702, 1686, 1655, 1618, 1544, 1508, 1499, 1459, 1426, 1386, 1220, 1019, 842, 723, 531, 558; ESI MS: calcd. for [C₂₄₈H₂₄₄N₁₆O₄Br₄Cu₄]⁴⁺ [M⁴⁺]: m/z 1021.6, found: m/z 1021.3; [M.PF₆³⁺]: m/z 1410.4, found: m/z 1410.7; Anal. Calcd. for

$C_{248}H_{244}Br_4Cu_4N_{16}O_4 \cdot 4PF_6 \cdot 4CH_2Cl_2$: C, 60.46; H, 5.07; N, 4.48. Found: C, 60.55; H, 5.35; N, 4.54; Yield: 89%.

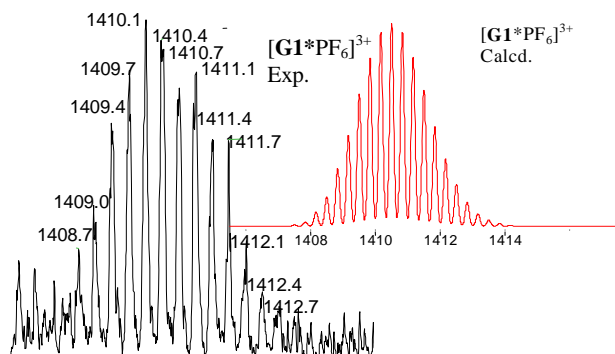


Figure S1. Experimental isotopic distribution of $[G1*PF_6]^{3+}$ charge species (dark) along with the theoretically expected one (red). See manuscript for 4^+ charge distribution.

G2: M.p. > 300 °C; 1H NMR (CD_2Cl_2 , 400 MHz): δ 8.68-8.75 (m, 8H, phen), 8.45-8.47 (m, 16H, phen), 8.08-8.22 (m, 4H, phen), 7.76-7.95 (m, 20H, phen), 7.07 (s, 4H, phenyl), 6.96 (s, 8H, phenyl), 4.00 (s, 8H, methoxy), 0.87-1.79 (m, 125H, benzyl and aliph.), 0.67 (s, 3H, aliph.); IR (KBr): ν 3278, 2846, 2209 (ν C \equiv C), 1721, 1701, 1669, 1621, 1552, 1508, 1484, 1434, 1426, 1399, 1230, 1021, 867, 714, 565, 557; ESI MS: calcd. for $[C_{224}H_{196}Br_4N_{16}O_4Cu_4]^{4+}$ [M^{4+}]: m/z 937.4, found: m/z 937.5; Anal. Calcd. for $C_{224}H_{198}Br_4N_{16}O_4Cu_4 \cdot 4PF_6 \cdot 4CH_2Cl_2$: C, 58.65; H, 4.40; N, 4.80. Found: C, 58.50; H, 4.44; N, 4.84; Yield: 94%.

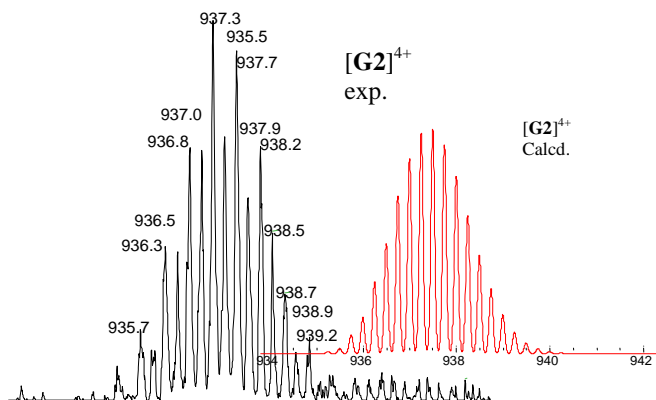


Figure S2. Experimental isotopic distribution of $G2^{4+}$ (dark) along with its theoretical one (red).

Procedure for metal-driven fabrication of G3-G4

General procedure for the Pt^{II} insertion in to the $[Cu(5)(6)]PF_6$ and R3-R4: Functional racks (**R3** and **R4**; 1 eq.) were treated with *trans*- $[Pt(PEt_3)_2]Cl_2$ (0.5 eq.) and triethylamine (TEA; 2 ml

for 5.8×10^{-3} mmol of **R3** or **R4**) in 50 ml of dry dichloromethane. The reaction was monitored by ESI MS and after 24 h the solvent was removed and the resulting dark red solid was washed with water (50 ml x 3). The organic layer was separated, dried over MgSO₄ and evaporated to dryness. The reaction mixture was analysed by ESI MS, ¹H NMR, COSY, elemental analysis, without any further purification. **R6** was prepared along the same procedure.

R6: M.p. 229-231 °C; ¹H NMR (CD₂Cl₂, 400 MHz): δ 8.60 (d, *J* = 3.9 Hz, 4H, phen.), 8.45 (s, 4H, phen.), 8.42 (d, *J* = 6.8 Hz, 4H, phen.), 8.01 (s (broad), 4H, phen.), 7.86 (s, 4H, phen.), 7.67-7.76 (m, 6H, phen.), 5.92 (s, 4H, mes.), 5.76 (s, 4H, mes.), 1.70 (s, 12H, benzyl), 1.66 (s, 12H, benzyl), 1.55 (s, 12H, benzyl), 1.52 (m, 12H, benzyl and aliph.), 0.77-0.81 (m, 18H, aliph.); ¹³C NMR (CD₂Cl₂, 100 MHz) : 160.6, 159.2, 147.9, 144.5, 143.4, 140.7, 138.2, 137.8, 137.4, 136.3, 136.1, 134.9, 132.0, 128.9, 128.4, 127.7, 127.5, 127.2, 127.0, 126.8, 126.4, 126.3, 126.0, 124.9, 119.7, 117.0 (arom.); 107.2, 91.1 (ethynyl); 20.5, 20.4, 20.1 (2C), 19.7 (2C), 16.0 (2C), 8.1 (2C) (aliph.); ³¹P{¹H} NMR (CD₂Cl₂, 162 MHz) : 13.30 (s); ESI MS: calcd. for [C₁₀₀H₁₀₀N₈P₂PtCu₂]⁺² [M⁺²]: *m/z* 899.1, found: *m/z* (%) 899.2(100); x-ray structure see the manuscript.

G3: M.p. > 224-226 °C; ¹H NMR (CD₂Cl₂, 400 MHz): δ 8.49 (d, *J* = 3.3 Hz, 4H, phen), 8.42 (m, 20H, phen), 8.1-8.2 (m, 6H, phen), 7.80-8.0 (m, 18H, phen), 7.05 (s, broad, 4H, phenyl), 5.98 (s, broad, 8H, phenyl), 4.11 (s, broad, 8H, methoxy), 1.00-1.80 (m, 200H, benzyl and aliph.), 0.70-0.90 (m, 36H, aliph.); ¹³C NMR (CD₂Cl₂, 100 MHz) : 171.3, 160.7, 159.3, 154.3, 149.3, 148.2, 144.4, 142.8, 141.5, 140 (2C), 138.1, 137.9, 137.7, 136.7, 134.9, 133.4, 132.6, 132.5, 129.2, 128.5, 128.2, 127 (3C), 126.7, 126.6, 126.4, 126.2, 125.1, 121.6, 117.1, 113.8, 106.1 (arom.), 92.9 (2C), 90.9 (2C) (ethynyl), 69.7 (2C), 32.3 (2C), 30.1 (2C), 29.9 (2C), 29.7 (2C), 29.5, 26.2 (2C), 23.1, 20.4 (2C), 20.2 (2C), 18.4 (2C), 15.9, 14.3; ³¹P{¹H} NMR (CD₂Cl₂, 162 MHz): 11.65 (s); IR (KBr): ν 3192, 2923, 2852, 2088 (ν C≡C), 1618, 1562, 1544, 1499, 1459, 1414, 1376, 1221, 1033, 910, 842, 769, 723, 636, 557; ESI MS: calcd. for [C₂₇₂H₃₀₄Br₄Cu₄N₁₆O₄P₄Pt₂]⁴⁺ [M⁴⁺]: *m/z* 1237.3, found: *m/z* 1236.6; [M.PF₆³⁺]: *m/z* 1698.08, found: *m/z* 1697.2; Anal. Calcd. for C₂₇₂H₃₀₄Br₄N₁₆O₄Cu₄Pt₂P₄.4PF₆*2CH₂Cl₂: C, 57.75; H, 5.45; N, 3.93. Found: C, 57.67; H, 5.47; N, 4.06; Yield: 91%.

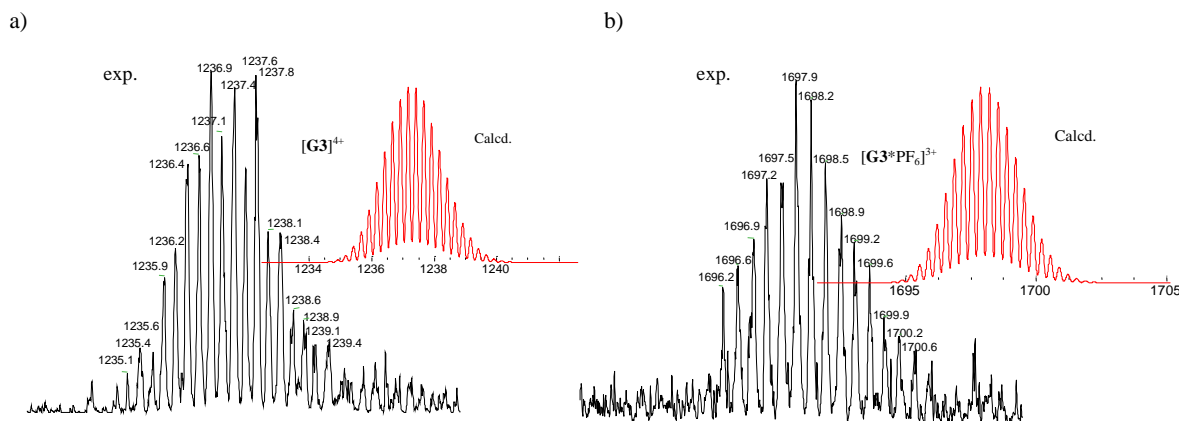


Figure S3. Experimental isotopic distributions of 4^+ (a) and 3^+ (b) charged species (dark) of **G3** along with their theoretical ones (red).

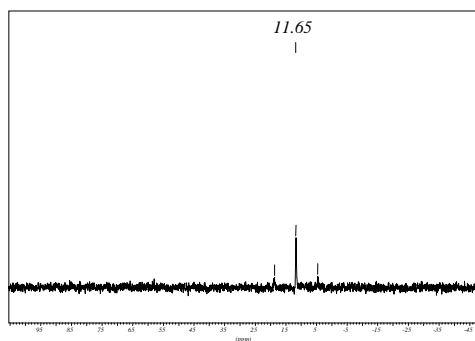


Figure S4. $^{31}\text{P}\{^1\text{H}\}$ NMR of **G3**.

G4: M.p. > 258-260 °C; ^1H NMR (CD_2Cl_2 , 400 MHz): δ 8.61 (d, $J = 3.5$ Hz, 4H, phen), 8.30-8.48 (m, 20H, phen), 8.01-8.11 (m, 6H, phen), 7.73-7.94 (m, 18H, phen), 7.05 (s, broad, 4H, phenyl), 5.95 (s, broad, 8H, phenyl), 3.99 (t, broad, $J = 6.1$ Hz, 8H, methoxy), 1.20-1.90 (m, 120H, benzyl and aliph.), 1.0-1.20 (m, 24H, aliph.), 0.62-0.86 (m, 44H, aliph.); ^{13}C NMR (CD_2Cl_2 , 100 MHz) : 193.6, 160.7, 154.3, 148.2 (2C), 144.4 (2C), 142.8 (2C), 141.5, 140.5, 137.0 (2C), 136.7 (2C), 135.0, 133.5 (2C), 133.4, 132.6, 129.3, 128.5, 128.3, 128.1, 127 (2C), 126.6, 126.5, 125.1, 121.6, 117.1, 113.8, 106.0 (2C) (arom.), 92.3 (2C), 92.1 (2C) (ethynyl), 31.7 (2C), 29.4, 25.9 (2C), 22.8 (2C), 20.4 (2C), 20.2, 18.4 (2C), 15.9 (2C), 14.1, 8.1; $^{31}\text{P}\{^1\text{H}\}$ NMR (CD_2Cl_2 , 162 MHz) : 11.66 (s); IR (KBr): ν 3525, 2921, 2087 (ν $\text{C}\equiv\text{C}$), 1686, 1562, 1544, 1499, 1461, 1414, 1388, 1220, 1034, 842, 767, 723, 557, 531; ESI MS: calcd. for $[\text{C}_{248}\text{H}_{256}\text{Br}_4\text{Cu}_4\text{N}_{16}\text{O}_4\text{P}_4\text{Pt}_2]^{4+}$ $[\text{M}^{4+}]$: m/z 1153.1, found: m/z 1153.5; $[\text{M}^{4+}]$: m/z 1585.8, found: m/z 1585.3; Anal. Calcd. for $\text{C}_{248}\text{H}_{256}\text{Br}_4\text{N}_{16}\text{O}_4\text{Cu}_4\text{P}_4\cdot 4\text{PF}_6\cdot 2\text{CH}_2\text{Cl}_2$: C, 56.00; H, 4.89; N, 4.80. Found: C, 55.85; H, 4.89; N, 4.25; Yield: 93%.

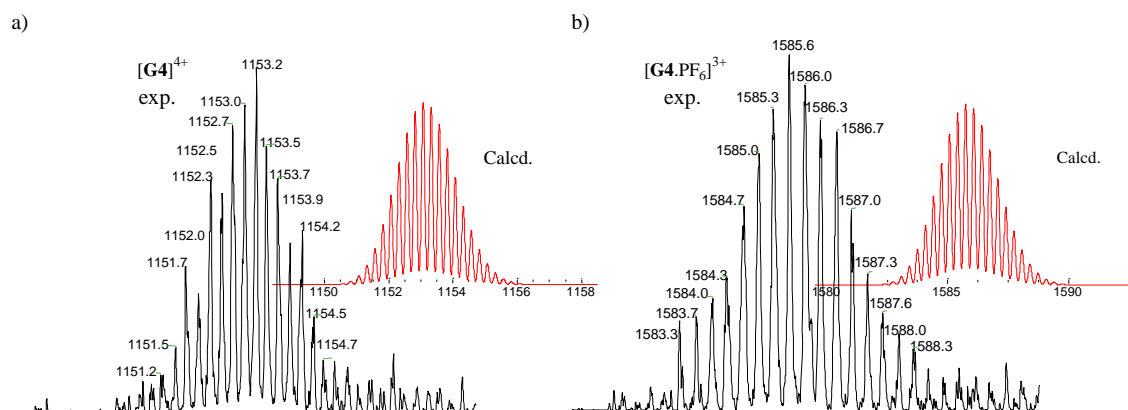


Figure S5. Experimental isotopic distributions of the 4⁺ (a) and 3⁺ (b) charged species of **G4** along with their theoretical ones.

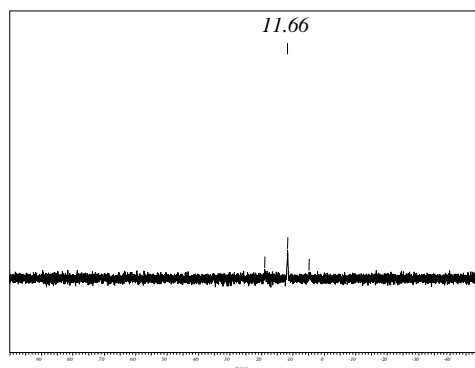


Figure S6. ³¹P{¹H} NMR of **G4**.

ESI MS titration of **7** and **1** with [Cu(MeCN)₄]PF₆ salt in dichloromethane.

Ligands **7** and **1** were titrated with Cu(I) salt in dichloromethane. All relevant signals appearing during the titration process could be identified and are listed in below table. As data in table 1 indicate, no homoleptic complexes of **1** were formed during the whole titration process. The data can be assigned to intermediates. The final spectrum contains only signals corresponding to the grid structure **G1**.

Titration Nr.	Stoichiometric ratio of 7 , 1 and Cu(I) salt	Observed m/z	Formula
1	1: 1: 0.2	851.2 (12%)	[1-H] ⁺
		909.4 (31%)	[(1)(Cu)] ⁺
		1066.0 (10%)	[7-H] ⁺
		1977.3 (100%)	[(7)(1)(Cu)] ⁺
2	1: 1: 0.4	851.2 (8%)	[1-H] ⁺
		909.4 (30%)	[(1)(Cu)] ⁺
		1022.0 (5%)	[(7)(1)(Cu)₂] ⁺
		1977.9 (100%)	[(7)(1)(Cu)] ⁺
3	1: 1: 0.6	851.2 (2%)	[1-H] ⁺
		909.4 (10%)	[(1)(Cu)] ⁺
		1022.0 (10%)	[(7)(1)(Cu)₂] ⁺
		1977.9 (100%)	[(7)(1)(Cu)] ⁺
4	1: 1: 0.8	851.2 (2%)	[1-H] ⁺
		909.4 (8%)	[(1)(Cu)] ⁺
		1022.0 (17%)	[(7)(1)(Cu)₂] ⁺
		1977.9 (100%)	[(7)(1)(Cu)] ⁺
5	1: 1: 1.0	909.4 (10%)	[(1)(Cu)] ⁺
		1022.0 (40%)	[(7)(1)(Cu)₂] ⁺ and [(7)₂(1)₂(Cu)₄] ⁴⁺
		1410.0 (10%)	[(7)₂(1)₂(Cu)₄.PF₆] ³⁺
		1977.9 (100%)	[(7)(1)(Cu)] ⁺
6	1: 1: 1.2	1022.0 (75%)	[(7)(1)(Cu)₂] ⁺ and [(7)₂(1)₂(Cu)₄] ⁴⁺
		1410.0 (20%)	[(7)₂(1)₂(Cu)₄.PF₆] ³⁺
		1977.9 (100%)	[(7)(1)(Cu)] ⁺
7	1: 1: 1.4	1021.8 (100%)	[(7)(1)(Cu)₂] ⁺ and [(7)₂(1)₂(Cu)₄] ⁴⁺
		1410.0 (55%)	[(7)₂(1)₂(Cu)₄.PF₆] ³⁺
		1977.9 (80%)	[(7)(1)(Cu)] ⁺
8	1: 1: 1.6	1021.8 (100%)	[(7)(1)(Cu)₂] ⁺ and [(7)₂(1)₂(Cu)₄] ⁴⁺
		1410.0 (80%)	[(7)₂(1)₂(Cu)₄.PF₆] ³⁺
		1977.9 (55%)	[(7)(1)(Cu)] ⁺
9	1: 1: 1.8	1021.8 (100%)	[(7)(1)(Cu)₂] ⁺ and [(7)₂(1)₂(Cu)₄] ⁴⁺
		1410.0 (65%)	[(7)₂(1)₂(Cu)₄.PF₆] ³⁺
		1977.9 (5%)	[(7)(1)(Cu)] ⁺
10	1: 1: 2.0	1021.8 (100%)	[(7)₂(1)₂(Cu)₄] ⁴⁺
		1410.0 (39%)	[(7)₂(1)₂(Cu)₄.PF₆] ³⁺
11	1: 1: 4.0	1021.8 (100%)	[(7)₂(1)₂(Cu)₄] ⁴⁺
		1410.0 (39%)	[(7)₂(1)₂(Cu)₄.PF₆] ³⁺

Table 1. ESI MS titration data along with their proposed formulas.

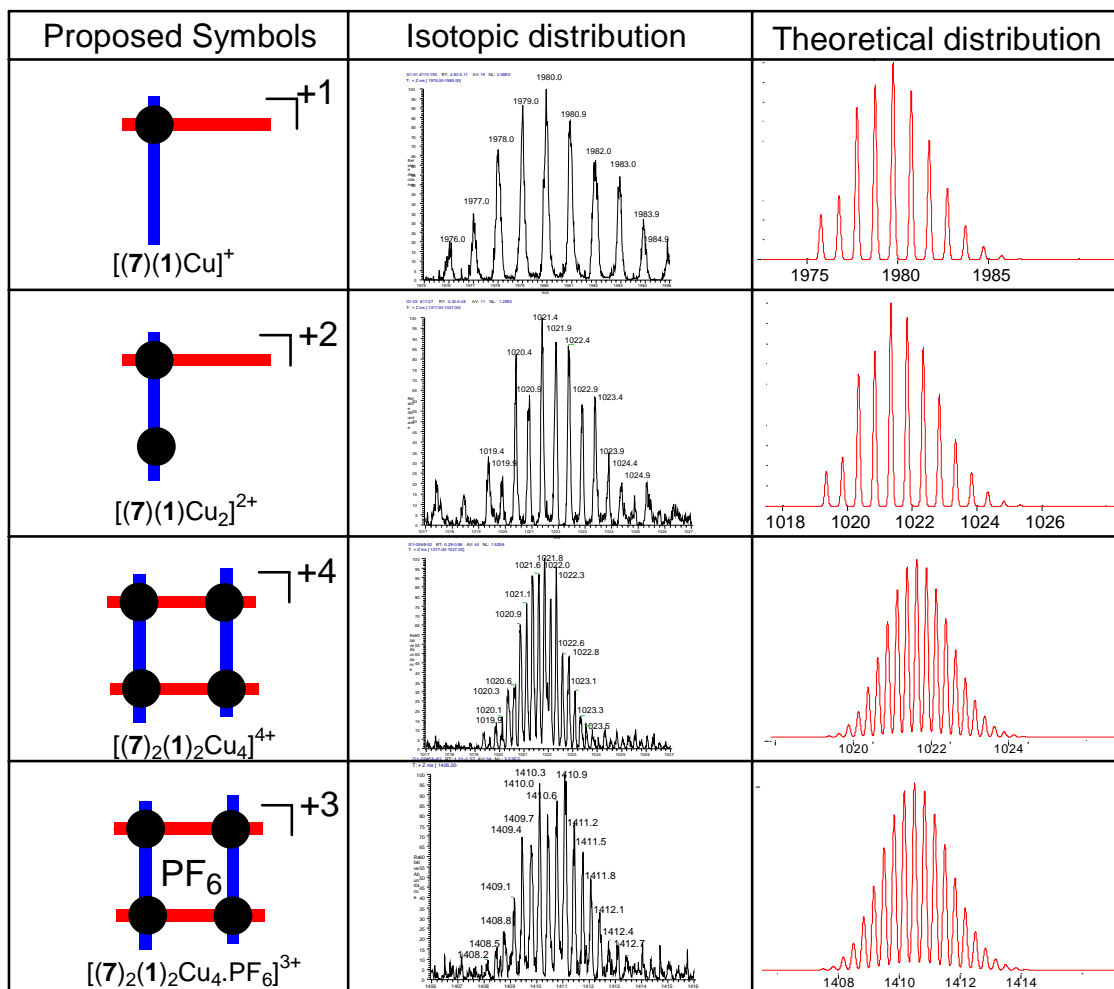
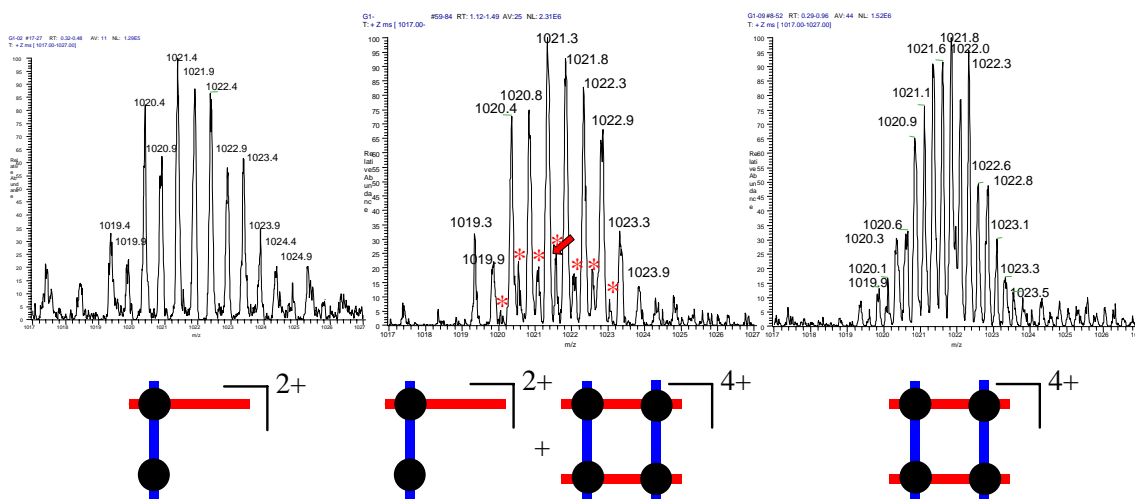


Fig. S7. Isotopic distributions of proposed compositions.


 Figure S8. Isotopic distribution changes during the titration at m/z : 1020.

Collisional activation study on G1

Fragmentation of the grid (G1) further confirmed the assignments. Fragmentation of $[(7)_2(1)_2(\text{Cu})_4\text{PF}_6]^{+3}$ produced the signals corresponding to $[(7)(1)(\text{Cu})]^+$ and $[(7)(1)(\text{Cu})_2]^{+2}$ with both the species being further confirmed by their isotopic distributions.

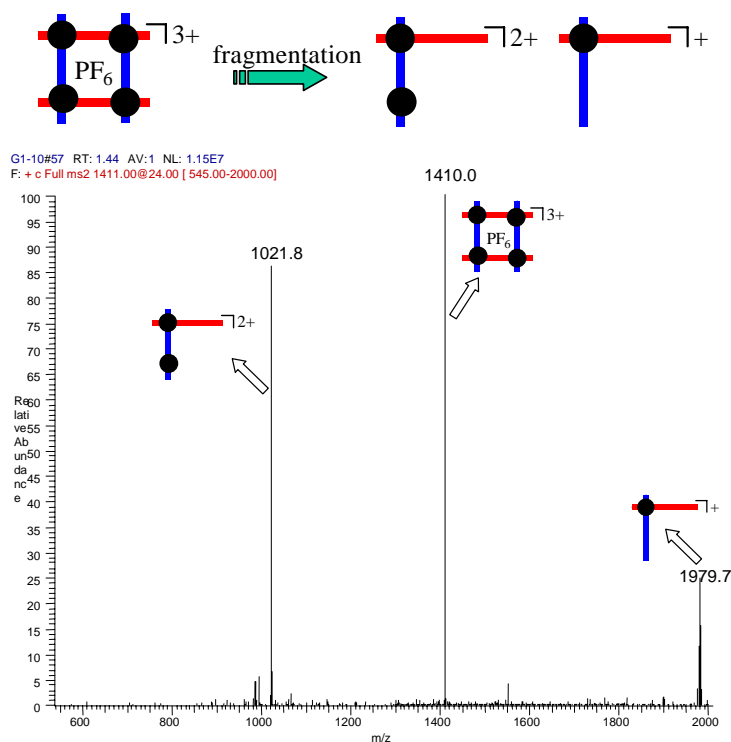


Figure S9.

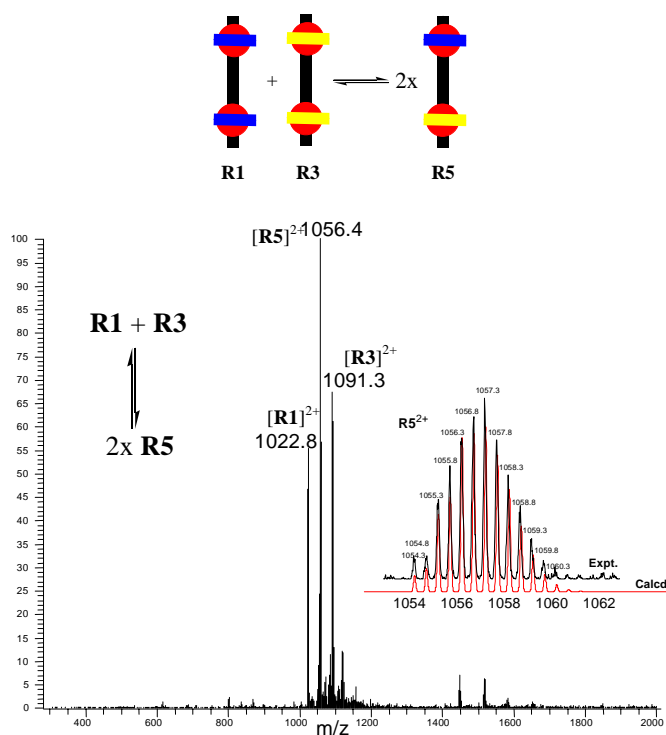
ESI MS of the reaction mixture when **R1** and **R3** are reacted in dichloromethane.

Figure S10. ESI MS of the reaction mixture when **R1** and **R3** are reacted in dichloromethane. Below is shown the experimental isotopic distribution of $\mathbf{R5}^{2+}$ species (dark) along with its theoretical one (red).

Fragmentation of the mixed rack, **R5** further confirmed the assignments. Fragmentation of $[(\mathbf{1})(\mathbf{3})(\mathbf{4})(\text{Cu})_2]^{2+}$ produced the signals corresponding to $[(\mathbf{1})(\mathbf{3})(\text{Cu})]^+$, $[(\mathbf{1})(\mathbf{4})(\text{Cu})]^+$, $[(\mathbf{3})(\text{Cu})]^+$ and $[(\mathbf{4})(\text{Cu})]^+$ with all the species being further confirmed by their isotopic distributions.

^1H NMR experiments for the **R1-R3-R5** equilibration could not be performed due to signal overlap. However, in a similar Cu(I) based rack system (**R7**) the dynamic nature could readily be observed by ^1H NMR. ^1H NMR of rack **R7** and **R8** showed singlets for all bridge phenyl protons because of their homotopic nature. When rack **R7** and **R8** were reacted together the mixed species **R9** was detected by ESI MS and ^1H NMR, similar to the equilibrium observed for **R1-R3-R5**. In the ^1H NMR of the mixed rack species **R9**, the bridge phenyl protons become constitutionally heterotopic; therefore, they appear as a pair of AB-doublets.

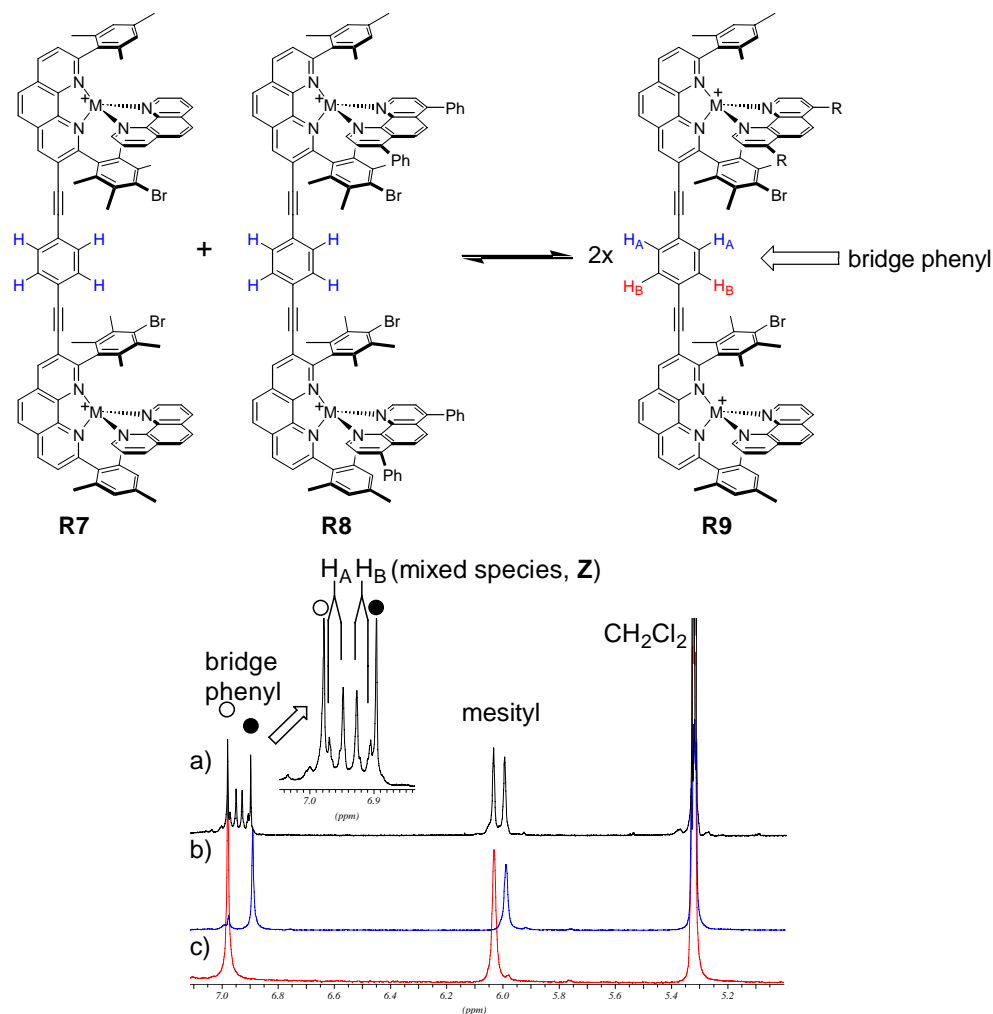


Figure S11. ^1H NMR aromatic region in dichloromethane at room temperature; a) **R7+R8** (dark, 400 MHz), b) **R7** (blue, 200 MHz, filled circles), c) **R8** (red, 200 MHz, empty circles). Inlet is the expansion of bridge phenyl region showing the new set of signals for heterotopic protons present in the mixed species **R9**.

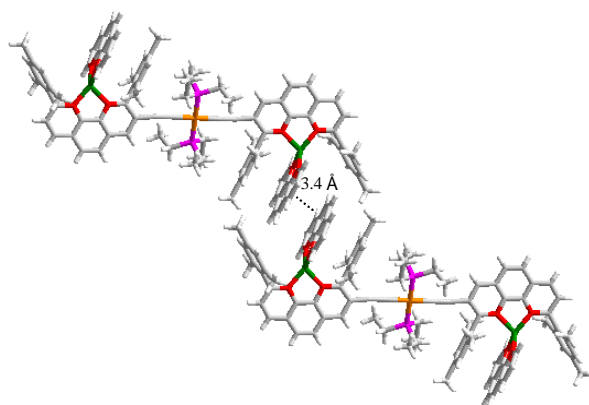


Figure S12. Part of the infinite intermolecular π - π (3.4 Å) interactions between neighbouring phenanthrolines in the solid state structure of **R6**.

- (1) Schmittel, M.; Kalsani, V. *Top. Curr. Chem.* **2004**, *245*, 1–53.
- (2) (a) Sleiman, H.; Baxter, P. N. W.; Lehn, J.-M.; Airola, K.; Rissanen, K. *Inorg. Chem.* **1997**, *36*, 4734–4742.
(b) Brown, D.; Zong, R.; Thummel, R. P. *Eur. J. Inorg. Chem.* **2004**, 3269–3272 and ref's therein.
- (3) Ruben, M.; Rojo, J.; Romero-Salguero, F. J.; Uppadine, L. H.; Lehn, J.-M. *Angew. Chem., Int. Ed.* **2004**, *43*, 3644–3662.
- (4) Schalley, C. A. *Angew. Chem., Int. Ed.* **2004**, *43*, 4399–4401.
- (5) The HETPHEN (heteroleptic bisphenanthroline) approach is based on steric and electronic effects originating from bulky aryl substituents at the bisimine coordination sites (as seen in **3-5**, **7** and **8**) to control the coordination equilibrium both kinetically and thermodynamically.
- (6) (a) Schmittel, M.; Ganz, A. *Chem. Commun.* **1997**, 999–1000. (b) Schmittel, M.; Lüning, U.; Meder, M.; Ganz, A.; Michel, C and Herderich, M. *Heterocycl. Commun.* **1997**, *3*, 493–494.
- (7) Kalsani, V.; Ammon, H.; Jäckel, F.; Rabe, J. P.; Schmittel, M. *Chem. Eur. J.* **2004**, *21*, 5481–5492.
- (8) Schmittel, M.; Ganz, A.; Fenske, D. *Org. Lett.* **2002**, *4*, 2289–2292.
- (9) Schmittel, M.; Ammon, H.; Kalsani, V.; Wiegrefe, A.; Michel, C. *Chem. Commun.* **2002**, 2566–2567.
- (10) (a) Schmittel, M.; Kalsani, V.; Fenske, D.; Wiegrefe, A. *Chem. Commun.* **2004**, 490–491. (b) Kalsani, V.; Bodenstedt, H.; Fenske, D.; Schmittel, M. *Eur. J. Inorg. Chem.* **2005**, accepted.
- (11) Schmittel, M.; Kalsani, V.; Kienle, L. *Chem. Commun.* **2004**, 1534–1535.
- (12) Benaglia, M.; Ponzini, F.; Woods, C. R.; Siegel, J. S. *Org. Lett.* **2001**, *3*, 967–969.
- (13) Schmittel, M.; Michel, C.; Wiegrefe, A.; Kalsani, V. *Synthesis* **2001**, 1561–1567.
- (14) Carina, R. F.; Dietrich-Buchecker, C.; Sauvage, J. P. *J. Am. Chem. Soc.* **1996**, *118*, 9110–9116.
- (15) Jiang, H.; Lin, W. *J. Am. Chem. Soc.* **2004**, *126*, 7426–7427 and ref's therein.
- (16) Crystal data for **R6**: Crystals were obtained by slow diffusion of toluene into a dichloromethane solution of the complex. $C_{100}H_{100}Cu_2N_8Pt*2PF_6*2$ toluene, triclinic, space group $P-1$, $a = 12.893(3) \text{ \AA}$, $b = 13.701(3) \text{ \AA}$, $c = 16.224(3) \text{ \AA}$, $\alpha = 76.032(17)^\circ$, $\beta = 80.039(17)^\circ$, $\gamma = 73.553(17)^\circ$, $V = 2650.4(9) \text{ \AA}^3$, $Z = 1$, $D_{\text{calcd}} = 1.424 \text{ Mg/m}^3$, $\mu = 1.847 \text{ mm}^{-1}$, Final R indices [$I > 2\sigma(I)$] $R1 = 0.0592$, $wR2 = 0.1195$, R indices (all data) $R1 = 0.1143$, $wR2 = 0.1361$.
- (17) Osakada, K.; Hamada, M.; Yamamoto, T. *Organomet.* **2000**, *19*, 458–468.
- (18) Petitjean, A.; Kyritsakas, N.; Lehn, J.-M. *Chem. Commun.* **2004**, 1168–1169 and ref's therein.
- (19) ^1H NMR experiments for the **R1-R3-R5** equilibration could not be performed due to signal overlap. However, in a similar Cu(I) based rack system the dynamic nature could readily be observed by ^1H NMR (see **R7**: supp. information).
- (20) Synthesis of a family of Pt-appended bis-phenanthrolines and their complexes will be described in detail in forthcoming paper. Schmittel, M.; Kalsani, V. Manuscript in preparation. ^1H -, ^{13}C -, ^{31}P -NMR, ESI-MS are in agreement with their structure.
- (21) Hyperchem[®] 6.02 Release for Windows by Hypercube, Inc. 2000. MM+ force field.
- (22) Kalsani, V.; Bodenstedt, H.; Fenske, D.; Schmittel, M. *Eur. J. Inorg. Chem.* **2005**, accepted for publication.
- (23) Carina, R. F.; Dietrich-Buchecker, C.; Sauvage, J. P. *J. Am. Chem. Soc.* **1996**, *118*, 9110–9116.

CHAPTER 5

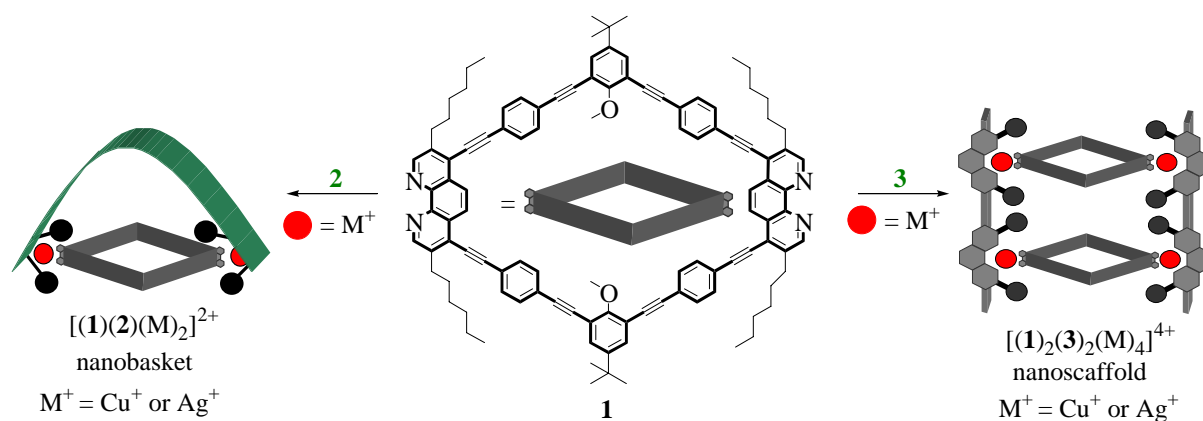
5. Multicomponent Aggregates of a Rigid Exotopic Bisphenanthroline Macrocycle and their Characterization in Solution and at Surfaces.....	229
5.1 Synthesis and Self-Assembly of a Rigid Exotopic Bisphenanthroline Macrocycle: Surface Patterning and a Supramolecular Nanobasket (Supp 5-1)	229
5.2.1 Introduction and Motivation.....	229
5.2.2 Self-Assembly of Macrocycle at Solid-Liquid Interfaces (in cooperation with Prof. J. P. Rabe, Humboldt University Berlin, Berlin)	229
5.2.3 Self-Assembly of a Nanobasket.	230
5.2.3 Mechanistic Insight	232
5.2 Self-Assembly of Nanoscaffolds and Their Characterization (Supp 5-2 and Supp 5-3)	232
5.2.1 Introduction and Motivation.....	232
5.2.2 Quantitative Formation and Clean Metal Exchange Processes of Large Void (~5000 Å ³) Nanobox Structures (Supp 5-2).....	233
5.2.3 Heteroleptic Bisphenanthroline Metallo-Nanoscaffolds – A Model Case for the Solution State Characterisation of Supramolecular Nano Edifices (Supp 5-3)	234
5.3 TEM and AFM Investigations of Nanoscaffolds (Supp 5-4)	235
5.3.1 TEM Investigations of Nanobox, Nanogrid and a Simple Bisheteroleptic Phenanthroline Copper Complex (in cooperation with Dr. L. Kienle, Max-Planck-Institut für Festkörperforschung, Stuttgart).	235
5.3.3 AFM Investigations of the Nanobox (in cooperation with Prof. J. P. Rabe, Humboldt University Berlin, Berlin)	237
5.4 Summary	239

5. Multicomponent Aggregates of a Rigid Exotopic Bisphenanthroline Macrocycle and their Characterization in Solution and at Surfaces

5.1 Synthesis and Self-Assembly of a Rigid Exotopic Bisphenanthroline Macrocycle: Surface Patterning and a Supramolecular Nanobasket (Supp 5-1)¹

5.2.1 Introduction and Motivation

The synthesis of rigid macrocycles² and their self-assembly in solution as well as at solid-liquid interfaces has attracted considerable attention over the last few years due to their potential to serve as 2D-templates for the construction of larger supramolecular 3D-assemblies and as matrix for the incorporation of guest molecules.³⁻⁵ The synthesis of macrocycle **1** has been described previously by Horst Ammon.⁶ In the present chapter, the self-assembly of **1** with various other phenanthroline building blocks to yield a variety of nanoscaffolds with unprecedented voids (Scheme 5-1) will be presented.



Scheme 5-1. Cartoon representation of multicomponent self-assembly reactions of macrocycle **1** yielding a nanobasket and nanoscaffold motifs.

5.2.2 Self-Assembly of Macrocycle at Solid-Liquid Interfaces (in cooperation with Prof. J. P. Rabe, Humboldt University Berlin, Berlin)

The self-assembly of macrocycle **1** at solid-liquid surfaces was studied by scanning tunnelling microscopy (STM). Figure 5-1a displays an STM current image of **1** at the solution-HOPG-interface (HOPG = highly oriented pyrolytic graphite) revealing the formation of a highly ordered monolayer of the macrocycle, the dimensions of which are in good agreement with the calculated structure. Due to the orientation and spacing of the phenanthroline units being

ideal for metal ion coordination, one might envisage using the monolayer to study the formation and the electronic properties of coordination polymers.

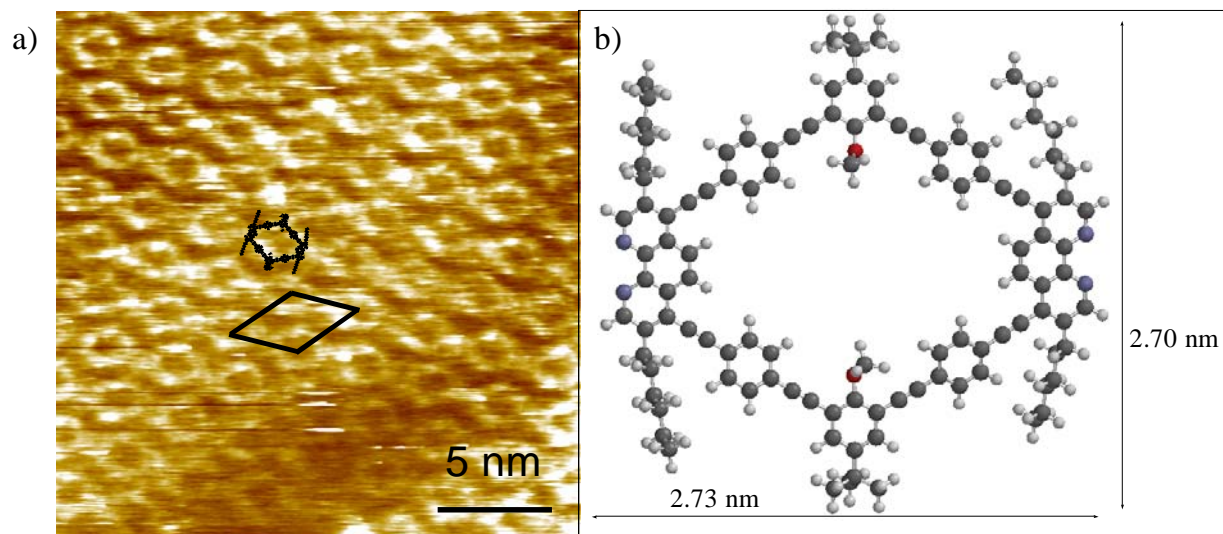
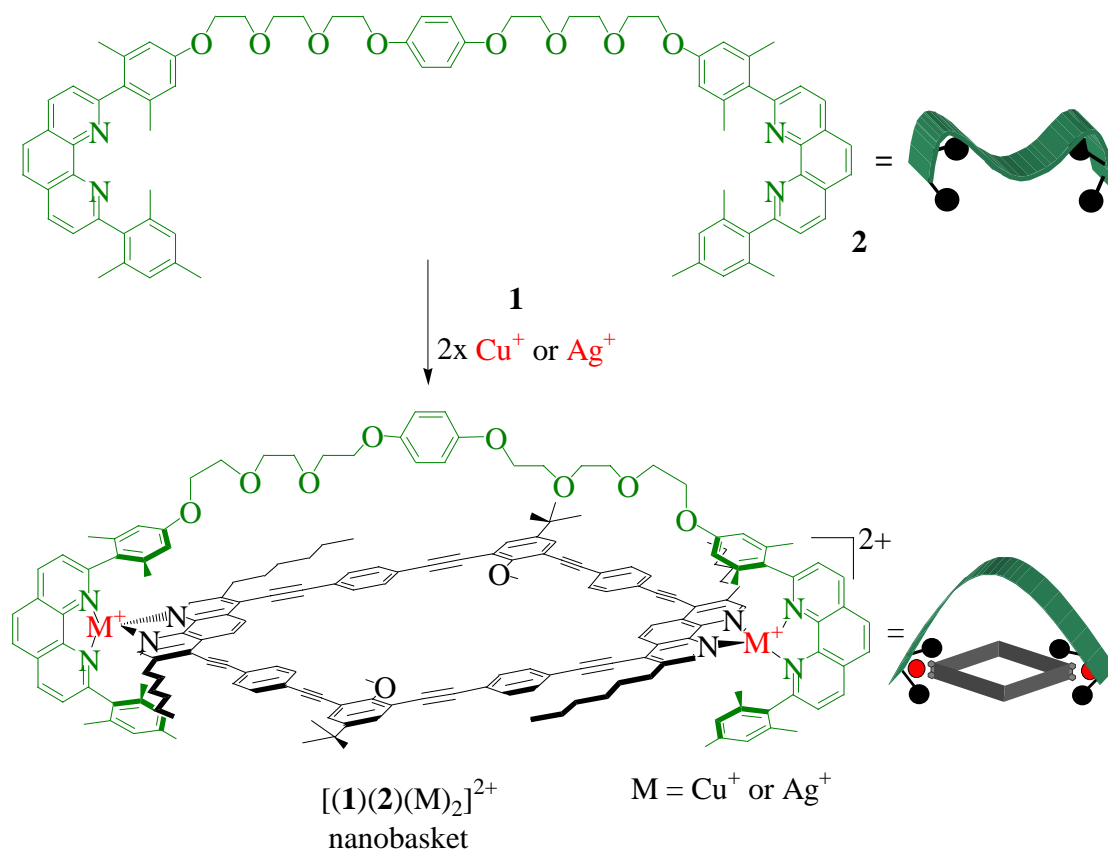


Figure 5-1. a) STM current image of a highly ordered monolayer of macrocycle **1** on highly oriented pyrolytic graphite (HOPG). b) PM3 minimized structure of the macrocycle. (in cooperation with F. Jäckel and Prof. J. P. Rabe, Humboldt University Berlin, Berlin)

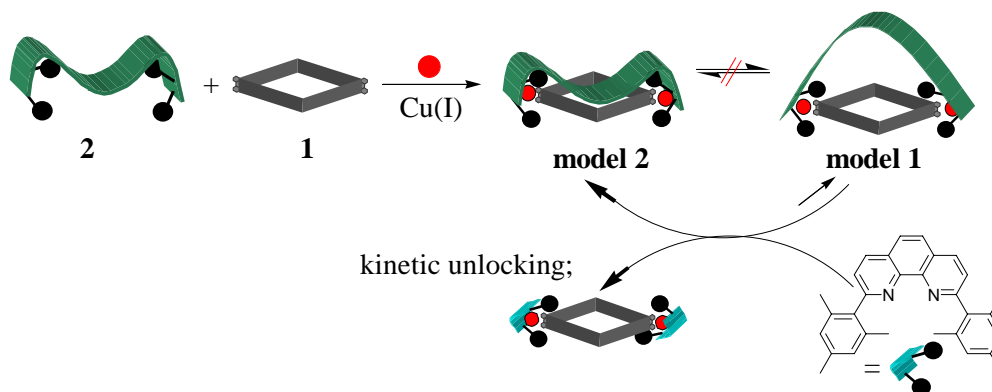
5.2.3 Self-Assembly of a Nanobasket.

The construction of well defined basket shaped molecules has attracted a great deal of interest among supramolecular chemists, due to their potential use in host-guest chemistry. While some first cyclophane assemblies have been reported to date,⁷ these are well below nanoscale dimensions. According to the HETPHEN concept, the reaction of **1** and **2** with appropriate tetrahedral metal ions (Cu^+ or Ag^+) is expected to yield a nanobasket assembly (Scheme 5-2).



Scheme 5-2. Programmed self-assembly of a nanobasket assembly.

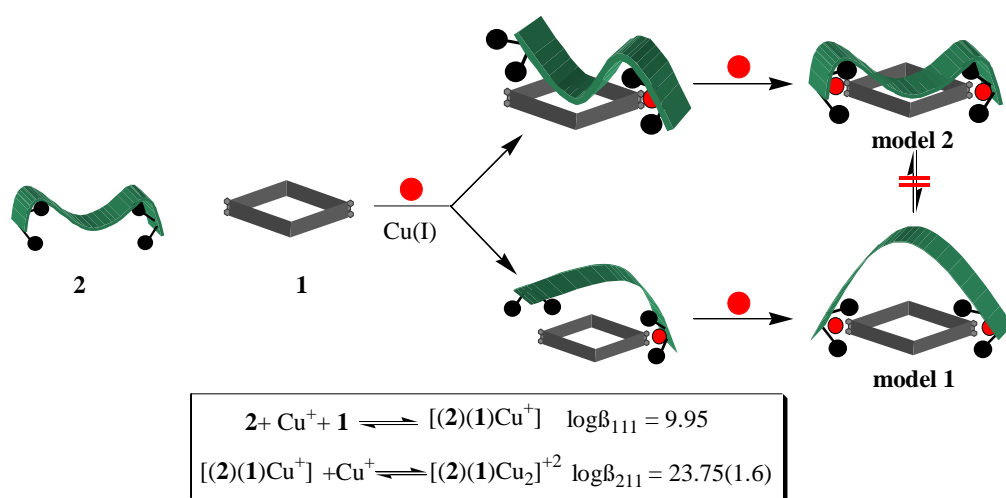
Upon complexation of macrocycle **1** with **2** and $[\text{Cu}(\text{MeCN})_4]\text{PF}_6$ (1:1:2 equiv.), the solution turned deep red. The ESI MS analysis of this solution indicated the formation of $[\mathbf{1}(\mathbf{2})(\text{Cu})_2]^{2+}$ as the exclusive species. The isotopic splitting pointing to a doubly charged species is in perfect agreement with its proposed composition. Interestingly, the ^1H NMR analysis showed three sets of signals, the relative intensities of which were not affected by temperature and the sequence of addition, suggesting very slow interconversion of three isomers. Structural characteristics and assignments of these three isomers (**model 1-2**) will be detailed in Supp 5-1 (Scheme 5-3).



Scheme 5-3. Self-assembly of a nanobasket assembly leading to the formation of non-equilibrating isomers **model 1-2** and kinetic unlocking of the equilibrium.

5.2.3 Mechanistic Insight

Thermodynamic and kinetic data on the formation of supramolecular entities provide deeper mechanistic insight thus facilitating the understanding of self-recognition phenomena and the construction of more complex supramolecular structures. Very few reports are at hand providing mechanistic insight into the heteroleptic organisation.^{7a,8} The present study makes use of ESI MS for qualitative analysis and spectrophotometry for quantitative analysis. From the results a two step pathway was postulated for the formation of the nanobasket assembly (Scheme 5-4).



Scheme 5-4. Proposed mechanistic pathway for the self-assembly of the nanobasket.

5.2 Self-Assembly of Nanoscaffolds and Their Characterization (Supp 5-2 and Supp 5-3)⁹

5.2.1 Introduction and Motivation

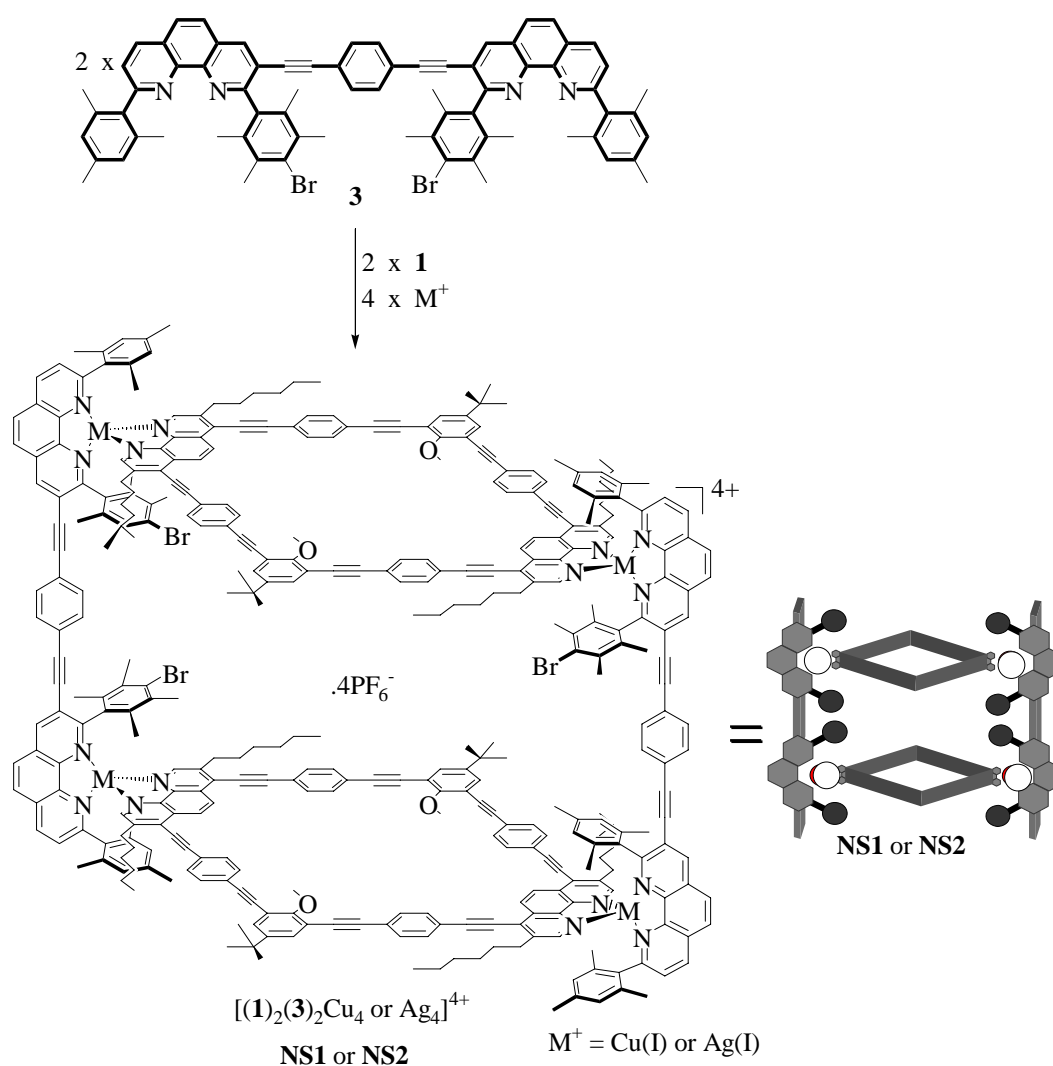
As discussed in chapter 2, rather few aggregates beyond 2 nm dimensions have been reported to date, due to the difficulties involving their construction and characterization. Because of our success with the HETPHEN approach, it was of our interest to pursue supramolecular aggregates with unprecedented voids and to use the internal void for potential host-guest chemistry and other purposes. In the following, the self-assembly of nanoscaffolds with volumes of $>5000 \text{ \AA}^3$ and their characterization in solution will be presented (Supp 5-2).

As the size and scale of the supramolecular aggregates augment it becomes increasingly difficult to characterise these nanoscale devices in the solid state, because the large size and huge void make it difficult to obtain X-ray suitable single crystals. Hence, it was very important to highlight the available solution state characterization techniques and to lay out a

model case for the characterisation of large supramolecular structures in the solution state (Supp 5-3).

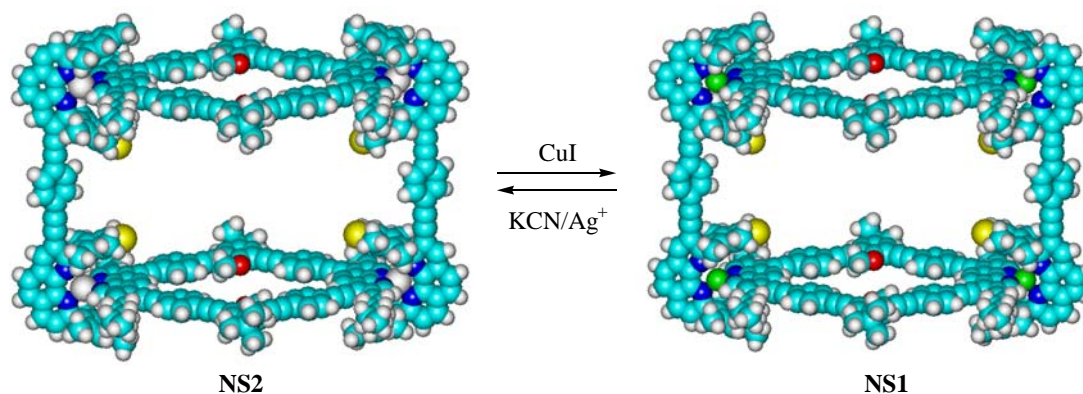
5.2.2 Quantitative Formation and Clean Metal Exchange Processes of Large Void (~5000 Å³) Nanobox Structures (Supp 5-2).

As suggested by the HETPHEN concept, the reaction of **1** and **3** with Cu(I) or Ag(I) produced multicomponent nanoscaffolds, quantitatively (Scheme 5-5). The resulting aggregates could be characterized in solution by ¹H NMR, ESI MS, analytical ultracentrifugation and elemental analysis. The nanoscopic nature of these aggregates was evident from model calculations that indicated the diagonal distance between two copper and two phenanthrolines to amount to 3.5 and 4.7 nm, respectively.



Scheme 5-5. Self-assembly of multicomponent nanoscaffolds NS1-2.

Due to their dynamic nature, the silver scaffolds could be converted to the corresponding copper scaffolds (Scheme 5-6). The silver scaffold could be regenerated by the treatment with KCN (aq.) and excess of Ag^+ . The transformations were readily monitored by ESI MS and UV/vis spectroscopy.



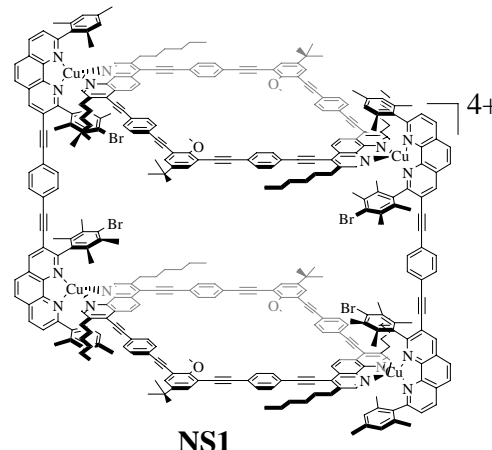
Scheme 5-6. Interconversion of copper (NS1) and silver nanoscaffolds (NS2).

5.2.3 Heteroleptic Bisphenanthroline Metallo-Nanoscaffolds – A Model Case for the Solution State Characterisation of Supramolecular Nano Edifices (Supp 5-3)

As discussed in the introduction, due to the problems associated with the characterization of nanoscaffolds in the solid state it was of interest to elaborate a model case for their solution state characterization. In the present subchapter (Supp 5-3), a battery of both direct and indirect solution state characterization techniques will be presented for nanoscaffolds. Copper nanoscaffold **NS1** was chosen as a model case, and the results are summarized in a tabular form (Table 5-1). As can be seen from Table 1, both direct and indirect methods provide an unambiguous characterization of the nanoscaffold **NS1**. A detailed discussion of each experiment is presented in Supp 5-3.

Table 5-1. A model case (NS1) for the solution state characterization of nanoscaffolds (> 3 nm).

direct methods	indirect methods
^1H NMR	model calculations
^{13}C NMR	chemical oxidation
ESI MS	ligand exchange experiments
analytical ultracentrifugation	metal exchange experiments
UV/vis	mechanistic insight (studied by ESI MS and UV/vis)
elemental analysis	self-recognition phenomena

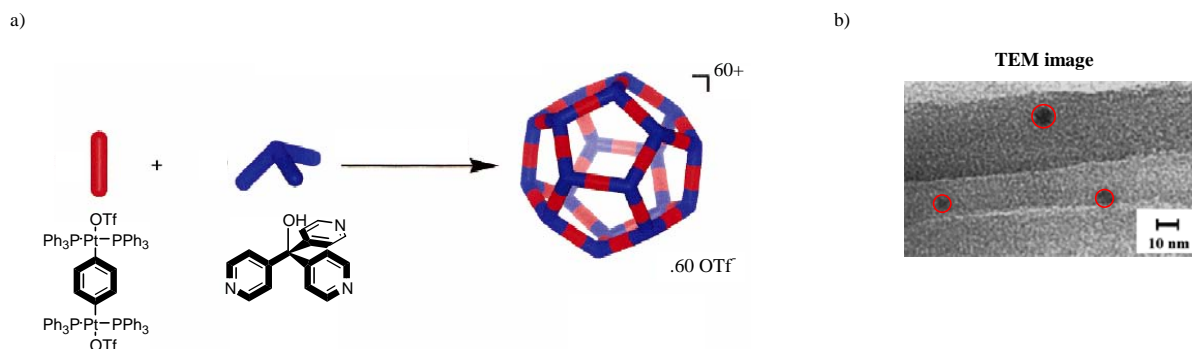


5.3 TEM and AFM Investigations of Nanoscaffolds (Supp 5-4)¹⁰

5.3.1 TEM Investigations of Nanobox, Nanogrid and a Simple Bisheteroleptic Phenanthroline Copper Complex (in cooperation with Dr. L. Kienle, Max-Planck-Institut für Festkörperforschung, Stuttgart).

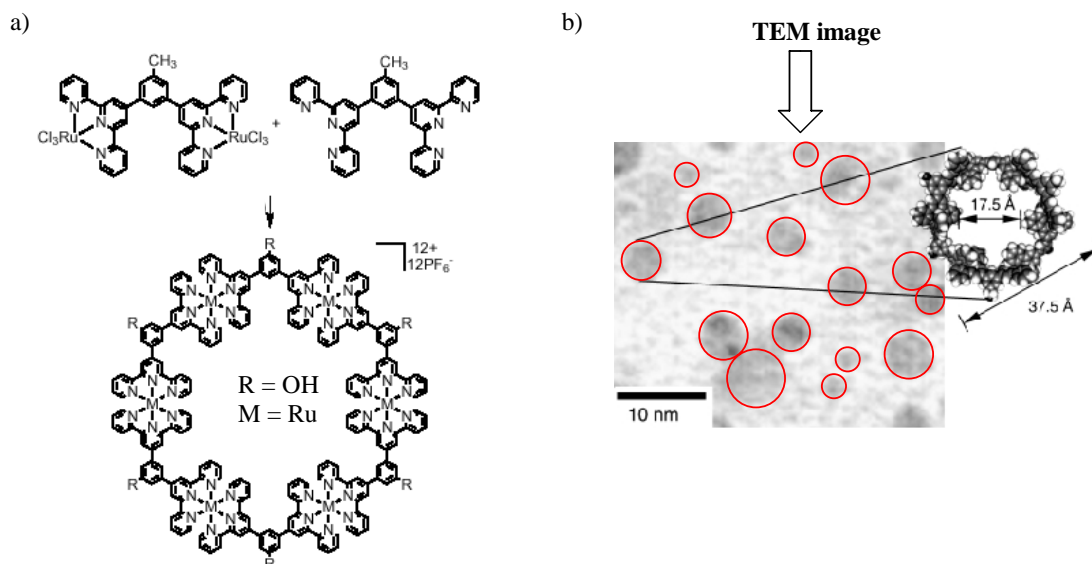
In absence of single crystal analysis, transmission electron microscopy (TEM), scanning tunnelling microscopy (STM) and atomic force microscopy (AFM) have become methods of choice to characterize large supramolecular aggregates. In the following we (in cooperation with Prof. J. P. Rabe and Dr. L. Kienle) studied a few supramolecular aggregates using TEM and AFM.

Literature known examples: Using the directional bonding strategy (see chapter 2 for different strategies) Stang *et al.*, reported on a fascinating self-assembled dodecahedra with outer dimensions of ca. 5 and 8 nm from 50 pre-designed components via 60 metal-ligand bonds.¹¹ Its structure was supported by TEM imaging (Scheme 5-7).



Scheme 5-7. Self-assembly of a dodecahedra and its TEM image. Reprinted with permission from ref. 11. Copyright 1999 American chemical society.

Newkome *et al.* demonstrated the self-assembly of terpyridine based molecular hexagons.¹² Apart from solution state characterization, here again TEM imaging was used to determine the dimensions of the hexagons (Scheme 5-8).



Scheme 5-8. Newkome's hexagon and the TEM image provided in support of the proposed structure. Reprinted with permission from ref. 12. Copyright, Wiley-VCH Verlag GmbH & Co KG.

Close inspection of the above two TEM images (scheme 5-7 and 5-8) revealed that all the particles are not of the same size (marked with red circles). Therefore, questions with regard to the assignments should be raised. We investigated the **NS1** and **G1** architectures using HRTEM. This work has been done in cooperation with Dr. Kienle, Max-Planck Institute, Stuttgart. The HRTEM investigations on **NS1**, **G1** provided nanoparticles of ~5 nm dimensions; however, closer inspection of these nanoparticles by selected angle X-ray diffraction (SAED)/HRTEM showed that these nanoparticles are composed of pure crystalline copper and do not represent the original suprastructure. In order to investigate the templating effect of the suprastructure we investigated the much simpler complex **4**. As shown in Figure 5-2, again copper nanoparticles of ~5 nm were generated, indicating no suprastructure templating effect.

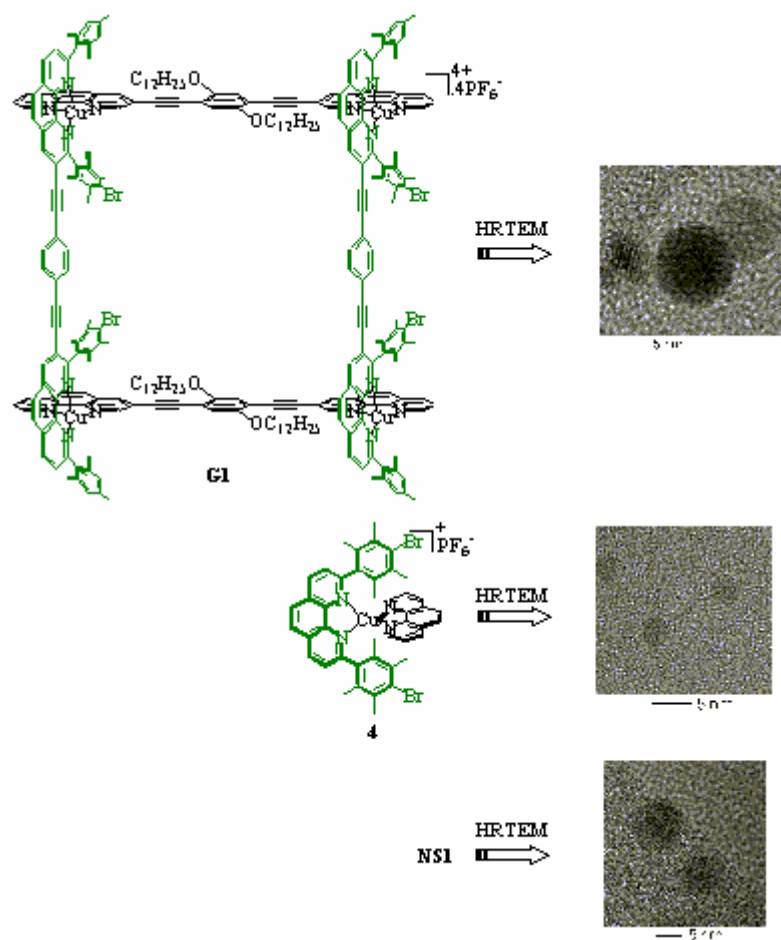


Figure 5-2. HRTEM imaging of NS1, G1 and 4 (in cooperation with Dr. Lorenz Kienle, Max-Planck-Institut für Festkörperforschung, Stuttgart).

The above results point to the following two conclusions:

- 1) Copper nanoparticles (~5 nm) can be generated from simple bisphenanthroline copper complexes under HRTEM conditions.
- 2) TEM imaging alone is not a good tool to characterise supramolecular aggregates. It has to be supported by SAED.

5.3.3 AFM Investigations of the Nanobox (in cooperation with Prof. J. P. Rabe, Humboldt University Berlin, Berlin)

Recently, atomic force microscopy (AFM) has been used to image discrete nanostructures.¹³ In a remarkable example by Kobuke *et al.*, a cyclic porphyrin nanohexamer was self-assembled that possesses structural similarities with the natural light harvesting systems (LH1, LH2 and LH3).^{13b} The structure of the nanohexamer was supported by an AFM image (Figure 5-3). Encouraged by these reports, we investigated the AFM images of NS1. Unfortunately, the results point to a strong aggregation of NS1, thus preventing single molecule imaging.

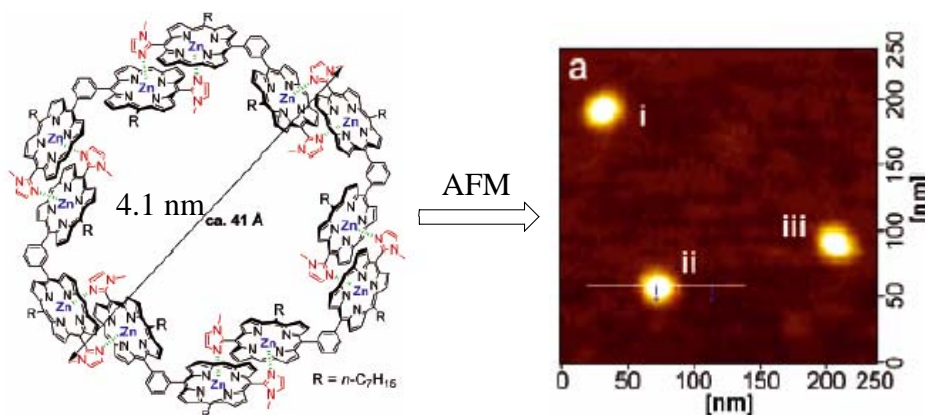


Figure 5-3. A self-assembled cyclic hexamer^{13b} and its AFM image. Reprinted with permission from ref. 13b. Copyright 1999 American chemical society.

Atomic force microscopy investigations on **NS1** were performed in the tapping mode under ambient conditions. Samples were prepared by spincoating solutions of the nanobox in trichlorobenzene at various concentrations onto substrates of freshly cleaved mica which was rinsed with milliQ-water and subsequently dried in a nitrogen flow. *Estimated* concentrations ranged from $\sim 10^{-3}$ M down to $\sim 10^{-10}$ M (error might be an order of magnitude!). Figure 5-4a-b shows the height images measured from samples of different **NS1** concentrations. At high concentrations large statistical (poorly defined) aggregates are observed. Dilution reduces, as expected, the number and size of the aggregates. In figure 5-4, the results of a statistical analysis of the images obtained from the two lowest concentrated samples investigated are shown. In particular, the height and the lateral dimensions (corrected for the tip broadening effect with an assumed tip radius of 10 nm) of the objects were determined. In both cases, the broadness of the distributions obtained, as well as the range of the width-distribution, strongly indicated that even at such low concentration aggregates rather than single **NS1** were visualized.

It seems not to be useful to further dilute, because, already at the lowest concentration used, very large uncovered substrate areas were found. This might be due to adsorption of the molecules to the substrate after the de-wetting of the solvent film during spin-coating. Thus, it will be increasingly difficult to find covered areas at further dilution. Secondly, the height images at lowest concentration used demonstrate that we approach the limits of the instrument. Thus we may doubt that further measurement would give reliable results.

In conclusion, AFM investigations of **NS1** showed strong aggregation even at very low concentration. Unfortunately, it was not possible to confirm any structural model of **NS1**.

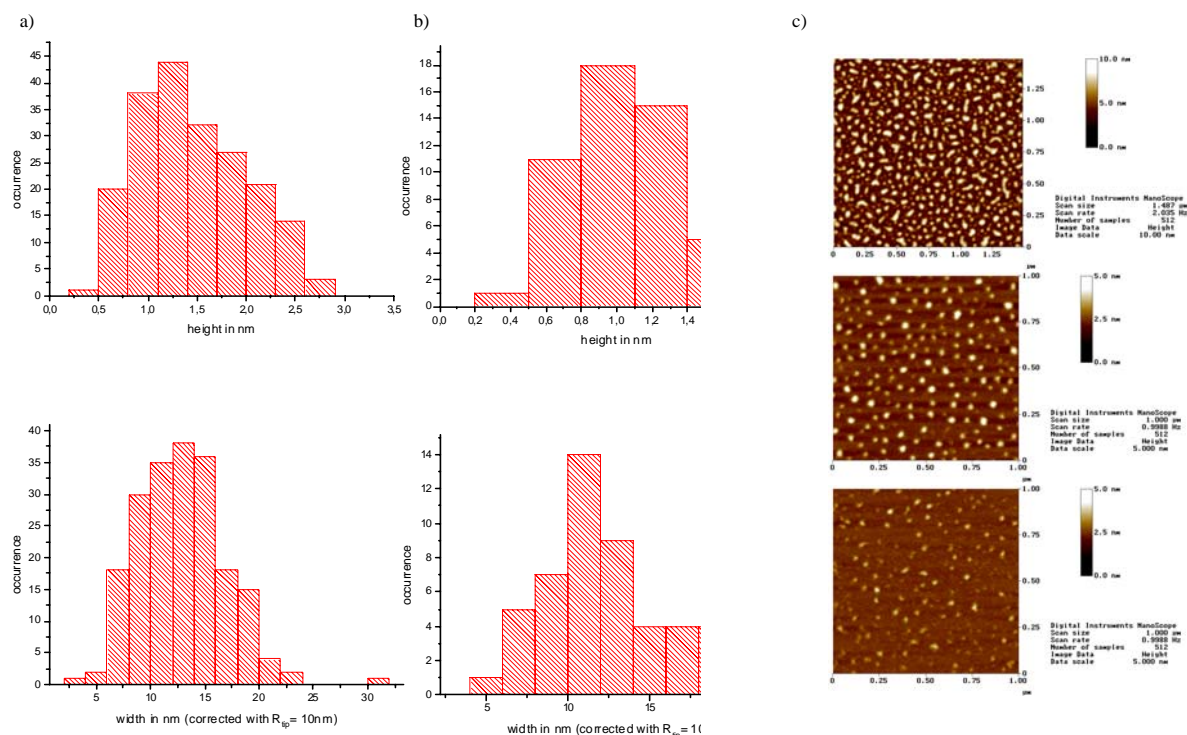


Figure 5-4. a) Histograms of height and width values as measured for samples with solution concentrations of $\sim 10^{-9}$ M. b) Histograms of height and width values as measured for samples with solution concentrations of $\sim 10^{-10}$ M. c) AFM height images of samples with different concentration. From top to bottom $\sim 10^{-3}$ M, $\sim 10^{-9}$ M and $\sim 10^{-10}$ M solutions used for spincoating. (in cooperation with Prof. J. P. Rabe, Humboldt University Berlin, Berlin)

5.4 Summary

The presence of two rigid exotopic bidentate chelating groups makes macrocycle **1** a useful building block to create multicomponent nanoscale architectures with interesting dynamic properties. Due to the large void present in these aggregates, it was not possible to obtain suitable single crystals for X-ray analysis. However, a battery of both direct and indirect solution state characterization techniques provided unambiguous evidence for the proposed structure. HRTEM investigations of **NS1**, **G1** and complex **4** led to the invention of a novel non-aqueous method to generate pure copper nanoparticles with 3-5 nm dimensions.

- (1) V. Kalsani, H. Ammon, F. Jäckel, J. P. Rabe, M. Schmittl, Synthesis and Self-Assembly of a Rigid Exotopic Bisphenanthroline Macrocycle: Surface Patterning and a Supramolecular Nanobasket, *Chem. Eur. J.* **2004**, *10*, 5481-5492.
- (2) a) B. Dietrich, P. Viout, J.-M. Lehn, *Macrocyclic Chemistry*, VCH, Weinheim **1993**. b) *Macrocyclic Synthesis*, Ed. D. Parker, Oxford University Press, Oxford **1996**.
- (3) S. Höger, K. Bonrad, A. Mourran, U. Beginn, M. Möller, Synthesis, Aggregation, and Adsorption Phenomena of Shape-Persistent Macrocycles with Extraannular Polyalkyl Substituents, *J. Am. Chem. Soc.* **2001**, *123*, 5651-5659.
- (4) E. Mena-Osteritz, P. Bäuerle, Self-Assembled Hexagonal Nanoarrays of Novel Macrocyclic Oligothiophene-Diacetylenes, *Adv. Mat.* **2001**, *13*, 243-246.
- (5) P. Samori, F. Jäckel, O. Unsal, A. Godt, J. P. Rabe, Ordered Nanostructures of a [2]Catenane Through Self-Assembly at Surfaces - An STM Study With Sub-Molecular Resolution, *Chem. Phys. Chem.* **2001**, *2*, 461-464.

-
-
- (6) M. Schmittel, H. Ammon, Preparation of a Rigid Macrocycle with two Exotopic Phenanthroline Binding Sites, *Synlett*, **1999**, 750-752.
 - (7) a) E. Leize, D. R. VanDorsselaer, R. Krämer, J.-M. Lehn, Electrospray Mass-Spectrometry of the Self-Assembly of a Capped Polymetallic Complex, *J. C. S. Chem. Commun.* **1993**, 990-993. b) T. Bark, T. Weyhermüller, F. Heitzler, Self-Assembly of a Helical Dicopper(I) Metallophane, *Chem. Commun.* **1998**, 1475-1476.
 - (8) A. Marquis-Rigault, A. Dupont-Gervais, P. N. W. Baxter, A. Van Dorsselaer, J.-M. Lehn, Self-Assembly of an 11-Component Cylindrical Inorganic Architecture : Electrospray Mass Spectrometry and Thermodynamic Studies, *Inorg. Chem.* **1996**, 35, 2307-2310.
 - (9) a) M. Schmittel, H. Ammon, V. Kalsani, A. Wiegrefe, C. Michel, Quantitative Formation and Clean Metal Exchange Processes of Large Void ($\sim 5000 \text{ \AA}^3$) Nanobox Structures, *Chem. Commun.* **2002**, 2566-2567. (b) M. Schmittel, V. Kalsani, C. Michel, A. Wiegrefe, **2005**, manuscript in preparation.
 - (10) a) M. Schmittel, V. Kalsani, L. Kienle, Simple and Supramolecular Copper Complexes as Precursors in the HRTEM Induced Formation of Crystalline Copper Nanoparticles, *Chem. Commun.* **2004**, 1534-1535. b) M. Schmittel, V. Kalsani, F. Jäckel, J. P. Rabe, **2005**, unpublished results.
 - (11) B. Olenyuk, M. D. Levin, J. A. Whiteford, J. E. Shield, P. J. Stang, Self-Assembly of Nanoscopic Dodecahedra from 50 Predesigned Components, *J. Am. Chem. Soc.* **1999**, 121, 10434-10435.
 - (12) G. R. Newkome, T. J. Cho, C. N. Moorefield, R. Cush, P. S. Russo, L. A. Godínez, M. J. Saunders, P. Mohapatra, Hexagonal Terpyridine-Ruthenium and -Iron Macrocylic Complexes by Stepwise and Self-Assembly Procedures, *Chem. Eur. J.* **2002**, 8, 2946-2954.
 - (13) a) C. M. Drain, F. Nifiatis, A. Vasenko and J. D. Batteas, Porphyrin Tessellation by Design: Metal-Mediated Self-Assembly of Large Arrays and Tapes, *Angew. Chem. Int. Ed.* **1998**, 37, 2344-2347. b) R. Takahashi and Y. Kobuke, Hexameric Macroring of Gable-Porphyrins as a Light-Harvesting Antenna Mimic, *J. Am. Chem. Soc.* **2003**, 125, 2372-1273.

Supp 5-1

Chem. Eur. J. **2004**, *10*, 5481-5492

Reproduced by permission of *Wiley-VCH Verlag GmbH & Co KG*

Synthesis and Self-Assembly of a Rigid Exotopic Bisphenanthroline Macrocycle: Surface Patterning and a Supramolecular Nanobasket

Venkateshwarlu Kalsani,^[a] Horst Ammon,^[b] Frank Jäckel,^[c] Jürgen P. Rabe,^[c] Michael Schmittel^{*[a]}

[a] Center of Micro and Nanochemistry and Engineering, Organische Chemie I, Universität Siegen, Adolf-Reichwein-Str., D-57068 Siegen (Germany), FAX: Int + 49 (0) 271 740 4356

E-mail: Schmittel@chemie.uni-siegen.de

[b] Institut für Organische Chemie der Universität Würzburg Am Hubland, D-97074 Würzburg (Germany)

[c] Humboldt University Berlin, Department of Physics, Newtonstraße 15, D-12489 Berlin (Germany)

Abstract: The synthesis and characterisation of a rigid nanoscale macrocycle with two exotopic phenanthroline binding sites is reported. Scanning tunnelling microscopy (STM) at the solid liquid interface reveals the formation of highly ordered monolayers of macrocycles with dimensions that are in good agreement with the calculated structure. Using the HETPHEN concept several bisheteroleptic coordination complexes with other phenanthrolines and a nanoscale basket assembly were prepared in presence of copper(I) ions. NMR, mass spectrometric data and elemental analysis point to three distinct isomers of the basket assembly in solution. A silver basket was prepared and readily converted to its copper analogue. Electrospray ionisation (ESI)-MS and spectrophotometric investigations provided additional mechanistic insight into the assembly process. Hence, the exotopic bisphenanthroline macrocycle in combination with HETPHEN concept proves to be very effective in controlling the compositional aspects of multicomponent self-assembly.

Introduction

Macrocycles^[1] have attracted increasing attention over the last years due to their applicability for surface patterning as well as components of supramolecular assemblies. Monolayers of macrocycles on solid supports or interfaces have been suggested to serve as 2D-templates for the construction of larger supramolecular 3D-assemblies and as matrix for the incorporation of guest molecules.^[2-4] These monolayers have been characterised with scanning tunnelling microscopy (STM), Langmuir-Blodgett-techniques, X-ray diffraction, photoelectron and infrared spectroscopy as well as ellipsometry.^[2-5]

Recently, the synthesis of rigid or shape-persistent macrocycles of nanometer scale has become an important avenue of research.^[6] In contrast to ring systems with flexible linkages a macrocycle with a rigid back bone is an attractive building block for supramolecular architectures to address defined interior and exterior spatial arrangements and relationships. Over the years, rigid macrocycles with or without coordinating ligand sites have been reported.^[6] In particular, macrocycles incorporating polypyridyl units have received ample interest due to their coordination properties in presence of suitable metal ions.^[7] Schlüter and Grave have reviewed the recent developments on rigid nano-sized macrocycles and outlined their assets.^[6h] Although many of the rigid macrocycles reported to date contain bipyridine and terpyridine units, most of them (bipyridine) still lack directionality in their coordination behaviour (Figure 1) due to rotational movements, thus allowing for both *exo* and *endo* coordination. For defined *exo* or *endo* coordination phenanthrolines appear superior to bipyridines as a free rotating bond in between chelating nitrogens is fixed. Sauvage, Lünig and others have used flexible macrocycles incorporating endotopic phenanthrolines to engineer functional catenanes, rotaxanes,^[8] concave reagents,^[9] and molecular knots.^[10] To the best of our knowledge, the only rigid macrocycle with phenanthroline units has been reported by Reahn.^[11] This macrocycle, however, exhibits endotopic coordination sites, hence prohibiting any access to extended oligomeric structures. Therefore we envisaged the synthesis of a rigid macrocycle with phenanthrolines having exotopic coordination sites.

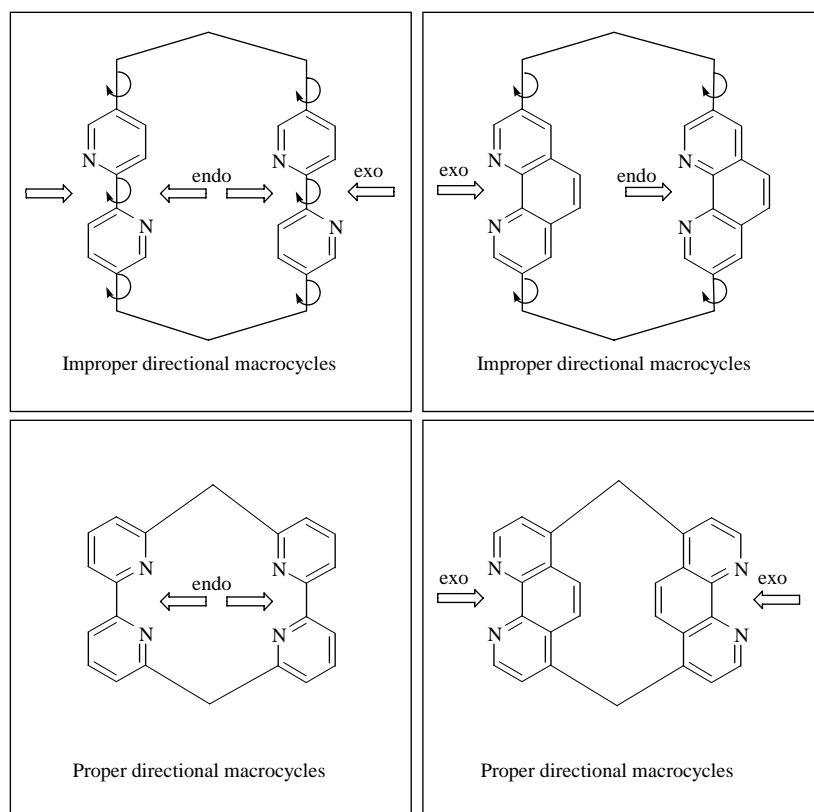
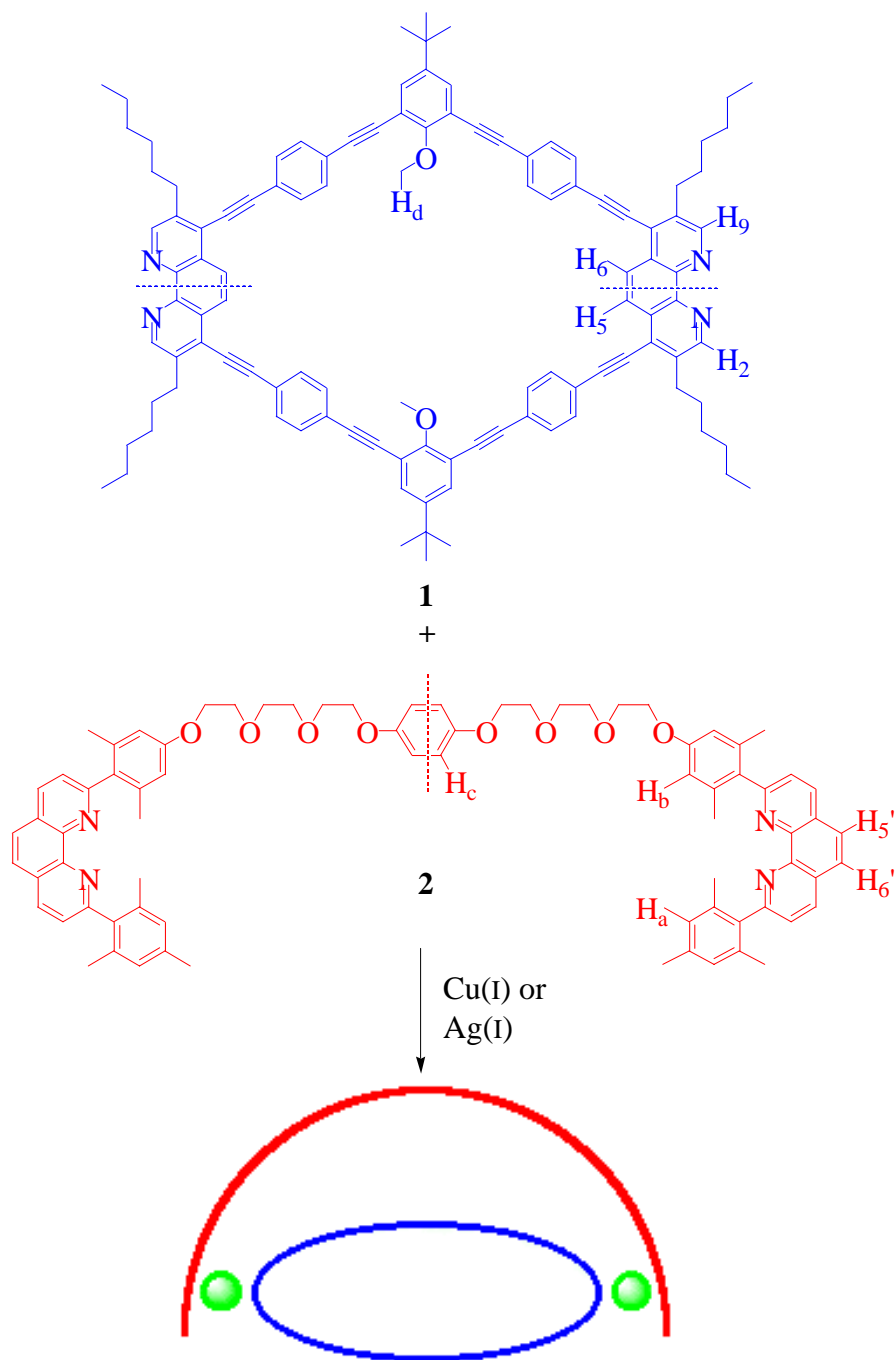


Figure 1. Schematic representation of binding motifs in macrocycles containing bipyridines and phenanthrolines as the coordinating ligands.

Herein, we present the experimental details of the synthesis^[12] of the rigid, nano-sized (ca. 2.70 nm length) macrocycle **1** with opposite exotopic phenanthroline sites, its self-assembly studied with scanning tunneling microscopy (STM) at a solid liquid interface and its potential as a useful building block for engineering a heteroleptic supramolecular basket structure *via* self-assembly in solution along the strategy outlined in Scheme 1.



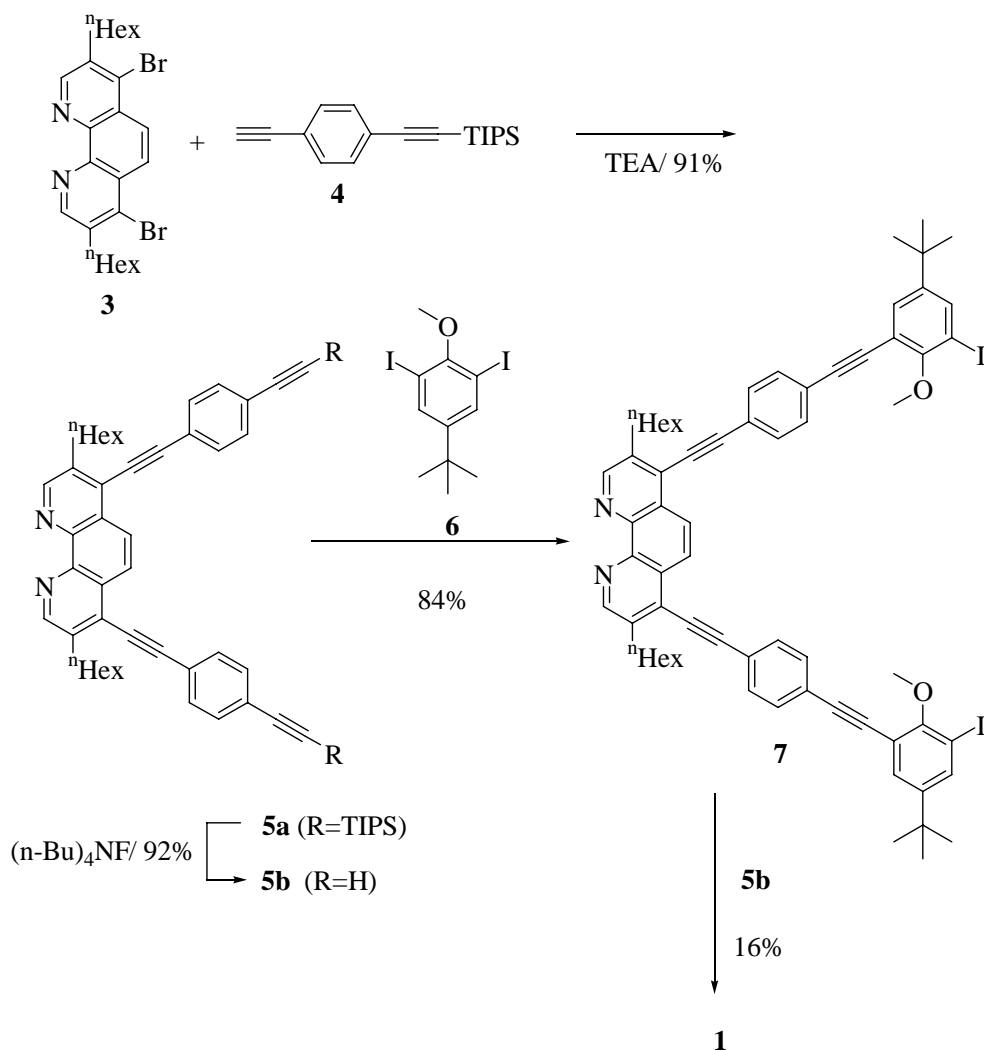
Scheme 1. Schematic representation of the strategy for the self-assembly of a three-component supramolecular basket.

Results and Discussion

Synthesis

Macrocycle **1** was prepared by combining three building blocks by a series of Sonogashira couplings as depicted in scheme 2 and as communicated earlier.^[12] The key building block **3**, equipped with solubilizing hexyl chains in 3,8-position,^[13] served as source

of the exotopic phenanthroline site. Following the synthetic protocol, phenanthroline **3** was first connected with the bisalkyne spacer **4**. After deprotection of **5a**, product **5b** was subsequently linked to two 1,3-diiodobenzene units **6**. Finally, the resultant compound **7** was coupled with **5b** to afford the macrocycle **1**.



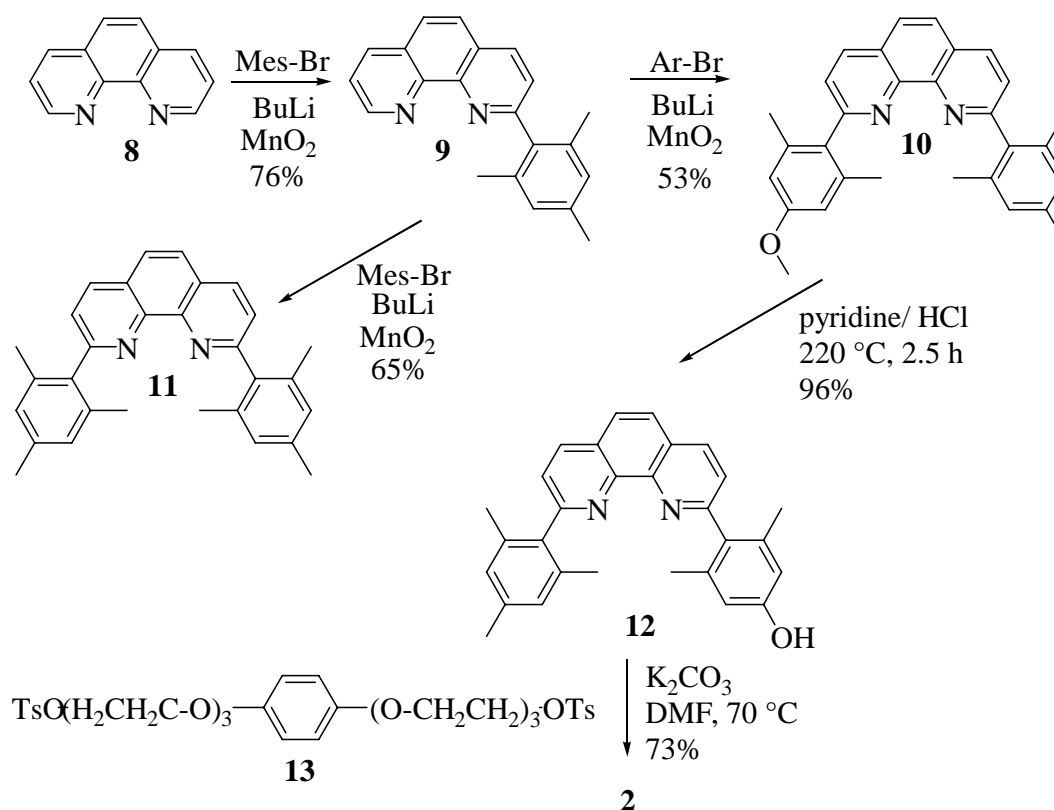
Scheme 2. Preparation of macrocycle **1**.

Macrocycle **1** precipitated as pale yellow microcrystals in trichloromethane, the structure of which was unambiguously assigned by elemental analysis, ^1H NMR, and ESI MS. The ring structure was convincingly visualised by STM.

Synthesis of a Handle for a Supramolecular Basket Assembly

The construction of well defined basket shaped molecules is of interest not only because of their potential use in host-guest chemistry but also to place defined functionalities

above a nanoscale array. While some first cyclophane assemblies have been reported to date,^[14] these are well below the nanoscale dimensions. Due to our earlier results with the HETPHEN concept (allowing for the selective preparation of heteroleptic bisphenanthroline copper/silver complexes) we have chosen **2** as a counter part to the macrocycle to prepare the nanoscale basket assembly. The HETPHEN approach^[15] utilises steric and electronic effects originating from bulky aryl substituents at one of the two phenanthroline ligands (as seen in **2** and in **10,11**) to steer the coordination equilibrium both kinetically and thermodynamically towards the heteroleptic bisphenanthroline complex. **2,10** and **11** are designed to carry steric stoppers at 2 and 9 positions of the phenanthroline. **2** was obtained in four steps starting from the parent [1,10]phenanthroline (**8**). The arene groups were added in 2- and 9-position according to Sauvage^[16] in a stepwise fashion as depicted in scheme 3. The addition products were isolated and oxidised with activated manganese dioxide to afford the 2,9-disubstituted [1,10]phenanthroline. After deprotection of **10** with pyridine and hydrochloric acid we obtained the free phenol **12** that was subsequently treated with **13** to yield **2** in 73%.



Scheme 3. Synthetic scheme for the preparation of **2**.

2 showed a ¹H NMR spectrum with a singlet at $\delta = 6.85$ ppm for the four protons of the 1,4-phenylene unit and a ESI MS spectrum with only two signals, one being centred at 1175.7 (25%) (**2**+H⁺) and the other at 588.8 (100%) (**2**+2H)²⁺. The isotopic patterns are in

agreement with the calculated ones. All other data is also in accordance with its structure (see experimental section).

Self-assembly at the solid-liquid interface

Figure 2 displays an STM current image of a highly ordered monolayer of the macrocycle **1** at the solution-HOPG-interface. The arrangement is characterised by an oblique unit cell containing one molecule ($a = 2.98 \pm 0.15$ nm, $b = 3.08 \pm 0.13$ nm and $\alpha = 47 \pm 6^\circ$). The area of the unit cell of $A = 6.6 \pm 0.3$ nm² is in good agreement with the space requirements of a single molecule lying completely flat on the substrate (~ 6.3 nm²). The bright areas of the image can be attributed to the conjugated parts of the macrocycle since the energy difference between the frontier orbital and the Fermi level of the graphite substrate is rather small.^[17] The dark areas of the image between the rings can be assigned to the aliphatic side chains that could not be visualised, probably due to their high conformational mobility on a time scale faster than the STM imaging. Notably, also the area inside the rings could be imaged which is probably dynamically occupied by solvent molecules. Due to the orientation and spacing of the phenanthroline units being ideal for metal ion coordination, one might envisage to use these monolayers to study the formation and the electronic properties of coordination polymers.

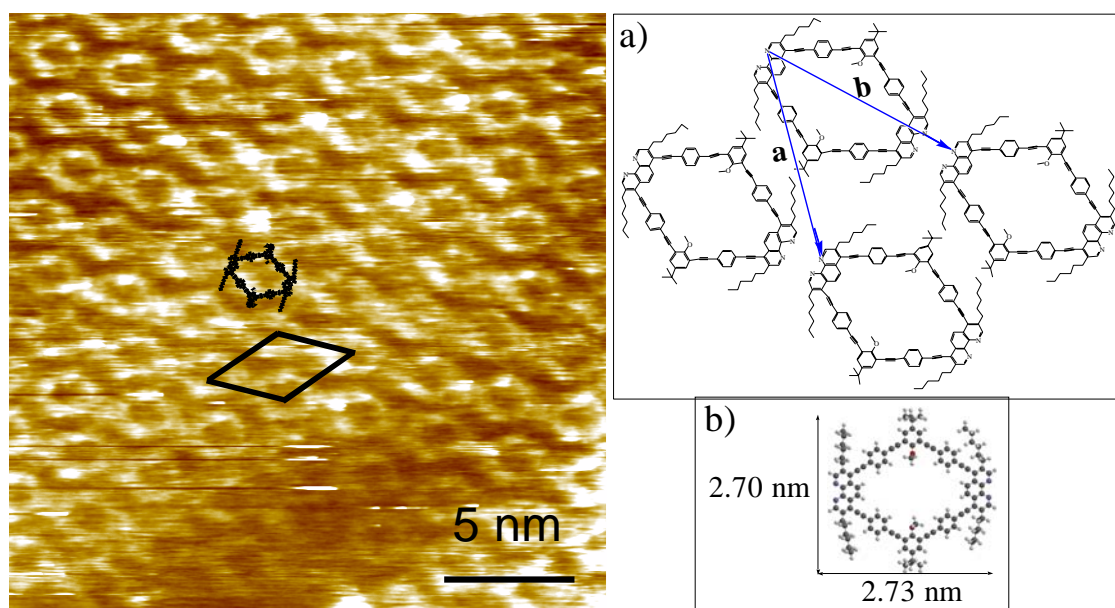
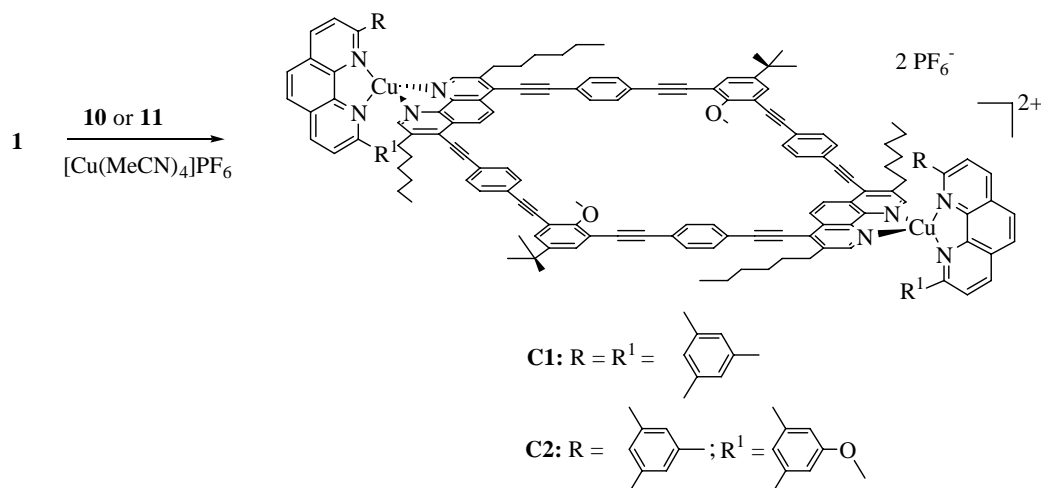


Figure 2. STM current image of a highly ordered monolayer of macrocycle **1**. Parameters were -1.4 V sample bias and 100 pA average tunneling current. Unit cell and macrocycle structure are indicated. a) Model for the arrangement. b) PM3 minimized dimensions of the macrocycle.

Self-assembly in solution

Complexation behaviour of the Macrocycle and of the Handle. The presence of two rigid exotopic binding sites renders macrocycle **1** an attractive building block for nanoscale assemblies, particularly in combination with tetrahedrally coordinating metal ions (Cu^+ or Ag^+)^[7a] and HETPHEN ligands **2**, **10** and **11**, which contain steric stopper groups in 2,9-position.^[15] First, the ability of macrocycle **1** to form complexes with **10** and **11**, respectively was probed in presence of Cu^+ (scheme 4). Rewardingly, only complexes **C1**, **C2**, but no oligomers of macrocycle could be detected by both ESI-MS and ^1H NMR, highlighting the utility of the HETPHEN concept in engineering heteroleptic supramolecular assemblies.

In the ESI-MS a characteristic signal is observed corresponding to **C1** and **C2**, respectively, with the experimental isotopic distributions being in good agreement with the calculated ones. Because of its symmetric structure and the sharp signals the ^1H NMR is readily rationalised. Characteristic high field shifts were observed for aryl protons of ligands **10** and **11** in the complexes **C1** or **C2**, respectively, a clear indication for the formation of heteroleptic complex as demonstrated earlier.^[15]

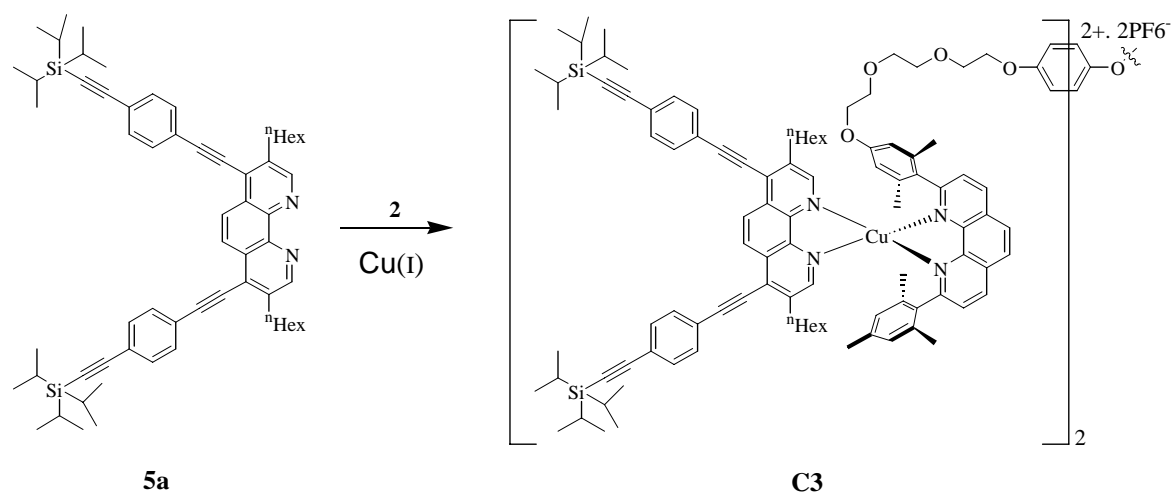


Scheme 4. Formation of complexes **C1** and **C2**

In the following we probed the complexation behaviour of the handle **2**. A mixture of $\mathbf{2}:\text{[Cu(MeCN)}_4\text{]PF}_6 = 1:1$ resulted in a yellow solution the analysis of which by ESI-MS and ^1H NMR indicated the presence of mainly $[(\mathbf{2})(\text{Cu})]^+$ along with unreacted (protonated in case of ESI MS) phenanthroline. The isotopic distribution of $[(\mathbf{2})(\text{Cu})]^+$ is in excellent agreement

with the calculated one. However, it is obvious from the yellow colour and the absence of any metal-to-ligand-charge-transfer (MLCT) band in the region of 450-500 nm that no macrocyclic structure with a [Phen-Cu-Phen]⁺ complex has formed.^[18] From these experiments it is clear that the two shielded phenanthroline sites act as expected, not allowing for ring closure by formation of a homoleptic ring architecture or any other oligomeric structures.

To create a model complex for comparison with the target basket (Scheme 2) we reacted **2** with **5a** in presence of [Cu(MeCN)₄]PF₆ (1:2:2) to furnish **C3** (scheme 5). ¹H NMR, ESI-MS and other spectroscopic data are in good agreement with the proposed structure (see experimental section).



Scheme 5. Assembly of **C3** complex from **2** and **5a**.

ESI MS shows a signal centred at m/z 1560.2 Da corresponding to the **C3** complex $[(\mathbf{2})(\mathbf{5a})_2(\text{Cu})_2]^{2+}$. Again, the experimental isotopic distribution is in good agreement with the calculated one. Formation of complex **C3** is further confirmed by collisional fragmentation of **C3** producing the fragment $[(\mathbf{2})(\mathbf{5a})(\text{Cu})_2]^{2+}$, whose isotopic distribution is in agreement with its proposed composition.

Self-assembly of a Nanoscale Basket Assembly and Its Metal Exchange. Following the proposal depicted in scheme 1 complexation of **1** and **2** with appropriate metal ions such as Cu^I or Ag^I ions should furnish a basket shaped heteroleptic metallo-assembly. Upon addition of macrocycle **1** to **2** and [Cu(MeCN)₄]PF₆ (1:1:2), the solution turned deep red. The analysis of this solution by ESI-MS indicated the formation of $[(\mathbf{1})(\mathbf{2})(\text{Cu})_2]^{2+}$ (**C4**) as the exclusive species. The isotopic splitting pointing to a doubly charged species is in perfect

agreement with its proposed composition (Figure 3). The ^1H NMR shows that a heteroleptic bisphenanthroline complex has formed at the copper ions, as can be seen from typical highfield shifts of the mesityl and dimethylphenoxy protons at about 5.5-6.3 ppm (Figure 4). The sharp signals in the ^1H NMR rule out the existence of any higher aggregates or oligomers.

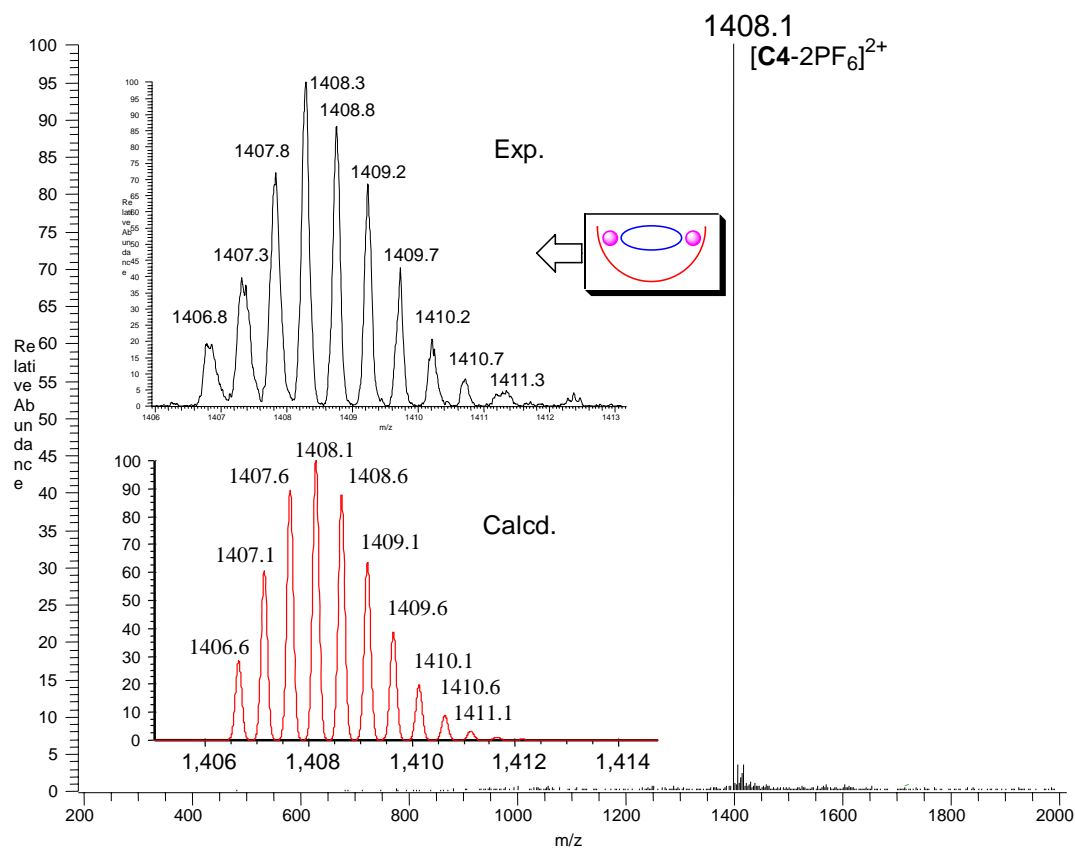


Figure 3. Positive ESI-MS spectrum of $[(1)(2)(\text{Cu})_2]^{2+}$ (**C4**) in dichloromethane. The insert shows the calculated (bottom) and experimental isotopic splittings (top).

Spectral comparison of C4 with C1-C3. The absorption spectra of the heteroleptic complexes **C1**, **C2** and **C4** (Figure 5) show the presence of similar bands. The strong bands at 250-400 nm correspond to ligand π - π transitions.^[19] The absorption band at 491 nm is assigned to the MLCT state which is responsible for the red colour of the complexes. These absorptions are in good agreement with those of other Cu^+ heteroleptic bisphenanthroline assemblies.^[20] The good match of the MLCT band for all three complexes is indicative of a similar environment at the metal centre. Moreover, the oscillator strength of the MLCT band at $\lambda = 491$ nm ($\epsilon_{\text{max}} = 23113$, 21395 and 18608 $\text{M}^{-1} \text{cm}^{-1}$ for **C1**, **C2** and **C4**, respectively) is in good agreement with the proposed two Cu^+ ions per complex. Analogous Cu^+ containing systems where one Cu^+ is present^[21] exhibit $\epsilon_{\text{max}} = 8500 \text{ M}^{-1} \text{cm}^{-1}$.

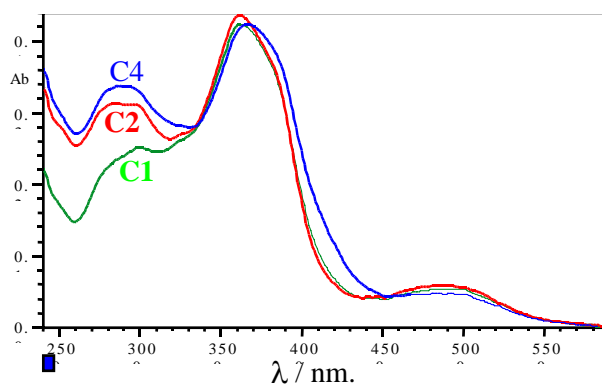


Figure 5. UV-vis absorption spectra of **C1**, **C2** and **C4** (basket assembly) in dichloromethane ($2.6 \cdot 10^{-6}$ M).

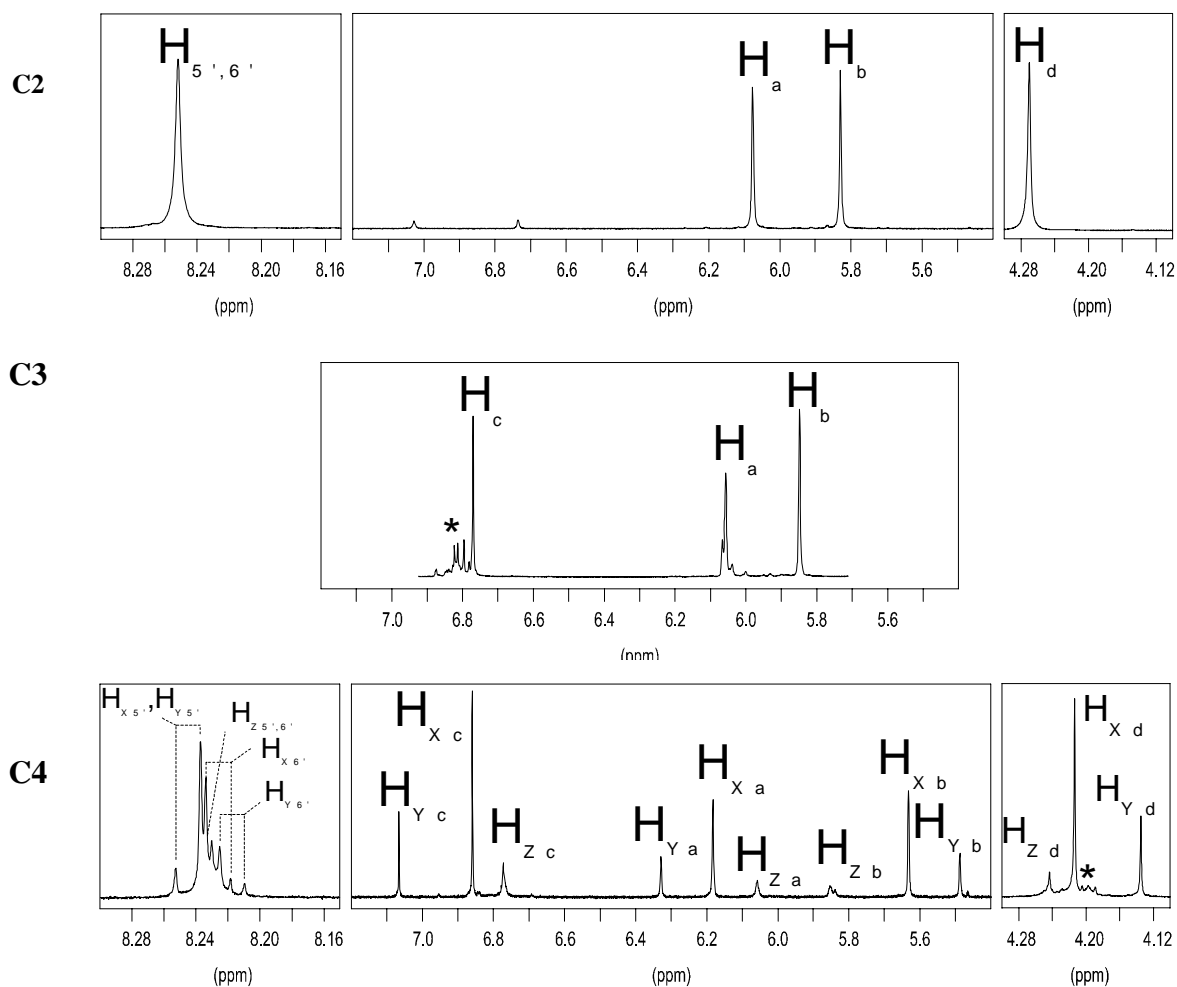


Figure 4. Parts of the NMR spectra (600 MHz) of **C2**, **C3** and **C4**. **C3** shows signals of conformational isomers at H_c and H_a (* = impurity).

Although ESI-MS and UV-vis data provide a clear and convincing picture for the composition of **C4** as $[(\mathbf{1})(\mathbf{2})(\text{Cu})_2]^{2+}$, the ^1H NMR spectra of the complex between 5.5-7 ppm is much more complex than expected revealing 3 well resolved sets of signals (in 59 : 24 : 17 ratio;^[22] Figure 4). In particular, protons H_a , H_b , H_c and H_d (see Scheme 1) appear well separated indicating only very slow interconversion between the different isomers. The isomers will be depicted as **C4x**, **C4y** and **C4z**.

Structural aspects. Further information about the structure of the isomers can be deduced from extensive Roesy investigations. For one set of the signals (indicated by z; assigned to **C4z**) there is no NOE effect between H_{zc} and H_{zd} , proposing that the ether bridge is well away from the macrocycle ($>6 \text{ \AA}$), in agreement with a basket type structure (Figure 6, **model I** in Scheme 6) of **C4z**. In addition, all signals of **C4z** show a remarkable similarity in the shifts with those of the complexes **C2** and **C3** (Figure 4), for which we have to assume an unconstrained polyether chain and a planar macrocycle, respectively. Hence, **C4z** is best described by the basket structure as depicted by an energy minimised structure using force field calculations.^[23]

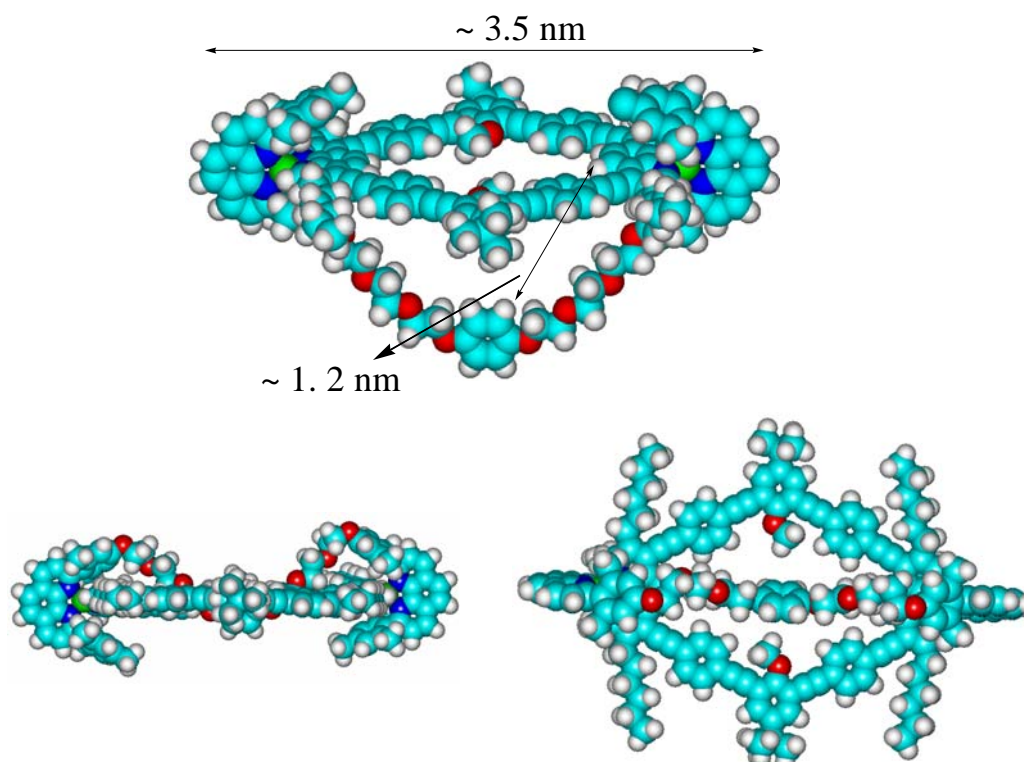
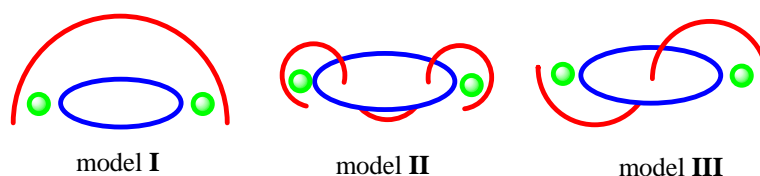


Figure 6. Energy minimised structure of the basket assembly **C4z** (top), proposing that H_{zc} of **2** and H_{zd} of **1** are far away from each other in line with NOESY data. The structure of **C4xy** is expected to look like the isomer shown in the two bottom pictures (left = side view; right = top view). Conformational motions of the entangled polyether chain in **C4xy** to generate **C4z** are prevented by a high barrier due to the restricted space in the core of the macrocycle.

However, **C4z** is only the minor constituent of three different complexes having the same composition $[(\mathbf{1})(\mathbf{2})(\text{Cu})_2]^{2+}$. By chromatography we could separate **C4z** from **C4x,y** and confirm the composition $[(\mathbf{1})(\mathbf{2})(\text{Cu})_2]^{2+}$ for both fractions by ESI-MS.

How can we rationalise the occurrence of various isomers of the composition $[(\mathbf{1})(\mathbf{2})(\text{Cu})_2]^{2+}$? Depending on the spatial arrangement of the polyether chain in **C4** there may exist different isomers as depicted in Scheme 6. From these choices the rotaxane-type **model III** can easily be discarded due to a rather high barrier (as predicted by molecular modelling^[23]) needed for threading the bulky diarylphenanthroline unit of **2** into macrocycle **1**. The high barrier is mainly due to repulsion of the 2,6-dimethylphenyl groups at phenanthroline of **2** and the methoxy groups in **1**.

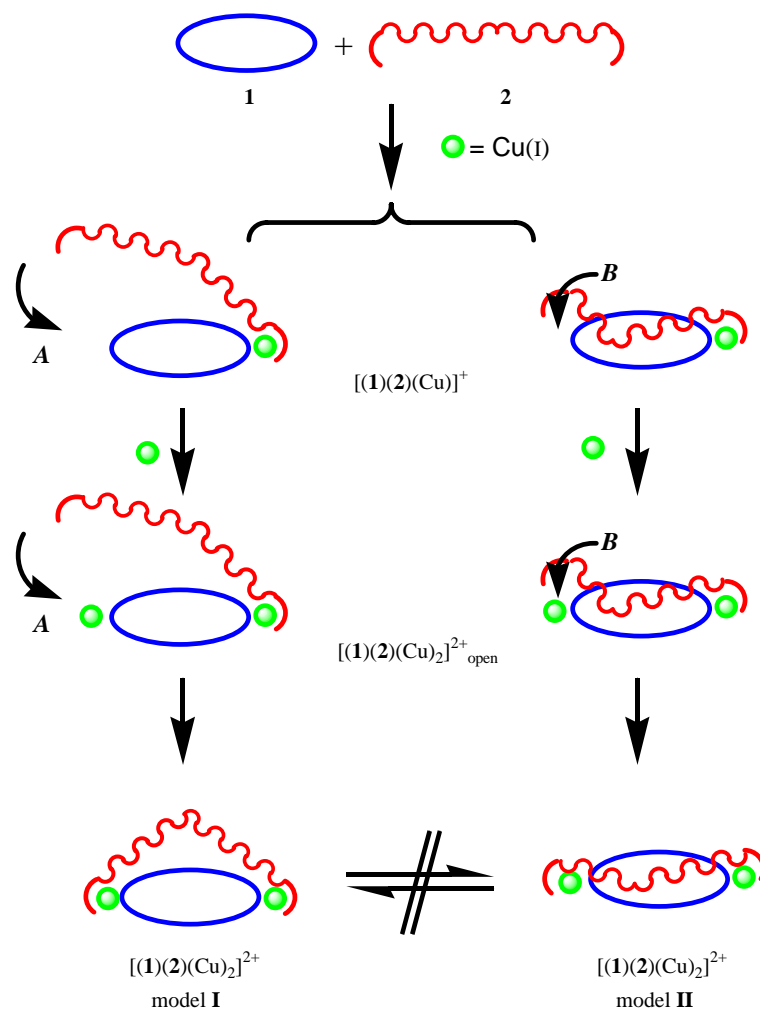


Scheme 6. Cartoon representation of possible isomers of $[(\mathbf{1})(\mathbf{2})(\text{Cu})_2]^{2+}$ (**C4**).

In contrast to signal set *z*, the other two sets of signals, *i.e.* for **C4x,y**, show notable NOE effects between H_c and H_d protons which proposes close proximity of the polyether bridge and the macrocycle as depicted in a cartoon-type fashion in **model II**. In support of a **model II** type structure for both **C4x** and **C4y** protons H_{xa} and H_{ya} are downfield to H_{za} while protons H_{xb} and H_{yb} are highfield to H_{zb} . This can only be rationalised by a distorted geometry at the copper(I) ion with the dimethylphenoxy unit being closer to the phenanthroline of **1** than the mesityl unit. This is due to a severe conformational pull exerted by the polyether chain that is entrapped in the macrocycle as shown in **model II**. It is, however, impossible to provide exact conformational differences along the polyether chain of **2** distinguishing the two isomers **C4x** and **C4y**, in particular, since also a slight folding of the macrocycle may be involved.^[24] The interconversion between **C4x** and **C4y** occurring at temperatures higher than -20 °C precluded chromatographic separation.

A key for further understanding is to picture the formation of the basket assembly. Upon formation of the mononuclear complex $[(\mathbf{1})(\mathbf{2})(\text{Cu})]^+$ (scheme 7) the free 2,9-diarylsubstituted phenanthroline site of **2** has actually only two major trajectories^[25] to move towards the second phenanthroline of macrocycle **1**: either it stretches the polyether chain to such an extent that approach of the loose phenanthroline along trajectory **A** is possible.

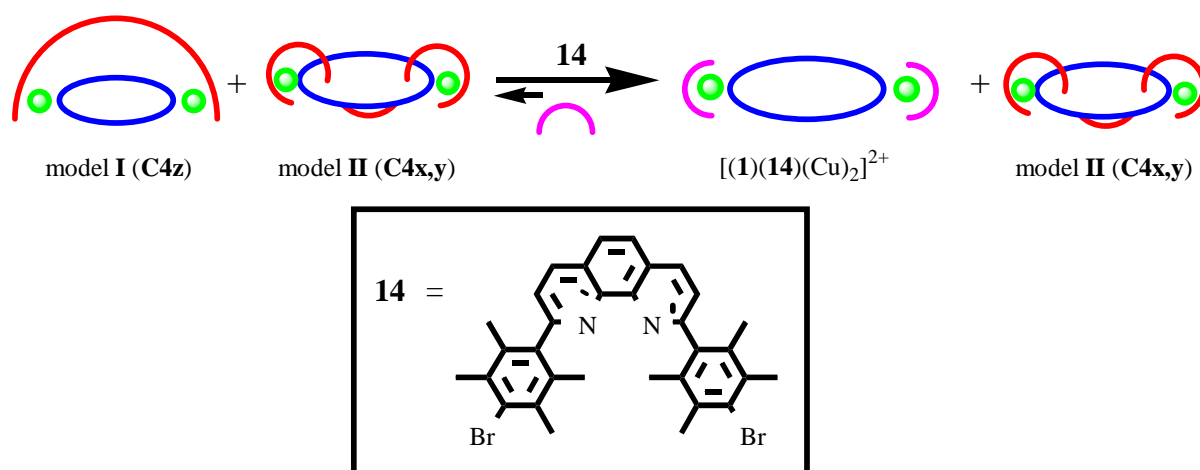
Alternatively, the polyether chain may fold partly into the macrocycle due to stabilizing interactions^[26] between the handle and the unsaturated macrocycle. This will severely limit the translational freedom of the loose binding site of **2** leaving only trajectory **B** to form the second copper complex.



Scheme 7. Cartoon representation of the formation of $[(1)(2)(Cu)_2]^{2+}$ (**C4**) leading to two sets of isomers (**model I** and **model II**).

It is, however, surprising to learn that even at temperatures as high as 60 °C interconversion between **C4_{x,y}** and **C4_z**, *i.e.* between **model I** and **II** isomers, remains completely shut down. Such a high barrier can only be rationalised if interconversion of **C4_{x,y}** and **C4_z** is not possible by conformational changes along the polyether chain. Molecular modelling indeed proposed that the entanglement of the cramped polyether chain within the void of the macrocycle will preclude conformational relaxation (Figure 6). Alternatively, a dissociation / association process connecting $[(1)(2)(Cu)_2]^{2+} \rightleftharpoons [(1)(2)(Cu)_2]^{2+}_{open}$ could potentially bring about the conformational flexibility needed for interconversion (*cf.* to Scheme 7), but apparently the exergonic association $[(1)(2)(Cu)_2]^{2+}_{open}$

→ $[(1)(2)(Cu)_2]^{2+}$ kinetically outruns the slow escape of the conformationally locked polyether chain. If the above rationale was correct, addition of ligand **14**^[27] to **C4** should lead to a competitive binding of **14** to $[(1)(2)(Cu)_2]^{2+}_{open}$ thereby freeing the hitherto kinetically locked equilibration between **C4_{x,y}** and **C4_z**. Indeed, after adding one mol equivalent of **14** to **C4_{x,y,z}** we saw enrichment of **C4_{x,y}** at the expense of **C4_z** while parallel the new complex $[(1)(14)_2Cu_2]^{2+}$ was formed (scheme 8). This result proposes that dissociation/association at the copper phenanthroline site in pure **C4_{x,y,z}** takes place but does not lead to interconversion of the isomers due to entrapment of the polyether chain in the void of the macrocycle. Moreover, this experiments indicates that **model II** structures are thermodynamically more stable than the basket (**model I**) due to attractive interactions.^[26]



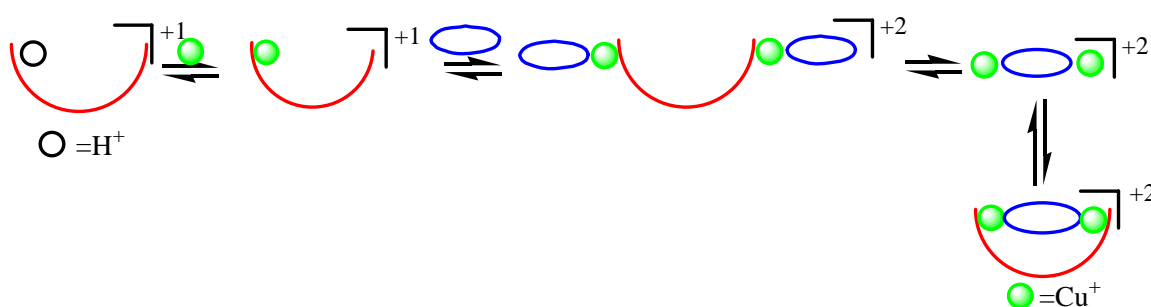
Scheme 8.

Metal Exchange. A silver-basket was made by mixing **1** and **2** with $AgBF_4$ in dichloromethane affording a yellowish solution. Analysis of this by ESI MS indicated a signal at $m/z = 1452.2$ with a charge 2+. Isotopic splitting was in good agreement with its proposed composition $[(1)(2)(Ag)_2]^{2+}$. The 1H NMR of $[(1)(2)(Ag)_2]^{2+}$ again indicated the presence of three isomers in a similar ratio as for $[(1)(2)(Cu)_2]^{2+}$. Upon the addition of $[Cu(MeCN)_4]^+$ in dichloromethane (2 eq., 8 additions, 30 min.) the $[(1)(2)(Ag)_2]^{2+}$ was quantitatively converted to $[(1)(2)(Cu)_2]^{2+}$. In the conversion process, signals of the intermediate species $[(Ag)(Cu)(2)(1)]^{+2}$ were detected. Importantly, the conversion of $[(1)(2)(Ag)_2]^{2+}$ to $[(1)(2)(Cu)_2]^{2+}$ does not entail detectable changes in the composition **C4_x:C4_y:C4_z**. Hence, metal exchange after dissociation followed by association is faster than conformation relaxation from **model I** to **model II**.

ESI MS investigations, thermodynamic and UV-vis Studies

Insight into the mechanistic pathways and thermodynamic features of supramolecular structures is of great interest to engineer well defined, discrete architectures and to understand the self-recognition phenomena. Very few reports are at hand providing mechanistic insight into the heteroleptic organisation.^[14a,28] The present study uses ESI MS for qualitative analysis and spectrophotometry for quantitative analysis. Both measurements were carried out in dichloromethane which we have found is a good solvent for such titrations.^[29] At first, a series of ESI MS titration experiments was carried out to obtain a qualitative picture about the intermediates on the way to $[(\mathbf{1})(\mathbf{2})(\text{Cu})_2]^{2+}$. In each case, it was ascertained that the thermodynamic equilibrium had been reached, as the spectra recorded proved to be constant over time.

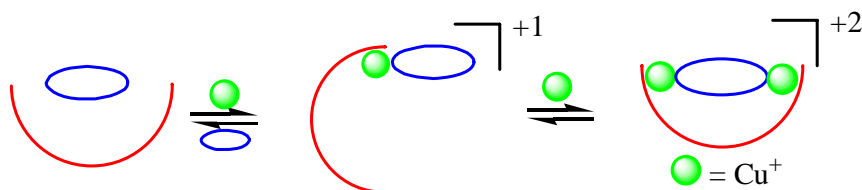
ESI-MS titration of $\mathbf{2}$ and Cu^+ with $\mathbf{1}$. In a first series of experiments $\mathbf{2}$ and Cu^{I} salt were titrated with $\mathbf{1}$. The titration was carried out in 5 additions and excess addition of $\mathbf{1}$ did not effect $[(\mathbf{1})(\mathbf{2})(\text{Cu})_2]^{2+}$, indicating a high stability of this assembly under the chosen conditions. During the course of titration four intermediates were observed apart from the final basket shape assembly. All the proposed intermediates (see the pictorial description in Scheme 9) were in good agreement with their isotopic splittings and served as models for the spectrophotometric titration using SPECFIT^[30] program.



Scheme 9. Proposed species (cartoons) in equilibrium when $\mathbf{2}$ and Cu^+ were titrated with $\mathbf{1}$.

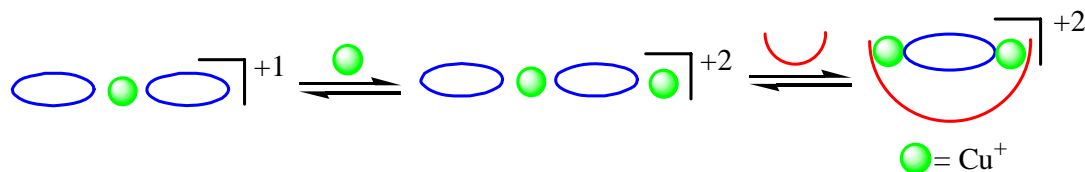
ESI-MS titration of $\mathbf{2}$ and $\mathbf{1}$ with Cu^+ . The second series of experiments was carried out by the titration of $\mathbf{2}$ and $\mathbf{1}$ with Cu^{I} salt. Cu^{I} salt (two equivalents) was added in five portion. Again, excess of addition did not change the spectrum. Though it was possible to detect three intermediates in minute amounts, the final basket assembly appeared as the major

component throughout the titration, indicating a strong tendency to form $[(1)(2)(Cu)_2]^{2+}$. The obtained results are presented in Scheme 10.



Scheme 10. Proposed species (cartoons) in equilibrium when **1** and **2** were titrated with Cu^+ .

ESI-MS titration of **1 and Cu^+ with **2**.** Finally in a third set of titrations, **1** and Cu^I salt were titrated with solution of **2** and the obtained results are depicted in Scheme 10 along with their proposed structures. Due to the starting conditions with macrocycle **1** being present along with Cu^+ homoleptic assemblies were observed in absence of **2**. These, however, readily disappeared upon addition of **2**, indicating the higher stability of the heteroleptic basket assembly.



Scheme 11. Proposed species (cartoons) in equilibrium when **1** and Cu^+ were titrated with **2**.

UV-vis titration of **2 and **1** with Cu^+ .** The ESI-MS titrations propose a qualitative picture of the intermediates in the self-assembly process. Though, the mechanistic pathways vary with the type of titration, they always lead to $[(1)(2)(Cu)_2]^{2+}$ as the final complex. Because of the simplicity observed with the second series of titration in ESI-MS, the same type of titration is carried out for spectrophotometric studies. Hence, these titration were performed by titrating **2** ($3.3 \cdot 10^{-6}$ M) and **1** ($3.3 \cdot 10^{-6}$ M), with aliquot amounts of Cu^I solution in 20 additions (total 4 eq. of Cu^+). Figure 7 displays UV-vis changes upon Cu^I salt addition with the solution turning red due to the MLCT transitions at ~ 490 nm. The insert shows the plots of absorbance changes at 490 nm for **2** and **1** vs. Cu^I salt, indicating that the complexation process is finished at 2 equiv. of Cu^I salt and excess addition of Cu^+ does not effect the already formed basket assembly. Fitting the model with UV-vis data using the SPECFIT program^[30] binding constants could readily be extracted for complexes $[(2)(1)(Cu)]^+$ and $[(2)(1)(Cu)_2]^{2+}$. As depicted in Scheme 10 a two step pathway is postulated

for the basket assembly process. Although the $\log \beta_{111}$ value is in the range of similar Cu^+ species^[25] the $\log \beta_{211}$ is relatively high, indicating the cooperativity in the final step.

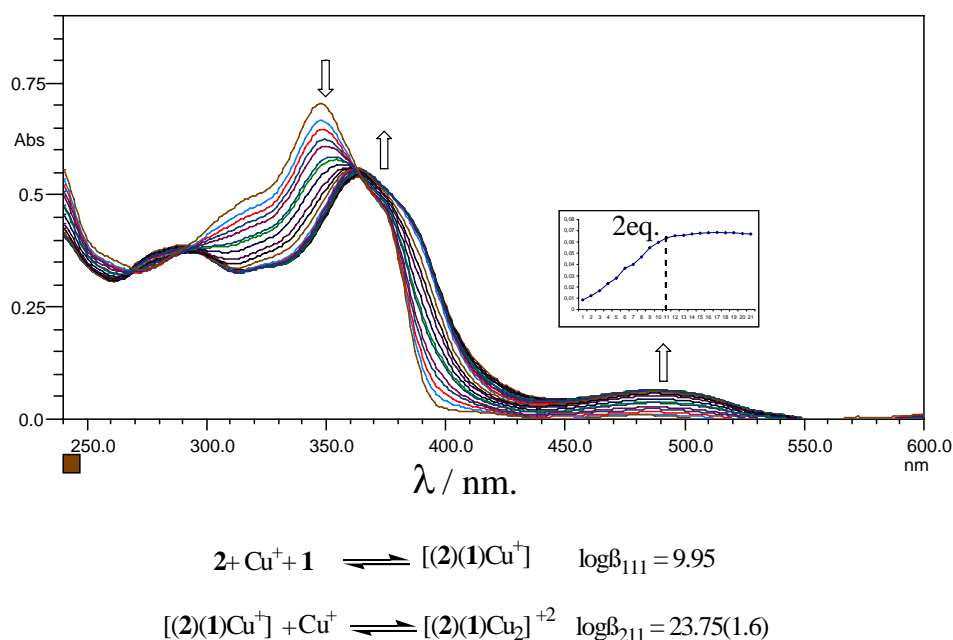


Figure 7. Spectrophotometric titration of **2** and **1** by aliquot amounts of Cu^+ salt in 20 additions. Solvent: dichloromethane. $T = 25(1)^\circ$; $[\mathbf{2}]$ and $[\mathbf{1}] = 3.30 \times 10^{-6}\text{M}$. Stability constants are given down to UV/vis spectra.

Conclusions

We report the synthesis of the rigid nanoscale macrocycle **1**, its self-assembly behaviour at a solid-liquid-interfaces and its usage in building a heteroleptic supramolecular nanoscale basket via self-assembly in solution. The presence of two rigid exotopic bidentate chelating groups makes **1** a useful building block to create nanoscale architectures. On one side, STM shows highly ordered monolayers of the macrocyclic system **1** at the solution-HOPG-interface. On the other side, there is a strong driving force for this macrocycle to form selectively heteroleptic Cu^+ and Ag^+ complexes with other phenanthrolines. The formation of these complexes is confirmed by a multitude of spectroscopic techniques (see experimental section). Most interesting is the formation of a heteroleptic self-assembled basket shaped aggregate that shows up in three different isomeric structures. The mechanistic investigations proposed a two step pathway for the self-assembly process. In addition, the conversion of the silver to the copper basket demonstrates the system to be dynamic. Further studies are in progress to study the interface behaviour of self-assembled structures of **1** with metal ions, host-guest properties of these assemblies and the construction of higher order supramolecular aggregates.

Experimental Section

Starting materials [1,10]-phenanthroline, ethynyltrimethylsilane, ethynyltriisopropylsilane, 2-bromo-1,3,5-trimethylbenzene, 2-bromo-5-methoxy-1,3-dimethylbenzene, 4-bromophenylamine, activated MnO₂ and 4-*tert*-butylphenol were purchased from Aldrich, Merck or Lancaster and used as received. [Pd(Ph₃P)₂Cl₂],^[31] [Pd(Ph₃P)₄],^[32] **3**,^[13] **9**^[15a], **11**^[15b], (4-Bromophenylethynyl)trimethylsilane^[34] and 5-*tert*-butyl-1,3-diiodo-2-methoxybenzene^[35] are prepared according to the literature procedures. Standard inert atmosphere and Schlenk techniques were employed for all the Heck reactions. Solvents were dried using typical drying procedures. ¹H NMR and ¹³C NMR were measured on a Bruker AC 200 (200 MHz) or Bruker AMX 600 (600 MHz). All the ¹H NMR was carried at room temperature in deuterio-trichloromethane unless specified otherwise. ESI MS was measured on a LCQ Deca Thermo Quest instrument. Typically, each time 25 scans were accumulated for one spectrum. UV-vis spectra were recorded on a Tidas II spectrophotometer using dichloromethane as the solvent. For full characterisation of **4** and its immediate precursor see ref.).^[33]

STM at the solid-liquid-interface^[34] was performed using a home-built beetle-type STM interfaced with a commercial controller (Omicron). STM tips have been prepared by mechanically cutting a 0.25 thick Pt/Ir (80%/20%) wire. A drop of an almost saturated solution of the macrocycle in 1,2,4-trichloro-benzene was applied to the basal plane of freshly cleaved highly oriented pyrolytic graphite (HOPG). The lattice of the underlying substrate could be visualised during measurements by simply changing the tunneling parameters to small tunneling impedance. This allows in-situ *x-y*-calibration of the piezo-scanner and drift-correction of the images recorded.

Molecular modelling was done with the MM+ force field as implemented in Hyperchem 6.02.^[23]

Spectrophotometric titrations

Equilibrium constants of complexes were determined in dichloromethane. Macrocycle **1** and **2** were titrated with aliquot amounts of a stock solution of copper(I) tetrakisacetonitrile hexafluorophosphate. All stock solutions were prepared by careful weighing on a µg analytical balance. Absorption spectra were recorded at 25.0±(0.1) °C. Since the formation is instantaneous as evidenced by proton NMR, ESI-MS analysis, and visible colour change, the

solutions were immediately analysed by the spectroscopy to avoid problems with the volatile solvent. The wavelength region from 240 nm to 600 nm was taken into account. Two equivalents (total) of metal salt in dichloromethane solution were added in 20 portions. The entire data sets comprising absorbances measured in one nanometer steps were decomposed in their principal components by factor analysis, and subsequently the formation constants including their standard deviation were calculated by using the SPECFIT^[30] program. Binding constants were determined from two independent titrations.

Synthesis of 6:

3,8-Dihexyl-4,7-bis-{4-[(trisisopropylsilyl)ethynyl]phenylethynyl}-[1,10]phenanthroline

(5a): 4,7-Dibromo-3,8-di-*n*-hexyl-[1,10]-phenanthroline^[13] (**3**) (1.00 g, 1.98 mmol), **4** (1.73 g, 6.12 mmol), PdCl₂(PPh₃)₂ (150 mg, 210 μmol) and CuI (300 mg, 1.60 mmol) were placed in a dry flask and dry benzene (20 ml) and dry triethylamine (10 ml) were added in an inert atmosphere. The resulting dark solution was refluxed for 3 d and the solvent was removed under reduced pressure. The residual material was dissolved in dichloromethane (50 ml) and washed with aqueous KCN (50 ml, 20%) and later by water. The solvent was then removed under reduced pressure. The residue was purified by column chromatography using dichloromethane and subsequently ethyl acetate as eluents to afford 1.64 g (90%) of **5a** as yellow powder. m.p. 67-70 °C; ¹H-NMR (200 MHz): δ = 0.87 (t, *J* = 6.9 Hz, 6 H, hexyl), 1.05 (s, 6 H, triisopropyl), 1.15 (s, 36 H, triisopropyl), 1.23-1.54 (m, 12 H, hexyl), 1.72-1.90 (m, 4H, hexyl), 3.07 (t, *J* = 6.6 Hz, 4 H, hexyl), 7.53 (d, *J* = 8.6 Hz, 4 H, phenyl), 7.60 (d, *J* = 8.6 Hz, 4 H, phenyl), 8.38 (s, 2H, phenanthroline), 9.04 (s, 2 H, phenanthroline); ¹³C-NMR (50 MHz): δ = 11.3, 14.0, 18.7, 22.6, 29.2, 30.6, 31.6, 32.6, 85.7, 93.8, 101.9, 106.4, 122.2, 124.5, 125.1, 127.6, 127.7, 131.5, 132.2, 138.9, 144.4, 151.2; IR (KBr): $\tilde{\nu}$ = 2941 cm⁻¹, 2863, 2204, 2153, 1560, 1508, 1459, 1420, 1382, 1232, 996, 882, 835, 677; Elemental analysis calcd (%) for C₆₂H₈₀N₂Si₂ • H₂O (927.52): C 80.29, H 8.91, N 3.02; found: C 80.21, H 8.62, N 3.14.

4,7-Bis-(4-ethynylphenylethynyl)-3,8-dihexyl-[1,10]phenanthroline (**5b**):

Tetrabutylammoniumfluoride trihydrate (1.04 g, 3.30 mmol) in THF (50 ml) was added to a solution of **5a** (1.25 g, 1.35 mmol) in THF (50 ml). The resulting mixture was stirred at room temperature for 30 min.; then the reaction was quenched by the addition of water (100 ml). The resulting solution was extracted with dichloromethane and the combined organic layers were dried over MgSO₄. The solvent was removed under reduced pressure and the residue was purified by column chromatography using dichloromethane and then ethyl acetate as eluents to give 750 mg of **5b** (92%) as ochre coloured crystals. M.p.173-174 °C; ¹H-NMR

(200 MHz): δ = 0.87 (t, J = 6.9 Hz, 6 H, hexyl), 1.21-1.56 (m, 12 H, hexyl), 1.73-1.95 (m, 4H, hexyl), 3.08 (t, J = 7.5 Hz, 4 H, hexyl), 3.23 (s, 2 H, ethynyl), 7.55 (d, J = 8.1 Hz, 4 H, phenyl), 7.63 (d, J = 8.1 Hz, 4 H, phenyl), 8.39 (s, 2H, phenanthroline), 9.06 (s, 2 H, phenanthroline); ^{13}C -NMR (50 MHz): δ = 14.0, 22.5, 29.1, 30.5, 31.6, 32.6, 79.5, 83.0, 85.7, 101.6, 123.0, 124.9, 125.0, 127.5, 131.6, 132.2, 132.5, 139.0, 144.3, 151.1; IR (KBr): $\tilde{\nu}$ = 3294 cm^{-1} , 3166, 2924, 2854, 2198, 2094, 1560, 1508, 1458, 1421, 1376, 1234, 1102, 893, 837, 754; Elemental analysis calcd (%) for $\text{C}_{44}\text{H}_{40}\text{N}_2 \cdot 0.5 \text{H}_2\text{O}$ (605.83): C 87.23, H 6.82, N 4.62; found: C 87.16, H 7.23, N 4.68.

4,7-Bis-[4-(5-*tert*-butyl-3-iodo-2-methoxyphenylethynyl)phenylethynyl]-3,8-

dihexyl[1,10]phenanthroline (7): A mixture of **5b** (200 mg (330 μmol)) and 5-*tert*-butyl-1,3-diiido-2-methoxybenzene^[35] (**6**) (1.56 g, 3.75 mmol), dry benzene (7 ml), dry triethylamine (2 ml), and $\text{Pd}(\text{PPh}_3)_4$ (200 mg, 170 μmol) was refluxed for 3 d. Then the solvent was removed under reduced pressure. After taking up the residue in dichloromethane (100 ml) it was washed with aqueous KCN (100 ml, 2%) and later with water. The organic layer was dried over MgSO_4 and the residual material subjected to column chromatography using at first dichloromethane and later methyl-*tert*-butylether as eluents to give 340 mg of **7** (88%) as colourless powder. M.p. 208-210 $^\circ\text{C}$; ^1H -NMR (200 MHz): δ = 0.89 (t, J = 6.9 Hz, 6 H, hexyl), 1.24-1.57 (m, 12 H, hexyl), 1.31 (s, 18 H, *tert*-butyl), 1.72-1.97 (m, 4 H, hexyl), 3.09 (t, J = 8.3 Hz, 4 H, hexyl), 4.02 (s, 6 H, methoxy), 7.51 (d, J = 2.3 Hz, 2 H, phenyl), 7.62 (d, J = 8.6 Hz, 4 H, phenyl), 7.69 (d, J = 8.6 Hz, 4 H, phenyl), 7.77 (d, J = 2.3 Hz, 2 H, phenyl), 8.38 (s, 2H, phenanthroline), 9.05 (s, 2 H, phenanthroline); ^{13}C NMR (50 MHz): δ = 14.0, 22.5, 29.1, 30.6, 31.2, 31.6, 32.6, 34.2, 61.0, 85.8, 88.1, 91.7, 93.2, 101.7, 116.2, 122.4, 124.0, 125.0, 127.5, 130.9, 131.6, 131.7, 131.9, 137.2, 138.9, 144.4, 148.6, 151.2, 158.1; IR (KBr): $\tilde{\nu}$ = 3054 cm^{-1} , 2924, 2855, 2202, 1560, 1509, 1466, 1435, 1420, 1256, 1097, 1000, 835, 746, 693; Elemental analysis calcd (%) for; $\text{C}_{66}\text{H}_{66}\text{I}_2\text{N}_2\text{O}_2$ (1173.07): C 67.58, H 5.67, N 2.39; found: C 67.68, H 5.86, N 2.41.

Synthesis of macrocycle 1: A solution of **7** (400 mg, 341 μmol) and **5b** (200 mg, 330 μmol) in dry benzene (20 ml) was added to a flask containing a mixture of $\text{Pd}(\text{PPh}_3)_4$ (350 mg, 300 μmol), dry benzene (60 ml) and dry triethylamine (20 ml) over a period of 32 h using an injection pump while keeping at reflux. The resulting dark solution was refluxed for 8 h and the solvent was removed under reduced pressure. The obtained dark residue was suspended in trichloromethane and washed with aqueous KCN (100 ml, 2%). The aqueous phase was extracted several times with trichloromethane. The combined organic phases were evaporated

to dryness under reduced pressure affording a residue which was then extracted twice with hot *n*-hexane (2 X 20 ml) and dried under reduced pressure. Subsequently, trichloromethane (5 ml) was added and after one night at room temperature colourless thin needles resulted which were washed several times with trichloromethane to yield analytically pure 80.0 mg of **1**. (16%). M.p. > 300 °C; ¹H-NMR (200 MHz, CDCl₃/5% TFA): δ = 0.93 (t, *J* = 6.9 Hz, 12 H, hexyl), 1.33-1.64 (m, 24 H, hexyl), 1.40 (s, 18 H, *tert*-butyl), 1.80-2.00 (m, 8 H, hexyl), 3.25 (t, *J* = 6.0 Hz, 8 H, hexyl), 4.30 (s, 6 H, methoxy), 7.61 (s, 4 H, phenyl), 7.72 (d, *J* = 8.6 Hz, 8 H, phenyl), 7.80 (d, *J* = 8.6 Hz, 8 H, phenyl), 8.74 (s, 4 H, phenanthroline), 9.10 (s, 4 H, phenanthroline); ¹³C-NMR (CDCl₃/5% TFA, 50 MHz): δ = 13.9, 22.5, 29.2, 30.2, 31.2, 31.5, 32.8, 34.6, 62.1, 84.2, 88.6, 93.2, 109.8, 120.6, 126.0, 126.3, 126.4, 129.3, 131.3, 132.0, 132.5, 134.9, 135.0, 142.4, 146.8, 148.1, 160.1; IR (KBr): $\tilde{\nu}$ = 3064 cm⁻¹, 3038, 2954, 2925, 2855, 2202, 1560, 1510, 1466, 1420, 1245, 1110, 1005, 880, 832, 752; ESI MS: *m/z* (%): 1515 (100, M+H⁺). Elemental analysis calcd (%) for C₁₁₀H₁₀₄N₄O₂ (1514.06): C 87.26, H 6.92, N 3.70; found: C 87.08, H 7.11, N 3.68.

2-(4-Methoxy-2,6-dimethylphenyl)-9-(2,4,6-trimethylphenyl)-[1,10]phenanthroline (10):

n-Butyllithium (2.5 M solution in hexane, 24.0 ml, 60.0 mmol) was added to a solution of 2-bromo-5-methoxy-1,3-dimethylbenzene (1.80 g, 8.37 mmol) in dry diethyl ether (20 ml) at 0 °C. The yellow solution was stirred at room temperature for 1 h providing a colourless turbid mixture. 2-(2,4,6-Trimethylphenyl)-[1,10]phenanthroline (**9**)³⁶ (1.00 g, 3.35 mmol) was then added slowly under nitrogen atmosphere over 15 minutes. The solution turned to a dark violet colour and was now stirred for 18 hours at room temperature. After quenching the reaction with H₂O (50 ml) the organic phase was separated. The aqueous phase layer was extracted with dichloromethane (50 ml), and the combined organic phases were dried over magnesium sulfate. The concentrated reaction mixture (volume: 50 ml) was subsequently oxidised with excess of activated MnO₂ (10 g) for 1 h and filtered through a pad of celite using dichloromethane as eluent. After concentration of the filtrate the crude product was purified by column chromatography using first dichloromethane and then diethyl ether to give a 770 mg of a colourless solid (52%) M. p. 262 °C; ¹H-NMR (200 MHz): δ = 2.17 (s, 6 H, benzyl), 2.20 (s, 6 H, benzyl), 2.33 (s, 3 H, benzyl), 3.82 (s, 3 H, methoxy), 6.68 (s, 2 H, phenyl), 6.94 (s, 2 H, phenyl), 7.57 (d, *J* = 8.1 Hz, 1 H, phenanthroline), 7.58 (d, *J* = 8.3 Hz, 1 H, phenanthroline), 7.84 (s, 2 H, phenanthroline), 8.27 (d, *J* = 8.1 Hz, 1 H, phenanthroline), 8.28 (d, *J* = 8.3 Hz, 1 H, phenanthroline); ¹³C-NMR (50 MHz): δ = 20.5, 20.9, 21.0, 55.1, 113.1, 124.9, 125.2, 126.1, 127.0, 128.4, 133.9, 135.6, 136.2, 137.3, 137.9, 138.1, 146.2, 158.9, 159.8, 160.1; IR (KBr): $\tilde{\nu}$ = 2953 cm⁻¹, 2915, 1606, 1583, 1541, 1479, 1375, 1356,

1319, 1194, 1156, 1100, 1074, 1039, 885, 858, 634; Elemental analysis calcd (%) for $C_{30}H_{28}N_2O \cdot 0.5 H_2O$ (441.56): C 81.60, H 6.62, N 6.34; found: C 81.3, H 6.54, N 6.03.

3,5-Dimethyl-4-[9-(2,4,6-trimethylphenyl)-[1,10]phenanthrolin-2-yl]phenol (12): Pyridine (9 ml) was added to conc. HCl (10.5 ml) and the resultant mixture was heated to reflux at 200 °C (water was removed completely). After cooling the mixture to 140 °C, **10** (400 mg, 906 μ mol) was added. The mixture was heated to 215-220 °C and kept there for 2.5 h. Subsequently, the mixture was cooled to 130 °C and a solution of water (20 ml) and conc. HCl (5 ml) was added affording a yellow solution. After cooling to room temperature, the reaction mixture was extracted several times with dichloromethane. The organic phases were combined, washed with water and finally neutralised with conc. KOH. The organic layer was dried over $MgSO_4$ and the solvent was removed under reduced pressure. The residue was then purified by column chromatography using dichloromethane as eluent, furnishing 370 mg of **12** (96%) as a colourless powder. M. p. > 280 °C; 1H -NMR (200 MHz): δ = 1.90 (s, 6 H, benzyl), 2.12 (s, 6 H, benzyl), 2.29 (s, 3 H, benzyl), 6.30 (s, 2 H, phenyl), 6.91 (s, 2 H, phenyl), 7.51 (d, J = 8.1 Hz, 1 H, phenanthroline), 7.58 (d, J = 8.3 Hz, 1 H, phenanthroline), 7.86 (s, 2 H, phenanthroline), 8.23 (d, J = 8.3 Hz, 1 H, phenanthroline), 8.34 (d, J = 8.1 Hz, 1 H, phenanthroline); ^{13}C -NMR (50 MHz): δ = 20.3, 20.4, 21.1, 114.8, 123.8, 124.7, 125.5, 125.6, 126.4, 126.8, 127.1, 128.2, 131.2, 135.4, 135.8, 136.1, 136.4, 137.7, 145.6, 146.0, 156.9, 160.5, 161.1; IR (KBr): $\tilde{\nu}$ = 3258 cm^{-1} , 3033, 2952, 2917, 2856, 1614, 1586, 1542, 1479, 1318, 1159, 1101, 1033, 887, 857, 756, 636; Elemental analysis calcd (%) for; $C_{29}H_{26}N_2O \cdot 0.5 H_2O$ (427.55): C 81.47, H 6.37, N 6.55; found: C 81.21, H 6.67, N 6.34.

Synthesis of 2: Anhydrous K_2CO_3 (300 mg, 2.17 mmol) was added at room temperature and in an inert atmosphere to a solution of **12** (600 mg, 1.43 mmol) 1,4-bis[2-[2-(2-tosyloxyethoxy)ethoxy]ethoxy]benzene (410 mg, 610 μ mol) (**13**)^[37] in dry DMF (50 ml). The resulting dark brown solution was stirred for 1 h at room temperature and then for 3 d at 60-70 °C. The solvent was evaporated under reduced pressure and taken up in a mixture of dichloromethane (100 ml) and water (100 ml). The organic layers were washed with water and dried over $MgSO_4$, then the solvent was evaporated to dryness. The residue was then subjected to column chromatography using at first diethylether and later ethyl acetate as eluents to afford 520 mg (69%) of a beige powder. M. p. 87-89°C; 1H -NMR (200 MHz): δ = 2.14 (s, 12 H, benzyl), 2.15 (s, 12 H, benzyl), 2.31 (s, 6 H, benzyl), 3.65-3.78 (m, 8 H, ethoxy), 3.80-3.94 (m, 8 H, ethoxy), 4.02-4.19 (m, 8 H, ethoxy), 6.66 (s, 4 H, phenyl), 6.85 (s, 4 H, phenyl), 6.93 (s, 4 H, phenyl), 7.55 (d, J = 8.1 Hz, 2 H, phenanthroline), 7.57 (d, J = 8.1

Hz, 2 H, phenanthroline), 7.84 (s, 4 H, phenanthroline), 8.26 (d, $J = 8.1$ Hz, 2 H, phenanthroline), 8.27 (d, $J = 8.1$ Hz, 2 H, phenanthroline); ^{13}C -NMR (50 MHz): $\delta = 20.5, 20.9, 21.0, 67.3, 68.1, 69.7, 69.8, 70.7, 70.8, 113.9, 115.6, 124.9, 125.2, 126.1, 127.0, 128.4, 134.0, 135.6, 136.1, 137.3, 137.9, 138, 146, 153.1, 158.1, 159.7, 160.1$; IR (KBr): $\tilde{\nu} = 3036\text{ cm}^{-1}, 2917, 2856, 1604, 1585, 1508, 1476, 1317, 1231, 1164, 1125, 1069, 857, 634$; Elemental analysis calcd (%) for $\text{C}_{76}\text{H}_{78}\text{N}_4\text{O}_8 \cdot 3\text{H}_2\text{O}$ (1229.52): C 74.24, H 6.89, N 4.56; found: C 74.50, H 6.51, N 4.30.

C1: To a mixture of macrocycle **1** (50.7 mg, 33.5 μmol) and 2,9-bis-(2,4,6-trimethylphenyl)-[1,10]phenanthroline (**11**)^[15b] (28.0 mg, 67.0 μmol), tetrakis(acetonitrile)copper(I) hexafluorophosphate (25.0 mg, 67.0 μmol) was added in 10 ml of dichloromethane. The resulting dark red solution was heated for several seconds, and the solvent was evaporated to give **C1**. After chromatography (silica gel; dichloromethane:methanol = 10:1) 40.0 mg (43%) of a dark red powder were received. M. p. > 300 °C; ^1H -NMR (600 MHz, CD_2Cl_2): $\delta = 0.90$ (t, $J = 7.1$ Hz, 12 H, hexyl), 1.32-1.44 (m, 16 H, hexyl), 1.38 (s, 18 H, *tert*-butyl), 1.45-1.52 (m, 8 H, hexyl), 1.72 (s, 12 H, benzyl), 1.74 (s, 24 H, benzyl), 1.77-1.85 (m, 8 H, hexyl), 3.08 (t, $J = 6.9$ Hz, 8 H, hexyl), 4.27 (s, 6 H, methoxy), 6.05 (s, 8 H, phenyl), 7.58 (s, 4 H, phenyl), 7.73 (d, $J = 7.9$ Hz, 8 H, phenyl), 7.81 (d, $J = 7.9$ Hz, 8 H, phenyl), 7.82 (d, $J = 8.1$ Hz, 4 H, phenanthroline), 8.27 (s, 4 H, phenanthroline), 8.37 (s, 4 H, phenanthroline), 8.50 (s, 4 H, phenanthroline), 8.74 (d, $J = 8.1$ Hz, 4 H, phenanthroline); ^{13}C -NMR (CD_2Cl_2 , 151 MHz): $\delta = 14.0, 20.0, 20.7, 22.5, 29.1, 30.7, 31.2, 31.6, 32.5, 34.4, 61.7, 84.7, 88.7, 92.9, 104.6, 116.5, 121.3, 125.1, 125.2, 126.4, 127.0, 127.9, 128.1, 131.0, 131.9, 132.1, 134.4, 137.0, 137.7, 137.8, 140.5, 141.4, 143.8, 146.7, 147.9, 158.7, 160.2$; IR (KBr): $\tilde{\nu} = 2965\text{ cm}^{-1}, 2922, 2854, 2194, 1582, 1509, 1458, 1420, 1244, 1105, 1008, 840, 557$; ESI MS: m/z (%): 1236.4 (100) [**M**-2PF₆]; Elemental analysis calcd (%) for $\text{C}_{170}\text{H}_{160}\text{N}_8\text{O}_2\text{Cu}_2\text{P}_2\text{F}_{12}$ (2764.21): C 73.87, H 5.83, N 4.05; found: C 73.41, H 6.22, N 4.07.

C2: **10** (33.9 mg, 78.3 μmol), $[\text{Cu}(\text{CH}_3\text{CN})_4]\text{PF}_6$ (29.2 mg, 78.3 μmol), and macrocycle **1** (59.3 mg, 39.1 μmol) were stirred for 1 h in dichloromethane (10 ml). The resulting dark red solution was evaporated to dryness to furnish **C2**. After chromatography (silica gel; dichloromethane : methanol = 10:1) 87.0 mg (80%) of a dark red powder containing water were received. M. p. > 300 °C; ^1H -NMR (600 MHz, CD_2Cl_2): $\delta = 0.91$ (t, $J = 7.2$ Hz, 12 H, hexyl), 1.33-1.45 (m, 16 H, hexyl), 1.40 (s, 18 H, *tert*-butyl), 1.48-1.54 (m, 8 H, hexyl), 1.73 (s, 12 H, benzyl), 1.75 (s, 12 H, benzyl), 1.81 (s, 12 H, benzyl), 1.82-1.86 (m, 8 H, hexyl), 3.11 (t, $J = 7.5$ Hz, 8 H, hexyl), 3.34 (s, 6 H, methoxy), 4.27 (s, 6 H, methoxy), 5.83 (s, 4 H,

phenyl), 6.07 (s, 4 H, phenyl), 7.63 (s, 4 H, phenyl), 7.77 (d, $J = 8.1$ Hz, 8 H, phenyl), 7.85 (d, $J = 8.1$ Hz, 8 H, phenyl), 7.86 (d, $J = 8.0$ Hz, 2 H, phenanthroline), 7.87 (d, $J = 8.0$ Hz, 2 H, phenanthroline), 8.25 (s, 4 H, phenanthroline), 8.40 (s, 4 H, phenanthroline), 8.53 (s, 4 H, phenanthroline), 8.72 (d, $J = 8.0$ Hz, 2 H, phenanthroline), 8.73 (d, $J = 8.0$ Hz, 2 H, phenanthroline); ^{13}C -NMR (CD_2Cl_2 , 151 MHz): $\delta = 14.2, 20.2, 20.6, 20.8, 23.0, 29.6, 31.1, 31.3, 32.0, 33.0, 34.7, 55.0, 62.0, 85.3, 89.1, 93.1, 104.8, 112.0, 116.9, 122.0, 125.5, 125.6, 126.9, 127.1, 127.4, 128.4, 128.5, 128.6, 131.6, 132.3, 132.5, 133.1, 134.9, 136.7, 137.5, 137.9, 138.3, 141.2, 141.9, 144.4, 147.4, 148.5, 159.2, 159.3, 159.5, 160.6$; IR (KBr): $\tilde{\nu} = 2954\text{ cm}^{-1}, 2923, 2855, 2195, 1654, 1570, 1508, 1475, 1458, 1420, 1320, 1245, 1156, 1104, 1011, 839, 558$; ESI MS: m/z (%): 1253.2 (100) [$\text{M}-2\text{PF}_6$]; Elemental analysis calcd (%) for $\text{C}_{170}\text{H}_{160}\text{N}_8\text{O}_4\text{Cu}_2\text{P}_2\text{F}_{12} \cdot 3\text{H}_2\text{O}$ (2796.21): C 71.64, H 5.87, N 3.93; found: C 71.75, H 5.93, N 4.29.

C3: **2** (49.0 mg, 40.9 μmol), **5a** (74.4 mg, 81.8 μmol) and $[\text{Cu}(\text{CH}_3\text{CN})_4]\text{PF}_6$ (30.5 mg (81.8 μmol)) were stirred in 10 ml of dry dichloromethane for 2 h. The resulting dark red solution was evaporated to afford crude **C3**. After chromatography (silica gel; dichloromethane : methanol = 10:1) 130 mg (85%) of a dark red powder containing dichloromethane were received. M. p.: $> 122-124\text{ }^\circ\text{C}$; ^1H -NMR (600 MHz, CD_2Cl_2): $\delta = 0.86-0.90$ (m, 12 H, hexyl), 1.15-1.20 (m, 84 H, triisopropyl), 1.31-1.40 (m, 16 H, hexyl), 1.43-1.49 (m, 8 H, hexyl), 1.70-1.72 (m, 6 H, benzyl), 1.72-1.74 (m, 12 H, benzyl), 1.77-1.82 (m, 8 H, hexyl), 1.79 (s, 12 H, benzyl), 3.07 (t, $J = 7.6$ Hz, 8 H, hexyl), 3.55-3.56 (m, 4 H, ethoxy), 3.57 (s, 4 H, ethoxy), 3.58 (s, 4 H, ethoxy), 3.60-3.68 (m, 4 H, ethoxy), 3.69-3.81 (m, 4 H, ethoxy), 3.95-4.05 (m, 4 H, ethoxy), 5.84 (s, 4 H, phenyl), 6.02-6.06 (m, 4 H, phenyl), 6.75-6.80 (m, 4 H, phenyl), 7.59-7.63 (m, 8 H, phenyl), 7.71-7.74 (m, 8 H, phenyl), 7.85-7.94 (m, 4 H, phenanthroline), 8.24 (s, 4 H, phenanthroline), 8.38-8.40 (m, 4 H, phenanthroline), 8.47-8.52 (m, 4 H, phenanthroline), 8.70-8.74 (m, 4 H, phenanthroline); ^{13}C -NMR (151 MHz): $\delta = 11.7, 14.2, 18.8, 20.3, 20.6, 20.8, 23.0, 29.6, 31.1, 32.0, 33.0, 67.2, 68.3, 69.8, 70.1, 71.0, 71.1, 85.2, 94.9, 104.7, 106.6, 112.6, 115.7, 122.0, 125.6, 127.0, 127.2, 127.4, 128.3, 128.4, 128.6, 129.1, 132.2, 132.7, 133.3, 134.8, 136.7, 137.4, 137.9, 138.2, 141.4, 141.9, 144.4, 148.4, 153.4, 158.3, 159.2, 159.4$; IR (KBr): $\tilde{\nu} = 2924\text{ cm}^{-1}, 2862, 2198, 2152, 1618, 1578, 1542, 1508, 1458, 1376, 1232, 1164, 1124, 1071, 839, 747, 557$; ESI MS: m/z (%): 1560.3 (100) [$\text{M}-2\text{PF}_6$]; Elemental analysis calcd (%) for $\text{C}_{200}\text{H}_{238}\text{N}_8\text{O}_8\text{Si}_4\text{Cu}_2\text{P}_2\text{F}_{12} \cdot 4\text{CH}_2\text{Cl}_2$ (3751.23): C 65.40, H 6.62, N 2.99; found: C 65.11, H 6.44, N 2.90.

Preparation of heteroleptic basket assembly C4: To a mixture of **1** (24.2 mg, 16.1 μmol) and **2** (18.7 mg, 16.1 μmol), tetrakis(acetonitrile)copper(I)hexafluorophosphate (12.0 mg, 32.2 μmol) was added in 10 ml of dichloromethane. The resulting dark red solution was heated (~ 35 $^{\circ}\text{C}$) for several seconds and then the solvent was evaporated to afford the basket assembly (**C4_{xyz}**) quantitatively as dark red powder (containing water). M. p. 225 $^{\circ}\text{C}$; IR (KBr): $\tilde{\nu} = 2924$ cm^{-1} , 2855, 2195, 1605, 1509, 1462, 1260, 1101, 1026, 839, 555; ESI MS (**C4_{xyz}**): m/z (%): 1408.4 (100) [M-2PF₆]; Elemental analysis calcd (%) for C₁₈₆H₁₈₂N₈O₁₀Cu₂P₂F₁₂ • 2 H₂O (3142.59): C 71.09, H 5.97, N 3.57; found: C 71.02, H 5.89, N 3.46. **C4_x:C4_y:C4_z** were formed in a 59:24:17 ratio. **C4_{x,y}** could be separated from **C4_z** by chromatography (silica gel, dichloromethane : methanol=100:1). Initial fractions contained **C4_{x,y}** as the sole products while later fractions furnished enriched **C4_z** (80 %).

Isomer C4_x: ¹H-NMR (600 MHz, CD₂Cl₂): $\delta = 0.88$ -0.93 (m, 12 H, hexyl), 1.32-1.45 (m, 16 H, hexyl), 1.39 (s, 18 H, *tert*-butyl), 1.47-1.56 (m, 8 H, hexyl), 1.58 (s, 6 H, benzyl), 1.68 (s, 12 H, benzyl), 1.80-1.86 (m, 8 H, hexyl), 1.87 (s, 12 H, benzyl), 3.02-3.20 (m, 8 H, hexyl), 3.50-3.52 (m, 4 H, ethoxy), 3.53-3.56 (m, 4 H, ethoxy), 3.57-3.59 (m, 4 H, ethoxy), 3.69-3.70 (m, 4 H, ethoxy), 4.01-4.02 (m, 4 H, ethoxy), 4.16-4.20 (m, 4 H, ethoxy), 4.21 (s, 6 H, methoxy; H_{Xd}), 5.64 (s, 4 H, phenyl; H_{Xb}), 6.19 (s, 4 H, phenyl; H_{Xa}), 6.87 (s, 4 H, phenyl; H_{Xc}), 7.63 (s, 4 H, phenyl), 7.76-7.77 (m, 8 H, phenyl), 7.83 (d, $J = 8.0$ Hz, 2 H, phenanthroline), 7.84-7.86 (m, 8 H, phenyl), 7.93 (d, $J = 8.2$ Hz, 2 H, phenanthroline), 8.21 (d, $J = 9.3$ Hz, 2 H, phenanthroline; H_{X6'}), 8.24 (d, $J = 9.3$ Hz, 2 H, phenanthroline; H_{X6}), 8.40 (s, 4 H, phenanthroline), 8.52 (s, 4 H, phenanthroline), 8.70 (d, $J = 8.0$ Hz, 2 H, phenanthroline), 8.74 (d, $J = 8.2$ Hz, 2 H, phenanthroline); ¹³C-NMR (CD₂Cl₂, 151 MHz): $\delta = 14.0, 20.0, 20.3, 20.4, 23.0, 29.1, 29.3, 30.9, 31.7, 32.7, 34.5, 61.7, 66.7, 68.0, 68.1, 69.3, 70.5, 70.9, 85.0, 88.9, 92.8, 104.6, 111.8, 115.5, 116.6, 121.7, 125.2, 125.4, 126.8, 126.9, 127.3, 128.0, 128.1, 128.3, 131.4, 132.0, 132.2, 132.6, 132.9, 134.7, 136.2, 136.4, 137.5, 137.6, 138.1, 140.9, 141.6, 144.1, 147.2, 148.2, 153.2, 153.3, 157.8, 158.7, 160.3$.

Isomer C4_y: ¹H-NMR (600 MHz, CD₂Cl₂): $\delta = 0.88$ -0.93 (m, 12 H, hexyl), 1.32-1.45 (m, 16 H, hexyl), 1.38 (s, 18 H, *tert*-butyl), 1.47-1.56 (m, 8 H, hexyl), 1.70 (s, 12 H, benzyl), 1.74 (s, 6 H, benzyl), 1.80-1.86 (m, 8 H, hexyl), 1.99 (s, 12 H, benzyl), 3.02-3.20 (m, 8 H, hexyl), 3.61-3.62 (m, 4 H, ethoxy), 3.63-3.65 (m, 4 H, ethoxy), 3.70-3.72 (m, 4 H, ethoxy), 3.78-3.80 (m, 4 H, ethoxy), 3.89-3.90 (m, 4 H, ethoxy), 3.96-3.98 (m, 4 H, ethoxy), 4.14 (s, 6 H, methoxy; H_{Yc}), 5.49 (s, 4 H, phenyl; H_{Yb}), 6.33 (s, 4 H, phenyl; H_{Ya}), 7.07 (s, 4 H, phenyl; H_{Yc}), 7.62 (s, 4 H, phenyl), 7.74-7.76 (m, 8 H, phenyl), 7.77 (d, $J = 8.1$ Hz, 2 H, phenanthroline), 7.87-7.88 (m, 8 H, phenyl), 7.97 (d, $J = 8.2$ Hz, 2 H, phenanthroline), 8.21

(d, $J = 9.3$ Hz, 2 H, phenanthroline; $H_{Y6'}$), 8.24 (d, $J = 9.3$ Hz, 2 H, phenanthroline; $H_{Y5'}$), 8.40 (s, 4 H, phenanthroline), 8.55 (s, 4 H, phenanthroline), 8.67 (d, $J = 8.1$ Hz, 2 H, phenanthroline), 8.76 (d, $J = 8.2$ Hz, 2 H, phenanthroline); ^{13}C -NMR (CD_2Cl_2 , 151 MHz): $\delta = 13.9, 20.1, 20.3, 20.4, 23.0, 29.1, 29.3, 30.9, 31.7, 32.7, 34.5, 61.6, 66.6, 69.8, 70.5, 70.8, 71.2, 71.3, 85.0, 88.9, 92.8, 104.6, 111.5, 115.7, 116.6, 121.8, 125.3, 125.4, 126.8, 127.6, 128.0, 128.1, 128.3, 131.3, 132.0, 132.2, 132.6, 132.9, 134.7, 136.2, 136.4, 137.5, 137.8, 138.1, 140.9, 141.6, 144.1, 147.2, 148.2, 153.2, 153.3, 157.8, 159.3, 160.4$.

Isomer C4z: ^1H -NMR (400 MHz, CD_2Cl_2): $\delta = 0.79$ - 0.83 (m, 12 H, hexyl), 1.32-1.45 (m, 16 H, hexyl), 1.38 (s, 18 H, *tert*-butyl), 1.47-1.56 (m, 8 H, hexyl), 1.70 (s, 12 H, benzyl), 1.74 (s, 6 H, benzyl), 1.80-1.86 (m, 8 H, hexyl), 1.99 (s, 12 H, benzyl), 2.91-3.01 (m, 8 H, hexyl), 3.61-3.62 (m, 4 H, ethoxy), 3.63-3.65 (m, 4 H, ethoxy), 3.70-3.72 (m, 4 H, ethoxy), 3.78-3.80 (m, 4 H, ethoxy), 3.89-3.90 (m, 4 H, ethoxy), 3.96-3.98 (m, 4 H, ethoxy), 4.24 (s, 6 H, methoxy; H_{Za}), 5.85 (s, 4 H, phenyl; H_{Zb}), 6.06 (s, 4 H, phenyl), 6.75 (s, 4 H, phenyl; H_{Zc}), 7.61 (s, 4 H, phenyl), 7.75-7.77 (m, 8 H, phenyl), 7.77 (d, $J = 8.1$ Hz, 2 H, phenanthroline), 7.87-7.88 (m, 8 H, phenyl), 7.97 (d, $J = 8.2$ Hz, 2 H, phenanthroline), 8.21 (d, $J = 9.3$ Hz, 2 H, phenanthroline; $H_{Z5'}$), 8.23 (s, 2 H, phenanthroline; $H_{Z6'}$), 8.38 (s, 4 H, phenanthroline), 8.53 (s, 4 H, phenanthroline), 8.67 (d, $J = 8.1$ Hz, 2 H, phenanthroline), 8.76 (d, $J = 8.2$ Hz, 2 H, phenanthroline).

Acknowledgements. We are indebted to the financial support from the DFG, the Fonds der Deutschen Chemie and the European Union (MAC-MES).

References

- [1] a) B. Dietrich, P. Viout, J.-M. Lehn, *Macrocyclic Chemistry*, VCH, Weinheim **1993**; b) *Macrocyclic Synthesis*, Ed. D. Parker, Oxford University Press, Oxford **1996**.
- [2] S. Höger, K. Bonrad, A. Mourran, U. Beginn, M. Möller, *J. Am. Chem. Soc.* **2001**, *123*, 5651-5659.
- [3] E. Mena-Osteritz, P. Bäuerle, *Adv. Mat.* **2001**, *13*, 243-246.
- [4] P. Samori, F. Jäckel, O. Unsal, A. Godt, J. P. Rabe, *Chem. Phys. Chem.* **2001**, *2*, 461-464.
- [5] a) A. S. Shetty, P. R. Fischer, K. F. Stork, P. W. Bohn, J. S. Moore, *J. Am. Chem. Soc.* **1996**, *118*, 9409-9414; b) O. Y. Mindyuk, M. R. Stetzer, D. Gidalevitz, P. A. Heiney, *Langmuir* **1999**, *15*, 6897-6900; c) Krömer, I. Rios-Carreras, G. Fuhrmann, C. Musch, M. Wunderlin, T. Debaerdemaeker, E. Mena-Osteritz, P. Bäuerle, *Angew. Chem. Int. Ed. Engl.* **2000**, *39*, 3481-3486.
- [6] a) S. Höger, *J. Polym. Sci. Part A: Polym. Chem.* **1999**, *37*, 2685-2698; b) F. Diederich, *Nature* **1994**, *369*, 199-207; c) J. M. Tour, *Chem. Rev.* **1996**, *96*, 537-553. d) J. S. Moore, *Acc. Chem. Res.* **1997**, *30*, 402-413; e) M. M. Haley, *Synlett* **1998**, 557-565; f) M. M. Haley, J. J. Pak, S. C. Brand, *Top. Curr. Chem.* **1999**, *201*, 81-130; g) F. Diederich, *Chem. Commun.* **2001**, 219-227; h) C. Grave, A. D. Schlüter, *Eur. J. Org. Chem.* **2002**, 3075-3098; P. N. W. Baxter, *Chem. Eur. J.* **2003**, *9*, 5011-5022; i) Y. Yamaguchi, Z. Yoshida, *Chem. Eur. J.* **2003**, *9*, 5430-5440; j) S. Höger, *Chem. Eur. J.* **2004**, *10*, 1320-1329.
- [7] a) M. Schmittel, H. Ammon, V. Kalsani, A. Wiegrefe, C. Michel, *Chem. Commun.* **2002**, 2566-2567; b) O. Henze, D. Lentz, A. Schäfer, P. Franke, A. D. Schlüter, *Chem. Eur. J.* **2002**, *8*, 357-365; c) K. Campbell, R. McDonald, N. R. Branda, R. R. Tykwinski, *Org. Lett.* **2001**, *3*, 1045-1048; d) K. Campbell, C. J. Kuehl, M. J.

- Ferguson, P. J. Stang, R. R. Tykwinski, *J. Am. Chem. Soc.* **2002**, *124*, 7266-7267; e) P. H. Ge, W. Fu, W.A. Herrmann, E. Herdtweck, C. Campana, R. D. Adams, U. H. F. Bunz, *Angew. Chem. Int. Ed. Engl.* **2000**, *39*, 3607-3610; f) S. Höger, V. Enkelmann, K. Bonrad, C. Tschierske, *Angew. Chem. Int. Ed. Engl.* **2000**, *39*, 2268-2270; g) O. Henze, D. Lentz, A. D. Schlüter, *Chem. Eur. J.* **2000**, *6*, 2362-2367; h) M. Ohkita, K. Ando, T. Suzuki, T. Tsuji, *J. Org. Chem.* **2000**, *65*, 4385-4390; i) M. J. Marsella, I. T. Kim, F. Tham, *J. Am. Chem. Soc.* **2000**, *122*, 974-975; j) Y. Tobe, T. Fujii, H. Matsumoto, K. Tsumuraya, D. Noguchi, N. Nakagawa, M. Sonoda, K. Naemura, Y. Achiba, T. Wakabayashi, *J. Am. Chem. Soc.* **2000**, *122*, 1762-1775; k) S. Eisler, R. R. Tykwinski, *Angew. Chem. Int. Ed. Engl.* **1999**, *38*, 1940-1943; l) T. Kawase, Y. Hosokawa, H. Kurata, M. Oda, *Chem. Lett.* **1999**, 745-746; m) M. Haley, S. C. Brand, J. J. Pak, *Angew. Chem. Int. Ed. Engl.* **1997**, *36*, 836-838; n) J. Anthony, A. M. Boldi, C. Boudon, J.-P. Gisselbrecht, M. Gross, P. Seiler, C. B. Knobler, F. Diederich, *Helv. Chim. Acta.* **1995**, *78*, 797-817.
- [8] a) C. Dietrich-Buchecker, J.-P. Sauvage, *Chem. Rev.* **1987**, *87*, 795-810; b) B. X. Colasson, C. Dietrich-Buchecker, M. C. Jimenez-Molero, J.-P. Sauvage, *J. Phys. Org. Chem.* **2002**, *15*, 476-483; c) V. Balzani, A. Credi, F. M. Raymo, J. F. Stoddart, *Angew. Chem. Int. Ed. Engl.* **2000**, *39*, 3348-3391.
- [9] B. Meynhardt, U. Lüning, C. Wolff, C. Näther, *Eur. J. Org. Chem.* **1999**, *9*, 2327-2335.
- [10] a) C. Dietrich-Buchecker, G. Rapenne, J.-P. Sauvage, *Coord. Chem. Rev.* **1999**, *185-186*, 167-176; b) H. J. Claude, C. Dietrich-Buchecker, J.-P. Sauvage, *Comprehensive Supramolecular Chemistry*, **1996**, *9*, 43-83.
- [11] U. Velten, M. Rehahn, *Macromol. Chem. Phys.* **1998**, *199*, 127-140.
- [12] M. Schmittel, H. Ammon, *Synlett* **1999**, 750-752.
- [13] M. Schmittel, H. Ammon, *Synlett* **1997**, 1096 - 1098.
- [14] a) E. Leize, D. R. Dorsselaer, R. Krämer, J.-M. Lehn, *J. C. S. Chem. Commun.* **1993**, 990-993; b) T. Bark, T. Weyhermüller, F. Heirtzler, *Chem. Commun.* **1998**, 1475-1476.
- [15] a) M. Schmittel, A. Ganz, *Chem. Commun.* **1997**, 99-100; b) M. Schmittel, U. Lüning, M. Meder, A. Ganz, C. Michel, M. Herderich, *Heterocycl. Commun.* **1997**, *3*, 493-498.
- [16] C. Dietrich-Buchecker, P. A. Marnot, J.-P. Sauvage, *Tetrahedron Lett.* **1982**, *23*, 5291-5294.
- [17] R. Lazzaroni, A. Calderone, J. L. Bredas, J. P. Rabe, *J. Chem. Phys.* **1997**, *107*, 99-105.
- [18] a) R. J. P. Williams, *J. Chem. Soc.* **1955**, 137-145; b) R. A. Palmer, T. S. Piper, *Inorg. Chem.* **1966**, *5*, 864-878; c) W. R. McWinnie, J. D. Miller, *Adv. Inorg. Chem. Radiochem.* **1969**, *12*, 135.
- [19] a) V. Gouille, R. P. Thummel, *Inorg. Chem.* **1990**, *29*, 1767-1772; b) M. Schmittel, C. Michel, S. X. Liu, D. Schilbach, D. Fenske, *Eur. J. Inorg. Chem.* **2001**, 1155-1166; c) X. Y. Li, J. Illigen, M. Nieger, S. Michel, C. A. Schalley, *Chem. Eur. J.* **2003**, *9*, 1332-1347.
- [20] P. N. W. Baxter, J.-M. Lehn, G. Baum, D. Fenske, *Chem. Eur. J.* **1999**, 102-112 and ref's therein.
- [21] N. Fatin Rouge, S. Blanc, A. Pfeil, A. Rigault, A. M. Albrecht-Gary, J.-M. Lehn, *Helv. Chim. Acta.* **2001**, *84*, 1694-1711.
- [22] Combining **1**, **2** and copper(I) salt at $-60\text{ }^{\circ}\text{C}$ leads to a ratio of **C4x**:**C4y**:**C4z** = 45 : 20 : 35 (determined at rt).
- [23] HyperchemTM 6.02 Release for Windows by Hypercube, Inc. 2000. MM+ force field.
- [24] The ¹H NMR data of **C4xy** for proton H_a, H_b and H_d suggest that in **C4y** the distortion at the Cu⁺ centre is even more pronounced than in **C4x**. This could be explained by assuming a planar macrocycle in **C4x** and a slightly folded one in **C4y**.
- [25] This limitation is due to the fact that 3,8-dihexyl groups at the phenanthroline of **1** are prohibiting a sideward slide-on motion.
- [26] Most likely, π - π and other attractive interactions as well as desolvation effects stabilize **model II** and its precursor complexes.
- [27] M. Schmittel, A. Ganz, *Org. Lett.* **2002**, *4*, 2289-2292.
- [28] A. Marquis-Rigault, A. Dupont-Gervais, P. N. W. Baxter, A. Van Dorsselaer, J.-M. Lehn, *Inorg. Chem.* **1996**, *35*, 2307-2310.
- [29] M. Schmittel, A. Ganz, V. Kalsani, *unpublished results*.
- [30] a) H. Gampp, M. Maeder, C. J. Meyer, A. D. Zuberbühler, *Talanta* **1985**, *32*, 95-100; b) F. J. C. Rossoti, H. S. Rossoti, R. J. Whewell, *J. Inorg. Nucl. Chem.* **1971**, *33*, 2051-2065; c) H. Gampp, M. Maeder, C. J. Meyer, A. D. Zuberbühler, *Talanta* **1985**, *32*, 257-264; d) H. Gampp, M. Maeder, C. J. Meyer, A. D. Zuberbühler, *Talanta* **1986**, *33*, 943-951.
- [31] J. L. Burmeister, F. Basolo, *Inorg. Chem.* **1964**, *3*, 1587-1593.
- [32] D. R. Coulson, *Inorg. Synth.* **1972**, *13*, 121-124.
- [33] A. Godt, *J. Org. Chem.* **1997**, *62*, 7471-7474.
- [34] J. P. Rabe, S. Buchholz, *Science* **1991**, *253*, 424-427.
- [35] R. C. Helgeson, B. J. Selle, I. Goldberg, C. B. Knobler, D. J. Cram, *J. Am. Chem. Soc.* **1993**, *115*, 11506-11511.
- [36] M. Schmittel, A. Ganz, D. Fenske, M. Herderich. *J. Chem. Soc. Dalton. Trans.* **2000**, 353-359.

[37] P. L. Anelli, P. R. Ashton, N. Spencer, A. M. Z. Slawin, J. F. Stoddart, D. J. Williams, *Angew. Chem. Int. Ed. Engl.* **1991**, *30*, 1036-1039.

Key words: exotopic, heteroleptic complex, basket, HETPHEN, self-assembly, STM.

Supp 5-2

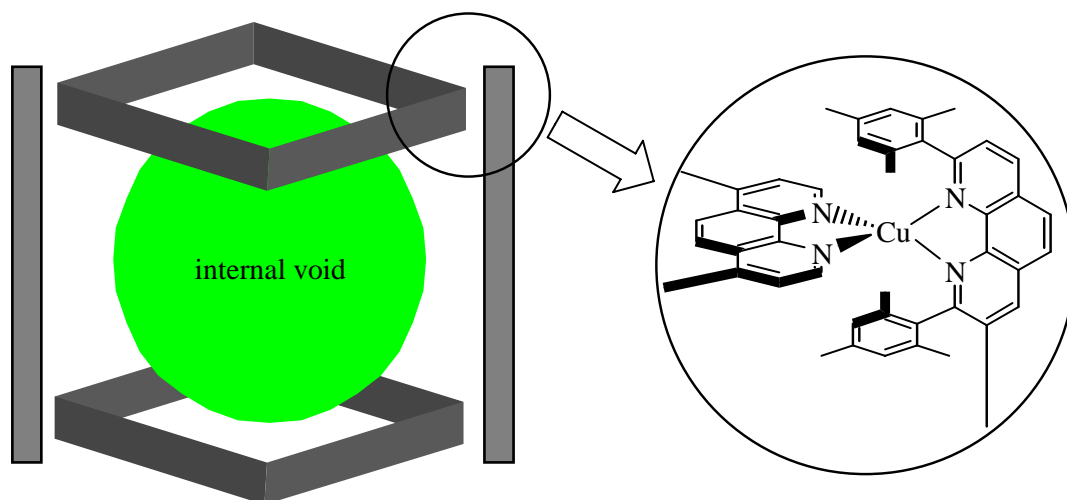
Chem. Commun. 2002, 2566-2567Reproduced by permission of *The Royal Society of Chemistry***Quantitative Formation and Clean Metal Exchange Processes of Large Void (>5000 Å³) Nanoscaffold Structures**Michael Schmittl,^{*a} Horst Ammon,^b Venkateshwarlu Kalsani,^a Andreas Wiegrefe^a and Christoph Michel^a^aFB8-OC1 Chemie-Biologie, Universität Siegen, Adolf-Reichwein-Str, D-57068 Siegen, Germany.

E-mail: schmittl@chemie.uni-siegen.de; Fax: (+49) 271 740 3270; Tel: (+49) 271 740 4356.

^bInstitut für Organische Chemie der Universität Würzburg, Am Hubland, D-97074 Würzburg, Germany.

Abstract. The metallosupramolecular assembly of linear and macro-cyclic bisphenanthrolines in the presence of Cu⁺ provides nanobox structures with internal volumes of >5000 Å³ when the ligands are designed along the HETPHEN approach.

The preparation of defined molecular architectures still represents a considerable synthetic challenge, although seminal contributions in the last decade have established highly efficient self-assembly processes,¹ increasingly based on metal-ligand coordination, to provide sparkling supramolecular structures, *e.g.* racks, ladders, grids, cages *etc.*² Our interest is to build large porous nano scaffolds in solution with a large internal void (free volume of >5000 Å³) the inside of which can be modelled at will (Figure 1).

**Figure 1.** Cartoon representation of programmed nanoscaffolds with large internal voids.

To prepare a sufficiently large and stable nanoscaffold by self-assembly we decided to rely on the thermodynamically stable and kinetically labile³ copper(I) bisphenanthroline complex as a key unit for the corners of the box. In addition, these complexes are also geometrically well-defined as demonstrated by Sauvage⁴ in many examples. However, when following the principle of maximum site occupancy and cooperativity, as successfully employed by Lehn⁵ for a related cylindrical architecture, the self-assembly process of **1** and **3** (Chart 1) in the presence of copper(I) ions afforded a variety of structures depicted schematically in Scheme 1. ESI-MS revealed that the desired box $[\text{Cu}_4(\mathbf{1})_2(\mathbf{3})_2]^{4+}$ (**A**) was only formed as a minor constituent beside the homoleptic oligomer $[\text{Cu}_n(\mathbf{1})_n]^{n+}$ ($n = 3,4$; **B**) and some trace amounts of the mixed triangular structure $[\text{Cu}_3(\mathbf{1})_2(\mathbf{3})]^{3+}$ (**C**). Hence, it is clear that a clean approach to nanobox **B** in solution cannot rely solely on cooperativity and maximum site occupancy effects.

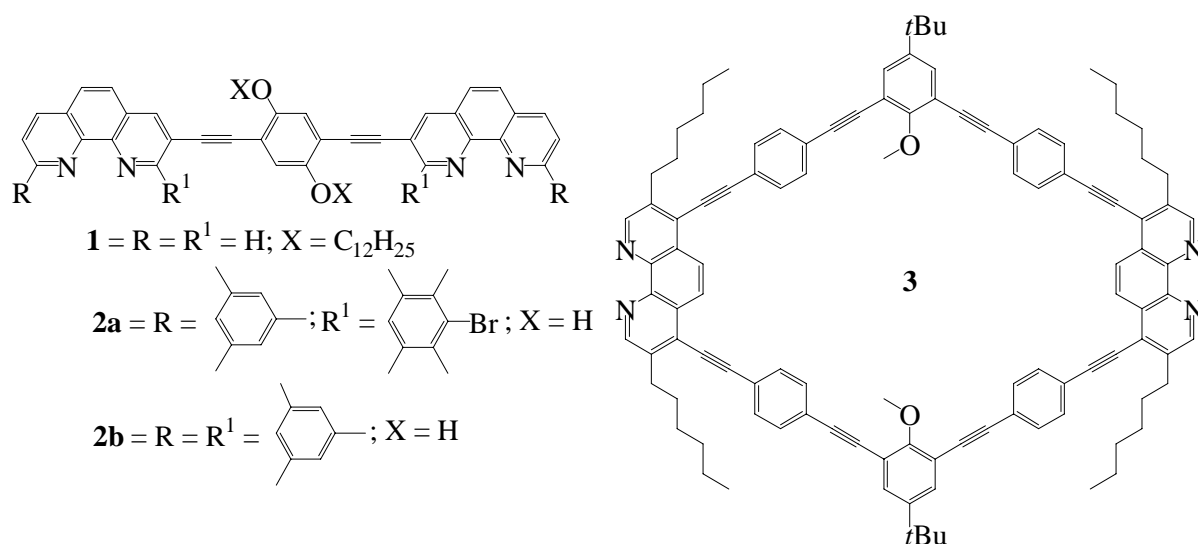
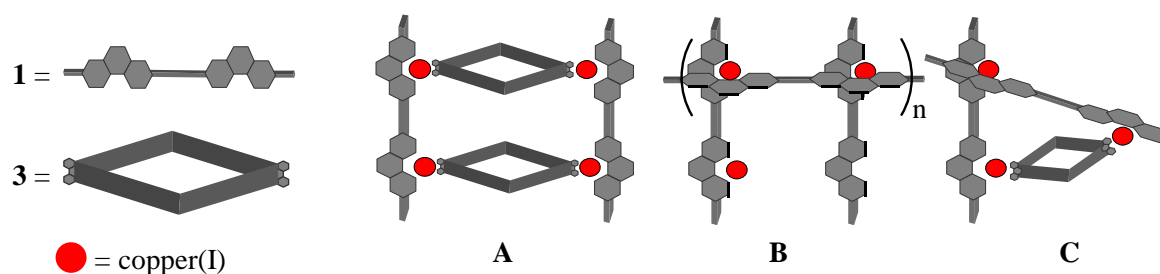


Chart 1. Ligands used for the present study.

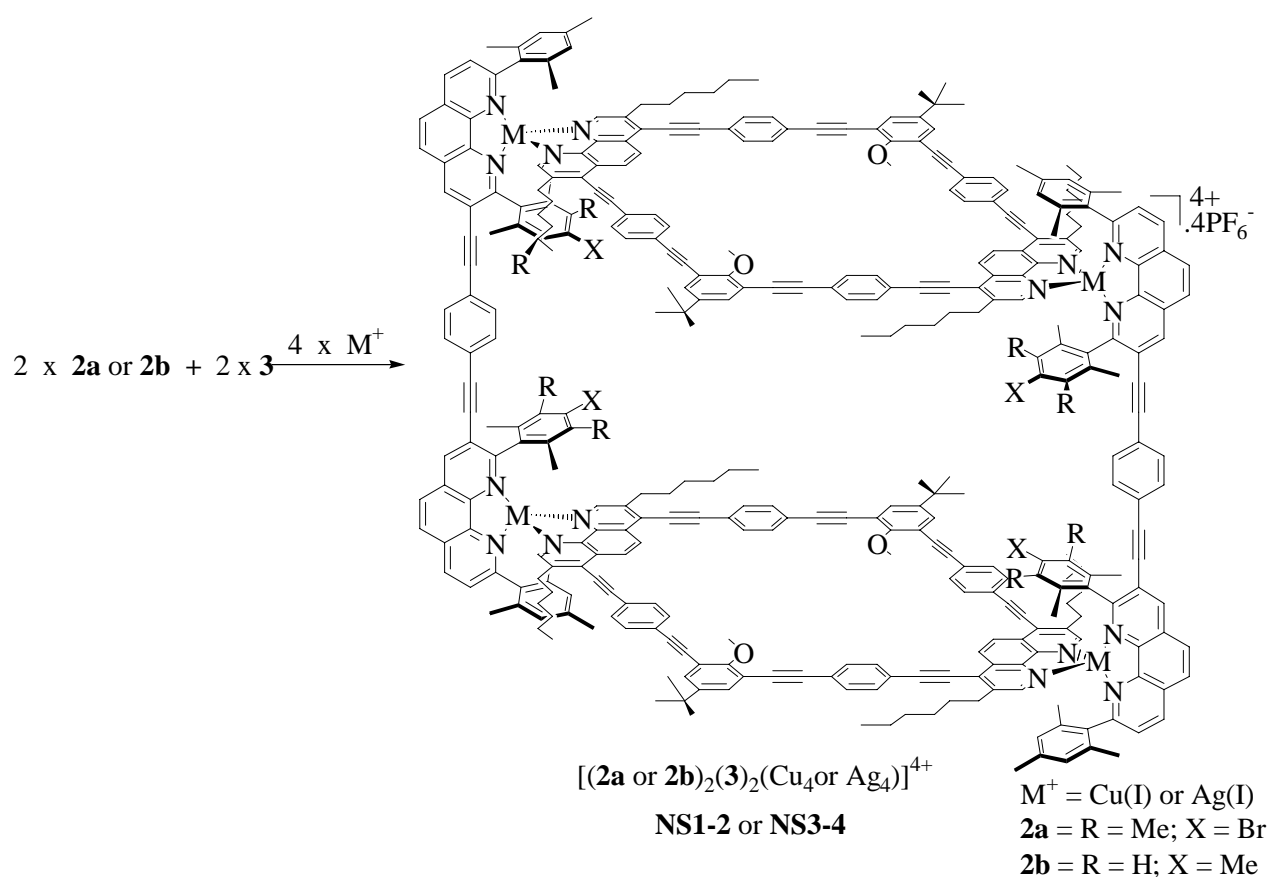


Scheme 1. Schematic representation of complexes A–C obtained in the reaction of **1** and **3**.

We argued, that it would be helpful (i) to prevent formation of any *homoleptic* bisphenanthroline complex in order to diminish the number of possible options in the self-

assembly process and (ii) to impose even more driving force than in the parent copper(I) bisphenanthroline complex. Hence, we made use of the HETPHEN approach (a quantitative approach to hetero-leptic bisphenanthroline metal complexes⁶) to build defined heteroleptic copper(I) complexes. This approach utilizes steric and electronic effects originating from bulky aryl substituents at the bisimine coordination sites (as seen in **2a,b**) to control the coordination equilibrium both kinetically and thermodynamically.

Quantitative self-assembly of the deep red supramolecular complexes **NS1,2**⁴⁺ (Scheme 2) indeed could be effected when the linear ligand **2a** or **2b**, the macrocyclic bisphenanthroline **3** and [Cu(MeCN)₄]PF₆ (stoichiometric ratio 2:2:4, respectively) were simply dissolved in dichloromethane at ambient temperature for a couple of seconds. Both, the ESI-MS and ¹H NMR spectra indicated the presence of just one single species.



Scheme 2. Self-assembly of nanoscaffolds, **NS1-4**.

For example, in the electrospray (ESI) mass spectra of complex [**NS2**](PF₆)₄ only one set of signals was observed in the mass range up to 4000 Dalton: $m/z = 2740$, 1777 and 1298, corresponding to [**NS2**](PF₆)₂²⁺, [**NS2**](PF₆)³⁺ and [**NS2**]⁴⁺ formed by successive loss of

counterions. For **NS1**⁴⁺ the ESI data were analogous. Moreover, the ¹H NMR revealed highly symmetric species **NS1**⁴⁺ and **NS2**⁴⁺, respectively. The distinct highfield shift of the mesitylene protons ($\delta = 6.10$) in **NS2**⁴⁺ (vs. in **2b**: $\delta = 6.93$) is clearly indicative of the formation of a heteroleptic complex as demonstrated earlier. Both, [**NS2**](PF₆)₄ and [**NS1**](PF₆)₄ display a single reversible Cu⁺/Cu²⁺ redox wave in cyclic voltammetry experiments ($E_{1/2} = 1.09$ VTPP and 1.12 VTPP, respectively. TPP = triphenylpyrylium), in line with the potentials of mononuclear heteroleptic copper(I) complexes. All our attempts to receive crystals of **NS1,b** suitable for X-ray analysis were met with failure. Such problems are well known for other metallocsupramolecular structures with a large void;⁷ those that can be obtained in a crystalline state usually exhibit voids <1000 Å³ and are most often filled with counter ions⁸ or are interpenetrating.⁹ Nevertheless, a complete characterisation was possible. As a first indication for the proposed structure we ascertained that the isotopic distribution patterns of **NS1,b**⁴⁺ matched the calculated compositions.

To further support our assignment and to rigorously exclude alternative catenated, oligomeric or polymeric complexes (e.g. [Cu₆(**2b**)₃(**3**)₃]⁶⁺), we investigated the sedimentation coefficient distribution using analytical ultra-centrifugation.¹⁰ Sedimentation velocity experiments in acetone at ambient temperature *showed clearly only one single species in solution* (Figure 3, solid line). From the density variation in two different solvents (acetone and d6-acetone) a dry molar mass of 5831 g mol⁻¹ was derived. This is in excellent agreement ($\pm 1\%$) with the calculated mass for [**NS2**](PF₆)₄ of 5772 g mol⁻¹. Moreover, the experimental hydrodynamic diameter of 4.2 nm (compare to 5.0 nm for Stang's cuboctahedron) correlates nicely with the calculated size of the box (the diagonal distance between two copper(I) centres amounts to 3.5 nm, the diagonal between two phenanthrolines to 4.7 nm, Figure 2a). From sedimentation velocity experiments a molecular mass for the solvated box of 19.8×10^3 g mol⁻¹ was obtained (Fig. 2, dotted line), which amounts to a solvation of 2.44 g g⁻¹. This means that the solvation of the box not only involves *240 molecules of acetone* but also accounts for 71% of the overall mass and for 80% of the volume. Knowing these numbers, the low tendency to form X-ray suited crystals is readily understood. The experimental volume of the solvated box **NS1** amounts to 38.8×10^3 Å³ that agrees nicely with the volume from MM+ calculations¹¹ (36.2×10^3 Å³). MM+ calculations of **NS1,2** predict an inner volume of 6×10^3 Å³, indicating that about 50 molecules of acetone fill the inner void (Figure 2b).

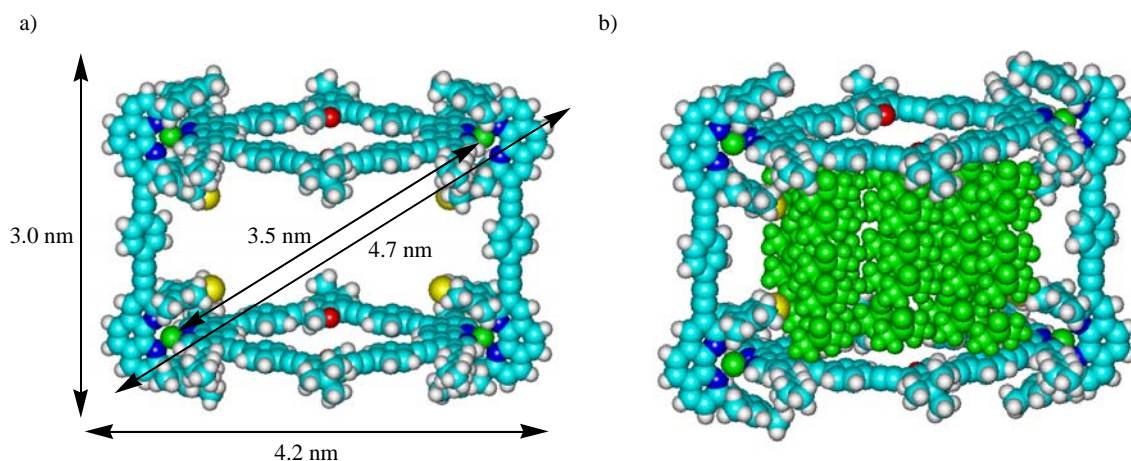


Figure 2. a) Hyperchem dimensions of NS1. (b) Hyperchem model of acetone (50 molecules) filled NS1.

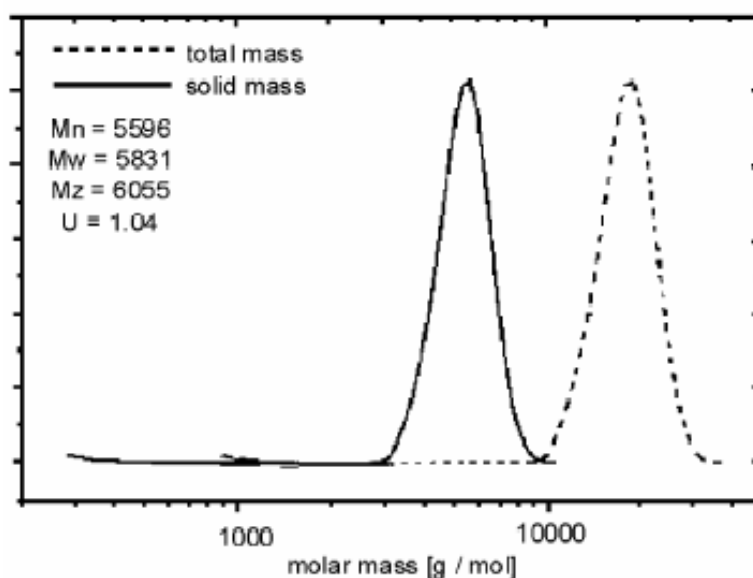


Figure 3. Determination of the molar mass of $[\text{NS2}](\text{PF}_6)_4$ in acetone in a sedimentation velocity experiment (solid line: dry weight; dotted line: weight of solvated box).

The tendency to form NS1,2^{4+} from its constituents is remarkable. When $[\text{NS2}](\text{PF}_6)_4$ was treated with trifluoroacetic acid, both the ESI-MS data and the loss of the red colour evidenced complete disintegration through protonation of the ligands. However, after addition of aqueous potassium hydroxide a red product reappeared, which dissolved in the dichloromethane layer. ESI-MS showed again the signal of NS2^{4+} .

Using the above procedure, the yellow silver(I) nanoboxes NS3,4^{4+} were also readily formed in quantitative yield from bisphenanthrolines **2a** or **2b**, **3** and AgPF_6 (2:2:4, respectively) as witnessed by ESI-MS and ^1H NMR data (Scheme 2). Because silver(I) phenanthroline complexes are usually less stable than the corresponding copper(I) complexes, we treated $[\text{NS3}](\text{PF}_6)_4$ (3.5 μmol) with CuI (14.7 μmol) at rt. The transformation NS3^{4+} to NS1^{4+} could

readily be followed by UV/Vis (disappearance of λ_{\max} (sh) = 389 nm) and by ESI-MS, as all intermediate $\text{Ag}_m\text{Cu}_n^{4+}$ complexes ($m+n = 4$) were observed by their characteristic mass signals. From the ESI signals at different times it appears that aggregates with m, n being even numbers are slightly favored thermodynamically, presumably because of cooperativity reasons. For example, after 90 min the various species were: NS3^{4+} (26%), $[\text{Ag}_3\text{Cu}(\mathbf{2b})_2(\mathbf{3})_2]^{4+}$ (23%), $[\text{Ag}_2\text{Cu}_2(\mathbf{2b})_2(\mathbf{3})_2]^{4+}$ (51%), but no $[\text{AgCu}_3(\mathbf{2b})_2(\mathbf{3})_2]^{4+}$. After 24 h NS1^{4+} was the only species present in solution. The silver box NS3^{4+} can be regenerated from NS1^{4+} in the presence of cyanide and excess Ag^+ (Figure 4).

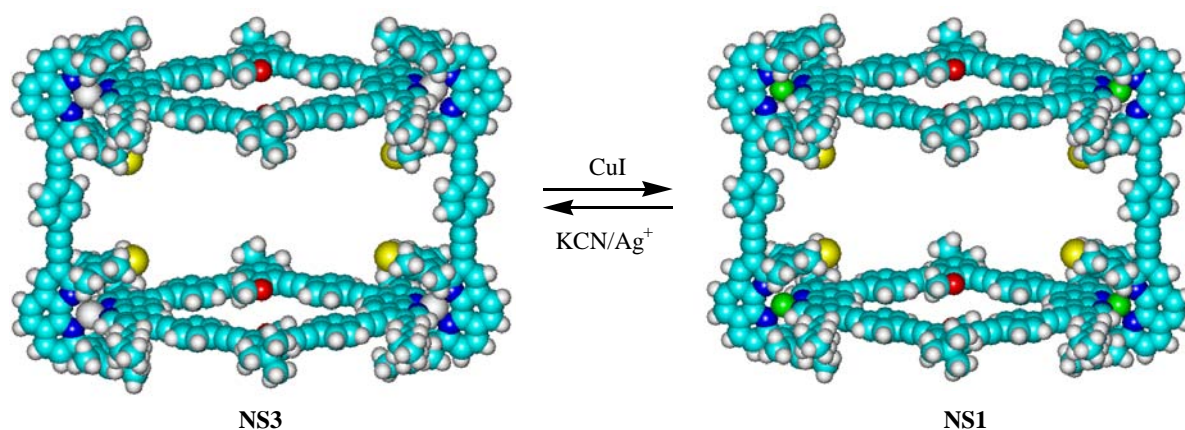


Figure 4. Hyperchem models of transmetalation experiment.

In conclusion, only a combination of the HETPHEN concept with maximum site occupancy and cooperativity allows to establish a quantitative self-assembly process in solution for copper phenanthroline nanoboxes. The large void aggregates are unambiguously characterized by ESI, NMR and ultra-centrifuge/light scattering techniques. From the size of the inner void ($6 \times 10^3 \text{ \AA}^3$) it is clear that in contrast to smaller analogous systems any templating effects by counter ions can be excluded. The large cavity of these boxes is ideally suited for future internal functionalisations. The unprecedented conversion of the Ag_4^{4+} to Cu_4^{4+} nanobox convincingly underlines the reliability, robustness and flexibility of our approach.

ACKNOWLEDGMENT: We would like to express our gratitude to the Deutsche Forschungsgemeinschaft, the Fonds der Chemischen Industrie, and Dr Schilling for the ultracentrifuge experiments.

References:

- (1) Recent books covering this wide field, see: (a) J.-M. Lehn, *Supramolecular Chemistry, Concepts and Perspectives*, VCH, New York, **1995**. (b) J. W. Steed and J. L. Atwood, *Supramolecular Chemistry*, Wiley, Chichester, **2000**.
- (2) M. Schmittel, V. Kalsani, *Top. Curr. Chem.* **2005**, *245*, 1-53 and ref's therein.
- (3) R. Colton, B. D. James, I. D. Potter, J. C. Traeger, *Inorg. Chem.* **1993**, *32*, 2626.
- (4) (a) A. Harriman, J.-P. Sauvage, *Chem. Soc. Rev.* **1996**, 41. (b) C. Dietrich-Buchecker, G. Rapenne, J.-P. Sauvage, *Coord. Chem. Rev.* **1999**, *185-186*, 167. (c) C. Dietrich-Buchecker, G. Rapenne, J.-P. Sauvage, A. De Cian, J. Fischer, *Chem. Eur. J.* **1999**, *5*, 1432.
- (5) (a) P. N. W. Baxter, J.-M. Lehn, B. O. Kneisel, G. Baum, D. Fenske, *Chem. Eur. J.* **1999**, *5*, 113. (b) A. M. Garcia, D. M. Bassani, J.-M. Lehn, G. Baum, D. Fenske, *Chem. Eur. J.* **1999**, *5*, 1234.
- (6) (a) M. Schmittel, A. Ganz, *Chem. Commun.* **1997**, 999. (b) M. Schmittel, U. Lüning, M. Meder, A. Ganz, C. Michel, M. Herderich, *Heterocycl. Commun.* **1997**, *3*, 493.
- (7) B. Olenyuk, J. A. Whiteford, A. Fechtenkötter, P. J. Stang, *Nature* **1999**, *398*, 796.
- (8) C. J. Kuehl, S. D. Huang, P. J. Stang, *J. Am. Chem. Soc.* **2001**, *123*, 9634.
- (9) G.-F. Liu, B.-H. Ye, Y.-H. Ling, X.-M. Chen, *Chem. Commun.* **2002**, 1442.
- (10) (a) J. Shen, J. Brodbelt, *J. Am. Soc. Mass. Spectrom.* **1998**, *10*, 126. (b) D. Schubert, C. Tzatzios, P. Schuck, U. S. Schubert, *Chem. Eur. J.* **1999**, *5*, 1377.
- (11) Molecular modeling is based on MM + , implemented in Hyperchem@.

Supp 5-3

Heteroleptic Bisphenanthroline Metallo-Nanoscaffolds – A Model Case for the Solution State Characterization of Supramolecular Nano-Edifices

Michael Schmittel,^{*a} Venkateshwarlu Kalsani,^a Andreas Wiegrefe,^a Christoph Michel,^a

^a *Center of Micro and Nanochemistry and Engineering, Organische Chemie I, Universität Siegen, Adolf-Reichwein-Str., D-57068 Siegen, Germany.*

Abstract. As supramolecular chemistry is expanding to nanoscale structures, it becomes increasingly important to have at hand variable and robust self-assembly protocols as well as reliable characterisation techniques. Herein, we describe the difficulties with the solid state structure elucidation of metallo-nanoscaffolds with large voids and lay out a battery of both direct and indirect solution state characterisation methods using ESI MS, ¹H NMR and UV/vis spectroscopy. These methods along with the conventional direct methods provide very useful tools to characterise nanoscaffold aggregates.

Introduction

While the development of self-assembly protocols to provide reliable access to supramolecular structures has been a major focus of the last two decades,¹ there is now growing interest to engineer aggregates at the > 3 nm scale. Leading pioneers in the area, such as Stang,² Lehn,³ Newkome,⁴ Reinhoudt,⁵ Fujita⁶ and others,⁷ for example have reported on sparkling nanoscale architectures, such as polygons/polyhedra and rosette aggregates. Despite this progress, it is well evident that there is still a rather limited number of discrete assemblies of > 3 nm size reported in the literature. Quite often this is due to problems with their characterisation, in particular in the solid state. Due to the large size and huge voids, that often bring along a multitude of disordered solvent molecules, X-ray suitable single crystals and hence diffraction data are difficult to obtain.^{2,3,4,5,7} Therefore solution state techniques (NMR, diffusion NMR spectroscopy,⁸ mass spectrometry and UV/vis) have become methods of choice to characterise nanoscale aggregates. In a few cases, vapor-phase osmometry has also

been used, but this technique is quite limited due to the required large sample concentration and low molecular mass range.⁹ As a supplementary technique, scanning probe microscopy techniques and high resolution TEM (HRTEM) have also shown some utility.¹⁰

In the following, we will describe our experience with the characterisation of dynamic heteroleptic nanoscale aggregates. Apart from conventional NMR and mass spectrometric characterisation, we outline the use of analytical ultracentrifugation to elucidate the structure, the size and the solvent content of the proposed nanoedifices.¹¹ Further control experiments, such as oxidation, ligand/metal exchange studies, and size selectivity phenomena were performed to increase our understanding of the proposed structures. Using a fruitful combination of ESI MS and UV/vis spectrometry, we were able to characterize three intermediates on the way to the final assembly.

Results and Discussion

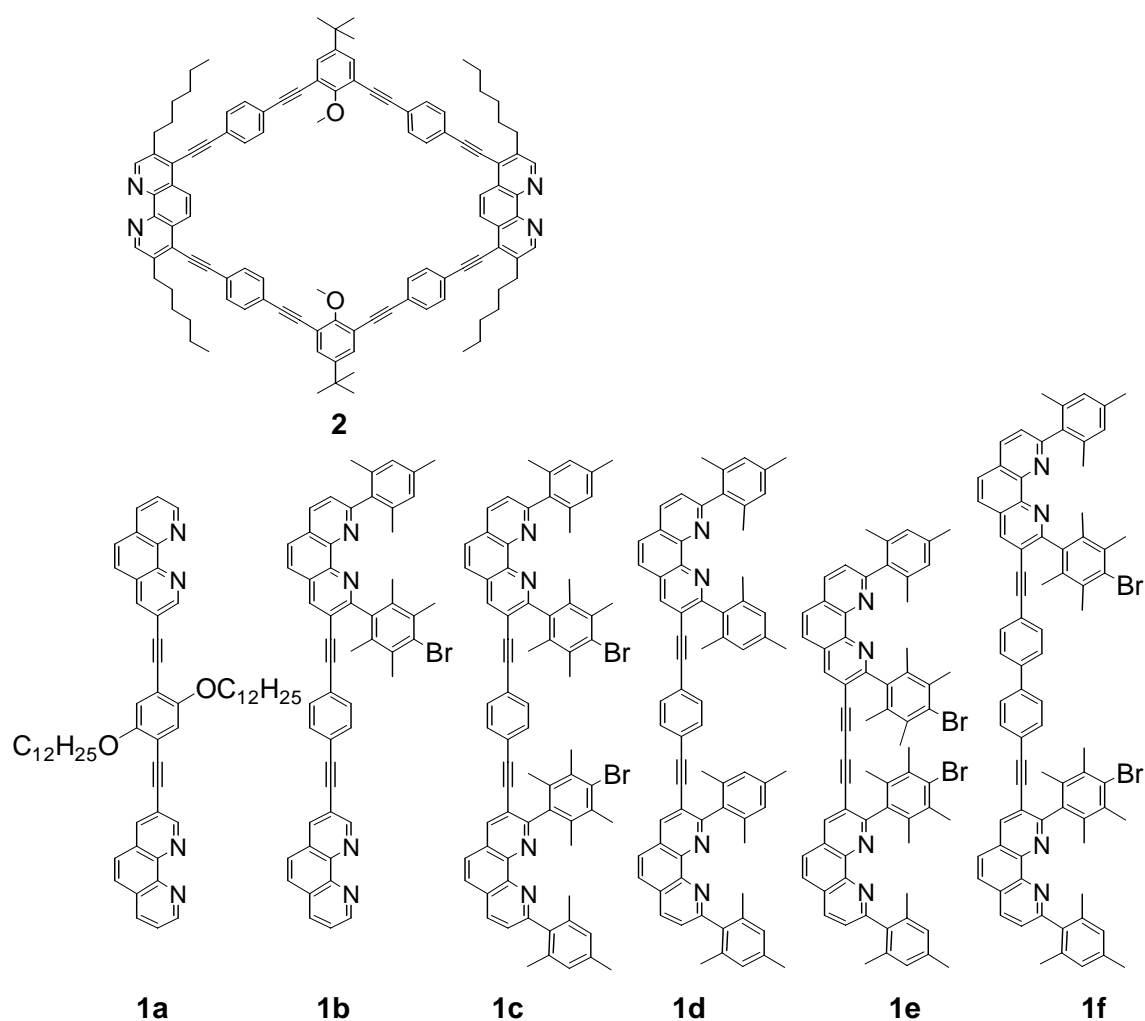
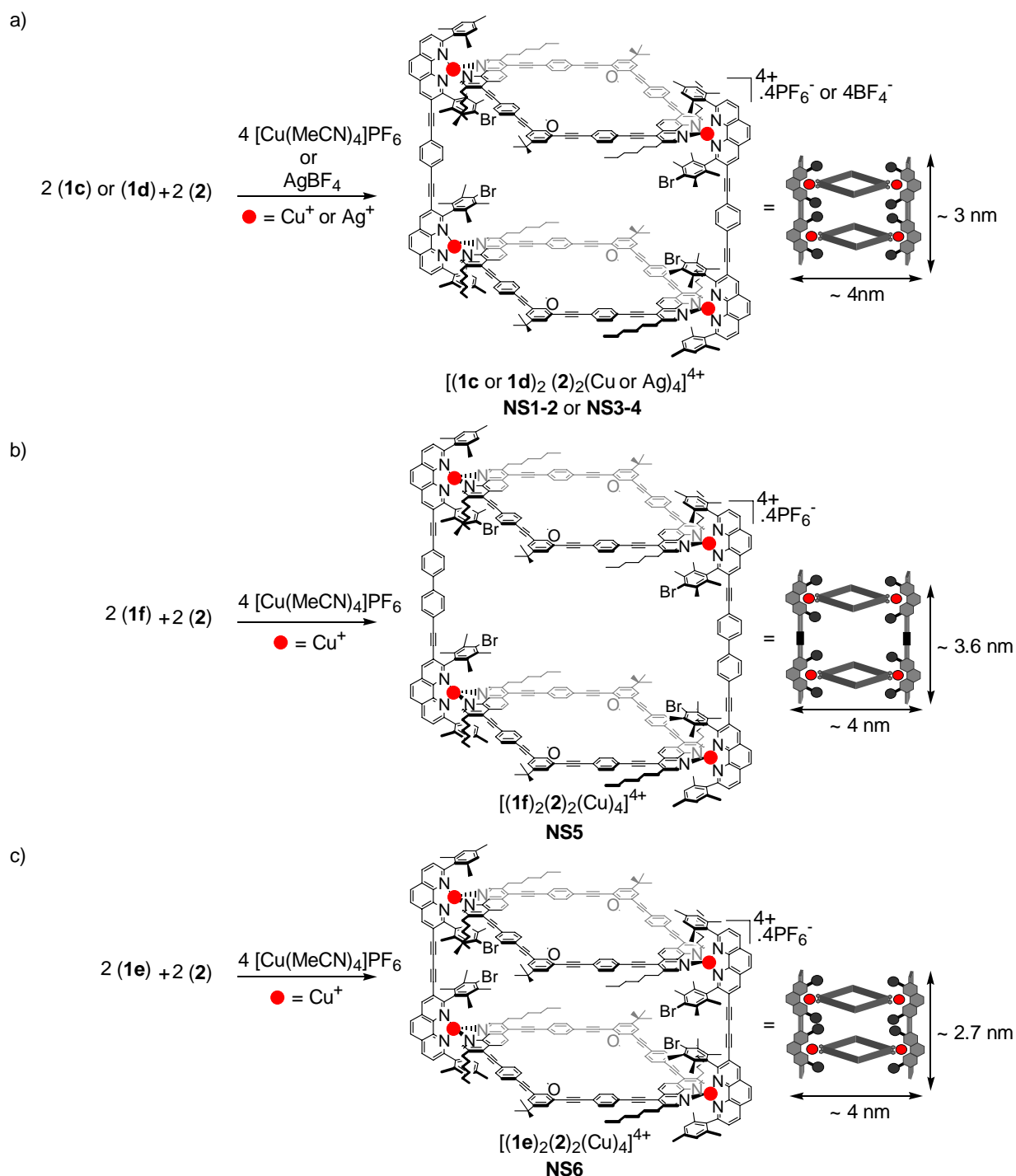


Chart 1. Ligands used for programming heteroleptic nanoscaffolds.

Recently, we have demonstrated the utility of the HETPHEN¹² approach to construct nanoscale devices. Complexation of **1a** or **1b** and **2** (Chart 1) in presence of appropriate metal ions such as Cu(I) or Ag(I) was expected to yield nanoscale heteroleptic metallo-assembly such as those depicted in Scheme 1. However, the assembly of **1a** or **1b** and **2** with Cu(I) afforded a variety of homoleptic and heteroleptic combinations. It seems to be clear that there is need of additional control to drive this equilibrium toward a single heteroleptic nanostructure.

Self-Assembly of Nanoscaffolds and their Characterisation

Ligand **1c-1f** designed according to the HETPHEN concept - were explored for the quantitative formation of heteroleptic aggregates. As demonstrated earlier,¹¹ mixing **1c** or **1d** and Cu(I) with **2** resulted in the formation of the dark red solid nanoscaffolds **NS1** and **NS2** in virtually quantitative yield (scheme 1a). The assemblies proved to be stable for more than a year and soluble in variety of solvents, such as dichloromethane, acetonitrile, nitromethane, dimethylformamide and dimethylsulfoxide. ¹H NMR spectra exhibited a single set of sharp signals indicative of a highly symmetric species. As already seen earlier in analogous mononuclear complexes, the mesityl protons in **NS1**, **NS2** showed a characteristic high field shift from ~7 to 6~ppm, characteristic for heteroleptic complex formation. Similar results were obtained for the silver nanoscaffolds, where mesityl protons experienced high field shifts from ~7 to ~6.2 ppm. **NS5** and **NS6** were prepared along the same procedures (Scheme 1b-c, see experimental section).



Scheme 1. Metal mediated self-assembly of nanoscaffolds, NS1-6.

UV/vis spectroscopy

The absorption spectra of the heteroleptic nanoscaffolds **NS1**, **NS2** are depicted in Figure 1. The strong absorption bands at 250-400 nm correspond to ligand π - π transitions,¹³ whereas the absorption band at 491 nm was assigned to the metal-to-ligand-charge-transfer (MLCT) that is responsible for their red colour. For both complexes the MLCT band is almost identical, what is indicative of a very similar environment at the metal centres in both

assemblies. Moreover, the absorptions are very much similar to those of analogous Cu(I) heteroleptic assemblies.¹⁴ The MLCT bands in the visible region at $\lambda = 484$ nm ($\epsilon_{\text{max}} = 27280$ for **NS1** and ($\epsilon_{\text{max}} = 27720$ M⁻¹ cm⁻¹ for **NS2**, respectively) account for four Cu(I) ions and are thus in good agreement with the proposed compositions. Analogous copper complexes show a $\epsilon_{\text{max}} = 7000\text{-}8000$ M⁻¹ cm⁻¹ for one copper centre.^[15]

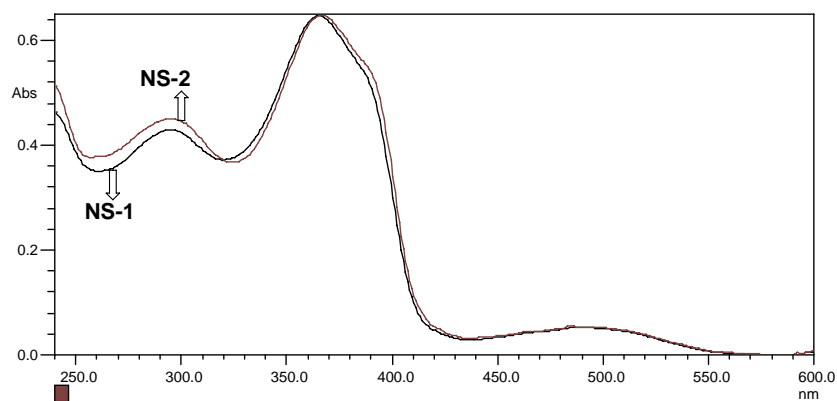


Figure 1. UV/vis spectra of **NS1** and **NS2** in dichloromethane at room temperature. $[M]^{+4} = 4.4 \times 10^{-6}$ M.

Analytical Ultracentrifugation analysis of **NS2**

Stang and others¹⁶ have utilised ¹H NMR diffusion experiments to investigate the hydrodynamic radius of nanoscale aggregates. In contrast, analytical ultracentrifugation can provide much more detailed information as will be shown below. Though it has recently become a recommended technique to study the solution integrity of metallocsupramolecular assemblies,¹⁷ very few reports are known utilising this method. Such investigations are very useful not only to obtain the molar mass and hydrodynamic radius of the aggregates but also to gather important information about number of solvent molecules associated with supramolecular aggregates.

The sedimentation velocity experiments of **NS2** in acetone using analytical ultracentrifugation further supported our assignment. At ambient temperature they showed clearly only one single species in solution (Figure 2, solid line). From the density variation in two different solvents (acetone and d₆-acetone) a dry molar mass of 5831 g mol⁻¹ was derived. This is in excellent agreement ($\pm 1\%$) with the calculated mass for **NS2** of 5772 g mol⁻¹. Moreover, the experimental hydrodynamic diameter of 4.2 nm is in excellent agreement with the calculated size of the box (the diagonal distance between two copper(I) centres amounts to 3.5 nm, the diagonal between two phenanthrolines to 4.7 nm). From sedimentation velocity experiments a molecular mass for the solvated box of 19.8×10^3 g mol⁻¹ was obtained (Figure

5, dotted line) that amounts to a solvation of 2.44 g/g. This indicates that the solvation shell of the box not only involves 240 molecules of acetone but in addition accounts for 71% of the overall mass and for 80% of the volume. Knowing these numbers, the low tendency to form X-ray suited crystals is readily understood. The experimental volume of the solvated box [NS2] amounts to $38.83 \times 10^3 \text{ \AA}^3$ agreeing nicely with the volume from MM⁺ calculations ($36.23 \times 10^3 \text{ \AA}^3$). MM⁺ calculations of [NS1] and [NS2] predict an inner volume of $6 \times 10^3 \text{ \AA}^3$, suggesting that about 50 molecules of acetone fill the inner void.

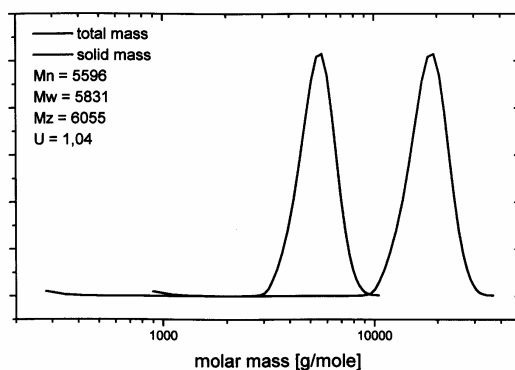


Figure 2. Molecular weight determination by sedimentation velocity experiment.

MM⁺ Calculations

MM⁺ calculations were performed to visualise the dimensions of the nanoscaffolds.¹⁸ The minimised space filling models of NS1, NS5 and NS6 are displayed in Figure 3. In, NS5, the external dimensions are $\sim 3.6 \text{ nm}$ along **1f** axis (height) and $\sim 4 \text{ nm}$ along **2** (width).

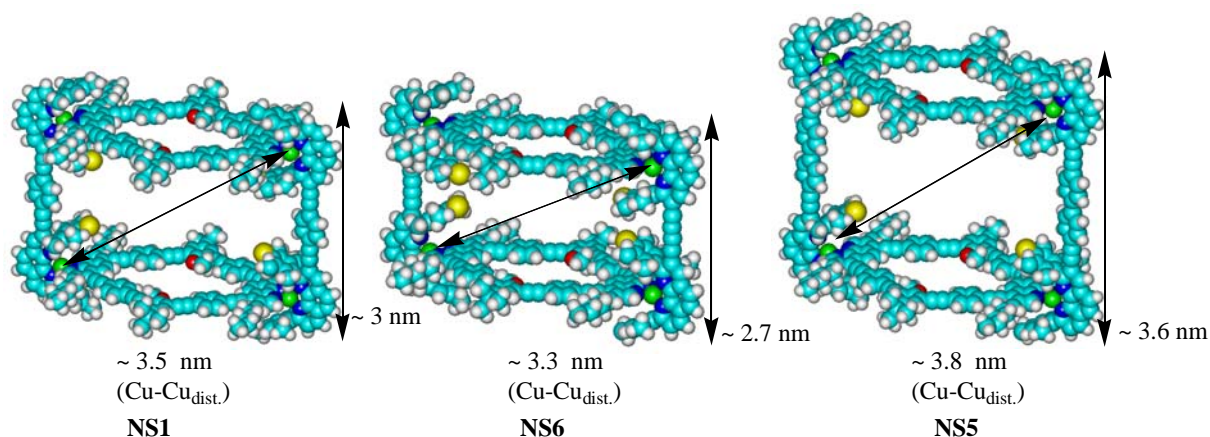


Figure 6. MM⁺ minimised space filling representations of NS1, NS5 and NS6.

Mass spectrometric (ESI MS) characterisation

ESI MS has been the method of choice to elucidate metallo-supramolecular structures in solution.¹⁹ ESI MS analysis of NS1, NS2 confirmed the proposed hetero aggregate

structures, composed out of 2 linear ligands (**1c** and **1d**), 2 macrocycles (**2**) and 4 copper(I) ions. No fragments were observable, even at higher voltages, indicative of a high stability of these assemblies. For example, an analysis of the hexafluorophosphate salt of **NS1** furnished signals corresponding to $[\text{NS1} - 4 \text{PF}_6]^{4+}$ and $[\text{NS1} - 3 \text{PF}_6]^{3+}$ centred at $m/z = 1391$ and 1903 Da, respectively. The experimental isotopic distributions are in excellent agreement with the calculated distributions (Figure 3, 4). Similar results were obtained for all other nanoscaffolds. Elemental analysis of all assemblies was in good agreement with the proposed composition.

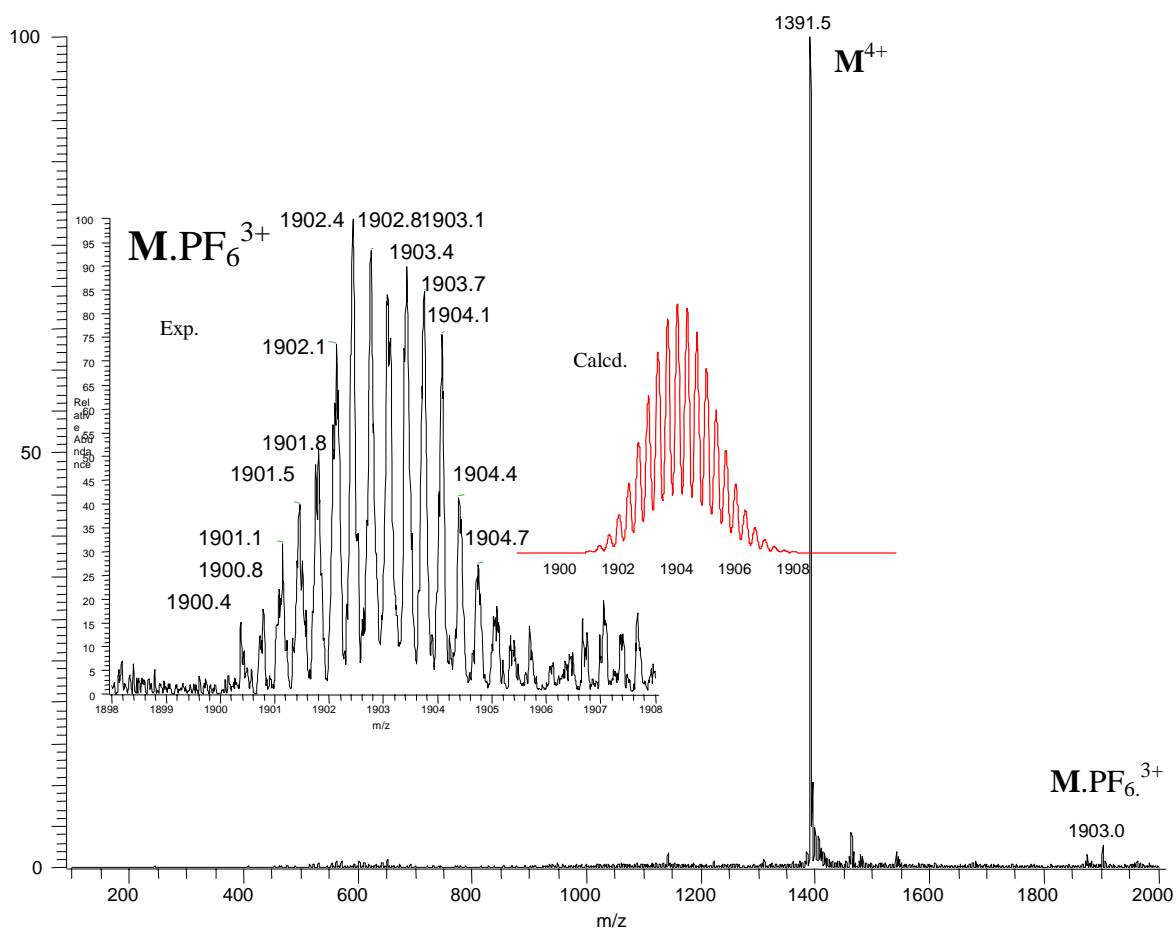


Figure 3. ESI MS of **NS1**. The inset shows the experimental isotopic distribution for the 3+ charged species along with its calculated one.

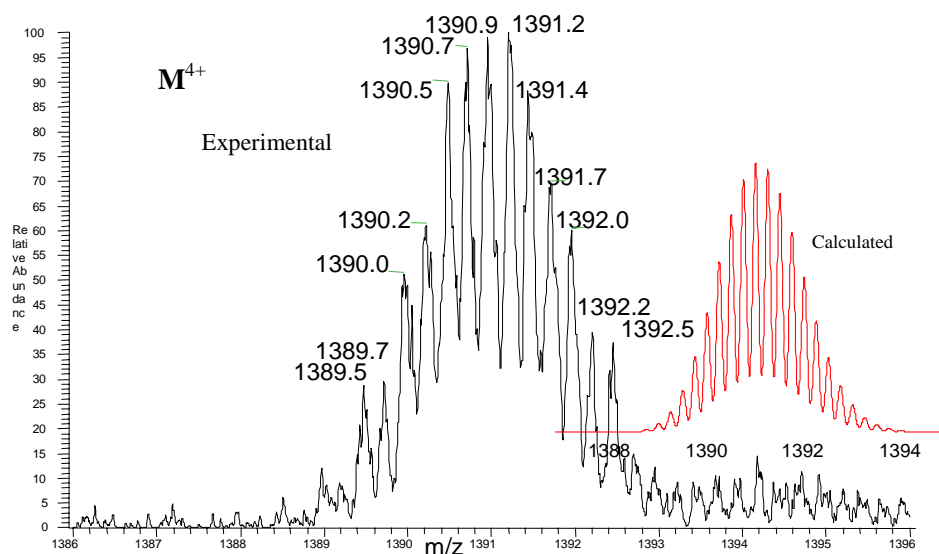


Figure 4. ESI MS of NS1. Experimental isotopic distribution for the 4+ charged species along with its calculated one.

The ESI MS assignments were further confirmed by collisional fragmentation experiments. Fragmentation of $NS1^{3+}$ produced the signal corresponding to $[Cu_2(\mathbf{1c})(\mathbf{2})]^{2+}$ with its isotopic distribution being in good agreement with the proposed composition (Figure 5).

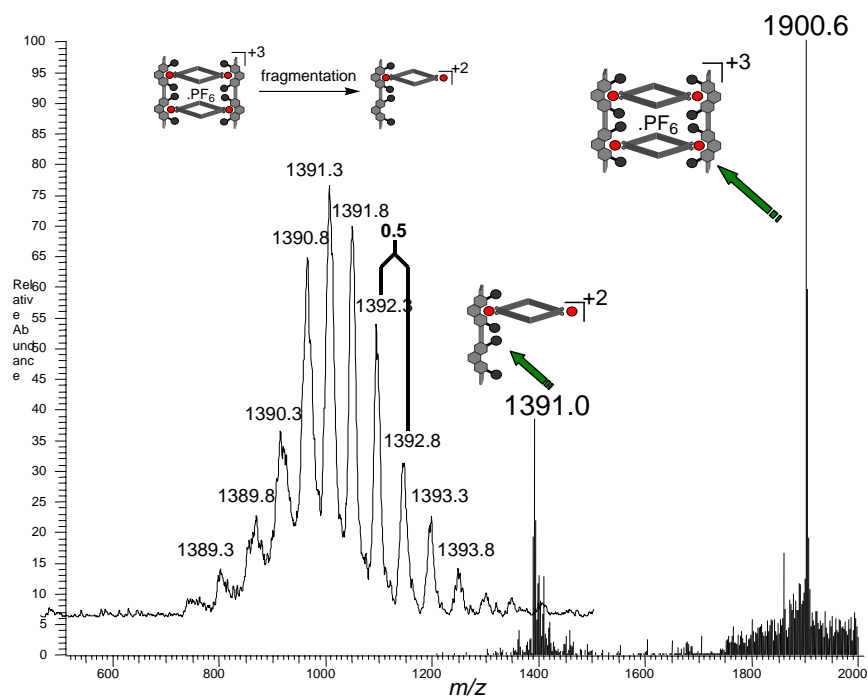


Figure 5. Collisional fragmentation of NS1. The inset shows the experimental isotopic distribution of the fragmented centred at $m/z = 1391$.

Control Experiments Studied by ESI MS and/or UV-vis

In the above section, the nanoscaffolds were characterised by standard techniques such as ^1H NMR, ESI MS, and UV/vis spectroscopies. In addition, analytical ultracentrifugation technique was used to understand their structure and solvation. In the following, we describe the use of indirect methods to further support the proposed nanoscaffold structures. For example, we have carried out investigations such as chemical oxidation of the nanoscaffolds, metal/ligand exchange studies, and size selectivity experiments.

D) Chemical Oxidation

NS1 and NS2 displayed a single reversible wave for the $\text{Cu}^+/\text{Cu}^{2+}$ redox couple in cyclic voltammetry experiments (at $E_{1/2} = 1.09 \text{ V}_{\text{TPP}}$ and $1.12 \text{ V}_{\text{TPP}}$, respectively. TPP = triphenylpyrylium), that are in line with redox potentials of analogous Phen-Cu(I)-Phen systems.²⁰ Oxidation in combination with ESI MS can now be used to interrogate the composition of the aggregates. For this purpose, a mixture of $\text{NS2}^{5+/6+/7+/8+}$ was generated through the successive addition of tris(*p*-bromophenyl) aminium hexachloroantimonate as a one-electron oxidant to effect the Cu(I) to Cu(II) oxidation. Depending on the amount of oxidant, the ESI-MS spectra showed all signals for $\text{NS2}^{5+/6+/7+/8+}$. The highly charged boxes ($> 4+$) were always associated with chloride ions stemming from the hexachloroantimonate (Figure 6). The found signals confirm the composition assigned to NS2. Most importantly, however, signals of oligomeric complexes could not be detected. These experiments also hint the potential use of these nanoscaffold structures as redoxactive hosts for large anionic structures.

Tabelle 1: Signals detected by ESI MS when NS2 $[\text{Cu}_4(\mathbf{1d})_2(\mathbf{2})_2(\text{PF}_6)_4]$ was oxidised with Tris(*p*-bromophenyl)aminium-hexachloroantimonat.

complex	calculated mass <i>m/z</i>	obtained mass <i>m/z</i> (%)
$[\mathbf{M} - 4 \text{ PF}_6 + 4(\text{Cl}^-)]^{4+}$	1333.6	1333.5 (100)
$[\mathbf{M} - 4 \text{ PF}_6 + 3(\text{Cl}^-)]^{4+}$	1324.8	1325.7 (36)
$[\mathbf{M} - 4 \text{ PF}_6 + 2(\text{Cl}^-)]^{4+}$	1315.9	1316.1 (32)
$[\mathbf{M} - 4 \text{ PF}_6 + (\text{Cl}^-)]^{4+}$	1307.1	1307.1 (8)
$[\mathbf{M} - 4 \text{ PF}_6 + 2(\text{TFA}^-)]^{4+}$	1354.7	1354.7 (32)
$[\mathbf{M} - 4 \text{ PF}_6 + 3(\text{TFA}^-)]^{4+}$	1383.0	1383.8 (4)

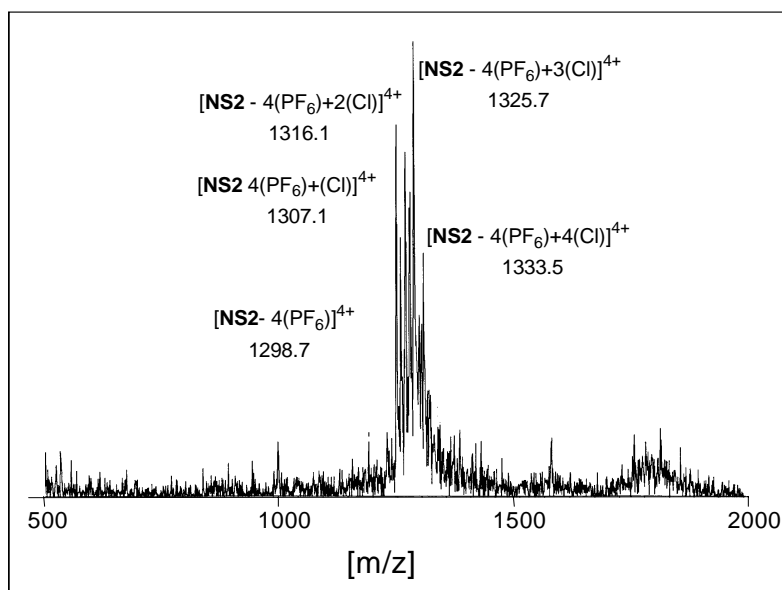
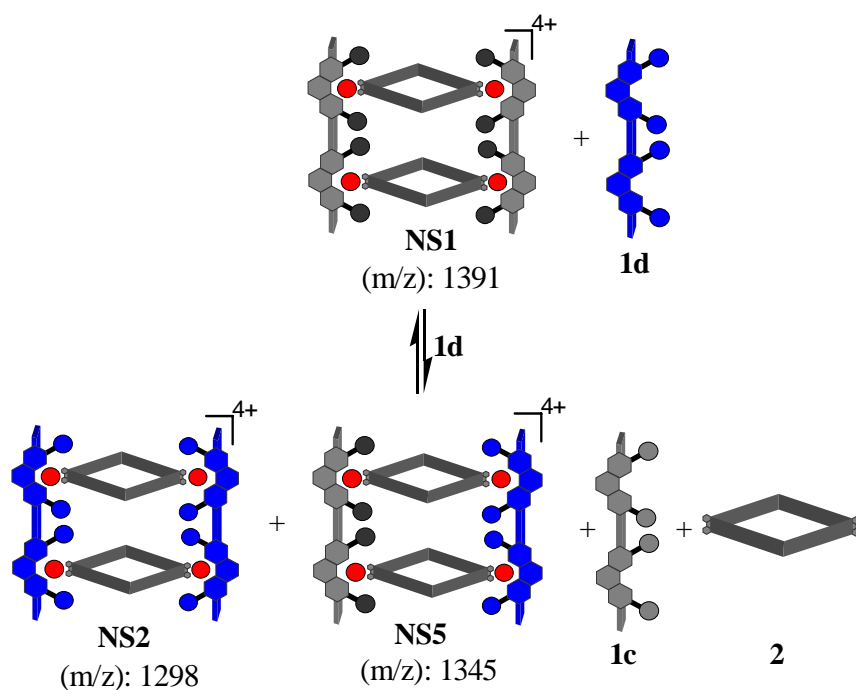


Figure 6. ESI MS after the chemical oxidation of NS2.

II) Ligand Exchange studies by ESI-MS

In thermochemically controlled self-assembly procedures exchange processes between competing topologies (*e.g.* cyclic *vs.* linear oligomers) are essential in order that the system can finally reach the most stable state. Interestingly, such exchange studies have rarely been used to support the suggested supramolecular structure.²¹ Insight into the nature of the exchange process of different nanoscaffolds **NS1**, **NS2** should provide information about the reversibility of the assembly pathway and additional structural insight into the aggregates. Hence, we decided to monitor the ligand exchange between **NS1** and ligand **1d** by using ESI MS. Ligand **1d** has the same length as the ligand **1c** and differs only at the steric stoppers of the linear bisphenanthroline. As **1c** and **1d** have different molecular weights, they should be well-suited for a study of the non-self recognition process by ESI MS techniques.

In an experiment, ligand **1d** and **NS1** were reacted in a 1:1 stoichiometry in dry dichloromethane. The ligand exchange processes were readily observed (after 5 min) by characteristic signals corresponding to a mixture of three boxes **NS1**, **NS2** and **NS5** (in m/z (%) = 100, 12 and 15, respectively) that are in equilibrium with each other (Scheme 2). All signals corresponding to scaffolds were isotopically resolved (Figure 7). Similar results were also obtained after the addition of 2 eqs. of ligand **1d** to **NS1** in dichloromethane. In presence of excess of ligand **1d** (6 eqs with respect to **NS1**) the boxes disassembled to furnish exclusively the monomeric building blocks.



Scheme 2: Schematic representation of products formed in the exchange equilibrium after mixing **NS1** with the linear ligand **1d**.

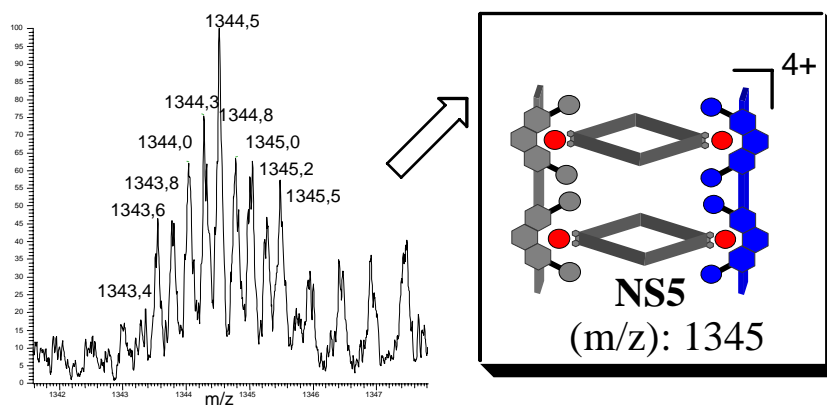


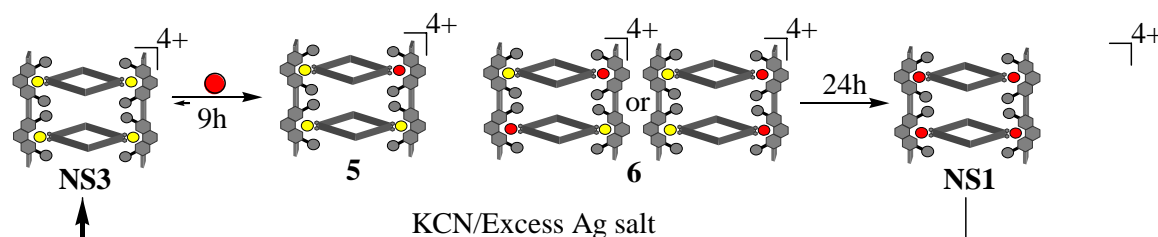
Figure 7: Isotopic distribution of the mixed box NS5^{4+} with $(\text{m/z}) = 1345$ Da.

These results clearly support the notion of the dynamic nature of the nanoscaffolds **NS1**, **NS2**. It is also clear that the absence of any other hetero nanoscaffold combinations in the ESI MS further supports the compositions proposed for **NS1-5**.

III) Metal Exchange Studies

Previous reports by Sauvage *et al.* have demonstrated the potential of metal exchange to effect motions in catenanes and rotaxanes.²² However, up to date such exchange studies have not been explored to confirm supramolecular structures and to provide insight into the mechanism of the dynamic processes. Herein, we present metal-exchange studies with **NS3**.

The silver nanoscaffolds **NS3** or **NS4** were obtained quantitatively by treating **1c** or **1d** and **2** with AgBF_4 . The resulting silver complexes were characterized by ESI MS, ^1H NMR, UV/vis and elemental analysis. Surprisingly, these silver complexes proved to be stable even after exposing them to atmosphere for several weeks. Since, silver complexes proved to be less stable than the corresponding copper complexes, the silver nanoscaffold **NS3** was readily converted to the copper nanoscaffold **NS1** upon addition of $[\text{Cu}(\text{MeCN})_4\text{PF}_6]$ in dichloromethane or CuI in acetonitrile (Figure 8). With CuI in dichloromethane crucial information about the possible intermediates could be smoothly extracted through ESI MS and UV/vis spectrometric investigations over a period of 24 h. ESI MS showed signals corresponding to all possible compositions: *e.g.*, after 90 min the various species detected were **NS1** (26%), $[\text{Ag}_3\text{Cu}(\mathbf{1c})_2(\mathbf{2})_2]^{4+}$ (**5**) (23%), $[\text{Ag}_2\text{Cu}_2(\mathbf{1c})_2(\mathbf{2})_2]^{4+}$ (**6**) (51%), but no $[\text{AgCu}_3(\mathbf{1c})_2(\mathbf{2})_2]^{4+}$. After 24 h **NS1** was the only species present in solution (Figure 8). The all silver species **NS3** could be regenerated by treating **NS1** with cyanide and excess $\text{Ag}(\text{I})$ salt. UV/vis provided equally a clear proof for the conversion as shown by the appearance of the MLCT band at ~ 500 nm (Cu-Phen-Cu) at the expense of λ_{max} (sh) = 389 nm (Ag-Phen-Ag). This inter-conversion also demonstrates the reversible nature of these assemblies.



Scheme 3. Cartoon representation of transmetalation experiment.

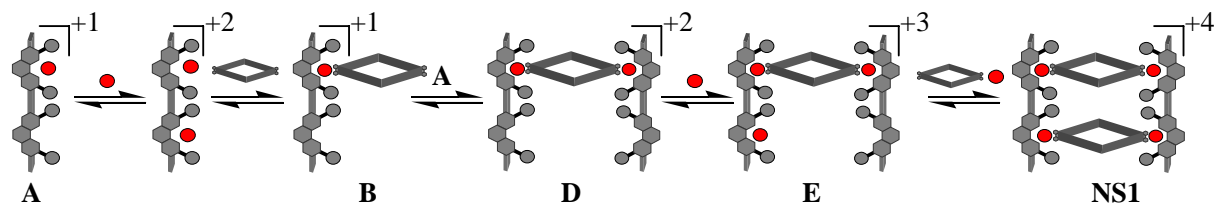
into the non-self-recognition interactions when two different ligands assemble together by means of metal-ion coordination. Since one of the ligands used in this study is able to form also a homoleptic assembly, the quantitative formation of a heteroleptic nanoscaffold should be the result of cooperativity. Very few reports about mechanistic pathways of self-assembled systems²³ are at hand, and investigations into nanoscale assemblies is even more rare.²⁴

NS1 was chosen for a detailed study using a combination of ESI and spectrophotometric titrations. Whereas the ESI MS studies provided the qualitative information about possible intermediates, the thermodynamic parameters of the intermediates and the nanoscaffold were obtained from spectrophotometric titrations. The spectrophotometric data were processed by the SPECFIT program,²⁵ which uses the factor analysis to reduce the absorption matrix and to extract the eigenvectors prior to the multiwavelength fit of the reduced data set according to the Marquardt algorithm.²⁶ Models that do not fit in the data were rejected. From the obtained association constants distribution curves were computed using the Haltafall program.²⁷

ESI MS Investigations ESI MS has been used as a powerful tool to identify the composition of intermediate species of metallo-self-assembly processes. Measurements were carried out in dichloromethane due to solubility reasons and to avoid any competitive coordination with the solvent.²⁸ At first a series of ESI MS titration experiments was carried out to obtain a qualitative road map of the intermediates on the way to the nanoscaffold assembly. Measurements were done after the spectra recorded were persistent with time thus assuring that complete thermodynamic equilibration had been achieved.

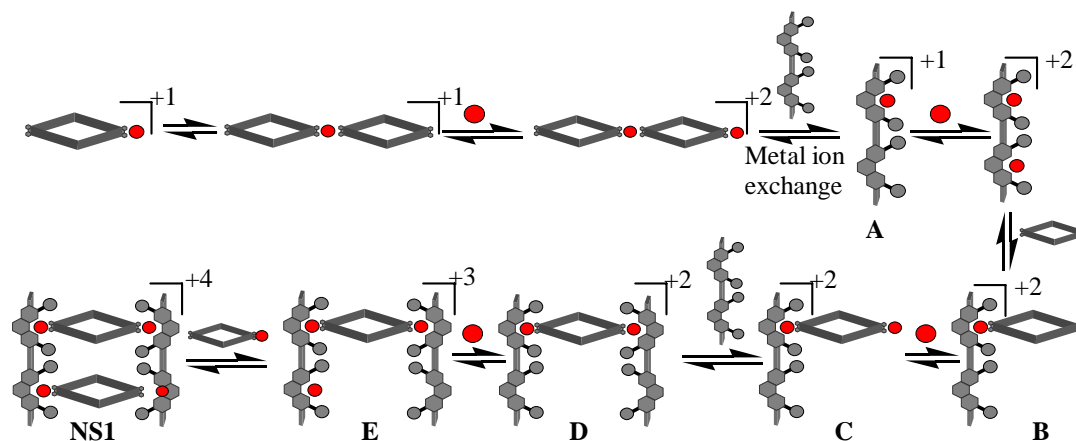
a) ESI-MS titration of 1c and Cu(I) by macrocycle 2. In a first series of experiments, **1c** (8.7×10^{-5} M) and Cu(I) (1.7×10^{-4} M) were titrated with aliquot amounts of **2** in 10 additions. Excess addition of **2** did not affect the nanoscaffold. During the course of the titration six intermediates were observed apart from the final nanoscaffold as depicted in Scheme 4. As the titration proceeded, signals corresponding to the nanoscaffold increased. After the final addition the spectrum contained only signals corresponding to the desired nanoscaffold. All intermediates were clearly identifiable through their m/z ratio, their isotopic splitting pattern and their collisional fragmentation processes. Equally, intermediates were searched with SPECFIT program using the spectrophotometric titration data. Only intermediates that agreed with the spectrophotometric data were taken into account. During the titration no oligomeric combinations were detected.

It became clear from the data that no homoleptic complexes of **1c** were formed during the whole titration process, highlighting the control exerted by the HETPHEN ligands in preparing heteroleptic assemblies. The observed data clearly point to a multistep assembling of nanoscaffold **NS1**. Ligand **1c** was always found associated with the metal ion, due to a stabilizing cation- π interactions between the metal ion and the aromatic groups in 2,9-positions.



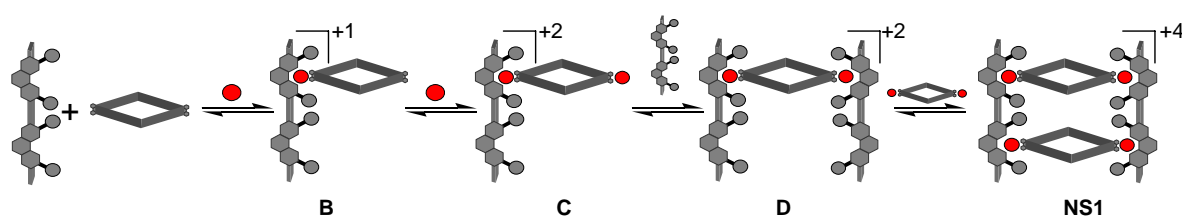
Scheme 4. Proposed intermediates (cartoon representation) for the species in assembly process when **1c** and Cu(I) were titrated with **2**.

b) ESI-MS titration of **2 and Cu(I) with **1c**.** The second set of experiments was carried out by the titration of **2** and Cu(I) salt with aliquot amounts of **1c** in dichloromethane. A total of one equivalent of **1c** was added in 10 additions. Here too, the excess addition of **1c** did not alter the finally furnished **NS1**. The analysis of the data indicated that even though $[\text{Cu}_n(\mathbf{2})_2]^{n+}$ ($n = 1,2$) was present at the initial stage of the titration, these homoleptic structures disassembled to furnish the nanoscaffold assembly as soon as **1c** was added (Scheme 5). In this titration, we were able to detect 8 intermediates apart from the final nanoscaffold. As the titration proceeded the signals corresponding to the nanoscaffold increased with the final spectrum only containing signals corresponding to the nanoscaffold. Interestingly, apart from $[\text{Cu}_n(\mathbf{2})_2]^{n+}$, that is present prior to addition of **1c**, the same intermediates were observed in both titrations. All the signals were in good agreement with their isotopic splittings.



Scheme 5. Proposed structures for the intermediate species on the way to the nanoscaffold assembly.

c) **ESI-MS titration of 2 and 1c with Cu(I) salt solution.** Finally, in a third titration, **2** and **1c** were titrated with Cu(I) in dichloromethane (Scheme 6). The analysis of the data emphasised the high affinity of the **1c** towards metal ion coordination. Otherwise, the intermediates were the same as in the titrations above (Figure 9). All suggested structures were in accordance with their isotopic splittings. A signal centred at $m/z = 1961$ Da was assigned to species **D**. Collisional fragmentation of **D** yielded species **C** with all signals showing the expected isotopic distributions. Intermediate **C** and the nanoscaffold have the same m/z value (1391 Da) but differ in their isotopic splitting. Model **C** is a 2+ charged species, whereas **D** contains four positive charges. Because of the largely reduced number of intermediates in titration c, this procedure (with Cu(I) salt as a titrant) was used for the spectrophotometric titrations.



Scheme 6. Suggested intermediates in the titration of **1c** and **2** with Cu(I) salt.

In conclusion, ESI-MS titrations allowed to identify possible intermediates in the self-assembly of **NS1**. Mechanistically, the assembly steps proved to be very similar independent of the type of titration except for the starting situation. Mainly four intermediates (**A**, **B**, **C**, **D**) were observed in all three titrations that were carefully assigned (Figure 10).

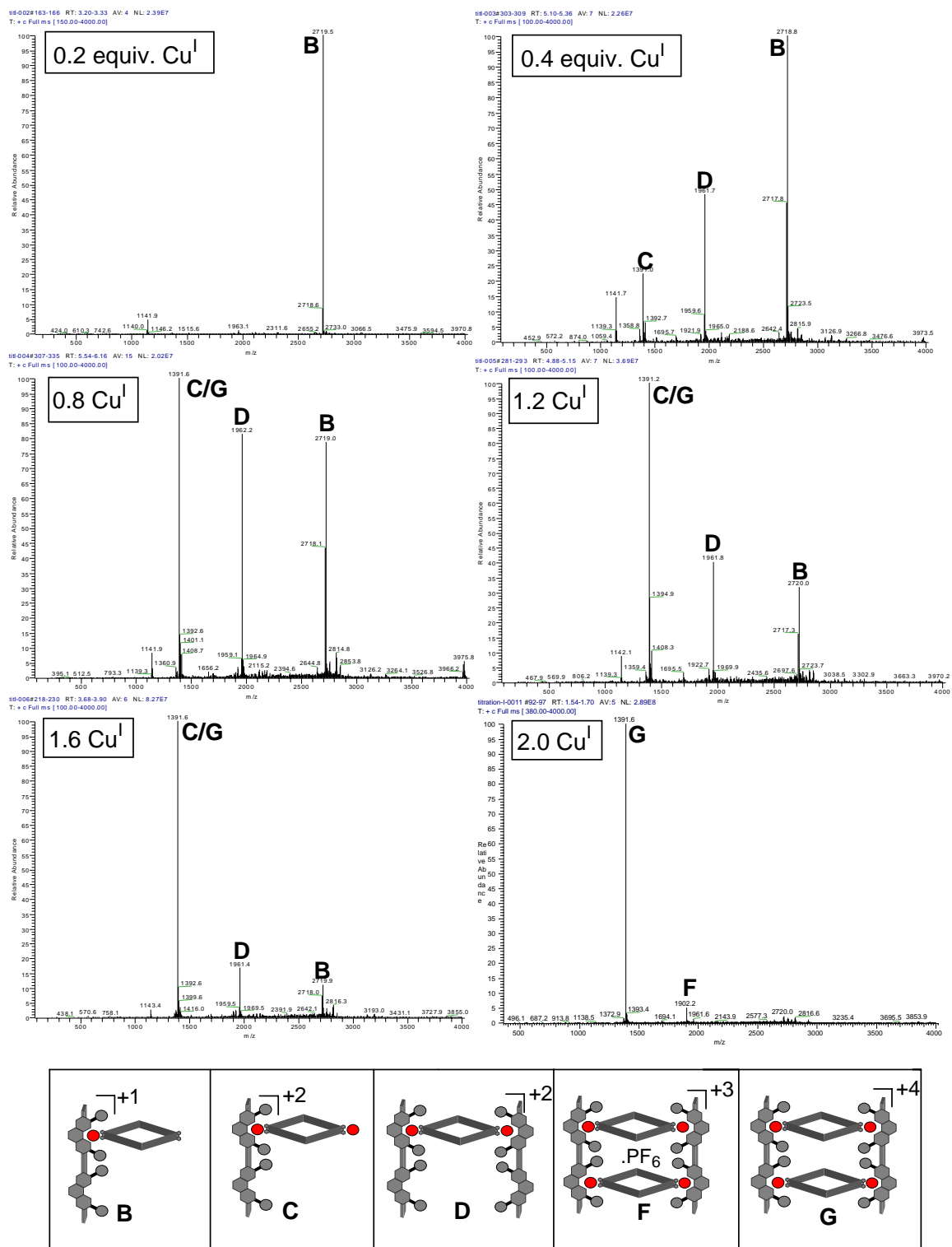


Figure 9. ESI MS changes during the addition of Cu(I) solution to a mixture of **1c** and **2** in dichloromethane.

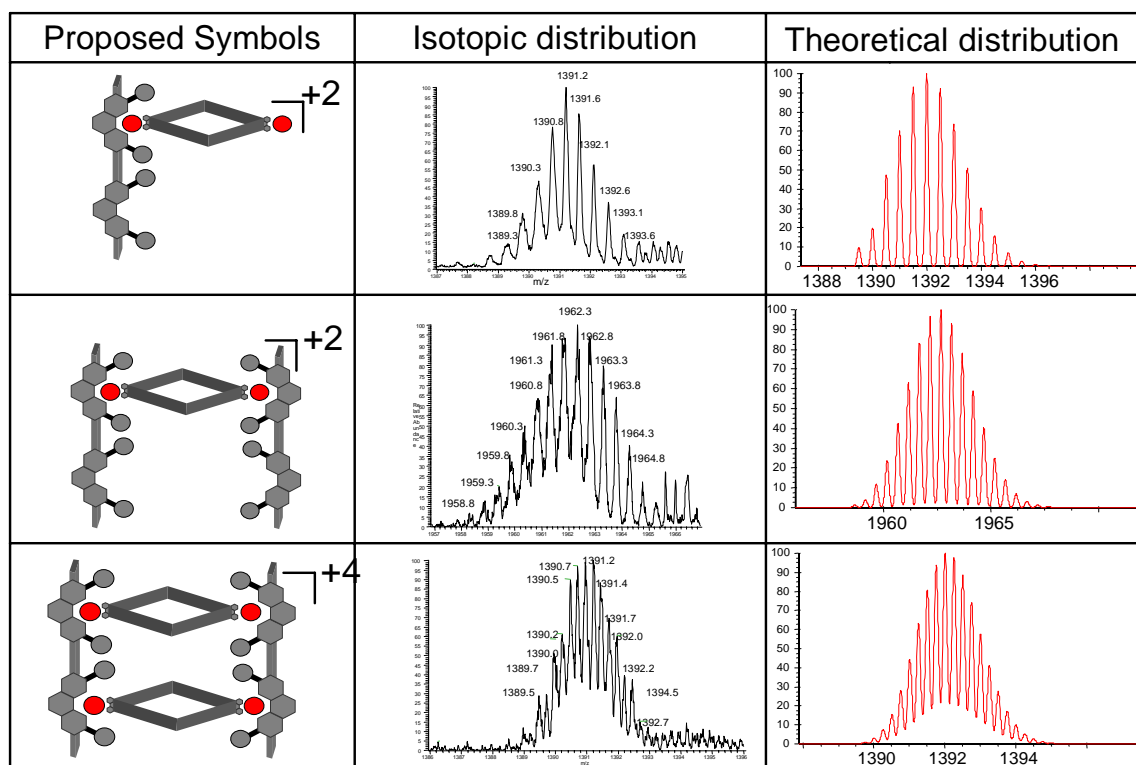


Figure 10. Proposed compositions of **C**, **D** and **F** (left), their experimental isotopic splittings (middle) and their theoretical isotopic distributions (right).

Spectrophotometric titration and thermodynamic parameters

1c and **2** were titrated with aliquot amounts of Cu(I) salt in dichloromethane at 25° C, resulting in significant changes in the UV/vis spectra. The characteristic MLCT band of **NS1** appeared at ~490 nm (Figure 11). As the titration proceeded, the $\pi - \pi^*$ transitions were red shifted due to the complex formation. Addition of more Cu(I) salt (beyond the nanoscaffold stoichiometry) did not lead to any further changes in the visible region in agreement with observations during the ESI MS titration. The inset in the spectrum below clearly indicates that the final complex **NS1** is realized at 2 equivalents of Cu(I) salt. The combined titration data were used to determine the binding constants of the intermediates and the nanoscaffold using the SPECFIT program (Table 2). It was only possible to determine the constants for 3 complexes including the final nanoscaffold. All those are in line with such from previous reports.^{23,14}

Distribution curves (Figure 12) were computed using the formation constants reported in Table 2. The curves suggest a strong cooperativity in the formation of the heteroleptic nanoscaffold. As a result, the two intermediates were formed only in very minor amounts. Again this observation is in line with the ESI MS results. During the early stages of the

titration complex [111] **B**? formed as the major species as detected by both in ESI MS and species distribution curves. In the final step two $[\text{Cu}_2(\mathbf{1c})(\mathbf{2})]^{+2}$ combine together to give final nanoscaffold. As soon as these two intermediates are formed they are rapidly converted to final **NS1**.

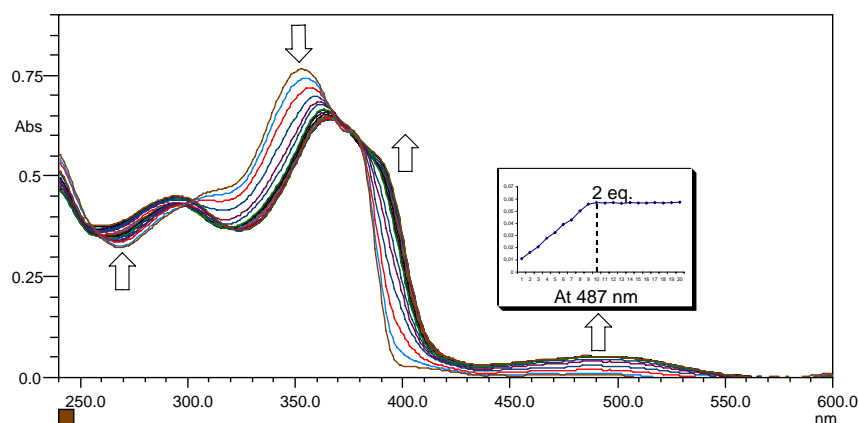


Figure 15. Spectrophotometric titration of **1c** and **2** by aliquot amounts of Cu(I) salt in 20 additions. Solvent: methylene chloride. $T = 25(1)^\circ$; $[\mathbf{1c}]$ and $[\text{Mac}] = 4.38 \times 10^{-6}\text{M}$.

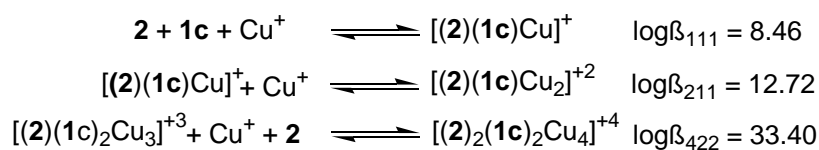


Table 2. Stability constants obtained for the formation of intermediates and of **NS1** when **1c** and **2** were titrated with aliquot amounts of Cu(I) salt in dichloromethane.

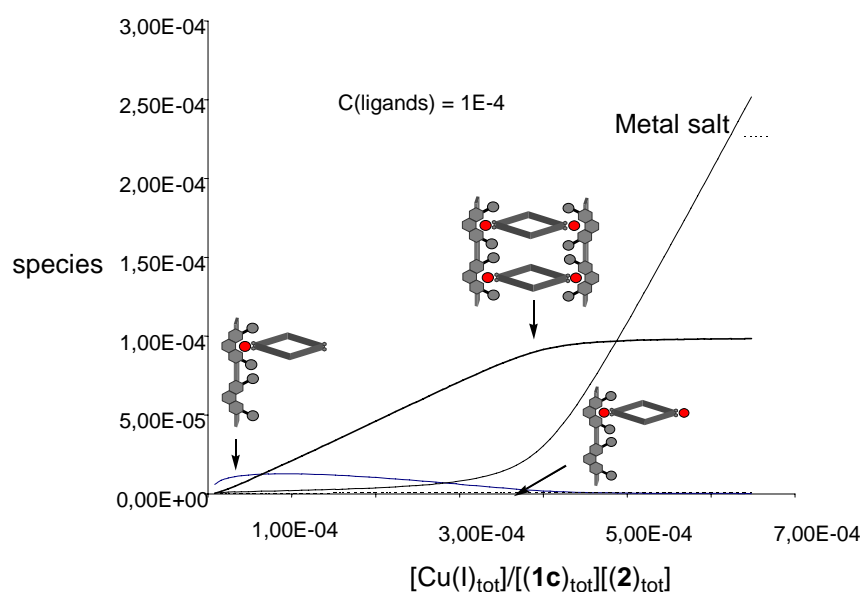


Figure 12. Distribution curves of Cu(I) complexes with **1c** and **2** versus Cu(I) salt. The stability constants are given in Table 2. Solvent: methylene chloride; $T = 25^\circ\text{C}$.

A four step formation process was proposed for the formation of the 8 component heteroleptic nanoscaffold assembly **NS1** (Scheme 6) on the basis of the titration data. These results demonstrate impressively the utility of the **HETPHEN** concept to construct quantitatively heteroleptic supramolecular architectures.

V) Size Selectivity Phenomena

It is well documented that a mixture of different ligands can be used for the self-recognition of helicate-type assemblies. In such cases, self-recognition leads to the exclusive formation of homoleptic coordination compounds.²⁹ Self-recognition can be controlled by the number of metal binding sites or by different spacer lengths. It would be interesting to probe this phenomenon in heteroleptic aggregates where multiple aggregation scenarios are possible.³⁰ Herein we present a size selectivity study (by ESI MS) of heteroleptic nanoscaffolds. Unfortunately, ¹H NMR studies were not able to resolve symmetric and unsymmetric nanoscaffolds due to signal overlap.

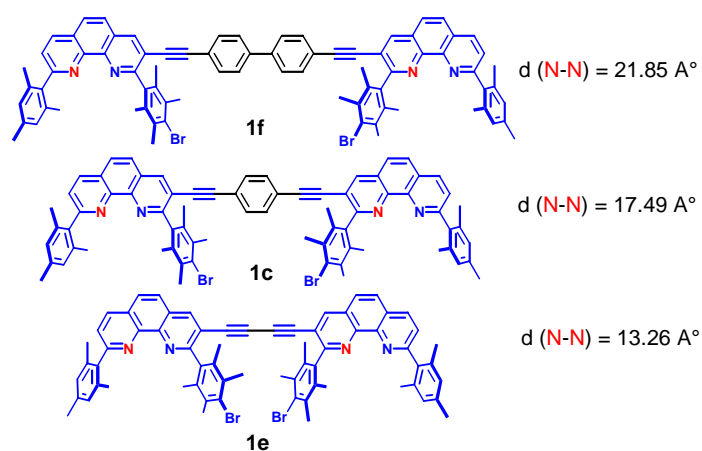
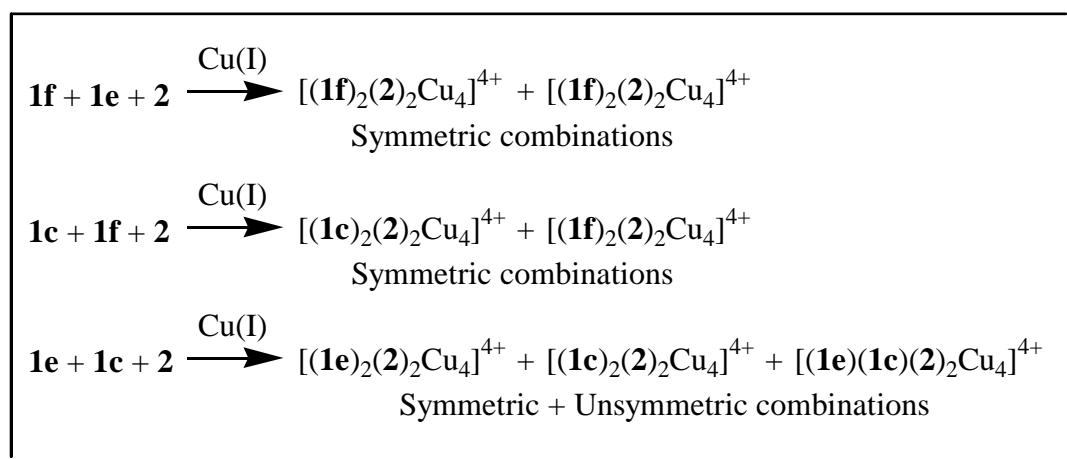


Chart 2. Ligands used for studying the size selection phenomenon.

As shown in Scheme 7, reacting a mixture of the ligands **1f**, **1e** (2 equiv. each) and **2** (2 equiv.) with Cu(I) salt (8 equiv.) in dichloromethane furnished only symmetric scaffolds. Equally, only symmetric combinations were found by ESI MS. when **1c**, **1f** and **2** were reacted with Cu(I) salt. In contrast, from the reaction of **1e**, **1c** and **2** with Cu(I) salt, both unsymmetric and symmetric combinations were detected.



Scheme 7.

How can we understand the size selection depicted in scheme 7? One approach suggests to consider macrocycle **2** as a stiff spacer ligand connecting the two opposing linear bisphenanthrolines via copper centers. In such a case, model calculations propose that up to a deviation of 4.1 degrees of ligand **2** unsymmetric combinations may form. In case of **1e,1f** the unsymmetric nanoscaffold is no longer observed as it would experience a deviation of 4.4 degrees from the ideal angle (Figure 13). However, all the complexes are again heteroleptic, as no homoleptic combinations were found. Again, the non-self-recognition of the ligands during the formation of the nanoscaffolds is reliably controlled by the HETPHEN concept.

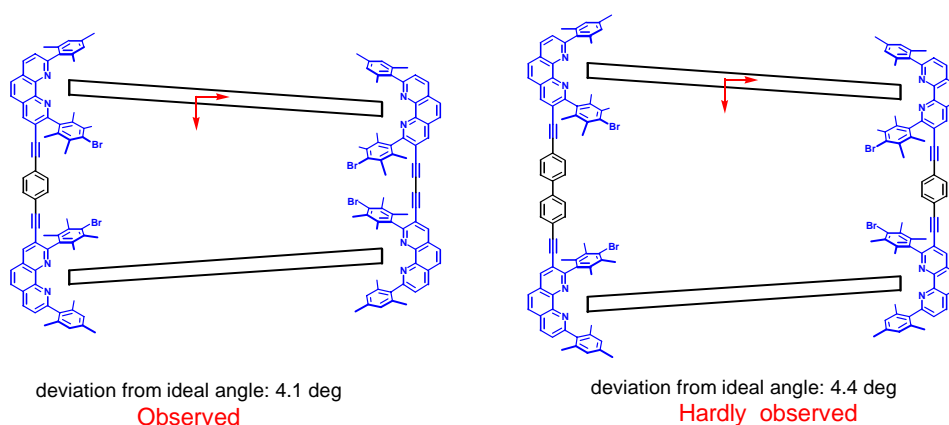


Figure 13. Deviation from the ideal angle obtained from model calculations.

Conclusions

As it is very difficult to obtain single crystal analysis for nanoscaffolds larger than ~3 nm containing large voids it is highly important to combine several solution characterisation techniques available to ascertain the proposed supramolecular structures. Herein, we have presented a battery of methods for dissolved nanoaggregates, both direct and indirect

experiments, to support our structural assignment. The assemblies possessing unprecedented voids were unambiguously characterized by several spectroscopic means and by control experiments. Metal and Ligand exchange studies demonstrated the reversibility of the assemblies and the absence of any indication for other oligomeric combinations further supports the proposed nanostructures. Silver and copper nanoscaffolds could readily be interconverted with no homoleptic complexes formed in between. Mechanistic insight into these assemblies allowed us to better understand the process occurring during the formation of the nanoscale heteroleptic assembly **NS1**. The analysis was performed based on the species observed by ESI MS and spectrophotometry. A four step pathway is postulated for the self-assembly of the nanoscaffold. The two main intermediates proposed were formed only in minor amounts and rapidly converted to the final nanoscaffold. The large void existing in these assemblies makes them an attractive host systems for nanoscopic guest molecules. In conclusion, we have presented a novel supramolecular strategy for heteroleptic programming of nanoscale assemblies outlining a series of solution state characterisation techniques to characterise metallo-supramolecular aggregates with large internal voids.

Experimental

Ligands **1a-f** were prepared according to known procedures.³¹ ¹H NMR and ¹³C NMR were measured on a Bruker AC 200 (200 MHz) or Bruker AC 400 (400 MHz). All the ¹H NMR was carried at room temperature in deuterated dichloromethane unless specified otherwise.

Spectrophotometric titrations: UV-vis spectra were recorded on a Tidas II spectrophotometer using dichloromethane as the solvent. Equilibrium constants of complexes were determined in dichloromethane. Ligands **1e** and **2** were titrated with aliquot amounts of a stock solution of the copper(I) tetrakisacetonitrile hexafluorophosphate. All stock solutions were prepared by careful weighing on a μg analytical balance. Absorption spectra were recorded at $25.0 \pm (0.1)^\circ\text{C}$. Since the formation is instantaneous as evidenced by proton NMR, ESI-MS analysis, and colour change, the solutions were immediately analysed to avoid problems with the volatile solvent. The wavelength region from 240 nm to 600 nm was taken into account. Two equivalents (total) of the metal salt in dichloromethane were added in 20 portions. The entire data sets comprising absorbances, measured in one nanometer steps, were decomposed in their principal components by factor analysis, and subsequently the formation constants including their standard deviation were calculated by using the SPECFIT^{ref} program. Binding constants were determined from two independent titrations.

ESI MS investigations: Positive ESI MS spectra were recorded on the LCQ Deca Thermo Quest instrument, scanning over the m/z range 200-4000. Each time a total of 25 scans was accumulated for the final spectrum. The samples were introduced in the ES source with a flow rate of 10 ml/min. Typical ESI MS conditions used in this study: the sheath gas flow rate, spray voltage, capillary voltage and tube lense offset were set at 50 (arb), 5 (kV), 200 °C, 41 (V) and 5 (V) respectively, in order to avoid any fragmentation. Assignment of ions was further confirmed by comparison of their isotopic splitting with the calculated ones and also by collisional fragmentations.

NS1 $[\text{Cu}_4(\mathbf{1b})_2(\mathbf{2})_2]^{4+}$: Mp.: 295-298 °C; $^1\text{H-NMR}$ (400 MHz, CD_2Cl_2): δ 8.81 (s, 4H, phenanthroline), 8.63 (d, $J = 7.6$ Hz, 4H, phenanthroline), 8.45 (s, 8H, phenanthroline), 8.28 (s, 8H, phenanthroline), 8.20 (d, $J = 9.2$ Hz, 4H, phenanthroline), 8.17 (d, $J = 9.2$ Hz 4H, phenanthroline), 7.81 (d, $J = 7.8$ Hz, 4H, phenanthroline), 7.69 (d, $J = 8.2$ Hz, 16H, phenyl), 7.64 (d, $J = 8.2$ Hz, 16H, phenyl), 7.54 (s, 8H, phenyl), 6.92 (s, 8H, phenyl), 5.96 (s, 8H, Mes-H), 4.16 (s, 12H, methoxy), 2.98 (m, 16H, aliph), 1.71 (s, 24H, benzyl), 1.64 (s, 12H, aliph), 1.54 (s, 24H, benzyl), 1.47 (s, 24H, aliph), 1.31 (s, 36H, *t*-Bu), 0.77 (t, $J = 7.2$ Hz, 24H, aliph); $^{13}\text{C-NMR}$ (CDCl_3 , 200 MHz): δ 163.4, 161.6, 160.1, 148.9 (2C), 146.2, 145.8, 144.4, 143.4 (2C), 138.9, 137.9, 137.5, 136.2, 135.4 (2C), 134.9 (2C), 134.2, 133.6, 133.1, 132.5, 132.0, 131.8, 131.3, 129.8 (2C), 129.1, 128.5, 128.2, 127.6, 127.3, 126.9, 126.5, 126.3 (2C), 126.0, 125.6, 125.0, 122.8, 121.6, 119.0, 109.1, 96.2 (arom), 93.8 (2C), 89.9 (2C), 88.6 (2C), 84.4 (2C) (ethynyl), 62.8 (methoxy), 34.1, 32.6, 31.8, 31.0, 30.2, 29.6, 22.5, 21.8, 21.2 (2C), 20.9 (2C), 20.2 (2C), 13.5 (aliph); IR (KBr): ν 2926, 2840, 2194 ($\text{C}\equiv\text{C}$), 1598, 1507, 1460, 1422, 1291, 1160, 1110, 1005, 842, 678, 548; ESI MS: calcd. for $[\text{Cu}_4\text{C}_{364}\text{H}_{328}\text{N}_{16}\text{Br}_4\text{O}_4]^{4+}$ $[\text{M}^{4+}]$ (%): m/z 1391.1, found: m/z 1391.5 (100), calcd. for $[\text{Cu}_4\text{C}_{364}\text{H}_{328}\text{N}_{16}\text{Br}_4\text{O}_4*\text{PF}_6]^{3+}$ $[\text{M}^{3+}]$ (%): m/z 1903.1, found: m/z 1903.0 (5); Elemental analysis: $[\text{Cu}_4\text{C}_{364}\text{H}_{328}\text{N}_{16}\text{Br}_4\text{O}_4*4\text{PF}_6]$: calcd. C 69.52, H 5.51, N 3.56; found: C 69.44, H 5.48, N 3.52.

NS2 $[\text{Ag}_4(\mathbf{1b})_2(\mathbf{2})_2]^{4+}$: Mp.: > 300 °C; $^1\text{H-NMR}$ (400 MHz, CD_2Cl_2): δ 8.77 (s, 4H, phenanthroline), 8.60 (d, $J = 7.6$ Hz, 4H, phenanthroline), 8.55 (s, 8H, phenanthroline), 8.28 (s, 8H, phenanthroline), 8.15 (d, $J = 9.2$ Hz, 4H, phenanthroline), 8.13 (d, $J = 9.2$ Hz 4H, phenanthroline), 7.84 (d, $J = 7.8$ Hz, 4H, phenanthroline), 7.69 (d, $J = 8.2$ Hz, 16H, phenyl), 7.65 (d, $J = 8.2$ Hz, 16H, phenyl), 7.54 (s, 8H, phenyl), 6.92 (s, 8H, phenyl), 5.96 (s, 8H, Mes-H), 4.16 (s, 12H, methoxy), 2.98 (m, 16H, aliph), 1.86 (s, 24H, benzyl), 1.81 (s, 12H, aliph), 1.61 (s, 24H, benzyl), 1.55 (s, 24H, benzyl), 1.31 (s, 36H, *t*-Bu), 0.82 (t, $J = 7.2$ Hz, 24H, benzyl); $^{13}\text{C-NMR}$ (CDCl_3 , 200 MHz): δ 165.4, 162.6, 159.1, 149.1, 146.7, 145.4, 144.9,

143.4 (2C), 138.9, 137.9, 137.5, 136.2, 135.4 (2C), 134.9 (2C), 135.3, 133.9, 133.4, 132.9, 132.0, 131.5, 131.2, 130.5 (2C), 129.3, 128.5, 128.0, 127.6, 127.3, 126.9, 126.5, 126.3 (2C), 126.0, 125.6, 125.0, 122.0, 121.6, 116.5, 107.5, 95.2 (arom), 93.8 (2C), 88.9 (2C), 87.1 (2C), 82.4 (2C) (ethynyl), 60.8 (methoxy), 35.9, 33.6, 31.4, 30.8, 29.7, 28.6, 22.0, 21.8, 21.2 (2C), 20.9 (2C), 19.5 (2C), 12.5 (aliph); IR (KBr): ν 2936, 2852, 2198 (C \equiv C), 1598, 1515, 1460, 1419, 1296, 1166, 1102, 1002, 838, 681, 552; ESI MS: calcd. for [Ag₄C₃₆₄H₃₂₈N₁₆Br₄O₄]⁴⁺ [M⁴⁺] (%): m/z 1435.2, found: m/z 1435.2 (100); Elemental analysis: [Cu₄C₃₆₄H₃₂₈N₁₆Br₄O₄*6PF₆]: calcd. C 68.00, H 5.33, N 3.49; found: C 67.98, H 5.31, N 3.46.

NS3 [Cu₄(**1b**)₂(**2**)₂]⁴⁺: Mp.: 280 °C; ¹H-NMR (400 MHz, CD₂Cl₂): δ 8.86 (s, 4H, phenanthroline), 8.70 (d, J = 7.8 Hz, 4H, phenanthroline), 8.51 (s, 8H, phenanthroline), 8.38 (s, 8H, phenanthroline), 8.24 (d, J = 9.6 Hz, 4H, phenanthroline), 8.21 (d, J = 9.6 Hz, 4H, phenanthroline), 7.84 (d, J = 7.8 Hz, 4H, phenanthroline), 7.82 (d, J = 8.2 Hz, 16H, phenyl), 7.74 (d, J = 8.2 Hz, 16H, phenyl), 7.60 (s, 8H, phenyl), 7.17 (s, 8H, phenyl), 6.10 (s, 8H, Mes-H), 5.99 (s, 8H, Mes-H), 4.23 (s, 12H, methoxy), 3.09 (t, J = 6.9 Hz, 16H, aliph), 1.80-1.90 (m, 16H, aliph), 1.72 (s, 48H, aliph), 1.67 (s, 12H, benzyl), 1.64 (s, 12H, benzyl), 1.45-1.60 (m, 16H, aliph), 1.37 (s, 36H, *t*-Bu), 1.30-1.42 (m, 32H, aliph), 0.88 (t, J = 7.2 Hz, 24H, aliph); IR (KBr): ν = 2922, 2848, 2194 (C \equiv C), 1591, 1509, 1460, 1419, 1296, 1166, 1102, 1002, 838, 681, 552; ESI MS: calcd. for [Cu₄C₃₆₀H₃₂₄N₁₆O₄]⁴⁺ [M⁴⁺] (%): m/z 1298.2, found: m/z 1298.1 (100); calcd. for [Cu₄C₃₆₀H₃₂₄N₁₆O₄*PF₆]³⁺ [M³⁺] (%): m/z 1778.2, found: m/z 1778.1 (20); Elemental analysis: [Cu₄C₃₆₀H₃₂₄N₁₆O₄*4PF₆*6H₂O]: calcd. C 73.53, H 5.76, N 3.81; found: C 73.59, H 6.35, N 3.80.

NS5 [Cu₄(**1f**)₂(**2**)₂]⁴⁺: ¹H-NMR (200 MHz, CD₂Cl₂): δ 8.83 (s, 4H, phenanthroline), 8.73 (d, J = 8.3 Hz, 4H, phenanthroline), 8.53 (s, 8H, phenanthroline), 8.34 (s, 8H, phenanthroline), 8.22 (d, J = 9.1 Hz, 8H, phenanthroline), 7.93 (d, J = 8.1 Hz, 4H, phenanthroline), 7.83 (d, J = 8.1 Hz, 16H, phenyl), 7.74 (d, J = 8.3 Hz, 16H, phenyl), 7.61 (s, 8H, phenyl), 7.55 (d, J = 8.6 Hz, 8H, phenyl), 7.43 (d, J = 8.6 Hz, 8H, phenyl), 6.11 (s, 8H, Mes-H), 4.24 (s, 12H, methoxy), 3.01-3.18 (m, 16H, aliph), 1.83 (s, 48H, benzyl), 1.63 (s, 36, benzyl), 1.35-1.37 (m, 100H, aliph), 0.89 (t, J = 6.6 Hz, 24H, aliph); ¹³C-NMR (CDCl₃, 50 MHz): δ 166.2, 158.7, 154.6, 153.9, 147.9, 147.1, 143.9, 142.1, 141.2, 140.6, 138.3, 138.1, 134.5, 133.2 (2C), 132.2, 131.9 (2C), 130.6, 130.3, 129.7, 128.6 (2C), 128.4 (2C), 128.0, 127.7, 125.8, 125.6 (2C), 125.1, 124.0, 121.6 (2C), 120.6, 119.8, 119.0, 116.5, (arom), 93.8 (2C), 84.5 (2C), 81.6 (2C), 84.8 (2C) (ethynyl), 64.3 (methoxy), 32.7, 31.6 (2C), 30.9 (2C), 29.2 (2C), 28.2, 23.9, 22.6 (2C), 13.8 (aliph); ESI MS: calcd. for [Cu₄C₃₇₆H₃₃₆Br₄N₁₆O₄]⁴⁺ [M⁴⁺] (%): m/z 1429.1, found: m/z 1429.4 (100).

NS6 $[\text{Cu}_4(\mathbf{1e})_2(\mathbf{2})_2]^{4+}$: Mp.: 289 °C; $^1\text{H-NMR}$ (200 MHz, CD_2Cl_2): δ 8.83 (s, 4H, phenanthroline), 8.73 (d, $J = 8.1$ Hz, 4H, phenanthroline), 8.52 (s, 8H, phenanthroline), 8.33 (s, 8H, phenanthroline), 8.22 (q, $J = 9.1$ Hz, 4H, phenanthroline), 8.10 (s, 4H, phenanthroline), 7.92 (d, $J = 8.4$ Hz, 4H, phenanthroline), 7.89 (s, 8H, phenyl), 7.83 (d, $J = 8.3$ Hz, 16H, phenyl), 7.74 (d, $J = 8.3$ Hz, 16H, phenyl), 7.61 (s, $J = 8.2$ Hz, 8H, phenyl), 6.10 (s, 8H, Mes-H), 4.23 (s, 12H, methoxy), 3.12 (t, $J = 7.9$ Hz, 16 H, aliph), 2.29 (m, 4H, aliph), 1.82 (s, 36 H, benzyl), 1.63 (s, 48H, benzyl), 1.36 (s, 36H, *t*-Bu), 0.88 (t, $J = 6.9$ Hz, 32H, aliph); $^{13}\text{C-NMR}$ (100 MHz, CD_2Cl_2): δ 160.6, 159.8, 159.2, 147.7, 146.8, 143.3, 142.4, 140.9, 140.5, 140.3, 138.1, 137.8, 137.3, 137.0, 134.2, 132.9, 131.9, 131.6 (2C), 131.0, 128.7, 128.2, 127.7, 127.4, 127.2, 126.8, 126.7, 125.8, 125.2, 124.8, 121.3, 121.1, 116.2, 104.4 (arom), 92.4 (2C), 88.3 (2C), 84.6 (2C), 84.5 (2C) (ethynyl), 61.4 (methoxy), 34.1, 32.4, 31.3, 30.6, 30.5, 28.9, 22.3, 19.9, 19.6, 19.5, 17.7, 13.5 (aliph); ESI MS: calcd. for $[\text{Cu}_4\text{C}_{352}\text{H}_{320}\text{N}_{16}\text{O}_4\text{Br}_4]^{4+}$ $[\text{M}^{4+}]$ (%): m/z 1353.1, found: m/z 1354.1 (100); calcd. for $[\text{Cu}_4\text{C}_{352}\text{H}_{320}\text{N}_{16}\text{O}_4\text{Br}_4*\text{PF}_6]^{3+}$ $[\text{M}^{3+}]$ (%): m/z 1852.4, found: m/z 1852.8 (14).

Acknowledgements. We are indebted to the Deutsche Forschungsgemeinschaft (Schm 647/12-1) and the Fonds der Chemischen Industrie for financial support. V. K. thanks Annie Marquis for helping with the fitting programm.

- (1) (a) Lehn, J.-M. Chair Ed.; Atwood, J. L.; Davis, J. E. D.; MacNicol, D. D.; Vögtle, V. Exec. Eds., *Comprehensive Supramolecular Chemistry*. Pergamon: Oxford, UK, **1996**, Vols. 1–11. (b) Schmittl, M.; Kalsani, V. *Topics in Current Chemistry*. **2004**, in press. (c) Schalley, C. A. *Angew. Chem. Int. Ed.* **2004**, *7*, 4399-4401 and ref's therein.
- (2) (a) Olenyuk, B.; Levin, M. D.; Whiteford, J. A.; Shield, J. E.; Stang, P. J. *J. Am. Chem. Soc.* **1999**, *121*, 10434-10435. (b) Stang, P. J.; Persky, N. E.; Manna, J. *J. Am. Chem. Soc.* **1997**, *119*, 4777-4778. (c) Manna, J.; Whiteford, J. S.; Stang, P. J. *J. Am. Chem. Soc.* **1996**, *118*, 8731-8732. (d) Kryshchenko, Y. K.; Seidel, S. R.; Muddiman, D.; Nepomuceno, A. I.; Stang, P. J. *J. Am. Chem. Soc.* **2003**, *125*, 9647-9652. (e) Stang, P. J.; Cao, D. H.; Chen, K.; Gray, G. M.; Muddiman, D. C.; Smith, R. D. *J. Am. Chem. Soc.* **1997**, *119*, 5163-5168. (f) Manna, J.; Kuehl, C. J.; Whiteford, J. A.; Stang, P. J.; Muddiman, D. C.; Hofstadler, S. A.; Smith, R. D. *J. Am. Chem. Soc.* **1997**, *119*, 11611-11619. (g) Fan, J.; Whiteford, J. A.; Olenyuk, B.; Levin, M. D.; Stang, P. J.; Fleischer, E. B. *J. Am. Chem. Soc.* **1999**, *121*, 2741-2752. (h) RadhaKrishnan, U.; Schweiger, M.; Stang, P. J. *Org. Lett.* **2001**, *3*, 3141-3143. (i) Kuehl, C. J.; Yamamoto, T.; Seidel, S. R.; Stang, P. J. *Org. Lett.* **2002**, *4*, 913-915. (j) Schweiger, M.; Seidel, S. R.; Schmitz, M.; Stang, P. J. *Org. Lett.* **2000**, *2*, 1255-1257. (k) Leininger, S.; Schmitz, M.; Stang, P. J. *Org. Lett.* **1999**, *1*, 1921-1923. (l) Leininger, S.; Fan, J.; Schmitz, M.; Stang, P. J. *Proc. Natl. Acad. Sci. USA.* **2000**, *97*, 1380-1384.
- (3) (a) Drain, C. M.; Lehn, J.-M. *J. Chem. Soc., Chem. Commun.* **1994**, 2313–2315. (b) Garcia, A. M.; Bassani, D. M.; Lehn, J.-M.; Baum, G.; Fenske, D. *Chem. Eur. J.* **1999**, *5*, 1234-1238. (c) Baxter, P. N. W.; Lehn, J.-M.; Baum, G.; Fenske, D. *Chem. Eur. J.* **1999**, *5*, 102-112.
- (4) (a) Newkome, G. R.; Cho, T. J.; Moorefield, C. N.; Baker, G. R.; Cush, R.; Russo, P. S. *Angew. Chem. Int. Ed.* **2001**, *38*, 3717-3721. (b) Newkome, G. R.; Cho, T. J.; Moorefield, C. N.; Cush, R.; Russo, P. S.; Godinez, L. A.; Saunders, M. J.; Mohapatra, P. *Chem. Eur. J.* **2002**, *8*, 2946-2954. (c) Newkome, G. R.; Cho, T. J.; Moorefield, C. N.; Mohapatra, P.; Godinez, L. A. *Chem. Eur. J.* **2004**, *10*, 1493-1500.
- (5) (a) Paraschiv, V.; Crego-Calama, M.; Fokkens, R. H.; Padberg, C. J.; Timmerman, P.; Reinhoudt, D. N.

- J. Org. Chem.* **2001**, *66*, 8297-8301. (b) Prins, L. J.; Neuteboom, E. E.; Paraschiv, V.; Crego-Calama, M.; Timmerman, P.; Reinhoudt, D. N. *J. Org. Chem.* **2002**, *67*, 4808-4820. (c) Paraschiv, V.; Crego-Calama, M.; Ishi-i, T.; Padberg, C. J.; Timmerman, P.; Reinhoudt, D. N. *J. Am. Chem. Soc.* **2002**, *124*, 7638-7639.
- (6) Fujita, M.; Tominaga, M.; Hori, A.; Therrien, B. *Acc. Chem. Res.* **2005**, ASAP article and ref's therein.
- (7) (a) Johannessen, S. C.; Brisbois, R. G. *J. Am. Chem. Soc.* **2001**, *123*, 3818-3819. (b) Sommer, R. D.; Rheingold, A. L.; Goshe, A. J.; Bosnich, B. *J. Am. Chem. Soc.* **2001**, *123*, 3940-3952. (c) Sautter, A.; Schmid, D. G.; Jung, G.; Wurthner, F. *J. Am. Chem. Soc.* **2001**, *123*, 5424-5430. (d) Wurthner, F.; Sautter, A. *Chem. Commun.* **2000**, 445-446. (e) Wurthner, F.; Sautter, A.; Schmid, D.; Weber, P. G. *Chem. Eur. J.* **2001**, *7*, 894-902. (f) Wurthner, F.; Sautter, A. *Org. Biomol. Chem.* **2003**, *1*, 240-243. (g) You, C. C.; Wurthner, F. *J. Am. Chem. Soc.* **2003**, *125*, 9716-9725. (h) Sun, S. S.; Lees, A. J. *Inorg. Chem.* **2001**, *40*, 3154-3160. (i) Merlau, M. L.; Mejia, M. P.; Nguyen, S. T.; Hupp, J. T. *Angew. Chem. Int. Ed.* **2001**, *40*, 4239-4242. (j) Ziessel, R. *Synthesis*, **1999**, 1839-1865. (k) Jiang, H.; Lin, W. *J. Am. Chem. Soc.* **2003**, *125*, 8084-8085. (l) Jiang, H.; Lin, W. *J. Am. Chem. Soc.* **2004**, *126*, 7426-7427. (m) Kuramochi, Y.; Satake, A.; Kobuke, Y. *J. Am. Chem. Soc.* **2004**, *126*, 8668-869. (n) Takahashi, R.; Kobuke, Y. *J. Am. Chem. Soc.* **2003**, *125*, 2372-2373. (o) Fenniri, H.; Deng, B. L.; Ribbe, A. E. *J. Am. Chem. Soc.* **2002**, *124*, 11064-11072. (p) Fenniri, H.; Deng, B. L.; Ribbe, A. E.; Hallenga, K.; Jacob, J.; Thiagarajan, P. *Proc. Natl. Acad. Sci. USA.* **2002**, *99*, 6487-6492. (q) Yamaguchi, T.; Tashiro, S.; Tominaga, M.; Kawano, M.; Ozeki, T.; Fujita, M. *J. Am. Chem. Soc.* **2004**, *126*, 10818-10819. (r) Tominaga, M.; Suzuki, K.; Kawano, M.; Kusukawa, T.; Ozeki, T.; Sakamoto, S.; Yamaguchi, K.; Fujita, M. *Angew. Chem. Int. Ed.* **2004**, early view. (s) Schalley, C. A. *Angew. Chem. Int. Ed.* **2004**, *34*, 4399-4401.
- (8) Cohen, Y.; Avram, L.; Frish, L. *Angew. Chem. Int. Ed.* **2005**, *44*, 520-554.
- (9) (a) Seto, C. T.; Whitesides, G. M. *J. Am. Chem. Soc.* **1993**, *115*, 905-916; (b) Nelson, J. C.; Saven, K. G.; Moore, J. S.; Wolynes, P. G. *Science* **1997**, *277*, 1793-1796; (c) Higler, I.; Grave, L.; Breuning, E.; Verboom, W.; De Jong, F.; Fyles, T. M.; Reinhoudt, D. N. *Eur. J. Org. Chem.* **2000**, 1727-1734.
- (10) Schmittel, M.; Kalsani, V.; Kienle, L. *Chem. Commun.* **2004**, 1534-1535 and ref's therein.
- (11) Schmittel, M.; Ammon, H.; Kalsani, V.; Wiegrefe, A.; Michel, C. *Chem. Commun.* **2002**, 2566-2567.
- (12) Schmittel, M.; Ganz, A. *Chem. Commun.* **1997**, 99-101; Schmittel, M.; Luning, U.; Meder, M.; Ganz, A.; Michel, C.; Herderich, M. *Heterocycl. Commun.* **1997**, *3*, 493-494.
- (13) (a) Goulle, V.; Thummel, R. P. *Inorg. Chem.* **1990**, *29*, 1767-1772; (b) Li, X. Y.; Illigen, J.; Nieger, M.; Michel, S.; Schalley, C. A. *Chem. Eur. J.* **2003**, *6*, 1332-1347.
- (14) Schmittel, M.; Kalsani, V.; Fenske, D.; Wiegrefe, A. *Chem. Commun.* **2004**, 490-491.
- (15) Fatin-Rouge, N.; Blanc, S.; Pfeil, A.; Rigault, A.; Albrecht-Gary, A. M.; Lehn, J.-M. *Helvetica chimica acta.* **2001**, 1694-1711.
- (16) Cohen, Y.; Avram, L.; Frish, L. *Angew. Chem. Int. Ed.* **2005**, *44*, 520-554 and ref's therein.
- (17) Schubert, D.; Tziatzios, C.; Schuck, P.; Schubert, U. S. *Chem. Eur. J.* **1999**, *5*, 1377-1383.
- (18) Molecular modelling was done with the MM+force field as implemented in Hyperchem 6.02. Hyperchem® 6.02 Release for Windows by Hypercube, Inc. 2000. MM+force field.
- (19) Russell, K. C.; Leize, E.; VanDorsselaer, A.; Lehn, J.-M. *Angew. Chem. Int. Ed. Engl.* **1995**, *34*, 209-213.
- (20) (a) Schmittel, M.; Ganz, A.; Liu, S. X.; Kalsani, V. unpublished results. (b) Poleschak, I.; Kern, J. M.; Sauvage, J. P. *Chem. Commun.* **2004**, 474-476 and ref's therein.
- (21) (a) Baxter, P. N. W. *Comprehensive, supramolecular chemistry.* **1996**, chapter 5, 165-211. (b) Olenyuk, B.; Fechtenkotter, A.; Stang, P. J. *J. Chem. Soc. Dalton. Trans.* **1998**, *11*, 1707-1728. (c) Leininger, S.; Olenyuk, B.; Stang, P. J. *Chem. Rev.* **2000**, *100*, 853-907.
- (22) Jimenez-Molero, M. C.; Dietrich-Buchecker, C.; Sauvage, J. P. *Chem. Commun.* **2003**, 1613-1616 and ref's therein.
- (23) (a) Marquis, A.; Kintzinger, J. P.; Graff, R.; Baxter, P. N. W.; Lehn, J.-M. *Angew. Chem. Int. Ed.* **2002**, *15*, 2760-2764; (b) Leize, E.; VanDorsselaer, A.; Kramer, R.; Lehn, J.-M. *Chem. Commun.* **1993**, 990-993; (c) Floquet, S.; Ouali, N.; Bocquet, B.; Bernardinelli, G.; Imbert, D.; Bunzli, J. C. G.; Hopfgartner, G.; Piguet, C. *Chem. Eur. J.* **2003**, *8*, 1860-1875; (d) Hamacek, J.; Blanc, S.; Elhabiri, M.; Leize, E.; VanDorsselaer, A.; Piguet, C.; Albrecht-Gary, A. M. *J. Am. Chem. Soc.* **2003**, *125*, 1541-1550; (e) Fatin-Rouge, N.; Blanc, S.; Leize, E.; VanDorsselaer, A.; Baret, P.; Pierre, J. L.; Albrecht-Gary, A. M. *Inorg. Chem.* **2000**, *39*, 5771-5778.
- (24) Levin, M. D.; Stang, P. J. *J. Am. Chem. Soc.* **2000**, *122*, 7428-7429.
- (25) (a) Gampp, H.; Maeder, M.; Meyer, C. J.; Zuberbuhler, A. D. *Talanta* **1985**, *32*, 95-101; (b) Rossotti, F. J. C.; Rossotti, H. S.; Whewell, R. J. *J. Inorg. Nucl. Chem.* **1971**, *33*, 2051; (c) Gampp, H.; Maeder, M.; Meyer, C. J.; Zuberbuhler, A. D. *Talanta* **1985**, *32*, 257-264; (d) Gampp, H.; Maeder, M.; Meyer, C. J.; Zuberbuhler, A. D. *Talanta* **1986**, *33*, 943-951.

- (26) (a) Marquardt, D. W. *J. Soc. Indust. Appl. Math.* **1963**, *11*, 431-441; (b) Maeder, M.; Zuberbuhler, A. D. *Anal. Chem.* **1990**, *62*, 2220-2224.
- (27) Ingri, N.; Kakolowicz, W.; Sillen, L. G.; Warnqvist, B. *Talanta* **1967**, *14*, 1261-1286.
- (28) (a) Schmittl, M.; Ganz, A.; Kalsani, V. unpublished results; (b) Stiller, R.; Lehn, J.-M. *Eur. J. Inorg. Chem.* **1998**, 977-982.
- (29) (a) Kramer, R.; Lehn, J.-M.; Marquis-Rigault, A. *Proc. Natl. Acad. Sci. USA.* **1993**, *90*, 5394-5398. (b) Albrecht, M.; Blau, O.; Frohlich, R. *Proc. Natl. Acad. Sci. USA.* **2002**, *99*, 4867-4872. (c) Caulder, D. L.; Raymond, K. N. *Angew. Chem. Int. Ed. Engl.* **1997**, *36*, 1440-1442. (d) Albrecht, M.; Blau, O.; Wegelius, E.; Rissanen, K. *New. J. Chem.* **1999**, *23*, 667-668.
- (30) Addicott, C.; Das, N.; Stang, P. J. *Inorg. Chem.* **2004**, *43*, 5335-5338.
- (31) Schmittl, M.; Michel, C.; Wiegrefe, A.; Kalsani, V. *Synthesis* **2001**, 1561-1567.

Supp 5-4

Chem. Commun. **2004**, 1534-1535

Reproduced by permission of *The Royal Society of Chemistry*

Simple and Supramolecular Copper Complexes as Precursors in the HRTEM Induced Formation of Crystalline Copper Nanoparticles

Michael Schmittel,^{*a} Venkateshwarlu Kalsani^a, Lorenz Kienle,^{*b}

^a Center of Micro and Nanochemistry and Engineering, Organische Chemie I, Universität Siegen, Adolf-Reichwein-Str., D-57068 Siegen, Germany, Fax: (+49) 271 740 3270; Tel: (+49) 271 740 4356; E-mail: schmittel@chemie.uni-siegen.de

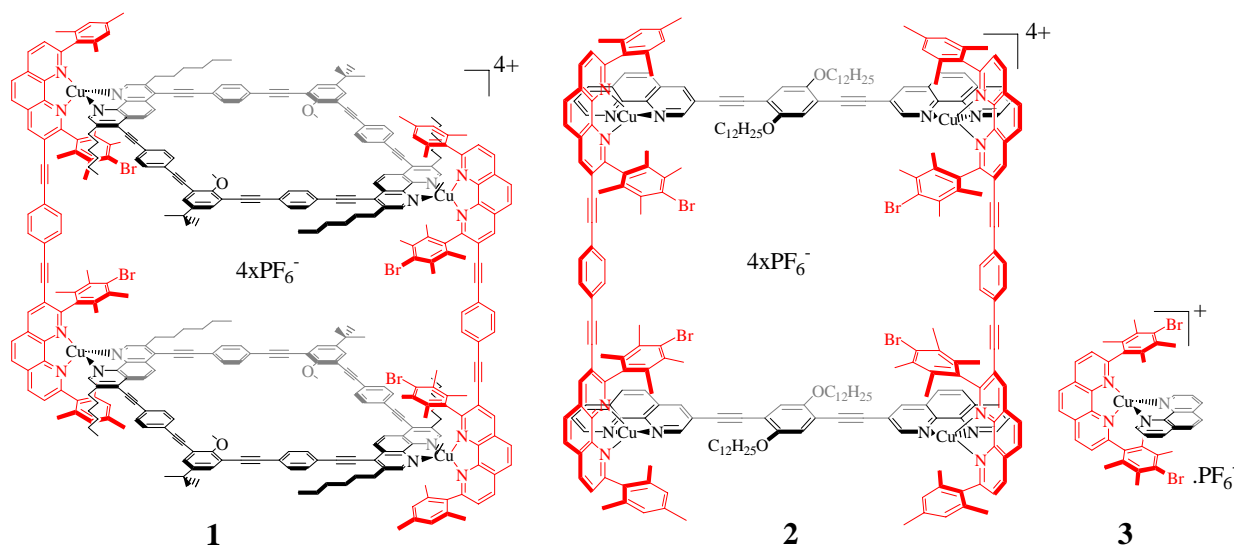
^b Max-Planck-Institut für Festkörperforschung, Heisenbergstraße 1, D-70569 Stuttgart, Germany.

Abstract. In the HRTEM investigations of copper(I) bisphenanthroline nanoscaffolds and simple precursor complexes nanoparticles were generated that upon closer inspection turned out to be pure crystalline copper nanoparticles.

The synthesis of discrete supramolecular assemblies in the 3-10 nm regime is a fascinating and rapidly growing area of research. Amazing structures, such as dodecahedra, hexagons and grids, have been reported in seminal contributions by Stang,¹ Newkome,² Lehn³ and others.⁴ Due to the large size and huge void of these structures, that mostly contain disordered solvent molecules, X-ray diffraction data are difficult to obtain. Hence, scanning probe microscopy techniques and high resolution TEM (HRTEM)⁵ have been serving as important supplementary tools for characterisation. Metallosupramolecular aggregates, a nanoscopic dodecahedron and a hexagonal metallocycle, were among the first to be structurally supported by HRTEM.^{1,2} In the following, we will describe our experience with HRTEM of copper(I) bisphenanthroline nanoscaffolds, showing that these investigations do not provide pictures of the nanostructures but instead lead to crystalline copper nanoparticles that can easily be confused with the original aggregates.

The formation and investigation of ordered and defined metal nanoparticles have been an actively pursued area of research. In particular, due to an increased surface to volume ratio their properties, *c.f.* to copper particles in heterogeneous catalysis, are different from those of

bulk materials.⁶ Metal nanoparticles have been generated by using reducing agents or reverse micelles, *via* photoreduction, and by γ -irradiation, sonochemical, radiolytic methods or thermal decomposition.⁷ Mostly their formation was effected in aqueous media. In contrast, the present study suggests to prepare copper nanoparticles from coordination precursors in non-aqueous media.



The compounds of the present study, the copper(I) bisphenanthroline nanoscaffolds (**1** and **2**), have been described earlier,⁸ while complex **3** was prepared along the same strategy.⁹

Nanoscaffold **1** ($M = \text{Cu}$) was prepared for HRTEM¹⁰ and SAED (selected area electron diffraction) investigations by either spreading the solid powder of **1** on Cu- or Al-grids (sample 1, 2) or a solution of **1** in acetone on a Al-grid (sample 3). The use of Al-grids was required for quantitative EDX measurements.

As samples 1 and 2 displayed no differences in the real structure, we will not separate them in the ensuing discussion. The HRTEM micrographs of samples 1 and 2 showed nanoaggregates of 5 nm size, roughly that expected for **1** ($d = 4.2$ nm). EDX spectra proved an enrichment of copper within the nanoaggregates of the matrix. As a consequence, such pictures may be interpreted as cast iron proof for the formation of the organic nanostructure **1**. However, these nanoaggregates are not present in the initially homogeneous matrix, they are formed after a short time of exposure. Ongoing exposure increases the crystal quality of the nanoaggregates, finally transforming them to perfect nanocrystals. The distribution and density of the copper nanoparticles within the matrix is random (see Figure. 1).

The exposed area and the region with massive formation of copper nanoparticles are quite apart. In some cases, the nanoparticles form a circle around the exposed area. Hence, the radiation damage of the material can easily be overlooked, as the loci of exposure and nanoparticles formation are different.

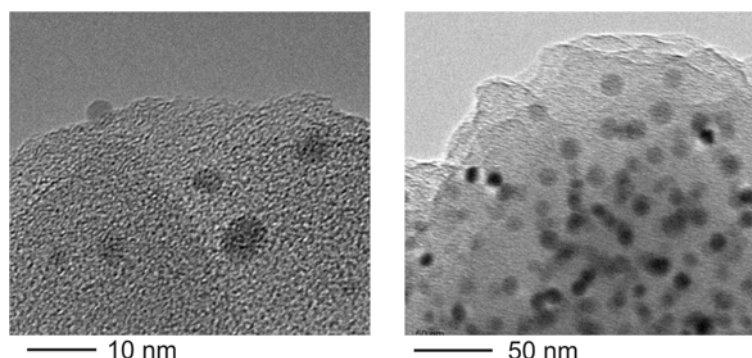


Figure 1. Bright field images of copper nanoparticles prepared from sample 1, 2.

A clear determination of the nanoparticles structure is possible by applying SAED and HRTEM combined with image processing. The SAED pattern depicted in Figure. 2 on the left was recorded on a region with many nanoparticles. The diffraction pattern exhibits sharp Bragg intensities as expected for perfect single crystals. The reflections were located on concentric circles due to unsystematic orientations of the nanoparticles. The diameters of the circles correspond to d-values expected for pure copper (d_{Cu} : $d_{111} \sim 2.09 \text{ \AA}$, $d_{200} \sim 1.81 \text{ \AA}$, $d_{220} \sim 1.28 \text{ \AA}$, $d_{311} \sim 1.09 \text{ \AA}$). The crystalline nature of the nanoparticles was also evidenced by HRTEM, see Figure. 2, right. The HRTEM micrographs display a periodic arrangement of stripes corresponding with net planes of copper, as evidenced by the FFT (fast Fourier transform) of this image. After massive exposure, it is possible to detach the nanoparticles from the surface of the matrix. As evidenced by EDX, these unattached nanoparticles consist of pure copper. Again, their structure can be attributed to the fcc structure of bulk copper by the above mentioned techniques.

Sample 3 was received after evaporating a thin liquid film of red **1** on the Al-grid. Before radiation damage, no Bragg intensities can be observed in electron diffraction patterns of this material – even not within nanosized regions.

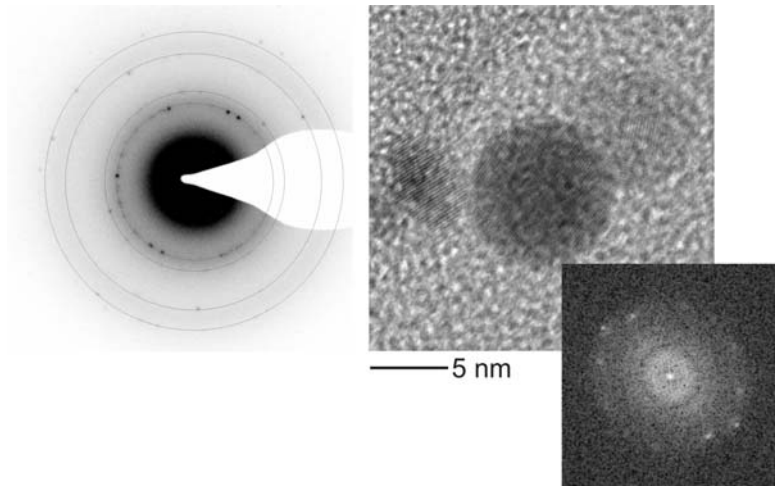


Figure 2. SAED (left) and HRTEM (right) of copper nanoparticles prepared from sample 3.

The SAED pattern and HRTEM micrograph of Figure. 3 were recorded after radiation damage of the amorphous film. Both are consistent with the formation of copper nanoparticles in sample 3. As described above, the composition of isolated nanoparticles was checked by EDX. In conclusion, the combination of HRTEM, SAED and EDX confirms nanoparticle formation in samples 1-3 as a result of radiation damage. Definitely, these particles do not show the suprastructure of nanoscaffold **1**.

As a control experiment we have investigated the supramolecular grid assembly **2**. Similar to **1**, assembly **2** proved also sensitive against radiation damage. The obtained results were again in line with formation of crystalline copper nanoparticles during the exposure. Following the procedures described earlier, the formation of copper nanoparticles was checked by SAED patterns recorded on aggregates of nanoparticles (see Figure. 3), EDX (not shown) and Fourier transformation of HRTEM images of individual nanoparticles (not shown).

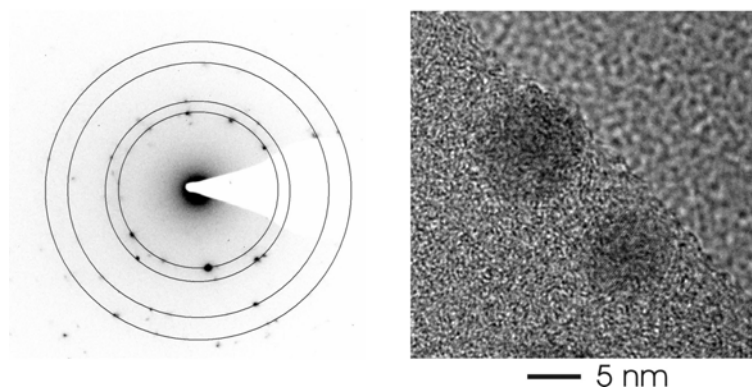


Figure 3: SAED pattern (left, with circles indicating d_{Cu}) and HRTEM micrograph of copper nanoparticles (right) obtained from grid assembly **2**.

To elucidate whether there is a unique templating effect of the supramolecular scaffolds **1** and **2**, the much simpler copper complex **3**¹¹ was investigated by HRTEM and SAED. As shown in Figure 4, the high resolution image again shows copper nanoparticles with a size of 4-5 nm. These findings led us to conclude that the nanoparticle size is independent of any unique templating effect of suprastructures **1** and **2**.

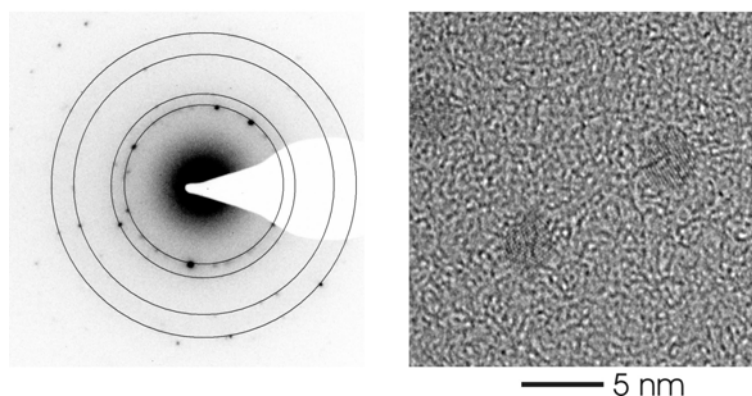


Figure 4. SAED pattern (left, with circles indicating d_{Cu}) and high resolution image of copper nanoparticles (right) of model complex **3**.

CONCLUSIONS: We have shown that copper nanoparticles form from several copper bisphenanthroline precursors. Surprisingly, the dimensions of the nanoparticles are independent of the size and shape of the precursor structure. The observed results point to a radiation damage mediated formation of crystalline copper nanoparticles and rule out any supramolecular template effect. These findings also raise serious questions on using TEM as a proof of metallo-supramolecular aggregates. Moreover, the formation of ordered nanoparticles in non-aqueous media certainly is an interesting aspect of our approach that does not require special reducing additives (*i.e.* detergents) due to the electron beam. Therefore, Cu(I) bisphenanthroline complexes can now be considered as precursors for crystalline copper nanoparticles.

ACKNOWLEDGMENT: We gratefully acknowledge financial support from the DFG and the Fonds der Chemischen Industrie. The authors would like to thank Viola Duppel for practical TEM work and Prof. Dr. Arndt Simon for helpful discussions.

References:

- (1) (a) B. Olenyuk, M. D. Levin, J. A. Whiteford, J. E. Shield, P. J. Stang, *J. Am. Chem. Soc.* **1999**, *121*,

10434. (b) S. R. Seidel, P. J. Stang, *Acc. Chem. Res.* **2002**, *35*, 972.
- (2) G. R. Newkome, T. J. Cho, C. N. Moorefield, R. Cush, P. S. Russo, L. A. Godinez, M. J. Saunders, P. Mohapatra, *Chem. Eur. J.* **2002**, *8*, 2946.
- (3) (a) D. P. Funeriu, J.-M. Lehn, K. M. Fromm, D. Fenske, *Chem. Eur. J.* **2000**, *6*, 2103. (b) M. Barboiu, G. Vaughan, R. Graff, J.-M. Lehn, *J. Am. Chem. Soc.* **2003**, *125*, 10257 and ref's therein.
- (4) (a) S. Leininger, B. Olenyuk, P. J. Stang, *Chem. Rev.* **2000**, *100*, 853. (b) M. Schmittel, V. Kalsani, *Top. Curr. Chem.* **2005**, *245*, 1-53.
- (5) **For example: TEM supported structures see;** (a) ref. 1-2. (b) W. T. S. Huck, B. H. M. Snellink-Ruel, J. W. T. Lichtenbelt, F. C. J. M. van Veggel, D. N. Reinhoudt, *Chem. Commun.* **1997**, *9*. **AFM and STM supported recent structures;** (a) C. M. Drain, F. Nifiatis, A. Vasenko, J. D. Batteas, *Angew. Chem. Int. Ed. Engl.* **1998**, *37*, 2344. (b) R. Takahashi, Y. Kobuke, *J. Am. Chem. Soc.* **2003**, *125*, 2372. (c) S. De Feyter, F. C. De Schryver, *Chem. Soc. Rev.* **2003**, *32*, 139. (d) A. Semenov, J. P. Spatz, M. Möller, J.-M. Lehn, B. Sell, D. Schubert, C. H. Weidl, U. S. Schubert, *Angew. Chem. Int. Ed. Engl.* **1999**, *38*, 2547. (e) U. Ziener, J.-M. Lehn, A. Mourran, M. Möller, *Chem. Eur. J.* **2002**, *8*, 951.
- (6) (a) A. P. Alivisatos, *Science* **1996**, *271*, 933. (b) H. Weller, *Angew. Chem. Int. Ed. Engl.* **1993**, *32*, 41. G. Schmid, Ed. *Clusters and Colloids*; VCH Press: New York, **1994**. (c) R. C. Ashoori, *Nature* **1996**, *379*, 413. (d) L. M. I. Billas, A. Chatelain, W. A. de Heer, *Science* **1994**, *265*, 1682. (d) C. B. Murray, D. J. Norris, M. G. Bawendi, *J. Am. Chem. Soc.* **1993**, *115*, 8706. (e) T. Vossmeier, L. Katsikas, M. Giersig, I. G. Popovic, K. Diesner, A. Chemseddine, Eychmueller, H. Weller, *J. Phys. Chem.* **1994**, *98*, 7665. (f) S. H. Tolbert, A. P. Alivisatos, *Science* **1994**, *265*, 373.
- (7) (a) M. P. Pileni, *Langmuir*, **1997**, *13*, 3266. (b) H. H. Huang, F. Q. Yan, Y. M. kek, C. H. Chew, G. Q. Xu, W. Ji, P. S. Oh, S. H. Tang, *Langmuir*, **1997**, *13*, 172 and ref's therein. (c) B. A. Korgel, K. P. Johnston, R. C. Doty, K. J. Ziegler, *J. Am. Chem. Soc.* **2001**, *123*, 7797. (d) J. Hambrock, A. Becker, J. Weiß, R. A. Fischer, *Chem. Commun.* **2002**, 68 and ref's therein. (e) L. Gou, C. J. Murphy, *Nano Lett.* **2003**, *2*, 231. (f) S. U. Son, I. K. Park, T. Hyeon, *Chem. Commun.* **2004**, 778.
- (8) (a) M. Schmittel, H. Ammon, V. Kalsani, A. Wiegrefe, C. Michel, *Chem. Commun.* **2002**, 2566. (b) M. Schmittel, V. Kalsani, D. Fenske, A. Wiegrefe, *Chem. Commun.* **2004**, 490.
- (9) Model complex **3** was prepared by mixing [Cu(MeCN)₄]PF₆, 2,9-bis(4-bromo-2,3,5,6-tetramethylphenyl)-[1,10]phenanthroline¹¹ and [1,10]phenanthroline (1:1:1 equiv.) in dichloromethane. The resulting dark red compound was identified by ¹H NMR, ESI MS and elemental analysis.
- (10) The electron microscope (Philips CM30ST, LaB₆-cathode) was operating at 300 kV (resolution: 1.9 Å). Fourier transforms (FFT) of high resolution micrographs were calculated with the software Digital Micrograph 3.6.1 (Gatan). EDX (Si-Li-Detector, Noran) was performed with a nanoprobe (point analyses) and in the scanning mode (spectral imaging).
- (11) M. Schmittel, A. Ganz, D. Fenske, *Org. Lett.* **2002**, *4*, 2289.

CHAPTER 6

6. The HETTAP Approach.....	311
6.1 Introduction	311
6.2 State of Knowledge and Motivation	311
6.3 Results and Discussion	313
6.3.1 The HETTAP Approach: Self-Assembly and Metal Ion Sensing of Dumbbell-Shaped Molecules and A Clip Molecule (Supp 6-1).....	313
6.3.2 A Facile Approach to Dynamic and Fluorescent Nanoscale Phenanthroline/Terpyridine Zinc(II) Ladders (Supp 6-2).....	316
6.3.3 Zn(II)/Ag(I) Nanoscale 2D Ladders with Internally Appended Pyrenes (Supp 6-3)	319
6.3.4 A Directional Approach to Functional Nanoscale Ladders (Supp 6-4)	320
6.3.5 Other Large Assemblies	323
6.4 Summary	324

6. The HETTAP Approach

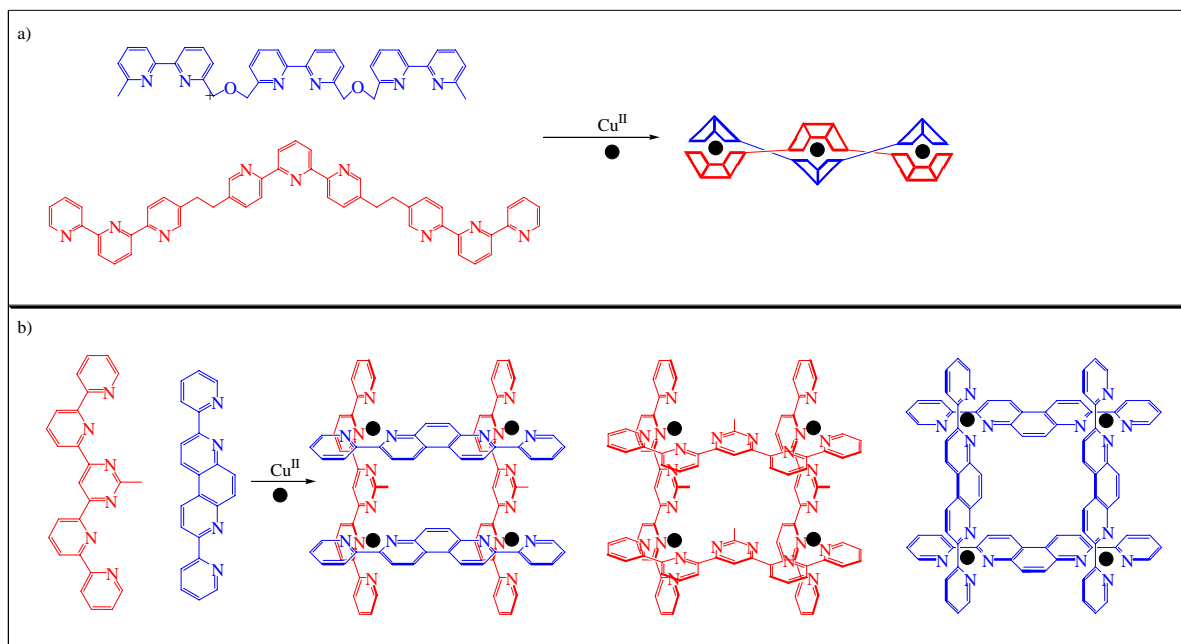
6.1 Introduction

As discussed in chapter 2, it is quite evident that currently rather few tools¹ are at hand to construct supramolecular aggregates in particular when we compare them to those of covalent organic synthesis. Moreover, our usual strategies for the construction of multitopic aggregations are still at rudimentary levels when compared to those used by nature for the construction of biological assemblies (*e.g.* the cell).

Over the years, heteroleptic aggregates have been rarely reported. They are unique not only in the structural sense but also since they lend access to arrays of self-assembled multiple functionalities. Inspired by our success with the HETPHEN approach (chapter 3), we searched to explore the possibility of self-assembled nanostructures composed of both bi- and tridentate ligands. In this chapter a novel supramolecular toolkit, the HETTAP (**h**eteroleptic **t**erpyridine **a**nd **p**henanthroline complexation) approach, and its functional consequences will be presented. Using the HETTAP methodology several multicomponent aggregates, such as dumbbell, clip, and ladder motifs, were realised and explored with regard to their properties.

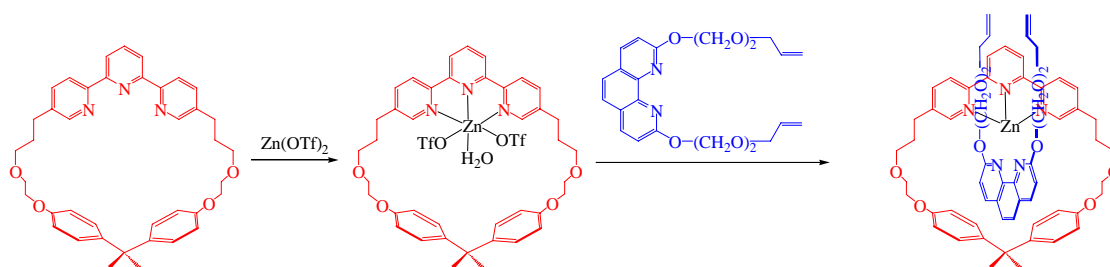
6.2 State of Knowledge and Motivation

In a dynamic multicomponent scenario, the main problem is the rapid ligand/metal exchange taking place interconverting homo and hetero combinations. This fact has become evident from previous investigations directed towards the self-assembly of bi and tridentate ligands in presence of appropriate metal cations (Scheme 6-1 and Scheme 6-2). A while ago Lehn *et al.* reported² on the self-assembly of a helicate composed of bi- and tridentate ligands with Cu²⁺ (prefers to have pentacoordination) using the maximum site coordination principle (Scheme 6-1a). However, later attempts by the same group to fabricate bi- and tridentate ligand aggregation in other structural motifs failed (Scheme 6-1b).^{3a}



Scheme 6-1. Lehn's attempts^{2,3a} to achieve multicomponent aggregates composed of bi and tridentate ligands.

Recently, Sauvage *et al.* utilised bi- and tridentate ligand aggregation in the construction of a interlocked molecule.⁴ However, this unique example is restricted to interlocked molecules and can not be generalised (Scheme 6-2).



Scheme 6-2. Sauvage's approach to endeavour multicomponent aggregation; exploration of ring-constraints.

Later studies by Constable,^{3b} Schubert^{3d} and Newkome^{3e} further suggested that there is need of a general construction strategy to make bi- and tridentate aggregates. Herein, we now present our results on the use of phenanthroline and terpyridine ligands as elements in multicomponent aggregation. The readily available HETPHEN building blocks **1-4** presented in chapter 2 were used in combination with terpyridine building blocks **5-6** and Zn(II) salts (Figure 6-1).

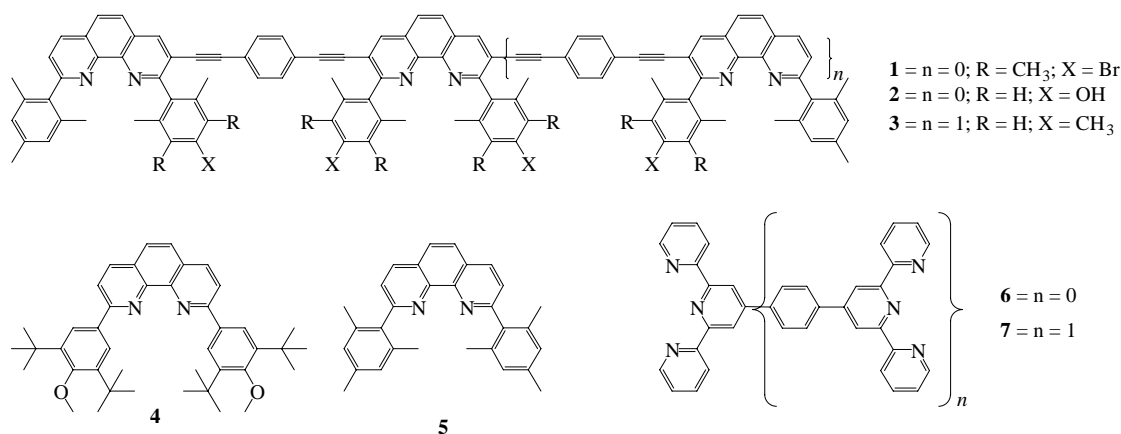


Figure 6-1. Ligands used for multicomponent aggregation.

6.3 Results and Discussion

6.3.1 The HETTAP Approach: Self-Assembly and Metal Ion Sensing of Dumbbell-Shaped Molecules and A Clip Molecule (Supp 6-1)

The exploration of HETPHEN building blocks in combination with other chelating ligands has led to the discovery of the HETTAP approach (**h**eteroleptic **t**erpyridine **a**nd **p**henanthroline) (Figure 6-2). In the following, the first examples of zinc(II) based multicomponent dumbbell-shaped structures and a clip structure both comprised of bisphenanthroline and tridentate (terpyridine) ligands will be presented and their ability to sense metal cations will be highlighted. This study provided access to fluorescent aggregates since zinc(II) complexes are known for their photophysical innocuousness.⁵

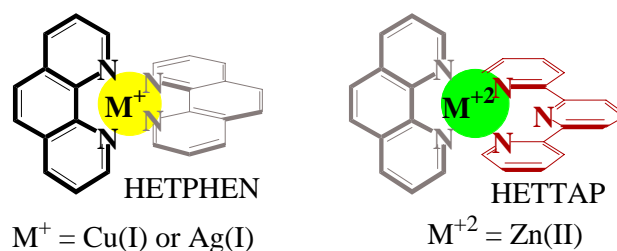
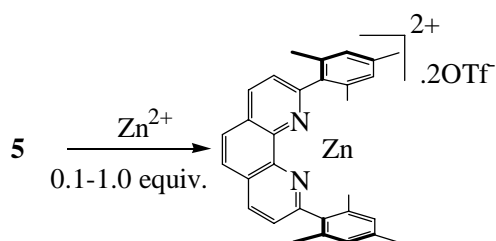


Figure 6-2. HETPHEN and HETTAP approaches.

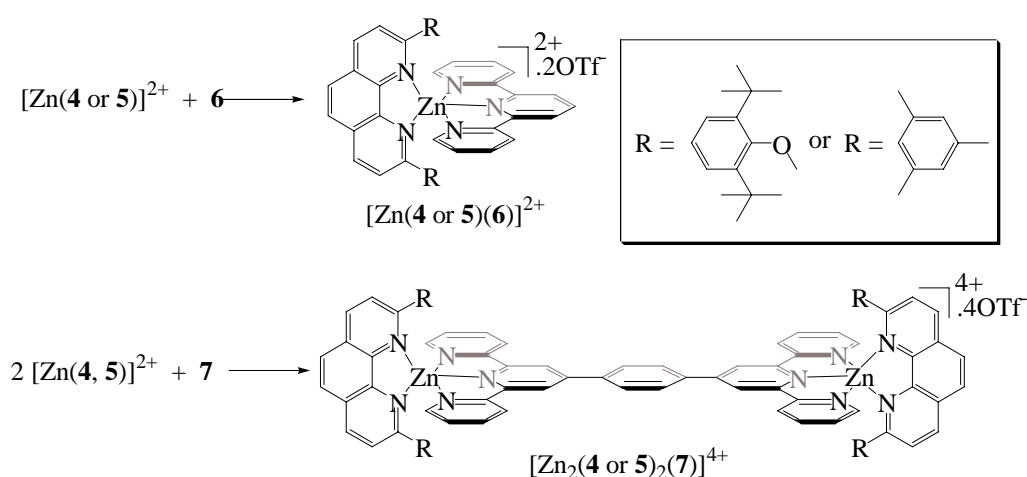
As with the HETPHEN approach, the appropriate combination of bi- and tridentate ligands and metal ions such as Zn(II) or Cu(II) is expected to yield preferentially heteroleptic combinations. At first, the nature of HETPHEN building blocks with Zn(II) was investigated. As shown in Scheme 6-1, no homoleptic complexes could be detected upon the titration of **5**

with Zn(II) salt. Thus, ligand **5** behaved similar towards Zn(II) as towards Cu(I) and Ag(I) cations (Scheme 6-3).



Scheme 6-3. Zn(II) coordination behaviour of **5**.

Rewardingly, the reaction of $[\text{Zn}(\mathbf{4},\mathbf{5})]^{2+}$ with terpyridine building blocks **6** or **7** produced quantitatively the multicomponent complexes $[\text{Zn}(\mathbf{4},\mathbf{5})(\mathbf{6})]^{2+}$ and $[\text{Zn}_2(\mathbf{4},\mathbf{5})_2(\mathbf{7})]^{4+}$, as demonstrated by NMR and ESI MS spectroscopic data. One of the dumbbell structures, $[\text{Zn}_2(\mathbf{4} \text{ or } \mathbf{5})_2(\mathbf{7})]^{4+}$, was further characterized by X-ray analysis (Figure 6-3).



Scheme 6-4. Self-assembly of heterotopic aggregates.

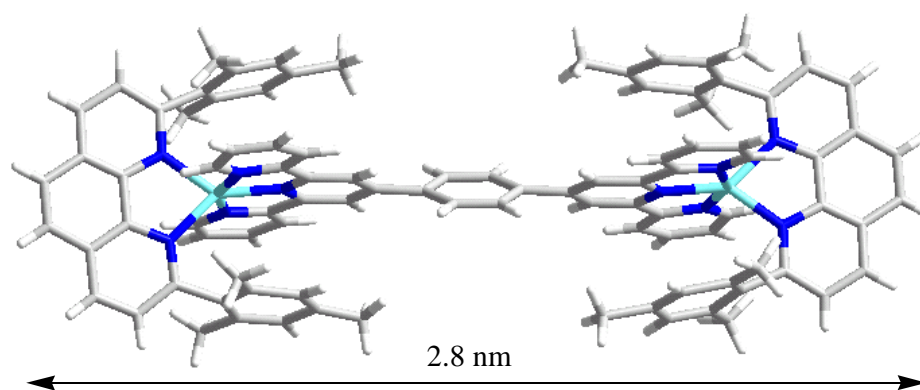
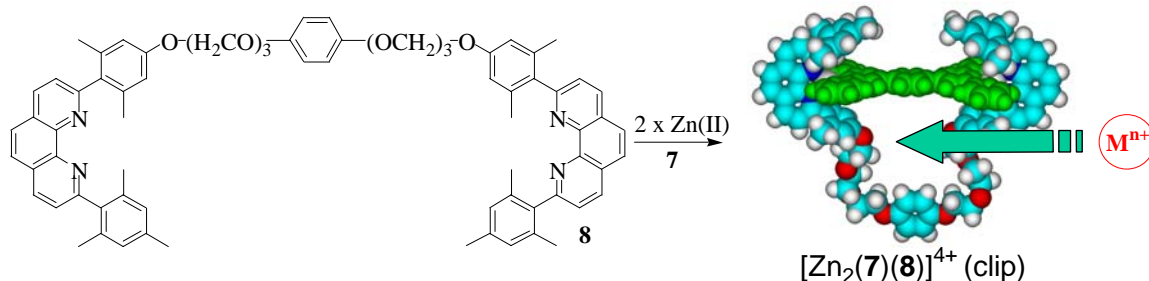


Figure 6-3. Single crystal structure of **C2** $[\text{Zn}_2(\mathbf{5})_2(\mathbf{7})]^{4+}$ (dumbbell-2).

Clip-like⁶ molecules have attracted considerable interest due to their rich host-guest chemistry.⁷ As shown in Scheme 6-3, a clip-shaped molecule was self-assembled by reacting **8**,⁸ **7** and Zn(OTf)₂. Since the supramolecular clip contains an oligoether unit, it is expected to sense metal cations.⁹



Scheme 6-5. Self-assembly of clip motif.

Metal ion sensing of the Clip assembly: The ability of $[Zn_2(7)(8)]^{4+}$ to act as a host for various metal cations was investigated using UV/vis and fluorescence spectroscopy. Within the small series of cations studied, the largest increase of the fluorescence response was observed for Pb^{2+} (25% increase with respect to $[Zn_2(7)(8)]^{2+}$).

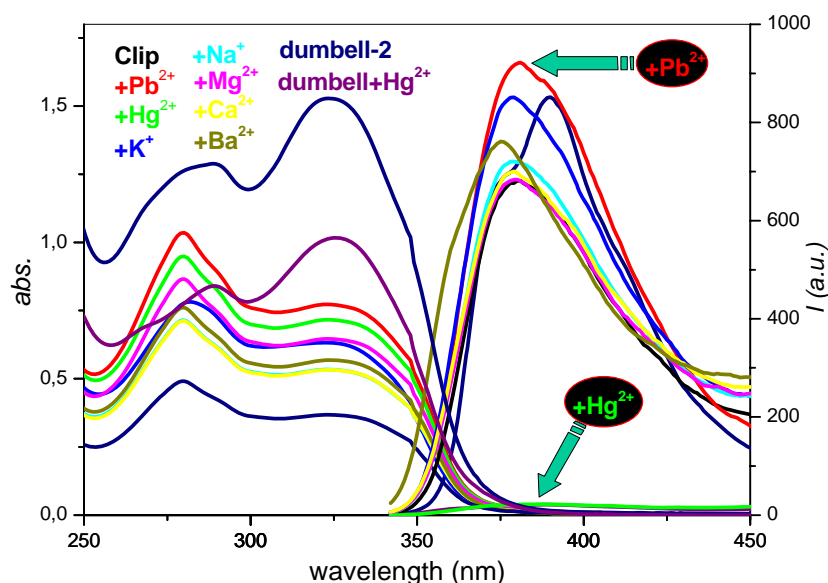


Figure 6-4. UV-vis and fluorescence spectra of $[Zn_2(7)(8)]^{4+}$ (2.04×10^{-5} M) and $[Zn_2(5)_2(7)]^{4+}$ (1.9×10^{-4} M) in the absence and in the presence of Na^+ , K^+ , Mg^{2+} , Ca^{2+} , Pb^{2+} , Ba^{2+} and Hg^{2+} in acetonitrile at rt (metal salts used as their perchlorate salts; ~10 equiv. of each metal ion was added). Excitation wavelength: 330 nm.

Interestingly, an almost complete fluorescence quenching was observed upon addition of Hg^{2+} to $[Zn_2(7)(8)]^{4+}$ (Figure 6-4 and Figure 6-5). When $[Zn_2(7)(8)]^{4+}$ was replaced by the dumbbell $[Zn_2(4 \text{ or } 5)_2(7)]^{2+}$, complete quenching of fluorescence was equally observed, ruling out any selective interaction between the oligoether chain and Hg^{2+} ions. The ESI MS analysis of the reaction mixture showed a complete transmetalation process and well resolved

signals corresponding to $[\text{Hg}_2(\mathbf{7})(\mathbf{8})]^{2+}$ (Hg-clip) with no signals of $[\text{Zn}_2(\mathbf{7})(\mathbf{8})]^{2+}$ being detectable. Therefore, the Zn(II) dumbbell and clip molecules can selectively sense Hg^{2+} through a metal exchange process. Fluorescence quenching is supposedly due to an electron transfer process from the fluorophore to the metal center.¹⁰

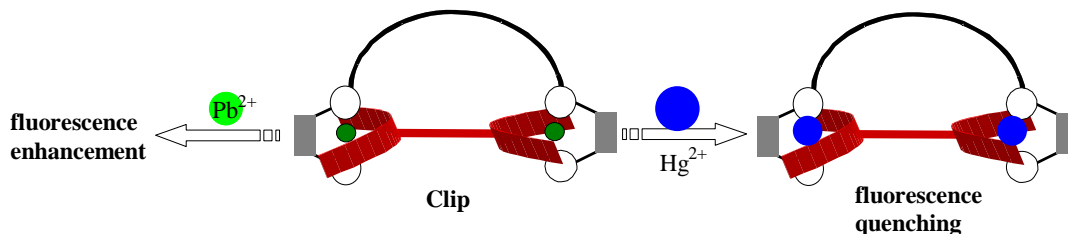
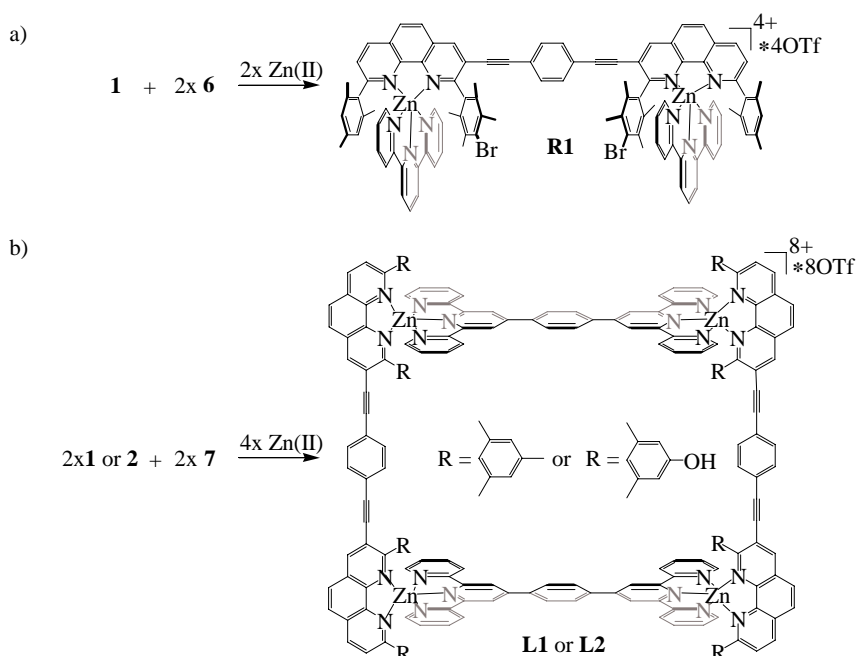


Figure 6-5. Metal ion sensing of Clip assembly.

6.3.2 A Facile Approach to Dynamic and Fluorescent Nanoscale Phenanthroline/Terpyridine Zinc(II) Ladders (Supp 6-2)

After the successful installation of the HETTAP methodology its utility to prepare nanoscale ladder motifs was probed. As shown in Scheme 6-6, several rack and ladder motifs were prepared quantitatively by mixing the appropriate phenanthroline and terpyridine building blocks with $\text{Zn}(\text{OTf})_2$. All racks and ladders exhibited at notable fluorescence at $\lambda_{\text{em}} \sim 460\text{-}480$ nm upon excitation at ~ 390 nm.



Scheme 6-6. Self-Assembly of rack and ladder motifs.

Aside of extensive solution state characterization of **R1** and **L1,L2**, **L2** was investigated by single crystal analysis furnishing a decisive proof of the suggested structure (Figure 6-6). **L2**

possesses a nanoscale ladder structure, in which two **2** and **7** assemble along with four Zn^{2+} ions (Figure 6-1). External dimensions (including van der Waals radii) are 2.7 and 3.2 nm. The terpyridine units of **7** are sandwiched in between the 2,9-aryl groups of the phenanthrolines of **2** allowing for stabilising π - π interactions ($d = 3.4 \text{ \AA}$). Hence, the presence of the 2,9-steric stoppers in **2** forces the Zn(II) ions to adapt a penta-coordination with three positions being filled from the terpyridine unit and two from the phenanthroline ligand. To the best of our knowledge this is the first structurally characterised nanoscale ladder assembly.

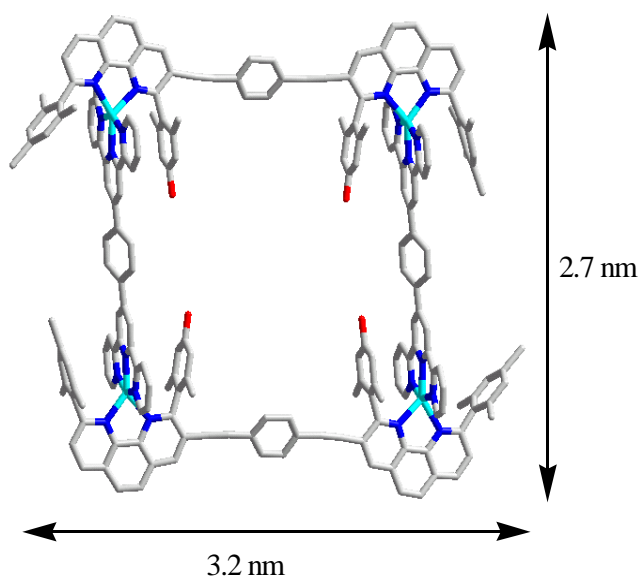


Figure 6-6. Single crystal structure of **L2**.

The dynamic nature of the aggregates became evident after mixing **L1** and **L2** in $\text{CH}_2\text{Cl}_2/\text{CH}_3\text{OH}$ (8:2). Within few (~5) minutes the formation of the mixed species **L3** = $[(\text{Zn})_4(\mathbf{1})(\mathbf{2})(\mathbf{7})_2]^{8+}$ aside of **L1** and **L2** was clearly indicated by the ESI-MS and $^1\text{H-NMR}$ data (Figure 6-7).

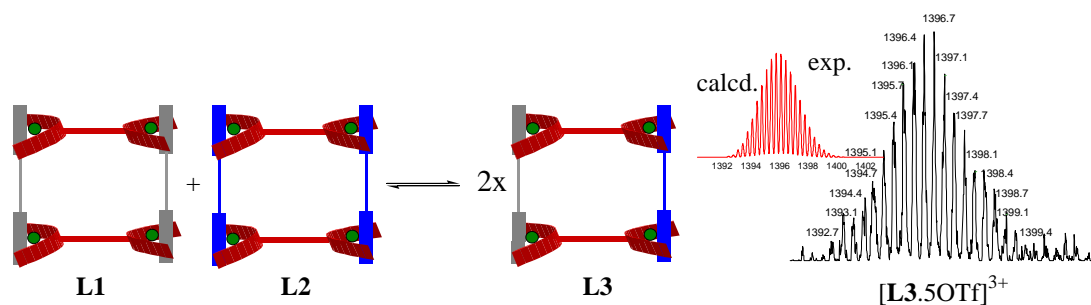
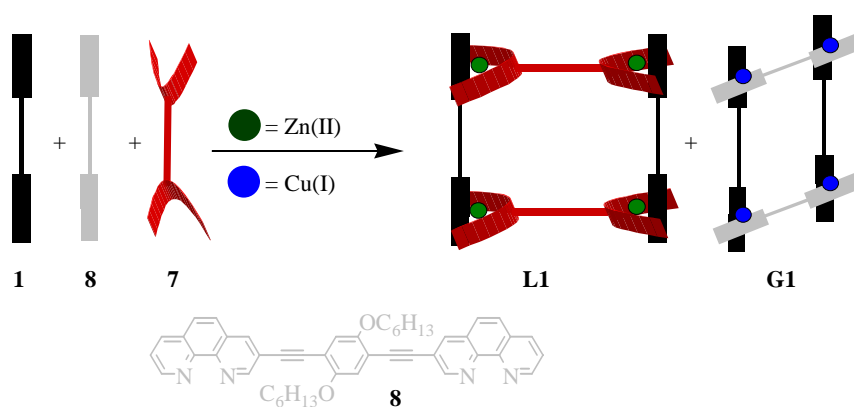


Figure 6-7. Dynamic nature of the ladder structures. Isotopic distribution (dark) of the mixed species $[\text{L3.5OTf}]^{3+}$ along with its theoretical one (red).

The dynamic nature of **L1,2** allowed us to conceive experiments with an unprecedented level of self-recognition.¹¹ Such phenomena had originally been studied by Lehn,^{11a} who was able to demonstrate that from a mixture of oligo-bipyridine strands and a mixture of Cu(I) and Ni(II) salts only helicates composed of *like* ligands and *like* metal ions were afforded. In contrast, combinations of *unlike* ligands and *unlike* metal ions never reached a high level of self-recognition. Using the conceptual insight gained from the HETPHEN and HETTAP strategies we interrogated the reaction of ligands **1**, **8** and **7** in presence of metal ions Zn²⁺ and Cu⁺ (1:1:1:2:2 stoichiometry). As conceived, only two discrete nanostructures emerged selectively from this mixture of ligands and metal ions, *i.e.* ladder **L1** and grid **G1** (Scheme 6-7), as indicated by ESI MS and ¹H NMR.



Scheme 6-7. Cartoon representation of the un-like ligand/metal ions recognition process.

The HETTAP concept was further extended to other metal ions and used for metal exchange scenarios. Along the general procedure we prepared the copper ladder **L4** = [(Cu)₄(**1**)₂(**7**)₂]⁴⁺ and the mercury ladder **L5** = [(Hg)₄(**1**)₂(**7**)₂]⁸⁺ both of which did not fluoresce quite in contrast to **L1** (Figure 6-8). From these observations a two step multi-transmetalation off-on-off system was designed. Upon addition of Zn(II) salt to **L4** (non fluorescent; OFF), **L1** was afforded (fluorescent; ON) that could be transformed further to **L5** (non fluorescent; OFF) upon the addition of Hg(II). The transmetalations were readily followed by ESI MS and fluorescence spectrometry.

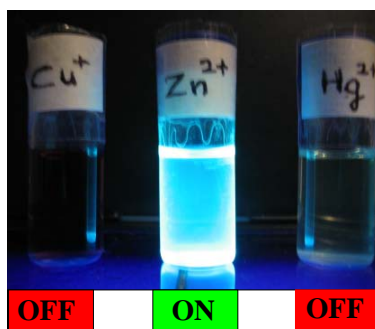


Figure 6-8. Photograph taken under a UV lamp (254 nm).

6.3.3 Zn(II)/Ag(I) Nanoscale 2D Ladders with Internally Appended Pyrenes (Supp 6-3)

There is growing interest to fabricates stacks of π -conjugated planar molecules due to their unique chemical and physical properties.¹² In order to realise stacks with quadruple pyrene in an discrete atmosphere we have explored self-assembly strategy 2 (Figure 6-9).

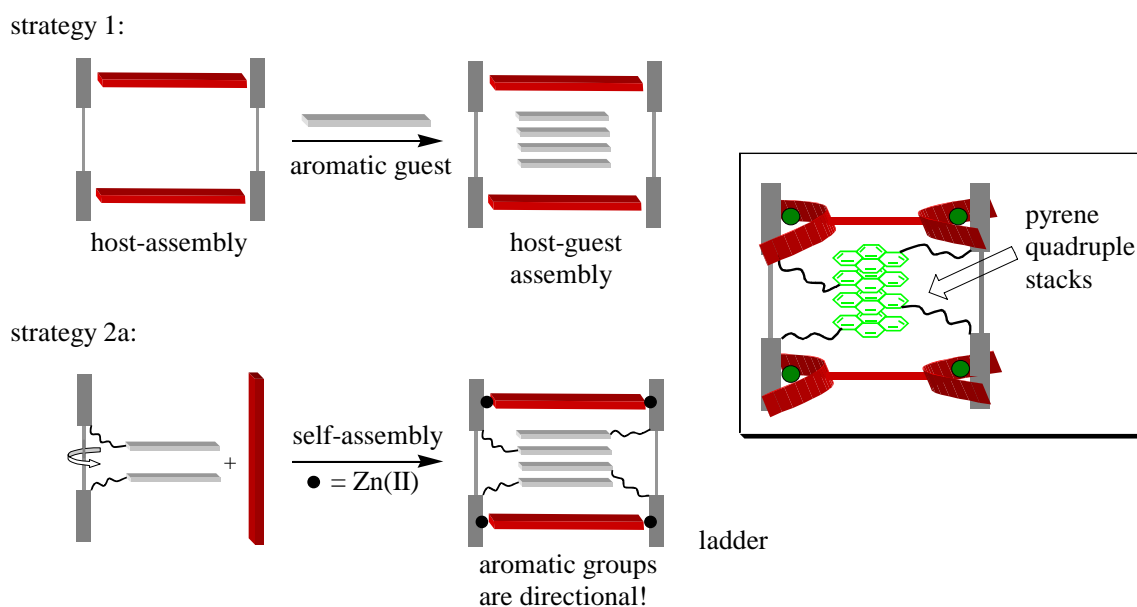
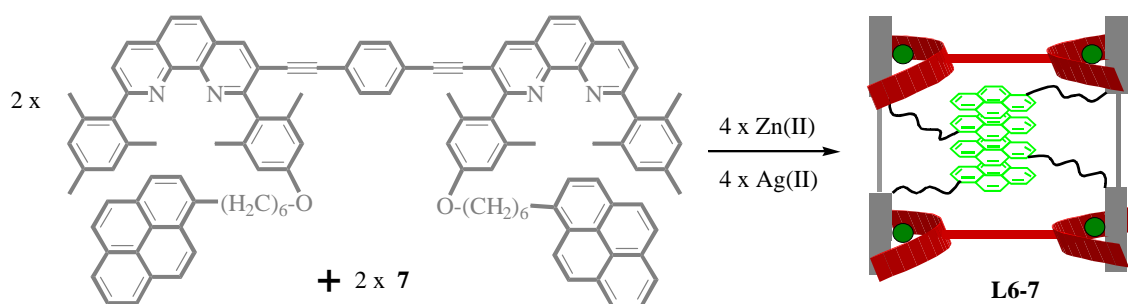


Figure 6-9. Available strategies to observe aromatic stacks in an discrete supramolecular atmosphere.¹³

As shown in Scheme 6-8, the ladder **L6** could readily be assembled by mixing **7**, **9**, and Zn(OTf)_2 (1:1:2 eq respectively) in a mixture of dichloromethane and methanol (8:2). Aside of solution state proof through NMR, ESI MS data, the pyrene ladder could also be characterized in the solid state.



Scheme 6-8. Self-assembly of the pyrene ladder **L6**.

The crystal structure analysis showed **L6** to possess the suggested structure, in which two molecules of **7** and **9** assemble by means of coordination to four metal (Zn^{2+}) ions. The structure reveals the nanoscale dimensions of **L6** with external distances (including van der Waals radii, along the ladder backbone) of 2.3, 2.6, 3.2 nm (Figure 6-10). The external distance (max) in-between two pyrenes is ~ 3.6 nm. Similarly to **L2**, π - π stacking interactions were detected ($d = 3.4 \text{ \AA}$) between the terpyridine units and the 2,9-alkylaryl groups at any phenanthroline ligand. However, no aromatic stacking of the pyrenes could be detected in the solid state, due to the limited space within the ladder enforcing the pyrene units to tilt away from the interior. Similarly, Ag(I) ladder (**L7**) were prepared and characterised. A discussion of the photophysical properties of these aggregates is presented in Supp 6-4.

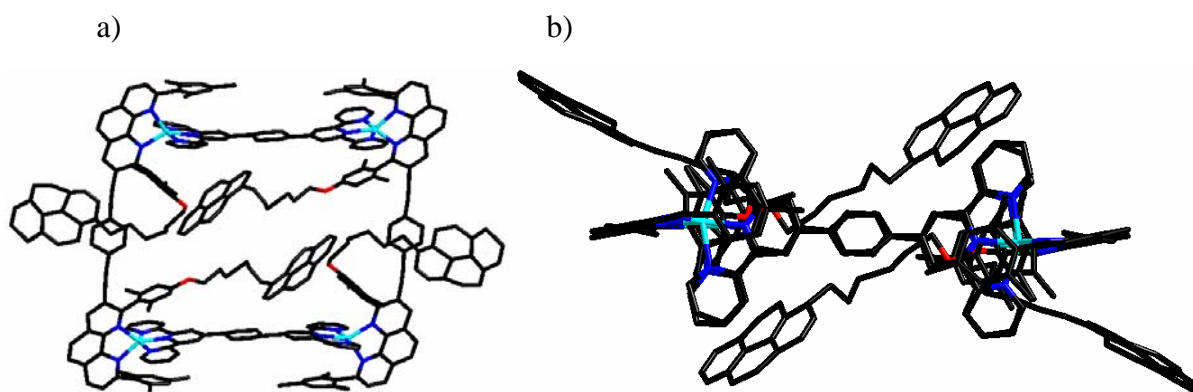


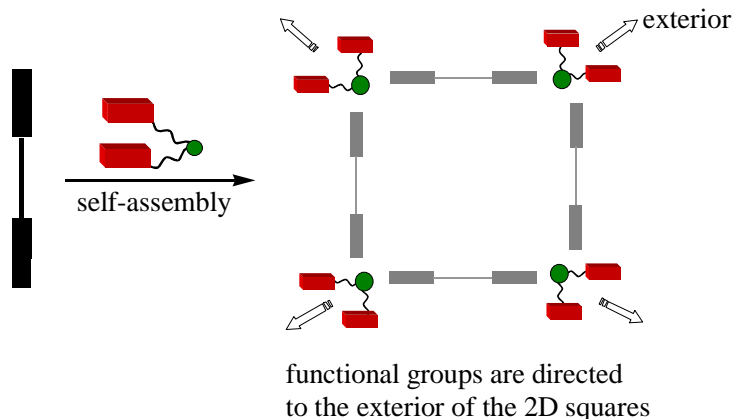
Figure 6-10. a) Stick representation of single crystal structure of **L6**. b) Side view

6.3.4 A Directional Approach to Functional Nanoscale Ladders (Supp 6-4)

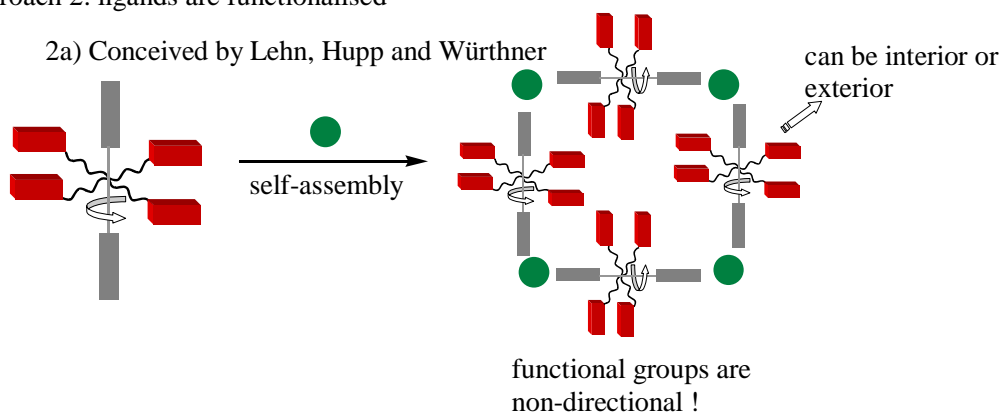
The incorporation of functional units into supramolecular aggregates has been achieved so far using two strategies (Figure 6-12). Due to its simplicity, approach 1 has become the method of choice to incorporate functionalities in supramolecular aggregates.^{14a} However, this scheme only lead to externally functionalized aggregates. On the other hand, internal functionalisation

should allow to generate superstructures in the inside with novel optical and electrical properties. This can be partly realized by the strategy followed up by Lehn, Hupp and Würthner^{14b-d} (Figure 6-12, 6-2a). As shown in Figure 6-12, 6-2b, however, the HETTAP approach should provide access to highly internally directed functional aggregates.

Approach 1: metal centers are functionalised; conceived by Stang



Approach 2: ligands are functionalised



2b) HETTAP principle; coined by Schmittel

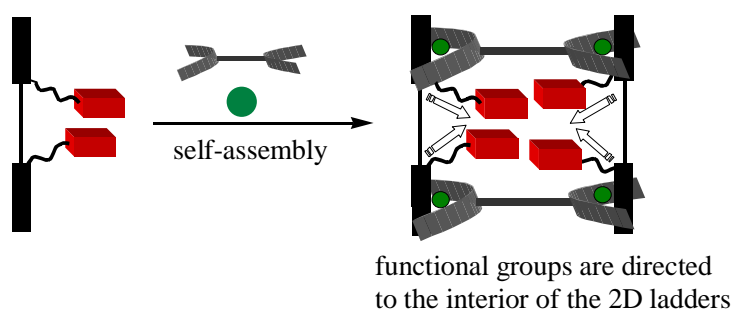
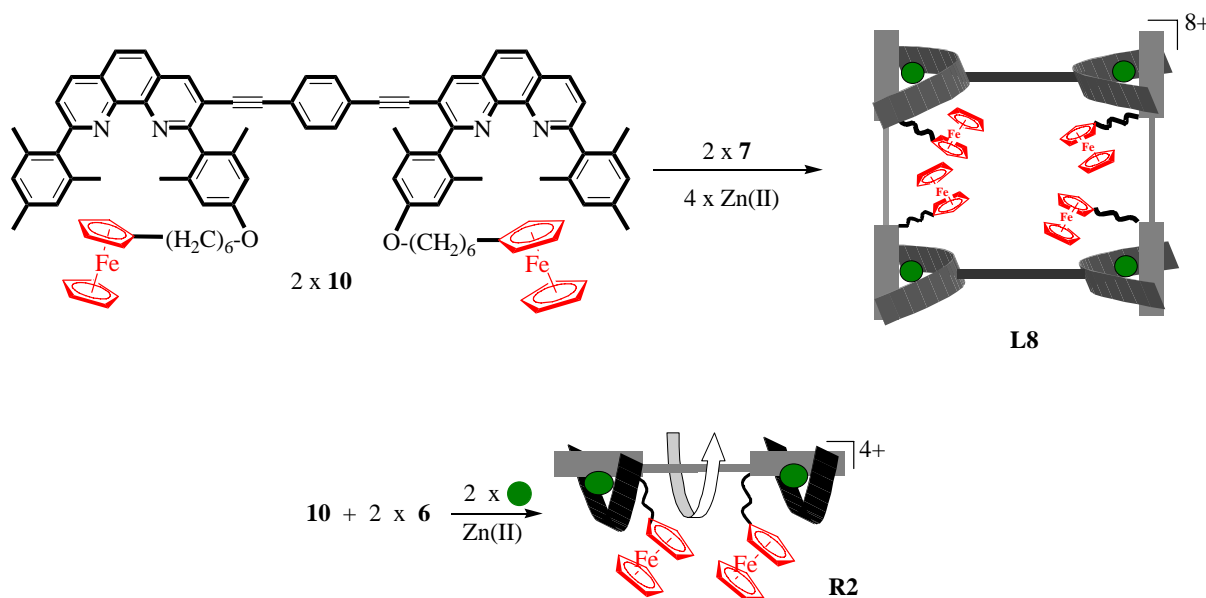


Figure 6-12. Available approaches for supramolecular functionalisation.¹⁴

As novel electrochemical properties¹⁵ may be accessible from the resulting nanoladders, ferrocene was chosen as a functional building block due to its role as a stable redox active entity. In the following, we describe the exploration of approach 2b to furnish internally ferrocene functionalised nanoaggregates, their characterization and their electrochemistry.

As shown in Scheme 6-8, **L8** and **R2** could readily be assembled by mixing **10** with **6** or **7**, respectively, and $\text{Zn}(\text{OTf})_2$ (1:1:2 or 1:2:2 equiv.) in a mixture of dichloromethane and methanol (8:2).



Scheme 6-8. Self-assembly of **L8** and **R2**.

The effect of the supramolecular framework **L8** on the redox properties of ferrocene in comparison of that in **10** was probed by cyclic voltammetry (CV) in dichloromethane/acetonitrile. In contrast to Würthner squares (a peak splitting was reported suggesting the presence of interior and exterior sets of ferrocene units),¹⁶ the CV of **L8** (also of **10** and **R2**) exhibited one single sharp reversible oxidation wave which suggested little or no interaction between the redox centers.¹⁷ Indeed, the Hyperchem minimized¹⁸ structure advocated a similar environment for all four ferrocene units in **L8** (Figure 6-13).

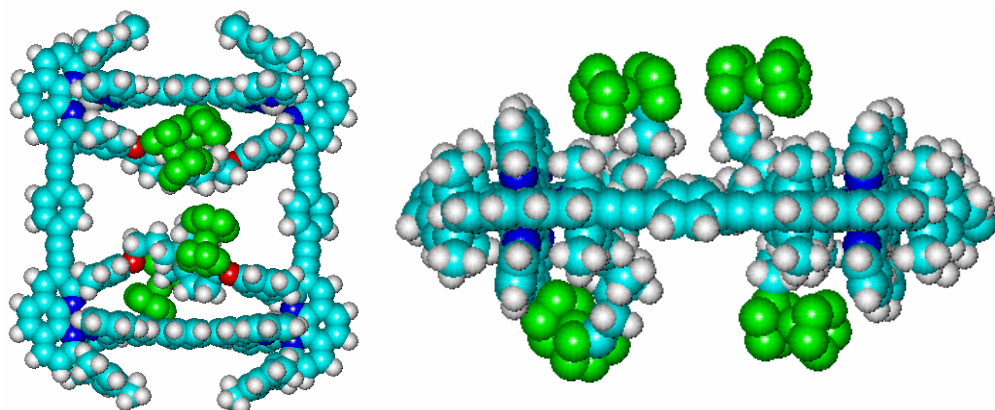


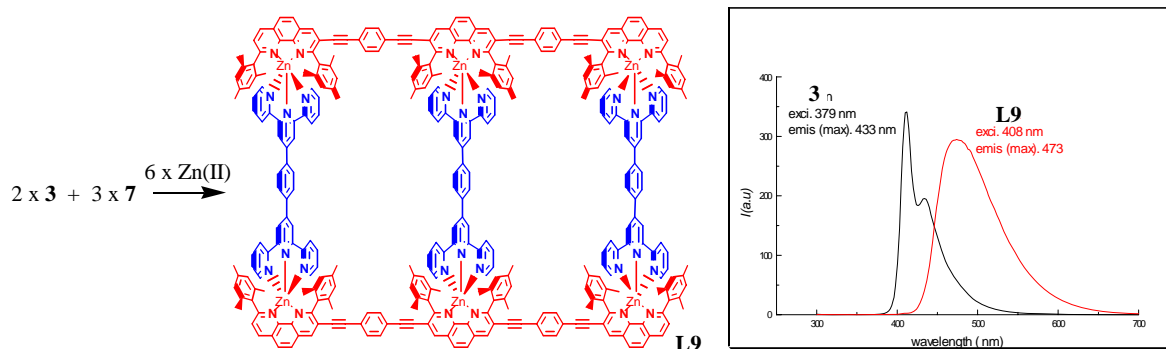
Figure 6-13. Front (left) and top (right) views of the energy minimised structure of **L8**. Ferrocenes are highlighted with green colour.

L8 showed a wave at $E_{1/2} = 0.47$ V (versus DMF/DMF⁺; DMF = decamethylferrocene) at all scan rates for the ferrocene couple. Interestingly, the potential in **L8** is anodically shifted (20 mV) compared to that of the free ligand **10** and that of **R2**, suggesting that the observed $\Delta E_{1/2}$ of **L8** is due to a supramolecular effect. Apparently, the oxidation of ferrocene (charge buildup) becomes thermodynamically hindered by the supramolecular ladder structure. Similarly, positive shifts were reported in supramolecular systems containing ferrocene as a host and equally in dendrimers with a ferrocene core.¹⁹ However, the observed positive shift is moderate (20 mV) suggesting only a slight shielding of the ferrocenes by the ladder skeleton. This fact is also clear from the minimised structure; due to the presence of long alkyl chains the ferrocenes were outside of the two dimensional plane that is opened up by the ladder structure, rendering the ferrocenes easily accessible for redox processes (see Figure 6-13b).

6.3.5 Other Large Assemblies

In the following, two logical extensions of the HETTAP strategy leading to the self-assembly of a [2x3] ladder motif and a [3x3] hexagon will be presented.

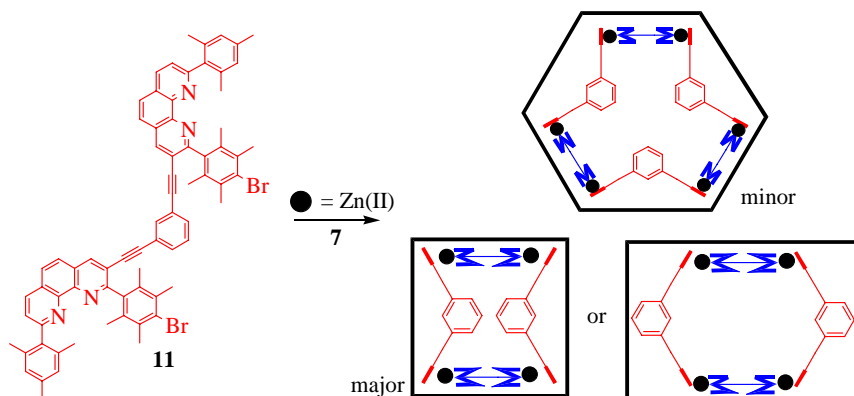
Self-assembly of a [2x3] ladder: Upon reacting **3** and **7** with Zn(II) salt (1:1.5:3 equiv. respectively) **L9** formed cleanly. **L9** was characterized by ESI MS and ¹H NMR. Similar to **L1,L2**, **L9** also exhibited intense emission (~480 nm) upon excitation at ~390 nm (Scheme 6-9).



Scheme 9. Self-assembly of [2x3]ladder **L9** and its fluorescence spectra.

Attempts to prepare hexagon: Attempts to prepare a hexagon as a pure compound were met with failure as the analysis of the reaction mixture by ESI MS and ¹H NMR indicated the

presence of both a [2x2] ladder motif (major species) and the desired hexagon (minor), suggesting the importance of entropic contributions in driving the equilibrium towards the less particle containing aggregates (Scheme 6-10).



Scheme 6-10. Self-assembly of a hexagon.

6.4 Summary

A systematic investigation led to the invention of a novel supramolecular toolkit, the HETTAP approach. Following the HETTAP strategy, several multicomponent supramolecular structures could be assembled. Since the resulting aggregates proved to be fluorescent, this approach gave ready access to novel photophysically active architectures. Hence, unlike the HETPHEN concept, the HETTAP approach is most useful in preparing fluorescent heterotopic supramolecular aggregates. A heterotopic dumbbell and a clip proved sensitive towards Hg^{2+} (driven by metal exchange) monitored by fluorescence quenching and towards Pb^{2+} shown through fluorescence enhancement. Due to the dynamic nature, ligand/metal exchange experiments could be performed in ladder aggregates. Using the HETTAP approach internally functionalised nanoladders were assembled and their properties explored as a function of the supramolecular environment.

- (1) M. Schmittel, V. Kalsani, Functional, Discrete, Nanoscale Supramolecular Assemblies, *Top. Curr. Chem.*, **2005**, 245, 1-53.
- (2) B. Hasenknopf, J. M. Lehn, G. Baum, D. Fenske, Self-assembly of a Heteroduplex Helicate from two Different Ligand Strands and Cu(II) Cations, *Proc. Natl. Acad. Sci. U. S. A.*, **1996**, 93, 1397-1400.
- (3) a) P. N. W. Baxter, R. G. Khoury, J.-M. Lehn, G. Baum, D. Fenske, Adaptive Self-Assembly: Environment-Induced Formation and Reversible Switching of Polynuclear Metallocyclophanes, *Chem. Eur. J.* **2000**, 6, 4140-4148. (b) C. B. Smith, E. C. Constable, C. E. Housecroft, B. M. Kariuki, Formation of a [1+1] Metallomacrocyclic from a Heterotopic Ligand Containing two Terpy and one Bipy Metal-Binding Domains, *Chem. Commun.* **2002**, 2068-2069. (c) F. Loiseau, C. Di Pietro, S. Serroni, S. Campagna, A. Licciardello, A. Manfredi, G. Pozzi, S. Quici, A New Polytopic Bis-diazacrown-ether-polypyridine Ligand and Its Complexes with Zn(II) Salts and Mononuclear and Dendritic Ru(II) Precursors. Synthesis, Absorption Spectra, Redox Behavior, and Luminescence

- Properties, *Inorg. Chem.* **2001**, *40*, 6901-6909. (d) H. Hofmeier, U. S. Schubert, Recent developments in the supramolecular chemistry of terpyridine–metal complexes, *Chem. Soc. Rev.* **2004**, 373-399. (e) P. Wang, C. N. Moorefield, M. Panzer, G. R. Newkome, Helical and Polymeric Nanostructures Assembled from Benzene Tri- and Tetracarboxylic Acids Associated with Terpyridine Copper(II) Complexes, *Chem. Commun.* **2005**, 465-467.
- (4) C. Hamann, J.-M. Kern, J.-P. Sauvage, Zinc(II)-Templated Synthesis of a [2]-Catenane Consisting of a 2,2',6',2''-Terpyridine-Incorporating Cycle and a 1,10-Phenanthroline-Containing Ring, *Inorg. Chem.* **2003**, *42*, 1877-1883.
- (5) J. Rojo, F. J. Romero-Salguero, J.-M. Lehn, G. Baum, D. Fenske, Self-Assembly, Structure, and Physical Properties of Tetranuclear Zn^{II} and Co^{II} Complexes of [2 × 2] Grid-Type, *Eur. J. Inorg. Chem.* **1999**, 1421-1428.
- (6) J. A. A. W. Elemans, M. B. Claase, P. P. M. Aarts, A. E. Rowan, Porphyrim Clips Derived from Diphenylglycoluril. Synthesis, Conformational Analysis, and Binding Properties, *J. Org. Chem.* **1999**, *64*, 7009-7016.
- (7) A. Wu, P. Mukhopadhyay, A. Chakraborty, J. C. Fetting, L. Isaacs, Molecular Clips Form Isostructural Dimeric Aggregates from Benzene to Water, *J. Am. Chem. Soc.* **2004**, *126*, 10035-10043 and ref's therein.
- (8) V. Kalsani, H. Ammon, F. Jäckel, J. P. Rabe, M. Schmittel, Synthesis and Self-Assembly of a Rigid Exotopic Bisphenanthroline Macrocyclic Surface Patterning and a Supramolecular Nanobasket, *Chem. Eur. J.* **2004**, *10*, 5481-5492.
- (9) (a) G. W. Gokel, W. M. Leevy, M. E. Weber, Crown Ethers: Sensors for Ions and Molecular Scaffolds for Materials and Biological Models, *Chem. Rev.* **2004**, *104*, 2723-2750. (b) Y. Liu, Z. Y. Duan, H. Y. Zhang, X. L. Jiang, J. R. Han, Selective Binding and Inverse Fluorescent Behavior of Magnesium Ion by Podand Possessing Plural Imidazo[4,5-f]-1,10-phenanthroline Groups and Its Ru(II) Complex, *J. Org. Chem.* **2005**, *70*, 1679-1683.
- (10) R. Métivier, I. Leray, B. Valeur, Lead and Mercury Sensing by Calixarene-Based Fluoroionophores Bearing Two or Four Dansyl Fluorophores, *Chem. Eur. J.* **2004**, *10*, 4480-4490.
- (11) a) R. Krämer, J.-M. Lehn, A. Marquis-Rigault, *Proc. Natl. Acad. Sci. USA*, Self-Recognition in Helicate Self-Assembly: Spontaneous Formation of Helical Metal Complexes from Mixtures of Ligands and Metal Ions, **1993**, *90*, 5394-5398. b) A. Wu, L. Isaacs, Self-Sorting: The Exception or the Rule?, *J. Am. Chem. Soc.* **2003**, *125*, 4831-4835 and ref's therein. c) B. Belgicir, X. Xing, K. Kumar, Programmed Self-Sorting of Coiled Coils with Leucine and Hexafluoroleucine Cores, *J. Am. Chem. Soc.* **2001**, *123*, 11815-11816.
- (12) A. Schmidt-Mende, A. Fechtenkötter, K. Müllen, E. Moons, R. H. Friend, D. MacKenzie, Self-Organized Discotic Liquid Crystals for High-Efficiency Organic Photovoltaics, *Science* **2001**, *293*, 1119 and ref's therein.
- (13) a) K. Kumazawa, Y. Yamanoi, M. Yoshizawa, T. Kusukawa, M. Fujita, A Palladium(II)-Clipped Aromatic Sandwich, *Angew. Chem. Int. Ed.* **2004**, *43*, 5936-5940. b) F. Wuerthner, A. Sautter, Energy transfer in multichromophoric self-assembled molecular squares, *Org. Biomol. Chem.* **2003**, 240-243. c) M. Schmittel, V. Kalsani, J. W. Bats, **2005**, unpublished results.
- (14) a) P. J. Stang, D. H. Cao, K. Chen, G. M. Gray, D. C. Muddiman, R. D. Smith, Molecular Architecture via Coordination: Marriage of Crown Ethers and Calixarenes with Molecular Squares, Unique Tetranuclear Metallamacrocycles from Metallacrown Ether and Metallacalixarene Complexes via Self-Assembly, *J. Am. Chem. Soc.* **1997**, *119*, 5163-5168. b) R. V. Slone, J. T. Hupp, Synthesis, Characterization, and Preliminary Host-Guest Binding Studies of Porphyrinic Molecular Squares Featuring fac-Tricarbonylrhenium(I) Chloro Corners, *Inorg. Chem.* **1997**, *36*, 5422-5423. c) C. M. Drain, J.-M. Lehn, Self-Assembly of Square Multiporphyrin Arrays by Metal Ion Coordination, *J. Chem. Soc. Chem. Commun.* **1994**, 2313-2315. d) F. Wuerthner, C.-C. You, C. R. Saha-Moeller, Metallosupramolecular Squares: From Structure to Function, *Chem. Soc. Rev.* **2004**, 133-146.
- (15) F. A. Cotton, C. Lin, C. A. Murillo, Supramolecular Arrays Based on Dimetal Building Units, *Acc. Chem. Res.* **2001**, *34*, 759-771.
- (16) C.-C. You, F. Würthner, Self-Assembly of Ferrocene-Functionalized Perylene Bisimide Bridging Ligands with Pt(II) Corner to Electrochemically Active Molecular Squares, *J. Am. Chem. Soc.* **2003**, *125*, 9716-9725.
- (17) S.-H. Hwang, C. N. Moorefield, F. R. Fronczek, O. Lukoyanova, L. Echeguyen, G. R. Newkome, Construction of Triangular Metallamacrocycles: [M₃(1,2bis(2,2'-6,2''-Terpyridin-4-yl-ethynyl)Benzene)₃][M = Ru(II), Fe(II), 2Ru(II)Fe(II)], *Chem. Commun.* **2005**, 713-715.
- (18) Hyperchem 6.02[®]. Release for Windows by Hypercube, Inc. **2000**. MM+ force field.
- (19) Similar anodic shifts were reported for inclusion complexes of ferrocenes in a supramolecular

atmosphere. a) W.-Y. Sun, T. Kusakawa, M. Fujita, Electrochemically Driven Clathration/Declathration of Ferrocene and Its Derivatives by a Nanometer-Sized Coordination Cage, *J. Am. Chem. Soc.* **2002**, *124*, 11570-11571. b) A. E. Kaifer, *Acc. Chem. Res.* **1999**, *32*, 62. c) C. M. Cardona, S. Mendoza, A. E. Kaifer, Electrochemistry of Encapsulated Redox Centers, *Chem. Soc. Rev.* **2000**, *29*, 37. d) D. L. Stone, D. K. Smith, P. T. McGrail, Ferrocene Encapsulated within Symmetric Dendrimers: A Deeper Understanding of Dendritic Effects on Redox Potential, *J. Am. Chem. Soc.* **2002**, *124*, 856-864.

Supp 6-1

The HETTAP Approach: Self-Assembly and Metal Ion Sensing of Dumbbell-Shaped Molecules and A Clip Molecule

Michael Schmittl,^{*a} Venkateshwarlu Kalsani,^a Jan W. Bats^b

^a Center of Micro and Nanochemistry and Engineering, Organische Chemie I, Universität Siegen, Adolf-Reichwein-Str., D-57068 Siegen, Germany, Fax: (+49) 271 740 3270; Tel: (+49) 271 740 4356; E-mail: schmittl@chemie.uni-siegen.de

^b Institut für Organische Chemie und Chemische Biologie, Johann Wolfgang Goethe-Universität, Marie-Curie-Strasse 11, D-60439 Frankfurt am Main, Germany.

Introduction

Stimulating research endeavours by Lehn¹ and Sauvage² have demonstrated a way to fabricate heteroleptic and heterotopic aggregates relying solely on maximum site occupancy and/or ring constraints. However, due to inherent constraints, their building principles do not open a general venue to a wide variety of architectures. Inspired by our recent success with the HETPHEN approach (Figure 1), we have explored the possibility of using the sterically shielded 2,9-diarylphenanthrolines in combination with tridentate ligands (terpyridine building blocks) and pentacoordinating metal ions to develop a *heteroleptic terpyridine and phenanthroline* toolkit in a systematic approach. In the following, the first report about zinc(II) based multicomponent dumbbell-shaped structures and a clip comprised of both bisphenanthroline and tridentate (terpyridine) ligands will be presented. The ability of these assemblies to sense metal cations will also be highlighted.

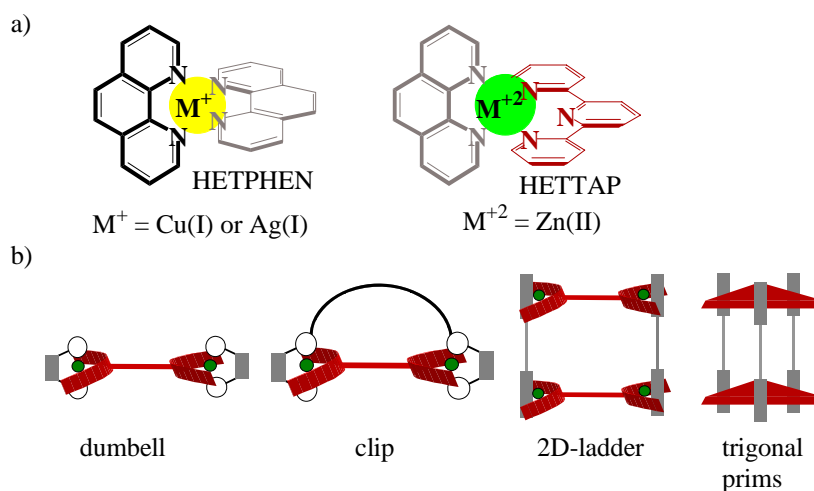


Figure 1. a) HETPHEN and HETTAP approaches. b) expected supramolecular structures from HETTAP approach.

The potential of the HETPHEN (heteroleptic phenanthroline complexation) concept³ has been demonstrated recently by the quantitative formation of several nanoscale heteroleptic assemblies. Since most of the structures were based on Cu(I) coordination chemistry, their photophysical properties proved to be limited.⁴ Therefore, it was tempting to explore other metal ions to access supramolecular aggregates with interesting photophysical properties. Few reports are at hand utilising Zn(II) coordination for fluorescent aggregates., although zinc(II) complexes are known for their photophysical innocuousness.⁵ With regard to structural variations, there is a great potential and flexibility to prepare a variety of supramolecular aggregates (Figure 1, 6 and 7) because terpyridine building blocks are readily available or easily accessible.

Results and Discussion

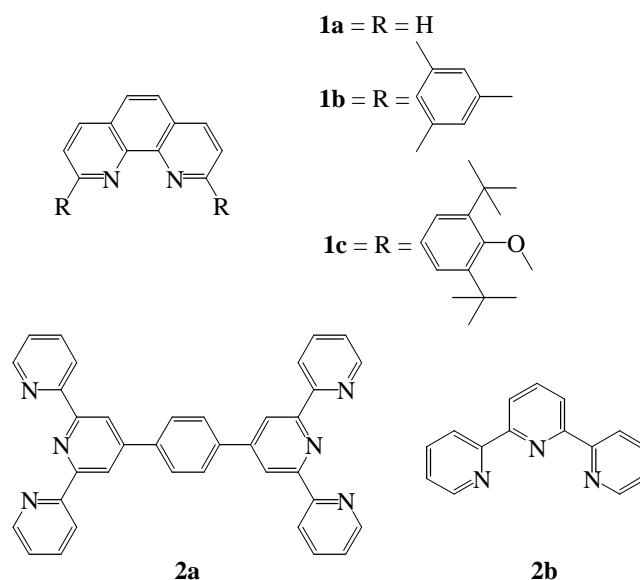


Figure 2. Ligands used for the HETTAP approach.

The phenanthroline building blocks **1b-c** were synthesised according to known procedures.⁶ Ligands **1b** and **1c** were encoded with the required control features to furnish exclusively heterotopic assemblies, *i.e.* the 2,9 positions of each phenanthroline unit in **1b** and **1c** are shielded with bulky alkylaryl groups thus preventing any self-association of these building blocks with metal cations. The terpyridine building blocks **2a** and **2b** were purchased and used as received. The appropriate combination of ligands **1b,c** with metal ions such as Zn(II) or Cu(II)⁷ in presence of **2a-b** is expected to yield heterotopic combinations preferred over homotopic ones.

Heterotopic aggregation. The factors governing heterotopic aggregation were systematically monitored. The reaction of the sterically unloaded (at 2,9-positions) phenanthroline **1a** with **2a** or **2b** and $\text{Zn}(\text{OTf})_2$ provided multiple sets of signals in the ^1H NMR, indicative of the presence of mixtures (Figure 3). ESI MS indeed showed signals corresponding to homo and heterotopic compositions. These results are in line with the previous attempts to assemble bipyridine and terpyridine building blocks by Lehn *et al.*⁸ Other conditions, e.g. sequential addition and change of temperature, did not affect the mixture. From these observations it was evident,⁹ that additional control would be required to drive selectively the thermodynamic equilibria to heterotopic ones.

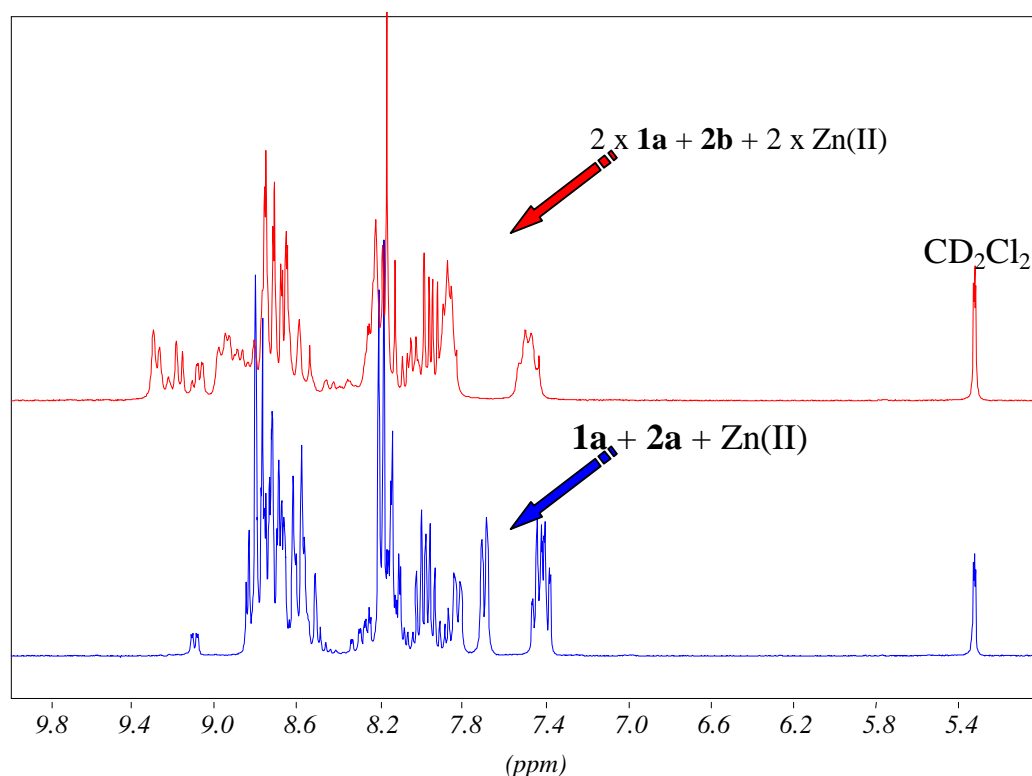
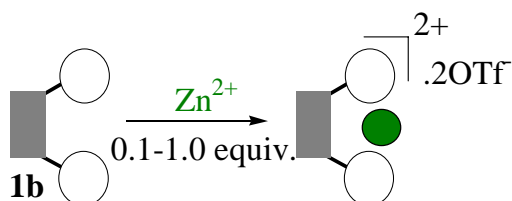


Figure 3. ^1H NMR aromatic region of reaction mixture of a). $2 \times \mathbf{1a} + \mathbf{2b} + 2 \times \text{Zn}(\text{II})$ and b). $\mathbf{1a} + \mathbf{2a} + \text{Zn}(\text{II})$.

Similar to previous observations with the HETPHEN approach, no homoleptic complexes could be detected by ^1H NMR upon reacting **1b** with $\text{Zn}(\text{II})$ salt (1:0-1eq., respectively). This can easily be seen by the absence of a signal at $\delta \sim 6$ ppm, which has been serving as a diagnostic signal¹⁰ for the formation of heteroleptic and heterotopic $\text{Zn}(\text{II})$ complexation (Figure 4a-f; depicted by a red arrow). Thus, ligand **1b** behaved similar towards $\text{Zn}(\text{II})$ as for $\text{Cu}(\text{I})$ and $\text{Ag}(\text{I})$ cations (Scheme 1). When **1b** was reacted with $\text{Zn}(\text{II})$ -ions (1: 1 equiv.) the molecular receptor **3a** could be isolated and characterised by ^1H NMR (Figure 4f).



Scheme 1. Zn(II) coordination behaviour of **1b**.

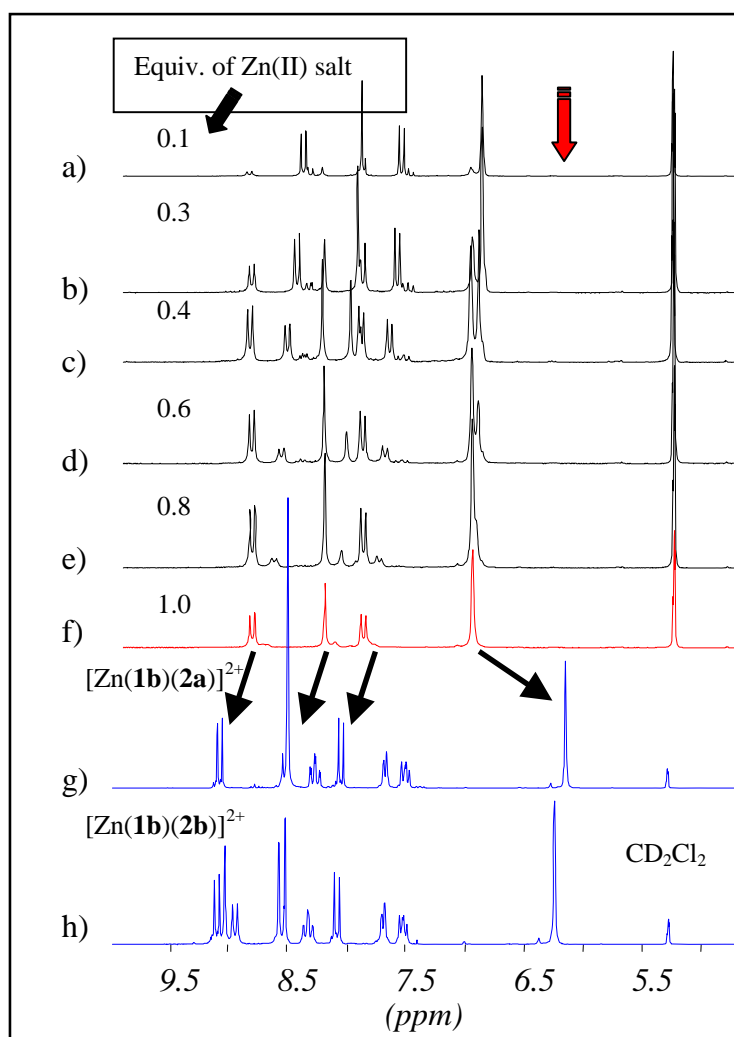
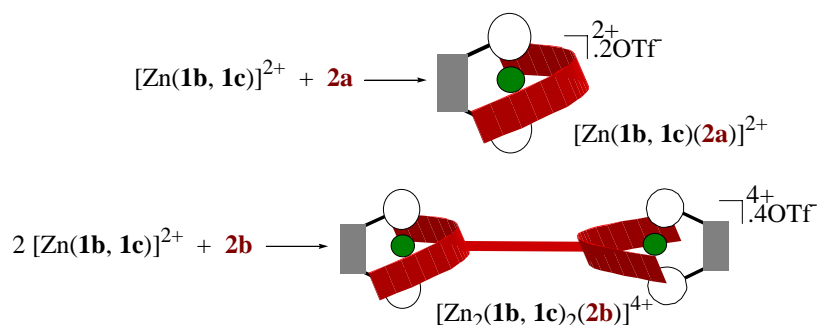


Figure 4. ^1H NMR aromatic region changes of **1b** upon Zn(II) coordination (0.1-1.0 equiv. of Zn(II), a-f) and selected region of heterotopic complexes $[\text{Zn}(\mathbf{1b})(\mathbf{2a})]^{2+}$ and $[\text{Zn}(\mathbf{1b})(\mathbf{2b})]^{2+}$.

Self-assembly of dumbbell-shaped molecules: Rewardingly, treatment of molecular receptors $[\text{Zn}(\mathbf{1b},\mathbf{c})]^{2+}$ with **2a** or **2b** (1:1 equiv., respectively) resulted in the quantitative formation of heterotopic assemblies in solution (Scheme 2). ESI MS analysis indicated the formation of $[\text{Zn}(\mathbf{1b},\mathbf{c})(\mathbf{2a})]^{2+}$ and $[\text{Zn}_2(\mathbf{1b},\mathbf{1c})_2(\mathbf{2b})]^{2+}$, respectively. All signals are isotopically well resolved (Figure 5). Each compound displays a sharp and single set of signals in the ^1H NMR, indicative of a highly symmetric species (Figure 4g-h). The chemical shifts of the mesityl protons ($\delta \sim 7.0$ in ligand, $\delta \sim 6.2$ ppm in complex) are most diagnostic for

the formation of a heterotopic complex. In summary, the observed ^1H -, ^{13}C -NMR, ESI-MS and the elemental analysis data are all consistent with the formation of single, highly symmetric heterotopic assemblies.



Scheme 2. Self-assembly of heterotopic aggregates.

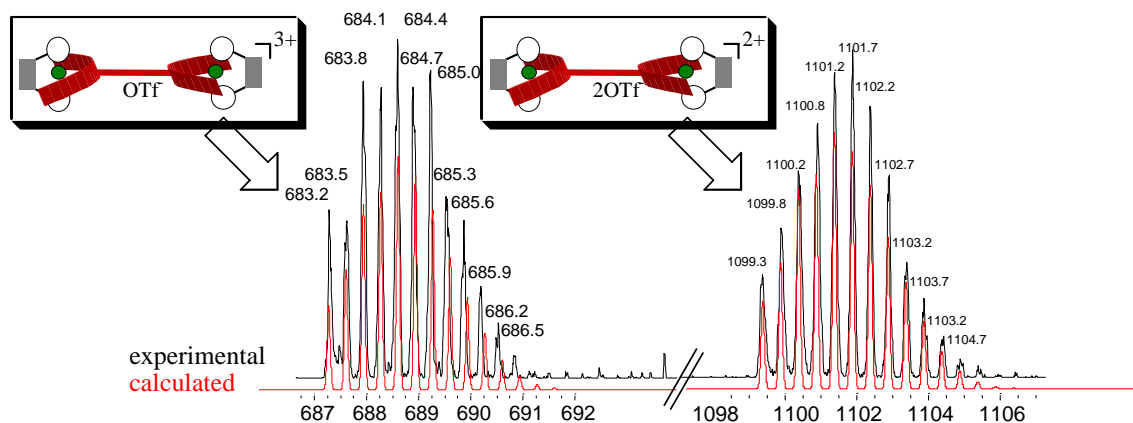


Figure 5. Isotopic distributions (red: calculated, dark: experimental) of $[\text{Zn}_2(\mathbf{1c})_2(\mathbf{2b})]^{3+}$ (left) and $[\text{Zn}_2(\mathbf{1c})_2(\mathbf{2b})]^{2+}$ (right).

This non-covalent approach of making dumbbell-shaped molecules should provide an alternative access to rotaxane molecules (Figure 6). Usual procedures¹¹ of making rotaxanes involve covalent stoppering of pseudorotaxanes, that may have a low yield (highest yield reported to date is 84%).¹² On the contrary, the present strategy could provide a quantitative strategy for dumbbell-shaped molecules and should give easy access to dynamic rotaxanes that exchange rings between axes.

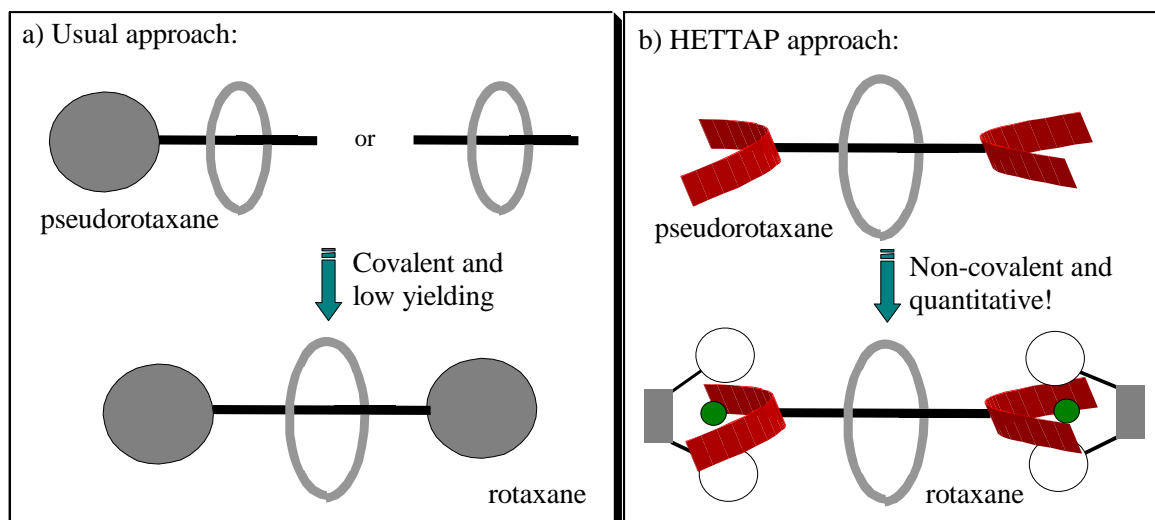


Figure 6. Strategies for the stoppering of rotaxane-type molecules.

Using this strategy, one may also design a light switchable molecular on-off rotor (Figure 7).

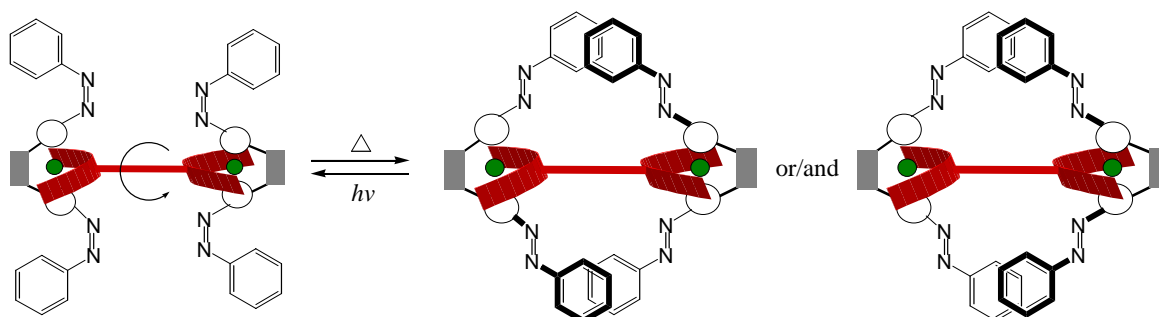


Figure 7. A light switchable molecular on-off rotor.

The ligands **1b-c**, **2a-b** and their complexes absorption and emission spectra were recorded in a mixture of dichloromethane and methanol (8:2) at rt. As shown in Figure 8, all ligands and their complexes display intense and well-resolved peaks, the absorptions lying at ~250-280 nm being assigned to essentially unshifted π - π^* bands of the phenanthroline subunits and phenyl rings.¹³ A red shift is observed for the Zn(II) complexes with respect to the ligands, indicating increased π conjugation. Interestingly, contrary to the absorption behaviour, Zn complexes of **1b-c** with **2a-b** exhibited an emission that was slightly blue shifted with high intensity. The observed fluorescence of the complexes is ascribed to emission from the lowest ligand-centered (LC) excited singlet level.¹⁴ The intense fluorescence makes these assemblies an attracting candidate to design the supramolecular sensors.

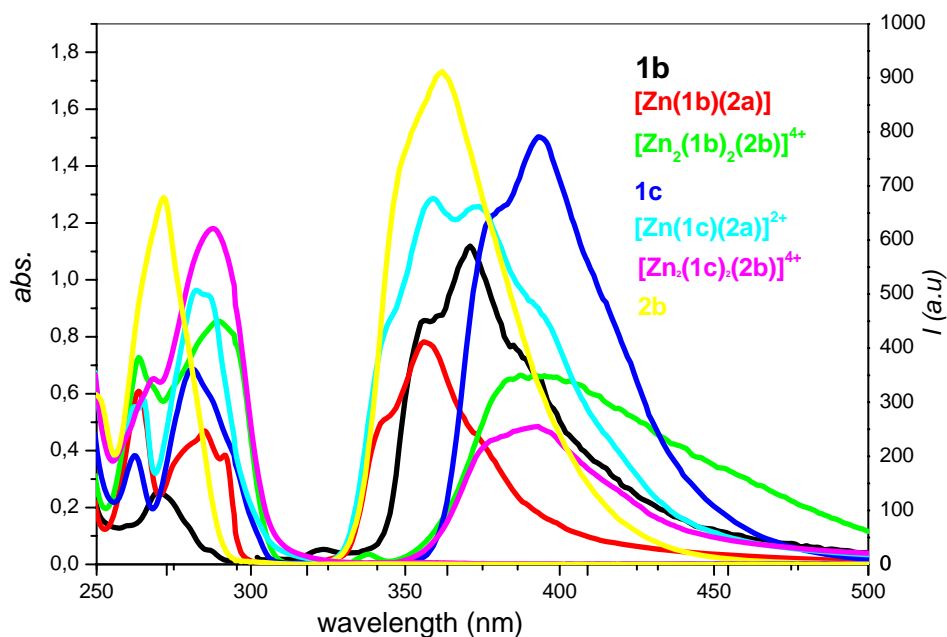


Figure 8. Absorption and Emission spectra of **1b**, **1c**, **2a** and **2b** and their Zn(II) complexes in dichloromethane / methanol (8:2) (2.4×10^{-5} M).

The dumbbell nature of $[\text{Zn}(\mathbf{1b}, \mathbf{1c})(\mathbf{2b})]$ was visualized from a single crystal measurement (Figure 9).¹⁵ As depicted in Figure 7, the distance between Zn atoms in the dumbbell is ~ 1.5 nm and external distance is 2.8 nm (including van der Waals radii) (Figure 9). The structure is centrosymmetric with an inversion center at the midpoint of the central benzene ring. This is one of the very few structurally characterized nanodumbbell's¹⁶ and the first example of dumbbell-shaped aggregate composed of phenanthroline and terpyridine building blocks.

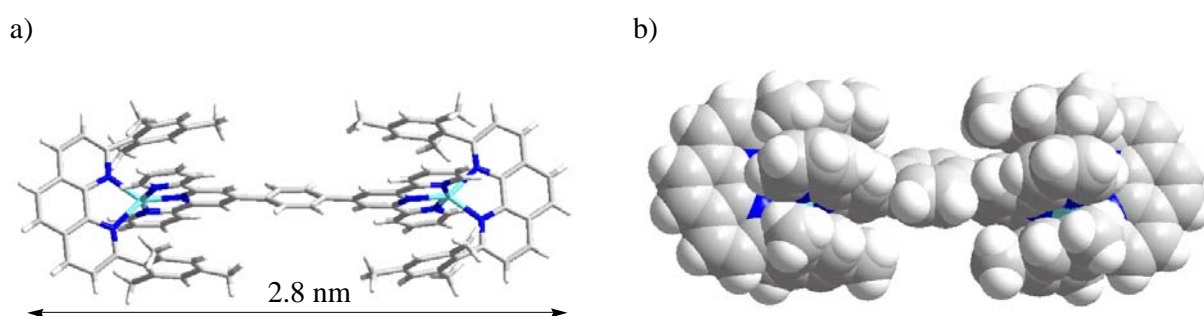


Figure 9. Single crystal structure of $[\text{Zn}_2(\mathbf{1b})(\mathbf{2b})]^{2+}$. a&b) stick and space filling representation, respectively.

Self-assembly of a Clip: Clip-like¹⁷ molecules have attracted considerable interest due to their rich host-guest chemistry.¹⁸ As shown in Figure 10, a clip-shaped molecule is expected when **1d**¹⁹ and **2b** are reacted with Zn(II) salt. Since the designed clip molecule contains an oligoether unit, it is expected to sense metal cations.²⁰

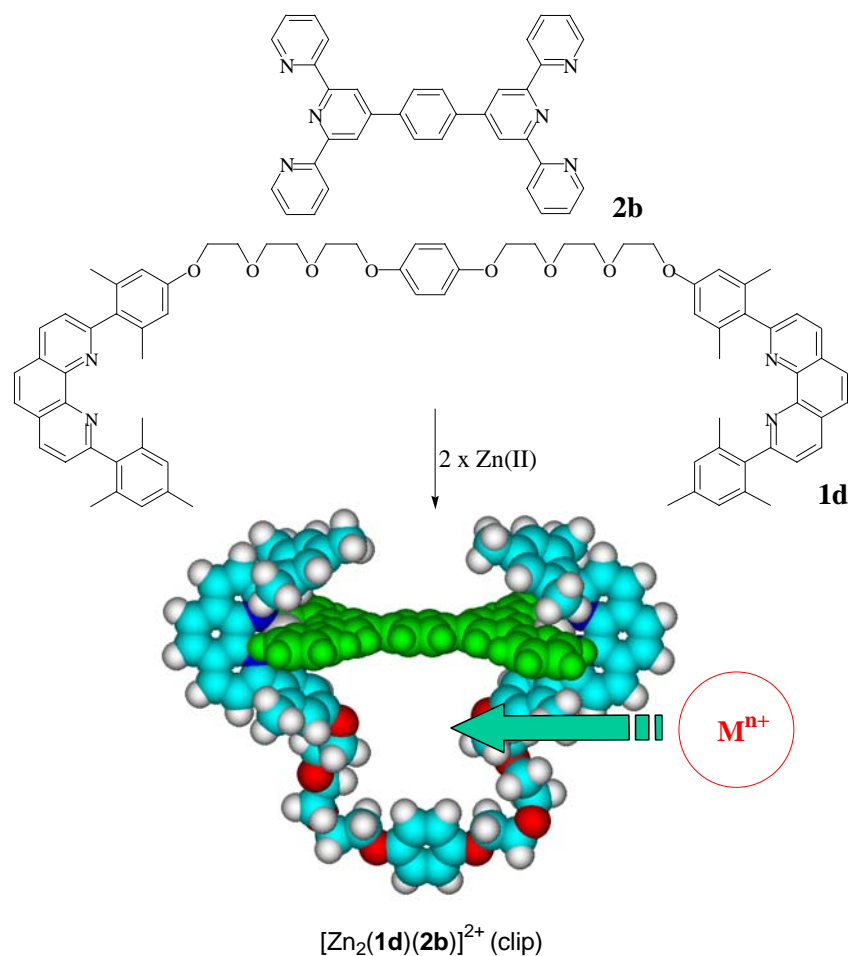


Figure 10. Self-assembly of a heterotopic clip molecule and its potential to function as a host for metal cations. The clip is represented as a spacefilling model obtained by HyperChem.

Upon mixing **1d**, **2b** and $[Zn(OTf)_2]$ (1:1:2), the solution turned light orange colour. Analysis of this solution by ESI-MS indicated the formation of $[Zn_2(\mathbf{1d})(\mathbf{2b})]^{2+}$ (clip) as the exclusive species. The isotopic splitting clearly showed a doubly charged species and is in perfect agreement with its proposed composition (Figure 11). The 1H NMR spectrum showed a sharp and single set of signals ruling out the presence of any higher aggregates. The formation of heterotopic aggregate was additionally ascertained by the appearance of characteristic high-field shifted mesityl protons and dimethylphenoxy protons at about $\delta \sim 6.0$ ppm.

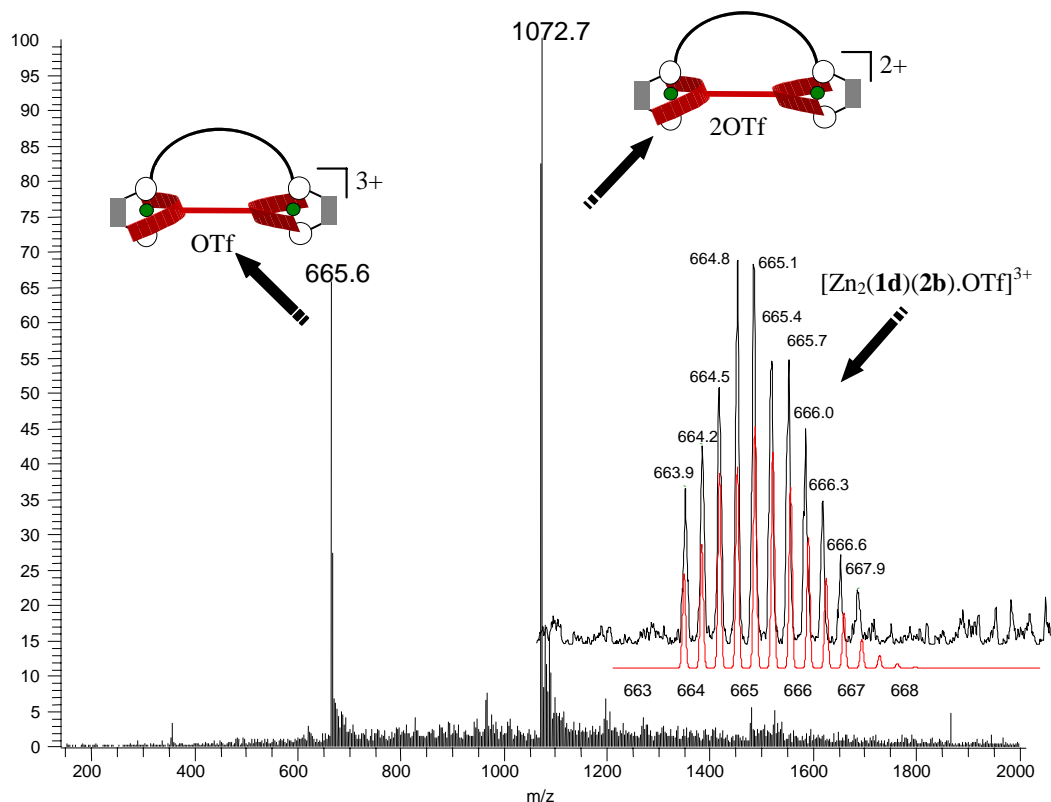


Figure 11. ESI MS of $[Zn_2(\mathbf{1d})(\mathbf{2b})]^{2+}$ and inset showing the isotopic distributions (red: calculated, dark: experimental) of 3+ charged species.

Metal ion sensing of the Clip assembly: The host ability of $[Zn_2(\mathbf{1d})(\mathbf{2b})]^{2+}$ was probed by its reaction with various metal cations using UV/vis and fluorescence spectroscopy. As can be seen from Figure 12, the absorption, emission intensity and emission wavelength of $[Zn_2(\mathbf{1d})(\mathbf{2b})]^{2+}$ changed when excess alkali metal and alkaline earth metal cations in acetonitrile were added to the acetonitrile solution of $[Zn_2(\mathbf{1d})(\mathbf{2b})]^{2+}$. Within the small series of cations studied the highest fluorescence increase was observed for Pb^{2+} cation (25% with respect to $[Zn_2(\mathbf{1d})(\mathbf{2b})]^{2+}$).

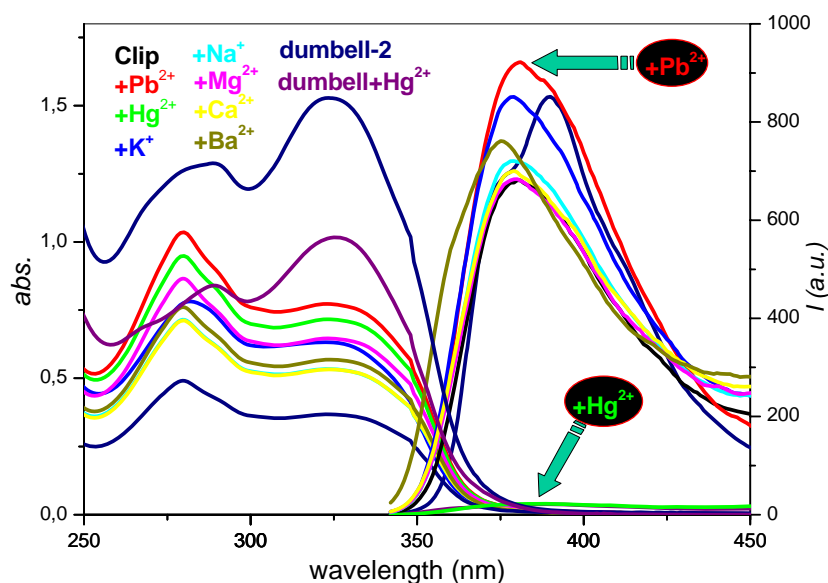


Figure 12. UV-vis and fluorescence spectra of **Clip** (2.04×10^{-5} M) and **dumbbell** (1.9×10^{-4} M) in the absence and in the presence of Na^+ , K^+ , Mg^{2+} , Ca^{2+} , Pb^{2+} , Ba^{2+} and Hg^{2+} in acetonitrile at rt (metal salts used as their perchlorate salts and ~ 10 equiv. of each metal ion was added). Excitation wavelength: 330 nm.

Fluorescence quenching of $[\text{Zn}_2(\mathbf{1d})(\mathbf{2b})]^{2+}$ was observed in case of addition of Hg^{2+} (Figure 12 and Figure 13). When the $[\text{Zn}_2(\mathbf{1d})(\mathbf{2b})]^{2+}$ was replaced by dumbbell $[\text{Zn}_2(\mathbf{1a}$ or $\mathbf{1b})_2(\mathbf{2b})]^{2+}$ equally quenching of fluorescence was observed, ruling out any selective interaction between the oligoether chain and Hg^{2+} . Nevertheless, it is clear that dumbbells and $[\text{Zn}_2(\mathbf{1d})(\mathbf{2b})]^{2+}$ can sense Hg^{2+} , selectively, within a small series of metal cations tested.

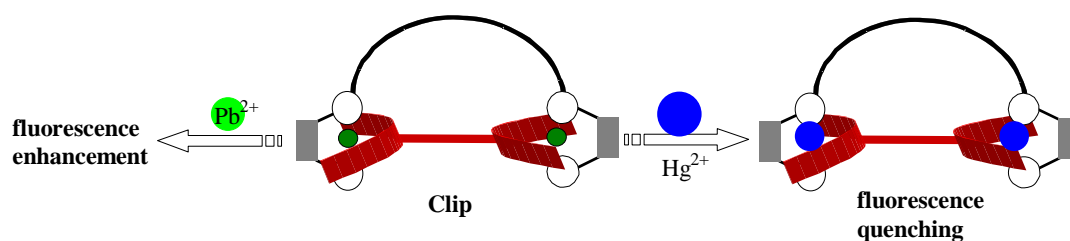


Figure 13. Metal ion sensing of **Clip** assembly.

ESI MS analysis of the mixture $[\text{Clip} + n \text{Hg}^{2+}]$ provided isotopically well resolved signals corresponding to $[\text{Hg}_2(\mathbf{1d})(\mathbf{2b})]^{2+}$ (Hg-clip) with no signals of $[\text{Zn}_2(\mathbf{1d})(\mathbf{2b})]^{2+}$ be detectable (Figure 14a-b). Obviously, the fluorescence quenching of dumbbells and $[\text{Zn}_2(\mathbf{1d})(\mathbf{2b})]^{2+}$ after addition of Hg^{2+} is driven by a metal exchange mechanism. The fluorescence quenching is believed to be due to an electron transfer process from the fluorophore to the metal center.²¹

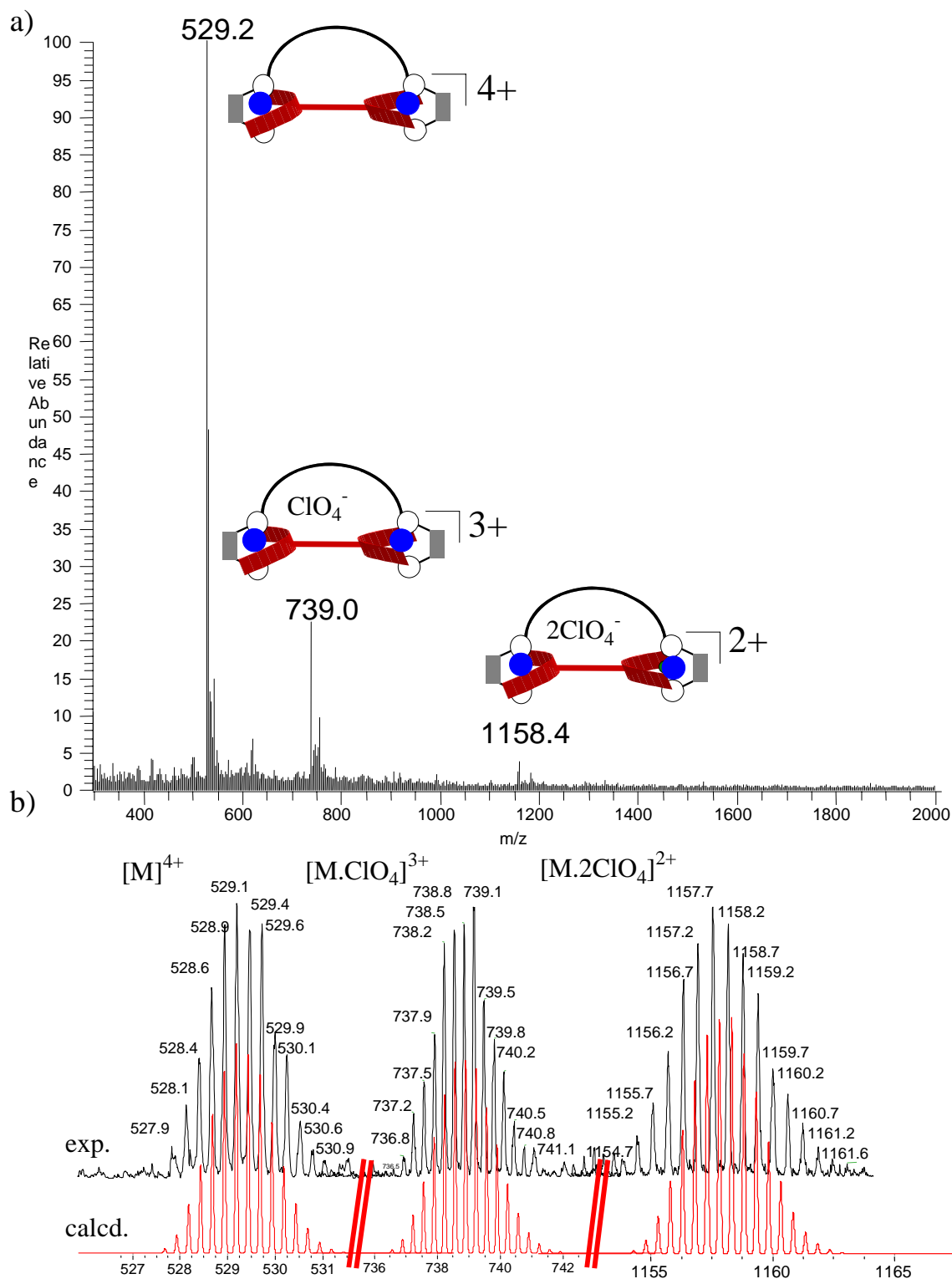


Figure 14. ESI MS of the reaction mixture obtained when $[Zn_2(\mathbf{1d})(\mathbf{2b})]^{2+}$ was reacted with $[Hg(ClO_4)_2]$ in acetonitrile at rt.

In conclusion, a novel and general supramolecular toolkit for dumbbell-shaped aggregates is presented. Since the resulting aggregates are fluorescent, this approach should give ready access to explore novel photophysically active architectures. Unlike the HETPHEN concept

the HETTAP approach is most useful in preparing fluorescent heterotopic supramolecular aggregates (Figure 1). Both, the heterotopic dumbbell and the clip show prove sensitive towards Hg^{2+} (fluorescence quenching, driven by metal exchange) and Pb^{2+} (fluorescence enhancement).

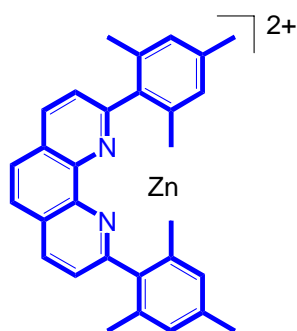
Acknowledgements. I would like to thank Prof. H. Ihmels for allowing me to access the Varian Cary 100 Bio UV/visible Spectrometer and Varian Cary Eclipse Fluorescence Spectrometer. We are grateful to the Deutsche Forschungsgemeinschaft and the Fonds der Chemischen Industrie.

Experimental:

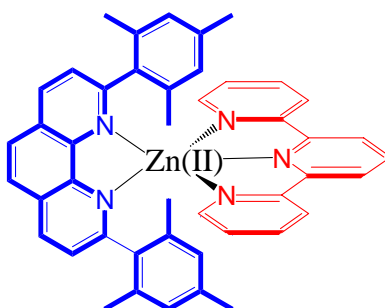
Phenanthroline building blocks **1b** and **1c** were prepared by known procedures. Terpyridine building blocks (**2a,b**) were purchased from Aldrich and used as received. ^1H NMR and ^{13}C NMR were measured on a Bruker AC 200 (200 MHz) unless specified otherwise. ESI MS spectra were measured on a LCQ Deca Thermo Quest instrument. Typically, each time 25 scans were accumulated for one spectrum. All complexes were characterized by ^1H -, ^{13}C and ESI MS. UV/vis spectra were recorded on a Varian Cary 100 Bio UV/visible Spectrometer and Varian Cary Eclipse Fluorescence Spectrometer.

General Procedure for the Heterotopic Assemblies:

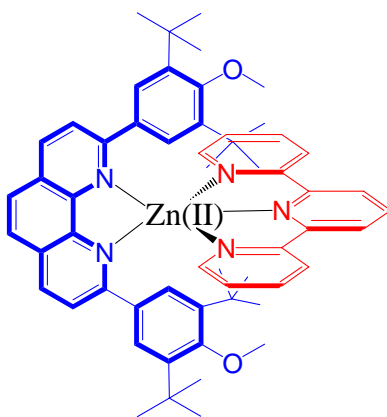
The molecular receptors $[\text{Zn}(\mathbf{1b,c})]$ were prepared by reacting **1b** or **1c** (10.0 mg, 2.40×10^{-2} mmol or 14.8 mg 2.40×10^{-2} mmol, respectively) with $[\text{Zn}(\text{OTf})_2]$ (8.72 mg, 2.40×10^{-2} mmol) (1:1 equiv.) in a dichloromethane/methanol mixture (8:2, respectively). The resulting solutions were analysed without any further purification by ^1H NMR and used directly for the preparation of heterotopic aggregates. In all cases no purification procedures were required for the characterization.



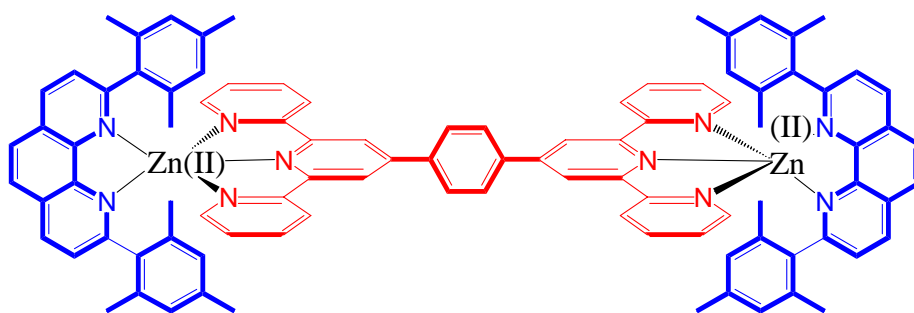
$[\text{Zn}(\mathbf{1b})]^{2+}$: ^1H NMR ($\text{CD}_2\text{Cl}_2/\text{CD}_3\text{OD}$ (8:2), 200 MHz): δ 8.90 (d, $J = 8.12$, 2H, phen), 8.28 (s, 2H, phen), 7.95 (d, $J = 8.37$, 2H, phen), 7.03 (s, 4H, phenyl), 2.32 (s, 6H, benzyl), 1.98 (s, 12H, benzyl).



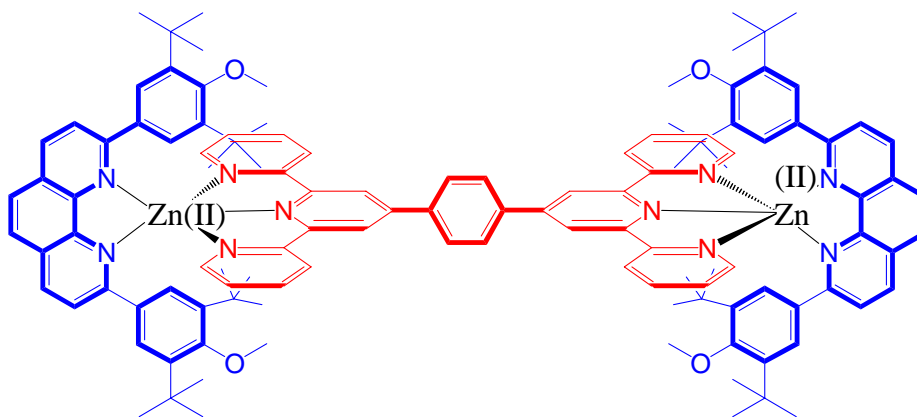
$[\text{Zn}(\mathbf{1b})(\mathbf{2a})]^{2+}$: ^1H NMR ($\text{CD}_2\text{Cl}_2/\text{CD}_3\text{OD}$ (8:2), 200 MHz): δ 9.10 (d, $J = 8.4$ Hz, 2H, phen), 8.56 (s, 2H, phen), 8.51 (s, 5H, terp), 8.29 (t, $J = 7.6$ Hz, 2H, terp), 8.07 (d, $J = 8.4$ Hz, 2H, phen), 7.70 (d, $J = 4.9$ Hz, 2H, terp), 7.53 (t, $J = 5.18$ Hz, 2H, terp), 1.78 (s, 6H, benzyl), 1.11 (s, 12H, benzyl); ^{13}C NMR ($\text{CD}_2\text{Cl}_2/\text{CD}_3\text{OD}$ (8:2), 50 MHz) : 161.3, 149.2 (2C), 147.6, 146.8, 144.8, 143.2 (2C), 140.4, 135.2 (2C), 134.7, 129.6, 128.4, 128.2, 127.9, 123.6, 123.3 (arom), 20.5, 19.4 (benzyl); ESI MS: calcd. for $[\text{ZnC}_{45}\text{H}_{39}\text{N}_5\cdot\text{OTf}]^+$ [M^+] (%): m/z 864.3, found: m/z 864.1 (100), calcd. for $[\text{ZnC}_{45}\text{H}_{39}\text{N}_5]^{2+}$ [M^{2+}] (%): m/z 357.6, found: m/z 357.2 (52).



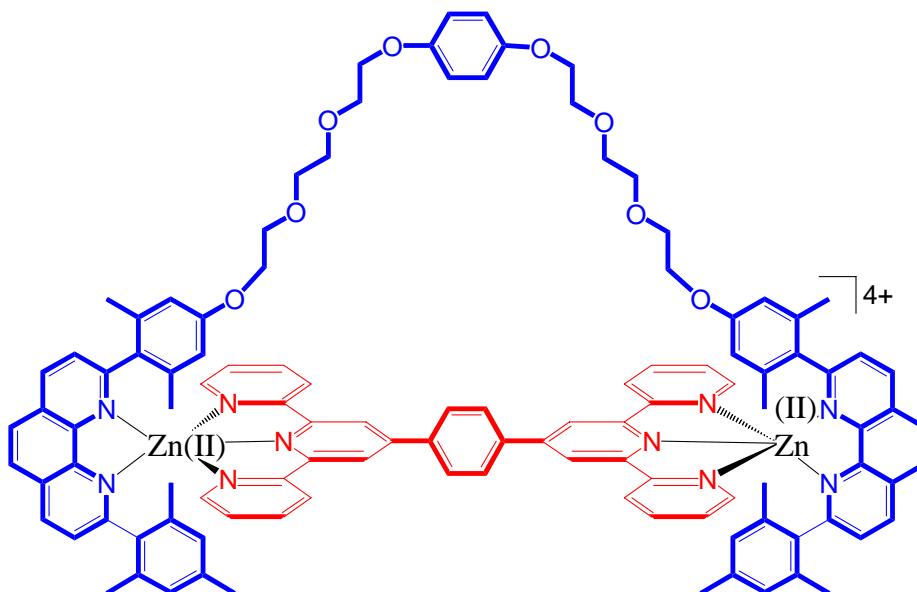
(Zn(**1b**)(**2a**)] : ^1H NMR ($\text{CD}_2\text{Cl}_2/\text{CD}_3\text{OD}$ (8:2), 200 MHz): δ 9.00 (d, 2H, $J = 8.4$ Hz, phen), 8.62 (d, $J = 8.8$ Hz, 2H, terp), 8.50 (d, $J = 5.7$ Hz, 3H, terp), 8.45 (s, 2H, phen), 8.24 (t, $J = 7.9$ Hz, 2H, terp), 8.05 (d, $J = 8.4$ Hz, 2H, phen), 7.71 (d, $J = 4.9$ Hz, 2H, terp), 8.24 (t, $J = 7.6$ Hz, 2H, terp), 6.75 (s, 4H, phenyl), 3.28 (s, 6H, methoxy), 0.90 (s, 36H, *t*-Bu); ^{13}C NMR ($\text{CD}_2\text{Cl}_2/\text{CD}_3\text{OD}$ (8:2), 50 MHz) : 162.8, 162.5, 149.4, 149.0, 147.6, 146.8, 146.4 (2C), 143.8, 143.4, 141.5, 140.7, 133.7 (2C), 130.1, 129.9, 128.9, 128.6, 126.2 (2C), 124.7, 124.2 (arom.), 65.9 (methoxy), 36.5, 32.1 (*t*-Bu); ESI MS: calcd. for $[\text{ZnC}_{57}\text{H}_{63}\text{N}_5\text{O}_2]^{2+}$ [M^+] (%): m/z 457.7, found: m/z 457.2 (100).



$[\text{Zn}_2(\mathbf{1b})(\mathbf{2b})]^{4+}$: ^1H NMR ($\text{CD}_2\text{Cl}_2/\text{CD}_3\text{OD}$ (8:2), 200 MHz): δ 9.10 (d, $J = 8.1$ Hz, 4H, phen), 9.04 (s, 4H, phenyl), 8.94 (d, $J = 8.1$ Hz, 4H, terp), 8.59 (s, 4H, terp), 8.55 (s, 4H, phen), 8.35 (t, $J = 7.9$ Hz, 4H, terp), 8.10 (d, $J = 8.4$ Hz, 4H, phen), 7.71 (d, $J = 4.2$ Hz, 4H, terp), 7.55 (t, $J = 5.4$ Hz, 4H, terp), 6.27 (s, 8H, phenyl), 1.79 (s, 12H, benzyl), 1.16 (s, 24H, benzyl); ^{13}C NMR ($\text{CD}_2\text{Cl}_2/\text{CD}_3\text{OD}$ (8:2), 50 MHz) : 161.5, 155.9, 149.0, 148.4, 147.2, 143.2, 141.5, 140.7, 137.9, 135.3, 134.7, 129.8, 129.6, 128.4, 128.3, 128.1, 124.3, 128.8 (arom), 20.6, 19.5 (aliph.); ESI MS: calcd. for $[\text{Zn}_2\text{C}_{96}\text{H}_{80}\text{N}_{10} \cdot 2\text{OTf}]^{2+}$ [M^{2+}] (%): m/z 901.3, found: m/z 901.5 (100), calcd. for $[\text{Zn}_2\text{C}_{96}\text{H}_{80}\text{N}_{10} \cdot \text{OTf}]^{3+}$ [M^{3+}] (%): m/z 551.2, found: m/z 551.4 (45). See single crystal structure.



$[\text{Zn}_2(\mathbf{1c})_2(\mathbf{2b})]^{4+}$: ^1H NMR ($\text{CD}_2\text{Cl}_2/\text{CD}_3\text{OD}$ (8:2), 200 MHz): δ 9.12 (s, 4H, terp), 9.05 (d, $J = 8.4$ Hz, 4H, phen), 8.97 (d, $J = 7.9$ Hz, 4H, terp), 8.49 (s, 4H, phen), 8.35 (s, 4H, phenyl), 8.29 (d, $J = 7.9$ Hz, 4H, terp), 8.10 (d, $J = 8.4$ Hz, 4H, phen), 7.72 (d, $J = 3.9$ Hz, 4H, terp), 7.60 (t, $J = 7.4$ Hz, 4H, terp), 6.82 (s, 8H, phenyl), 3.28 (s, 12H, methoxy, 0.96 (s, 72H, *t*-Bu); ^{13}C NMR ($\text{CD}_2\text{Cl}_2/\text{CD}_3\text{OD}$ (8:2), 50 MHz) : 162.3, 162.0, 156.8, 149.1, 148.4, 147.2, 145.9, 143.2, 142.7, 140.9, 137.6, 133.1, 129.8, 129.4, 129.1, 128.2, 125.6, 124.4 (arom.), 65.2 (methoxy), 35.9, 31.4 (*t*-Bu); ESI MS: calcd. for $[\text{ZnC}_{120}\text{H}_{128}\text{N}_{10}\text{O}_4 \cdot 2\text{OTf}]^{2+} [\text{M}^{2+}]$ (%): m/z 1101.6, found: m/z 1101.5 (100), calcd. for $[\text{ZnC}_{120}\text{H}_{128}\text{N}_{10}\text{O}_4 \cdot \text{OTf}]^{3+} [\text{M}^{3+}]$ (%): m/z 684.7, found: m/z 684.8 (15).



$[\text{Zn}_2(\mathbf{1d})(\mathbf{2b})]^{4+}$: ^1H NMR ($\text{CD}_2\text{Cl}_2/\text{CD}_3\text{OD}$ (8:2), 400 MHz): δ 9.23 (d, $J = 7.9$ Hz, 4H, phen), 9.12 (s, 4H, terp), 8.92 (d, $J = 8.2$ Hz, 4H, phen), 8.49 (s, 8H, terp and phenyl), 8.41 (d, $J = 8.1$ Hz, 4H, phen), 8.31 (t, $J = 7.8$ Hz, 4H, terp), 7.71 (d, $J = 5.8$ Hz, 4H, terp), 7.54 (t, $J = 5.3$ Hz, 4H, terp), 6.68 (s, 4H, phenyl), 6.24 (s, 4H, phenyl), 5.99 (s, 4H, phenyl), 3.42-3.70 (m, 24H, ether), 1.68 (s, 6H, benzyl), 1.23 (s, 12H, benzyl), 1.13 (s, 12H, benzyl); ^{13}C NMR ($\text{CD}_2\text{Cl}_2/\text{CD}_3\text{OD}$ (8:2), 100 MHz) : 161.7, 161.5, 160.2, 155.9, 153.8, 153.7, 149.3, 148.7,

147.5, 145.8, 143.4, 141.8, 140.8, 138.2, 137.5, 135.5, 135.1, 130.6, 129.9, 129.7, 129.0, 128.6, 128.2, 124.5, 122.7, 121.1, 119.6, 116.7, 116.1, 113.7, 113.6 (arom.), 71.1, 70.3, 68.8, 68.1, 61.7, 60.6 (methoxy), 20.8, 20.0, 19.4 (benzyl); ESI MS: calcd. for $[\text{Zn}_2\text{C}_{112}\text{H}_{102}\text{N}_{10}\text{O}_8 \cdot 2\text{OTf}]^{2+} [\text{M}^{2+}]$ (%): m/z 1072.5, found: m/z 1072.7 (100), calcd. for $[\text{Zn}_2\text{C}_{112}\text{H}_{102}\text{N}_{10}\text{O}_8 \cdot \text{OTf}]^{3+} [\text{M}^{3+}]$ (%): m/z 665.3, found: m/z 665.5 (70).

- (1) M. Schmittel, V. Kalsani, *Topics in Current Chemistry* **2004**, *245*, 1-53 and ref's therein.
- (2) C. Hamann, J.-M. Kern, J.-P. Sauvage, *Inorg. Chem.* **2003**, *42*, 1877-1883.
- (3) HETPHEN concept: quantitative approach to heteroleptic bisphenanthroline metal complexes.⁶ This approach utilizes steric and electronic effects originating from bulky aryl substituents at the bisimine coordination sites (as seen in **1** and **5**) to control the coordination equilibrium both kinetically and thermodynamically.
- (4) N. Armaroli, *Chem. Soc. Rev.* **2001**, 113-124.
- (5) J. Rojo, F. J. Romero-Salguero, J.-M. Lehn, G. Baum, D. Fenske, *Eur. J. Inorg. Chem.* **1999**, 1421-1428.
- (6) (a) M. Schmittel, U. Lüning, M. Meder, A. Ganz, C. Michel, M. Herderich, *Heterocyclic Communications* **1997**, *3*, 493-498. (b) M. Schmittel, V. Kalsani, **2005**, unpublished results.
- (7) B. Hasenknopf, J.-M. Lehn, G. Baum, D. Fenske, *Proc. Natl. Acad. Sci. USA* **1996**, *93*, 1397-1400.
- (8) P. N. W. Baxter, R. G. Khoury, J.-M. Lehn, G. Baum, D. Fenske, *Chem. Eur. J.* **2000**, *6*, 4140-4148.
- (9) M. Schmittel, A. Ganz, M. Schlosser, H.-J. Deiseroth, V. Kalsani, unpublished results.
- (10) M. Schmittel, A. Ganz, D. Fenske, M. Herderich, *Dalton Trans.* **2000**, 353-359.
- (11) S. H. Chiu, S. J. Rowan, S. J. Cantrill, J. F. Stoddart, A. J. P. White, D. J. Williams, *Chem. Eur. J.* **2002**, *8*, 5170-5183 and ref's therein.
- (12) A. G. Kolchinski, N. W. Alcock, R. A. Roesner, D. H. Busch, *Chem. Commun.* **1998**, 1437-1438.
- (13) S. Goeb, A. De Nicola, R. Ziesel, *J. Org. Chem.* **2005**, ASAP.
- (14) J. Rojo, F. J. R.-Salguero, J.-M. Lehn, G. Baum, D. Fenske, *Eur. J. Inorg. Chem.* **1999**, 1421-1428.
- (15) A single crystal (pale yellow plate with dimensions 0.10 x 0.32 x 0.36 mm) was measured on a SIEMENS SMART diffractometer at a temperature of about -117 °C. Repeatedly measured reflections remained stable. An empirical absorption correction with program SADABS (Sheldrick, **2000**) gave a correction factor between 0.615 and 1.000. Equivalent reflections were averaged. $R(\text{I})_{\text{internal}} = 0.158$. The structure was determined by direct methods using program SIR97. The unit cell contains a solvent accessible area of about 936 Å³. Only a few solvate groups, probably methanol could be seen in the solvate region. Program PLATON/SQUEEZE (van der Sluis & Spek, *Acta Cryst.*, **1990**, *A46*, 194-201) was used to model the solvate density. The solvent electron count was estimated as about 357 electrons/cell. The H atoms were geometrically positioned and were constrained. The non-H atoms were refined with anisotropic thermal parameters. The structure was refined on F² values using program SHELXL-97. The final difference density was between -0.69 and +1.07 e/Å. $\text{C}_{100}\text{H}_{80}\text{F}_{12}\text{N}_{10}\text{O}_{12}\text{S}_4\text{Zn}_2$, $M = 2100.79$, Triclinic, space group $P-1$, $a = 11.521(2)$, $b = 17.185(4)$, $c = 18.164(4)$, $V = 3074.0(11)$ Å³, $T = -117$ °C, $Z = 1$, $D_c = 1.135$ g/cm³, $\lambda(\text{Mo K}\alpha) = 0.71073$, 30425 reflexions measured, 11341 unique ($R_{\text{int}} = 0.1577$) which were used in all calculations. $R_1 = 0.2382$ ($I > \sigma_2(I)$), $wR_2 = 0.2930$, GOF = 0.988; max/min residual density 1.069/-0.690 e.Å⁻³. CCDC reference number xxxxx. See also supporting information.
- (16) (a) M. Lu, Y. Wie, B. Xu, C. F.-C. Cheung, Z. Peng, D. R. Powell, *Angew. Chem. Int. Ed.* **2002**, *41*, 1566-1568. (b) J. Fan, W.-Y. Sun, T.-A. Okamura, J. Xie, W.-X. Tang, N. Ueyama, *New. J. Chem.* **2002**, 199-201. (c) O. Lukin, J. Recker, A. Böhmer, W. M. Müller, T. Kubota, Y. Okamoto, M. Nieger, R. Fröhlich, F. Vögtle, *Angew. Chem. Int. Ed.* **2003**, *42*, 442-445.
- (17) J. A. A. W. Elemans, M. B. Claase, P. P. M. Aarts, A. E. Rowan, *J. Org. Chem.* **1999**, *64*, 7009-7016.
- (18) A. Wu, P. Mukhopadhyay, A. Chakraborty, J. C. Fetters, L. Isaacs, *J. Am. Chem. Soc.* **2004**, *126*, 10035-10043 and ref's therein.
- (19) V. Kalsani, H. Ammon, F. Jäckel, J. P. Rabe, M. Schmittel, *Chem. Eur. J.* **2004**, *10*, 5481-5492.
- (20) (a) G. W. Gokel, W. M. Leevy, M. E. Weber, *Chem. Rev.* **2004**, *104*, 2723-2750. (b) Y. Liu, Z. Y. Duan, H. Y. Zhang, X. L. Jiang, J. R. Han, *J. Org. Chem.* **2005**, ASAP.
- (21) R. Métivier, I. Leray, B. Valeur, *Chem. Eur. J.* **2004**, *10*, 4480-4490.

Supp 6-2

A Facile Approach to Dynamic and Fluorescent Nanoscale Phenanthroline/Terpyridine Zinc(II) Ladders

Michael Schmittel,*[‡] Venkateshwarlu Kalsani,[‡] Helmut Cölfen,[§] Jan W. Bats[†]

[‡]Contribution from the Center of Micro and Nanochemistry and Engineering, Organische Chemie I, Universität Siegen, Adolf-Reichwein-Str., D-57068 Siegen, Germany, [§]The Max-Planck-Institut für Kolloid- und Grenzflächenforschung, Golm, 14424 Potsdam, Germany, and [†]Institut für Organische Chemie und Chemische Biologie, Johann Wolfgang Goethe-Universität, Marie-Curie-Strasse 11, D-60439 Frankfurt am Main, Germany.

E-mail: schmittel@chemie.uni-siegen.de

Metallosupramolecular assemblies are at the heart of many current investigations due to their great potential as novel functional materials with redox-active, magnetic, catalytic, photochemical, optical and mechanical properties.¹ As a consequence, variable strategies for their fabrication have been developed,^{2a} some of which (*i.e.* with Pt/Pd-pyridine; Pt-C≡C-; Rh- linkages) were the basis for astounding nanoscale architectures,^{2b-d} most of which rely on homoleptic (same ligand) aggregation. For functional metallosupramolecular systems, however, strategies to build defined heteroleptic aggregates should be superior due to the possibility to incorporate variable functionalities at defined locations. A few multicomponent aggregates have been reported by Lehn, Mirkin and Shionoya *et al.*^{1,3} Recently, Sauvage *et al.* have shown bi- and tridentate ligands to associate,⁴ but this unique example was restricted to interlocked molecules.⁵ Otherwise, attempts to assemble multicomponent grid motifs from bi- and tridentate ligands have failed.^{12a} An attempt by Newkome *et al.* along this line has only led to polymeric structures.^{12f} As a consequence, although ladder motifs are structurally rather similar to grid and square motifs, their chemistry is very much restricted to one single report,⁶ due to the problems associated with multicomponent aggregation

In this investigation, it was of interest to elucidate whether the self-assembly of tridentate ligands with HETPHEN bidentate phenanthrolines in presence of Zn(II) corners would afford discrete multicomponent aggregation. Herein, we describe a robust approach to supramolecular ladders with unique fluorescence properties that undergo, due their dynamic nature, interesting metal exchange and *unlike* ligand selection processes. Moreover, Hg(II) and Cu(I) could also be used as a metal centers for the construction of ladder like structures. Solution and solid state characterisation results unambiguously confirm the suggested structures.

According to the HETPHEN concept⁷ phenanthroline building blocks loaded with steric stoppers (*e.g.* 2,9-dimesityl/2,9-diduryl; as seen in **2-3**) are instructed to avoid self-association in presence of Cu(I), Ag(I) and Zn(II) ions (chart 1).⁸ Thus, in combination with sterically innocent phenanthrolines, only heteroleptic phenanthroline aggregates form.

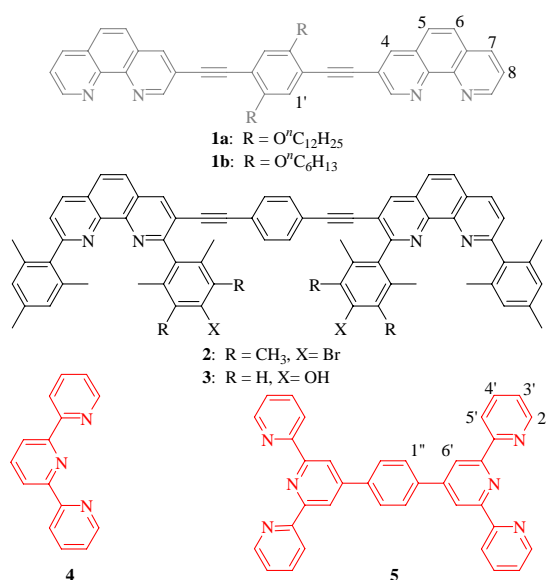
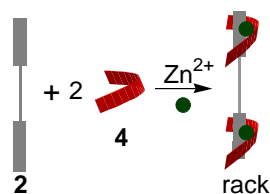


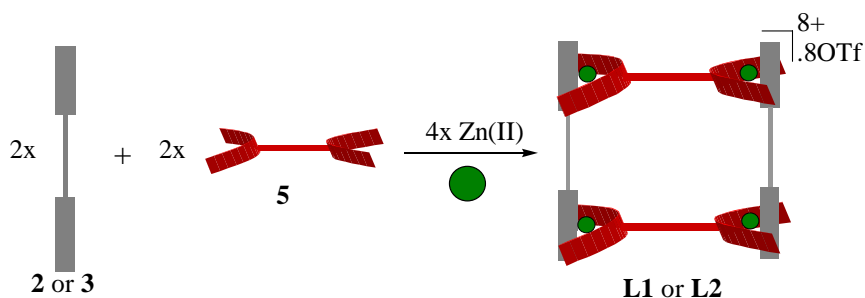
Chart 1. Ligands used for the heterotopic aggregation.

Ligands **1-3**⁹ were designed and tested for their ability to recognise ligands **4-5**¹⁰ in presence of Zn(II) ion.¹¹ Only homoleptic combinations dominated in the self-assembly of **1a** and **5** in presence of zinc(II) metal salt, as detected by ESI MS and ¹H NMR (Figure 3a). Apparently, self-recognition is the dominating phenomena, as also seen in earlier reports.¹² In contrast, only the rack assembly **R1** was afforded from the reaction of **2**, **4** and Zn(II) salt, as evidenced by ESI MS, ¹H NMR, UV/vis and elemental analysis (Scheme 1). The ¹H NMR showed typical high field shifts for the mesityl protons of 2,9-aryl-stoppers ($\delta = 7.1$ to 6.2 ppm) upon coordination.¹³ UV/vis investigations showed bathochromically shifted absorption envelopes at $\lambda \sim 220$ -400 nm, typical of Zn(II) coordinated systems.¹⁴ Interestingly, **R1** is fluorescent with an emission at ~ 460 nm (excitation at ~ 390 nm, Figure 5).



Scheme 1. Self assembly of multicomponent rack.

Rewardingly, along the same strategy **L1** = $[(\text{Zn})_4(\mathbf{2})_2(\mathbf{5})_2]^{8+}$ and **L2** = $[(\text{Zn})_4(\mathbf{3})_2(\mathbf{5})_2]^{8+}$ were formed in quantitative yields upon the reaction of **2** or **3** with **5** with Zn(II) salt (1:1:2 eq. respectively, Scheme 2).



Scheme 2. Self assembly of heterotopic ladders **L1** and **L2**.

All spectroscopic data in solution confirmed the clean formation and the integrity of ladders **L1-L2**. The ^1H NMR showed a single set of sharp signals, with the high field shifts of the mesityl protons (δ ~7.2 to ~6.1 ppm; Figure 1b) being most characteristic. Peaks assignment were further corroborated by COSY experiments. ^{13}C NMR showed single sets of the expected 36 and 35 signals for **L1** and **L2**, respectively.

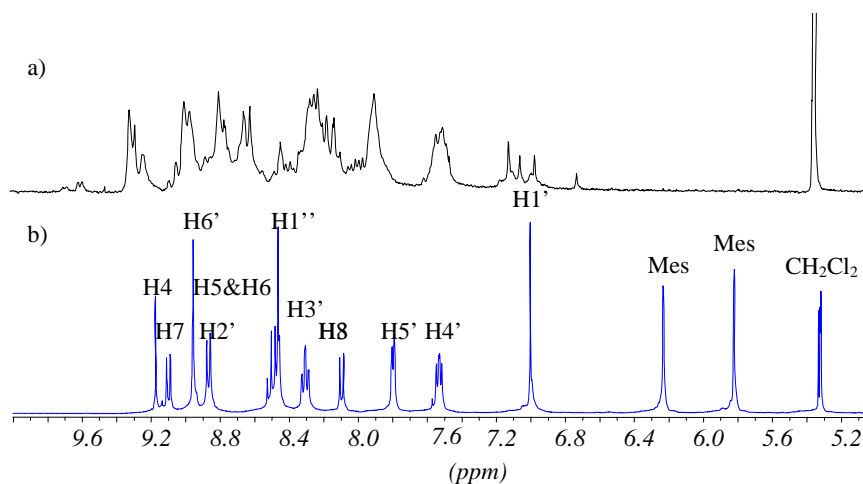


Figure 1. Aromatic region of the ^1H NMR spectra (400 MHz, CD_2Cl_2 - CD_3OD (8:2), rt). (a) An oligomeric homoleptic mixture was obtained from **1a**, **5** and Zn(II) salt. (b) **L2**.

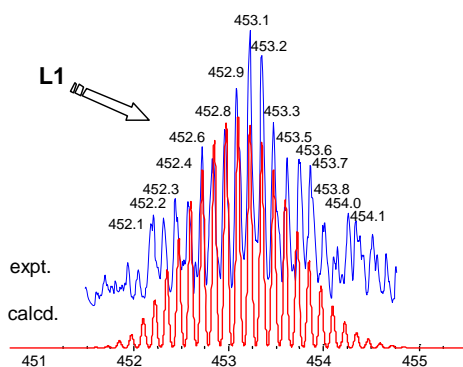


Figure 2. The isotopic distribution pattern (top) for $[(\text{Zn})_4(\mathbf{2})_2(\mathbf{5})_2]^{8+}$ and its calculated pattern (bottom).

Also ESI MS analysis of **L1,L2** substantiated the proposed ladder structures. For example, ESI MS of **L1** contained isotopically resolved signals at $m/z = 485.1, 539.2, 653.9, 814.4, 1055.3, 1455.8$ corresponding to the ions $[(Zn)_4(2)_2(5)_2]^{8+}$, $[(Zn)_4(2)_2(5)_2*OTf]^{7+}$, $[(Zn)_4(2)_2(5)_2*2OTf]^{6+}$, $[(Zn)_4(2)_2(5)_2*3OTf]^{5+}$, $[(Zn)_4(2)_2(5)_2*4OTf]^{4+}$, $[(Zn)_4(2)_2(5)_2*5OTf]^{3+}$, respectively. The isotopic distribution for $[(Zn)_4(2)_2(5)_2]^{8+}$ is shown in Figure 2. This is, to our knowledge, the second example of such a highly splitted pattern, reported for any supramolecular structure.¹⁵

The ultimate proof for the ladder structures was obtained from a single crystal analysis of **L2**.¹⁶ The crystal analysis showed the proposed structure, with two molecules of each **3** and **5** assembled by means of four metal (Zn^{2+}) ions (Figure. 3). The structure reveals the nanoscale nature of these unique supramolecular aggregates with overall external dimensions (including van der Waals radii) of 2.3, 2.7, 3.2 nm (Figure 3). The terpyridine units are sandwiched in between the 2,9-aryl groups of the phenanthroline unit taking profit from stabilizing π - π interactions (3.4 Å). The presence of 2,9-steric stoppers enforce $Zn(II)$ to undergo pentacoordination, in which three positions are occupied by the nitrogen atoms of the terpyridine nucleus and two are occupied by the nitrogen atoms of the phenanthroline unit. To the best of our knowledge this is the first structurally characterised nanoscale multicomponent ladder assembly combining both bi- (**2** or **3**) and tri-dentate ligands (**5**).

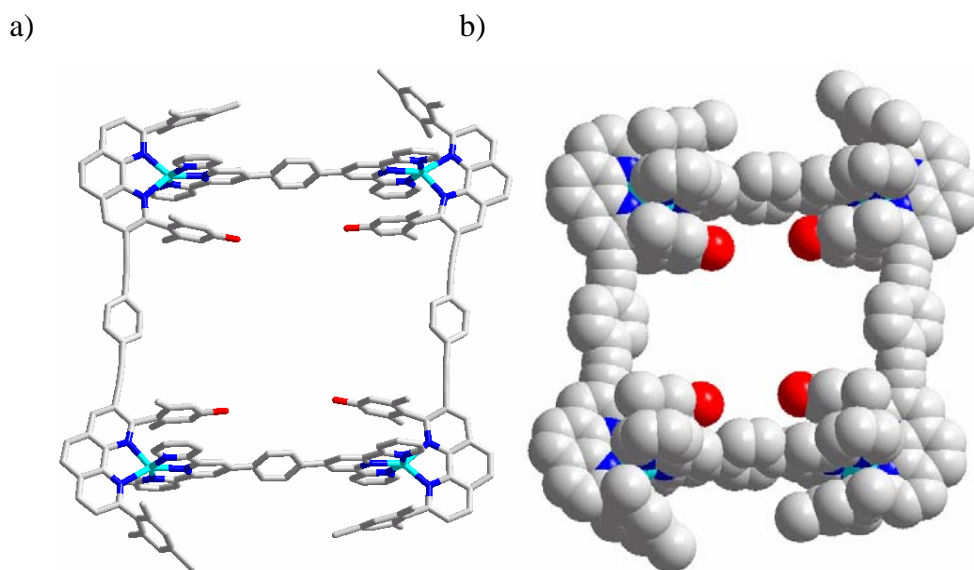
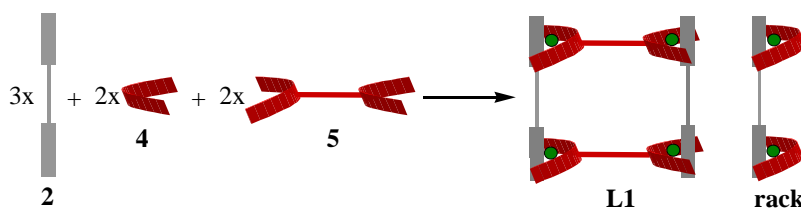


Figure 3. a) Single crystal structure of **L2**. b) Space filling representation. For clarity, H atoms, solvent molecules and anions are omitted.

The dynamic nature of these aggregates becomes evident after mixing **L1** and **L2**. ESI MS and ^1H NMR analysis indicated the formation of mixed species **L3** = $[(\text{Zn})_4(\mathbf{2})(\mathbf{3})(\mathbf{5})_2]^{8+}$ aside of **L1** and **L2**. A ligand selection experiment was performed by reacting **2,4,5** and Zn(II) salt in one pot (3:2:2:6 equiv., respectively, s. Scheme 3). As shown by ESI MS and ^1H NMR, **L1** and **R1** were formed, selectively with no other combinations being detected. This finding highlights the control of the present approach to yield dynamic multicomponent systems.



Scheme 3. Ligand selection driven multicomponent self-assembly.

This strategy could also be used to build the Cu(I)-ladder **L4** by reacting **2**, **5** and $[\text{Cu}(\text{MeCN})_4\text{PF}_6]$ salt (1:1:2 equiv.). Preliminary metal-exchange studies suggested that, in contrast to related earlier reports,¹⁷ the Zn(II)-ladder **L1** could not be converted to its Cu(I) analogue **L4**. On the contrary, **L4** (non fluorescent; Off) could be converted to **L1** (fluorescent; on) when reacted with excess of Zn(II) salt (Figure 5).¹⁸ The transformation **L1** to **L4** could readily be followed by UV/vis (disappearance of $\text{MLCT}_{\text{phenCu}}$ band at ~ 500 nm) and ESI MS (appearance of signals corresponding to **L1**). Interestingly, the fluorescent Zn(II) ladder **L2** could be further converted to the Hg(II)-ladder **L5** (non fluorescent; Off) by reacting it with excess (10 equiv.) of $\text{Hg}(\text{ClO}_4)_2$ (acetonitrile/12 h, Figure 5). As evidenced by ESI MS and fluorescence spectroscopy, the Zn(II)-ladders do not have an affinity for other metal ions (Na^+ , K^+ , Ca^{2+} , Mg^{2+} , Pb^{2+} , Cu^+), but exclusively recognize Hg^{2+} . Therefore, the Zn(II) based ladders act as novel ion recognition systems operating by exchange of metal ions. The fluorescence of the Zn(II)-assemblies is ascribed to emission from the lowest ligand-centered (LC) excited singlet level. Due to the intrinsic quenching nature of the $\text{Hg}(\text{II})$ ¹⁹ and $\text{Cu}(\text{I})$ ²⁰ ions, **L4** and **L5** were non emissive.

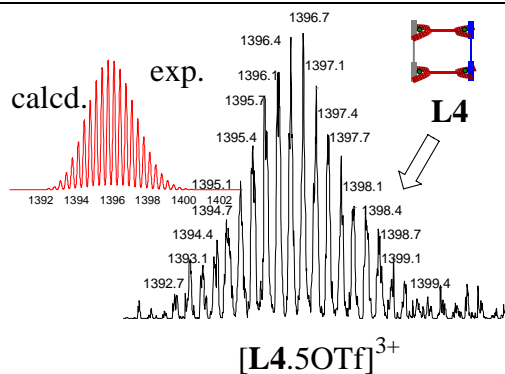


Figure 4. Cartoon representation of the mixed species and its isotopic distribution (dark) $[L4.5OTf]^{3+}$ along with its theoretical one (red).

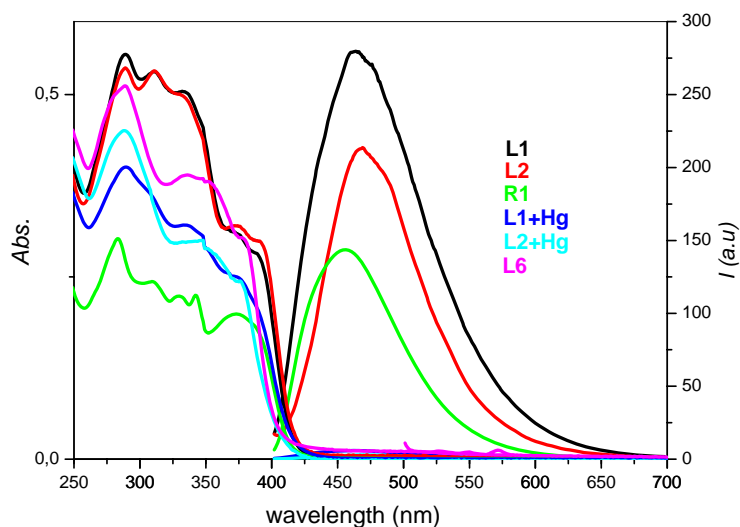
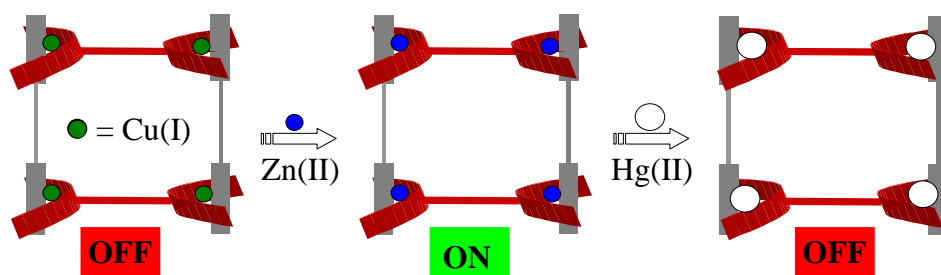


Figure 5. Absorption and emission spectra of **L1**, **L2**, **R1**, **L1+Hg**, **L2+Hg** (λ_{exc} . 389 nm) and **L6** (λ_{exc} . 490 nm) in acetonitrile at rt (1.3×10^{-5} M).

From the above observations, a two step transmetalation off-on-off system based on fluorescence was designed. As shown in Scheme 4, upon addition of Zn(II) salt to **L4** (non fluorescent; off), **L1** formed (fluorescent; On) which could be again transformed to **L5** (non fluorescent; off) upon addition of Hg(II). These transmetalations could be readily followed by ESI MS and fluorescence spectrometries.



Scheme 4. A two-step transmetalation off-on-off fluorescence system.

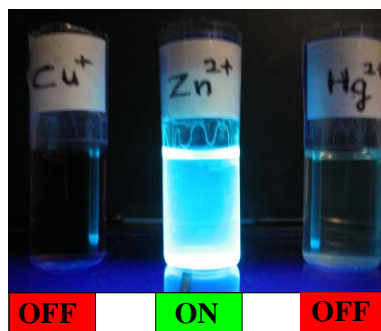
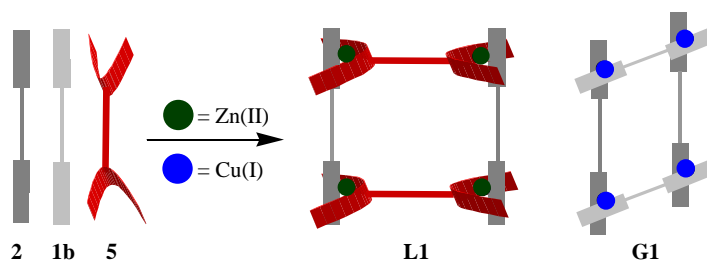


Figure 6. Photo: Taken under a UV lamp (254 nm).

A while ago Lehn *et al.* showed^{21a} self-recognition phenomena in helicate aggregates that was later also studied by others.^{21b} It was demonstrated that from the reaction of a mixture of oligobipyridine strands with a mixture of metal ions (Cu(I) and Ni(II)) only helicates composed of *like* ligands and *like* metal ions were formed, selectively. However, *unlike* ligand and *unlike/like* metal ions combination have never been studied in detail. Therefore, it was of interest to study this phenomena in multicomponent (*unlike* ligand scenario) aggregates. As the Cu(I) ladder **L4** could readily be converted to Zn(II) ladder (**L1**), we reasoned that upon mixing of **1b**, **2** and **5** with Cu(I) and Zn(II) salt both the Zn(II) ladder **L1** and grid **G1**^{8b} should emerge. Indeed, as shown in Scheme 5, **L1** and **G1** were formed selectively since no other combinations could be detected by ESI MS and ¹H NMR. This process represents a unique example of self/nonself-discrimination involving the preferential binding of like metal ions by *unlike* ligands from a mixture to assemble into respective multicomponent aggregates, selectively.



Scheme 5. Cartoon representation of un-like ligand and like metal ions recognition phenomena.

Conclusions

A new supramolecular toolkit allows to prepare cleanly heterotopic aggregates combining both phenanthroline and terpyridine building blocks at various metal centers. Since many terpyridine and phenanthroline/bipyridine building blocks are easily accessible, these

findings should open an effective way to diverse supramolecular aggregates. Due to their dynamic nature a two-step transmetalation and an *unlike* ligand/ *like* metal selection experiment could be realised. Further studies are in progress to study the host-guest and photophysical properties of these unique multicomponent ladder structures.

Acknowledgments. We are indebted to the Deutsche Forschungsgemeinschaft for continued support. We also would like to thank Prof. H. Ihmels for allowing us to access the Varian Cary 100 Bio UV/visible Spectrometer and Varian Cary Eclipse Fluorescence Spectrometer.

Supporting Information Available: Experimental details including ¹H NMR, ESI MS, elemental analysis and crystallographic data (PDF). This material is available free of charge via the Internet at <http://pubs.acs.org>.

-
- (1) Schmittel, M.; Kalsani, V. *Top. Curr. Chem.* **2005**, *245*, 1-53 and ref's therein.
 - (2) (a) Holliday, B. J.; Mirkin, C. A. *Angew. Chem. Int. Ed. Engl.* **2001**, *40*, 2022-2043. (b) Seidel, S. R.; Stang, P. J. *Acc. Chem. Res.* **2002**, *35*, 972-983 (c) Fujita, M.; Oguro, D.; Miyazawa, M.; Oka, H.; Yamaguchi, K.; Ogura, K. *Nature* **1995**, *378*, 469-471. (d) Fujita, M.; Tominaga, M.; Hori, A.; Therrien B.; *Acc. Chem. Res.* **2005**, ASAP.
 - (3) (a) Hasenknopf, B.; Lehn, J.-M.; Baum, G.; Fenske, D. *Proc. Natl. Acad. Sci. USA* **1996**, *93*, 1397-1400. (b) Ovchinnikov, M. V.; Brown, A. M.; Liu, X.; Mirkin, C. A.; Zakharov, L. N.; Rheingold, A. L. *Inorg. Chem.* **2004**, *43*, 8233-8235. (c) Hiraoka, S.; Hirata, K.; Shionoya, M. *Angew. Chem. Int. Ed.* **2004**, *43*, 3814-3818. (d) Hiraoka, S.; Shiro, M.; Shionoya, M. *J. Am. Chem. Soc.* **2004**, *126*, 1214-1218.
 - (4) Hamann, C.; Kern, J.-M.; Sauvage, J. P. *Inorg. Chem.* **2003**, *42*, 1877-1883.
 - (5) (a) Cantrill, S. J.; Chichak, K.; Peters, A. J.; Stoddart, J. F. *Acc. Chem. Res.* **2005**, *38*, 1-9. (b) Lukin, O.; Vögtle, F. *Angew. Chem. Int. Ed.* **2005**, ASAP.
 - (6) Baxter, P. N. W.; Hanan, G. S.; Lehn, J.-M. *Chem. Commun.* **1996**, 2019-2020.
 - (7) HETPHEN: This strategy makes use of steric and electronic effects originating from bulky aryl substituents at the bisimine coordination sites (as seen in 1) to control the coordination equilibrium both kinetically and thermodynamically. The steric stoppers at coordinations sites (2, 9 positions) of bis-phenanthroline site prevent any competitive homoleptic combination of itself, therefore leading to just hetero combinations; (a) Schmittel, M.; Ganz, A. *Chem. Commun.* **1997**, 999-1000. (b) Schmittel, M.; Lünig, U.; Meder, M.; Ganz, A.; Michel, C.; Herderich, M. *Heterocycl. Commun.* **1997**, *3*, 493-498.
 - (8) (a) Kalsani, V.; Ammon, H.; Jäckel, F.; Rabe, J. P.; Schmittel, M. *Chem. Eur. J.* **2004**, *21*, 5481-5492. (b) Schmittel, M.; Kalsani, V.; Fenske, D.; Wiegrefe, A. *Chem. Commun.* **2004**, 490-491. (c) Schmittel, M.; Ganz, A.; Fenske, D. *Org. Lett.* **2003**, *4*, 2289-2292. (d) Schmittel, M.; Ammon, H.; Kalsani, V.; Michel, C.; Wiegrefe, A. *Chem. Commun.* **2002**, 2566-2567. (e) Kalsani, V.; Bodenstedt, H.; Fenske, D.; Schmittel, M. *Eur. J. Inorg. Chem.* **2005**, in press.
 - (9) Schmittel, M.; Michel, C.; Wiegrefe, A.; Kalsani, V. *Synthesis* **2001**, 1561-1567.
 - (10) Purchased from Aldrich and used as received.
 - (11) In a typical experiment, ligands **1/2** or **4/5** and Zn(II) salts were mixed in dichloromethane-methanol (4:1) and heated for few minutes to get a clear solution. Thereafter, the resulting solution was analysed without any further purification.
 - (12) (a) Baxter, P. N. W.; Khoury, R. G.; Lehn, J.-M.; Baum, G.; Fenske, D. *Chem. Eur. J.* **2000**, *6*, 4140-4148. (b) Smith, C. B.; Constable, E. C.; Housecroft, C. E.; Kariuki, B. M. *Chem. Commun.* **2002**, 2068-2069. (d) Loiseau, F.; Di Pietro, C.; Serroni, S.; Campagna, S.; Licciardello, A.; Manfredi, A.; Pozzi, G.; Quici, S. *Inorg. Chem.* **2001**, *40*, 6901-6909. (e) Hofmeier, H.; Schubert, U. S. *Chem. Soc. Rev.* **2004**, 373-399. (f) Wang, P.; Moorefield, C. N.; Panzer, M.; Newkome, G. R. *Chem. Commun.* **2005**, 465-467.

- (13) Schmittel, M.; Ganz, A.; Fenske, D.; Herderich, M. *J. Chem. Soc. Dalton Trans.* **2000**, 353-359.
- (14) Rojo, J.; Romero-Salguero, F. J.; Lehn, J.-M.; Baum, G.; Fenske, D. *Eur. J. Inorg. Chem.* **1999**, 1421-1428.
- (15) Tominaga, M.; Suzuki, K.; Kawano, M.; Kusukawa, T.; Ozeki, T.; Sakamoto, S.; Yamaguchi, K.; Fujita, M. *Angew. Chem. Int. Ed.* **2004**, *43*, 5621-5625.
- (16) Slow evaporation of a dichloromethane/methanol mixture (5:1) containing **L2** produced X-ray quality crystals. The crystals were only surviving in the solvent and diffracted very poorly. A single crystal (yellow block with dimensions 0.20 x 0.35 x 0.50 mm) was measured on a SIEMENS SMART diffractometer. Crystal data of **L2**: C₂₁₆H₁₅₆F₂₄N₂₀O₂₈S₈Zn₄, *M* = 4453.57, Monoclinic, space group *P21/n*, *a* = 21.715(6) Å, *b* = 19.196(6) Å and *c* = 28.620(7) Å, *V* = 11887 (5) Å³, *T* = 157 (2) K, *Z* = 2, *D_c* = 1.244 g/cm³, λ(Mo Kα) = 0.71073 Å, 101150 reflexions measured, 17215 unique (*R*_{int} = 0.2147) which were used in all calculations. The structure was determined by direct methods using program SIR98 and refined on *F*² values using program SHELXL-97. *R*₁ = 0.2315 (*I* > 2 σ(*I*)) and *wR*₂ = 0.3967, GOF = 1.638; max/min residual density 1.272/-0.556 e Å⁻³. CCDC reference number **xxxx**. See also supp. information.
- (17) Jimenez-Molero, M. C.; Dietrich-Buchecker, C.; Sauvage, J. P. *Chem. Eur. J.* **2002**, *8*, 1456-1466.
- (18) Toyota, S.; Woods, C. R.; Benaglia, M.; Haldimann, R.; Wärnmark, K.; Hardcastle, K.; Siegel, J. S. *Angew. Chem. Int. Ed.* **2001**, *40*, 751-754.
- (19) (a) Ramachandram, B.; Samanta, A. *Chem. Phys. Lett.* **1998**, *290*, 9-16. (b) Rurack, K. *Spectrochim. Acta Part A* **2001**, *57*, 2161-2195.
- (20) Armaroli, N. *Chem. Soc. Rev.* **2001**, *30*, 113-124.
- (21) (a) Krämer, R.; Lehn, J.-M.; Marquis-Rigault, A. *Proc. Natl. Acad. Sci. USA* **1993**, *90*, 5394-5398. (b) Wu, A.; Isaacs, L. *J. Am. Chem. Soc.* **2003**, *125*, 4831-4835 and ref's therein.

Supp 6-3**Zn(II)/Ag(I) Nanoscale 2D Ladders Containing Pyrene Units**Michael Schmittel,^{*a} Venkateshwarlu Kalsani,^a Bice He,^a Jan W. Bats^b

^a Center of Micro and Nanochemistry and Engineering, Organische Chemie I, Universität Siegen, Adolf-Reichwein-Str., D-57068 Siegen, Germany, Fax: (+49) 271 740 3270; Tel: (+49) 271 740 4356; E-mail: schmittel@chemie.uni-siegen.de

^b Institut für Organische Chemie und Chemische Biologie, Johann Wolfgang Goethe-Universität, Marie-Curie-Strasse 11, D-60439 Frankfurt am Main, Germany.

Introduction

As discotic liquid crystals,¹ composed of a columnar arrangement of aromatics, and natural light harvesting systems (LHS) containing porphyrine dyes allow for a precise positioning in space,² there has recently been growing interest to interrogate the chemical and physical properties of aromatic stacks.³ Consequently, stacks with an undefined or infinite number of constituents have been well studied,⁴ whereas stacks composed of a defined number are much less explored.⁵ Discrete assemblies are anticipated to show different properties from those of an isolated molecule or infinitely stacked π -systems, thus allowing to probe the communication as a function of the number of constituents.

Two different strategies have been explored to realise π -stacked systems within a discrete supramolecular environment (Figure 1), *i.e.* host-guest complexation and preorganization.^{3,6} Recently, Fujita *et al.* have assembled a small aromatic π -stack utilising supramolecular host-guest chemistry (strategy 1). The alternative strategy 2 has been utilized first by Würthner *et al.* in perylene based squares,⁶ but due to free rotation about the perylene spacer unit carrying pyrene units their approach lacked the needed directionality (Figure 1; strategy 2a). In contrast, strategy 2b (Figure 1) should provide a high degree of directionality to position the appended aromatics in aromatic π -stacks, but this requires a multicomponent supramolecular aggregation.

For some time, we have designed novel multicomponent aggregation systems, the HETPHEN⁷ and HETTAP (**H**eteroleptic **T**erpyridine **A**nd **P**henanthroline aggregation)⁸ concept that might be able to give access to discrete π -stacked aromatic systems. Herein, we present our attempts to generate an aromatic π -stack in a nanoladder aggregate following strategy 2b.

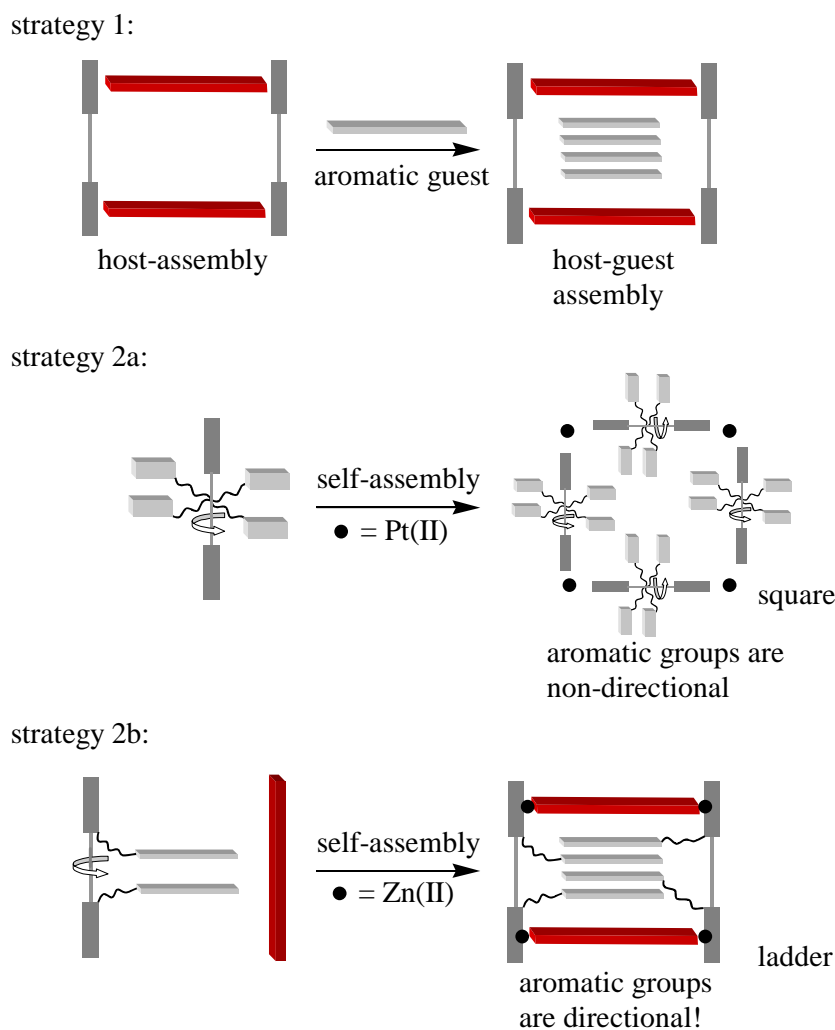


Figure 1. Strategies to prepare aromatic π -stacks in a discrete environment.

As indicated above, the self-assembly process was conceived applying the HETTAP concept. Ligand **1** (Chart 1) was encoded with the required control features to furnish exclusively the heteroleptic assembly, *i.e.* the 2,9 positions of each phenanthroline unit in **1** were shielded with bulky methylaryl groups, thus preventing any association to homoleptic complexes. The appropriate combination of this ligand with **1** or **3** and Zn(II)/Cu(I)/Ag(I) was expected to yield the heteroleptic rack or ladder.⁹ Pyrene was selected as a test case to test strategy 2b because of its well known properties as a spectroscopic probe.¹⁰ As shown in Scheme 1,2b, upon nanoladder formation the pyrene units were expected to form a quadruple aromatic stack. In the following, we present the self-assembly of a pyrene enriched nanoladder, single crystal structure and preliminary photophysical properties.

Results and Discussion

Ligand **1** was synthesised utilising sequential Sonogashira coupling protocols that will be published elsewhere.¹¹ Ligands **2** and **3** were purchased from Aldrich and used as received (Chart 1).

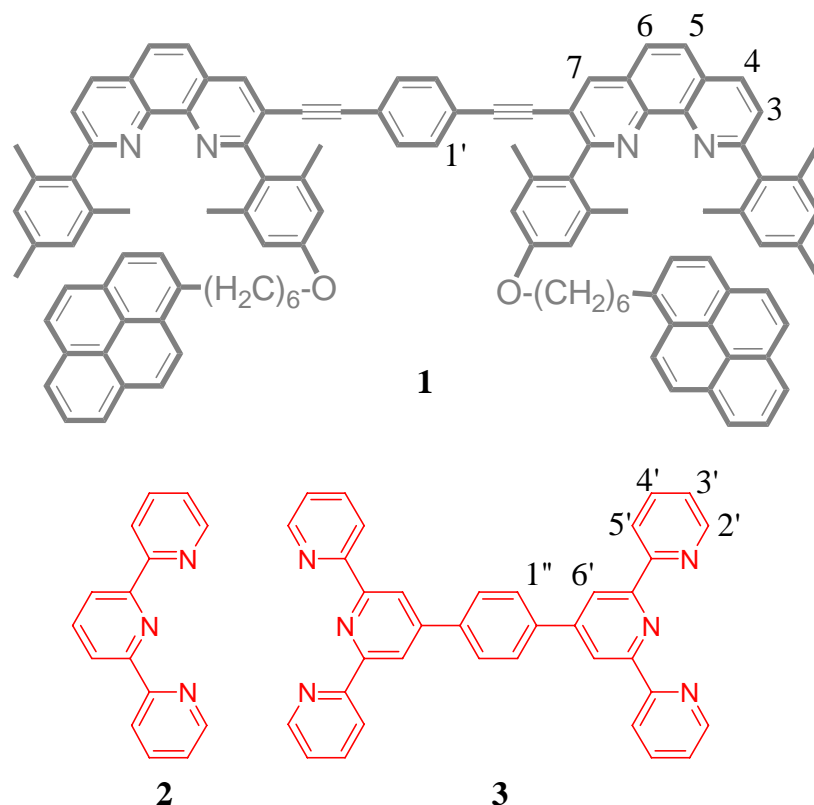
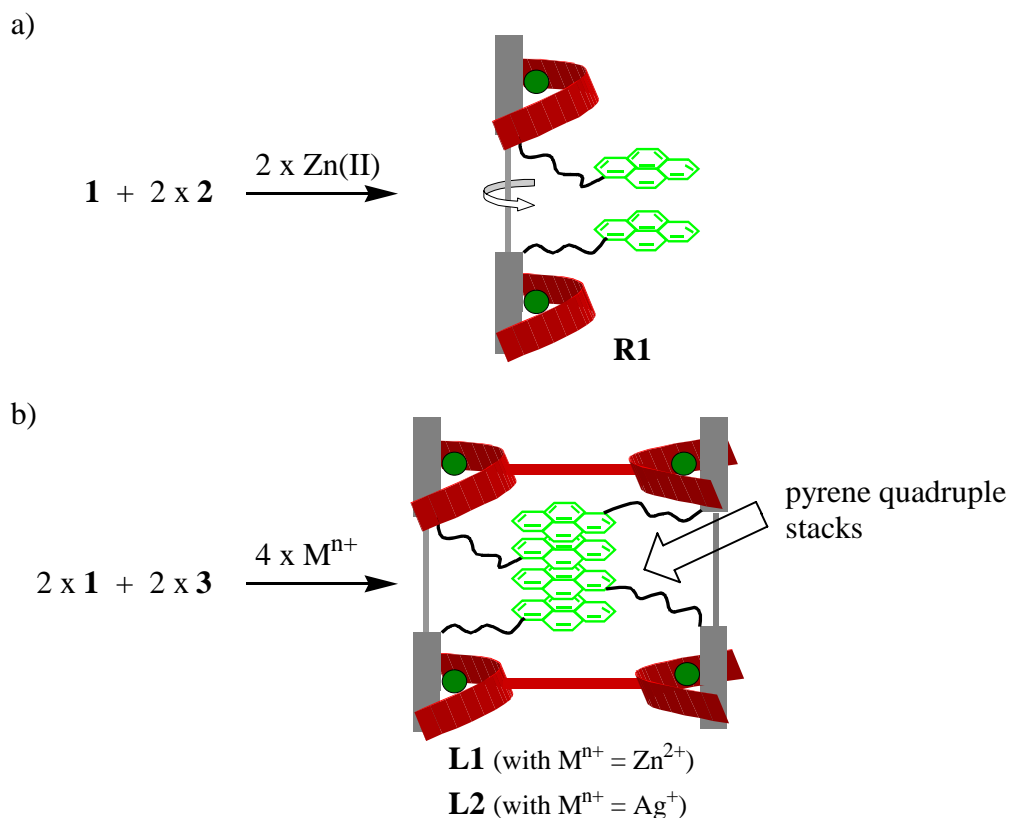


Chart 1. Ligands used for the heterotopic aggregation.

As shown in Scheme 1b, ladder **L1** was readily assembled by mixing **1**, **3** and $\text{Zn}(\text{OTf})_2$ (1:1:2 eqs.) in dichloromethane / methanol (8:2). The ^1H NMR showed a single set of signals and was in full accordance with a highly symmetric structure. For example, typical^{7,8,9} high field shifts ($\delta \sim 7$ to ~ 6 ppm) were observed for the mesityl protons upon formation of the phen-Zn-terpyridine complex. The ^1H NMR signals of the pyrene units in **L1** were shifted downfield ($\delta \sim 7.6$ - 8.1 to 7.9 - 8.3 ppm). **R1** was prepared using an analogous procedure (Scheme 1a, see experimental section).



Scheme 1. Self-assembly of racks and ladders.

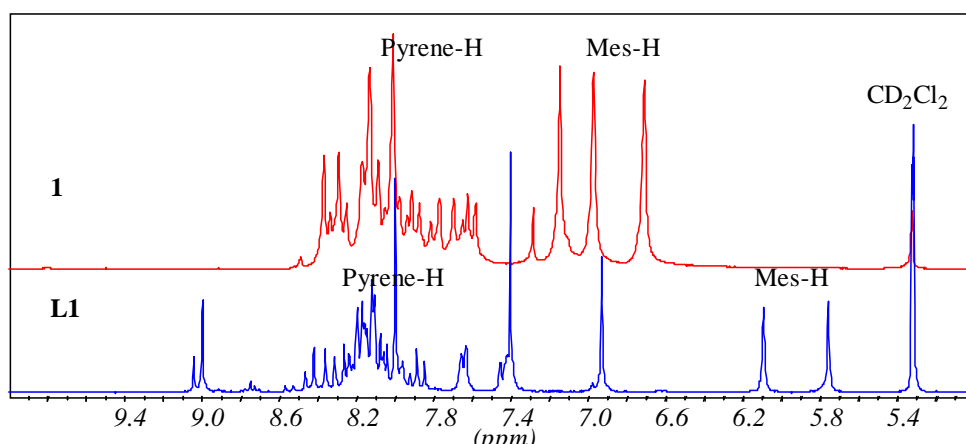


Figure 2. Changes in the ^1H NMR of the aromatic region of **1** upon ladder formation (see experimental section for detailed assignments).

ESI MS measurements provided unequivocal evidence for the assignment of the **R1** and **L1** structures (Figure 3). For example, the ESI MS of the **L1** showed isotopically resolved signals at $m/z = 969.2$, 1247.9 , 1714.5 corresponding to the ions $[(\text{Zn})_4(\mathbf{1})_2(\mathbf{3})_2 \cdot 3\text{OTf}]^{5+}$, $[(\text{Zn})_4(\mathbf{1})_2(\mathbf{3})_2 \cdot 4\text{OTf}]^{4+}$, and $[(\text{Zn})_4(\mathbf{1})_2(\mathbf{3})_2 \cdot 5\text{OTf}]^{3+}$, respectively (Figure 3).

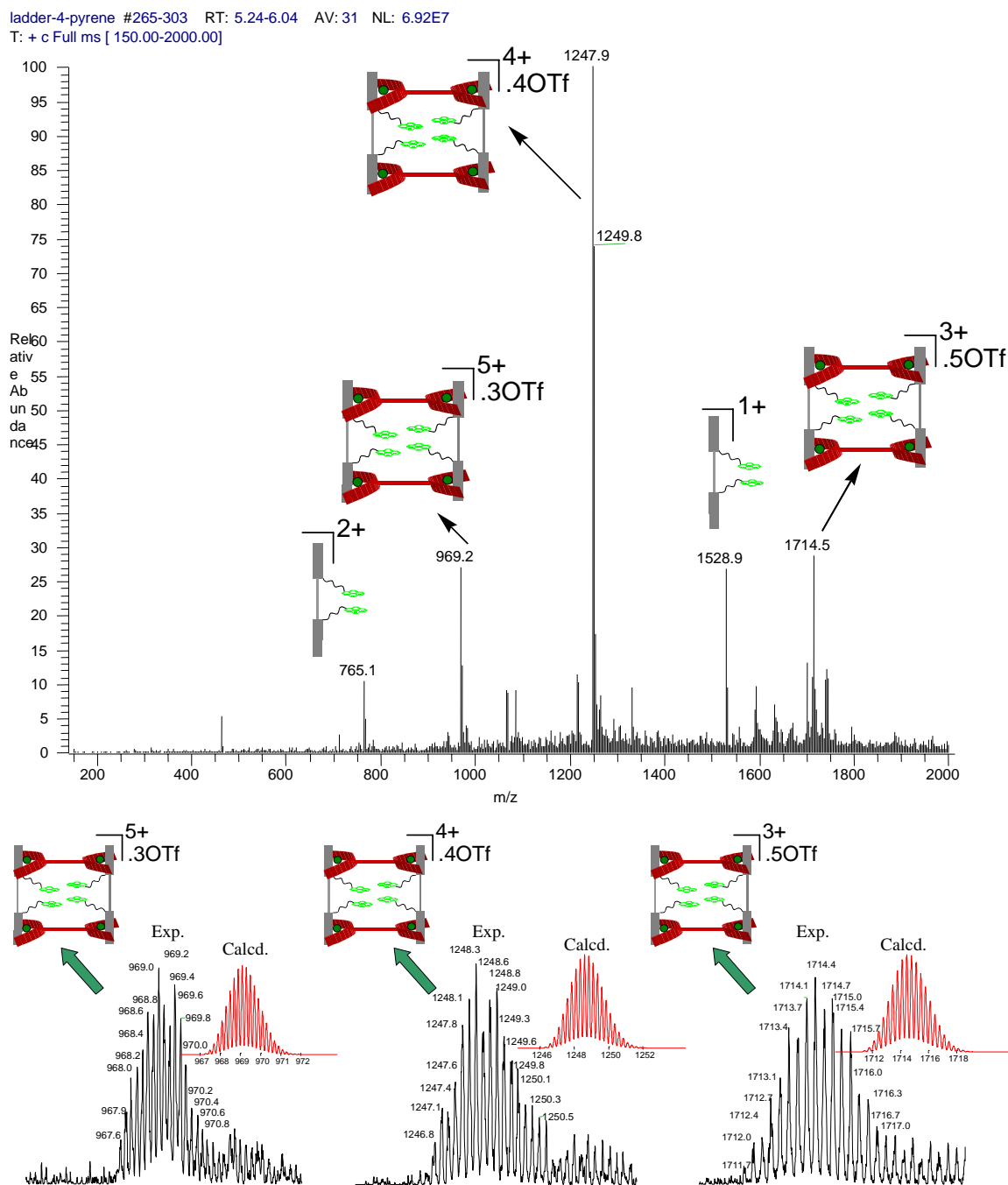


Figure 3. (a) ESI MS of the pyrene Zn(II) ladder (L1). (b) Isotopic distributions (dark) along with their theoretical ones (red).

The ultimate proof of the ladder structures was obtained from a single crystal analysis of L1 (Figure 4).¹² It showed the complex possessing the proposed structure, in which two molecules of each **1** and **3** assemble by means of four metal (Zn^{2+}) ions. The structure reveals the nanoscale nature of these unique supramolecular aggregates with overall external dimensions (including van der Waals radii) of 2.3, 2.6, 3.2 nm (Figure 4). The terpyridine units are sandwiched in between two alkylaryl groups of the phenanthroline units and are

stabilised by π - π interactions (3.4 Å). The presence of the 2,9-steric stoppers forces the Zn(II) to accept a pentacoordination in which three positions are occupied by the nitrogen atoms of the terpyridine ligand and two are occupied by the nitrogen atoms of the phenanthroline unit. The programmed aromatic stackings, however, could not be detected, possibly due to the limited internal space that forces the pyrene moieties to tilt away from the internal area thus preventing formation of pyrene-pyrene stacks in the solid state.

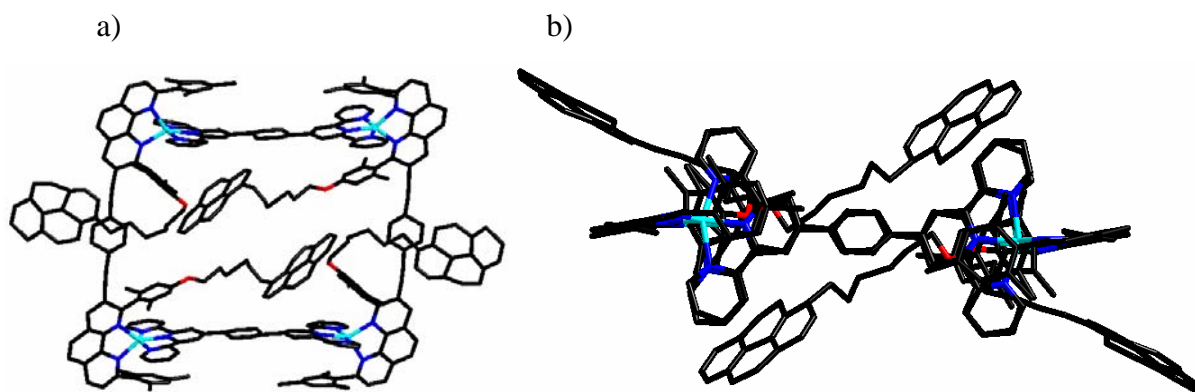
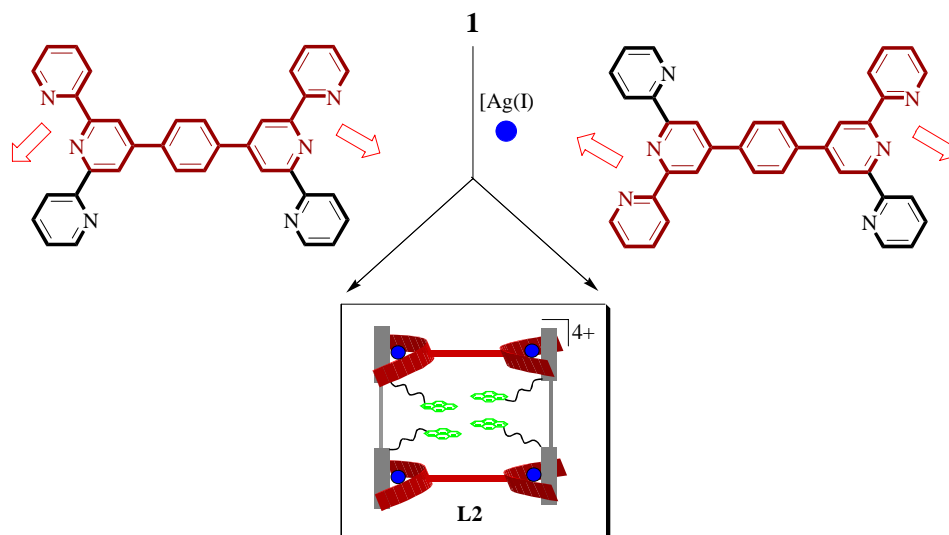


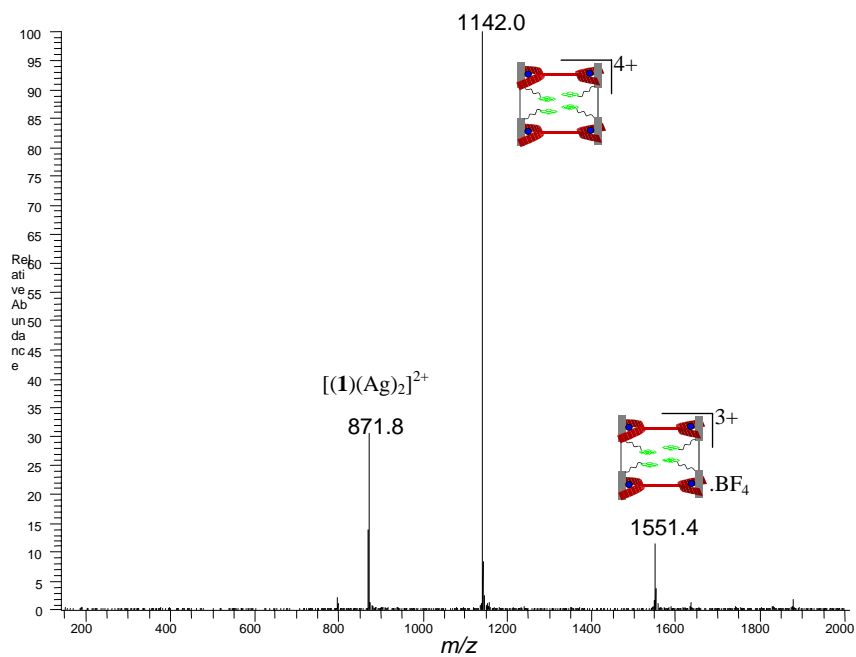
Figure 4. a) Stick representation of single crystal structure of **L1**⁸⁺. b) Side view

Following the procedure as described for **L1**, the silver(I) ladder **L2** was prepared by reacting **1** and **3** with AgBF_4 in dichloromethane/methanol (8:2) (Scheme 2). The clean and sharp peaks in the ^1H NMR spectra suggested the presence of a single species in the solution by excluding the possibility of the formation of polymeric or oligomeric structures. Similar to **L1**, also in **L2** characteristic highfield shifts were observed for the mesityl protons ($\delta \sim 7$ to 6 ppm). Further direct evidence for the ladder structure was obtained from electrospray ionization (ESI) mass spectrometry. Figure 5 illustrates the ESI MS spectrum and the isotopic distributions of the **L2**ⁿ⁺. As Ag(I) prefers tetrahedral coordination and due to the orientation of bipyridine units (showed with arrows in Scheme 2), one may expect different conformational and configurational isomers (see Scheme 2) for **L2**, however, there was no mixture detectable in the ^1H NMR either due to rapid equilibria or to enforced pentacoordination at the silver(I) ions.



Scheme 2. Self-assembly of silver(I) ladder L2.

a)



b)

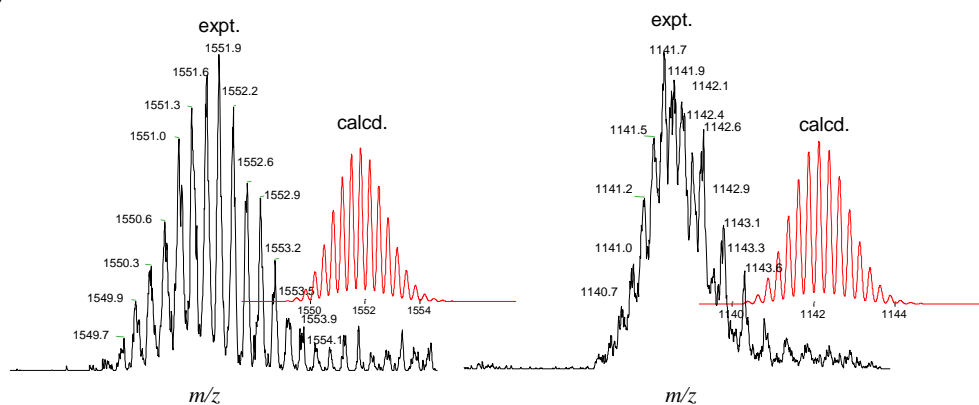


Figure 5. (a) ESI MS of pyrene silver ladder (L2). (b) Isotopic distributions (dark) along with their theoretical ones (red).

UV-vis of Ligands and Rack (R1) and Ladder Motifs (L1-2):

The optical properties of the ligands **1-3** and their aggregates **R1**, **L1-2** were investigated by UV/vis spectroscopy and fluorescence measurements in dichloromethane/methanol (8:2). The UV/vis spectra of **1-3** and **R1**, **L1-L2** exhibited intense absorption bands ranging from 250 to 410 nm (due to π - π^* transitions), which are characteristic for the phenanthroline building blocks.^{7b} Additionally, three sharp and intense transitions at 309, 328 and 344 nm were observed for the pyrene chromophore, which were not affected in **R1** and **L1-L2** with respect to the free ligand **1**. The absorption maxima of **L1-L2** were bathochromically shifted by about 8 to 10 nm with respect to the free ligand **1** (Figures 6) due to coordination of the phenanthroline/terpyridine groups to Zn(II) or Ag(I). As can be seen in Figure 6, almost double intensity was observed for **L1-L2** with respect to **1** and **R1**, supporting the proposed composition for ladders **L1-2** that contain four pyrene moieties.

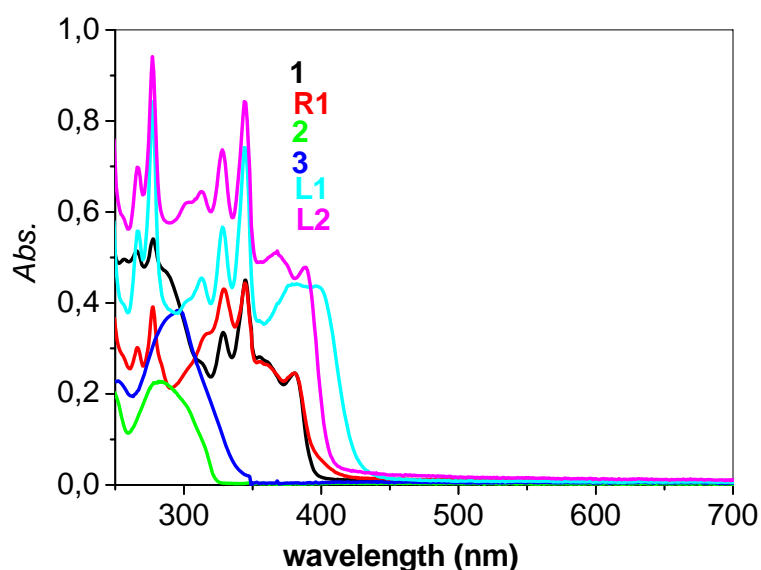


Figure 6. Absorption spectra of **1-3** and **R1**, **L1-2** in dichloromethane / methanol (8:2) (6.5×10^{-6} M).

Preliminary fluorescence studies indicated that the emission of **1** is slightly quenched upon formation of the multicomponent aggregates **R1** and **L1**. The weak fluorescence of **L2** with respect to ligand **1** can be attributed to the *heavy atom effect*¹³ caused by the coordination of **1** and **3** to the silver(I) cations.

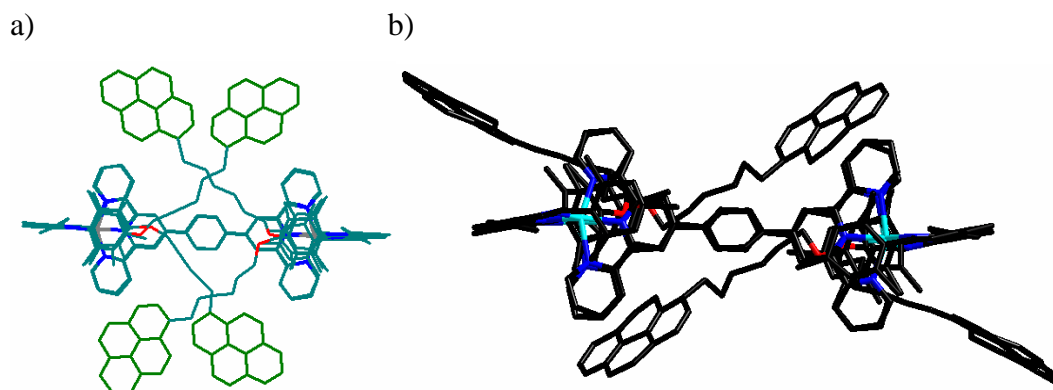


Figure 8. Structural relationship of **L1** in gaseous and solid state: a) Hyperchem calculated structure. b) single crystal structure.

In conclusion, we have shown that pyrene ladders can be assembled using the HETTAP concept. The resulting structures were characterised in solution, and in one case, by a single crystal analysis. As shown by the single crystal analysis, strategy 2b offers an interesting route to preorganise pyrene residues in a discrete atmosphere. It is also clear from model calculations¹⁴ and the solid state structure that the long alkyl chains preclude organisation of the pyrene units within the ladder framework of **L1**. Instead they lead to an expulsion of the pyrene units from the internal space. This suggests to use either a more spacious ladder system or to resort to very short alkyl chains connecting the pyrenes and the phenanthrolines. Further studies in this direction are in progress. Studies are also in progress to understand the quenching process of **1**, **2** and **3** in **R1**, **L1-L2**.

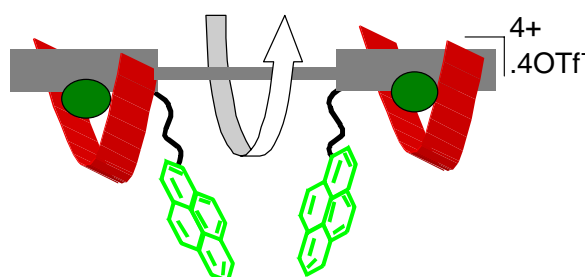
Acknowledgements. We are grateful to the Deutsche Forschungsgemeinschaft and the Fonds der Chemischen Industrie. We thank Prof. H. Ihmels for providing access to fluorescence spectrometers.

Experimental:

The synthesis of ligand **1** will be published elsewhere. Terpyridine building blocks **2,3** were purchased from Aldrich and used as received. ¹H NMR and ¹³C NMR were measured on a Bruker AC 200 (200 MHz), unless specified otherwise. ESI MS spectra were measured on a LCQ Deca ThermoQuest instrument. Typically, 25 scans were accumulated for a spectrum. All complexes were characterized by ¹H-, ¹³C, ESI MS and elemental analysis. UV/vis spectra were recorded on a Varian Cary 100 Bio UV/visible Spectrometer and Varian Cary Eclipse Fluorescence Spectrometer.

General Procedure for the Heterotopic Assemblies:

Ladder motifs, **L1** or **L2** were prepared by mixing **1** (2.50 mg, 1.63×10^{-3} mmol) and **3** (0.88 mg, 1.63×10^{-3} mmol) with $\text{Zn}(\text{OTf})_2$ (1.16 mg, 3.27×10^{-3} mmol) or AgBF_4 (0.63 mg, 3.27×10^{-3} mmol) in dichloromethane/methanol mixture (8:2).¹⁵ The resulting suspension was heated for a few minutes until a clear solution had formed. It was analysed by ESI MS, ^1H NMR, ^{13}C NMR and UV/vis spectroscopy without any further purification. In addition, **L1** could be characterised in solid state. With Ag^+ a light yellow precipitate formed that could be dissolved in acetonitrile. Along the same line rack **R1** was prepared by reacting **1** (2.50 mg, 1.63×10^{-3} mmol), **2** (0.76 mg, 1.63×10^{-3} mmol) and $\text{Zn}(\text{OTf})_2$ (1.18 mg, 3.27×10^{-3} mmol) in a dichloromethane /methanol mixture (8:2).



$[\text{Zn}_2(\mathbf{1})(\mathbf{2})_2]^{4+}$: ^1H NMR ($\text{CD}_2\text{Cl}_2/\text{CD}_3\text{OD}$ (8:2), 200 MHz): δ 9.00 (s, 2H, phen), 8.42 (q, $J = 9.1$ Hz, 4H, phen), 7.98-8.31 (m, 24H, pyrene&phen&terp), 7.91 (t, $J = 6.6$ Hz, 4H, terp), 7.68 (d, $J = 4.9$ Hz, 2H, phen), 7.46 (t, $J = 6.2$ Hz, 4H, terp), 6.94 (s, 4H, phenyl), 6.11 (s, 4H, phenyl), 5.78 (s, 4H, phenyl), 3.29-3.40 (m, 12H, alkyl), 1.75 (s, 6H, benzyl), 1.40-1.53 (m, 12H, alkyl), 1.06 (s, 12H, benzyl), 1.04 (s, 12H, benzyl); ^{13}C NMR ($\text{CD}_2\text{Cl}_2/\text{CD}_3\text{OD}$ (8:2), 50 MHz) : 162.3, 161.1, 160.9, 160.5, 159.5, 157.6, 155.4, 149.6, 149.0, 148.9, 147.0, 146.2, 145.0, 144.1, 142.7, 140.7, 140.0, 137.3, 136.8, 134.8, 134.3, 131.6, 131.4, 129.7, 129.4, 129.1, 128.5, 127.8, 127.5, 127.4, 127.1, 126.5, 125.9, 124.7, 124.0, 123.5, 122.2, 112.2 (arom), 86.1, 81.8 (ethynyl), 67.9 (alkoxy), 33.7, 32.8, 32.1, 29.7, 26.2, 19.3, 19.1 (2C) (aliph); ESI MS: calcd. for $[\text{Zn}_2\text{C}_{142}\text{H}_{116}\text{N}_{10}\text{O}_2]^{4+}$ [M^{4+}] (%): m/z 531.3, found: m/z 531.6 (100), calcd. for $[\text{Zn}_2\text{C}_{142}\text{H}_{116}\text{N}_{10}\text{O}_2 \cdot \text{OTf}]^{3+}$ [M^{3+}] (%): m/z 758.1, found: m/z 761.2 (80), calcd. for $[\text{Zn}_2\text{C}_{142}\text{H}_{116}\text{N}_{10}\text{O}_2 \cdot 2\text{OTf}]^{2+}$ [M^{2+}] (%): m/z 1211.7, found: m/z 1212.2 (12).

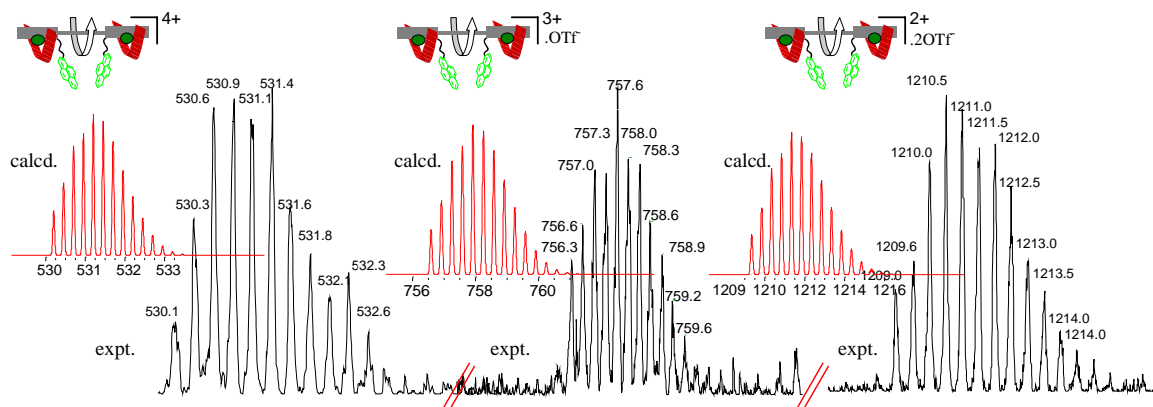
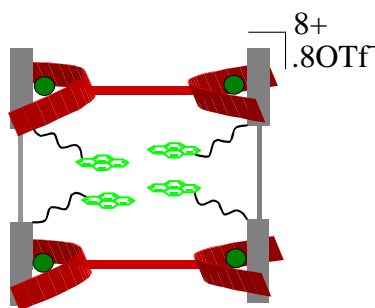
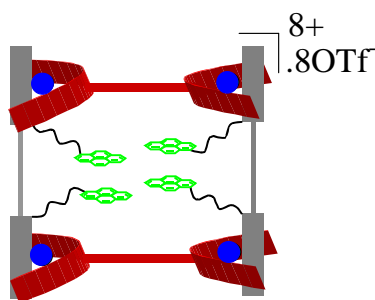


Figure 9. Isotopic distributions of the pyrene Zn rack **R1**; experimental (dark), theoretical (red).



$[\text{Zn}_4(\mathbf{1})_2(\mathbf{3})_2]^{8+}$: ^1H NMR ($\text{CD}_2\text{Cl}_2/\text{CD}_3\text{OD}$ (8:2), 200 MHz): δ 9.04 (s, 4H, phen), 8.56 (q, $J = 9.1$ Hz, 8H, phen), 8.12-8.26 (m, 48H, pyrene&phen&terp), 8.07 (s, 8H, phenyl), 7.99 (s, 8H, terp), 7.84 (d, $J = 6.9$ Hz, 4H, phen), 7.65 (t, $J = 4.42$ Hz, 8H, terp), 7.45 (t, 6H, $J = 9.12$ Hz, terp), 7.40 (s, 8H, terp) 6.93 (s, 8H, phenyl), 6.09 (s, 8H, phenyl), 5.75 (s, 8H, phenyl), 3.32-3.36 (m, 24H, alkyl), 1.96 (s, 16H, alkyl), 1.51-1.53 (m, 8H, alkyl), 1.72 (s, 12H, benzyl), 1.01 (s, 48H, benzyl); ^{13}C NMR ($\text{CD}_2\text{Cl}_2/\text{CD}_3\text{OD}$ (8:2), 100 MHz) : 163.6, 162.0, 159.0, 156.4, 149.5, 148.5, 147.6, 144.6, 144.1, 143.3, 141.7, 140.8, 140.1, 138.5, 137.4, 135.5, 135.1, 134.1, 132.3, 130.1, 129.8, 129.2, 128.5, 128.3, 128.2, 127.1, 126.0, 124.9, 124.3, 123.0, 122.7, 121.2, 119.6, 117.7, 115.2, 114.0, 112.5, 111.0, 106.8, 100.4 (arom), 98.0, 86.6 (ethynyl), 60.6 (alkoxy), 28.6, 26.2, 24.1, 23.4, 23.2, 20.6, 19.4, 19.1 (aliph); ESI MS: calcd. for $[\text{Zn}_4\text{C}_{296}\text{H}_{236}\text{N}_{20}\text{O}_4 \cdot 3\text{OTf}]^{5+} [\text{M}^{5+}]$ (%): m/z 969.2, found: m/z 969.2 (30), calcd. for $[\text{Zn}_4\text{C}_{296}\text{H}_{236}\text{N}_{20}\text{O}_4 \cdot 4\text{OTf}]^{4+} [\text{M}^{4+}]$ (%): m/z 1248.7, found: m/z 1247.9 (100), calcd. for $[\text{Zn}_4\text{C}_{296}\text{H}_{236}\text{N}_{20}\text{O}_4 \cdot 5\text{OTf}]^{3+} [\text{M}^{3+}]$ (%): m/z 1714.7, found: m/z 1714.5 (30). See also single crystal structure.



$[\text{Ag}_4(\mathbf{1})_2(\mathbf{3})_2]^{4+}$: ^1H NMR ($\text{CD}_2\text{Cl}_2/\text{CD}_3\text{OD}$ (8:2), 400 MHz): δ 8.62 (d, 4H, $J = 8.3$ Hz, phen), 8.55 (s, 4H, phen), 8.30 (bs, 8H, terp), 8.20 (d, $J = 9.4$ Hz, 4H, phen), 8.11 (t, $J = 8.3$ Hz, 8H, terp), 8.08 (dt, $J = 8.4$ Hz, $J = 1.7$ Hz, 8H, terp), 8.04 (q, $J = 8.4$ Hz, 8H, phen), 7.80-8.01 (m, 44H, pyrene&terp), 7.80 (dd, $J = 8.3$ Hz, 8H, phen), 7.48 (s, 8H, phenyl), 7.41 (bs, 8H, terp), 6.95 (s, 8H, phenyl), 6.68 (bs, 8H, phenyl), 6.39 (s, 8H, phenyl), 3.76 (bs, 8H, methoxy), 3.25 (t, $J = 7.5$ Hz, 8H, aliph), 2.38 (bs, 12H, aliph), 2.11 (s, 12H, benzyl), 1.77 (s, 24H, benzyl), 1.74 (s, 24H, benzyl), 1.58 (bs, 8H, aliph), 1.41 (bs, 12H, aliph); ^{13}C NMR ($\text{CD}_2\text{Cl}_2/\text{CD}_3\text{OD}$ (8:2), 100 MHz): 162.6, 161.6, 159.8, 152.2, 150.7, 143.0, 142.0, 141.2, 140.5, 139.7, 139.6, 139.0, 138.3, 138.2, 136.3, 133.3, 132.3 (2C), 132.2, 131.7, 130.4, 129.3 (2C), 129.0, 128.8, 128.4, 128.3, 128.2, 127.9, 127.3, 127.0, 126.9, 126.1, 125.7, 125.5 (2C), 124.4, 123.3, 121.9, 95.8 (arom.), 93.9, 88.7 (ethynyl), 68.2 (methoxy), 33.8, 32.5, 29.9, 29.5, 26.5, 21.0, 20.1 (2C) (aliph.); ESI MS: calcd. for $[\text{Ag}_4\text{C}_{296}\text{H}_{236}\text{N}_{20}\text{O}_4]^{4+}$ $[\text{M}^{4+}]$ (%): m/z 1142.2, found: m/z 1141.0 (100), calcd. for $[\text{Ag}_4\text{C}_{296}\text{H}_{236}\text{N}_{20}\text{O}_4\cdot\text{BF}_4]^{3+}$ $[\text{M}^{3+}]$ (%): m/z 1551.8, found: m/z 1551.4 (10).

- (1) S. Chandrasekhar, B. K. Sadashiva, K. A. Suresh, *Pramana* **1977**, 9, 471.
- (2) R. J. Bushby, O. R. Lozman, *Curr. Opin. Colloid Interface Sci.* **2002**, 7, 343 and ref's therein.
- (3) A. Schmidt-Mende, A. Fechtenkötter, K. Müllen, E. Moons, R. H. Friend, D. MacKenzie, *Science* **2001**, 293, 1119 and ref's therein.
- (4) V. Lemaur, D. A. da Silva Filho, V. Coropceanu, M. Lehmann, Y. Geerts, J. Piris, M. G. Debije, A. M. van de Craats, K. Senthilkumar, L. D. A. Siebbeles, J. M. Warman, J.-L. Bredas, J. Cornil, *J. Am. Chem. Soc.* **2004**, 126, 3271-3279 and ref's therein.
- (5) (a) K. Kumazawa, Y. Yamanoi, M. Yoshizawa, T. Kusukawa, M. Fujita, *Angew. Chem. Int. Ed.* **2004**, 43, 5936-5940. (b) M. Yoshizawa, J. Nakagawa, K. Kumazawa, M. Nagao, M. Kawano, T. Ozeki, M. Fujita, *Angew. Chem. Int. Ed.* **2005**, ASAP. (c) X. Peng, N. Aratani, A. Takagi, T. Matsumoto, T. Kawai, I.-W. Hwang, T. K. Ahn, D. Kim, A. Osuka, *J. Am. Chem. Soc.* **2004**, 126, 4468-4469 and ref's therein.
- (6) (a) F. Würthner, A. Sautter, *Org. Biomol. Chem.* **2003**, 240-243. (b) F. Würthner, C. C. You, C. R. Saha-Moeller, *Chem. Rev.* **2004**, 133-146.
- (7) (a) M. Schmittel, V. Kalsani, *Topics in Current Chemistry* **2005**, 245, 1-53. (b) V. Kalsani, H. Ammon, F. Jäckel, J. P. Rabe, M. Schmittel, *Chem. Eur. J.* **2004**, 21, 5481-5492. (c) M. Schmittel, V. Kalsani, D. Fenske, A. Wiegrefe, *Chem. Commun.* **2004**, 490-491. (d) M. Schmittel, V. Kalsani, L. Kienle, *Chem. Commun.* **2004**, 1534-1535. (e) M. Schmittel, A. Ganz, D. Fenske, *Org. Lett.* **2003**, 4, 2289-2292. (f) M. Schmittel, H. Ammon, V. Kalsani, C. Michel, A. Wiegrefe, *Chem. Commun.* **2002**, 2566-2567. (g) V. Kalsani, H. Bodenstedt, D. Fenske, M. Schmittel, *Eur. J. Inorg. Chem.* **2005**, in press.
- (8) HETTAP: This strategy makes use of steric and electronic effects originating from bulky aryl substituents at the bisimine coordination sites (as seen in **1**) to control the coordination equilibrium both kinetically and thermodynamically. The steric stoppers at coordinations sites (2, 9 positions) of bis-

-
- phenanthroline site prevent any competitive homoleptic combination of itself, therefore leading to just hetero combinations; (a) M. Schmittel, V. Kalsani, J. W. Bats, **2005**, manuscript in preparation.
- (9) M. Schmittel, V. Kalsani, J. W. Bats, H. Cölfen, **2005**, manuscript in preparation.
- (10) C. W. Rogers, M. O. Wolf, *Angew. Chem. Int. Ed.* **2002**, *41*, 1898-1900.
- (11) M. Schmittel, B. He, **2005**, unpublished results.
- (12) Slow evaporation of methylene chloride and methanol mixture (5:1) containing **L3** produced X-ray quality crystals. Only poor quality crystals could be obtained therefore the crystal analysis is poor. However, it was possible to obtain the structure skeleton for this ladder. The crystals were extremely solvent dependent and diffracted very poorly. No intensity was found below a resolution of about 2 Å. Nevertheless it was possible to measure the data up to about 1 Å. Of 20064 independent reflections, only 5594 were observed. The structure contains a very large amount of disordered solvent which we do not see. Only one triflate group is visible in the difference map, the rest is disordered.
- (13) (a) R. S. Drago, *Physical Methods in Chemistry*; W. B. Saunders Company: Philadelphia, **1977**; Chapter 5. (b) F. Masetti, U. Mazzucato, G. Galiazzo, *J. Lumin.* **1971**, *4*, 8. (c) T. C. Werner, W. Hawkins, J. Facci, R. Torrisi, T. Trembath, *J. Phys. Chem.* **1978**, *82*, 298.
- (14) Hyperchem 6.02[®]. Release for Windows by Hypercube, Inc. 2000. MM+ force field.
- (15) C. Hamann, J.-M. Kern, J.-P. Sauvage, *Inorg. Chem.* **2003**, *42*, 1877-1883.

Supp 6-4

A Functional Nanoscale Ladder Containing Ferrocene Units

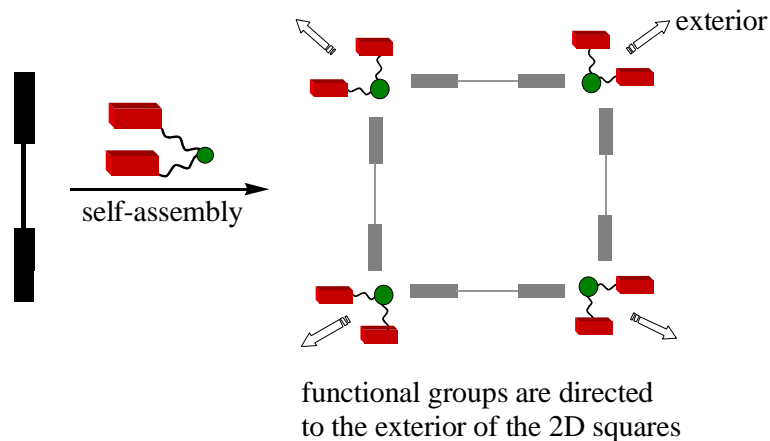
Michael Schmittel,^{*a} Venkateshwarlu Kalsani,^a Bice He,^a Jan W. Bats^b^aContribution from the Center of Micro and Nanochemistry and Engineering, Organische Chemie I, Universität Siegen, Adolf-Reichwein-Str., D-57068 Siegen, Germany.^bInstitute für Organische Chemie und Chemische Biologie, Johann Wolfgang Goethe-Universität, Marie-Curie-Strasse 11, D-60439, Frankfurt an Main, Germany.E-mail: schmittel@chemie.uni-siegen.de**Introduction**

Due to their great potential as novel redox-active, catalytic, optical and mechanical materials,¹ the construction of supramolecular^{2,3} assemblies is a main topic of current interest. While considerable progress has been made to fabricate spectacular supramolecular structures,⁴ their design as functional working models is still in its early stages. As shown in Figure 1, functional supramolecules may be accessed by two approaches. For some time, approach 1 was the method of choice to make functional aggregates, mainly due to the simplicity of the construction because the functional groups were incorporated at the metal corners.⁵ Other researchers, such as Lehn, Stang, Hupp⁶ and Würthner *et al.*,⁷ have explored approach 2a to square motifs, in which functional units were introduced with the organic spacers. However, due to the presence of free rotation^{7c} about the central ligand axis these unique examples lacked any directionality as both external and internal positions may be occupied by the functional unit (Figure 1; approach 2a). In contrast, ladder motifs⁸ may provide a way to a high directionality, but this approach requires multicomponent aggregation (Figure 1; approach 2b).

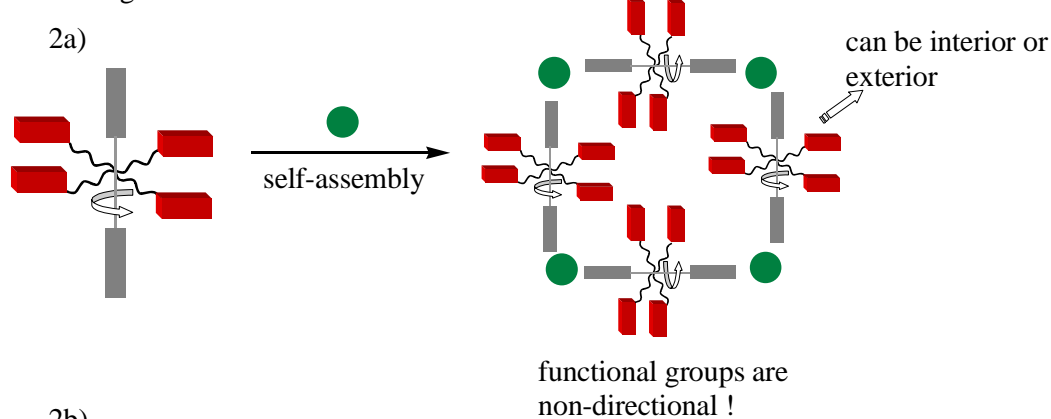
Recently, we have developed self-assembly strategies for multicomponent ladder aggregates using the HETPHEN (**h**eteroleptic **p**henanthroline complexes)⁹ and HETTAP (**h**eteroleptic **t**erpyridine **a**nd **p**henanthroline complexes)¹⁰ concepts. The resultant aggregates were explored to access pure copper nanoparticles in organic media¹¹ and for metal sensing.¹² The beauty of our concepts is that they not only provide an entry to multi-component aggregates, but they also provide directionality to the appended functional systems (Figure 1; approach 2b). Ferrocene was chosen as a functional building block due to its role as a stable redox active unit. Due to interaction of the ferrocenes in the nanoladder novel electrochemical

properties^{5,13} may emerge. In the following, we describe the preparation of ferrocene functionalised nanoracks and nanoladders, their characterization and their electrochemistry.

Approach 1: metal centers are functionalised



Approach 2: ligands are functionalised



2b)

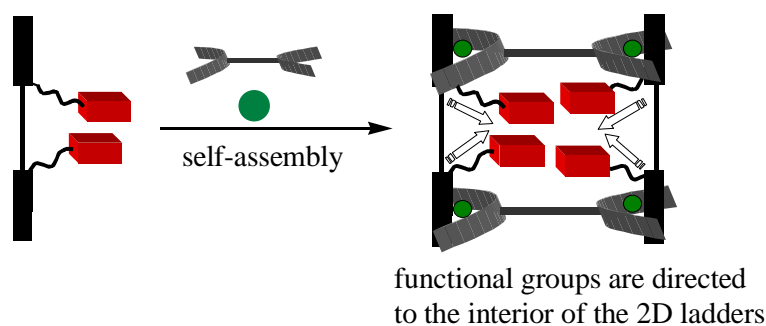


Figure 1. Approaches currently used for supramolecular functionalisation.

Self-assembly of the ferrocene nanorack R1 and nanoladder L1:

Terpyridine ligands **2** and **3** were purchased from Aldrich and used as received (Chart 1). The synthesis of ligand **1** will be published elsewhere.¹⁴ Along with the solution state

characterization of **1**, it was also possible to characterise it by the single crystal structure analysis¹⁵ (Figure 2). As expected, molecule was identified in its transoid conformation, in solid state. As depicted in Figure 3, the external dimensions between two ferrocenes is 3.5 nm and 2.9 nm along the bis-phenanthroline axis. The structure is centrosymmetric with an inversion center at the midpoint of the central benzene ring. The crystal packing shows a number of weak intermolecular C-H... π interactions.

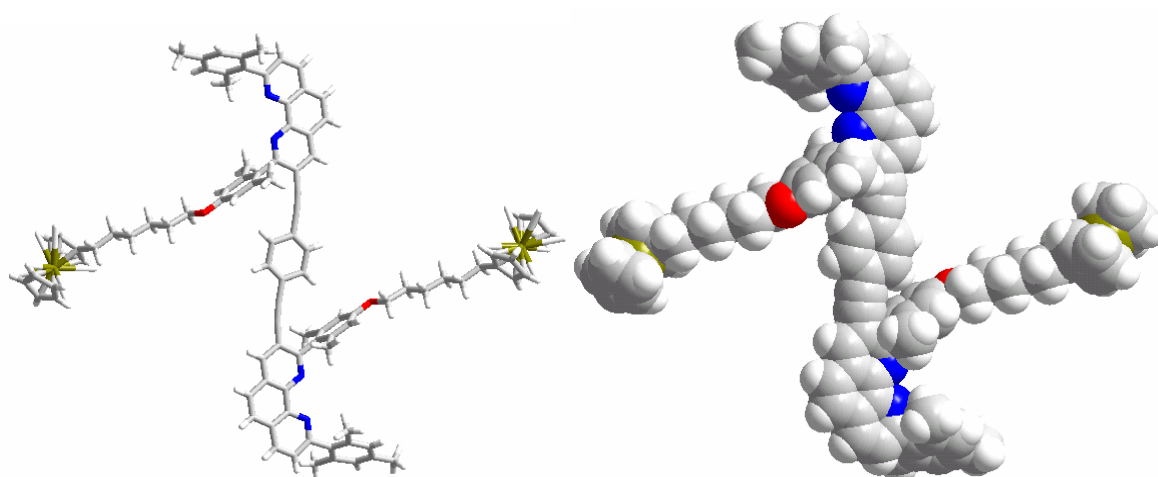


Figure 2. Single crystal structure of ferrocene appended rigid bis-phenanthroline **1**; Stick (left) and space filling representation (rite).

The self-assembly process is guided by the HETTAP principles, as described earlier,¹⁶ suggesting to react ligands **1** and **2** with Zn(II) triflate to afford the desired heteroleptic nanoladder.¹⁷ As depicted in a cartoon in Scheme 1, the ferrocene units are expected to be directed into the interior space of the nanoladder. Indeed, treatment of **1** and **2** with Zn(OTf)₂ (1:1:2 eqs.) in a mixture of dichloromethane / methanol (8:2) afforded the ladder **L1**, quantitatively. **R1** was prepared along the same strategy (Figure 6, see experimental section).

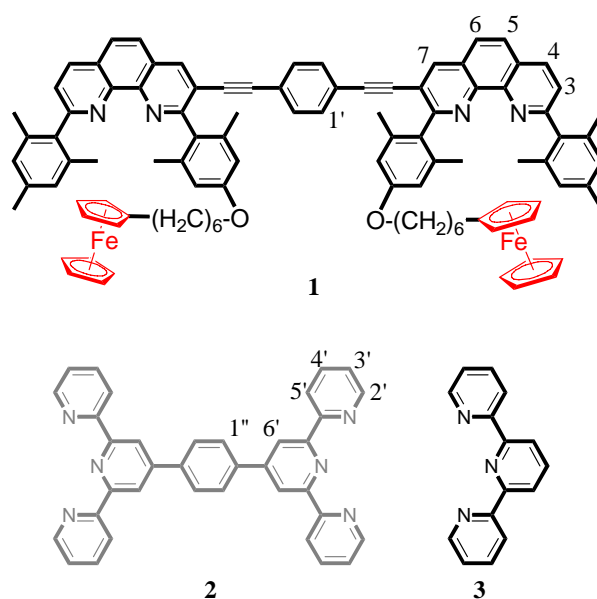
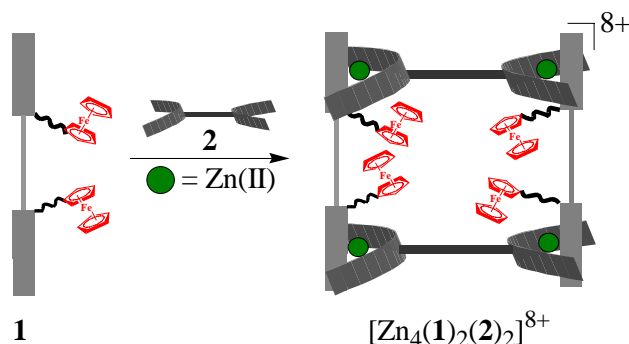


Chart 1. Ligands used for the heterotopic aggregation of **R1** and **L1**.**Scheme 1.** self-assembly of the nanoladder, **L1**.

All spectral data, the ^1H -, ^{13}C -NMR, ESI MS and elemental analysis, point to a single species **L1**. For example, the ^1H NMR spectrum of **L1** in dichloromethane/methanol (8:2) showed a single set of signals for the ligands **1** and **2**, indicative of the formation of a highly symmetrical species. Characteristic high field shifts of the mesityl protons (from $\delta \sim 6.7$ and 6.9 to 5.9 and 6.3 ppm, respectively) and low field shifts of the phenanthroline protons ($\Delta\delta \sim 1.0$ ppm) are in strong support of the formation of the Phen(**1**)-Zn(II)-Terp(**2**) complex, in analogy to earlier results. Upon formation of **L1** the ^1H NMR signals of the ferrocenyl protons were shifted high field (from $\delta = 4.12$ to 3.85 ppm) with the splitting pattern remaining the same. The peaks assignment was further confirmed by COSY 2D proton NMR spectra.

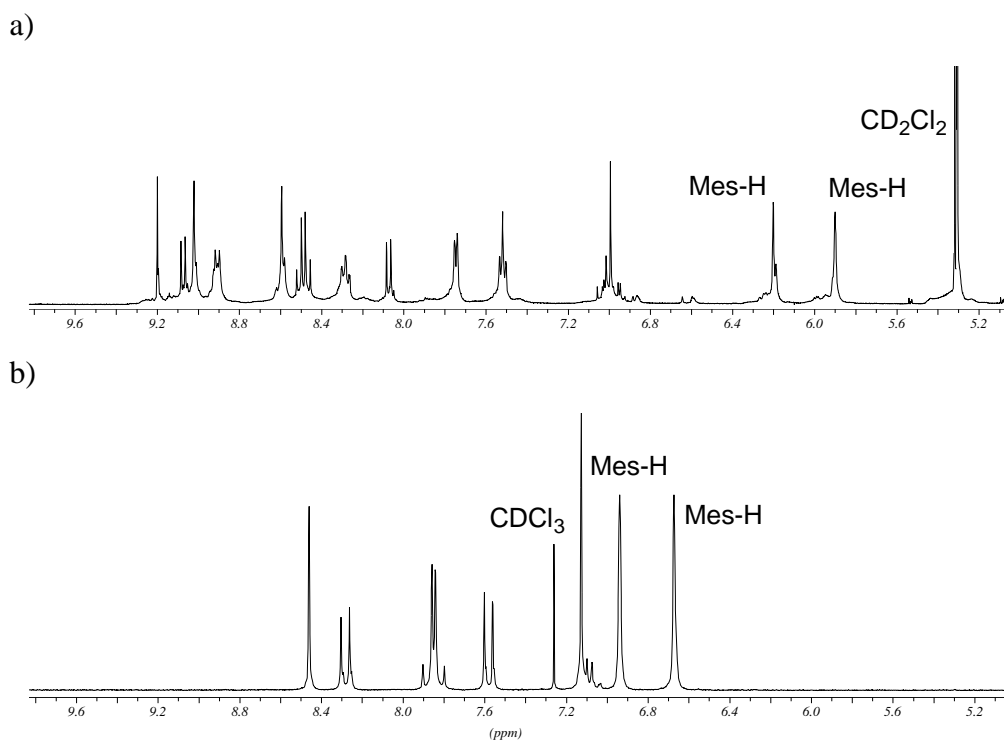


Figure 3. Aromatic region of the ^1H NMR spectra of a) **L1**. b) ligand **1**.

The ESI MS spectra of the ferrocene ladder **L1** showed only peaks attributable to the proposed nanoaggregate. It showed several signals, such as those of $[\text{Zn}_4(\mathbf{1})_2(\mathbf{2})_2](\text{OTf})_3]^{5+}$, $[\text{Zn}_4(\mathbf{1})_2(\mathbf{2})_2](\text{OTf})_4]^{4+}$ and $[\text{Zn}_4(\mathbf{1})_2(\mathbf{2})_2](\text{OTf})_3]^{3+}$ (Figure 4), arising from the consecutive loss of OTf^- counterions from **L1**. Furthermore, the isotopic distribution of these fragments was in excellent agreement with the calculated ones (Figure 5). Hence, the combination of ^1H , ^{13}C -NMR, ESI MS, and elemental analysis, furnished strong evidence for the proposed structure.

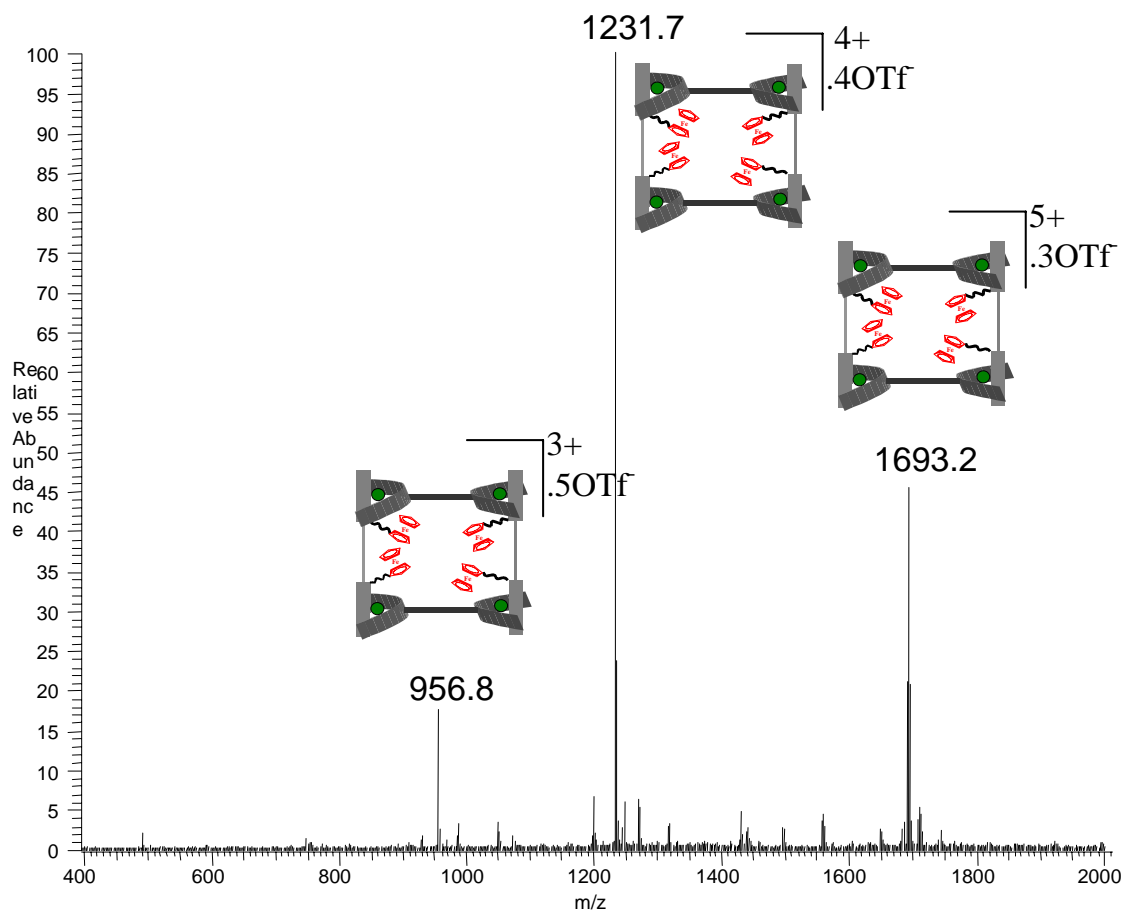


Figure 4. ESI MS of the **L1**.

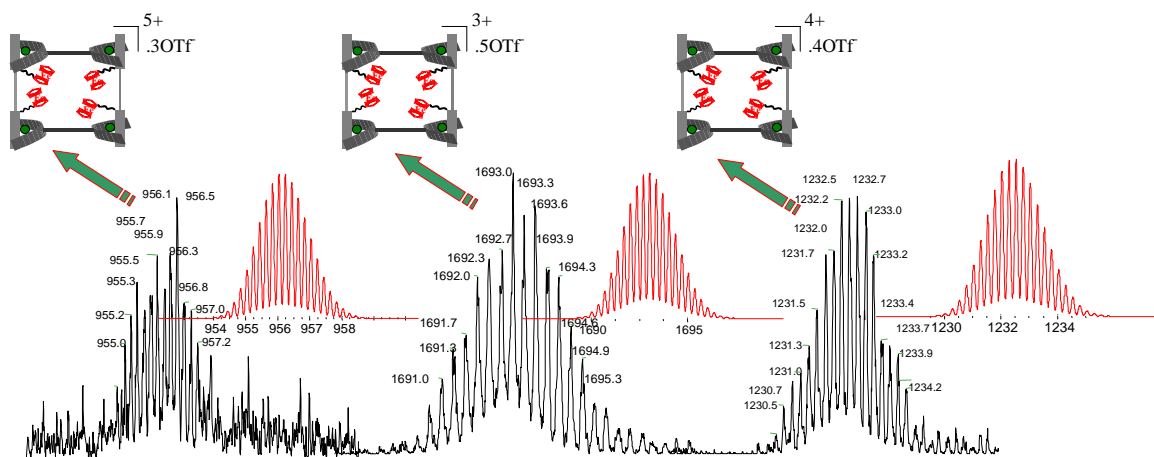


Figure 5. Isotopic distributions (dark = experimental, red = calculated) of 5, 3 and 4 charged species of **L1**.

The effect of the supramolecular frame of **L1** on the redox properties of the ferrocene units was probed by cyclic voltammetry (CV) in dichloromethane/acetonitrile and compared to those of **1** (results are listed in Table 1). The CV analysis of **1** exhibited a single sharp reversible oxidation wave of the ferrocenes at $E_{1/2} = 0.47$ V (versus DMFc/DMFc⁺; DMFc = decamethylferrocene). In contrast to Würthner's squares, for which a peak splitting had been

reported suggesting the presence of internal and external ferrocene units, a single oxidation wave was observed for the Fc/Fc⁺ couple in **1**, **R1** and **L1** at all scan rates. This result proposed that all ferrocene units in the various structures are oxidized at the same potential, as expected for non-interacting redox centers in identical environments.¹⁸ Indeed, the force field minimised¹⁹ structure of **L1** suggests that all four ferrocene units are positioned outside of the nanoladder plane in a rather similar environment with little to no interaction between the redox centers (Figure 6).

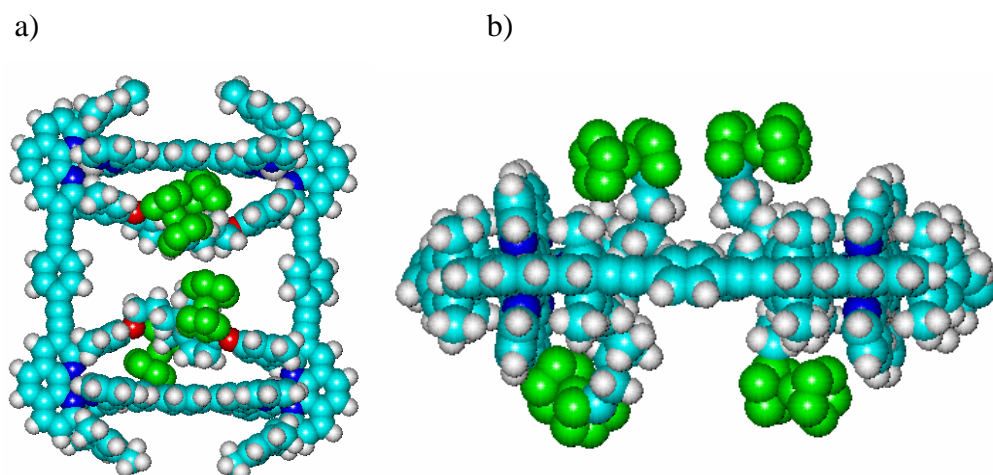


Figure 6. Front (a) and side (b) views of the energy minimised structure of **L1**. Ferrocenes are highlighted with green colour.

In all cases the oxidative couple is with ΔE_p (peak separation) of 59 mV. Interestingly, as can be seen in Table 1, the oxidation potential corresponding to ferrocene couple in **L1** is anodically shifted (20 mV) compared to that of the corresponding free ligand **1**. In order to probe the supramolecular effect on the ferrocene redox process, the rack assembly **R1** = [Zn₂(**1**)(**3**)₂]⁴⁺ was prepared (Figure 6). The CV analysis of **R1** showed an identical redox potential as ligand **1**, suggesting that the observed anodic shift of the oxidation potential of **L1** is due to a supramolecular effect. The anodic shift indicates that oxidation to the ferrocenium (charge build-up) becomes thermodynamically hindered by the supramolecular ladder. Similar anodic shifts had been reported in host-guest chemistry of ferrocene-supramolecules and also in dendrimers containing a ferrocene core.²⁰ However, the observed anodic shift is moderate (20 mV) suggesting only a slight shielding of the ferrocenes by the ladder skeleton. This fact is also clear from the minimised structure; due to the presence of long alkyl chains the ferrocenes were stretched away from the two dimensional plane of ladder rendering the ferrocenes more easily accessible for redox processes (see Figure 5b).

Table 1. Oxidation potentials of ligand **1** and its multicomponent rack **R1** and ladder motifs **L1** in TBAPF₆-CH₃CN at glassy carbon electrode, scan rate = 100 mV s⁻¹.

Compound	$E_{1/2(\text{ox.})}$ (V)	ΔE_p (mV)
1	0.47	59
L1	0.49	59
R1	0.47	59

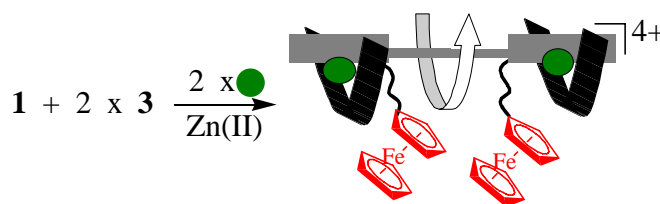


Figure 6. Self-assembly of **R1**.

In conclusion, we have demonstrated the proof of principle for the directional approach to functionalised aggregates using strategy 2b. This approach can therefore be used for internal functionalisation of supramolecular assemblies. Using the HETTAP concept, a nanoscale rack **R1** and a nanoladder **L1**, composed of two and four ferrocenes, respectively, were self-assembled, quantitatively. The redox potential of **R1** corresponded to that of **1**, whereas the redox wave of **L1** was anodically shifted, due to the supramolecular effect present in **L1**. The reversible redox properties and the heterometallic nature of these aggregates suggest some potential for energy storage devices and nanomachinery.

Acknowledgements. We are grateful to the Deutsche Forschungsgemeinschaft and the Fonds der Chemischen Industrie. We would like to thank Prof. H. Ihmels for access to fluorescence spectrometers.

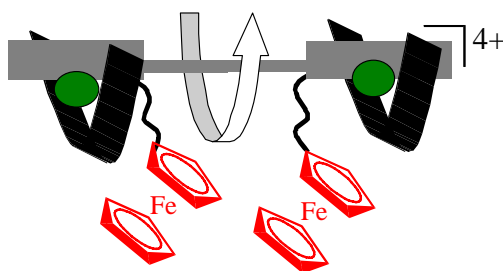
Experimental:

Ligand **1** synthesis will be published elsewhere. Terpyridine building blocks (**2** and **3**) were purchased from Aldrich and used as received. ¹H NMR and ¹³C NMR were measured on a Bruker AC 200 (200 MHz), unless specified otherwise. ESI MS spectra were measured on a LCQ Deca Thermo Quest instrument. Typically, 25 scans were accumulated each time for one spectrum. All complexes were characterized by ¹H-, ¹³C-NMR and ESI MS. UV/vis spectra

were recorded on a Varian Cary 100 Bio UV/visible Spectrometer and Varian Cary Eclipse Fluorescence Spectrometer.

General Procedure for the HETTAP Assemblies:

Rack (**R1**) and ladder motifs (**L1**) were prepared by mixing **1** (2.50 mg, 1.67×10^{-3} mmol) and **3** (0.77 mg, 3.34×10^{-3} mmol) or **2** (0.90 mg, 1.67×10^{-3} mmol) with $\text{Zn}(\text{OTf})_2$ (1.21 mg, 3.34×10^{-3} mmol) (1:2:2 or 1:1:2 equiv., respectively) in a dichloromethane/methanol mixture (8:2).²¹ The resulting suspension was heated for a few minutes until a clear solution had formed. It was analysed by ESI MS, ^1H -, ^{13}C NMR and elemental analysis without any further purification.



$[\text{Zn}_2(\mathbf{1})(\mathbf{3})_2]^{4+}$ (**R1**): ^1H NMR ($\text{CD}_2\text{Cl}_2/\text{CD}_3\text{OD}$ (8:2), 200 MHz): δ 9.13 (s, 2H, phen), 8.71 (d, $J = 7.9$ Hz, 4H, terp), 8.64 (d, 2H, $J = 8.2$ Hz, phen), 8.51 (dd, 4H, $J = 7.8$ Hz, phen), 8.21-8.40 (m, 4H, terp), 8.17 (dt, $J = 9.1$ Hz, $J = 1.7$ Hz, 2H, terp), 7.81-7.90 (m, 2H, terp), 7.75 (d, $J = 4.2$ Hz, 4H, terp), 7.71 (d, $J = 8.1$ Hz, 2H, phen), 7.43-7.49 (m, 4H, terp), 7.43 (dt, $J = 8.8$ Hz, $J = 1.6$ Hz, 2H, terp), 7.37 (s, 4H, phenyl), 5.90 (s, 4H, phenyl), 5.85 (s, 4H, phenyl), 4.32-4.39 (m, 18H, ferrocene), 3.42-3.50 (m, 4H, alkoxy), 1.99 (t, $J = 4.5$ Hz, 4H, alkyl), 1.77 (s, 6H, benzyl), 1.36-1.48 (m, 16H, aliph), 1.15 (s, 12H, benzyl), 1.11 (s, 12H, benzyl); ^{13}C NMR ($\text{CD}_2\text{Cl}_2/\text{CD}_3\text{OD}$ (8:2), 100 MHz): 162.2, 161.0, 159.5, 149.8, 147.4, 147.0, 146.2, 144.1, 143.6, 142.7, 142.6, 141.3, 140.8, 139.9, 139.2, 136.7, 134.7, 134.1, 131.5, 129.3, 129.0, 128.5, 128.4, 127.9, 127.7, 127.4, 127.3, 123.9, 123.6, 123.0, 122.5, 122.1, 121.8, 118.6, 112.1 (arom), 97.2, 85.6 (ethynyl), 67.5 (methoxy), 30.2, 28.9, 28.8, 28.7, 25.6, 20.0, 18.8, 18.6 (aliph); ESI MS: calcd. for $[\text{Zn}_2\text{C}_{130}\text{H}_{116}\text{N}_{10}\text{O}_2\text{Fe}_2]^{4+}$ [M^{4+}] (%): m/z 523.2, found: m/z 523.0 (100), calcd. for $[\text{Zn}_2\text{C}_{130}\text{H}_{116}\text{N}_{10}\text{O}_2\text{Fe}_2 \cdot \text{OTf}]^{3+}$ [M^{3+}] (%): m/z 747.3, found: m/z 747.8 (33), calcd. for $[\text{Zn}_2\text{C}_{130}\text{H}_{116}\text{N}_{10}\text{O}_2\text{Fe}_2 \cdot 2\text{OTf}]^{2+}$ [M^{2+}] (%): m/z 1195.4, found: m/z 1195.4 (55).

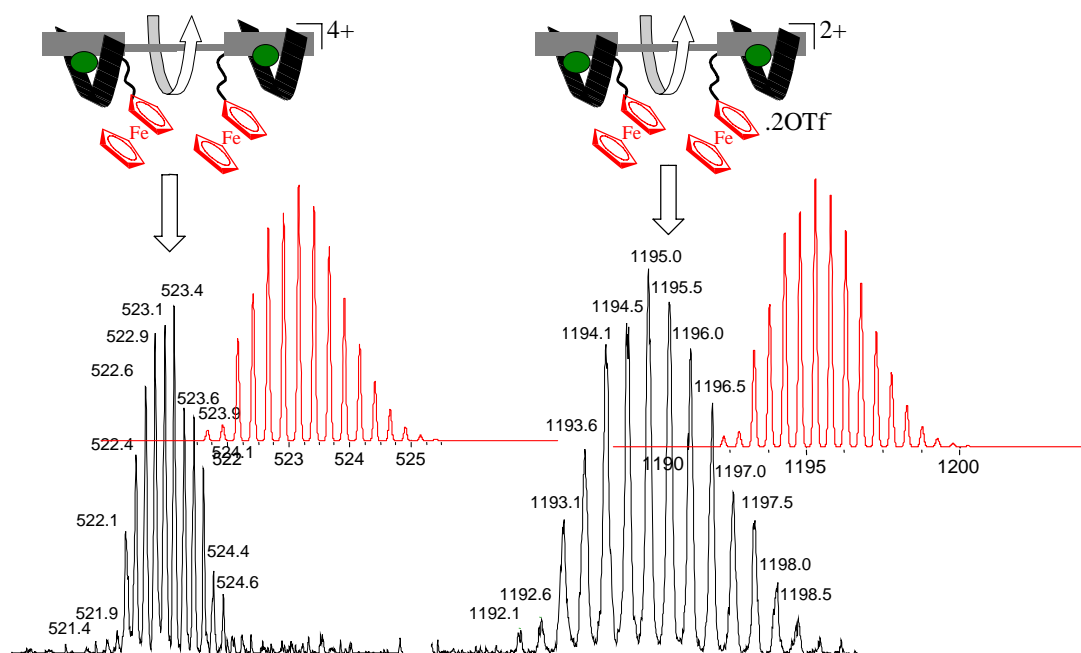
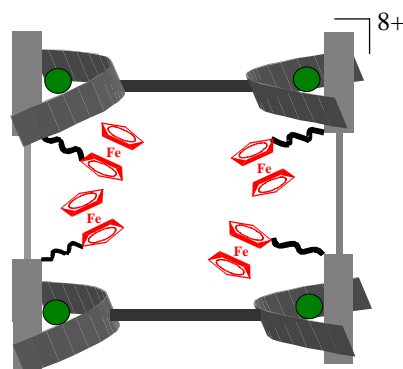


Figure 4. Isotopic distributions (dark = experimental, red = calculated) of 4 and 2 charged species of $\mathbf{R1}^{n+}$.



$[\text{Zn}_4(\mathbf{1})_2(\mathbf{2})_2]^{8+}$ (**L1**): ^1H NMR ($\text{CD}_2\text{Cl}_2/\text{CD}_3\text{OD}$ (8:2), 400 MHz): δ 9.23 (s, 4H, phen), 9.08 (d, $J = 8.2$ Hz, 4H, phen), 9.02 (s, 8H, phenyl), 8.92 (d, $J = 8.1$ Hz, 8H, terp), 8.58 (s, 8H, terp), 8.49 (q, $J = 7.6$ Hz, 8H, phen), 8.30 (dt, $J = 7.8$ Hz, $J = 1.2$ Hz, 8H, terp), 8.07 (d, $J = 8.1$ Hz, 4H, phen), 7.74 (d, $J = 5.1$ Hz, 8H, terp), 7.51 (dt, $J = 5.3$ Hz, $J = 1.2$ Hz, 8H, terp), 6.99 (s, 8H, phenyl), 6.20 (s, 8H, phenyl), 5.90 (s, 8H, phenyl), 3.85-3.96 (m, 36H, ferrocene), 3.43 (t, $J = 6.4$ Hz, 8H, alkoxy), 1.69-1.73 (m, 8H, aliph), 1.73 (s, 12H, benzyl), 1.19-1.36 (m, 32H, aliph), 1.08 (s, 24H, benzyl), 1.07 (s, 24H, benzyl); ^{13}C NMR ($\text{CD}_2\text{Cl}_2/\text{CD}_3\text{OD}$ (8:2), 50 MHz): 162.6, 161.7, 161.2, 155.3 (2C), 149.2, 148.3, 147.1 (2C), 146.6, 144.5, 143.3, 142.0, 141.3, 140.6, 139.8 (2C), 137.8, 137.4, 135.2, 134.7, 132.2, 129.9, 129.1, 128.3, 127.9, 125.7, 124.3, 122.6, 120.4, 119.3, 116.2, 112.7, 109.0, 101.2 (arom.), 97.7, 86.2 (ethynyl), 68.8, 68.4, 68.1, 67.5 (ferrocene), 61.4 (alkoxy), 31.1, 29.7, 25.8, 25.0, 20.5, 20.0, 19.6, 19.2 (aliph); ESI MS: calcd. for $[\text{Zn}_4\text{C}_{272}\text{H}_{236}\text{N}_{20}\text{O}_4\text{Fe}_4 \cdot 3\text{OTf}]^{5+}$ [M^{5+}] (%): m/z 956.2, found: m/z

956.8 (20), calcd. for $[\text{Zn}_4\text{C}_{272}\text{H}_{236}\text{N}_{20}\text{O}_4\text{Fe}_4*4\text{OTf}]^{4+} [\text{M}^{4+}]$ (%): m/z 1232.5, found: m/z 1231.7 (100), calcd. for $[\text{Zn}_4\text{C}_{272}\text{H}_{236}\text{N}_{20}\text{O}_4\text{Fe}_4*5\text{OTf}]^{3+} [\text{M}^{3+}]$ (%): m/z 1693.1, found: m/z 1693.2 (50).

- (1) M. Schmittel, V. Kalsani, *Topics in Current Chemistry*, **2005**, 245, 1-53.
- (2) J.-M. Lehn, *Supramolecular Chemistry: Concepts and Perspectives*, VCH, Weinheim, **1995**.
- (3) L. J. Prins, D. N. Reinhoudt, P. Timmerman, *Angew. Chem. Int. Ed.* **2001**, 40, 2382-2426.
- (4) (a) B. J. Holliday, C. A. Mirkin, *Angew. Chem. Int. Ed. Engl.* **2001**, 40, 2022-2043. (b) S. R. Seidel, P. J. Stang, *Acc. Chem. Res.* **2002**, 35, 972-983. (c) M. Fujita, D. Oguro, M. Miyazawa, H. Oka, K. Yamaguchi, K. Ogura, *Nature* **1995**, 378, 469-471. (d) M. Fujita, M. Tominaga, A. Hori, B. Therrien *Acc. Chem. Res.* **2005**, ASAP. (e) F. Wuerthner, C.-C. You, C. R. Saha-Moeller, *Chem. Soc. Rev.* **2004**, 133-146. (f) M. Ruben, J. Rojo, F. J. Romero-Salguero, L. H. Uppadine, J.-M. Lehn, *Angew. Chem. Int. Ed.* **2004**, 43, 3644-3662.
- (5) (a) P. J. Stang, D. H. Cao, K. Chen, G. M. Gray, D. C. Muddiman, R. D. Smith, *J. Am. Chem. Soc.* **1997**, 119, 5163-5168. (b) P. J. Stang, B. Olenyuk, J. Fan, A. M. Arif, *Organometallics* **1996**, 15, 904-908. (c) S.-S. Sun, J. A. Anspach, A. J. Lees, *Inorg. Chem.* **2002**, 41, 1862-1869.
- (6) (a) O. Shoji, S. Okada, A. Satake, Y. Kobuke, *J. Am. Chem. Soc.* **2005**, 127, 2201-2210. (b) B. Quinodoz, G. Labat, H. Stoeckli-Evans, A. Von Zelewsky, *Inorg. Chem.* **2004**, 43, 7994-8004. (c) J. Fan, J. A. Whiteford, B. Olenyuk, M. D. Levin, P. J. Stang, *J. Am. Chem. Soc.* **1999**, 121, 2741-2752. (d) R. V. Slone, J. T. Hupp, *Inorg. Chem.* **1997**, 36, 5422-5423. (e) C. M. Drain, J.-M. Lehn. *J. Chem. Soc. Chem. Commun.* **1994**, 2313-2315.
- (7) (a) C.-C. You, F. Würthner, *J. Am. Chem. Soc.* **2003**, 125, 9716-9725. (b) F. Wuerthner, A. Sautter, *Org. Biomol. Chem.* **2003**, 240-243. (c) F. Wuerthner, C.-C. You, C. R. Saha-Moeller, *Chem. Soc. Rev.* **2004**, 133-146.
- (8) P. N. W. Baxter, G. S. Hanan, J.-M. Lehn, *Chem. Commun.* **1996**, 2019-2020.
- (9) (a) M. Schmittel, A. Ganz, *Chem. Commun.* **1997**, 999-1000. (b) M. Schmittel, U. Lüning, M. Meder, A. Ganz, C. Michel, M. Herderich, M. *Heterocycl. Commun.* **1997**, 3, 493-498.
- (10) M. Schmittel, V. Kalsani, J. W. Bats, **2005**, manuscript in preparation.
- (11) M. Schmittel, V. Kalsani, L. Kienle, *Chem. Commun.* **2004**, 1534-1535.
- (12) M. Schmittel, V. Kalsani, J. W. Bats, **2005**, manuscript in preparation.
- (13) F. A. Cotton, C. Lin, C. A. Murillo, *Acc. Chem. Res.* **2001**, 34, 759-771.
- (14) M. Schmittel, B. He, **2005**, unpublished results.
- (15) Crystal data for **1**: Suitable single crystals of **1** were obtained by the slow evaporation of dichloromethane/acetonitrile (9.1) solution containing **1**. $\text{C}_{100}\text{H}_{94}\text{N}_4\text{O}_2\text{Fe}_2$, $M = 1495.49$, Monoclinic, space group $P 2_1/c$, $a = 22.789(7) \text{ \AA}$, $b = 13.891(4) \text{ \AA}$ and $c = 13.212(3) \text{ \AA}$, $V = 4101(19) \text{ \AA}^3$, $T = 170(2) \text{ K}$, $Z = 2$, $D_c = 1.211 \text{ g/cm}^3$, $\lambda(\text{Mo K}\alpha) = 0.71073 \text{ \AA}$, 24981 reflexions measured, 7531 unique ($R_{\text{int}} = 0.2864$) which were used in all calculations. $R_1 = 0.3741$ ($I > 2 \sigma(I)$) and $wR_2 = 0.2998$, GOF = 0.872; max/min residual density 0.345/-0.319 e \AA^{-3} . See also supp. information. The R-values are rather large due to the limited scattering power of the crystal.
- (16) HETTAP: This strategy makes use of steric and electronic effects originating from bulky aryl substituents at the bisimine coordination sites (as seen in **1**) to control the coordination equilibrium both kinetically and thermodynamically. The steric stoppers at coordinations sites (2, 9 positions) of bisphenanthroline site prevent any competitive homoleptic combination of itself, therefore leading to just hetero combinations; (a) M. Schmittel, V. Kalsani, J. W. Bats, **2005**, manuscript in preparation.
- (17) M. Schmittel, V. Kalsani, J. W. Bats, H. Cölfen, **2005**, manuscript in preparation.
- (18) S.-H. Hwang, C. N. Moorefield, F. R. Fronczek, O. Lukoyanova, L. Echeguyen, G. R. Newkome, *Chem. Commun.* **2005**, 713-715.
- (19) Hyperchem 6.02[®]. Release for Windows by Hypercube, Inc. 2000. MM+ force field.
- (20) Similar anodic shifts were reported for inclusion complexes of ferrocenes in a supramolecular atmosphere. (a) W.-Y. Sun, T. Kusukawa, M. Fujita, *J. Am. Chem. Soc.* **2002**, 124, 11570-11571. (b) A. E. Kaifer, *Acc. Chem. Res.* **1999**, 32, 62. (c) C. M. Cardona, S. Mendoza, A. E. Kaifer, *Chem. Soc. Rev.* **2000**, 29, 37. (d) D. L. Stone, D. K. Smith, P. T. McGrail, *J. Am. Chem. Soc.* **2002**, 124, 856-864.
- (21) C. Hamann, J.-M. Kern, J.-P. Sauvage, *Inorg. Chem.* **2003**, 42, 1877-1883.

Chapter 7

7 Crystal Structure Data.....	377
7.1 Crystal Structure Data of 1 (In Cooperation with Prof. Martin U. Schmidt, Johann Wolfgang Goethe-University, Frankfurt am Main, Germany).	377
7.2 Crystal Structure Data of 2 (In Cooperation with Marc Schlosser, Prof. Hans-Jorg Deiseroth, University of Siegen, Germany).	380
7.3 Crystal Structure Data of 3 (In Cooperation with Marc Schlosser, Prof. Hans-Jorg Deiseroth, University of Siegen, Germany). ²	386
7.4 Crystal Structure Data of 4 (In Cooperation with Dr. Jan W. Bats, Johann Wolfgang Goethe-University, Frankfurt an Main, Germany).	390
7.5 Crystal Structure Data of 5 (In Cooperation with Prof. Dieter Fenske, University of Karlsruhe, Germany). ³	392
7.6 Crystal Structure Data of 6 (In Cooperation with Prof. Dieter Fenske, University of Karlsruhe, Germany). ³	397
7.7 Crystal Structure Data of 7 (In Cooperation with Dr. Jan W. Bats, Johann Wolfgang Goethe-University, Frankfurt am Main, Germany).	401
7.8 Crystal Structure Data of 8 (In Cooperation with Prof. Dieter Fenske, University of Karlsruhe, Germany).	403
7.9 Crystal Structure Data of 9 (In Cooperation with Prof. Dieter Fenske, University of Karlsruhe, Germany).	408
7.10 Crystal Structure Data of 10 (In Cooperation with Prof. Dieter Fenske, University of Karlsruhe, Germany). ⁵	412
7.11 Crystal Structure Data of 11 (In Cooperation with Dr. Jan W. Bats, Johann Wolfgang Goethe-University, Frankfurt am Main, Germany).	418
7.12 Crystal Structure Data of 12 (In Cooperation with Dr. Jan W. Bats, Johann Wolfgang Goethe-University, Frankfurt am Main, Germany).	422
7.13 Crystal Structure Data of 13 (In Cooperation with Dr. Jan W. Bats, Johann Wolfgang Goethe-University, Frankfurt am Main, Germany).	426
7.14 Crystal Structure Data of 14 (In Cooperation with Dr. Jan W. Bats, Johann Goethe-University, Frankfurt am Main, Germany).	431

7 Crystal Structure Data

Single crystal analysis has become an important method of characterising supramolecular arrangements in solid state.¹ As discussed in chapter 5 (Supp 5-3), it is not always easy to obtain suitable single crystals for X-ray analysis, in particular of aggregates with large internal voids. However, a few single crystals can be obtained for some ligands and their metallo-aggregates. In the following, crystal structure data of this type structures will be presented. In most cases, due to the large size and unsolved solvent, counter ions resulted poor diffraction data with large R values. However, their basic structure could be undoubtedly solved. Detailed discussion of the structures can be found in the manuscripts.

7.1 Crystal Structure Data of **1** (In Cooperation with Prof. Martin U. Schmidt, Johann Wolfgang Goethe-University, Frankfurt am Main, Germany).

Suitable single crystals were obtained by slow evaporation of the dichloromethane/acetonitrile (1:1) solution containing **1**. As shown in Figure 1, intermolecular hydrogen bondings were observed between **1** and acetonitrile (solvent); however, It was interesting to see the selective binding of acetonitrile with **1** over dichloromethane.

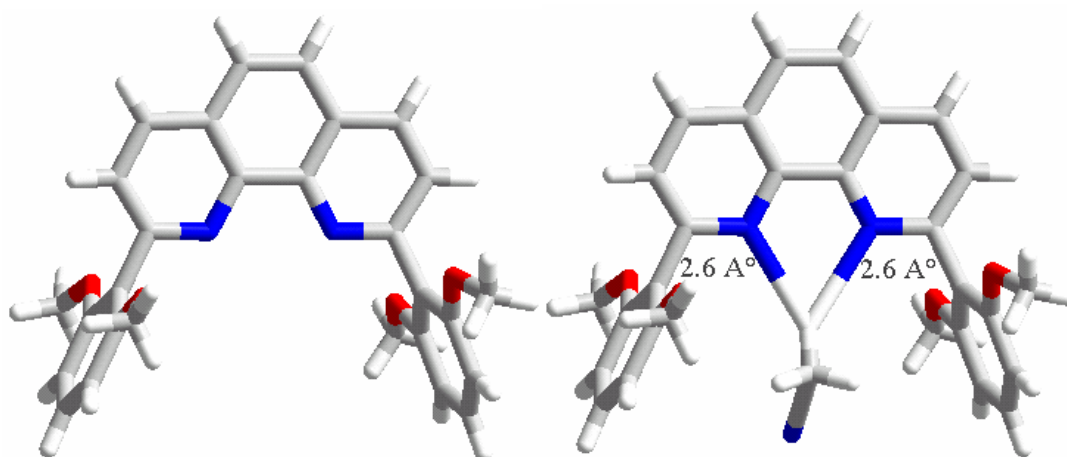


Figure 1-1. Stick representation of ligand **1** (left) and its hydrogen bonding (2.6 Å) with solvent, acetonitrile (rite).

Crystal Structure Data

Table 1-1: Crystal data and structure refinement for **1**.

Substance	1
Sum formula	C32H30N4O4
Formula weight /g·mol ⁻¹	534.6
Temperature /K	100(2)
Wavelength	0.71073 Å
Crystal system, space group	Triclinic, <i>P</i> -1
Unit cell dimensions	a = 8.2800 (19) Å b = 11.194 (3) Å c = 16.043 (4) Å B = 101.009 (19) °
Volume /Å ³	1426.9(6)
Z, Calculated density /Mg·m ⁻³	2, 1.244
Absorption coefficient /mm ⁻¹	0.083
F(000)	564
Crystal size /mm ³	0.34 x 0.19 x 0.03
Reflections collected / unique / R _{int}	5041 / 2285 / 0.0931
Refinement method	Full-matrix least-squares on <i>F</i> ²
Data / restraints / parameters	5041 / 0 / 367
Goodness-of-fit on <i>F</i> ²	0.914
Final <i>R</i> indices [<i>I</i> >2σ(<i>I</i>)]	<i>R</i> 1 = 0.0654, <i>wR</i> 2 = 0.141
<i>R</i> indices (all data)	<i>R</i> 1 = 0.1512, <i>wR</i> 2 = 0.1835

Table 1-2: Atomic coordinates (x 10⁵) and equivalent isotropic displacement parameters (Å² x 10⁴) for **1**. *U*(eq) is defined as one third of the trace of the orthogonalized *U*_{ij} tensor.

Atom	x	y	z	U_{eq}
N11	0.6217(4)	0.2944(3)	0.8207(2)	0.0255(7)
C12	0.7510(5)	0.3515(3)	0.8830(2)	0.0223(8)
C13	0.8153(5)	0.2956(3)	0.9558(3)	0.0262(9)
H13	0.9048	0.34	0.9995	0.031
C14	0.7461(5)	0.1765(3)	0.9619(2)	0.0266(9)
H14	0.788	0.1374	1.0095	0.032
C15	0.6118(5)	0.1128(3)	0.8964(2)	0.0226(8)
C16	0.5523(5)	0.1763(3)	0.8271(2)	0.0223(8)
C17	0.5400(5)	-0.0161(3)	0.8959(3)	0.0253(9)
H17	0.5798	-0.0581	0.9423	0.03
N21	0.3593(4)	0.1756(3)	0.6913(2)	0.0243(7)
C22	0.2346(5)	0.1144(3)	0.6274(2)	0.0240(8)
C23	0.1644(5)	-0.0090(3)	0.6240(3)	0.0264(9)
H23	0.0777	-0.0481	0.577	0.032
C24	0.2214(5)	-0.0743(4)	0.6892(3)	0.0279(9)
H24	0.1744	-0.1583	0.6876	0.033
C25	0.3514(5)	-0.0139(3)	0.7586(2)	0.0235(8)
C26	0.4172(5)	0.1117(3)	0.7577(2)	0.0216(8)
C27	0.4172(5)	-0.0765(3)	0.8300(3)	0.0267(9)
H27	0.3735	-0.1607	0.8304	0.032
C31	0.8309(5)	0.4780(3)	0.8693(3)	0.0245(8)
C32	0.7579(5)	0.5787(3)	0.8869(3)	0.0250(9)
C33	0.8247(5)	0.6956(4)	0.8669(3)	0.0299(10)

Crystal Structure Data

H33	0.7751	0.7641	0.878	0.036
C34	0.9649(5)	0.7068(4)	0.8306(3)	0.0305(9)
H34	1.009	0.7843	0.8156	0.037
C35	1.0444(5)	0.6089(4)	0.8151(3)	0.0298(9)
H35	1.1416	0.6199	0.7911	0.036
C36	0.9766(5)	0.4939(3)	0.8359(2)	0.0272(9)
O32	0.6213(4)	0.5544(2)	0.92345(19)	0.0323(7)
C37	0.5502(6)	0.6561(4)	0.9529(3)	0.0415(12)
H37A	0.6383	0.7163	0.9918	0.062
H37B	0.4618	0.6261	0.9831	0.062
H37C	0.5026	0.6944	0.9037	0.062
O36	1.0415(4)	0.3894(2)	0.8245(2)	0.0336(7)
C38	1.2032(6)	0.4029(4)	0.8009(4)	0.0481(13)
H38A	1.195	0.4326	0.7448	0.072
H38B	1.2382	0.3236	0.7981	0.072
H38C	1.286	0.4615	0.8437	0.072
C41	0.1803(5)	0.1877(3)	0.5559(3)	0.0259(9)
C42	0.2623(5)	0.1938(4)	0.4872(3)	0.0292(9)
C43	0.2149(5)	0.2626(4)	0.4199(3)	0.0317(9)
H43	0.2696	0.2652	0.3729	0.038
C44	0.0856(6)	0.3267(4)	0.4241(3)	0.0336(10)
H44	0.0554	0.3754	0.3801	0.04
C45	0.0000(6)	0.3216(4)	0.4903(3)	0.0319(10)
H45	-0.0889	0.3649	0.491	0.038
C46	0.0463(5)	0.2516(4)	0.5565(3)	0.0279(9)
O42	0.3873(4)	0.1256(3)	0.49004(19)	0.0362(7)
C47	0.4524(7)	0.1056(5)	0.4137(3)	0.0493(13)
H47A	0.3596	0.0704	0.3655	0.074
H47B	0.5306	0.0491	0.4227	0.074
H47C	0.5112	0.1836	0.4012	0.074
O46	-0.0325(4)	0.2353(3)	0.62404(19)	0.0368(8)
C48	-0.1765(6)	0.2922(5)	0.6255(3)	0.0438(13)
H48A	-0.1425	0.3809	0.6276	0.066
H48B	-0.2218	0.2736	0.6761	0.066
H48C	-0.2628	0.2607	0.5737	0.066
N51	0.3549(7)	0.6359(4)	0.6796(4)	0.0687(15)
C51	0.4330(6)	0.5623(4)	0.6691(3)	0.0406(11)
C52	0.5304(6)	0.4668(4)	0.6547(3)	0.0433(12)
H52A	0.5033	0.4009	0.6892	0.065
H52B	0.6505	0.502	0.6713	0.065
H52C	0.5022	0.4339	0.594	0.065
N61	0.1548(6)	0.0789(4)	0.9339(3)	0.0523(12)
C61	0.0586(6)	0.0787(4)	0.8718(3)	0.0358(10)
C62	-0.0630(7)	0.0820(4)	0.7935(3)	0.0437(12)
H62A	-0.1093	0.1565	0.7984	0.066
H62B	-0.1538	0.0104	0.7848	0.066
H62C	-0.0075	0.0813	0.7448	0.066

Table 1-3: Anisotropic displacement parameters ($\text{\AA}^2 \times 10^4$) for **1**. The anisotropic displacement factor exponent takes the form: $\{-2 \pi^2 [h^2 a^{*2} U_{11} + \dots + 2 hka^*b^*U_{12}]$

Atom	U_{11}	U_{22}	U_{33}	U_{23}	U_{13}	U_{12}
N11	0.0266(17)	0.0242(15)	0.0282(18)	0.0056(14)	0.0080(15)	0.0081(13)
C12	0.0203(19)	0.0264(18)	0.0206(18)	0.0000(15)	0.0042(16)	0.0066(15)
C13	0.024(2)	0.029(2)	0.024(2)	-0.0012(16)	0.0038(17)	0.0060(16)
C14	0.031(2)	0.031(2)	0.0213(19)	0.0083(16)	0.0042(18)	0.0131(17)
C15	0.026(2)	0.0234(18)	0.0216(18)	0.0053(15)	0.0083(17)	0.0080(16)
C16	0.0224(19)	0.0233(18)	0.0242(19)	0.0045(16)	0.0092(17)	0.0069(15)
C17	0.028(2)	0.0259(19)	0.024(2)	0.0069(16)	0.0075(18)	0.0060(16)
N21	0.0256(17)	0.0269(16)	0.0226(16)	0.0054(13)	0.0054(15)	0.0099(14)
C22	0.0231(19)	0.0280(19)	0.0240(19)	0.0051(16)	0.0077(17)	0.0101(16)

Crystal Structure Data

C23	0.028(2)	0.0274(19)	0.024(2)	0.0013(16)	0.0050(18)	0.0068(17)
C24	0.030(2)	0.0255(19)	0.030(2)	0.0062(17)	0.0094(18)	0.0067(17)
C25	0.025(2)	0.0248(18)	0.0221(19)	0.0017(16)	0.0061(17)	0.0084(16)
C26	0.023(2)	0.0224(18)	0.0215(19)	0.0037(15)	0.0079(17)	0.0074(15)
C27	0.032(2)	0.0216(18)	0.030(2)	0.0062(16)	0.0103(19)	0.0075(16)
C31	0.025(2)	0.0233(18)	0.0230(19)	0.0025(15)	0.0021(17)	0.0019(15)
C32	0.0214(19)	0.0263(19)	0.027(2)	0.0064(16)	0.0055(17)	0.0026(16)
C33	0.030(2)	0.030(2)	0.030(2)	0.0041(17)	0.0039(19)	0.0088(18)
C34	0.036(2)	0.0253(19)	0.030(2)	0.0072(17)	0.0060(19)	0.0041(17)
C35	0.029(2)	0.034(2)	0.026(2)	0.0001(17)	0.0093(18)	0.0029(18)
C36	0.031(2)	0.0267(19)	0.023(2)	0.0004(16)	0.0051(18)	0.0059(17)
O32	0.0320(16)	0.0250(14)	0.0458(18)	0.0089(13)	0.0163(14)	0.0105(12)
C37	0.044(3)	0.033(2)	0.057(3)	0.009(2)	0.024(2)	0.016(2)
O36	0.0320(16)	0.0282(14)	0.0451(18)	-0.0002(13)	0.0187(14)	0.0089(12)
C38	0.039(3)	0.038(2)	0.074(4)	-0.003(2)	0.031(3)	0.008(2)
C41	0.026(2)	0.0269(19)	0.0229(19)	0.0037(16)	0.0001(18)	0.0044(16)
C42	0.030(2)	0.0284(19)	0.031(2)	0.0067(17)	0.0037(19)	0.0104(17)
C43	0.033(2)	0.035(2)	0.030(2)	0.0107(18)	0.012(2)	0.0056(18)
C44	0.040(2)	0.029(2)	0.031(2)	0.0088(18)	0.001(2)	0.0094(18)
C45	0.039(2)	0.028(2)	0.030(2)	0.0042(17)	0.002(2)	0.0132(18)
C46	0.031(2)	0.030(2)	0.023(2)	0.0034(16)	0.0044(18)	0.0113(17)
O42	0.0349(17)	0.0480(17)	0.0334(16)	0.0148(14)	0.0123(14)	0.0186(14)
C47	0.059(3)	0.058(3)	0.047(3)	0.021(2)	0.030(3)	0.029(3)
O46	0.0392(18)	0.0442(17)	0.0340(16)	0.0066(14)	0.0098(14)	0.0237(15)
C48	0.045(3)	0.061(3)	0.036(2)	0.009(2)	0.010(2)	0.035(3)
N51	0.075(3)	0.058(3)	0.102(4)	0.040(3)	0.054(3)	0.037(3)
C51	0.043(3)	0.038(2)	0.050(3)	0.018(2)	0.023(2)	0.011(2)
C52	0.050(3)	0.032(2)	0.054(3)	0.014(2)	0.017(3)	0.016(2)
N61	0.063(3)	0.052(2)	0.046(3)	0.009(2)	0.008(2)	0.025(2)
C61	0.040(3)	0.036(2)	0.035(2)	0.0061(19)	0.010(2)	0.015(2)
C62	0.046(3)	0.047(3)	0.040(3)	0.006(2)	0.008(2)	0.016(2)

7. 2 Crystal Structure Data of **2** (In Cooperation with Marc Schlosser, Prof. Hans-Jorg Deiseroth, University of Siegen, Germany).²

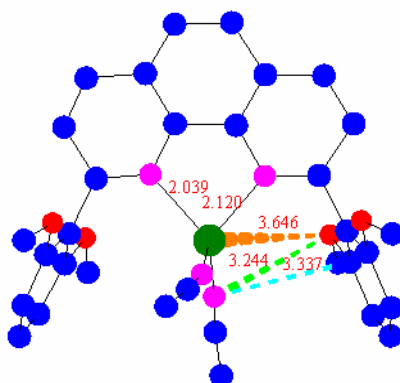


Figure 2-1. Ball and stick representation of **2**.

Crystal Structure Data

Table 2-1: Crystal data and structure refinement for **2**.

Substance	2
Sum formula	C ₃₂ H ₃₀ CuF ₆ N ₄ O ₄ P
Formula weight /g·mol ⁻¹	743.11
Temperature /K	173(2)
Wavelength	0.71073 Å
Crystal system, space group	Triclinic, <i>P</i> -1
Unit cell dimensions	a = 11.496 (2) Å b = 12.177 (2) Å c = 13.345 (3) Å B = 103.92 (3) °
Volume /Å ³	1623.0(6)
Z, Calculated density /Mg·m ⁻³	2, 1.521
Absorption coefficient /mm ⁻¹	0.8
F(000)	760
Reflections collected / unique / R _{int}	8912 / 3727 / 0.1906
Refinement method	Full-matrix least-squares on <i>F</i> ²
Data / restraints / parameters	8912 / 3 / 878
Goodness-of-fit on <i>F</i> ²	0.526
Final <i>R</i> indices [<i>I</i> > 2σ(<i>I</i>)]	<i>R</i> 1 = 0.0412, <i>wR</i> 2 = 0.0935
<i>R</i> indices (all data)	<i>R</i> 1 = 0.1184, <i>wR</i> 2 = 0.1199

Table 2-2: Atomic coordinates (× 10⁵) and equivalent isotropic displacement parameters (Å² × 10⁴) for **2**. *U*(eq) is defined as one third of the trace of the orthogonalized *U*_{ij} tensor.

Atom	x	y	z	U _{eq}
Cu1	0.84502(3)	0.93364(3)	0.40909(3)	0.02479(12)
Cu2	0.84710(3)	1.31027(3)	1.00052(3)	0.02462(14)
P3	0.52112(13)	0.43119(11)	0.51737(10)	0.0500(4)
N2	0.9829(2)	1.0214(2)	0.3720(2)	0.0202(8)
N3	0.9408(2)	1.3543(2)	1.1667(2)	0.0180(8)
N4	0.7554(3)	0.8920(3)	0.2395(2)	0.0191(9)
N5	0.7061(2)	1.2189(3)	1.0393(2)	0.0198(9)
O6	1.2246(2)	1.3031(2)	1.1419(2)	0.0368(9)
O7	0.4683(2)	0.9368(3)	0.2640(2)	0.0331(9)
O8	1.0235(2)	1.6205(2)	1.2061(2)	0.0316(8)
C9	0.5649(3)	0.7773(3)	0.2394(3)	0.0198(10)
O10	0.6672(3)	0.6226(2)	0.2053(2)	0.0348(9)
O11	0.5227(2)	1.3341(2)	0.92390(19)	0.0289(8)
C13	1.0532(3)	1.4141(3)	1.2277(2)	0.0170(9)
O14	1.1665(3)	0.9098(3)	0.4898(2)	0.0347(9)
C15	0.8216(3)	0.9376(3)	0.1890(3)	0.0173(9)
N16	0.8666(2)	0.8037(3)	0.4574(2)	0.0245(9)
C17	0.9115(3)	1.3191(3)	1.3283(3)	0.0235(10)
C18	0.4377(3)	0.6939(4)	0.3584(3)	0.0300(11)
H18	0.3933	0.6651	0.3988	0.036
C19	0.8668(3)	1.3035(3)	1.2149(2)	0.0196(10)
C20	1.0990(3)	1.0954(3)	0.4384(2)	0.0229(10)
C21	0.7769(3)	0.9239(3)	0.0771(3)	0.0208(10)
O22	1.0904(3)	1.2992(2)	0.6197(2)	0.0392(9)

Crystal Structure Data

O23	0.5925(3)	0.9426(3)	0.7887(2)	0.0385(10)
N24	0.8304(3)	1.4417(3)	0.9540(3)	0.0321(11)
C25	0.4803(3)	0.8362(3)	0.2840(2)	0.0193(9)
C26	1.1277(3)	1.4645(3)	1.1702(3)	0.0222(11)
C27	0.6524(3)	0.8575(3)	0.0159(3)	0.0245(10)
H27	0.615	0.8447	-0.0607	0.029
C28	0.6334(3)	0.8267(3)	0.1782(3)	0.0260(12)
C29	0.8198(3)	1.5132(3)	0.9188(3)	0.0270(11)
N30	0.7968(3)	1.0632(4)	0.5212(3)	0.0501(12)
C31	0.5260(4)	0.6304(4)	0.3143(3)	0.0368(13)
H31	0.5424	0.561	0.326	0.044
C32	1.2466(4)	1.5569(4)	1.0540(3)	0.0358(13)
H32	1.2848	1.5867	1.0105	0.043
C33	0.7404(3)	1.2318(3)	1.1484(3)	0.0207(10)
C34	1.1369(3)	1.1040(3)	0.5591(3)	0.0240(11)
C35	0.5874(3)	0.8122(3)	0.0721(3)	0.0256(10)
H35	0.5036	0.7674	0.0315	0.031
C36	0.5599(3)	1.1371(4)	0.8503(3)	0.0260(11)
C37	1.1099(3)	1.4335(4)	1.3479(3)	0.0239(11)
H37	1.1936	1.477	1.3908	0.029
C38	0.5240(3)	1.2313(3)	0.8283(3)	0.0271(11)
C39	0.5983(3)	1.1507(3)	0.9691(3)	0.0229(11)
C40	0.9428(3)	1.0082(3)	0.2616(3)	0.0159(9)
C41	0.7119(3)	1.1921(3)	1.3047(3)	0.0283(11)
H41	0.6593	1.1577	1.3359	0.034
C42	1.2113(4)	1.4070(4)	1.1285(4)	0.0334(14)
C43	0.5842(3)	0.6762(3)	0.2548(2)	0.0242(10)
C44	0.9697(3)	1.0468(3)	0.0972(2)	0.0237(11)
H44	1.019	1.0847	0.0658	0.028
C45	1.1729(3)	1.0082(4)	0.5830(3)	0.0268(12)
C46	0.8677(4)	0.7281(4)	0.4857(3)	0.0322(14)
C47	1.1061(4)	1.5705(3)	1.1566(3)	0.0254(12)
C48	0.8551(3)	0.9809(3)	0.0345(2)	0.0181(9)
H48	0.8246	0.9715	-0.0418	0.022
C49	1.1783(3)	1.1569(3)	0.4053(2)	0.0211(10)
H49	1.2564	1.2094	0.4566	0.025
C50	1.0333(4)	1.3847(4)	1.3920(3)	0.0308(12)
H50	1.0641	1.3958	1.4689	0.037
C51	0.4190(3)	0.7935(3)	0.3419(3)	0.0283(11)
H51	0.3618	0.8347	0.3715	0.034
C52	0.8281(4)	1.2599(4)	1.3725(3)	0.0366(13)
H52	0.8563	1.2695	1.4491	0.044
C53	1.0212(3)	1.0619(3)	0.2155(3)	0.0209(10)
C54	0.6678(3)	1.1717(3)	1.1918(3)	0.0216(10)
C55	0.5544(3)	1.0282(4)	0.7598(3)	0.0270(11)
C56	1.1307(4)	1.2075(4)	0.6504(4)	0.0346(14)
C57	1.1370(3)	1.1378(3)	0.2889(3)	0.0304(11)
H57	1.1893	1.1774	0.261	0.036
C58	0.5182(3)	1.0920(4)	1.0134(4)	0.0320(12)
H58	0.4377	1.0442	0.9634	0.038
C59	1.2774(4)	1.4541(4)	1.0671(3)	0.0314(13)
H59	1.3375	1.4179	1.0379	0.038
C60	0.3638(3)	0.9872(4)	0.2849(3)	0.0361(13)
H60A	0.2873	0.9214	0.2454	0.054
H60B	0.3578	1.0501	0.2563	0.054
H60C	0.3761	1.0241	0.3672	0.054
C61	0.8795(5)	0.6312(4)	0.5301(4)	0.0545(16)
H61A	0.9374	0.5858	0.5009	0.082
H61B	0.7983	0.5745	0.5042	0.082
H61C	0.9105	0.6708	0.6138	0.082
C62	0.5496(3)	1.1008(3)	1.1170(3)	0.0231(11)

Crystal Structure Data

H62	0.4938	1.0602	1.1415	0.028
C63	1.3267(4)	1.2594(4)	1.1259(3)	0.0398(14)
H63A	1.3351	1.2537	1.0529	0.06
H63B	1.3164	1.1779	1.1253	0.06
H63C	1.4012	1.3155	1.1883	0.06
C64	0.7897(4)	1.1540(4)	0.5880(3)	0.0401(13)
C65	0.9057(4)	0.9676(4)	0.7363(4)	0.0567(17)
H65A	0.8891	0.9042	0.7629	0.085
H65B	0.9872	0.9727	0.7253	0.085
H65C	0.8421	0.9464	0.6636	0.085
C66	0.4834(3)	1.2220(4)	0.7201(3)	0.0310(12)
H66	0.4527	1.2848	0.7054	0.037
C67	0.9038(4)	1.0889(3)	0.8234(3)	0.0284(12)
F1	1.1213(3)	1.8328(3)	0.9996(2)	0.0795(11)
C70	0.5030(4)	1.4369(4)	0.9028(3)	0.0371(13)
H70A	0.5573	1.453	0.8609	0.056
H70B	0.5215	1.5089	0.9757	0.056
H70C	0.4165	1.4198	0.8572	0.056
C71	1.1700(4)	1.6142(4)	1.0965(3)	0.0277(12)
H71	1.1572	1.6856	1.0869	0.033
C72	1.2049(4)	1.0195(5)	0.6945(3)	0.0431(15)
H72	1.2238	0.9527	0.7099	0.052
C73	0.4888(4)	1.1155(4)	0.6307(3)	0.0478(16)
H73	0.4688	1.1089	0.555	0.057
C74	1.1938(4)	0.8028(4)	0.5020(4)	0.0364(13)
H74A	1.2797	0.8233	0.5507	0.055
H74B	1.1826	0.7377	0.4266	0.055
H74C	1.1379	0.7745	0.5371	0.055
C76	0.5233(4)	1.0205(4)	0.6537(3)	0.0378(13)
H76	0.5249	0.9483	0.5926	0.045
F2	1.1826(3)	1.95277(19)	0.9170(2)	0.0633(9)
C79	1.2092(4)	1.1270(4)	0.7815(3)	0.0381(15)
H79	1.239	1.1353	0.8576	0.046
C80	1.0080(4)	1.7363(4)	1.2042(3)	0.0439(14)
H80A	1.0894	1.7938	1.233	0.066
H80B	0.9582	1.7708	1.2528	0.066
H80C	0.9661	1.7225	1.1257	0.066
C81	1.1736(4)	1.2224(5)	0.7664(3)	0.0394(15)
H81	1.1767	1.2955	0.829	0.047
C82	0.6894(5)	0.5121(3)	0.2077(4)	0.0390(15)
H82A	0.6998	0.5171	0.2845	0.059
H82B	0.7647	0.4991	0.1878	0.059
H82C	0.619	0.4435	0.1523	0.059
F3	0.5241(7)	0.2983(5)	0.4930(6)	0.323(3)
C85	1.1237(5)	1.4194(4)	0.7068(3)	0.0550(16)
H85A	1.0737	1.4244	0.7576	0.083
H85B	1.1092	1.4768	0.6727	0.083
H85C	1.2116	1.4406	0.7507	0.083
C86	0.5769(5)	0.8214(5)	0.6955(5)	0.0590(19)
H86A	0.4893	0.7771	0.6635	0.089
H86B	0.6258	0.7743	0.7255	0.089
H86C	0.6051	0.8325	0.6355	0.089
F7	1.0225(3)	1.7956(3)	0.8279(4)	0.1259(14)
F4	0.4032(4)	0.3742(5)	0.4070(3)	0.129(2)
F5	0.5974(3)	0.4219(4)	0.4364(5)	0.216(2)
F6	1.2064(6)	1.7934(5)	0.7897(3)	0.256(2)
C91	0.7804(5)	1.2631(4)	0.6691(4)	0.0424(15)
H91A	0.7494	1.2463	0.7254	0.064
H91B	0.7232	1.2987	0.6311	0.064
H91C	0.8622	1.321	0.7078	0.064
C93	0.8186(5)	1.6008(5)	0.8793(4)	0.0577(19)

Crystal Structure Data

H93A	0.8906	1.6102	0.8534	0.087
H93B	0.8218	1.6789	0.9407	0.087
H93C	0.7426	1.5764	0.8153	0.087
F9	0.5471(4)	0.5717(3)	0.5424(3)	0.1031(16)
F8	1.1641(8)	1.6854(4)	0.8707(5)	0.208(3)
F10	0.6174(6)	0.4754(6)	0.6235(4)	0.263(3)
F11	0.4437(6)	0.4298(6)	0.5951(5)	0.222(3)
N110	0.8969(3)	1.1777(3)	0.8906(2)	0.0233(9)
P1	1.16725(12)	1.81531(12)	0.89448(11)	0.0444(4)
F12	1.2963(3)	1.8265(5)	0.9568(6)	0.188(3)

Table 2-3: Anisotropic displacement parameters ($\text{\AA}^2 \times 10^4$) for **1**. The anisotropic displacement factor exponent takes the form: $\{-2 \pi^2 [h^2 a^{*2} U_{11} + \dots + 2 hka^*b^*U_{12}]\}$

Atom	U_{11}	U_{22}	U_{33}	U_{23}	U_{13}	U_{12}
Cu1	0.02740(18)	0.0286(2)	0.01922(14)	0.01127(14)	0.00861(13)	0.00434(15)
Cu2	0.0276(2)	0.0273(2)	0.01861(16)	0.00998(16)	0.00805(15)	0.00403(17)
P3	0.0682(8)	0.0335(6)	0.0407(5)	0.0220(5)	-0.0014(5)	0.0044(5)
N2	0.0333(12)	0.0198(12)	0.0182(9)	0.0150(9)	0.0120(9)	0.0120(10)
N3	0.0238(11)	0.0179(12)	0.0152(9)	0.0084(9)	0.0096(8)	0.0044(10)
N4	0.0190(12)	0.0136(13)	0.0227(12)	0.0049(11)	0.0057(10)	0.0087(10)
N5	0.0143(12)	0.0178(14)	0.0221(13)	0.0019(11)	0.0069(10)	0.0066(10)
O6	0.0396(12)	0.0333(13)	0.0549(13)	0.0277(11)	0.0257(10)	0.0175(10)
O7	0.0296(12)	0.0405(15)	0.0492(13)	0.0272(12)	0.0258(10)	0.0237(10)
O8	0.0380(12)	0.0223(12)	0.0346(11)	0.0088(10)	0.0147(9)	0.0120(10)
C9	0.0167(13)	0.0114(13)	0.0237(13)	0.0046(12)	0.0026(11)	-0.0051(11)
O10	0.0509(16)	0.0219(13)	0.0382(13)	0.0161(11)	0.0165(12)	0.0160(12)
O11	0.0270(11)	0.0308(13)	0.0214(10)	0.0078(9)	0.0028(9)	0.0025(10)
C13	0.0281(14)	0.0130(13)	0.0143(10)	0.0118(10)	0.0039(10)	0.0060(11)
O14	0.0461(15)	0.0290(13)	0.0415(13)	0.0227(11)	0.0165(11)	0.0204(11)
C15	0.0207(12)	0.0036(12)	0.0270(13)	0.0047(11)	0.0115(10)	-0.0006(10)
N16	0.0209(12)	0.0234(14)	0.0269(12)	0.0117(11)	0.0041(10)	0.0020(11)
C17	0.0222(14)	0.0177(15)	0.0269(14)	0.0063(13)	0.0058(12)	0.0072(12)
C18	0.0130(13)	0.038(2)	0.0228(14)	0.0030(14)	0.0040(11)	-0.0096(13)
C19	0.0288(15)	0.0296(17)	0.0096(11)	0.0128(12)	0.0081(11)	0.0195(13)
C20	0.0295(14)	0.0297(16)	0.0141(11)	0.0104(11)	0.0076(10)	0.0179(12)
C21	0.0376(18)	0.0247(17)	0.0104(11)	0.0132(12)	0.0113(11)	0.0167(14)
O22	0.0505(14)	0.0260(13)	0.0323(12)	0.0038(11)	0.0110(11)	0.0122(11)
O23	0.0489(17)	0.0296(15)	0.0251(13)	0.0071(12)	-0.0015(12)	0.0115(13)
N24	0.0394(17)	0.0324(19)	0.0200(13)	0.0060(14)	0.0112(12)	0.0075(15)
C25	0.0171(12)	0.0309(16)	0.0166(10)	0.0133(11)	0.0114(9)	0.0064(11)
C26	0.0234(16)	0.0259(18)	0.0172(13)	0.0100(13)	0.0049(12)	0.0067(14)
C27	0.0166(13)	0.0368(18)	0.0165(12)	0.0083(13)	0.0003(10)	0.0149(12)
C28	0.0193(15)	0.0206(18)	0.0324(18)	0.0039(15)	0.0085(13)	0.0091(13)
C29	0.0320(17)	0.0211(16)	0.0266(14)	0.0136(13)	0.0029(13)	0.0037(13)
N30	0.0377(17)	0.083(2)	0.0431(14)	0.0469(14)	0.0073(13)	0.0088(16)
C31	0.0359(19)	0.0211(17)	0.046(2)	0.0161(16)	-0.0009(16)	0.0062(15)
C32	0.056(3)	0.036(2)	0.0205(14)	0.0213(14)	0.0110(15)	0.0040(18)
C33	0.0200(13)	0.0118(14)	0.0219(13)	0.0019(12)	0.0015(11)	0.0037(11)
C34	0.0160(13)	0.0300(18)	0.0152(12)	0.0032(13)	0.0011(11)	-0.0010(13)
C35	0.0240(15)	0.0214(16)	0.0269(14)	0.0104(13)	0.0048(12)	-0.0025(13)
C36	0.0240(17)	0.0310(19)	0.0280(15)	0.0202(14)	0.0055(13)	0.0050(14)
C37	0.0213(16)	0.0323(19)	0.0091(12)	0.0053(13)	-0.0068(12)	0.0111(14)
C38	0.0199(15)	0.0287(17)	0.0314(14)	0.0182(13)	0.0011(12)	-0.0018(13)
C39	0.0193(15)	0.0088(14)	0.0355(17)	0.0056(14)	0.0087(13)	-0.0007(12)
C40	0.0250(13)	0.0187(15)	0.0196(11)	0.0144(11)	0.0187(10)	0.0146(11)
C41	0.0234(13)	0.0273(16)	0.0475(16)	0.0233(14)	0.0184(12)	0.0129(12)
C42	0.0258(19)	0.0173(18)	0.035(2)	0.0040(17)	-0.0102(16)	-0.0052(15)

Crystal Structure Data

C43	0.0169(14)	0.0366(19)	0.0126(11)	0.0099(12)	-0.0006(10)	-0.0019(13)
C44	0.0421(19)	0.0263(18)	0.0089(11)	0.0092(12)	0.0154(11)	0.0095(15)
C45	0.0173(16)	0.032(2)	0.0245(16)	0.0078(15)	0.0043(13)	0.0032(14)
C46	0.033(2)	0.030(2)	0.0237(17)	0.0063(17)	0.0041(15)	0.0031(17)
C47	0.0345(19)	0.0048(14)	0.0260(17)	0.0001(14)	0.0035(15)	0.0016(13)
C48	0.0190(13)	0.0201(14)	0.0183(11)	0.0124(11)	0.0039(10)	0.0061(11)
C49	0.0240(13)	0.0295(16)	0.0095(11)	0.0056(11)	0.0063(10)	0.0123(12)
C50	0.055(2)	0.0243(19)	0.0158(13)	0.0135(13)	0.0091(14)	0.0087(17)
C51	0.0254(14)	0.0315(18)	0.0326(15)	0.0151(14)	0.0123(12)	0.0121(13)
C52	0.065(2)	0.041(2)	0.0242(14)	0.0225(15)	0.0263(14)	0.0296(18)
C53	0.0205(13)	0.0114(13)	0.0321(14)	0.0073(12)	0.0124(11)	0.0073(11)
C54	0.0307(16)	0.0259(17)	0.0241(13)	0.0195(12)	0.0172(12)	0.0146(13)
C55	0.0251(15)	0.0378(19)	0.0139(11)	0.0100(12)	0.0045(11)	0.0009(14)
C56	0.0266(19)	0.0215(19)	0.042(2)	0.0080(17)	-0.0006(16)	0.0025(15)
C57	0.0347(14)	0.0332(18)	0.0422(14)	0.0233(13)	0.0286(12)	0.0159(13)
C58	0.0193(16)	0.0195(17)	0.057(2)	0.0201(16)	0.0112(15)	-0.0044(14)
C59	0.0279(18)	0.041(2)	0.0191(14)	0.0122(15)	0.0058(13)	-0.0066(17)
C60	0.0312(16)	0.044(2)	0.0445(17)	0.0256(16)	0.0158(14)	0.0185(15)
C61	0.098(3)	0.0302(19)	0.058(2)	0.0362(17)	0.028(2)	0.0307(19)
C62	0.0211(16)	0.0164(16)	0.0331(17)	0.0123(14)	0.0084(13)	0.0044(13)
C63	0.0448(19)	0.055(2)	0.0335(18)	0.0188(18)	0.0226(15)	0.0373(17)
C64	0.0338(18)	0.067(2)	0.0306(15)	0.0338(15)	0.0041(13)	0.0194(17)
C65	0.071(2)	0.048(3)	0.036(2)	-0.006(2)	0.0243(18)	0.027(2)
C66	0.0270(16)	0.0295(18)	0.0300(15)	0.0143(14)	-0.0015(13)	0.0013(14)
C67	0.0406(19)	0.0180(17)	0.0271(16)	0.0052(14)	0.0199(14)	0.0052(15)
F1	0.166(2)	0.0684(15)	0.0510(10)	0.0500(10)	0.0527(13)	0.0683(15)
C70	0.0309(17)	0.0338(19)	0.0417(19)	0.0159(17)	0.0003(15)	0.0141(15)
C71	0.040(2)	0.0241(19)	0.0107(12)	0.0080(13)	0.0024(13)	-0.0089(16)
C72	0.049(3)	0.059(3)	0.0313(16)	0.0347(17)	0.0074(16)	0.007(2)
C73	0.044(2)	0.063(3)	0.0281(16)	0.0227(18)	-0.0022(16)	0.004(2)
C74	0.046(2)	0.034(2)	0.0498(18)	0.0333(16)	0.0218(16)	0.0134(17)
C76	0.040(2)	0.035(2)	0.0244(16)	0.0082(15)	-0.0035(15)	0.0021(17)
F2	0.0818(17)	0.0184(9)	0.0678(14)	0.0297(10)	-0.0135(13)	-0.0223(11)
C79	0.043(2)	0.040(2)	0.0179(16)	0.0115(16)	-0.0024(16)	-0.008(2)
C80	0.065(2)	0.044(2)	0.0383(17)	0.0232(16)	0.0238(16)	0.0311(17)
C81	0.037(2)	0.052(3)	0.0159(15)	0.0051(17)	0.0074(14)	0.003(2)
C82	0.060(3)	0.0078(16)	0.043(2)	0.0090(17)	0.008(2)	0.0089(17)
F3	0.652(6)	0.236(3)	0.475(4)	0.308(3)	0.473(4)	0.335(3)
C85	0.098(3)	0.030(2)	0.0236(17)	0.0043(17)	0.000(2)	0.032(2)
C86	0.049(3)	0.035(3)	0.050(3)	-0.015(2)	0.008(2)	-0.007(2)
F7	0.075(2)	0.135(2)	0.184(2)	0.1360(18)	-0.0293(18)	-0.0003(17)
F4	0.117(3)	0.161(4)	0.0601(19)	0.035(2)	-0.020(2)	0.007(3)
F5	0.1853(18)	0.098(3)	0.471(4)	0.121(3)	0.2746(19)	0.064(2)
F6	0.553(5)	0.273(4)	0.2221(17)	0.2275(18)	0.304(2)	0.280(4)
C91	0.061(3)	0.0219(19)	0.050(2)	0.0164(18)	0.024(2)	0.0141(18)
C93	0.058(3)	0.039(3)	0.049(3)	0.020(2)	-0.017(2)	-0.012(2)
F9	0.235(4)	0.0283(13)	0.0511(14)	0.0159(12)	0.0489(19)	0.0484(18)
F8	0.482(9)	0.075(3)	0.150(3)	0.078(2)	0.169(4)	0.114(4)
F10	0.271(5)	0.133(4)	0.165(3)	0.023(3)	-0.192(3)	-0.038(4)
F11	0.437(5)	0.151(4)	0.230(3)	0.113(3)	0.274(3)	0.149(4)
N110	0.0358(13)	0.0158(13)	0.0210(12)	0.0004(11)	0.0213(10)	0.0152(11)
P1	0.0518(7)	0.0414(7)	0.0454(6)	0.0240(5)	0.0155(5)	0.0118(5)
F12	0.0231(15)	0.236(4)	0.348(6)	0.202(4)	0.003(2)	0.0368(19)

7. 3 Crystal Structure Data of 3 (In Cooperation with Marc Schlosser, Prof. Hans-Jorg Deiseroth, University of Siegen, Germany).

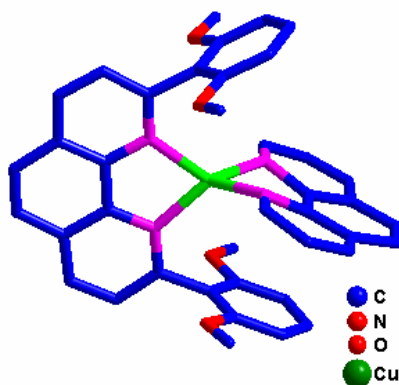


Figure 3-1. Stick representation of 3.

Table 3-1: Crystal data and structure refinement for 3.

Substance	3
Sum formula	C ₄₀ H ₃₀ CuF ₆ N ₄ O ₄ P
Formula weight /g·mol ⁻¹	839.19
Temperature /K	153(2)
Wavelength	0.71073 Å
Crystal system, space group	Triclinic, <i>P</i> -1
Unit cell dimensions	a = 14.046 (3) Å b = 21.352 (4) Å c = 14.052 (3) Å B = 118.57 (3) °
Volume /Å ³	3701.2(13)
Z, Calculated density /Mg·m ⁻³	4, 1.506
Absorption coefficient /mm ⁻¹	0.712
F(000)	1712
Reflections collected / unique / R _{int}	8022 / 4320 / 0.0761
Refinement method	Full-matrix least-squares on <i>F</i> ²
Data / restraints / parameters	8022 / 0 / 602
Goodness-of-fit on <i>F</i> ²	0.921
Final <i>R</i> indices [<i>I</i> > 2σ(<i>I</i>)]	<i>R</i> 1 = 0.0707, <i>wR</i> 2 = 0.1907
<i>R</i> indices (all data)	<i>R</i> 1 = 0.1269, <i>wR</i> 2 = 0.2168

Crystal Structure Data

Table 3–2: Atomic coordinates ($\times 10^5$) and equivalent isotropic displacement parameters ($\text{\AA}^2 \times 10^4$) for **1**. $U(\text{eq})$ is defined as one third of the trace of the orthogonalized U_{ij} tensor.

Atom	x	y	z	U_{eq}
Cu1	0.70264(5)	0.00016(3)	0.29737(5)	0.03227(19)
N1	0.7914(3)	-0.05976(17)	0.2595(3)	0.0261(8)
N2	0.7405(3)	0.06016(17)	0.2084(3)	0.0262(8)
N3	0.7292(4)	0.0218(3)	0.4463(4)	0.0710(18)
N4	0.5548(4)	-0.0226(4)	0.2720(4)	0.0723(19)
O1	0.6163(3)	-0.17816(17)	0.1988(3)	0.0438(9)
O2	0.8010(3)	0.17815(17)	0.3845(3)	0.0444(9)
O3	0.9298(3)	-0.1120(2)	0.5012(3)	0.0513(10)
O4	0.4982(3)	0.1123(2)	0.0705(3)	0.0514(10)
C1	0.7159(4)	0.1205(2)	0.1874(3)	0.0305(10)
C2	0.7538(4)	0.1562(2)	0.1286(4)	0.0394(12)
H2	0.7358	0.1993	0.1154	0.047
C3	0.8167(5)	0.1287(3)	0.0904(4)	0.0460(14)
H3	0.8422	0.1528	0.0503	0.055
C4	0.8436(5)	0.0652(3)	0.1101(4)	0.0427(13)
C5	0.9071(6)	0.0315(3)	0.0726(5)	0.0611(19)
H5	0.9367	0.053	0.0336	0.073
C6	0.9256(5)	-0.0303(3)	0.0914(6)	0.0605(19)
H6	0.9642	-0.0519	0.0613	0.073
C7	0.8890(4)	-0.0644(3)	0.1556(4)	0.0428(13)
C8	0.9089(4)	-0.1278(3)	0.1818(5)	0.0462(14)
H8	0.9483	-0.1517	0.1553	0.055
C9	0.8716(4)	-0.1558(3)	0.2459(4)	0.0390(12)
H9	0.8853	-0.1989	0.2641	0.047
C10	0.8133(4)	-0.1201(2)	0.2838(4)	0.0309(10)
C11	0.8031(4)	0.0329(2)	0.1705(4)	0.0318(11)
C12	0.8292(4)	-0.0320(2)	0.1964(4)	0.0313(11)
C13	0.6455(4)	0.1479(2)	0.2288(4)	0.0313(10)
C14	0.6896(4)	0.1775(2)	0.3301(4)	0.0361(11)
C15	0.6225(5)	0.2015(2)	0.3688(5)	0.0453(13)
H15	0.6525	0.2211	0.4378	0.054
C16	0.5119(5)	0.1962(3)	0.3053(5)	0.0495(14)
H16	0.4659	0.213	0.331	0.059
C17	0.4655(5)	0.1669(3)	0.2048(5)	0.0501(14)
H17	0.389	0.1636	0.1624	0.06
C18	0.5331(4)	0.1427(2)	0.1677(4)	0.0411(12)
C19	0.8514(6)	0.2116(4)	0.4853(5)	0.072(2)
H19A	0.8306	0.2558	0.4724	0.109
H19B	0.9303	0.2079	0.5177	0.109
H19C	0.8276	0.1938	0.5348	0.109
C20	0.3853(5)	0.0967(3)	0.0101(6)	0.0652(18)
H20A	0.3641	0.072	0.0558	0.098
H20B	0.3723	0.0722	-0.0539	0.098
H20C	0.3422	0.1353	-0.0127	0.098
C21	0.7718(4)	-0.1475(2)	0.3546(4)	0.0309(10)
C22	0.6704(4)	-0.1773(2)	0.3107(4)	0.0371(11)
C23	0.6322(5)	-0.2015(2)	0.3770(5)	0.0467(13)
H23	0.5636	-0.2216	0.3469	0.056
C24	0.6954(5)	-0.1959(3)	0.4881(5)	0.0486(14)
H24	0.6694	-0.2125	0.534	0.058
C25	0.7958(5)	-0.1667(3)	0.5343(4)	0.0491(14)
H25	0.8382	-0.1635	0.6108	0.059
C26	0.8333(4)	-0.1424(2)	0.4669(4)	0.0402(12)
C27	0.5162(6)	-0.2120(4)	0.1487(6)	0.074(2)
H27A	0.5296	-0.256	0.1711	0.11
H27B	0.4846	-0.2093	0.0697	0.11
H27C	0.4658	-0.1939	0.1709	0.11
C28	0.9906(6)	-0.0960(3)	0.6144(4)	0.0645(19)

Crystal Structure Data

H28A	0.9446	-0.0718	0.6357	0.097
H28B	1.054	-0.071	0.6268	0.097
H28C	1.0145	-0.1345	0.6577	0.097
C29	0.4696(5)	-0.0468(4)	0.1862(5)	0.075(3)
C30	0.3891(10)	-0.0897(6)	0.1968(10)	0.055(5)
C31	0.3971(9)	-0.1019(5)	0.2959(10)	0.055(4)
C32	0.4893(8)	-0.0804(4)	0.3927(9)	0.043(4)
C33	0.5003(6)	-0.0908(3)	0.5001(6)	0.053(2)
C34	0.5890(6)	-0.0676(3)	0.5885(6)	0.056(3)
C35	0.6735(8)	-0.0327(5)	0.5759(8)	0.048(4)
C36	0.7629(9)	-0.0061(6)	0.6629(8)	0.054(4)
C37	0.8348(10)	0.0282(6)	0.6457(9)	0.055(5)
C38	0.8147(6)	0.0459(4)	0.5311(5)	0.078(4)
C39	0.5685(8)	-0.0472(4)	0.3780(8)	0.034(3)
C40	0.6601(8)	-0.0230(4)	0.4700(7)	0.036(3)
C41	0.3553(10)	-0.0285(7)	0.1650(11)	0.057(5)
C42	0.6227(9)	0.0475(4)	0.4326(8)	0.037(4)
C43	0.7049(11)	0.1019(5)	0.6033(9)	0.051(5)
C44	0.8028(11)	0.0896(6)	0.6107(9)	0.049(5)
C45	0.3919(10)	-0.0807(4)	0.4886(8)	0.043(4)
C46	0.4697(8)	-0.0232(5)	0.6602(8)	0.037(4)
C47	0.5755(9)	-0.0333(5)	0.6730(9)	0.049(4)
C48	0.6627(9)	-0.0060(6)	0.7631(9)	0.053(5)
P2	0.13225(12)	0.18791(8)	0.13265(11)	0.0469(4)
F1	0.0623(4)	0.1834(3)	0.1922(3)	0.0946(16)
F2	0.1918(3)	0.1831(3)	0.0631(3)	0.0933(16)
F3	0.0220(4)	0.1703(3)	0.0224(4)	0.1085(19)
F4	0.0996(8)	0.2542(2)	0.0998(7)	0.170(4)
F5	0.1464(6)	0.1123(3)	0.1471(6)	0.140(2)
F6	0.2398(3)	0.1889(3)	0.2406(3)	0.114(2)

Table 3-3: Anisotropic displacement parameters ($\text{\AA}^2 \times 10^4$) for **1**. The anisotropic displacement factor exponent takes the form: $\{-2 \pi^2 [h^2 a^{*2} U_{11} + \dots + 2 hka^*b^*U_{12}]\}$

Atom	U_{11}	U_{22}	U_{33}	U_{23}	U_{13}	U_{12}
Cu1	0.0338(3)	0.0403(3)	0.0326(3)	-0.0003(3)	0.0238(2)	-0.0002(3)
N1	0.0193(18)	0.037(2)	0.0209(17)	-0.0081(15)	0.0086(15)	-0.0035(15)
N2	0.0213(19)	0.037(2)	0.0187(16)	-0.0055(15)	0.0083(15)	-0.0089(16)
N3	0.037(3)	0.153(6)	0.031(2)	-0.032(3)	0.023(2)	-0.031(3)
N4	0.034(3)	0.155(6)	0.036(2)	-0.031(3)	0.024(2)	-0.032(3)
O1	0.036(2)	0.055(2)	0.0329(18)	-0.0040(16)	0.0098(16)	-0.0160(16)
O2	0.035(2)	0.054(2)	0.0341(18)	-0.0184(16)	0.0087(16)	-0.0049(16)
O3	0.036(2)	0.081(3)	0.0258(17)	-0.0154(17)	0.0060(16)	-0.0002(19)
O4	0.0256(19)	0.080(3)	0.036(2)	-0.0008(18)	0.0038(16)	-0.0162(18)
C1	0.024(2)	0.042(3)	0.021(2)	-0.0058(18)	0.0071(18)	-0.0129(19)
C2	0.044(3)	0.042(3)	0.028(2)	-0.003(2)	0.013(2)	-0.016(2)
C3	0.056(4)	0.056(3)	0.033(3)	-0.011(2)	0.027(3)	-0.031(3)
C4	0.048(3)	0.057(3)	0.035(3)	-0.019(2)	0.030(2)	-0.030(3)
C5	0.082(5)	0.070(5)	0.068(4)	-0.032(3)	0.065(4)	-0.038(4)
C6	0.062(4)	0.076(5)	0.076(4)	-0.039(4)	0.059(4)	-0.031(3)
C7	0.037(3)	0.057(3)	0.046(3)	-0.029(3)	0.029(3)	-0.021(2)
C8	0.033(3)	0.059(3)	0.052(3)	-0.031(3)	0.025(3)	-0.011(2)
C9	0.030(3)	0.046(3)	0.041(3)	-0.018(2)	0.017(2)	-0.006(2)
C10	0.023(2)	0.041(3)	0.025(2)	-0.0134(19)	0.0082(19)	-0.0058(19)
C11	0.030(3)	0.046(3)	0.023(2)	-0.0139(19)	0.0147(19)	-0.018(2)
C12	0.023(2)	0.046(3)	0.031(2)	-0.018(2)	0.0173(19)	-0.013(2)
C13	0.030(3)	0.032(2)	0.030(2)	0.0042(18)	0.013(2)	-0.0022(19)
C14	0.033(3)	0.033(3)	0.040(3)	0.001(2)	0.017(2)	0.002(2)
C15	0.062(4)	0.035(3)	0.048(3)	0.002(2)	0.034(3)	0.004(2)

Crystal Structure Data

C16	0.049(4)	0.043(3)	0.071(4)	0.019(3)	0.040(3)	0.014(3)
C17	0.035(3)	0.057(3)	0.059(4)	0.020(3)	0.023(3)	0.005(2)
C18	0.036(3)	0.047(3)	0.036(3)	0.016(2)	0.014(2)	-0.002(2)
C19	0.055(4)	0.093(5)	0.053(4)	-0.042(4)	0.013(3)	-0.011(4)
C20	0.029(3)	0.081(4)	0.062(4)	0.009(3)	0.003(3)	-0.016(3)
C21	0.028(2)	0.033(2)	0.030(2)	-0.0024(18)	0.013(2)	0.0029(19)
C22	0.043(3)	0.032(2)	0.033(3)	0.0003(19)	0.016(2)	0.001(2)
C23	0.048(3)	0.039(3)	0.062(4)	0.006(2)	0.034(3)	0.001(2)
C24	0.071(4)	0.040(3)	0.050(3)	0.011(2)	0.041(3)	0.018(3)
C25	0.061(4)	0.054(3)	0.034(3)	0.012(2)	0.025(3)	0.021(3)
C26	0.037(3)	0.047(3)	0.031(3)	0.000(2)	0.012(2)	0.015(2)
C27	0.053(4)	0.091(5)	0.058(4)	-0.012(4)	0.011(3)	-0.047(4)
C28	0.057(4)	0.083(4)	0.026(3)	-0.016(3)	-0.002(3)	0.009(3)
C29	0.036(4)	0.141(8)	0.046(4)	-0.022(4)	0.019(3)	-0.028(4)
C30	0.045(8)	0.057(8)	0.063(9)	-0.007(6)	0.026(6)	-0.009(5)
C31	0.043(7)	0.044(6)	0.081(9)	0.001(5)	0.033(6)	-0.003(4)
C32	0.045(7)	0.034(5)	0.065(7)	-0.003(4)	0.037(6)	0.002(4)
C33	0.067(5)	0.043(3)	0.067(4)	0.016(3)	0.046(4)	0.016(3)
C34	0.070(5)	0.054(4)	0.067(5)	0.020(3)	0.050(4)	0.019(3)
C35	0.047(7)	0.060(7)	0.044(6)	0.005(4)	0.028(5)	0.017(5)
C36	0.053(7)	0.077(9)	0.030(5)	0.006(5)	0.019(5)	0.026(6)
C37	0.046(8)	0.076(9)	0.043(7)	-0.012(6)	0.023(6)	0.004(6)
C38	0.047(4)	0.149(9)	0.037(4)	-0.029(4)	0.020(3)	-0.022(4)
C39	0.040(6)	0.028(5)	0.044(6)	-0.002(4)	0.028(5)	0.005(4)
C40	0.042(6)	0.038(5)	0.034(5)	0.009(4)	0.023(4)	0.016(4)
C41	0.033(7)	0.080(10)	0.052(8)	0.008(6)	0.016(6)	-0.012(6)
C42	0.057(7)	0.028(5)	0.041(6)	0.006(4)	0.034(5)	0.001(4)
C43	0.076(10)	0.042(7)	0.042(7)	-0.012(4)	0.033(6)	-0.002(5)
C44	0.057(9)	0.052(8)	0.039(7)	-0.012(5)	0.023(6)	-0.013(6)
C45	0.070(9)	0.032(6)	0.046(7)	0.003(4)	0.042(6)	-0.001(5)
C46	0.032(6)	0.040(6)	0.042(6)	0.013(4)	0.021(5)	0.005(4)
C47	0.051(7)	0.059(8)	0.048(7)	0.018(5)	0.032(6)	0.005(5)
C48	0.043(7)	0.072(9)	0.047(7)	0.021(6)	0.022(5)	0.007(6)
P2	0.0370(8)	0.0719(10)	0.0365(7)	0.0139(7)	0.0215(6)	0.0137(7)
F1	0.062(3)	0.178(5)	0.056(2)	0.034(3)	0.039(2)	0.026(3)
F2	0.058(3)	0.175(5)	0.059(2)	0.021(3)	0.038(2)	0.032(3)
F3	0.063(3)	0.204(6)	0.057(3)	-0.008(3)	0.027(2)	-0.008(3)
F4	0.291(10)	0.061(3)	0.274(9)	0.053(4)	0.229(9)	0.054(4)
F5	0.177(7)	0.075(3)	0.171(6)	0.021(4)	0.084(5)	0.020(4)
F6	0.044(2)	0.242(6)	0.045(2)	-0.009(3)	0.0131(19)	-0.010(3)

7.4 Crystal Structure Data of 4 (In Cooperation with Dr. Jan W. Bats, Johann Wolfgang Goethe-University, Frankfurt an Main, Germany).³

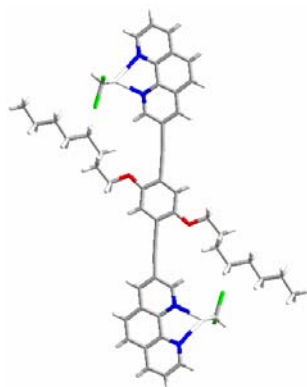


Figure 4-1. Stick representation of 4.

Table 4-1: Crystal data and structure refinement for 4.

Substance	4
Sum formula	C ₅₀ H ₅₀ N ₄ O ₂ *2CH ₂ Cl ₂
Formula weight /g·mol ⁻¹	908.79
Temperature /K	155(2)
Wavelength	0.71073 Å
Crystal system, space group	Triclinic, <i>P</i> -1
Unit cell dimensions	a = 10.8660 (16) Å b = 10.987 (2) Å c = 12.019 (2) Å β = 105.003 (12) °
Volume /Å ³	1173.4 (4)
Z, Calculated density /Mg·m ⁻³	1, 1.286
Absorption coefficient /mm ⁻¹	0.297
F(000)	478
Crystal size (mm)	0.60 x 0.22 x 0.18
Reflections collected / unique / R _{int}	20884 / 7645 / 0.0428
Refinement method	Full-matrix least-squares on F ²
Data / restraints / parameters	7645 / 0 / 280
Goodness-of-fit on F ²	1.028
Final R indices [I > 2σ(I)]	R1 = 0.0458, wR2 = 0.1167
R indices (all data)	R1 = 0.0659, wR2 = 0.1300
Largest diff. peak and hole	0.587 and -0.337 e/Å ³

Crystal Structure Data

Table 4-2: Atomic coordinates ($\times 10^5$) and equivalent isotropic displacement parameters ($\text{\AA}^2 \times 10^4$) for **4**. $U(\text{eq})$ is defined as one third of the trace of the orthogonalized U_{ij} tensor.

Atom	x	y	z	U_{eq}
O(1)	57724(12)	44608(10)	71416(8)	293(2)
N(1)	90617(12)	94391(11)	117851(10)	239(2)
C(2)	95751(13)	108776(12)	120981(11)	209(2)
C(16)	53726(14)	46645(13)	60573(11)	215(2)
N(2)	105857(13)	111691(12)	142390(10)	278(2)
C(13)	72000(13)	81124(13)	83890(11)	228(2)
C(12)	80135(13)	91247(13)	96350(11)	212(2)
C(14)	65264(13)	71969(13)	73732(11)	214(2)
C(17)	46431(14)	35909(12)	48891(11)	216(2)
C(11)	85391(13)	105866(13)	99561(11)	229(2)
C(1)	83194(14)	86141(13)	106019(11)	238(2)
C(15)	57394(13)	60893(12)	61718(11)	199(2)
C(8)	106683(15)	138775(14)	128095(13)	300(3)
C(3)	103799(13)	117904(13)	134001(11)	231(2)
C(10)	93431(13)	114981(13)	112063(11)	219(2)
C(23)	65336(14)	25304(14)	120925(11)	250(2)
C(7)	108977(14)	132848(13)	137388(12)	263(3)
C(22)	59405(15)	23062(14)	107261(12)	262(3)
C(9)	99264(15)	130287(14)	115923(13)	281(3)
C(6)	116294(16)	141355(15)	150173(13)	330(3)
C(24)	62432(17)	11444(16)	123161(13)	322(3)
C(4)	112894(16)	120161(16)	154304(13)	332(3)
C(18)	55694(19)	30698(15)	70817(13)	332(3)
C(25)	68770(20)	13820(20)	136824(15)	422(4)
C(20)	53480(20)	34526(19)	91530(15)	384(3)
C(5)	118189(17)	135022(17)	158577(13)	365(3)
C(21)	60260(20)	36526(17)	105182(14)	378(3)
C(19)	61915(18)	31648(16)	84016(13)	324(3)
Cl(1)	130989(5)	95397(4)	134863(4)	435(1)
Cl(2)	103402(5)	68707(5)	119358(5)	500(1)
C(26)	112438(19)	84679(19)	132552(15)	398(3)

Table 4-3. Anisotropic displacement parameters ($\text{\AA}^2 \times 10^4$) for **4**. The anisotropic displacement factor exponent takes the form: $\{-2 \pi^2 [h^2 a^{*2} U_{11} + \dots + 2 hka^*b^*U_{12}]\}$.

Atom	U_{11}	U_{22}	U_{33}	U_{23}	U_{13}	U_{12}
O(1)	451(6)	213(4)	171(4)	89(3)	67(4)	152(4)
N(1)	270(5)	196(5)	186(5)	46(4)	56(4)	92(4)
C(2)	204(5)	188(5)	184(5)	31(4)	67(4)	79(4)
C(16)	254(6)	200(5)	169(5)	75(4)	63(4)	102(4)
N(2)	298(5)	271(5)	178(5)	43(4)	72(4)	97(4)
C(13)	229(5)	228(5)	202(5)	70(4)	69(5)	106(5)
C(12)	202(5)	221(5)	163(5)	34(4)	54(4)	91(4)
C(14)	223(5)	196(5)	205(5)	75(4)	73(4)	95(4)
C(17)	264(6)	171(5)	180(5)	65(4)	71(4)	88(4)
C(11)	239(5)	227(5)	202(5)	68(4)	74(5)	113(5)
C(1)	266(6)	187(5)	189(5)	34(4)	54(5)	89(5)
C(15)	213(5)	182(5)	164(5)	52(4)	56(4)	82(4)
C(8)	317(7)	180(5)	325(7)	41(5)	113(6)	89(5)
C(3)	220(5)	211(5)	190(5)	24(4)	80(4)	72(4)
C(10)	218(5)	196(5)	214(5)	51(4)	84(5)	90(4)
C(23)	257(6)	292(6)	193(5)	95(5)	87(5)	127(5)

Crystal Structure Data

C(7)	240(6)	213(5)	241(6)	10(5)	93(5)	69(5)
C(22)	325(6)	276(6)	204(6)	97(5)	100(5)	163(5)
C(9)	310(6)	214(6)	293(6)	86(5)	104(5)	120(5)
C(6)	332(7)	239(6)	260(6)	-24(5)	108(6)	66(5)
C(24)	392(7)	340(7)	252(6)	149(6)	120(6)	183(6)
C(4)	342(7)	345(7)	185(6)	45(5)	86(5)	101(6)
C(18)	543(9)	267(6)	245(6)	132(5)	147(6)	238(6)
C(25)	490(9)	487(9)	314(8)	236(7)	146(7)	228(8)
C(20)	518(9)	507(9)	355(8)	259(7)	232(7)	365(8)
C(5)	354(7)	335(7)	197(6)	-34(5)	89(6)	66(6)
C(21)	626(10)	370(7)	274(7)	159(6)	218(7)	320(8)
C(19)	458(8)	372(7)	267(6)	179(6)	165(6)	271(7)
Cl(1)	521(2)	336(2)	479(2)	165(2)	245(2)	204(2)
Cl(2)	525(3)	370(2)	569(3)	182(2)	177(2)	210(2)
C(26)	464(9)	529(9)	315(7)	190(7)	160(7)	324(8)

7.5 Crystal Structure Data of 5 (In Cooperation with Prof. Dieter Fenske, University of Karlsruhe, Germany).

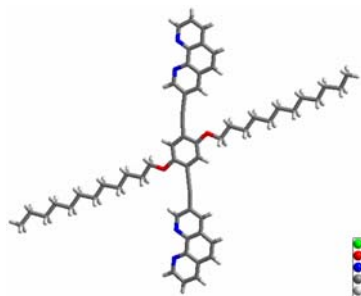


Figure 5-1. Stick representation of 5.

Table 5-1: Crystal data and structure refinement for **5**.

Substance	5
Sum formula	$C_{60}H_{66}C_{14}N_4O_2$
Formula weight /g·mol ⁻¹	1016.97
Temperature /K	193(2)
Wavelength	0.71073 Å
Crystal system, space group	Triclinic, <i>P</i> -1
Unit cell dimensions	a = 11.973 (2) Å b = 13.924 (3) Å c = 18.606 (4) Å $\beta = 82.81 (6)^\circ$
Volume /Å ³	2872 (2)
Z, Calculated density /Mg·m ⁻³	2, 1.176
Absorption coefficient /mm ⁻¹	0.250
F(000)	1076
Crystal size (mm)	0.30 x 0.15 x 0.05
Reflections collected / unique / R _{int}	12600 / 8519 / 0.0377
Refinement method	Full-matrix least-squares on <i>F</i> ²
Data / restraints / parameters	19983 / 0 / 725
Goodness-of-fit on <i>F</i> ²	1.041
Final <i>R</i> indices [<i>I</i> > 2σ(<i>I</i>)]	<i>R</i> 1 = 0.0912, <i>wR</i> 2 = 0.2854
<i>R</i> indices (all data)	<i>R</i> 1 = 0.1138, <i>wR</i> 2 = 0.3082
Largest diff. peak and hole	0.482 and -0.030 e/Å ³

Table 5-2: Atomic coordinates (x 10⁵) and equivalent isotropic displacement parameters (Å² x 10⁴) for **5**. *U*(eq) is defined as one third of the trace of the orthogonalized *U*_{ij} tensor.

Atom	x	y	z	<i>U</i> _{eq}
Cl1C	-0.1606(2)	0.57200(19)	0.12154(15)	0.0539(6)
Cl1B	-0.1382(3)	0.5286(3)	0.2031(3)	0.0953(14)
Cl1A	-0.0646(3)	0.4900(2)	0.26351(15)	0.0696(7)
Cl2C	-0.0011(3)	0.4659(3)	0.07806(19)	0.0705(8)
Cl2B	0.0564(3)	0.4179(2)	0.1345(3)	0.0886(12)
Cl2A	0.1038(3)	0.4053(2)	0.2164(2)	0.0853(10)
Cl3	0.3388(7)	1.1142(5)	0.0098(5)	0.0388(11)
Cl4	0.4373(6)	1.0375(4)	0.1532(4)	0.0357(9)
Cl5	0.2769(4)	1.2371(4)	0.1184(3)	0.0354(7)
Cl3A	0.3672(7)	1.0912(5)	0.0040(5)	0.0407(12)
Cl4A	0.4618(6)	1.0128(4)	0.1498(4)	0.0397(10)
Cl5A	0.3042(4)	1.2168(5)	0.1121(4)	0.0440(10)
O1	0.2082(2)	0.46238(16)	0.48826(12)	0.0507(5)
O2	0.4835(2)	0.60371(18)	0.63007(12)	0.0530(5)
N1	0.1304(2)	0.6552(2)	0.18348(14)	0.0466(6)
N2	0.0260(2)	0.7182(2)	0.05155(16)	0.0540(7)
N3	0.5050(2)	0.2892(2)	0.96499(15)	0.0506(6)
N4	0.5951(3)	0.2330(2)	1.10157(15)	0.0594(7)
C1	0.2782(2)	0.4915(2)	0.52705(16)	0.0412(6)

Crystal Structure Data

C2	0.3245(3)	0.5714(2)	0.48520(16)	0.0419(6)
C3	0.3940(3)	0.6097(2)	0.51887(16)	0.0433(6)
H3B	0.425	0.6643	0.4909	0.052
C4	0.4183(2)	0.5699(2)	0.59174(16)	0.0418(6)
C5	0.3741(3)	0.4885(2)	0.63313(16)	0.0435(6)
C6	0.3042(3)	0.4504(2)	0.59934(17)	0.0447(6)
H6A	0.2742	0.395	0.627	0.054
C7	0.3005(3)	0.6125(2)	0.40884(16)	0.0445(6)
C8	0.2812(3)	0.6470(2)	0.34457(16)	0.0452(6)
C9	0.2453(3)	0.6806(2)	0.27037(16)	0.0430(6)
C10	0.1751(3)	0.6289(2)	0.24882(17)	0.0460(7)
H10A	0.1588	0.5711	0.2836	0.055
C11	0.2720(3)	0.7609(2)	0.21937(16)	0.0454(7)
H11A	0.3216	0.7962	0.2315	0.054
C12	0.2261(3)	0.7918(2)	0.14846(16)	0.0433(6)
C13	0.1531(2)	0.7368(2)	0.13373(15)	0.0392(6)
C14	0.2488(3)	0.8763(3)	0.09318(19)	0.0579(8)
H14A	0.2992	0.9126	0.103	0.069
C15	0.1999(4)	0.9054(3)	0.0271(2)	0.0638(9)
H15A	0.2166	0.9619	-0.009	0.077
C16	0.0995(3)	0.7696(2)	0.06307(16)	0.0425(6)
C17	0.1239(3)	0.8534(2)	0.01032(18)	0.0528(8)
C18	0.0696(4)	0.8835(3)	-0.0571(2)	0.0675(10)
H18A	0.0841	0.9398	-0.0944	0.081
C19	-0.0049(4)	0.8307(3)	-0.0687(2)	0.0729(11)
H19A	-0.0424	0.8491	-0.1141	0.088
C20	-0.0238(3)	0.7506(3)	-0.0127(2)	0.0643(9)
H20A	-0.0769	0.7158	-0.0208	0.077
C21	0.4042(3)	0.4482(2)	0.70909(17)	0.0480(7)
C22	0.4364(3)	0.4235(2)	0.77077(17)	0.0466(7)
C23	0.4817(3)	0.3995(2)	0.84213(16)	0.0449(6)
C24	0.4621(3)	0.3166(3)	0.89799(17)	0.0516(7)
H24A	0.4155	0.2775	0.8874	0.062
C25	0.5493(3)	0.4558(2)	0.85803(17)	0.0455(7)
H25A	0.5636	0.5132	0.8218	0.055
C26	0.5966(2)	0.4287(2)	0.92708(17)	0.0438(6)
C27	0.5721(2)	0.3444(2)	0.97966(16)	0.0421(6)
C28	0.6680(3)	0.4840(3)	0.9459(2)	0.0548(8)
H28A	0.684	0.5414	0.9104	0.066
C29	0.7129(3)	0.4564(3)	1.0129(2)	0.0603(9)
H29A	0.761	0.4939	1.024	0.072
C30	0.6192(3)	0.3146(2)	1.05216(17)	0.0452(6)
C31	0.6893(3)	0.3707(3)	1.06807(18)	0.0516(7)
C32	0.7325(3)	0.3405(3)	1.1396(2)	0.0652(9)
H32A	0.7807	0.3763	1.1528	0.078
C33	0.7049(4)	0.2601(4)	1.1896(2)	0.0738(11)
H33A	0.7311	0.2403	1.2386	0.089
C34	0.6383(4)	0.2079(3)	1.1678(2)	0.0703(11)
H34A	0.6222	0.15	1.2025	0.084
C35	0.1566(3)	0.3809(2)	0.52433(18)	0.0453(7)
H35A	0.1086	0.3972	0.5693	0.054
H35B	0.2178	0.3158	0.5393	0.054
C36	0.0818(3)	0.3714(2)	0.46884(18)	0.0468(7)
H36A	0.1308	0.3597	0.4233	0.056
H36B	0.0209	0.4372	0.4552	0.056
C37	0.0229(3)	0.2848(2)	0.49716(18)	0.0491(7)
H37A	-0.0293	0.2981	0.5413	0.059
H37B	0.0833	0.2193	0.5129	0.059
C38	-0.0481(3)	0.2738(2)	0.43825(18)	0.0461(7)
H38A	-0.1095	0.3389	0.4234	0.055
H38B	0.0039	0.2623	0.3937	0.055

Crystal Structure Data

C39	-0.1049(3)	0.1866(2)	0.46501(19)	0.0498(7)
H39A	-0.1581	0.1991	0.5089	0.06
H39B	-0.0435	0.1219	0.4812	0.06
C40	-0.1735(3)	0.1725(2)	0.40688(17)	0.0456(7)
H40A	-0.2356	0.2366	0.3911	0.055
H40B	-0.1206	0.1603	0.3628	0.055
C41	-0.2285(3)	0.0839(2)	0.43489(18)	0.0495(7)
H41A	-0.2821	0.097	0.4785	0.059
H41B	-0.1661	0.0204	0.452	0.059
C42	-0.2961(3)	0.0654(2)	0.37806(17)	0.0461(7)
H42A	-0.3594	0.1282	0.3613	0.055
H42B	-0.243	0.0521	0.3342	0.055
C43	-0.3487(3)	-0.0246(2)	0.40866(19)	0.0503(7)
H43A	-0.2851	-0.087	0.426	0.06
H43B	-0.4016	-0.0109	0.4524	0.06
C44	-0.4163(3)	-0.0463(2)	0.35350(18)	0.0464(7)
H44A	-0.3638	-0.0598	0.3095	0.056
H44B	-0.4808	0.0155	0.3366	0.056
C45	-0.4668(3)	-0.1377(3)	0.3861(2)	0.0578(8)
H45A	-0.523	-0.1224	0.4281	0.069
H45B	-0.4029	-0.1986	0.4058	0.069
C46	-0.5283(4)	-0.1634(3)	0.3293(2)	0.0668(10)
H46A	-0.5592	-0.2224	0.353	0.1
H46B	-0.4727	-0.1802	0.2881	0.1
H46C	-0.5927	-0.1039	0.3103	0.1
C47	0.5339(3)	0.6844(2)	0.59126(16)	0.0450(6)
H47A	0.4721	0.7469	0.5714	0.054
H47B	0.5866	0.6635	0.5492	0.054
C48	0.6015(3)	0.7053(3)	0.64602(18)	0.0500(7)
H48A	0.6656	0.6432	0.663	0.06
H48B	0.5492	0.7192	0.69	0.06
C49	0.6525(3)	0.7960(2)	0.61326(17)	0.0475(7)
H49A	0.7048	0.7822	0.5693	0.057
H49B	0.5884	0.8582	0.5964	0.057
C50	0.7205(3)	0.8163(3)	0.66865(19)	0.0536(8)
H50A	0.7839	0.7535	0.6855	0.064
H50B	0.6678	0.8295	0.7126	0.064
C51	0.7736(3)	0.9060(3)	0.63895(19)	0.0523(7)
H51A	0.7106	0.9695	0.6233	0.063
H51B	0.8259	0.8938	0.5946	0.063
C52	0.8428(3)	0.9211(3)	0.69684(19)	0.0540(8)
H52A	0.7902	0.9317	0.7413	0.065
H52B	0.9056	0.8573	0.7121	0.065
C53	0.8971(3)	1.0103(2)	0.67099(19)	0.0526(7)
H53A	0.9473	1.0017	0.6253	0.063
H53B	0.8343	1.075	0.6583	0.063
C54	0.9694(3)	1.0193(2)	0.7289(2)	0.0524(8)
H54A	1.0315	0.9542	0.7417	0.063
H54B	0.9188	1.0276	0.7745	0.063
C55	1.0261(3)	1.1077(2)	0.7053(2)	0.0538(8)
H55A	1.0761	1.1003	0.6594	0.065
H55B	0.9643	1.1732	0.6936	0.065
C56	1.0989(3)	1.1127(3)	0.7639(2)	0.0575(8)
H56A	1.1619	1.0478	0.7744	0.069
H56B	1.0492	1.1174	0.8103	0.069
C57	1.1539(3)	1.2024(3)	0.7433(3)	0.0699(11)
H57A	1.2015	1.1998	0.696	0.084
H57B	1.0914	1.2678	0.7355	0.084
C58	1.2300(4)	1.2005(4)	0.8025(3)	0.0929(15)
H58A	1.2641	1.2591	0.787	0.139
H58B	1.2926	1.1363	0.81	0.139

Crystal Structure Data

H58C	1.1828	1.2049	0.8492	0.139
C59	-0.0140(4)	0.5114(4)	0.1654(3)	0.0821(13)
C60	0.4027(3)	1.1349(3)	0.08002(19)	0.0571(8)
C83	0.1582(4)	0.6077(3)	0.5388(4)	0.0648(16)
C84	0.1350(3)	0.5749(3)	0.6931(4)	0.0612(15)
C85	0.1269(6)	0.5901(6)	0.5568(7)	0.065(2)

Table 5-3: Anisotropic displacement parameters ($\text{\AA}^2 \times 10^4$) for **5**. The anisotropic displacement factor exponent takes the form: $\{-2 \pi^2 [h^2 a^{*2} U_{11} + \dots + 2 hka^*b^*U_{12}]\}$

Atom	U_{11}	U_{22}	U_{33}	U_{23}	U_{13}	U_{12}
Cl1C	0.0459(11)	0.0609(13)	0.0686(15)	-0.0211(11)	-0.0107(10)	-0.0268(10)
Cl1B	0.0592(16)	0.090(2)	0.169(4)	-0.087(3)	0.053(2)	-0.0452(16)
Cl1A	0.089(2)	0.0807(18)	0.0421(13)	-0.0009(12)	0.0092(13)	-0.0436(16)
Cl2C	0.0731(18)	0.0834(19)	0.0780(19)	-0.0369(16)	-0.0005(15)	-0.0418(15)
Cl2B	0.0685(18)	0.0643(17)	0.137(3)	-0.056(2)	0.030(2)	-0.0110(14)
Cl2A	0.099(2)	0.0448(13)	0.092(2)	0.0133(14)	-0.0339(19)	-0.0007(14)
Cl3	0.057(3)	0.029(3)	0.0378(18)	-0.0106(16)	-0.0100(19)	-0.0158(19)
Cl4	0.041(2)	0.009(2)	0.0425(13)	0.0047(16)	-0.0079(15)	0.0086(15)
Cl5	0.017(2)	0.0312(18)	0.0473(16)	-0.0190(12)	0.0063(15)	0.0149(14)
Cl3A	0.068(4)	0.029(3)	0.0321(14)	-0.0095(17)	-0.005(2)	-0.022(2)
Cl4A	0.049(3)	0.012(2)	0.0466(17)	0.0062(16)	-0.0196(19)	0.0061(16)
Cl5A	0.019(2)	0.047(3)	0.0505(16)	-0.0237(15)	0.0098(14)	0.0215(14)
O1	0.0586(13)	0.0512(12)	0.0477(12)	-0.0073(9)	-0.0113(10)	-0.0230(10)
O2	0.0621(14)	0.0595(13)	0.0449(12)	-0.0071(10)	-0.0119(10)	-0.0280(11)
N1	0.0511(14)	0.0488(14)	0.0430(13)	-0.0041(11)	-0.0089(11)	-0.0209(11)
N2	0.0573(16)	0.0577(16)	0.0511(15)	-0.0084(12)	-0.0155(12)	-0.0197(13)
N3	0.0529(15)	0.0583(15)	0.0449(14)	-0.0028(12)	-0.0078(11)	-0.0270(12)
N4	0.0657(18)	0.0720(18)	0.0441(15)	0.0017(13)	-0.0121(13)	-0.0327(15)
C1	0.0409(14)	0.0409(14)	0.0444(15)	-0.0139(12)	-0.0065(11)	-0.0097(11)
C2	0.0458(15)	0.0404(14)	0.0385(14)	-0.0096(11)	-0.0030(11)	-0.0089(12)
C3	0.0481(16)	0.0397(14)	0.0422(15)	-0.0083(12)	-0.0024(12)	-0.0126(12)
C4	0.0429(15)	0.0453(15)	0.0392(14)	-0.0116(12)	-0.0038(11)	-0.0122(12)
C5	0.0470(15)	0.0440(15)	0.0380(14)	-0.0085(12)	-0.0025(12)	-0.0103(12)
C6	0.0472(16)	0.0449(15)	0.0426(15)	-0.0099(12)	-0.0007(12)	-0.0141(12)
C7	0.0483(16)	0.0454(15)	0.0425(15)	-0.0124(12)	-0.0032(12)	-0.0145(12)
C8	0.0475(16)	0.0496(16)	0.0393(15)	-0.0090(12)	-0.0036(12)	-0.0147(13)
C9	0.0424(15)	0.0500(16)	0.0366(14)	-0.0110(12)	-0.0048(11)	-0.0101(12)
C10	0.0499(16)	0.0466(15)	0.0424(15)	-0.0029(12)	-0.0048(12)	-0.0195(13)
C11	0.0517(16)	0.0465(15)	0.0438(15)	-0.0106(12)	-0.0065(13)	-0.0206(13)
C12	0.0489(16)	0.0424(14)	0.0410(15)	-0.0087(12)	-0.0043(12)	-0.0159(12)
C13	0.0410(14)	0.0402(14)	0.0373(14)	-0.0079(11)	-0.0006(11)	-0.0138(11)
C14	0.077(2)	0.0529(18)	0.0523(18)	-0.0022(15)	-0.0116(16)	-0.0358(17)
C15	0.087(3)	0.0545(19)	0.0535(19)	0.0042(15)	-0.0115(18)	-0.0362(19)
C16	0.0432(15)	0.0426(15)	0.0417(15)	-0.0083(12)	-0.0043(12)	-0.0117(12)
C17	0.066(2)	0.0453(16)	0.0456(16)	-0.0026(13)	-0.0133(15)	-0.0140(14)
C18	0.091(3)	0.063(2)	0.0454(18)	0.0071(16)	-0.0194(18)	-0.026(2)
C19	0.082(3)	0.081(3)	0.056(2)	0.0007(19)	-0.0303(19)	-0.025(2)
C20	0.068(2)	0.070(2)	0.059(2)	-0.0070(17)	-0.0241(17)	-0.0226(18)
C21	0.0502(17)	0.0497(16)	0.0442(16)	-0.0097(13)	-0.0014(13)	-0.0149(13)
C22	0.0472(16)	0.0532(17)	0.0390(15)	-0.0057(13)	-0.0043(12)	-0.0164(13)
C23	0.0435(15)	0.0524(16)	0.0365(14)	-0.0054(12)	-0.0015(11)	-0.0135(13)
C24	0.0555(18)	0.0615(19)	0.0435(16)	-0.0049(14)	-0.0071(13)	-0.0287(15)
C25	0.0474(16)	0.0463(15)	0.0412(15)	-0.0046(12)	-0.0016(12)	-0.0148(13)
C26	0.0419(15)	0.0452(15)	0.0446(15)	-0.0088(12)	-0.0005(12)	-0.0141(12)

Crystal Structure Data

C27	0.0371(14)	0.0515(16)	0.0397(14)	-0.0089(12)	-0.0023(11)	-0.0158(12)
C28	0.0568(18)	0.0566(18)	0.0553(19)	-0.0057(15)	-0.0050(15)	-0.0269(15)
C29	0.066(2)	0.065(2)	0.061(2)	-0.0100(17)	-0.0109(17)	-0.0350(17)
C30	0.0432(15)	0.0533(16)	0.0405(15)	-0.0056(13)	-0.0022(12)	-0.0196(13)
C31	0.0503(17)	0.0608(19)	0.0489(17)	-0.0124(14)	-0.0069(14)	-0.0213(15)
C32	0.071(2)	0.079(2)	0.055(2)	-0.0075(18)	-0.0170(17)	-0.037(2)
C33	0.083(3)	0.095(3)	0.051(2)	0.000(2)	-0.0249(19)	-0.041(2)
C34	0.083(3)	0.083(3)	0.0480(19)	0.0100(18)	-0.0179(18)	-0.042(2)
C35	0.0436(15)	0.0409(14)	0.0520(17)	-0.0104(13)	-0.0041(13)	-0.0117(12)
C36	0.0467(16)	0.0401(14)	0.0533(17)	-0.0093(13)	-0.0095(13)	-0.0094(12)
C37	0.0471(16)	0.0488(16)	0.0540(18)	-0.0114(14)	-0.0059(13)	-0.0158(13)
C38	0.0455(16)	0.0431(15)	0.0510(17)	-0.0098(13)	-0.0057(13)	-0.0131(12)
C39	0.0459(16)	0.0500(17)	0.0550(18)	-0.0104(14)	-0.0040(14)	-0.0161(13)
C40	0.0426(15)	0.0433(15)	0.0507(17)	-0.0092(13)	-0.0024(13)	-0.0123(12)
C41	0.0476(16)	0.0496(16)	0.0536(18)	-0.0089(14)	-0.0053(13)	-0.0180(13)
C42	0.0451(15)	0.0434(15)	0.0503(17)	-0.0092(13)	-0.0032(13)	-0.0132(12)
C43	0.0473(16)	0.0496(17)	0.0546(18)	-0.0063(14)	-0.0044(14)	-0.0178(13)
C44	0.0467(16)	0.0425(15)	0.0510(17)	-0.0103(13)	-0.0022(13)	-0.0138(12)
C45	0.0577(19)	0.0514(18)	0.066(2)	-0.0050(16)	-0.0103(16)	-0.0214(15)
C46	0.070(2)	0.062(2)	0.078(3)	-0.0120(19)	-0.0100(19)	-0.0325(18)
C47	0.0477(16)	0.0476(15)	0.0426(15)	-0.0120(12)	-0.0015(12)	-0.0159(13)
C48	0.0514(17)	0.0559(18)	0.0484(17)	-0.0135(14)	-0.0065(13)	-0.0202(14)
C49	0.0477(16)	0.0515(17)	0.0468(16)	-0.0143(13)	-0.0024(13)	-0.0159(13)
C50	0.0542(18)	0.0601(19)	0.0545(18)	-0.0169(15)	-0.0012(14)	-0.0250(15)
C51	0.0501(17)	0.0541(18)	0.0565(19)	-0.0175(15)	0.0010(14)	-0.0169(14)
C52	0.0548(18)	0.0582(18)	0.0553(19)	-0.0137(15)	0.0013(15)	-0.0258(15)
C53	0.0513(17)	0.0479(16)	0.0592(19)	-0.0105(14)	0.0023(15)	-0.0177(14)
C54	0.0532(18)	0.0472(16)	0.061(2)	-0.0148(14)	0.0037(15)	-0.0205(14)
C55	0.0483(17)	0.0443(16)	0.068(2)	-0.0121(15)	0.0033(15)	-0.0139(13)
C56	0.0530(18)	0.0530(18)	0.071(2)	-0.0231(16)	0.0062(16)	-0.0180(15)
C57	0.0516(19)	0.058(2)	0.109(3)	-0.035(2)	0.004(2)	-0.0176(16)
C58	0.080(3)	0.101(3)	0.124(4)	-0.063(3)	0.015(3)	-0.042(3)
C59	0.103(3)	0.081(3)	0.079(3)	-0.005(2)	-0.016(2)	-0.056(3)
C60	0.070(2)	0.0566(18)	0.0488(17)	-0.0048(14)	-0.0069(15)	-0.0273(16)

7.6 Crystal Structure Data of 6 (In Cooperation with Prof. Dieter Fenske, University of Karlsruhe, Germany).

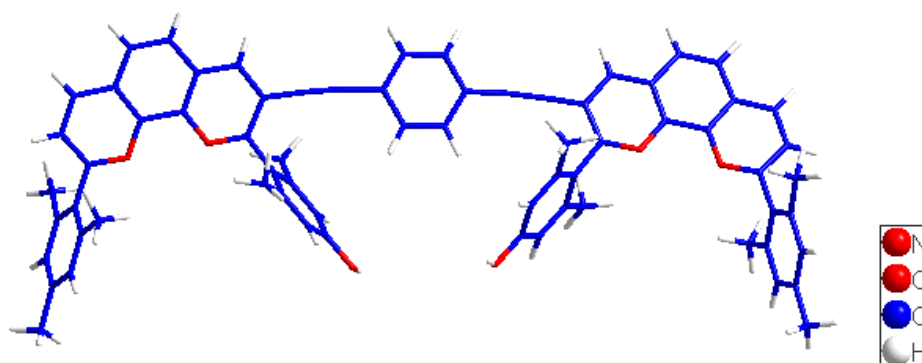


Figure 6-1. Stick representation of 6.

Crystal Structure Data

Table 6-1: Crystal data and structure refinement for **6**.

Substance	6
Sum formula	C80H82N8O6
Formula weight /g·mol ⁻¹	1251.54
Temperature /K	443(2)
Wavelength	0.71703 Å
Crystal system, space group	Triclinic, <i>P</i> -1
Unit cell dimensions	a = 32.113 (6) Å b = 15.049 (3) Å c = 14.506 (3) Å B = 93.72 (3) °
Volume /Å ³	6996 (2)
Z, Calculated density /Mg·m ⁻³	4, 1.188
Absorption coefficient /mm ⁻¹	0.076
F(000)	2664
Reflections collected / unique / R _{int}	8207 / 5570 / 0.0415
Refinement method	Full-matrix least-squares on <i>F</i> ²
Data / restraints / parameters	8207 / 0 / 572
Goodness-of-fit on <i>F</i> ²	1.075
Final <i>R</i> indices [<i>I</i> > 2σ(<i>I</i>)]	<i>R</i> 1 = 0.0558, <i>wR</i> 2 = 0.1556
<i>R</i> indices (all data)	<i>R</i> 1 = 0.0781, <i>wR</i> 2 = 0.1679

Table 6-2: Atomic coordinates (x 10⁵) and equivalent isotropic displacement parameters (Å² x 10⁴) for **6**. *U*(eq) is defined as one third of the trace of the orthogonalized *U*_{ij} tensor.

Atom	x	y	z	<i>U</i> _{eq}
N1	0.37812(4)	0.77927(8)	0.15623(7)	0.0409(3)
N2	0.32862(4)	0.74589(9)	0.30016(7)	0.0435(3)
N3	0.32382(7)	0.47134(13)	0.65800(10)	0.0699(5)
N4	0.42998(6)	0.26484(16)	0.06227(16)	0.0889(7)
O1	0.44670(5)	0.50911(10)	-0.13966(11)	0.0700(4)
O2	0.38966(6)	0.50662(12)	0.70952(10)	0.0858(5)
O3	0.38744(7)	0.16747(14)	0.12602(15)	0.1045(6)
C1	0.30510(5)	0.72996(11)	0.37052(9)	0.0488(4)
C2	0.29760(7)	0.79490(14)	0.43738(12)	0.0656(5)
C3	0.31373(7)	0.87779(14)	0.42983(12)	0.0676(5)
C4	0.33785(6)	0.89824(12)	0.35490(10)	0.0525(4)
C5	0.35476(6)	0.98467(12)	0.34132(11)	0.0582(4)
C6	0.37691(6)	1.00301(12)	0.26748(11)	0.0523(4)
C7	0.38476(5)	0.93428(10)	0.20199(9)	0.0447(3)
C8	0.40786(5)	0.95129(11)	0.12428(10)	0.0463(3)
C9	0.41611(5)	0.88205(10)	0.06498(9)	0.0434(3)
C10	0.40085(5)	0.79551(10)	0.08490(8)	0.0404(3)
C11	0.37001(5)	0.84744(10)	0.21430(8)	0.0419(3)
C12	0.34471(5)	0.82868(10)	0.29199(9)	0.0440(3)
C13	0.43993(5)	0.89558(10)	-0.01411(9)	0.0459(3)
C14	0.28765(5)	0.63821(11)	0.37736(9)	0.0475(4)
C15	0.31410(5)	0.56893(12)	0.40835(9)	0.0500(4)

Crystal Structure Data

C16	0.29835(6)	0.48280(13)	0.41093(10)	0.0534(4)
C17	0.25655(6)	0.46378(12)	0.38582(10)	0.0553(4)
C18	0.23088(6)	0.53393(13)	0.35676(10)	0.0548(4)
C19	0.24558(5)	0.62094(12)	0.35105(9)	0.0511(4)
C20	0.21677(7)	0.69231(17)	0.31284(14)	0.0655(5)
C21	0.24009(9)	0.36987(16)	0.38890(16)	0.0738(6)
C22	0.35884(6)	0.58648(15)	0.43993(14)	0.0616(4)
C23	0.41121(5)	0.71812(9)	0.02574(8)	0.0405(3)
C24	0.39087(5)	0.70651(10)	-0.06202(9)	0.0440(3)
C25	0.40274(6)	0.63639(11)	-0.11735(10)	0.0504(4)
C26	0.43389(6)	0.57814(11)	-0.08665(11)	0.0528(4)
C27	0.45313(6)	0.58828(12)	0.00141(12)	0.0539(4)
C28	0.44218(5)	0.65812(11)	0.05789(9)	0.0467(3)
C29	0.35657(7)	0.76763(13)	-0.09798(12)	0.0591(4)
C30	0.46497(7)	0.66859(16)	0.15206(12)	0.0632(5)
C31	0.45856(5)	0.90367(11)	-0.08292(10)	0.0469(3)
C32	0.47971(5)	0.90575(11)	-0.16699(9)	0.0450(3)
C33	0.48994(6)	0.82573(12)	-0.20919(10)	0.0528(4)
C34	0.49005(5)	0.98594(12)	-0.20890(10)	0.0516(4)
C35	0.30934(12)	0.5633(2)	0.65838(16)	0.0934(9)
C36	0.29383(10)	0.4014(2)	0.63648(15)	0.0867(8)
C37	0.36262(8)	0.45077(15)	0.68606(12)	0.0672(5)
C38	0.45030(15)	0.3482(4)	0.0669(6)	0.181(3)
C39	0.43810(14)	0.2071(4)	-0.0142(2)	0.159(2)
C40	0.40558(8)	0.23820(18)	0.12579(19)	0.0812(6)
H18	0.2005(8)	0.5221(15)	0.3397(14)	0.071(6)
H16	0.3179(7)	0.4319(16)	0.4332(15)	0.070(6)
H8	0.4171(6)	1.0133(14)	0.1153(13)	0.057(5)
H3	0.3095(8)	0.9223(18)	0.4753(18)	0.089(8)
H5	0.3497(8)	1.0318(18)	0.3906(17)	0.084(7)
H2	0.2824(8)	0.7794(15)	0.4897(16)	0.072(6)
H27	0.4759(8)	0.5445(16)	0.0210(16)	0.079(6)
H25	0.3876(7)	0.6286(14)	-0.1741(13)	0.056(5)
H6	0.3866(7)	1.0594(16)	0.2605(14)	0.067(6)
H33	0.4825(7)	0.7676(15)	-0.1790(13)	0.064(6)
H34	0.4838(6)	1.0419(14)	-0.1790(13)	0.058(5)
H222	0.3749(9)	0.6021(18)	0.3840(19)	0.093(8)
H221	0.3713(8)	0.5295(18)	0.4724(16)	0.082(7)
H291	0.3701(13)	0.819(3)	-0.123(2)	0.140(13)
H212	0.2150(11)	0.370(2)	0.423(2)	0.119(10)
H211	0.2610(14)	0.328(3)	0.429(3)	0.144(13)
H1	0.4284(11)	0.510(2)	-0.193(2)	0.113(11)
H37	0.3671(7)	0.3843(16)	0.6864(14)	0.067(6)
H292	0.3394(10)	0.737(2)	-0.144(2)	0.101(9)
H301	0.4761(9)	0.733(2)	0.1568(18)	0.097(8)
H302	0.4452(9)	0.6659(18)	0.2015(18)	0.087(8)
H223	0.3601(9)	0.6408(19)	0.4840(18)	0.092(8)
H201	0.2245(11)	0.703(2)	0.251(2)	0.116(10)
H293	0.3378(11)	0.783(2)	-0.047(2)	0.115(10)
H303	0.4915(10)	0.628(2)	0.1534(18)	0.099(8)
H362	0.3090(13)	0.338(3)	0.638(2)	0.136(13)
H202	0.1915(11)	0.685(2)	0.330(2)	0.107(10)
H213	0.2339(11)	0.347(2)	0.324(2)	0.122(10)
H203	0.2242(12)	0.749(3)	0.345(2)	0.121(11)
H361	0.2804(8)	0.4087(17)	0.5714(18)	0.084(7)
H351	0.2970(11)	0.570(2)	0.594(2)	0.123(10)
H352	0.2912(11)	0.578(2)	0.706(2)	0.125(10)
H40	0.4028(11)	0.284(3)	0.175(2)	0.127(12)
H381	0.4529(10)	0.354(2)	0.1245(18)	0.066(9)
H382	0.4482(16)	0.379(3)	0.013(3)	0.177(17)
H353	0.3434(18)	0.597(4)	0.666(3)	0.21(2)

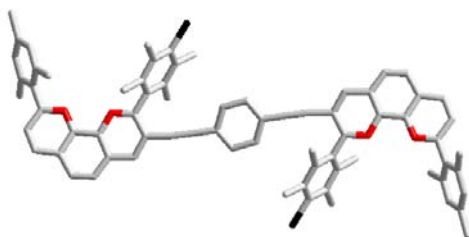
Crystal Structure Data

H363	0.2694(11)	0.403(2)	0.672(2)	0.114(10)
------	------------	----------	----------	-----------

Table 6-3: Anisotropic displacement parameters ($\text{\AA}^2 \times 10^4$) for **6**. The anisotropic displacement factor exponent takes the form: $\{-2 \pi^2 [h^2 a^{*2} U_{11} + \dots + 2 hka^*b^*U_{12}]\}$

Atom	U_{11}	U_{22}	U_{33}	U_{23}	U_{13}	U_{12}
N1	0.0473(7)	0.0446(6)	0.0317(5)	-0.0005(4)	0.0088(4)	-0.0003(5)
N2	0.0481(7)	0.0516(7)	0.0319(5)	-0.0003(4)	0.0111(5)	-0.0022(5)
N3	0.0924(13)	0.0750(11)	0.0433(7)	0.0047(6)	0.0119(7)	0.0139(10)
N4	0.0574(11)	0.0971(15)	0.1137(15)	0.0503(12)	0.0153(10)	0.0038(10)
O1	0.0757(10)	0.0631(8)	0.0730(8)	-0.0204(6)	0.0176(7)	0.0133(7)
O2	0.1092(14)	0.0788(11)	0.0688(8)	-0.0246(7)	0.0029(8)	0.0028(9)
O3	0.0932(13)	0.0921(13)	0.1307(15)	0.0393(11)	0.0258(11)	-0.0115(10)
C1	0.0523(9)	0.0601(9)	0.0354(6)	-0.0020(6)	0.0134(6)	-0.0060(7)
C2	0.0779(13)	0.0748(12)	0.0477(8)	-0.0121(8)	0.0323(8)	-0.0169(10)
C3	0.0861(14)	0.0694(11)	0.0511(8)	-0.0194(8)	0.0343(9)	-0.0139(10)
C4	0.0610(10)	0.0571(9)	0.0412(7)	-0.0106(6)	0.0172(7)	-0.0061(8)
C5	0.0726(12)	0.0558(9)	0.0481(8)	-0.0158(7)	0.0180(8)	-0.0075(8)
C6	0.0628(10)	0.0481(9)	0.0470(7)	-0.0087(6)	0.0121(7)	-0.0066(8)
C7	0.0506(9)	0.0475(8)	0.0366(6)	-0.0033(5)	0.0091(6)	-0.0032(6)
C8	0.0541(9)	0.0453(8)	0.0405(6)	-0.0008(5)	0.0105(6)	-0.0054(7)
C9	0.0473(8)	0.0487(8)	0.0349(6)	0.0015(5)	0.0093(5)	-0.0021(6)
C10	0.0432(8)	0.0462(7)	0.0324(5)	0.0014(5)	0.0072(5)	0.0012(6)
C11	0.0481(8)	0.0466(7)	0.0318(5)	-0.0023(5)	0.0081(5)	-0.0012(6)
C12	0.0495(8)	0.0503(8)	0.0331(6)	-0.0034(5)	0.0100(5)	-0.0027(6)
C13	0.0491(9)	0.0491(8)	0.0402(6)	0.0008(5)	0.0091(6)	-0.0045(6)
C14	0.0520(9)	0.0611(9)	0.0305(5)	-0.0001(5)	0.0122(5)	-0.0051(7)
C15	0.0508(9)	0.0646(10)	0.0355(6)	-0.0018(6)	0.0109(6)	-0.0066(7)
C16	0.0596(10)	0.0617(10)	0.0396(6)	0.0001(6)	0.0090(6)	-0.0032(8)
C17	0.0634(11)	0.0643(10)	0.0390(6)	-0.0006(6)	0.0104(6)	-0.0124(8)
C18	0.0535(10)	0.0730(11)	0.0384(7)	0.0008(6)	0.0062(6)	-0.0134(8)
C19	0.0522(9)	0.0675(10)	0.0345(6)	0.0032(6)	0.0090(6)	-0.0058(8)
C20	0.0602(12)	0.0809(14)	0.0557(9)	0.0117(9)	0.0062(8)	0.0014(10)
C21	0.0869(16)	0.0674(13)	0.0673(11)	-0.0012(9)	0.0064(11)	-0.0200(11)
C22	0.0539(11)	0.0734(12)	0.0578(9)	0.0002(9)	0.0059(8)	-0.0044(9)
C23	0.0454(8)	0.0437(7)	0.0334(5)	0.0021(5)	0.0112(5)	0.0004(6)
C24	0.0533(9)	0.0431(7)	0.0362(6)	0.0009(5)	0.0066(6)	0.0010(6)
C25	0.0628(10)	0.0501(9)	0.0389(6)	-0.0043(6)	0.0072(6)	0.0014(7)
C26	0.0552(10)	0.0497(9)	0.0554(8)	-0.0083(6)	0.0179(7)	0.0028(7)
C27	0.0487(9)	0.0558(9)	0.0581(8)	0.0004(7)	0.0113(7)	0.0109(8)
C28	0.0436(8)	0.0551(9)	0.0422(6)	0.0032(6)	0.0086(6)	0.0043(7)
C29	0.0725(12)	0.0518(9)	0.0509(8)	-0.0029(7)	-0.0115(8)	0.0096(9)
C30	0.0598(11)	0.0785(14)	0.0505(8)	0.0008(8)	-0.0036(8)	0.0133(10)
C31	0.0485(9)	0.0530(8)	0.0401(6)	0.0024(6)	0.0097(6)	-0.0027(7)
C32	0.0452(8)	0.0542(8)	0.0365(6)	0.0012(5)	0.0089(5)	-0.0022(6)
C33	0.0632(11)	0.0506(9)	0.0460(7)	0.0037(6)	0.0144(7)	-0.0019(7)
C34	0.0599(10)	0.0505(9)	0.0466(7)	-0.0029(6)	0.0208(7)	-0.0006(7)
C35	0.131(2)	0.0976(18)	0.0543(11)	0.0078(11)	0.0227(13)	0.0479(18)
C36	0.0916(18)	0.119(2)	0.0492(10)	0.0236(11)	0.0028(10)	-0.0107(16)
C37	0.0928(16)	0.0656(12)	0.0435(8)	-0.0120(7)	0.0067(8)	0.0112(11)
C38	0.102(3)	0.164(4)	0.267(7)	0.136(5)	-0.056(4)	-0.060(3)
C39	0.135(3)	0.251(6)	0.094(2)	0.046(3)	0.038(2)	0.097(4)
C40	0.0757(15)	0.0738(14)	0.0959(15)	0.0220(12)	0.0199(12)	0.0051(12)

7.7 Crystal Structure Data of 7 (In Cooperation with Dr. Jan W. Bats, Johann Wolfgang Goethe-University, Frankfurt am Main, Germany).⁴



A single crystal (yellow rod with dimensions 0.04 x 0.12 x 1.6 mm) was measured on a SIEMENS SMART diffractometer at a temperature of about -112 °C. An empirical absorption correction with program SADABS (Sheldrick, 1996) gave a correction factor between 0.525 and 1.000. Equivalent reflections were averaged. $R(I)_{\text{internal}} = 0.367$. The structure was determined by direct methods using program SIR92. A solvate molecule was considered to be methanol. The Br atom was refined with anisotropic thermal parameters. The H atoms at the methyl groups could not be located. The structure was refined on F^2 values using program SHELXL-97. The final difference density was between -0.49 and +0.57 e/Å³. The R-values are very large due to many weak reflections in the data set.

Table 7-1: Crystal data and structure refinement for **7**.

Substance	7
Sum formula	C ₇₄ H ₆₈ Br ₂ N ₄ O ₂
Formula weight /g·mol ⁻¹	1205.14
Temperature /K	161(2)
Wavelength /pm	0.71073 Å
Crystal system, space group	Triclinic, <i>P</i> -1
Unit cell dimensions	a = 8.216 (5) Å b = 14.101 (9) Å c = 14.470 (10) Å β = 76.30 (3) °
Volume /Å ³	1571.2 (18)
Z, Calculated density /Mg·m ⁻³	1, 1.274
Absorption coefficient /mm ⁻¹	1.339
F(000)	626
Crystal size (mm)	1.6 x 0.12 x 0.04 mm
Reflections collected / unique / R _{int}	9014 / 4044 / 0.3671
Refinement method	Full-matrix least-squares on <i>F</i> ²
Data / restraints / parameters	4044 / 0 / 170
Goodness-of-fit on <i>F</i> ²	0.964
Final <i>R</i> indices [<i>I</i> > 2σ(<i>I</i>)]	<i>R</i> 1 = 0.1723, <i>wR</i> 2 = 0.3136
<i>R</i> indices (all data)	<i>R</i> 1 = 0.4696, <i>wR</i> 2 = 0.4169
Largest diff. peak and hole	0.568 and -0.492 e/Å ³

Table 7-2: Atomic coordinates (x 10⁵) and equivalent isotropic displacement parameters (Å² x 10⁴) for **7**. *U*(eq) is defined as one third of the trace of the orthogonalized *U*_{ij} tensor.

Atom	x	y	z	U _{eq}
Br(1)	4516(4)	4040(4)	-1587(3)	122(2)
C(15)	4620(30)	1607(18)	4910(17)	35(7)
N(1)	4220(20)	1772(13)	3265(13)	32(5)
C(19)	4930(30)	1689(17)	819(16)	24(6)
C(21)	4340(30)	3260(20)	-314(19)	56(9)
C(34)	4960(30)	4555(17)	4004(16)	44(7)
N(2)	5650(20)	2357(14)	4521(13)	37(6)
C(12)	4700(30)	1596(17)	6583(18)	44(8)
C(10)	2880(30)	320(17)	6310(16)	32(7)
C(17)	3550(30)	1480(17)	2649(16)	30(7)
C(20)	4940(30)	2340(20)	-106(19)	46(8)
C(18)	3830(30)	2058(17)	1620(16)	25(6)
C(16)	3820(30)	1244(17)	4252(17)	31(7)
C(8)	2700(30)	406(17)	4697(16)	29(7)
C(29)	6940(30)	4410(20)	4077(19)	54(8)
C(13)	5780(30)	2300(19)	6174(18)	53(8)
C(32)	10040(30)	4298(18)	4181(16)	41(7)
C(9)	2350(30)	-15(17)	5709(16)	32(7)
C(7)	2080(30)	78(19)	3965(17)	50(8)

Crystal Structure Data

C(6)	2330(30)	665(17)	3007(17)	34(7)
C(3)	810(30)	836(18)	-54(17)	42(7)
C(28)	7450(30)	3560(20)	4612(18)	48(8)
C(22)	3350(40)	3600(20)	490(20)	74(10)
C(23)	3120(30)	2986(18)	1454(17)	36(7)
C(25)	6050(30)	1940(20)	-969(19)	67(9)
C(1)	-300(30)	-805(18)	911(17)	40(7)
O(1)	1820(30)	7809(19)	-2513(18)	143(9)
C(30)	7950(30)	5151(19)	3574(18)	52(8)
C(33)	9230(30)	3440(20)	4696(18)	53(8)
C(2)	590(30)	35(18)	803(17)	43(8)
C(31)	9580(30)	5140(20)	3614(19)	60(9)
C(26)	2480(40)	4660(30)	300(20)	124(13)
C(37)	2070(40)	6950(20)	-1700(20)	101(12)
C(11)	4010(30)	1168(18)	5975(18)	46(8)
C(14)	6300(30)	2694(18)	5124(18)	43(8)
C(36)	9790(30)	2540(20)	5192(18)	53(8)
C(24)	5640(30)	710(20)	1100(18)	57(8)
C(35)	10770(30)	6040(20)	2998(19)	74(10)
C(4)	1170(30)	218(17)	1629(18)	40(7)
C(5)	1640(30)	378(18)	2278(19)	50(8)
C(27)	1960(30)	3360(20)	2338(19)	70(9)

Table 7-3. Anisotropic displacement parameters ($\text{\AA}^2 \times 10^4$) for **7**. The anisotropic displacement factor exponent takes the form: $\{-2 \pi^2 [h^2 a^{*2} U_{11} + \dots + 2 hka^*b^*U_{12}]\}$.

Atom	U_{11}	U_{22}	U_{33}	U_{23}	U_{13}	U_{12}
Br(1)	57(2)	228(5)	56(2)	-20(3)	23(2)	-17(3)

7.8 Crystal Structure Data of **8** (In Cooperation with Prof. Dieter Fenske, University of Karlsruhe, Germany).⁵



Figure 8-1. Stick representation of **8**.

Crystal Structure Data

Table 8-1: Crystal data and structure refinement for **8**.

Substance	8
Sum formula	C ₈₄ H ₆₈ Br ₂ Cl ₂ Cu ₂ F ₁₂ N ₆ P ₂
Formula weight /g·mol ⁻¹	1809.18
Temperature /K	453(2)
Wavelength /pm	71.073
Crystal system, space group	Triclinic, <i>P</i> -1
Unit cell dimensions	a = 21.297 (4) Å b = 22.658 (5) Å c = 17.044 (3) Å B = 104.29 (3) °
Volume /Å ³	7970 (3)
Z, Calculated density /Mg·m ⁻³	4, 1.508
Absorption coefficient /mm ⁻¹	1.72
F(000)	3656
Crystal size /mm ³	0.30 × 0.15 × 0.10
Reflections collected / unique / R _{int}	20487 / 13759 / 0.503
Refinement method	Full-matrix least-squares on <i>F</i> ²
Data / restraints / parameters	20487 / 0 / 900
Goodness-of-fit on <i>F</i> ²	1.564
Final <i>R</i> indices [<i>I</i> > 2σ(<i>I</i>)]	<i>R</i> 1 = 0.0919, <i>wR</i> 2 = 0.2404
<i>R</i> indices (all data)	<i>R</i> 1 = 0.1259, <i>wR</i> 2 = 0.2558

Table 8-2: Atomic coordinates (× 10⁵) and equivalent isotropic displacement parameters (Å² × 10⁴) for **8**. *U*(eq) is defined as one third of the trace of the orthogonalized *U*_{ij} tensor.

Atom	<i>x</i>	<i>y</i>	<i>z</i>	<i>U</i> _{eq}
Cu1	-0.14825(3)	0.33474(3)	1.17228(4)	0.04444(17)
Cu2	0.41915(3)	0.34759(3)	0.53180(3)	0.03761(15)
Br1	0.13617(3)	0.20926(3)	1.21766(5)	0.0653(2)
Br2	0.12099(4)	0.25363(4)	0.45730(5)	0.0779(3)
N1	-0.23637(19)	0.37277(18)	1.1358(3)	0.0370(8)
N2	-0.12968(18)	0.38286(17)	1.0786(2)	0.0343(8)
N3	0.40657(18)	0.38472(17)	0.6380(2)	0.0319(7)
N4	0.51050(17)	0.37717(17)	0.5748(2)	0.0304(7)
N5	-0.0989(2)	0.2770(2)	1.2364(3)	0.0512(11)
N6	0.3698(2)	0.2937(2)	0.4598(3)	0.0403(9)
Cl1	0.36419(11)	0.44742(8)	0.44168(11)	0.0732(5)
Cl2	0.32402(16)	0.40437(14)	0.27618(15)	0.1094(9)
C1	-0.2857(2)	0.3197(2)	1.2289(3)	0.0405(10)
C2	-0.2959(3)	0.3389(3)	1.3030(4)	0.0502(12)
C3	-0.2947(3)	0.2969(3)	1.3634(4)	0.0552(14)
C4	-0.2842(3)	0.2371(3)	1.3507(4)	0.0530(13)
C5	-0.2741(3)	0.2197(3)	1.2772(4)	0.0481(12)
C6	-0.2749(2)	0.2597(2)	1.2154(3)	0.0413(10)
C7	-0.3064(4)	0.4033(3)	1.3204(5)	0.0691(19)
C8	-0.2850(4)	0.1921(4)	1.4169(5)	0.075(2)
C9	-0.2654(3)	0.2374(3)	1.1348(4)	0.0518(13)
C10	-0.2894(2)	0.3638(2)	1.1622(3)	0.0413(10)
C11	-0.3489(2)	0.3931(2)	1.1269(4)	0.0439(11)

Crystal Structure Data

C12	-0.3526(2)	0.4313(2)	1.0632(3)	0.0422(11)
C13	-0.2969(2)	0.4407(2)	1.0336(3)	0.0378(10)
C14	-0.2967(2)	0.4769(2)	0.9638(3)	0.0397(10)
C15	-0.2436(2)	0.4815(2)	0.9344(3)	0.0384(10)
C16	-0.1845(2)	0.4501(2)	0.9721(3)	0.0368(9)
C17	-0.1281(2)	0.4520(2)	0.9439(3)	0.0387(10)
C18	-0.0736(2)	0.4204(2)	0.9827(3)	0.0345(9)
C19	-0.0770(2)	0.3843(2)	1.0503(3)	0.0350(9)
C20	-0.1832(2)	0.4156(2)	1.0412(3)	0.0336(9)
C21	-0.2399(2)	0.4101(2)	1.0717(3)	0.0347(9)
C22	-0.0152(2)	0.4224(2)	0.9552(3)	0.0365(9)
C23	0.0308(2)	0.4267(2)	0.9274(3)	0.0354(9)
C24	0.0854(2)	0.4296(2)	0.8921(3)	0.0341(9)
C25	0.0779(2)	0.4436(3)	0.8100(3)	0.0415(11)
C26	0.1300(3)	0.4443(3)	0.7773(3)	0.0427(11)
C27	0.1927(2)	0.4317(2)	0.8242(3)	0.0352(9)
C28	0.2013(2)	0.4191(2)	0.9077(3)	0.0358(9)
C29	-0.0233(2)	0.3428(2)	1.0890(3)	0.0348(9)
C30	0.1477(2)	0.4174(2)	0.9400(3)	0.0368(9)
C31	-0.0310(2)	0.2826(2)	1.0697(3)	0.0418(11)
C32	0.0164(3)	0.2420(2)	1.1094(4)	0.0453(11)
C33	0.0701(3)	0.2641(3)	1.1647(4)	0.0485(13)
C34	0.0795(2)	0.3232(3)	1.1847(3)	0.0441(12)
C35	0.0314(2)	0.3635(2)	1.1475(3)	0.0399(10)
C36	0.0366(3)	0.4282(3)	1.1690(4)	0.0559(15)
C37	0.1408(3)	0.3451(3)	1.2462(4)	0.0648(18)
C38	0.0077(4)	0.1761(3)	1.0885(6)	0.073(2)
C39	-0.0901(3)	0.2602(3)	1.0060(4)	0.0580(16)
C40	0.2484(2)	0.4293(2)	0.7908(3)	0.0382(10)
C41	0.2963(2)	0.4239(2)	0.7668(3)	0.0376(9)
C42	0.3550(2)	0.4182(2)	0.7401(3)	0.0349(9)
C43	0.4140(2)	0.4398(2)	0.7871(3)	0.0381(10)
C44	0.4694(2)	0.4344(2)	0.7590(3)	0.0352(9)
C45	0.5332(3)	0.4556(3)	0.8036(3)	0.0451(12)
C46	0.5851(3)	0.4502(3)	0.7721(3)	0.0479(13)
C47	0.5803(2)	0.4240(2)	0.6939(3)	0.0363(10)
C48	0.6327(2)	0.4188(2)	0.6588(3)	0.0413(10)
C49	0.6230(2)	0.3939(2)	0.5822(3)	0.0374(10)
C50	0.5608(2)	0.3728(2)	0.5419(3)	0.0325(8)
C51	0.5193(2)	0.40272(19)	0.6495(2)	0.0296(8)
C52	0.4643(2)	0.4076(2)	0.6828(2)	0.0303(8)
C53	0.3542(2)	0.3888(2)	0.6655(3)	0.0320(8)
C54	0.2949(2)	0.3578(2)	0.6177(3)	0.0357(9)
C55	0.2437(2)	0.3897(2)	0.5689(3)	0.0402(10)
C56	0.1899(2)	0.3585(3)	0.5211(3)	0.0479(12)
C57	0.1927(3)	0.2966(3)	0.5241(4)	0.0515(14)
C58	0.2423(3)	0.2641(3)	0.5721(4)	0.0472(12)
C59	0.2943(2)	0.2959(2)	0.6210(3)	0.0397(10)
C60	0.2437(3)	0.4563(3)	0.5684(4)	0.0537(15)
C61	0.1325(3)	0.3934(4)	0.4710(5)	0.070(2)
C62	0.2428(4)	0.1973(3)	0.5757(5)	0.071(2)
C63	0.3508(3)	0.2612(3)	0.6761(4)	0.0523(13)
C64	0.5503(2)	0.3427(2)	0.4615(3)	0.0326(8)
C65	0.5500(2)	0.2810(2)	0.4581(3)	0.0356(9)
C66	0.5421(2)	0.2538(2)	0.3829(3)	0.0406(10)
C67	0.5338(3)	0.2863(3)	0.3118(3)	0.0426(11)
C68	0.5320(3)	0.3472(3)	0.3164(3)	0.0430(11)
C69	0.5402(3)	0.3773(2)	0.3904(3)	0.0391(10)
C70	0.5376(4)	0.4439(3)	0.3936(4)	0.0549(15)
C71	0.5317(3)	0.2562(3)	0.2318(3)	0.0596(16)
C72	0.5575(3)	0.2441(2)	0.5337(3)	0.0459(12)

Crystal Structure Data

C73	-0.0671(3)	0.2394(3)	1.2688(4)	0.0513(13)
C74	-0.0260(4)	0.1910(3)	1.3086(5)	0.069(2)
C75	0.3396(3)	0.2585(2)	0.4200(3)	0.0453(12)
C76	0.2993(5)	0.2127(3)	0.3712(4)	0.079(3)
C77	0.2988(4)	0.4217(4)	0.3633(5)	0.0701(19)
P1	0.15850(7)	0.56184(8)	0.30926(12)	0.0586(4)
P2	-0.43198(6)	0.60520(6)	0.96281(8)	0.0414(3)
F1	0.1423(5)	0.5066(5)	0.3513(6)	0.174(4)
F2	0.1330(4)	0.6169(4)	0.3453(5)	0.144(3)
F3	0.2247(3)	0.5649(3)	0.3779(4)	0.1067(18)
F4	0.0942(3)	0.5563(2)	0.2390(3)	0.0847(13)
F5	0.1874(4)	0.5103(4)	0.2615(5)	0.145(3)
F6	0.1840(6)	0.6059(5)	0.2548(7)	0.187(4)
F7	-0.4128(3)	0.6709(3)	0.9531(3)	0.0947(15)
F8	-0.3667(3)	0.5926(2)	1.0294(3)	0.0854(13)
F9	-0.4493(3)	0.5376(3)	0.9733(3)	0.0909(14)
F10	-0.4642(3)	0.6242(3)	1.0326(3)	0.0890(14)
F11	-0.4984(2)	0.6146(2)	0.8984(3)	0.0719(11)
F12	-0.3995(2)	0.5845(2)	0.8921(3)	0.0744(11)
C78	0.1211(6)	0.6116(6)	0.6292(7)	0.102(3)
C80	0.0190(7)	0.5261(7)	0.6093(9)	0.122(4)
C79	0.071(2)	0.589(2)	0.663(3)	0.074(16)
C82	0.070(3)	0.545(3)	0.530(3)	0.09(2)
C81	0.023(2)	0.516(2)	0.532(3)	0.073(17)
C83	0.1582(4)	0.6077(3)	0.5388(4)	0.0648(16)
C84	0.1350(3)	0.5749(3)	0.6931(4)	0.0612(15)
C85	0.1269(6)	0.5901(6)	0.5568(7)	0.065(2)

Table 8-3: Anisotropic displacement parameters ($\text{\AA}^2 \times 10^4$) for **8**. The anisotropic displacement factor exponent takes the form: $\{-2 \pi^2 [h^2 a^{*2} U_{11} + \dots + 2 hka^*b^*U_{12}]\}$

Atom	U_{11}	U_{22}	U_{33}	U_{23}	U_{13}	U_{12}
Cu1	0.0387(3)	0.0399(3)	0.0577(4)	0.0159(3)	0.0178(3)	0.0083(2)
Cu2	0.0369(3)	0.0397(3)	0.0365(3)	-0.0098(2)	0.0095(2)	-0.0067(2)
Br1	0.0570(3)	0.0572(4)	0.0785(4)	0.0172(3)	0.0104(3)	0.0236(3)
Br2	0.0597(4)	0.0857(6)	0.0820(5)	-0.0244(4)	0.0055(4)	-0.0292(4)
N1	0.0333(17)	0.031(2)	0.051(2)	0.0072(16)	0.0190(16)	0.0034(14)
N2	0.0300(16)	0.0311(19)	0.0441(19)	0.0042(15)	0.0137(15)	0.0043(14)
N3	0.0340(17)	0.0312(19)	0.0321(16)	-0.0038(14)	0.0110(14)	-0.0003(14)
N4	0.0323(16)	0.0306(19)	0.0300(15)	-0.0029(13)	0.0108(13)	-0.0015(13)
N5	0.048(2)	0.049(3)	0.063(3)	0.021(2)	0.025(2)	0.012(2)
N6	0.042(2)	0.038(2)	0.0418(19)	-0.0055(16)	0.0111(17)	-0.0053(17)
Cl1	0.0931(13)	0.0488(9)	0.0671(9)	0.0072(7)	-0.0005(9)	-0.0003(8)
Cl2	0.132(2)	0.113(2)	0.0765(13)	-0.0237(13)	0.0144(14)	0.0108(17)
C1	0.038(2)	0.033(2)	0.057(3)	0.002(2)	0.023(2)	-0.0019(18)
C2	0.056(3)	0.039(3)	0.067(3)	0.001(2)	0.036(3)	-0.001(2)
C3	0.063(3)	0.053(4)	0.059(3)	0.001(3)	0.035(3)	-0.007(3)
C4	0.055(3)	0.046(3)	0.062(3)	0.011(3)	0.022(3)	0.003(2)
C5	0.044(3)	0.040(3)	0.064(3)	0.004(2)	0.020(2)	0.000(2)
C6	0.039(2)	0.035(2)	0.054(3)	0.000(2)	0.020(2)	-0.0026(18)
C7	0.098(5)	0.040(3)	0.088(5)	-0.007(3)	0.057(4)	-0.001(3)
C8	0.087(5)	0.065(5)	0.081(4)	0.036(4)	0.035(4)	0.016(4)
C9	0.061(3)	0.037(3)	0.063(3)	-0.007(2)	0.025(3)	-0.001(2)
C10	0.038(2)	0.030(2)	0.061(3)	-0.001(2)	0.024(2)	-0.0010(18)
C11	0.033(2)	0.040(3)	0.064(3)	0.001(2)	0.022(2)	0.0029(19)
C12	0.032(2)	0.038(3)	0.059(3)	-0.001(2)	0.017(2)	0.0029(17)
C13	0.032(2)	0.033(2)	0.049(2)	-0.0028(19)	0.0110(19)	0.0036(17)
C14	0.037(2)	0.038(2)	0.044(2)	-0.0023(19)	0.0091(19)	0.0092(18)
C15	0.035(2)	0.038(3)	0.041(2)	-0.0021(19)	0.0083(18)	0.0043(18)

Crystal Structure Data

C16	0.037(2)	0.031(2)	0.042(2)	0.0015(18)	0.0110(18)	0.0030(17)
C17	0.037(2)	0.036(2)	0.045(2)	0.0040(19)	0.0135(19)	0.0013(18)
C18	0.0280(18)	0.031(2)	0.048(2)	-0.0014(18)	0.0153(17)	-0.0018(15)
C19	0.0311(19)	0.029(2)	0.047(2)	0.0029(17)	0.0138(18)	-0.0002(15)
C20	0.0293(18)	0.028(2)	0.045(2)	0.0023(17)	0.0127(17)	0.0024(15)
C21	0.034(2)	0.034(2)	0.039(2)	0.0007(17)	0.0143(17)	0.0042(17)
C22	0.035(2)	0.033(2)	0.044(2)	0.0011(18)	0.0125(18)	-0.0033(17)
C23	0.032(2)	0.031(2)	0.044(2)	-0.0001(18)	0.0106(18)	0.0010(16)
C24	0.0328(19)	0.031(2)	0.043(2)	-0.0031(17)	0.0167(17)	-0.0030(16)
C25	0.035(2)	0.049(3)	0.042(2)	0.004(2)	0.0117(18)	0.0049(19)
C26	0.042(2)	0.050(3)	0.037(2)	0.005(2)	0.0127(19)	0.006(2)
C27	0.036(2)	0.033(2)	0.041(2)	-0.0049(17)	0.0176(18)	0.0004(17)
C28	0.032(2)	0.039(2)	0.038(2)	-0.0002(17)	0.0117(17)	0.0021(17)
C29	0.0267(18)	0.032(2)	0.048(2)	0.0066(18)	0.0141(17)	0.0015(15)
C30	0.034(2)	0.041(3)	0.037(2)	0.0009(18)	0.0137(17)	0.0045(17)
C31	0.035(2)	0.034(3)	0.057(3)	0.001(2)	0.014(2)	0.0018(18)
C32	0.044(3)	0.033(3)	0.065(3)	0.006(2)	0.024(2)	0.0050(19)
C33	0.038(2)	0.046(3)	0.061(3)	0.014(2)	0.013(2)	0.016(2)
C34	0.035(2)	0.043(3)	0.055(3)	0.006(2)	0.012(2)	0.000(2)
C35	0.036(2)	0.037(3)	0.047(2)	0.005(2)	0.0111(19)	-0.0018(18)
C36	0.062(3)	0.032(3)	0.067(3)	0.000(2)	0.003(3)	-0.001(2)
C37	0.048(3)	0.066(4)	0.069(4)	0.001(3)	-0.008(3)	0.000(3)
C38	0.075(4)	0.030(3)	0.115(6)	-0.009(3)	0.022(4)	0.006(3)
C39	0.049(3)	0.045(3)	0.074(4)	-0.013(3)	0.004(3)	-0.002(2)
C40	0.041(2)	0.035(2)	0.042(2)	-0.0019(19)	0.0172(19)	0.0047(18)
C41	0.041(2)	0.035(2)	0.040(2)	-0.0005(18)	0.0171(18)	0.0030(18)
C42	0.043(2)	0.032(2)	0.035(2)	-0.0018(17)	0.0209(18)	0.0034(18)
C43	0.046(2)	0.038(2)	0.0333(19)	-0.0048(17)	0.0147(18)	0.0011(19)
C44	0.037(2)	0.037(2)	0.0322(19)	-0.0041(17)	0.0100(16)	-0.0026(17)
C45	0.044(2)	0.056(3)	0.036(2)	-0.011(2)	0.0104(19)	-0.008(2)
C46	0.042(2)	0.063(4)	0.036(2)	-0.014(2)	0.0064(19)	-0.011(2)
C47	0.034(2)	0.040(3)	0.0333(19)	-0.0036(18)	0.0058(17)	-0.0051(18)
C48	0.033(2)	0.049(3)	0.043(2)	-0.003(2)	0.0105(18)	-0.0082(19)
C49	0.0314(19)	0.042(3)	0.041(2)	-0.0032(19)	0.0136(17)	-0.0029(17)
C50	0.0333(19)	0.034(2)	0.0337(19)	0.0012(16)	0.0144(16)	0.0005(16)
C51	0.0296(18)	0.030(2)	0.0311(18)	-0.0026(15)	0.0108(15)	-0.0032(15)
C52	0.0320(19)	0.030(2)	0.0313(18)	-0.0014(16)	0.0128(15)	-0.0013(15)
C53	0.0347(19)	0.029(2)	0.0345(19)	0.0007(16)	0.0131(16)	0.0000(16)
C54	0.0323(19)	0.038(2)	0.041(2)	-0.0073(18)	0.0165(17)	-0.0027(17)
C55	0.037(2)	0.043(3)	0.043(2)	-0.0032(19)	0.0145(19)	-0.0032(19)
C56	0.035(2)	0.059(3)	0.048(3)	-0.006(2)	0.009(2)	-0.002(2)
C57	0.043(3)	0.056(4)	0.058(3)	-0.017(3)	0.018(2)	-0.017(2)
C58	0.046(3)	0.045(3)	0.054(3)	-0.009(2)	0.020(2)	-0.011(2)
C59	0.040(2)	0.035(2)	0.049(2)	-0.0042(19)	0.020(2)	-0.0035(18)
C60	0.054(3)	0.041(3)	0.061(3)	0.003(3)	0.005(3)	0.007(2)
C61	0.045(3)	0.085(5)	0.072(4)	0.002(4)	-0.005(3)	0.004(3)
C62	0.083(5)	0.041(3)	0.092(5)	-0.017(3)	0.027(4)	-0.016(3)
C63	0.054(3)	0.040(3)	0.064(3)	0.004(2)	0.016(3)	0.007(2)
C64	0.0326(19)	0.034(2)	0.0334(18)	-0.0012(16)	0.0120(16)	0.0034(16)
C65	0.036(2)	0.035(2)	0.038(2)	0.0018(18)	0.0112(17)	-0.0031(17)
C66	0.041(2)	0.039(3)	0.042(2)	-0.006(2)	0.0124(19)	-0.0035(19)
C67	0.043(2)	0.053(3)	0.035(2)	-0.010(2)	0.0174(19)	-0.002(2)
C68	0.050(3)	0.049(3)	0.033(2)	0.004(2)	0.0169(19)	0.004(2)
C69	0.047(2)	0.037(3)	0.036(2)	0.0025(18)	0.0144(19)	0.0035(19)
C70	0.081(4)	0.034(3)	0.052(3)	0.007(2)	0.021(3)	0.011(3)
C71	0.068(4)	0.077(5)	0.035(2)	-0.019(3)	0.015(2)	0.001(3)
C72	0.059(3)	0.039(3)	0.040(2)	0.006(2)	0.012(2)	-0.008(2)

Crystal Structure Data

C73	0.050(3)	0.046(3)	0.057(3)	0.013(2)	0.011(2)	0.004(2)
C74	0.066(4)	0.043(3)	0.085(4)	0.018(3)	-0.002(4)	0.011(3)
C75	0.056(3)	0.039(3)	0.038(2)	-0.0005(19)	0.005(2)	-0.008(2)
C76	0.111(6)	0.058(4)	0.055(3)	-0.002(3)	-0.006(4)	-0.039(4)
C77	0.068(4)	0.067(5)	0.072(4)	0.002(3)	0.011(4)	0.009(3)
P1	0.0403(7)	0.0508(9)	0.0809(11)	0.0097(8)	0.0078(7)	-0.0031(6)
P2	0.0406(6)	0.0367(7)	0.0455(6)	-0.0001(5)	0.0079(5)	0.0061(5)

7.9 Crystal Structure Data of 9 (In Cooperation with Prof. Dieter Fenske, University of Karlsruhe, Germany).⁶

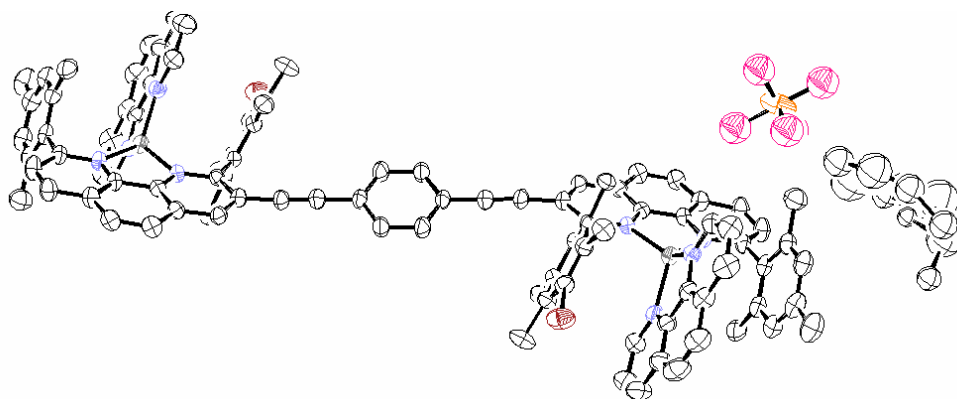


Figure 9-1.

Crystal Structure Data

Table 9-1: Crystal data and structure refinement for **9**.

Substance	9
Sum formula	Cu2P2Br2N8C116F6
Formula weight /g·mol ⁻¹	1968.167
Temperature /K	180 (2)
Wavelength /pm	71.073
Crystal system, space group	Triclinic, <i>P</i> -1
Unit cell dimensions	a = 10.4460 (21) Å b = 14.0790 (28) Å c = 16.8010 (34) Å B = 80.32 (3) °
Volume /Å ³	2425.2 (141)
Z, Calculated density /Mg·m ⁻³	1 /1.314
Absorption coefficient /mm ⁻¹	1.365
F(000)	974
Crystal size /mm ³	0.3 x 0.15 x 0.1
Reflections collected / unique / R _{int}	10608 / 8577 / 0.0277
Refinement method	Full-matrix least-squares on <i>F</i> ²
Data / restraints / parameters	10608 / 0 / 552
Goodness-of-fit on <i>F</i> ²	2.614
Final <i>R</i> indices [<i>I</i> >2σ(<i>I</i>)]	<i>R</i> 1 = 1084, <i>wR</i> 2 = 0.3341
<i>R</i> indices (all data)	<i>R</i> 1 = 0.1176, <i>wR</i> 2 = 0.3407

Table 9-2: Atomic coordinates (× 10⁵) and equivalent isotropic displacement parameters (Å² × 10⁴) for **9**. *U*(eq) is defined as one third of the trace of the orthogonalized *U*_{ij} tensor.

Atom	x	y	z
CU1	0.3074	0.7668	0.2889
P1	0.3121	0.2716	0.2531
BR1	-0.0336	0.8741	0.0473
N1	0.4257	0.7367	0.3732
N2	0.178	0.7889	0.3916
N3	0.3214	0.8737	0.1972
N4	0.3122	0.6841	0.1954
C1	0.6041	0.694	0.2756
C2	0.6312	0.7727	0.2194
C3	0.661	0.7589	0.1372
C4	0.6664	0.6681	0.1105
C5	0.6447	0.5897	0.1682
C6	0.6125	0.6015	0.2496
C7	0.6337	0.8718	0.2475
C8	0.6998	0.655	0.0218
C9	0.5845	0.5153	0.31
C10	0.5495	0.7076	0.3604
C11	0.6199	0.692	0.4262
C12	0.5589	0.7008	0.5035
C13	0.4265	0.7283	0.5176
C14	0.3544	0.7404	0.5974
C15	0.2276	0.7674	0.6071

Crystal Structure Data

C16	0.1628	0.7852	0.5368
C17	0.0319	0.8146	0.5429
C18	-0.0205	0.834	0.473
C19	0.0547	0.8188	0.3971
C20	0.2309	0.7756	0.4599
C21	0.3657	0.7463	0.4495
C22	-0.1498	0.8718	0.478
C23	-0.2535	0.9108	0.4831
C24	-0.378	0.9561	0.4918
C25	-0.4589	0.9506	0.5671
C26	-0.4192	1.0069	0.4249
C27	0.0089	0.8339	0.3184
C28	-0.0063	0.7536	0.2775
C29	-0.0179	0.7642	0.1961
C30	-0.0241	0.8565	0.1596
C31	-0.0248	0.9384	0.2014
C32	-0.003	0.9259	0.2819
C33	-0.007	0.6552	0.3217
C34	-0.0186	0.6778	0.1499
C35	-0.0445	1.038	0.1621
C36	0.0129	1.0124	0.3262
C37	0.3127	0.5893	0.1946
C38	0.3296	0.5427	0.1229
C39	0.3454	0.597	0.0498
C40	0.3434	0.6972	0.0485
C41	0.3579	0.7591	-0.0258
C42	0.3557	0.8531	-0.0245
C43	0.3403	0.8964	0.0505
C44	0.3374	0.9957	0.0559
C45	0.3274	1.0325	0.1306
C46	0.3217	0.9689	0.1989
C47	0.3297	0.8392	0.124
C48	0.3286	0.7369	0.123
C49	0.9825	0.4489	0.4497
C50	1.0829	0.5043	0.4801
C51	0.8697	0.4503	0.4634
C52	1.1073	0.4417	0.4269
C53	1.2069	0.4962	0.4554
C54	0.9987	0.3872	0.1449
C55	0.8181	0.3144	0.1818
C56	0.9262	0.3231	0.0921
C57	0.9702	0.4481	0.0584
C58	0.909	0.4153	0.2367
F1	0.3974	0.1782	0.2516
F2	0.3306	0.2781	0.1627
F3	0.2315	0.367	0.2526
F4	0.261	0.264	0.3546
F5	0.1941	0.2104	0.2578
F6	0.415	0.328	0.2734

Table 9-3: Anisotropic displacement parameters ($\text{\AA}^2 \times 10^4$) for **1**. The anisotropic displacement factor exponent takes the form: $\{-2 \pi^2 [h^2 a^{*2} U_{11} + \dots + 2 hka^*b^*U_{12}]\}$

Atom	U_{11}	U_{22}	U_{33}	U_{12}	U_{13}	U_{23}
CU1	0.03346	0.04395	0.03121	0.00185	-0.00654	-0.00613
P1	0.12961	0.05562	0.06323	-0.02309	-0.05567	0.00866
BR1	0.07398	0.07446	0.03942	-0.0148	-0.01743	0.01139
N1	0.02937	0.04013	0.0378	0.00343	-0.00871	-0.00854
N2	0.029	0.0316	0.0333	0.00408	-0.00711	-0.00512

Crystal Structure Data

N3	0.0368	0.03764	0.04436	-0.00012	-0.00145	-0.00618
N4	0.03222	0.03906	0.03246	-0.00014	-0.00804	-0.00326
C1	0.02599	0.05171	0.03967	0.00416	-0.0062	-0.01479
C2	0.0301	0.04999	0.05078	0.00041	-0.00238	-0.01271
C3	0.03922	0.06252	0.04968	0.00266	-0.00621	-0.00917
C4	0.03924	0.07739	0.04552	-0.0014	-0.00566	-0.01781
C5	0.03731	0.06483	0.05324	0.00277	-0.01007	-0.0203
C6	0.03361	0.04646	0.04919	0.00184	-0.00924	-0.01094
C7	0.04527	0.04331	0.07757	-0.00539	-0.00125	-0.00895
C8	0.05798	0.09954	0.04893	0.00341	-0.00542	-0.02729
C9	0.0668	0.05178	0.05997	-0.00097	-0.0072	-0.00371
C10	0.02668	0.04086	0.04375	0.00246	-0.00877	-0.00843
C11	0.03528	0.06537	0.05025	0.00916	-0.01595	-0.01705
C12	0.04064	0.05971	0.04763	0.00871	-0.01644	-0.00794
C13	0.03803	0.04668	0.0363	0.0025	-0.01325	-0.01052
C14	0.04951	0.04713	0.0377	0.00404	-0.01435	-0.00622
C15	0.05074	0.04683	0.03273	0.00392	-0.01049	-0.01119
C16	0.03838	0.03186	0.03595	0.0033	-0.00746	-0.00629
C17	0.03514	0.03314	0.04069	0.00282	-0.00063	-0.00731
C18	0.03221	0.038	0.03867	0.0048	-0.00455	-0.00782
C19	0.03074	0.02612	0.04078	0.00268	-0.00511	-0.00555
C20	0.03358	0.03022	0.03403	-0.00023	-0.0087	-0.00486
C21	0.03055	0.0337	0.03466	0.00307	-0.00824	-0.00719
C22	0.03433	0.04037	0.0441	0.00674	-0.00015	-0.00869
C23	0.03612	0.04092	0.04327	0.00546	-0.00495	-0.00857
C24	0.03031	0.03844	0.04178	0.0062	-0.00174	-0.00941
C25	0.04008	0.05209	0.03966	0.01223	-0.003	-0.0004
C26	0.03811	0.05071	0.0393	0.01068	0.00068	-0.00687
C27	0.02663	0.03132	0.03654	0.0027	-0.00357	-0.00181
C28	0.02644	0.03334	0.03845	0.00252	-0.00902	-0.00178
C29	0.03209	0.04197	0.03587	0.00035	-0.01145	-0.00411
C30	0.03716	0.05457	0.0316	-0.00311	-0.00842	0.00373
C31	0.04016	0.03855	0.04765	-0.00038	-0.00959	0.00716
C32	0.03547	0.03555	0.04253	0.00428	-0.00405	-0.00063
C33	0.0408	0.02935	0.04866	-0.00033	-0.00864	0.00109
C34	0.05314	0.0463	0.04469	-0.00154	-0.01703	-0.01094
C35	0.08838	0.042	0.06735	0.00431	-0.01928	0.01889
C36	0.05444	0.03364	0.06017	0.00164	-0.00416	-0.00882
C37	0.04161	0.04236	0.05155	-0.00137	-0.00993	-0.011
C38	0.06122	0.05439	0.05766	-0.00702	-0.01195	-0.02073
C39	0.06756	0.06347	0.0454	-0.01129	-0.0143	-0.02015
C40	0.04556	0.063	0.03984	-0.00634	-0.00777	-0.01125
C41	0.06456	0.07975	0.03821	-0.00681	-0.00979	-0.00547
C42	0.06632	0.08953	0.03819	-0.01372	-0.00977	0.00844
C43	0.0521	0.05758	0.04686	-0.00245	-0.00893	0.00902
C44	0.071	0.06062	0.07277	-0.00857	-0.00754	0.02234
C45	0.07456	0.04392	0.08234	-0.00241	-0.00244	0.00355
C46	0.05023	0.04339	0.06306	0.00221	-0.00339	-0.00151
C47	0.03638	0.0445	0.03987	-0.00312	-0.00544	0.00168
C48	0.03161	0.04714	0.03458	-0.00401	-0.00721	-0.00442

7.10 Crystal Structure Data of 10 (In Cooperation with Prof. Dieter Fenske, University of Karlsruhe, Germany).

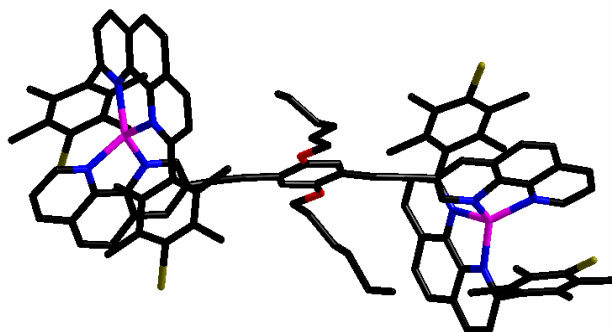


Figure 10-1. Stick representation of 10.

Table 10-1: Crystal data and structure refinement for 10.

Substance	10
Sum formula	C ₁₃₁ H ₁₃₄ Br ₄ Cu ₂ F ₁₂ N ₈ O ₂ P ₂
Formula weight /g·mol ⁻¹	2589.12
Temperature /K	373(2)
Wavelength	0.71073 Å
Crystal system, space group	Triclinic, <i>P</i> -1
Unit cell dimensions	a = 13.067 (8) Å b = 21.259 (15) Å c = 23.75 (2) Å β = 95.39 (3) °
Volume /Å ³	5995(8)
Z, Calculated density /Mg·m ⁻³	2, 1.434
Absorption coefficient /mm ⁻¹	1.788
F(000)	2664
Crystal size /mm ³	0.3 × 0.15 × 0.1
Reflections collected / unique / R _{int}	22023 / 7708 / 0.141
Refinement method	Full-matrix least-squares on <i>F</i> ²
Data / restraints / parameters	11341 / 0 / 1285
Goodness-of-fit on <i>F</i> ²	1.234
Final <i>R</i> indices [<i>I</i> > 2σ(<i>I</i>)]	<i>R</i> 1 = 0.1281, <i>wR</i> 2 = 0.296
<i>R</i> indices (all data)	<i>R</i> 1 = 0.2317, <i>wR</i> 2 = 0.3352

Crystal Structure Data

Table 10-2: Atomic coordinates ($\times 10^5$) and equivalent isotropic displacement parameters ($\text{\AA}^2 \times 10^4$) for **10**. $U(\text{eq})$ is defined as one third of the trace of the orthogonalized U_{ij} tensor.

Atom	x	y	z	U_{eq}
Cu1	1.62665(10)	-0.03955(8)	0.29525(7)	0.0847(5)
Cu2	1.17401(11)	0.70136(9)	0.89861(8)	0.0906(5)
Br1	1.83335(10)	-0.17795(9)	0.45012(8)	0.1133(6)
Br2	1.96698(10)	0.22728(9)	0.41409(9)	0.1220(6)
Br3	0.88888(11)	0.66431(10)	0.67457(9)	0.1216(6)
Br4	0.93727(13)	0.42957(9)	0.86475(9)	0.1225(6)
O1	1.3626(6)	0.2574(5)	0.4784(5)	0.095(3)
O2	1.4732(9)	0.4079(6)	0.7281(6)	0.121(3)
N1	1.5510(8)	0.0035(6)	0.2410(5)	0.096(3)
N2	1.5049(6)	-0.1134(5)	0.2543(5)	0.079(3)
N3	1.7760(7)	-0.0570(6)	0.3131(5)	0.082(3)
N4	1.6602(6)	0.0327(6)	0.3818(5)	0.090(3)
N5	1.0161(8)	0.6972(6)	0.8962(5)	0.084(3)
N6	1.1374(7)	0.6120(5)	0.8227(5)	0.087(3)
N7	1.2852(8)	0.7067(6)	0.9675(6)	0.102(3)
N8	1.2666(7)	0.7871(6)	0.9075(5)	0.088(3)
C1	1.7198(9)	-0.1803(8)	0.3931(7)	0.083(3)
C2	1.7142(8)	-0.2233(7)	0.3338(7)	0.078(3)
C3	1.6349(9)	-0.2261(7)	0.2886(7)	0.088(4)
C4	1.5579(8)	-0.1780(7)	0.3114(6)	0.078(3)
C5	1.5596(8)	-0.1394(7)	0.3722(6)	0.082(3)
C6	1.6432(9)	-0.1351(7)	0.4168(7)	0.088(4)
C7	1.7956(10)	-0.2750(8)	0.3080(8)	0.119(5)
C8	1.6283(9)	-0.2694(7)	0.2210(7)	0.096(4)
C9	1.4713(9)	-0.0925(7)	0.3956(6)	0.096(4)
C10	1.6538(10)	-0.0869(8)	0.4852(7)	0.107(4)
C11	1.4807(8)	-0.1690(7)	0.2654(6)	0.081(3)
C12	1.3880(9)	-0.2146(8)	0.2351(7)	0.097(4)
C13	1.3221(9)	-0.2010(8)	0.1935(7)	0.092(4)
C14	1.3495(8)	-0.1445(8)	0.1806(6)	0.086(4)
C15	1.2844(10)	-0.1241(9)	0.1370(7)	0.104(4)
C16	1.3076(10)	-0.0675(9)	0.1310(7)	0.103(4)
C17	1.4004(10)	-0.0199(8)	0.1649(6)	0.092(4)
C18	1.4229(10)	0.0467(9)	0.1631(6)	0.097(4)
C19	1.5116(9)	0.0891(8)	0.2012(7)	0.104(4)
C20	1.5780(10)	0.0664(8)	0.2389(6)	0.089(4)
C21	1.4629(8)	-0.0393(8)	0.2050(6)	0.088(4)
C22	1.4379(9)	-0.1013(7)	0.2116(6)	0.083(3)
C23	1.6715(8)	0.1076(7)	0.2771(7)	0.080(3)
C24	1.7684(9)	0.0851(8)	0.2641(7)	0.100(4)
C25	1.8582(8)	0.1216(8)	0.3060(7)	0.094(4)
C26	1.8467(9)	0.1786(8)	0.3563(8)	0.098(4)
C27	1.7506(9)	0.2059(7)	0.3704(7)	0.095(4)
C28	1.6642(8)	0.1676(8)	0.3275(7)	0.090(4)
C29	1.7778(9)	0.0203(7)	0.2051(7)	0.099(4)
C30	1.9629(9)	0.0954(8)	0.2937(7)	0.103(4)
C31	1.7435(11)	0.2714(8)	0.4255(7)	0.113(5)
C32	1.5567(9)	0.1932(7)	0.3428(7)	0.101(4)
C33	1.8256(8)	-0.1099(7)	0.2783(6)	0.087(4)
C34	1.9271(9)	-0.1160(7)	0.3008(7)	0.086(4)
C35	1.9731(9)	-0.0737(8)	0.3547(7)	0.087(4)
C36	1.9251(8)	-0.0169(8)	0.3928(7)	0.090(4)
C37	1.9700(9)	0.0358(7)	0.4527(7)	0.091(4)
C38	1.9164(8)	0.0866(7)	0.4879(7)	0.094(4)
C39	1.8084(9)	0.0865(7)	0.4640(7)	0.084(3)
C40	1.7527(8)	0.1392(7)	0.4999(6)	0.086(4)
C41	1.6495(8)	0.1373(7)	0.4740(6)	0.082(3)
C42	1.6067(8)	0.0842(8)	0.4169(6)	0.084(4)

Crystal Structure Data

C43	1.7660(8)	0.0389(7)	0.4069(6)	0.080(3)
C44	1.8203(8)	-0.0145(7)	0.3705(6)	0.076(3)
C45	1.5883(8)	0.1877(6)	0.5063(6)	0.083(4)
C46	1.5356(8)	0.2314(8)	0.5324(6)	0.087(4)
C47	1.4770(8)	0.2872(6)	0.5705(7)	0.083(4)
C48	1.5091(9)	0.3226(7)	0.6322(7)	0.084(3)
C49	1.4505(9)	0.3718(7)	0.6672(7)	0.081(3)
C50	1.3552(10)	0.3782(8)	0.6369(8)	0.100(4)
C51	1.3224(9)	0.3441(7)	0.5742(7)	0.090(4)
C52	1.3848(8)	0.2933(7)	0.5382(7)	0.083(4)
C53	1.2679(8)	0.2671(7)	0.4481(6)	0.095(4)
C54	1.2620(9)	0.2122(8)	0.3783(7)	0.105(4)
C55	1.2553(9)	0.1353(7)	0.3723(7)	0.093(4)
C56	1.2490(10)	0.0871(8)	0.3051(7)	0.098(4)
C57	1.2172(15)	0.0066(11)	0.2946(9)	0.146(6)
C58	1.2806(18)	-0.0129(11)	0.3348(10)	0.168(8)
C59	1.5689(13)	0.3986(11)	0.7592(8)	0.137(6)
C60	1.5627(14)	0.4483(15)	0.8263(11)	0.181(10)
C61	1.6516(16)	0.4503(14)	0.8645(13)	0.179(9)
C62	1.6422(14)	0.4955(13)	0.9358(8)	0.152(8)
C63	1.6393(13)	0.5734(12)	0.9522(10)	0.139(6)
C64	1.6462(12)	0.6102(10)	1.0239(9)	0.133(6)
C65	1.2878(10)	0.4286(8)	0.6749(7)	0.108(4)
C66	1.2294(10)	0.4652(7)	0.7037(7)	0.095(4)
C67	1.1593(9)	0.5073(8)	0.7378(7)	0.085(4)
C68	1.0509(9)	0.4861(7)	0.7239(6)	0.090(4)
C69	0.9879(9)	0.5334(8)	0.7604(7)	0.091(4)
C70	0.8709(9)	0.5123(8)	0.7449(7)	0.101(4)
C71	0.8140(10)	0.5633(8)	0.7849(7)	0.095(4)
C72	0.8575(10)	0.6214(8)	0.8326(8)	0.096(4)
C73	0.8013(11)	0.6761(9)	0.8744(8)	0.108(5)
C74	0.8495(10)	0.7317(9)	0.9243(9)	0.108(5)
C75	0.9603(10)	0.7447(7)	0.9351(7)	0.103(4)
C76	0.9703(9)	0.6406(8)	0.8490(7)	0.090(4)
C77	1.0322(8)	0.5937(7)	0.8108(6)	0.080(3)
C78	1.1986(9)	0.5691(7)	0.7872(7)	0.084(3)
C79	1.0505(10)	0.4994(8)	0.9094(7)	0.098(4)
C80	1.1459(11)	0.4860(9)	0.8905(7)	0.107(5)
C81	1.2335(10)	0.5403(8)	0.9247(7)	0.098(4)
C82	1.2112(10)	0.5998(8)	0.9683(7)	0.092(4)
C83	1.1153(10)	0.6138(8)	0.9905(7)	0.095(4)
C84	1.0308(12)	0.5610(8)	0.9581(7)	0.103(4)
C85	1.1626(14)	0.4172(8)	0.8414(7)	0.129(6)
C86	1.3388(10)	0.5286(8)	0.9038(7)	0.104(4)
C87	1.0984(11)	0.6779(8)	1.0404(7)	0.108(4)
C88	0.9179(10)	0.5721(8)	0.9747(7)	0.111(5)
C89	1.2941(10)	0.6621(7)	0.9937(7)	0.096(4)
C90	1.3751(12)	0.6729(9)	1.0422(7)	0.112(5)
C91	1.4481(11)	0.7319(9)	1.0631(9)	0.120(5)
C92	1.4374(11)	0.7767(8)	1.0346(7)	0.098(4)
C93	1.5099(9)	0.8395(8)	1.0515(7)	0.093(4)
C94	1.4969(10)	0.8823(8)	1.0210(8)	0.105(4)
C95	1.4160(10)	0.8655(7)	0.9729(7)	0.090(4)
C96	1.4008(10)	0.9051(8)	0.9367(8)	0.105(5)
C97	1.3229(11)	0.8855(7)	0.8881(8)	0.104(5)
C98	1.2549(9)	0.8231(8)	0.8737(7)	0.092(4)
C99	1.3425(9)	0.8057(7)	0.9545(6)	0.085(4)
C100	1.3563(9)	0.7623(8)	0.9862(6)	0.085(4)
C101	1.1678(9)	0.7942(8)	0.8202(7)	0.090(4)
C102	1.0695(10)	0.8170(8)	0.8299(7)	0.094(4)
C103	0.9912(10)	0.7794(9)	0.7826(8)	0.098(4)

Crystal Structure Data

C104	1.0061(10)	0.7216(8)	0.7323(7)	0.096(4)
C105	1.1034(10)	0.7001(9)	0.7200(7)	0.099(4)
C106	1.1849(10)	0.7383(8)	0.7659(8)	0.100(4)
C107	1.0538(10)	0.8781(8)	0.8866(8)	0.113(5)
C108	0.8743(9)	0.7996(9)	0.7897(9)	0.128(6)
C109	1.1176(12)	0.6402(9)	0.6646(7)	0.113(5)
C110	1.2957(10)	0.7216(8)	0.7577(8)	0.113(5)
C111	-0.0187(14)	0.0594(10)	0.8721(8)	0.144(6)
C112	0.0363(11)	0.1260(8)	0.8720(7)	0.109(4)
C113	0.1388(13)	0.1492(10)	0.9030(8)	0.131(5)
C114	0.1937(14)	0.2104(10)	0.9078(8)	0.136(6)
C115	0.1407(13)	0.2489(9)	0.8804(8)	0.125(5)
C116	0.0412(12)	0.2244(9)	0.8478(7)	0.118(5)
C117	-0.0124(11)	0.1625(9)	0.8442(7)	0.111(4)
C118	0.451(2)	0.4354(19)	0.3085(15)	0.246(12)
C119	0.4520(13)	0.3750(10)	0.2473(9)	0.133(5)
C120	0.4969(12)	0.3826(9)	0.2023(8)	0.124(5)
C121	0.4953(12)	0.3250(10)	0.1467(8)	0.124(5)
C122	0.4488(13)	0.2631(10)	0.1359(8)	0.133(5)
C123	0.4026(13)	0.2543(10)	0.1837(8)	0.133(5)
C124	0.4029(13)	0.3113(10)	0.2426(8)	0.129(5)
C125	0.0457(16)	0.4173(11)	0.5506(9)	0.154(7)
C126	-0.069(3)	0.422(2)	0.5663(16)	0.263(15)
C127	-0.1085(16)	0.3631(12)	0.5749(9)	0.157(7)
C128	-0.220(2)	0.3722(16)	0.5864(12)	0.209(10)
C129	-0.275(2)	0.4238(16)	0.5817(12)	0.199(9)
C130	-0.215(2)	0.4785(16)	0.5657(13)	0.221(11)
C131	-0.102(3)	0.4714(18)	0.5622(13)	0.219(11)
P1	0.8570(3)	0.2639(2)	0.6968(2)	0.0992(11)
P2	1.7679(3)	-0.0591(2)	-0.0234(2)	0.1043(12)
F1	0.9021(7)	0.2308(5)	0.6339(4)	0.146(3)
F2	0.8781(8)	0.3388(6)	0.6979(5)	0.151(3)
F3	0.7440(8)	0.2532(6)	0.6634(5)	0.159(4)
F4	0.8370(7)	0.1916(6)	0.7001(5)	0.151(3)
F5	0.9681(7)	0.2730(5)	0.7337(4)	0.130(3)
F6	0.8122(6)	0.2961(5)	0.7611(4)	0.124(3)
F7	1.7198(7)	-0.1336(6)	-0.0274(4)	0.146(3)
F8	1.8098(8)	0.0132(6)	-0.0189(5)	0.156(3)
F9	1.8787(7)	-0.0770(5)	-0.0118(4)	0.144(3)
F10	1.7713(7)	-0.0879(5)	-0.0955(5)	0.143(3)
F11	1.6520(6)	-0.0431(5)	-0.0364(4)	0.120(2)
F12	1.7604(6)	-0.0300(4)	0.0474(4)	0.109(2)

Table 10-3: Anisotropic displacement parameters ($\text{\AA}^2 \times 10^4$) for **10**. The anisotropic displacement factor exponent takes the form: $\{-2 \pi^2 [h^2 a^{*2} U_{11} + \dots + 2 hka^*b^*U_{12}]\}$

Atom	U_{11}	U_{22}	U_{33}	U_{23}	U_{13}	U_{12}
Cu1	0.0598(7)	0.0853(12)	0.1071(12)	0.0338(10)	0.0170(7)	0.0187(7)
Cu2	0.0734(8)	0.0768(12)	0.1222(13)	0.0374(10)	0.0232(8)	0.0159(7)
Br1	0.0733(8)	0.1290(15)	0.1445(14)	0.0657(12)	0.0057(8)	0.0047(8)
Br2	0.0765(8)	0.1153(14)	0.1722(16)	0.0596(12)	0.0060(9)	0.0028(8)
Br3	0.0927(9)	0.1189(15)	0.1605(15)	0.0661(12)	0.0064(9)	0.0121(8)
Br4	0.1259(12)	0.0976(14)	0.1430(14)	0.0520(11)	0.0087(10)	-0.0031(9)
O1	0.066(5)	0.106(8)	0.103(7)	0.026(6)	0.023(5)	0.032(4)
O2	0.126(8)	0.112(9)	0.122(9)	0.035(7)	0.050(7)	0.030(6)
N1	0.081(7)	0.092(9)	0.113(8)	0.027(7)	0.024(6)	0.055(6)
N2	0.062(5)	0.069(8)	0.097(7)	0.023(6)	0.006(5)	0.013(5)
N3	0.066(5)	0.085(8)	0.096(8)	0.031(7)	0.030(5)	0.022(5)
N4	0.052(5)	0.124(10)	0.124(8)	0.075(8)	0.026(5)	0.022(5)
N5	0.090(6)	0.061(8)	0.097(8)	0.024(7)	0.024(6)	0.018(6)

Crystal Structure Data

N6	0.056(5)	0.087(8)	0.120(8)	0.039(7)	0.020(5)	0.019(5)
N7	0.085(7)	0.075(9)	0.159(11)	0.056(9)	0.027(7)	0.015(6)
N8	0.073(6)	0.099(9)	0.098(8)	0.046(7)	0.015(6)	0.013(5)
C1	0.070(7)	0.093(11)	0.095(10)	0.046(9)	0.020(7)	0.002(7)
C2	0.055(6)	0.077(10)	0.112(11)	0.046(9)	0.014(7)	0.014(5)
C3	0.080(8)	0.063(9)	0.122(12)	0.035(9)	0.034(8)	0.004(6)
C4	0.072(7)	0.081(10)	0.083(9)	0.033(8)	0.017(6)	0.003(6)
C5	0.065(7)	0.093(11)	0.092(10)	0.041(8)	0.011(6)	0.013(6)
C6	0.074(7)	0.089(11)	0.106(11)	0.047(9)	0.015(7)	-0.002(7)
C7	0.080(8)	0.128(14)	0.170(14)	0.069(12)	0.044(9)	0.058(8)
C8	0.087(8)	0.085(11)	0.103(11)	0.021(9)	0.016(7)	0.021(7)
C9	0.077(7)	0.084(10)	0.122(11)	0.028(8)	0.029(7)	0.034(7)
C10	0.093(9)	0.122(14)	0.100(11)	0.045(10)	-0.001(8)	0.001(8)
C11	0.068(7)	0.089(11)	0.085(9)	0.029(8)	0.021(6)	0.019(7)
C12	0.070(7)	0.099(12)	0.117(11)	0.037(9)	0.020(7)	0.004(7)
C13	0.062(7)	0.095(12)	0.111(11)	0.031(9)	0.016(7)	0.014(7)
C14	0.060(7)	0.106(12)	0.089(9)	0.034(9)	0.009(6)	0.018(7)
C15	0.078(8)	0.106(14)	0.123(12)	0.036(11)	0.030(8)	0.014(8)
C16	0.067(8)	0.097(13)	0.141(13)	0.036(11)	0.028(8)	0.030(8)
C17	0.083(8)	0.101(13)	0.083(9)	0.022(9)	0.019(7)	0.025(8)
C18	0.094(9)	0.113(14)	0.089(10)	0.035(9)	0.030(8)	0.044(9)
C19	0.060(7)	0.137(14)	0.107(10)	0.038(10)	0.019(7)	0.021(8)
C20	0.097(9)	0.087(11)	0.095(10)	0.041(9)	0.033(8)	0.041(8)
C21	0.055(6)	0.111(13)	0.091(9)	0.030(9)	0.005(6)	0.026(7)
C22	0.068(7)	0.062(9)	0.111(10)	0.026(8)	0.016(7)	0.006(6)
C23	0.051(6)	0.081(10)	0.115(10)	0.044(9)	0.010(6)	0.015(6)
C24	0.074(8)	0.115(13)	0.140(12)	0.073(11)	0.043(8)	0.023(8)
C25	0.055(7)	0.097(12)	0.135(12)	0.049(10)	0.030(7)	0.013(7)
C26	0.063(7)	0.094(12)	0.141(12)	0.051(10)	0.020(7)	0.012(7)
C27	0.078(8)	0.075(11)	0.131(12)	0.037(9)	0.032(8)	0.009(7)
C28	0.061(7)	0.087(11)	0.129(11)	0.049(10)	0.019(7)	0.020(7)
C29	0.084(8)	0.081(11)	0.117(11)	0.016(9)	0.040(7)	0.025(7)
C30	0.066(7)	0.116(12)	0.139(12)	0.059(10)	0.022(7)	0.034(7)
C31	0.111(10)	0.075(12)	0.125(12)	0.010(10)	0.016(9)	0.003(8)
C32	0.067(7)	0.101(11)	0.126(11)	0.029(9)	0.034(7)	0.036(7)
C33	0.070(7)	0.069(9)	0.123(10)	0.033(8)	0.035(7)	0.010(6)
C34	0.065(7)	0.094(11)	0.096(10)	0.034(9)	0.004(7)	0.022(6)
C35	0.076(7)	0.096(11)	0.092(10)	0.037(9)	0.014(7)	0.035(7)
C36	0.057(6)	0.106(12)	0.114(11)	0.047(10)	0.013(7)	0.030(7)
C37	0.066(7)	0.079(10)	0.115(11)	0.026(9)	0.009(7)	0.011(6)
C38	0.060(6)	0.092(11)	0.137(11)	0.051(9)	0.017(7)	0.022(6)
C39	0.069(7)	0.075(10)	0.105(10)	0.026(8)	0.027(7)	0.029(6)
C40	0.066(6)	0.100(11)	0.106(9)	0.052(8)	0.025(6)	0.025(6)
C41	0.058(6)	0.081(10)	0.112(10)	0.038(9)	0.028(7)	0.024(6)
C42	0.053(6)	0.105(11)	0.085(9)	0.025(8)	0.014(6)	0.021(6)
C43	0.061(6)	0.081(10)	0.100(10)	0.035(8)	0.015(6)	0.020(6)
C44	0.070(6)	0.073(9)	0.079(9)	0.020(7)	0.015(6)	0.024(6)
C45	0.050(5)	0.064(9)	0.119(10)	0.017(7)	0.027(6)	0.010(5)
C46	0.061(6)	0.104(12)	0.100(9)	0.048(9)	0.006(6)	-0.004(7)
C47	0.063(6)	0.054(9)	0.127(12)	0.024(8)	0.038(7)	0.023(6)
C48	0.081(7)	0.073(10)	0.090(10)	0.018(8)	0.030(7)	0.017(6)
C49	0.085(8)	0.081(10)	0.078(9)	0.028(8)	0.021(7)	0.018(7)
C50	0.079(8)	0.083(11)	0.153(15)	0.053(11)	0.049(9)	0.032(7)
C51	0.086(8)	0.079(11)	0.094(10)	0.019(8)	0.021(7)	0.021(7)
C52	0.055(6)	0.076(10)	0.115(11)	0.026(8)	0.032(7)	0.027(6)
C53	0.063(7)	0.103(12)	0.113(11)	0.032(9)	0.013(7)	0.034(7)
C54	0.072(7)	0.119(14)	0.128(12)	0.052(11)	0.019(7)	0.020(7)

Crystal Structure Data

C55	0.088(8)	0.080(11)	0.107(11)	0.033(9)	0.013(7)	0.019(7)
C56	0.085(8)	0.105(13)	0.098(11)	0.033(9)	0.017(7)	0.020(7)
C57	0.151(15)	0.122(18)	0.149(16)	0.035(13)	0.007(12)	0.043(12)
C58	0.20(2)	0.119(18)	0.158(17)	0.033(14)	-0.014(15)	0.037(14)
C59	0.120(13)	0.172(19)	0.079(11)	0.010(11)	0.012(9)	0.001(12)
C60	0.088(11)	0.29(3)	0.18(2)	0.12(2)	0.008(12)	0.021(14)
C61	0.129(16)	0.21(3)	0.23(3)	0.13(2)	0.028(16)	-0.011(15)
C62	0.161(16)	0.19(2)	0.076(11)	0.033(13)	0.005(10)	-0.050(14)
C63	0.119(12)	0.131(18)	0.168(19)	0.064(15)	0.018(11)	-0.006(11)
C64	0.123(12)	0.127(16)	0.128(14)	0.033(12)	0.005(10)	0.014(10)
C65	0.080(8)	0.082(11)	0.143(13)	0.024(10)	0.019(8)	0.012(7)
C66	0.085(8)	0.066(10)	0.132(12)	0.031(8)	0.039(8)	0.023(7)
C67	0.076(7)	0.091(11)	0.104(10)	0.046(9)	0.034(7)	0.033(7)
C68	0.079(7)	0.088(10)	0.114(10)	0.048(9)	0.028(7)	0.022(7)
C69	0.068(7)	0.095(12)	0.122(11)	0.047(10)	0.035(7)	0.036(7)
C70	0.079(8)	0.122(13)	0.137(12)	0.079(11)	0.044(8)	0.038(8)
C71	0.086(8)	0.072(11)	0.124(12)	0.037(10)	0.014(8)	0.011(7)
C72	0.077(8)	0.070(11)	0.151(13)	0.044(10)	0.038(8)	0.031(7)
C73	0.083(9)	0.114(14)	0.150(14)	0.065(12)	0.044(9)	0.038(9)
C74	0.066(8)	0.109(14)	0.166(15)	0.068(12)	0.029(9)	0.029(8)
C75	0.098(9)	0.080(11)	0.149(13)	0.053(10)	0.043(9)	0.045(8)
C76	0.067(7)	0.095(12)	0.102(10)	0.030(9)	0.013(7)	0.030(7)
C77	0.062(6)	0.072(10)	0.111(10)	0.039(9)	0.020(7)	0.021(6)
C78	0.072(7)	0.075(10)	0.103(10)	0.029(9)	0.019(7)	0.021(7)
C79	0.088(8)	0.075(11)	0.148(13)	0.064(10)	0.013(8)	0.000(7)
C80	0.095(10)	0.120(14)	0.122(12)	0.059(11)	0.021(9)	0.036(9)
C81	0.097(9)	0.082(12)	0.123(12)	0.050(10)	0.011(9)	0.015(8)
C82	0.105(10)	0.066(11)	0.107(10)	0.032(9)	0.020(8)	0.028(8)
C83	0.079(8)	0.086(12)	0.137(12)	0.061(10)	0.026(8)	0.010(8)
C84	0.121(11)	0.074(12)	0.125(12)	0.041(10)	0.047(9)	0.041(9)
C85	0.188(16)	0.072(12)	0.112(12)	0.014(9)	0.013(11)	0.058(11)
C86	0.089(8)	0.097(11)	0.142(12)	0.056(10)	0.038(8)	0.041(8)
C87	0.110(10)	0.077(12)	0.126(12)	0.023(10)	0.035(9)	0.019(8)
C88	0.088(9)	0.107(13)	0.145(13)	0.055(11)	0.026(8)	0.007(8)
C89	0.086(8)	0.053(10)	0.137(12)	0.025(9)	0.009(8)	0.008(6)
C90	0.099(10)	0.123(15)	0.099(11)	0.024(10)	0.025(9)	0.028(10)
C91	0.088(9)	0.090(13)	0.181(17)	0.048(13)	0.035(10)	0.019(9)
C92	0.096(10)	0.088(12)	0.095(10)	0.019(9)	0.021(8)	0.025(8)
C93	0.073(7)	0.077(11)	0.110(11)	0.014(9)	0.032(7)	0.007(7)
C94	0.070(8)	0.114(13)	0.141(13)	0.059(11)	0.019(8)	0.023(7)
C95	0.075(8)	0.064(10)	0.130(12)	0.031(9)	0.035(8)	0.020(7)
C96	0.066(8)	0.121(14)	0.131(12)	0.049(11)	0.022(8)	0.021(8)
C97	0.084(8)	0.060(10)	0.177(15)	0.050(10)	0.041(10)	0.023(7)
C98	0.081(8)	0.093(11)	0.116(11)	0.048(10)	0.030(8)	0.038(8)
C99	0.077(8)	0.094(11)	0.094(10)	0.044(9)	0.025(7)	0.020(7)
C100	0.075(7)	0.092(11)	0.091(9)	0.036(9)	0.017(7)	0.031(7)
C101	0.069(7)	0.092(11)	0.130(12)	0.064(10)	0.018(8)	0.016(7)
C102	0.078(8)	0.084(11)	0.125(12)	0.042(10)	0.027(8)	0.010(7)
C103	0.088(9)	0.099(13)	0.127(13)	0.060(11)	0.028(9)	0.029(8)
C104	0.083(8)	0.102(13)	0.094(10)	0.031(9)	0.002(7)	0.017(8)
C105	0.072(8)	0.114(13)	0.118(12)	0.057(11)	0.000(8)	0.010(8)
C106	0.087(9)	0.083(11)	0.143(13)	0.054(10)	0.029(9)	0.031(8)
C107	0.087(8)	0.088(12)	0.153(13)	0.032(11)	0.040(9)	0.019(7)
C108	0.065(7)	0.125(14)	0.209(17)	0.075(13)	0.038(9)	0.034(8)
C109	0.120(11)	0.099(13)	0.110(12)	0.029(10)	0.011(9)	0.027(9)
C110	0.079(8)	0.112(13)	0.173(14)	0.069(11)	0.050(9)	0.051(8)
P1	0.0721(19)	0.090(3)	0.129(3)	0.038(3)	0.0094(19)	0.0107(17)

P2	0.072(2)	0.117(4)	0.124(3)	0.046(3)	0.0107(19)	0.025(2)
----	----------	----------	----------	----------	------------	----------

7.11 Crystal Structure Data of 11 (In Cooperation with Dr. Jan W. Bats, Johann Wolfgang Goethe-University, Frankfurt am Main, Germany).⁷

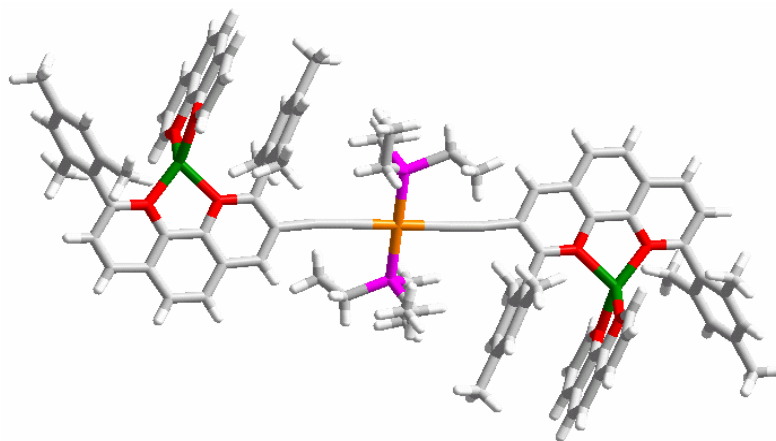


Figure 11-1. Stick representation of **11**.

Table 11-1: Crystal data and structure refinement for **11**.

Substance	11
Sum formula	Cu ₂ PtC ₁₁₄ H ₁₁₆ F ₁₂ N ₈ P ₄
Formula weight /g·mol ⁻¹	2272.20
Temperature /K	156(2)
Wavelength /pm	0.71073 Å
Crystal system, space group	Triclinic, <i>P</i> -1
Unit cell dimensions	a = 12.893 (3) Å b = 13.701 (3) Å c = 16.224 (3) Å β = 80.039 (17) °
Volume /Å ³	2650.4(9)
Z, Calculated density /Mg·m ⁻³	1, 1.424
Absorption coefficient /mm ⁻¹	1.847
F(000)	1160
Crystal size (mm)	0.32 x 0.20 x 0.10
Reflections collected / unique / R _{int}	29482 / 10610 / 0.0801
Refinement method	Full-matrix least-squares on <i>F</i> ²
Data / restraints / parameters	10610 / 0 / 644
Goodness-of-fit on <i>F</i> ²	0.998
Final <i>R</i> indices [<i>I</i> > 2σ(<i>I</i>)]	<i>R</i> 1 = 0.0592, <i>wR</i> 2 = 0.1195
<i>R</i> indices (all data)	<i>R</i> 1 = 0.1143, <i>wR</i> 2 = 0.1361
Largest diff. peak and hole	1.814 and -0.725 e/Å ³

Table 11-2: Atomic coordinates (× 10⁵) and equivalent isotropic displacement parameters (Å² × 10⁴) for **11**.

U(eq) is defined as one third of the trace of the orthogonalized *U*_{ij} tensor.

Atom	x	y	z	<i>U</i> _{eq.}
Pt(1)	0	0	0	386(1)
Cu(1)	15511(6)	-28470(6)	51517(5)	435(2)
P(1)	-17671(13)	-559(14)	201(10)	441(4)
N(4)	30120(40)	-25590(40)	49500(30)	334(11)
P(2)	-53697(14)	-8813(14)	72589(12)	506(5)
C(2)	-1010(50)	-8090(50)	20220(40)	371(15)
C(15)	17420(40)	-18660(50)	30220(30)	314(14)
C(5)	-5950(40)	-18720(40)	46800(30)	328(14)
N(1)	4470(40)	-20230(40)	42710(30)	339(12)
C(1)	-490(40)	-5060(40)	12510(40)	339(14)
C(6)	-7280(50)	-22540(40)	55820(30)	329(14)
F(5)	-41680(30)	-8000(40)	72320(30)	759(13)
N(2)	1940(40)	-27310(40)	59850(30)	367(12)
C(49)	37760(50)	-32580(50)	45410(40)	404(16)
C(24)	10960(50)	-35260(50)	72570(30)	359(15)
N(3)	24320(50)	-42060(40)	47760(40)	551(16)

Crystal Structure Data

C(29)	16470(50)	-28390(50)	73870(40)	389(15)
C(48)	33340(50)	-17520(50)	50380(40)	491(17)
C(3)	-2900(50)	-11720(40)	29340(30)	337(14)
F(2)	-54240(40)	-11800(50)	82640(30)	1290(20)
C(14)	-13450(50)	-10130(40)	33590(30)	361(15)
C(20)	23270(50)	-11540(50)	30070(40)	385(15)
C(11)	-26980(50)	-16030(40)	55590(40)	377(15)
C(28)	25920(50)	-32610(50)	77930(40)	444(16)
C(13)	-15200(50)	-13560(40)	42440(40)	334(14)
C(4)	5940(40)	-16800(40)	34350(30)	312(13)
C(17)	32750(50)	-28800(50)	22690(40)	425(16)
C(27)	29790(50)	-43120(50)	80700(40)	456(17)
C(18)	38820(50)	-21800(50)	22330(40)	449(17)
C(50)	34580(60)	-41440(50)	44530(40)	497(18)
C(9)	-18600(50)	-25440(50)	69030(40)	413(15)
F(6)	-65710(30)	-9540(30)	73110(40)	1110(20)
F(1)	-52780(30)	-5370(30)	62490(30)	774(13)
C(12)	-25820(50)	-12360(50)	47200(40)	367(15)
C(7)	830(50)	-30790(40)	68240(40)	356(14)
F(4)	-58480(30)	3120(30)	73020(30)	735(12)
C(16)	22010(50)	-27280(50)	26490(40)	405(16)
F(3)	-48970(30)	-20620(30)	71790(30)	861(15)
C(45)	48500(50)	-31440(60)	42210(40)	538(19)
C(26)	24230(50)	-49670(50)	79300(40)	491(18)
C(10)	-17790(50)	-21410(40)	60250(40)	348(14)
C(25)	14860(50)	-46020(50)	75250(40)	457(17)
C(19)	34030(50)	-13320(50)	26120(40)	460(17)
C(8)	-9490(50)	-30160(50)	72970(40)	407(15)
C(21)	15480(60)	-34850(50)	26520(50)	584(19)
C(37)	-24250(50)	-6610(50)	10200(40)	485(17)
C(23)	18380(50)	-2020(50)	33820(40)	508(18)
C(31)	40130(50)	-47210(60)	85180(50)	660(20)
C(22)	50390(50)	-23280(60)	17890(50)	650(20)
C(32)	12330(60)	-16790(50)	71310(50)	573(19)
C(47)	43620(60)	-15720(60)	47260(50)	610(20)
C(46)	51030(60)	-22540(70)	43160(50)	670(20)
C(30)	9040(70)	-53430(60)	73740(50)	730(20)
C(42)	42130(90)	-49100(70)	40440(50)	750(30)
C(44)	55890(70)	-39370(80)	38080(50)	780(30)
C(38)	-19610(60)	-18220(50)	12870(40)	575(19)
C(57)	76320(110)	-53360(110)	91790(80)	1200(40)
C(35)	-26490(60)	12570(60)	-2070(60)	760(30)
C(39)	21290(90)	-50190(70)	47110(60)	890(30)
C(56)	68120(110)	-45230(120)	88640(70)	1230(40)
C(33)	-19410(70)	-6770(80)	-8110(50)	840(30)
C(53)	82400(300)	-44000(300)	98440(180)	2700(200)
C(43)	52710(100)	-47820(80)	37450(50)	960(40)
C(41)	38460(130)	-57630(90)	39820(70)	1150(50)
C(40)	28380(140)	-58070(90)	42970(90)	1300(60)
C(36)	-25490(80)	19310(70)	3470(70)	1190(40)
C(52)	83060(170)	-52900(200)	97020(110)	1590(90)
C(55)	66510(120)	-35610(110)	90580(80)	1360(50)
C(34)	-31420(110)	-7140(110)	-7900(70)	1630(60)
C(51)	92410(120)	-61700(150)	100910(100)	2370(100)
C(54)	74400(200)	-35600(200)	96180(120)	2370(160)

Crystal Structure Data

Table 11-3. Anisotropic displacement parameters ($\text{\AA}^2 \times 10^4$) for **11**. The anisotropic displacement factor exponent takes the form: $\{-2 \pi^2 [h^2 a^{*2} U_{11} + \dots + 2 hka^*b^*U_{12}]\}$.

Atom	U_{11}	U_{22}	U_{33}	U_{23}	U_{13}	U_{12}
Pt(1)	274(2)	506(3)	298(2)	-20(2)	-52(2)	-15(2)
Cu(1)	291(4)	533(5)	431(5)	31(4)	-105(4)	-97(4)
P(1)	331(9)	583(12)	352(9)	5(8)	-85(7)	-82(9)
N(4)	290(30)	310(30)	400(30)	-110(20)	-90(20)	-20(20)
P(2)	292(9)	548(12)	581(12)	-41(9)	8(8)	-50(9)
C(2)	250(30)	430(40)	400(40)	-100(30)	-70(30)	-10(30)
C(15)	240(30)	350(40)	290(30)	20(30)	-80(20)	-20(30)
C(5)	220(30)	420(40)	330(30)	-20(30)	-60(30)	-90(30)
N(1)	240(30)	380(30)	360(30)	10(20)	-60(20)	-80(20)
C(1)	220(30)	340(30)	420(40)	-110(30)	-30(30)	30(30)
C(6)	290(30)	390(40)	310(30)	-10(30)	-70(30)	-120(30)
F(5)	400(20)	1000(30)	1010(30)	-510(30)	-140(20)	-80(20)
N(2)	310(30)	440(30)	340(30)	20(20)	-100(20)	-110(20)
C(49)	350(40)	470(40)	340(30)	-80(30)	-140(30)	30(30)
C(24)	340(30)	440(40)	260(30)	20(30)	-60(30)	-100(30)
N(3)	780(50)	370(30)	630(40)	10(30)	-380(30)	-260(30)
C(29)	360(40)	420(40)	360(30)	-70(30)	-40(30)	-60(30)
C(48)	450(40)	550(50)	510(40)	-130(30)	-120(30)	-120(40)
C(3)	300(30)	370(40)	310(30)	-10(30)	-110(30)	-50(30)
F(2)	910(40)	1530(50)	660(30)	170(30)	180(30)	430(40)
C(14)	270(30)	450(40)	330(30)	-30(30)	-110(30)	-20(30)
C(20)	260(30)	440(40)	380(40)	30(30)	-80(30)	-30(30)
C(11)	310(30)	440(40)	370(40)	-60(30)	-50(30)	-110(30)
C(28)	370(40)	520(40)	470(40)	-140(30)	-130(30)	-80(30)
C(13)	310(30)	340(30)	360(30)	-20(30)	-100(30)	-110(30)
C(4)	290(30)	320(30)	330(30)	-30(30)	-100(30)	-80(30)
C(17)	380(40)	430(40)	400(40)	-90(30)	-90(30)	50(30)
C(27)	330(40)	560(50)	420(40)	-90(30)	-110(30)	20(30)
C(18)	260(30)	530(40)	400(40)	30(30)	-50(30)	40(30)
C(50)	630(50)	380(40)	440(40)	-70(30)	-250(40)	40(40)
C(9)	400(40)	490(40)	350(40)	-50(30)	0(30)	-160(30)
F(6)	290(20)	670(30)	2290(60)	-160(30)	-30(30)	-170(20)
F(1)	720(30)	840(30)	650(30)	-210(20)	-200(20)	110(20)
C(12)	230(30)	450(40)	400(40)	-80(30)	-80(30)	-40(30)
C(7)	390(40)	340(30)	330(30)	40(30)	-90(30)	-150(30)
F(4)	580(30)	620(30)	900(30)	-270(20)	90(20)	10(20)
C(16)	350(40)	440(40)	350(30)	50(30)	-110(30)	-60(30)
F(3)	470(30)	460(30)	1560(40)	-160(30)	-90(30)	-10(20)
C(45)	380(40)	670(50)	400(40)	-50(40)	-90(30)	110(40)
C(26)	550(50)	380(40)	450(40)	-20(30)	-150(30)	20(30)
C(10)	370(40)	350(30)	350(30)	-60(30)	-40(30)	-120(30)
C(25)	470(40)	470(40)	420(40)	30(30)	-150(30)	-140(30)
C(19)	350(40)	490(40)	490(40)	40(30)	-110(30)	-110(30)
C(8)	450(40)	500(40)	260(30)	30(30)	-40(30)	-200(30)
C(21)	550(50)	540(50)	680(50)	-150(40)	-100(40)	-130(40)
C(37)	330(40)	630(50)	440(40)	-50(30)	-70(30)	-80(30)
C(23)	320(40)	440(40)	740(50)	-90(40)	-60(30)	-90(30)
C(31)	420(40)	790(50)	700(50)	-150(40)	-260(40)	90(40)
C(22)	310(40)	680(50)	730(50)	10(40)	10(30)	30(40)
C(32)	520(40)	440(40)	820(50)	-120(40)	-280(40)	-90(30)
C(47)	500(50)	820(60)	660(50)	-190(40)	-80(40)	-360(50)
C(46)	430(50)	1020(70)	610(50)	-100(50)	-90(40)	-300(50)
C(30)	770(60)	500(50)	960(60)	50(40)	-340(50)	-270(40)

Crystal Structure Data

C(42)	1020(80)	600(60)	480(50)	-170(40)	-290(50)	230(60)
C(44)	500(50)	1020(70)	500(50)	-100(50)	-90(40)	310(50)
C(38)	520(50)	620(50)	550(40)	-40(40)	-120(40)	-120(40)
C(57)	1040(90)	1660(120)	970(90)	-480(80)	-60(70)	-290(90)
C(35)	350(40)	730(60)	880(60)	230(50)	-130(40)	40(40)
C(39)	1190(80)	520(60)	1040(70)	10(50)	-640(60)	-180(60)
C(56)	1170(110)	1570(120)	1040(90)	-440(90)	-200(80)	-310(90)
C(33)	900(60)	1520(80)	400(40)	-120(50)	-160(40)	-780(60)
C(53)	2200(300)	4700(600)	1440(190)	600(300)	-600(170)	-1900(400)
C(43)	1110(90)	860(70)	430(50)	-130(50)	-230(50)	570(70)
C(41)	1880(140)	550(70)	960(80)	-280(60)	-800(100)	260(90)
C(40)	2160(160)	530(70)	1470(120)	-280(70)	-1160(130)	-150(100)
C(36)	1010(80)	610(60)	1600(110)	-170(70)	180(70)	80(60)
C(52)	1310(130)	3000(300)	850(100)	-450(140)	210(90)	-1380(170)
C(55)	1710(130)	1100(100)	1070(100)	-300(80)	570(90)	-380(90)
C(34)	2050(150)	2030(140)	1170(100)	70(90)	-780(100)	-1050(120)
C(51)	1240(130)	3400(300)	1670(150)	190(150)	-550(110)	200(140)
C(54)	3900(400)	3500(300)	1180(140)	-1500(190)	1030(180)	-3100(300)

7.12 Crystal Structure Data of **12** (In Cooperation with Dr. Jan W. Bats, Johann Wolfgang Goethe-University, Frankfurt am Main, Germany).⁸

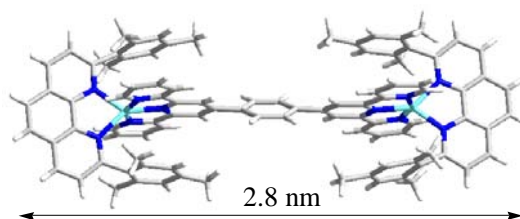


Figure 12-1. Stick representation of **12**.

Table 12-1: Crystal data and structure refinement for **12**.

Substance	12
Sum formula	Zn ₂ C ₁₀₀ H ₈₀ F ₁₂ N ₁₀ O ₁₂ S ₄
Formula weight /g·mol ⁻¹	2100.72
Temperature /K	-156(2)
Wavelength /pm	71.073
Crystal system, space group	Triclinic, <i>P</i> -1
Unit cell dimensions	a = 11.521 (2) Å b = 17.185 (4) Å c = 18.164 (4) Å B = 94.469 (19) °
Volume /Å ³	3074.0 (11)
Z, Calculated density /Mg·m ⁻³	1, 1.135
Absorption coefficient /mm ⁻¹	0.529
F(000)	1078
Crystal size /mm ³	0.36 × 0.32 × 0.10
Reflections collected / unique / R _{int}	30425 / 11341 / 0.1577
Refinement method	Full-matrix least-squares on <i>F</i> ²
Data / restraints / parameters	11341 / 4 / 637
Goodness-of-fit on <i>F</i> ²	0.988
Final <i>R</i> indices [<i>I</i> > 2σ(<i>I</i>)]	<i>R</i> 1 = 0.1166, <i>wR</i> 2 = 0.2564
<i>R</i> indices (all data)	<i>R</i> 1 = 0.2382, <i>wR</i> 2 = 0.2930
Extinction coefficient	0.0039(7)
Largest diff. peak and hole	1.069 and -0.690 e/Å ³

Table 12-2: Atomic coordinates (× 10⁵) and equivalent isotropic displacement parameters (Å² × 10⁴) for **12**. *U*(eq) is defined as one third of the trace of the orthogonalized *U*_{ij} tensor.

Atom	x	y	z	U _{eq}
Zn	74098(10)	48050(7)	24279(7)	221(4)
S(1)	82420(30)	78600(30)	66330(20)	677(11)
S(2)	73420(60)	121320(40)	90460(40)	1480(20)
N(1)	80200(60)	61710(50)	30450(40)	114(16)
N(3)	89340(60)	51580(50)	19000(40)	217(18)
N(2)	61640(70)	51220(50)	32920(50)	270(20)
N(5)	77200(60)	37230(50)	25110(50)	212(18)
C(45)	89090(90)	50950(70)	42470(60)	300(30)
N(4)	60930(70)	37880(60)	14660(50)	320(20)
C(18)	93670(90)	46040(70)	12920(60)	390(30)
C(36)	63360(80)	50930(70)	7790(50)	300(30)
C(31)	54770(90)	48270(60)	11030(60)	300(30)
C(14)	94790(90)	60400(70)	22250(60)	340(30)
C(7)	89990(80)	66540(60)	29100(60)	240(20)
C(15)	105140(90)	64340(70)	19370(60)	380(30)
O(1)	79990(80)	69290(60)	62480(60)	860(30)
C(12)	44450(90)	47770(70)	39040(60)	340(30)
C(40)	94910(90)	46990(70)	36560(70)	440(30)

Crystal Structure Data

C(5)	79340(90)	75180(70)	41420(60)	400(30)
C(6)	74580(80)	66060(60)	36600(60)	280(20)
C(19)	59840(90)	29280(60)	13580(60)	280(20)
O(2)	95590(80)	83930(60)	68280(70)	1090(40)
C(3)	95260(100)	90250(80)	45090(70)	520(30)
C(30)	69290(100)	28980(70)	19380(50)	360(30)
C(9)	64070(90)	60070(60)	37430(60)	260(20)
C(8)	95030(80)	75820(60)	33650(60)	340(30)
C(32)	48380(90)	53630(70)	16050(60)	360(30)
C(17)	103340(100)	48970(80)	9730(70)	550(30)
C(1)	104950(120)	105140(80)	46150(80)	750(40)
C(26)	69400(120)	20630(70)	18870(70)	520(30)
C(20)	52370(100)	38540(60)	9500(60)	390(30)
C(11)	47200(100)	56640(90)	43580(70)	510(30)
C(33)	52440(100)	62820(70)	18800(60)	410(30)
C(4)	89750(90)	80230(60)	39670(70)	420(30)
C(29)	86040(90)	37340(70)	30320(60)	370(30)
C(28)	87340(100)	28860(80)	29870(70)	450(30)
C(48)	79430(100)	48070(70)	45570(60)	530(30)
C(34)	62830(110)	66720(70)	16160(70)	460(30)
C(2)	100220(110)	95860(70)	41620(70)	540(30)
C(16)	109110(100)	58310(80)	13370(70)	530(30)
F(3)	81920(110)	90100(70)	81360(60)	1670(60)
C(13)	52680(100)	45440(70)	33740(60)	390(30)
O(3)	74550(90)	81870(80)	62670(60)	1050(30)
C(22)	42470(120)	22060(80)	2800(80)	680(40)
C(43)	107010(170)	65630(120)	45830(120)	910(60)
C(41)	105960(100)	50340(110)	34590(80)	660(40)
C(39)	69920(100)	46500(80)	1510(60)	580(40)
C(35)	67850(100)	61690(70)	11170(60)	440(30)
C(10)	57050(90)	63420(80)	43370(70)	500(30)
C(21)	42510(120)	30840(90)	3780(70)	680(40)
C(23)	51220(110)	21430(70)	8110(70)	440(30)
C(25)	60230(130)	12590(80)	12460(70)	590(40)
C(37)	37600(100)	49130(80)	18990(70)	640(40)
O(5)	75510(100)	125200(80)	99860(70)	1660(60)
O(6)	86600(130)	121410(100)	88330(100)	1900(60)
C(44)	96680(150)	61710(100)	47690(80)	790(40)
F(4)	53480(120)	108200(70)	87910(80)	1940(60)
C(42)	111760(120)	59940(130)	39550(110)	870(60)
C(46)	110920(120)	44160(110)	27660(90)	1080(60)
C(27)	78930(120)	20500(90)	24210(80)	620(40)
C(49)	79200(200)	80730(180)	76520(120)	1220(70)
F(1)	68860(120)	76210(70)	76340(70)	1950(70)
C(38)	67470(120)	77360(90)	19490(80)	920(50)
O(4)	63780(150)	122130(140)	85770(140)	3060(150)
C(24)	50930(130)	12760(90)	7550(90)	700(40)
F(2)	87380(130)	78760(80)	80690(70)	1650(50)
F(6)	64710(120)	104210(80)	79500(70)	2100(60)
C(50)	66870(180)	109100(120)	88290(120)	2600(200)
C(47)	115000(150)	75020(110)	50440(110)	1320(70)
F(5)	72100(300)	106800(300)	92100(300)	6400(400)

Table 12-3: Anisotropic displacement parameters ($\text{\AA}^2 \times 10^4$) for **12**. The anisotropic displacement factor exponent takes the form: $\{-2 \pi^2 [h^2 a^{*2} U_{11} + \dots + 2 hka^*b^*U_{12}]\}$

Atom	U_{11}	U_{22}	U_{33}	U_{23}	U_{13}	U_{12}
Zn	210(6)	261(7)	271(7)	163(6)	128(5)	111(5)
S(1)	600(20)	620(30)	720(30)	310(20)	200(20)	50(20)
S(2)	1160(50)	1110(40)	1620(60)	180(40)	630(40)	210(40)
N(1)	60(40)	360(50)	40(40)	160(30)	-10(30)	140(30)

Crystal Structure Data

N(3)	240(50)	220(50)	250(50)	130(40)	140(40)	100(40)
N(2)	200(50)	250(50)	330(50)	140(40)	70(40)	0(40)
N(5)	110(40)	370(50)	280(50)	260(40)	50(40)	80(40)
C(45)	530(70)	550(80)	310(60)	410(60)	350(60)	480(60)
N(4)	160(40)	510(60)	280(50)	190(50)	30(40)	100(40)
C(18)	410(70)	460(70)	460(70)	320(60)	180(60)	160(60)
C(36)	140(50)	770(90)	40(50)	170(50)	50(40)	250(50)
C(31)	280(60)	380(70)	270(60)	240(50)	-110(50)	50(50)
C(14)	420(70)	370(70)	340(60)	230(50)	90(50)	180(50)
C(7)	170(50)	270(60)	310(60)	120(50)	190(50)	100(40)
C(15)	270(60)	440(70)	510(70)	290(60)	260(50)	90(50)
O(1)	750(70)	660(70)	1120(80)	520(60)	180(60)	-40(50)
C(12)	320(60)	450(80)	190(60)	140(60)	120(50)	20(60)
C(40)	250(60)	520(80)	590(80)	450(70)	-50(60)	-120(60)
C(5)	420(70)	360(70)	430(70)	150(60)	250(60)	150(60)
C(6)	360(60)	170(60)	390(60)	140(50)	240(50)	150(50)
C(19)	410(60)	210(60)	280(60)	150(50)	130(50)	90(50)
O(2)	450(60)	1010(80)	1460(90)	290(70)	230(60)	140(50)
C(3)	450(70)	590(80)	490(80)	240(70)	330(60)	50(60)
C(30)	470(70)	530(80)	0(50)	80(50)	110(50)	100(60)
C(9)	330(60)	210(60)	200(60)	70(50)	80(50)	40(50)
C(8)	280(60)	330(70)	400(70)	110(50)	290(50)	130(50)
C(32)	280(60)	550(80)	230(60)	70(60)	160(50)	280(60)
C(17)	410(70)	720(100)	570(80)	340(70)	360(70)	120(70)
C(1)	1130(120)	290(70)	750(100)	210(70)	480(90)	70(70)
C(26)	740(90)	120(60)	620(90)	60(60)	310(80)	150(60)
C(20)	430(70)	190(60)	290(70)	-70(50)	230(60)	-40(50)
C(11)	430(70)	810(100)	390(70)	300(70)	280(60)	300(70)
C(33)	490(70)	430(80)	170(60)	-70(50)	50(50)	300(60)
C(4)	360(60)	220(60)	550(70)	140(60)	100(60)	-60(50)
C(29)	400(70)	650(80)	330(70)	370(60)	280(60)	310(60)
C(28)	440(70)	640(90)	440(80)	310(70)	100(60)	330(70)
C(48)	690(90)	610(80)	290(70)	280(60)	10(60)	120(70)
C(34)	580(80)	320(70)	370(70)	100(60)	100(60)	30(60)
C(2)	770(90)	440(80)	360(70)	170(60)	260(70)	80(70)
C(16)	370(70)	570(80)	860(100)	470(80)	420(70)	170(60)
F(3)	2180(130)	950(70)	1140(80)	-100(70)	850(80)	250(80)
C(13)	500(70)	370(70)	260(60)	90(50)	-10(60)	220(60)
O(3)	860(70)	1730(100)	1030(80)	840(80)	280(60)	800(70)
C(22)	810(100)	560(90)	520(80)	400(70)	10(80)	-210(70)
C(43)	870(140)	890(140)	840(130)	600(120)	-220(110)	-140(110)
C(41)	240(70)	1600(150)	620(90)	980(100)	180(70)	210(90)
C(39)	590(80)	940(100)	280(70)	220(70)	210(60)	420(70)
C(35)	440(70)	390(70)	400(70)	150(60)	150(60)	60(60)
C(10)	310(70)	460(70)	570(80)	160(60)	60(60)	-10(60)
C(21)	650(90)	660(100)	540(90)	340(80)	-180(70)	-110(80)
C(23)	590(80)	240(70)	310(70)	40(60)	30(60)	20(60)
C(25)	940(110)	380(80)	470(80)	210(70)	230(80)	160(80)
C(37)	480(80)	970(100)	630(90)	450(80)	190(70)	300(70)
O(5)	1040(90)	1400(100)	1010(90)	-530(80)	490(70)	-210(80)
O(6)	1480(120)	1970(140)	2400(160)	1010(120)	1300(120)	500(100)
C(44)	1210(140)	930(120)	650(100)	570(90)	220(100)	620(110)
F(4)	1630(110)	1120(80)	1940(120)	-10(80)	640(100)	-130(80)
C(42)	310(80)	1340(150)	1100(140)	1160(130)	-350(90)	-400(100)
C(46)	480(90)	1770(170)	1100(130)	820(130)	330(90)	210(100)
C(27)	670(90)	820(110)	580(90)	440(80)	80(80)	390(80)
C(49)	1030(160)	2100(200)	900(150)	990(170)	250(130)	530(170)

Crystal Structure Data

F(1)	1960(120)	1450(90)	1410(90)	220(70)	1210(100)	-520(90)
C(38)	680(100)	1210(140)	660(100)	250(100)	100(80)	290(100)
O(4)	1180(120)	3200(200)	3800(300)	400(200)	-700(150)	1540(150)
C(24)	650(100)	480(90)	700(100)	130(80)	30(80)	50(70)
F(2)	1990(130)	2110(130)	1220(90)	1110(90)	550(90)	550(100)
F(6)	2130(130)	1670(110)	1320(100)	90(90)	420(100)	-170(100)
C(50)	1300(180)	1800(200)	1440(180)	-1320(180)	1170(160)	-1070(170)
C(47)	1030(140)	1170(150)	1410(160)	780(130)	-370(120)	-300(120)
F(5)	6600(500)	12500(900)	8800(700)	9400(800)	5300(500)	7700(600)

7.13 Crystal Structure Data of 13 (In Cooperation with Dr. Jan W. Bats, Johann Wolfgang Goethe-University, Frankfurt am Main, Germany).⁹

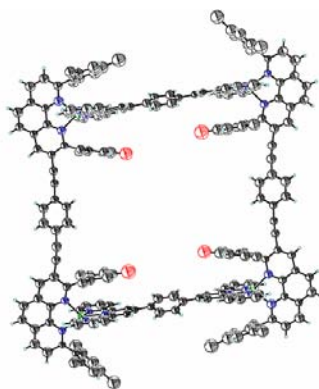


Figure 13-1.

Table 13-1: Crystal data and structure refinement for **13**.

Substance	13
Sum formula	Zn ₄ C ₂₁₆ H ₁₅₆ F ₂₄ N ₂₀ O ₂₈ S ₈
Formula weight /g·mol ⁻¹	4453.57
Temperature /K	157(2) K
Wavelength /pm	0.71073 Å
Crystal system, space group	Monoclinic, <i>P</i> 21/n
Unit cell dimensions	a = 21.715 (6) Å b = 19.196 (6) Å c = 28.620 (7) Å $\beta = 94.851(17)^\circ$
Volume /Å ³	11887 (5)
Z, Calculated density /Mg·m ⁻³	2, 1.244
Absorption coefficient /mm ⁻¹	0.552
F(000)	4560
Crystal size (mm)	0.50 x 0.35 x 0.20
Reflections collected / unique / R _{int}	101150 / 17215 / 0.2147
Refinement method	Full-matrix least-squares on <i>F</i> ²
Data / restraints / parameters	17215 / 0 / 643
Goodness-of-fit on <i>F</i> ²	1.638
Final <i>R</i> indices [<i>I</i> > 2σ(<i>I</i>)]	<i>R</i> 1 = 0.2315, <i>wR</i> 2 = 0.3967
<i>R</i> indices (all data)	<i>R</i> 1 = 0.3733, <i>wR</i> 2 = 0.4456
Largest diff. peak and hole	1.272 and -0.556 e/Å ³

Table 13-2: Atomic coordinates (× 10⁵) and equivalent isotropic displacement parameters (Å² × 10⁴) for **13**. *U*(eq) is defined as one third of the trace of the orthogonalized *U*_{ij} tensor.

Atom	x	y	z	U _{eq}
Zn(2)	72125(10)	8470(11)	31247(7)	545(7)
Zn(1)	128159(10)	73154(11)	16473(7)	477(7)
N(9)	71390(60)	23910(70)	76460(40)	430(40)
C(100)	67480(70)	24660(70)	68890(50)	330(40)
N(10)	64110(60)	32510(70)	80040(50)	420(40)
C(101)	67330(80)	26340(90)	73290(60)	460(50)
N(5)	79380(60)	1860(70)	34440(50)	480(40)
C(77)	76770(70)	9410(80)	45930(50)	340(40)
N(2)	124140(60)	64530(70)	13200(50)	490(40)
C(47)	67820(80)	-3000(90)	18660(60)	460(50)
C(52)	74670(80)	6590(90)	21680(60)	520(50)
C(76)	76550(80)	7980(90)	41280(60)	430(50)
N(6)	72400(60)	10830(60)	38130(40)	360(40)
C(75)	80900(80)	2770(80)	39030(60)	380(50)
C(39)	92850(80)	24810(90)	19790(60)	450(50)
C(51)	69980(80)	1310(90)	22370(60)	420(50)
C(10)	134850(70)	79650(80)	8360(50)	350(40)
N(4)	67940(70)	1380(80)	26720(50)	710(50)

Crystal Structure Data

C(36)	97520(80)	29610(90)	18750(60)	460(50)
N(8)	79280(60)	19290(70)	83560(50)	470(40)
N(3)	76510(70)	10930(70)	25380(50)	570(40)
C(79)	68340(80)	17190(90)	44220(60)	510(50)
C(37)	101820(80)	32000(90)	22190(60)	560(50)
C(9)	136520(90)	79520(110)	3430(70)	810(70)
C(23)	142720(80)	84880(90)	13680(60)	520(50)
C(96)	80230(70)	16700(80)	79290(60)	370(50)
C(90)	67110(90)	19540(90)	59350(70)	660(60)
C(82)	59770(90)	23380(100)	36350(70)	630(60)
C(13)	119500(90)	61000(100)	20420(70)	610(60)
C(89)	72270(80)	18690(80)	62460(60)	410(50)
O(60)	82750(80)	30660(90)	41810(60)	1320(60)
C(35)	98000(90)	32080(100)	14200(70)	660(60)
C(102)	63180(80)	31490(80)	75300(60)	370(50)
O(20)	116350(90)	67740(110)	33390(70)	1660(80)
C(45)	75150(80)	2330(90)	13640(60)	510(50)
C(97)	75960(80)	19170(80)	75340(60)	390(50)
C(42)	83640(80)	16250(90)	20840(60)	440(50)
C(86)	72320(90)	15580(90)	52520(70)	580(60)
N(1)	131390(60)	74710(70)	9660(40)	430(40)
C(7)	130660(90)	69050(100)	2070(70)	640(60)
C(78)	72640(80)	14190(80)	47490(60)	420(50)
C(43)	81800(80)	12210(90)	17120(60)	490(50)
C(22)	136910(80)	85260(90)	11370(60)	420(50)
C(28)	147240(90)	77950(110)	13610(70)	800(70)
C(103)	58670(90)	35120(100)	72810(70)	650(60)
C(12)	125440(80)	64020(100)	8570(60)	520(50)
C(33)	106210(100)	39390(110)	16700(70)	720(60)
C(41)	80920(80)	16000(80)	25040(60)	420(50)
C(98)	76030(70)	17340(80)	70670(50)	320(40)
C(62)	61770(90)	-3160(90)	32850(60)	550(50)
N(7)	65100(70)	15860(70)	31550(50)	550(40)
C(44)	77270(80)	7050(90)	17210(60)	430(50)
C(99)	71930(70)	20200(80)	67310(50)	340(40)
C(92)	83230(80)	17810(90)	87310(70)	580(60)
C(59)	91200(80)	12870(90)	32030(60)	560(50)
C(4)	123250(90)	58890(100)	5800(70)	620(60)
C(24)	145580(110)	90340(120)	16530(80)	1000(80)
C(32)	110670(100)	44540(110)	15650(70)	720(60)
C(54)	86490(80)	18650(90)	32730(60)	470(50)
C(105)	56300(90)	40950(100)	79640(70)	690(60)
C(25)	141700(120)	96220(130)	16590(80)	990(80)
C(95)	85160(90)	12400(100)	78630(70)	650(60)
C(34)	102370(90)	36610(100)	13110(70)	760(70)
C(40)	88800(90)	21240(90)	20280(60)	530(50)
C(16)	117520(110)	65050(120)	28710(80)	850(70)
C(48)	63680(90)	-8190(110)	19730(70)	750(60)
C(46)	70540(90)	-2180(100)	14160(70)	740(60)
C(38)	106500(90)	36800(100)	21280(70)	710(60)
C(93)	88080(110)	13120(120)	86950(80)	950(80)
C(87)	77470(100)	14650(100)	55800(70)	790(70)
C(18)	123180(100)	57790(110)	23600(70)	700(60)
C(68)	53080(110)	4740(120)	29900(80)	970(80)
C(2)	118260(90)	54250(100)	12280(70)	680(60)
C(58)	77500(100)	26200(110)	29790(80)	840(70)
C(8)	134260(90)	74330(110)	590(70)	780(70)

Crystal Structure Data

C(31)	114090(90)	48870(100)	14340(60)	620(60)
C(1)	120880(80)	60010(90)	15030(60)	500(50)
C(11)	128960(80)	69570(90)	6770(60)	500(50)
C(104)	55280(100)	40000(110)	74810(70)	840(70)
C(80)	68400(70)	15440(70)	39520(50)	260(40)
C(66)	63720(120)	-6360(130)	40700(90)	1140(90)
C(71)	83110(90)	-2260(100)	31990(70)	680(60)
C(55)	87000(90)	21950(100)	36990(70)	640(60)
C(53)	81830(80)	20470(80)	29180(50)	360(50)
C(74)	85380(90)	-680(100)	41610(70)	670(60)
C(27)	133430(110)	91510(120)	11530(80)	860(70)
C(91)	67150(90)	17800(80)	54570(60)	530(50)
C(106)	60660(90)	37250(90)	82190(70)	620(60)
C(5)	125030(90)	58660(110)	1190(70)	690(60)
C(72)	87770(100)	-6080(110)	34420(80)	880(70)
C(88)	77310(100)	16250(100)	60640(70)	730(60)
C(67)	65450(90)	-7530(100)	35980(70)	630(60)
C(21)	127830(100)	52960(110)	22850(70)	760(70)
C(49)	61760(90)	-8260(100)	24350(70)	700(60)
C(65)	59680(130)	-2010(140)	41990(100)	1150(90)
C(83)	56160(90)	25930(110)	32520(70)	770(70)
C(50)	63810(90)	-3590(100)	27720(60)	560(60)
C(85)	61410(100)	18280(110)	27990(80)	780(70)
C(3)	119880(90)	53850(100)	7770(70)	660(60)
C(57)	78120(100)	29460(110)	34210(70)	810(70)
C(63)	57160(100)	1000(110)	33300(80)	780(70)
C(26)	135830(120)	96790(130)	13950(80)	1010(80)
C(19)	109630(110)	68060(120)	16730(80)	1030(80)
C(14)	113770(100)	65630(110)	20730(80)	830(70)
C(15)	113120(120)	67560(120)	25260(90)	1050(80)
C(29)	144780(130)	103210(150)	19550(100)	1380(100)
C(73)	89200(100)	-5060(110)	39270(70)	820(70)
C(56)	82500(110)	27070(130)	37460(90)	980(80)
C(81)	64040(90)	18410(100)	35750(70)	600(60)
C(61)	72960(90)	28650(100)	25860(70)	750(60)
C(84)	57050(90)	23340(110)	28150(70)	790(70)
C(94)	88990(100)	10490(110)	82530(70)	780(70)
C(17)	122310(110)	60450(120)	28680(80)	980(80)
C(70)	70530(100)	-12820(110)	35150(70)	860(70)
C(64)	56350(110)	1760(130)	38390(90)	1110(90)
C(6)	128360(80)	63260(100)	-590(70)	580(60)
C(30)	127480(140)	92730(140)	8610(100)	1380(100)
C(69)	57610(140)	-1150(150)	47390(110)	1510(110)
S(1)	58940(30)	50140(30)	92900(20)	818(19)
S(2)	58150(60)	45200(70)	29480(40)	1170(40)
S(2')	55810(70)	47310(80)	35840(50)	1470(50)
F(3)	56640(80)	40260(90)	98920(60)	1680(70)
F(2)	49170(70)	45490(70)	95970(40)	1190(50)
O(4)	53900(90)	41290(90)	27570(60)	1250(60)
F(1)	54010(80)	38130(100)	91970(70)	1720(70)
O(3)	60840(70)	53500(80)	97110(60)	1170(60)
O(4')	54970(90)	40890(110)	37630(60)	1490(70)
O(5)	63710(90)	41970(100)	30370(60)	1410(70)
O(1)	54320(100)	54120(120)	89980(80)	1870(90)
O(5')	60840(80)	50690(80)	38180(50)	1070(50)
C(107)	55290(140)	42700(170)	94420(120)	1310(110)
O(2)	63750(90)	46670(100)	91430(60)	1480(70)

Crystal Structure Data

O(6)	59310(70)	51370(90)	27740(50)	1170(60)
O(6')	50260(120)	51070(120)	34980(80)	1950(90)
O(1A)	61050(120)	17310(160)	12830(100)	1930(100)
O(2A)	108630(80)	70530(90)	1580(60)	1100(60)
O(3A)	60160(90)	59750(100)	81690(60)	1420(70)
O(5A)	92900(100)	26960(120)	47760(70)	1750(80)
O(7')	98880(120)	72930(150)	960(90)	2180(100)
C(10')	107560(170)	68100(200)	-2990(140)	1980(150)
C(11')	60320(180)	12600(200)	15870(140)	2100(170)
C(14')	113720(170)	70420(170)	4460(120)	1690(130)
C(20')	62350(140)	14090(170)	8380(120)	1620(120)
O(1B)	65140(130)	22160(150)	13710(90)	2140(110)
O(2B)	55200(120)	33940(130)	60240(90)	2300(110)
O(4B)	59540(120)	26730(140)	16890(90)	2270(110)
O(8')	123220(160)	62780(180)	39970(130)	3120(160)
C(6B)	100800(200)	66000(300)	3770(170)	2800(200)
C(7B)	70500(200)	38900(200)	44930(140)	2320(170)
C(8B)	58420(150)	27130(170)	10130(110)	1700(120)
C(9B)	63700(200)	35800(200)	45450(150)	2500(190)
C(10B)	55970(170)	64390(190)	81480(120)	1830(140)
C(11B)	120000(200)	79000(200)	-5750(150)	2240(180)
C(12B)	103600(200)	79600(200)	2160(140)	2340(180)
C(110)	94000(200)	19600(200)	50370(150)	2490(190)
C(18B)	118200(200)	84500(300)	-4440(160)	2600(200)
C(109)	123200(300)	63800(300)	45800(200)	3900(300)
C(26B)	111800(400)	76700(500)	-400(300)	4800(400)

Table 13-3: Anisotropic displacement parameters ($\text{\AA}^2 \times 10^4$) for **13**. The anisotropic displacement factor exponent takes the form: $\{-2 \pi^2 [h^2 a^{*2} U_{11} + \dots + 2 hka^*b^*U_{12}]$

Atom	U_{11}	U_{22}	U_{33}	U_{23}	U_{13}	U_{12}
Zn(2)	608(17)	617(16)	421(14)	10(12)	107(12)	-21(13)
Zn(1)	505(15)	519(14)	425(14)	-33(12)	143(11)	-17(13)

Table 13-4: Hydrogen coordinates ($\times 10^4$) and isotropic displacement parameters ($\text{\AA}^2 \times 10^3$) for **13**.

Atom	x	y	z	U_{eq}
H(10A)	6444	2656	6666	39
H(77A)	7972	717	4808	41
H(79A)	6538	2042	4520	61
H(37A)	10162	3035	2530	67
H(9A)	13912	8301	230	97
H(90A)	6343	2134	6047	80
H(82A)	5926	2511	3941	75
H(35A)	9510	3047	1176	80
H(45A)	7706	235	1077	61
H(43A)	8369	1292	1429	59
H(10B)	5787	3421	6955	79
H(98A)	7897	1403	6977	39
H(92A)	8272	1998	9023	70
H(24A)	14956	9003	1816	120
H(10D)	5389	4425	8115	83
H(95A)	8592	1080	7559	78
H(34A)	10279	3786	994	91
H(48A)	6221	-1154	1747	91
H(46A)	6900	-492	1156	89

Crystal Structure Data

H(38A)	10962	3817	2362	85
H(93A)	9068	1177	8964	114
H(87A)	8120	1290	5474	95
H(8A)	13521	7435	-259	94
H(10C)	5230	4271	7299	101
H(66A)	6580	-910	4310	136
H(71A)	8251	-251	2866	82
H(55A)	9012	2086	3941	77
H(74A)	8591	-15	4492	81
H(91A)	6339	1819	5264	63
H(10E)	6131	3795	8548	74
H(5A)	12367	5482	-72	82
H(72A)	9002	-941	3280	106
H(88A)	8095	1554	6267	88
H(49A)	5890	-1174	2512	84
H(83A)	5313	2941	3291	93
H(85A)	6187	1627	2500	94
H(3A)	11860	4991	593	79
H(57A)	7552	3324	3489	97
H(26A)	13364	10107	1394	121
H(15A)	10982	7048	2604	126
H(73A)	9265	-729	4089	98
H(84A)	5475	2498	2540	95
H(94A)	9229	733	8218	94
H(17A)	12481	5904	3140	117
H(64A)	5338	503	3928	133
H(6A)	12931	6280	-375	69

7.14 Crystal Structure Data of 14 (In Cooperation with Dr. Jan W. Bats, Johann Goethe-University, Frankfurt am Main, Germany).¹⁰

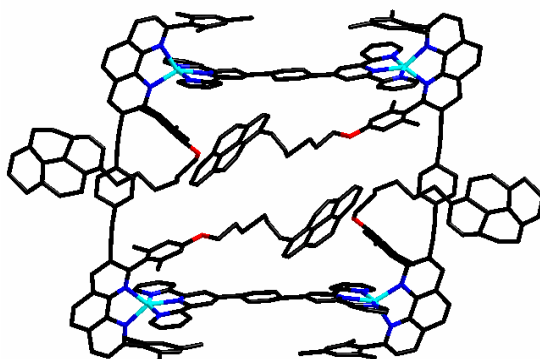


Figure 14-1. Stick representation of 14.

Table 14-1: Crystal data and structure refinement for **14**.

Substance	14
Sum formula	Zn ₄ C ₃₀₄ H ₂₃₆ F ₂₄ N ₂₀ O ₂₈ S ₈
Formula weight /g·mol ⁻¹	5591.09
Temperature /K	162(2)
Wavelength /pm	0.71073 Å
Crystal system, space group	Triclinic, <i>P</i> -1
Unit cell dimensions	a = 14.275 (2) Å b = 23.700 (4) Å c = 26.119 (5) Å $\beta = 78.716 (6)^\circ$
Volume /Å ³	7788 (2)
Z, Calculated density /Mg·m ⁻³	1, 1.192
Absorption coefficient /mm ⁻¹	0.435
F(000)	2888
Crystal size (mm)	0.30 x 0.15 x 0.05
Reflections collected / unique / R _{int}	41110 / 19983 / 0.2854
Refinement method	Full-matrix least-squares on <i>F</i> ²
Data / restraints / parameters	19983 / 0 / 725
Goodness-of-fit on <i>F</i> ²	1.014
Final <i>R</i> indices [<i>I</i> > 2σ(<i>I</i>)]	<i>R</i> 1 = 0.1758, <i>wR</i> 2 = 0.3395
<i>R</i> indices (all data)	<i>R</i> 1 = 0.3631, <i>wR</i> 2 = 0.4143
Largest diff. peak and hole	0.750 and -0.515 e/Å ³

Table 14-2: Atomic coordinates (x 10⁵) and equivalent isotropic displacement parameters (Å² x 10⁴) for **14**. *U*(eq) is defined as one third of the trace of the orthogonalized *U*_{ij} tensor.

Atom	x	y	z	<i>U</i> _{eq}
S(2)	9329(8)	-3431(4)	3902(5)	170(4)
O(6)	9379(11)	-4049(8)	4367(7)	91(5)
O(7)	8722(17)	-2982(12)	4092(10)	189(10)
C(150)	9980(30)	-3190(20)	3307(19)	204(18)
F(4)	11008(17)	-3489(12)	3749(10)	235(10)
F(5)	10590(20)	-2722(14)	3587(12)	295(13)
S(1)	2074(5)	1110(3)	-691(3)	85(2)
O(4)	2186(8)	1144(5)	-1263(5)	47(4)
O(5)	1326(10)	1562(7)	-604(6)	84(5)
O(3)	2011(14)	453(9)	-174(8)	142(7)
F(3)	3324(13)	1986(10)	-1160(9)	170(8)
F(1)	3924(11)	1073(7)	-791(6)	134(6)
F(2)	3172(16)	1481(10)	-203(11)	202(10)
C(149)	3250(20)	1572(17)	-640(18)	138(13)
Zn(1)	7316(2)	300(1)	1903(1)	46(1)
Zn(2)	94(2)	5163(1)	2642(1)	43(1)
C(79)	1377(12)	-6077(8)	7305(7)	26(5)
N(1)	6244(9)	886(6)	2052(6)	26(4)

Crystal Structure Data

N(4)	957(11)	4420(7)	2600(7)	45(5)
C(83)	-3215(17)	-5250(11)	8321(11)	79(8)
N(5)	719(12)	4841(8)	3400(7)	63(5)
N(7)	8642(11)	320(7)	1417(7)	54(5)
C(87)	-4080(16)	-4761(10)	8456(9)	72(7)
C(74)	743(12)	-7079(7)	8089(7)	25(5)
N(9)	1267(11)	-5366(7)	7004(6)	49(5)
C(24)	2130(15)	3538(10)	2546(9)	61(6)
N(8)	7604(11)	-667(6)	2293(6)	35(4)
C(70)	3072(15)	-6005(10)	6792(8)	59(6)
C(85)	-2463(18)	-5868(11)	7918(10)	86(8)
C(1)	5693(12)	1095(7)	1725(7)	22(4)
C(52)	7226(14)	2416(9)	465(8)	56(6)
C(18)	3157(13)	3057(8)	1878(8)	41(5)
C(71)	2258(13)	-6358(8)	7214(7)	32(5)
C(120)	1896(14)	-3942(9)	6543(8)	50(6)
C(84)	-3219(17)	-5372(11)	7912(11)	87(8)
O(1)	3438(11)	-118(7)	3195(7)	96(5)
C(21)	3870(15)	2148(10)	2858(9)	64(7)
N(3)	6467(11)	523(7)	1239(6)	42(4)
N(6)	-257(10)	5074(6)	1889(6)	37(4)
C(78)	571(12)	-6416(8)	7753(7)	27(5)
C(92)	4430(15)	-346(9)	3065(8)	50(6)
C(69)	2924(19)	-5338(13)	6443(11)	94(9)
C(68)	2004(14)	-5033(8)	6587(7)	40(5)
C(26)	984(12)	4292(7)	2189(7)	24(5)
C(96)	5547(12)	-985(8)	2039(7)	31(5)
C(75)	-76(14)	-7412(9)	8530(8)	49(6)
C(53)	7463(15)	2041(10)	151(8)	59(6)
N(10)	-311(11)	-6141(6)	7841(6)	36(4)
C(8)	7950(20)	652(13)	3547(11)	101(9)
C(119)	1698(13)	-4337(9)	6275(8)	42(5)
C(104)	715(19)	2822(13)	1581(13)	108(10)
C(125)	2076(14)	-4177(9)	7112(8)	51(6)
C(124)	1582(14)	-4201(9)	5709(8)	53(6)
C(41)	9949(17)	-1426(11)	2030(10)	74(7)
C(66)	4061(14)	-4564(10)	5639(9)	47(6)
C(32)	264(14)	4586(9)	1761(8)	50(6)
C(33)	275(17)	4586(11)	1244(11)	91(8)
C(117)	-1160(20)	3777(12)	715(11)	104(9)
C(22)	1465(15)	4140(10)	2972(9)	59(6)
C(59)	6330(15)	-2645(10)	3823(10)	59(6)
C(93)	4498(15)	-511(9)	2578(9)	64(7)
C(42)	10481(13)	-1035(9)	1622(8)	42(5)
C(35)	-978(15)	5368(10)	1054(9)	69(7)
N(2)	7759(13)	409(8)	2638(7)	68(5)
C(43)	10053(13)	-415(8)	1353(7)	39(5)
C(17)	3854(13)	2624(8)	1862(7)	36(5)
C(47)	9061(17)	-313(11)	1597(9)	77(7)
C(116)	-2160(30)	3949(15)	760(15)	154(13)
C(67)	3522(16)	-4929(10)	6002(10)	59(6)
C(25)	1622(14)	3828(9)	2078(8)	56(6)
C(100)	670(30)	969(19)	3339(17)	198(16)
C(51)	7661(15)	2178(10)	1009(9)	67(7)
C(19)	2940(14)	3054(9)	2413(8)	50(6)
C(63)	4632(18)	-4057(12)	5167(10)	86(8)
C(107)	-1181(16)	3004(10)	1772(10)	65(7)

Crystal Structure Data

C(89)	6050(13)	-878(8)	2880(7)	32(5)
C(95)	6576(14)	-869(9)	3772(8)	62(6)
C(40)	8838(13)	-1328(9)	2283(7)	38(5)
C(20)	3156(15)	2608(10)	2948(9)	64(7)
C(134)	3587(18)	-4043(13)	3825(11)	91(8)
C(14)	6114(17)	452(11)	432(10)	78(8)
C(30)	1010(20)	4887(13)	4254(12)	113(10)
C(60)	5764(19)	-3071(12)	4281(11)	90(8)
C(48)	8422(14)	-782(8)	2092(8)	35(5)
C(38)	7402(15)	-1721(9)	2950(8)	54(6)
C(36)	-901(14)	5435(9)	1574(8)	55(6)
C(34)	-464(18)	4973(12)	848(11)	100(9)
C(147)	4390(20)	-5411(18)	3544(14)	156(13)
C(50)	8383(14)	1706(9)	1084(8)	57(6)
C(11)	5712(18)	850(11)	1224(10)	76(7)
C(108)	-794(17)	2652(11)	2247(10)	73(7)
C(31)	607(13)	5101(8)	3761(8)	40(5)
C(65)	6053(14)	-3750(9)	4435(8)	51(6)
C(102)	710(20)	1969(16)	2693(13)	141(12)
C(140)	5930(20)	-3462(18)	1931(15)	170(14)
C(57)	8373(14)	1207(9)	-135(8)	59(6)
C(39)	8435(15)	-1849(10)	2753(9)	62(7)
C(3)	4906(13)	1646(8)	2262(8)	40(5)
C(97)	3308(18)	110(11)	3670(10)	94(8)
C(146)	4830(20)	-5666(14)	3198(15)	124(11)
C(64)	5480(14)	-4208(9)	4883(8)	46(6)
C(9)	8650(20)	265(13)	3448(12)	115(10)
C(4)	5545(14)	1451(8)	2592(8)	42(5)
C(123)	1480(17)	-3510(12)	5395(10)	80(8)
C(55)	8969(14)	1577(9)	1586(8)	55(6)
C(37)	6993(14)	-1040(9)	2702(8)	44(6)
C(121)	1682(18)	-3298(12)	6158(12)	99(9)
C(126)	1626(15)	-4591(10)	5396(9)	76(7)
C(73)	1680(14)	-7360(9)	7980(8)	46(6)
C(62)	4440(20)	-3453(16)	5048(13)	123(11)
C(82)	-2817(15)	-5440(10)	8791(9)	60(6)
C(46)	9141(15)	819(9)	913(8)	54(6)
C(54)	8146(16)	1561(11)	289(10)	75(7)
C(5)	6293(15)	1046(9)	2521(8)	57(6)
C(23)	2212(14)	3654(9)	3015(8)	59(6)
C(2)	4869(14)	1486(9)	1777(8)	54(6)
C(80)	-1860(20)	-6034(13)	8336(13)	120(10)
C(12)	5141(17)	1058(11)	861(10)	80(8)
C(135)	3623(16)	-4609(11)	3880(9)	66(7)
C(112)	-3850(20)	2967(15)	2541(13)	131(11)
C(106)	-610(20)	3323(12)	1138(11)	91(8)
C(27)	1384(13)	4366(8)	3443(7)	34(5)
C(77)	-1020(15)	-6452(10)	8233(9)	53(6)
C(114)	-3660(20)	3639(13)	1504(12)	111(10)
C(72)	2352(13)	-7036(8)	7591(7)	35(5)
C(15)	6603(15)	239(10)	835(9)	65(7)
C(49)	8551(15)	1363(10)	770(9)	58(6)
C(99)	1990(30)	790(20)	3143(18)	211(18)
O(2)	1448(16)	-2471(11)	5357(11)	160(8)
C(58)	6790(13)	-2239(9)	3404(8)	41(5)
C(56)	6363(16)	2854(10)	370(9)	76(7)
C(113)	-4229(19)	3334(13)	2079(13)	105(9)

Crystal Structure Data

C(6)	7006(14)	731(8)	2869(8)	43(6)
C(103)	170(20)	2484(14)	2241(13)	126(11)
C(129)	2440(30)	-1805(16)	3757(16)	175(14)
C(145)	5370(30)	-5284(19)	2710(17)	151(13)
C(28)	1768(18)	4075(12)	3952(12)	107(9)
C(131)	3310(20)	-2740(17)	3560(14)	168(14)
C(141)	6000(30)	-4120(20)	1981(18)	164(14)
C(61)	5000(20)	-2999(13)	4610(13)	109(10)
C(90)	5878(12)	-744(7)	3349(7)	25(5)
C(44)	10518(13)	226(9)	844(8)	46(6)
C(91)	4921(15)	-478(9)	3459(9)	63(7)
C(81)	-2007(16)	-5850(10)	8794(10)	73(7)
C(94)	5478(13)	-776(8)	2519(7)	36(5)
C(111)	-2800(20)	2828(13)	2487(12)	103(9)
C(29)	1607(18)	4354(12)	4339(10)	95(9)
C(7)	7193(16)	855(10)	3319(9)	64(7)
C(76)	-854(16)	-7066(11)	8575(9)	69(7)
C(88)	-2325(12)	-6076(8)	7415(7)	39(5)
C(137)	4860(20)	-4416(14)	2983(13)	122(10)
C(133)	4190(20)	-3581(14)	3314(13)	108(10)
C(139)	5270(20)	-3206(13)	2329(12)	109(9)
C(13)	5324(19)	857(12)	441(11)	99(9)
C(86)	-1387(14)	-6142(9)	9251(8)	55(6)
C(127)	1470(20)	-2175(16)	4797(16)	161(14)
C(118)	-2290(20)	3176(13)	1860(13)	116(10)
C(136)	4050(30)	-4830(18)	3594(15)	151(13)
C(16)	4153(14)	2118(9)	2318(8)	51(6)
C(132)	4200(20)	-2864(17)	3136(14)	158(13)
C(110)	-2210(20)	2409(13)	2891(11)	105(9)
C(45)	10018(14)	787(9)	617(8)	46(6)
C(115)	-2680(20)	3612(13)	1360(13)	107(10)
C(143)	6590(20)	-4850(18)	1624(15)	170(14)
C(130)	3310(20)	-2021(16)	3411(13)	144(12)
C(128)	2640(20)	-2186(15)	4462(14)	159(13)
C(142)	6660(30)	-4090(20)	1512(18)	205(17)
C(138)	4710(20)	-3700(15)	2955(14)	126(11)
C(101)	520(20)	1379(16)	2715(14)	137(11)
C(10)	8506(18)	197(11)	2921(11)	93(8)
C(105)	370(20)	3146(14)	1129(13)	127(11)
C(148)	5450(30)	-4620(30)	2480(20)	220(19)
C(144)	6010(20)	-5351(13)	2211(13)	116(10)
C(98)	2130(30)	290(20)	3640(20)	240(20)
C(122)	1610(20)	-3171(14)	5592(13)	110(10)
C(109)	-1260(20)	2331(13)	2886(12)	117(10)

Table 14-3. Anisotropic displacement parameters ($\text{\AA}^2 \times 10^4$) for **14**. The anisotropic displacement factor exponent takes the form: $\{-2 \pi^2 [h^2 a^{*2} U_{11} + \dots + 2 hka^*b^*U_{12}]\}$.

Atom	U_{11}	U_{22}	U_{33}	U_{23}	U_{13}	U_{12}
S(2)	216(12)	83(7)	174(10)	-36(7)	-9(9)	20(7)
S(1)	122(7)	53(5)	52(4)	-11(4)	9(4)	22(4)
Zn(1)	51(2)	37(2)	46(2)	-18(1)	-3(1)	13(1)
Zn(2)	56(2)	28(2)	39(2)	-14(1)	-7(1)	19(1)

- (1) (a) G.R.Desiraju, *Crystal Engineering. The Design of Organic Solids*; Elsevier, Amsterdam, **1989**. (b) *Encyclopedia of Supramolecular Chemistry*, J.L.Atwood and J. Steed (Eds.), Marcel Dekker, New York, **2004**. (c) D. Braga, *Chem. Commun.* **2003**, 2751.
- (2) **Supp 3-1.**
- (3) **Supp 4-2.**
- (4) **Chapter IV.**
- (5) **Supp 4-3.**
- (6) **Supp 4-4.**
- (7) **Supp 4-5.**
- (8) **Supp 6-1.**
- (9) **Supp 6-2.**
- (10) **Supp 6-3.**

CHAPTER 8

8. Summary and Keywords

Keywords: Self-assembly, HETPHEN, HETTAP, nanostructures, dynamic, sensors, crystal structures and STM.

The key-results of the present thesis are:

- (1) **Mechanistic Insight into the HETPHEN Approach**
- (2) **Synthesis of a Variety of Rigid Bisphenanthrolines and Study of their Self-Assembly Behavior in Solution, in the Solid state and at Solid-Liquid Interfaces**
- (3) **Multicomponent Self-Assembly Using a Nanoscale Macrocyclic**
- (4) **The HETTAP Concept**

(1) Detailed mechanistic investigations by ^1H NMR and UV-vis into the HETPHEN (**heteroleptic phenanthroline** complexes) approach led to a deeper understanding about the bias present between homo and heteroleptic copper(I) bisphenanthroline complexes. Interestingly, two scenarios were found in the small series of ligands investigated.

a) In case of ligands with arylmethyl steric stoppers, a high kinetic barrier, due to the sterically bulky *ortho*-methyl groups, prevents the formation of the homoleptic combination. As a consequence, the principle of maximum occupancy drives the coordination equilibrium towards the heteroleptic complex .

b) In contrast, in case of ligands with arylmethoxy steric stoppers, the situation is completely different as the homoleptic complex becomes the only product in nitrile-free solvents. In presence of a second phenanthroline, the heteroleptic complex becomes thermochemically preferred because the homoleptic complexes are sterically destabilized.

Further exploration of these principles paved the way to realize the first kinetically stable copper(I)bisphenanthroline complex. The photophysical properties of this complex were found to be very promising and suggesting a design for more efficient photoactive copper(I) based complexes.

(2) A family of rigid linear bisphenanthrolines with or without bulky groups at the bisimine site has been synthesized. Four of these nanoscale bisphenanthrolines were characterised in the solid state. A small family of the bisphenanthrolines could be imaged on surface,

which makes them very attractive candidates for surface chemistry. Using these bisphenanthrolines a family of multicomponent nanoracks, nanogrids and nanoscaffolds was self-assembled for the first time.

- (3) The macrocycle that had earlier been synthesised by Horst Ammon was used to prepare multicomponent nanoedifices, nanobasket and nanoscaffolds. However, due to the large void present in these aggregates, it was not possible to obtain suitable single crystals for X-ray analysis. This forced us to investigate and develop a battery of both direct and indirect solution state characterization techniques, which provided unambiguous evidence for the proposed structures.

HRTEM investigations of a few nanoscaffolds and a simple bisphenanthroline copper(I) complex led to the invention of a novel non-aqueous method to generate pure copper nanoparticles with 3-5 nm dimensions.

- (4) Inspired by the success of the HETPHEN approach, a novel multicomponent strategy HETTAP (**h**eteroleptic **t**erpyridine **a**nd **p**henanthroline complexes) was developed. Following the HETTAP strategy, several multicomponent supramolecular structures could be assembled. Since the resulting aggregates proved to be fluorescent, this approach gave ready access to novel photophysically active architectures. Although both approaches are conceptually very similar, unlike the HETPHEN concept, the HETTAP approach is more useful in preparing fluorescent heterotopic supramolecular aggregates.

A heteroleptic dumbbell and a clip proved sensitive towards Hg^{2+} (driven by metal exchange) monitored by fluorescence quenching and towards Pb^{2+} shown through fluorescence enhancement. Due to their dynamic nature, ligand/metal exchange experiments could be performed in ladder, clip and dumbbell aggregates.

Using the HETTAP approach, internally functionalised nanoladders were assembled and their properties explored as a function of the supramolecular environment.

CHAPTER 8

8. Zusammenfassung and Keywords

Keywords: Self-assembly, HETPHEN, HETTAP, nanostructures, dynamic, sensors, crystal structures and STM.

Die wichtigsten Ergebnisse der vorgelegten Dissertation sind:

- (1) **Mechanistische Einblicke in des HETPHEN-Konzept.**
- (2) **Synthese einer Vielzahl von starren Bisphenanthrolinen und Studien ihres Selbstassemblierungsverhaltens in Lösung, im Feststoff und an der Fest-Flüssig Grenzfläche.**
- (3) **Multikomponenten Selbsassemblierungsreaktionen unter Nutzung eines Nanomacrozyklus.**
- (4) **Das HETTAP-Konzept.**

(1) Detaillierte mechanistische Untersuchungen mittels $^1\text{H-NMR}$ and UV-Vis zum HETPHEN (**heteroleptic phen**anthroline complexes) Konzept führten zu einem tieferen Verständnis über die vorhandenen Unterschiede von homo- und heteroleptischen Kupfer-(I)-Bisphenanthrolin-Komplexen. Interessanterweise wurden innerhalb der Serie der untersuchten Liganden zwei Szenarien gefunden:

a) Im Fall von Liganden mit Arylmethyl-Gruppen als sterische Stopper verhindert eine hohe kinetische Barriere, aufgrund der sterisch anspruchsvollen *ortho*-Methyl-Gruppen, die Bildung der homoleptischen Kombination. Als Konsequenz wird durch das Prinzip der maximalen Besetzung (“principle of maximum occupancy”) das Komplexbildegleichgewicht auf die Seite des heteroleptischen Komplexes verschoben.

b) Im Fall von Liganden mit Arylmethoxy-Gruppen als sterische Stopper ist die Situation völlig anders und der homoleptische Komplex wird jetzt zum einzigen Produkt in Nitril-freien Lösungsmitteln. Es ist zu beachten, dass in Gegenwart eines zweiten Phenanthrolins der heteroleptische Komplex thermodynamisch bevorzugt wird, weil die homoleptischen Komplexe sterisch destabilisiert sind.

Die weitere Aufklärung dieser Prinzipien ebnete den Weg zur Realisierung des ersten kinetisch stabilen Kupfer-(I)-Bisphenanthrolin-Komplexes. Die photophysikalischen Eigenschaften dieses Komplexes erwiesen sich als sehr vielversprechend für das Design effizienterer photoaktiver Kupfer-(I)-basierter Komplexe.

(2) Es wurde eine Reihe von starren, linearen Bisphenanthrolinen, mit und ohne sterische Gruppen an der Bisimin-Koordinationstelle synthetisiert. Vier dieser nanoskalierten Bisphenanthroline wurden im Feststoff charakterisiert. Eine kleine Gruppe von Bisphenanthrolinen konnte auf der Oberfläche abgebildet werden, was diese zu sehr attraktiven Kandidaten für die Oberflächen-Chemie macht. Durch Verwendung dieser Bisphenanthroline wurde erstmals eine Reihe von multikomponenten “Nanoregalen”, “Nanogittern” und “Nanogerüsten” durch Selbstassemblierung dargestellt.

(3) Der zuvor von Horst Ammon synthetisierte Makrozyklus wurde zur Darstellung von Multikomponenten-Nanogefügen verwendet, wie etwa eines “Nanokorbs” und “Nanogerüsten”. Aufgrund des großen Hohlraums in diesen Aggregaten war es allerdings nicht möglich, verwertbare Einkristalle für die Röntgenstrukturanalyse zu erhalten. Dies zwang uns zur Entwicklung einer Reihe von sowohl direkten als auch indirekten Charakterisierungs-techniken in Lösung, durch die unzweideutig die vorgeschlagenen Strukturen bestätigt werden konnten.

HRTEM-Untersuchungen einer Reihe von “Nanogerüsten” und eines einfachen Bisphenanthrolin-Kupfer-(I)-Komplexes führten zur Entwicklung einer neuen, nicht-wässrigen Methode für die Erzeugung reiner Kupfer-Nanopartikel mit Dimensionen von 3-5 nm.

(4) Angeregt durch den Erfolg des HETPHEN-Konzepts, wurde die neue Multikomponenten Strategie HETTAP (**h**eteroleptic **t**erpyridine **a**nd **p**henanthroline complexes) entwickelt. Durch die Anwendung der HETTAP-Strategie konnten verschiedenste supramolekulare Multikomponenten-Strukturen assembliert werden. Da sich die resultierenden Aggregate als fluoreszierend erwiesen, ermöglichte dieser Ansatz den leichten Zugang zu neuen photophysikalischaktiven Architekturen. Obwohl beide Ansätze konzeptionell sehr ähnlich sind, ist das HETTAP-Konzept, ganz im Unterschied zum HETPHEN-Ansatz, eher brauchbar für die Darstellung fluoreszierender, heterotoper supramolekularer Aggregate.

Eine heteroleptische Hantel (“dumbbell”) und eine Klammer (“clip”) erwiesen sich als empfindlich gegenüber Hg^{2+} (getrieben durch Metall-Austausch), was durch eine Fluoreszenz-Löschung beobachtbar war und erwiesen sich als ebenfalls empfindlich

gegenüber Pb^{2+} , was in Form einer Fluoreszenz-Verstärkung sichtbar wurde. Aufgrund ihrer dynamischen Natur konnten Liganden/Metall-Austausch-Experimente sowohl in "Leiter"-, "Klammer"-, als auch in "Hantel"-Aggregaten ausgeführt werden.

Unter Verwendung des HETTAP-Ansatzes wurden intern funktionalisierte "Nanoleiterstrukturen" assembliert und ihre Eigenschaften als eine Funktion der supramolekularen Umgebung aufgeklärt.

Resume

Name Venkateshwarlu Kalsani
Date of Birth 10-06-1973
Fathers Name Rama Chandraiah Kalsani
Educational Qualification M. Sc.
Specialisation Organic Medicinal Chemistry
Present Occupation PhD student at Uni-Siegen

Educational Background:

Educational Level	University/Board	Year of Passing	Grades/Div obtained
High School (10 th)	Board of Secondary Education, Andhra Pradesh	March-1989	63.1 %/ First Div
Senior School (12 th)	Board of Intermediate Education, Andhra Pradesh	April-1991	53.5 %/Second Div
BSc (BZC) ^a	Kakatiya University, Warangal, India	June-1994	69.1 %/First Div.
MSc (Chem.) ^b	Kakatiya University, Warangal, India	April-1997	77.7%/Distinction with University Second Rank
PhD courses (2 sem.)	IIT-Powai, Mumbai	June-1999	7.10 ^(cpi) /First

^a BSc (BZC) = Bachelors of Science with Botany, Zoology and Chemistry as main subjects, ^b MSc (Chem.) = Masters of Science with Chemistry and specialising in Organic and Medicinal Chemistry. ^(cpi) = Cumulative Performance Index.

Work Experience:

Institute/Company	Address	Duration	Position
Indian Institute of Chemical Technology	Hyderabad, India	January-1998 to June-1998	Project Assistant

(IICT)-Hyderabad			
IIT-Powai	Powai, Mumbai	August-1998 to November- 1999	Junior Research Fellow at Chemistry Dept.
University of Siegen	Siegen, Germany	February- 2000-till date	Research Associate at University of Siegen

Languages Known Telugu, Hindi, English, German.

Marital Status Single

Permanent Address c/o: B Sanjeeva Reddy, 1-7-1384 F, Dr. B. Reddy
Bhavan, Advocates Colony-Hanamkonda,
Warangal, Andhra Pradesh 506001, India.

Present Address Engsbach Strasse 56, 237
Siegen-57068, Germany
Tel: +49-271-4058330 or +49-179-3209566
e.mail: kalsani@chemie.uni-siegen.de or
kalsaniv@yahoo.com

Publications:

-
- 1 M. Schmittel, C. Michel, A. Wiegrefe, **V. Kalsani**
"Synthesis of Soluble, Linear Bisphenanthrolines for the Construction of Heteroleptic NanoGrids and Nanoboxes"
Synthesis **2001**, 1561-1567.
 - 2 M. Schmittel, H. Ammon, **V. Kalsani**, A. Wiegrefe, C. Michel
"Quantitative Formation and Clean Metal Exchange Processes of Large Void (> 5000 Å³) Nanobox Structures"
Chem. Commun. **2002**, 2566-2567.
 - 3 M. Schmittel, **V. Kalsani**, D. Fenske, A. Wiegrefe
"Self-assembly of Heteroleptic [2x2] and [2x3] Nanogrids"
Chem. Commun. **2004**, 490-491.
 - 4 **V. Kalsani**, H. Ammon, F. Jäckel, J. P. Rabe, M. Schmittel
"Synthesis and Self-Assembly of a Rigid Exotopic Bisphenanthroline Macrocyclic: Surface Patterning and a Supramolecular Nanobasket"
Chem. Eur. J. **2004**, *10*, 5481-5492.
 - 5 M. Schmittel, **V. Kalsani**, L. Kienle
"Simple and Supramolecular Copper Complexes as Precursors in the HRTEM Induced Formation of Crystalline Copper Nanoparticles"
Chem. Commun. **2004**, 1534-1535.
 - 6 M. Schmittel, **V. Kalsani**
"Functional, Discrete, Nanoscale Supramolecular Assemblies"
Topics in Current Chemistry. **2005**, *245*, 1-53.
-

-
- 7 **V. Kalsani**, H. Bodenstedt, D. Fenske, M. Schmittel
“Supramolecular Copper Phenanthroline Racks: Structures, Mechanistic Insight and Dynamic Nature”
Eur. J. Inorg. Chem. **2005**, 1841-1849.
 - 8 M. Schmittel, **V. Kalsani**, J. W. Bats
“Metal-Driven and Covalent Synthesis of Supramolecular Grids from Dynamic Racks: A Convergent Approach to Heterometallic and Heteroleptic Nanostructures”
Inorg. Chem. **2005**, 44, 4115-4117.
Also, featured in the most-accessed articles: April-June, **2005**, *Inorg. Chem.*-ACS publications.
 - 9 M. Schmittel, **V. Kalsani**, R. S. K. Kishore, H. Cölfen, J. W. Bats
“Dynamic and Fluorescent Nanoscale Phenanthroline/Terpyridine Zinc(II) Ladders. Self Recognition in Unlike Ligand/Like Metal Coordination Scenarios”
J. Am. Chem. Soc. **2005**, 127, 11545-11546.
 - 10 **V. Kalsani**, M. Schmittel, A. Listorti, G. Accorsi, N. Armaroli
“Novel Phenanthroline Ligands and Their Kinetically Locked Copper(I) Complexes with Unexpected Photophysical Properties”
Inorg. Chem. **2006**, 45, 2061-2067.
 - 11 M. Schmittel, **V. Kalsani**, F. Jackel, J.-P. Rabe, J. W. Bats, D. Fenske
“Rigid Bisphenanthrolines: Synthesis, Structure and Self-Assembly at the Solid-Liquid Interface”
Eur. J. Org. Chem. **2006**, in early view. Also, chosen for the cover page.
-

Accepted for Publication:

- 12 “M. Schmittel, **V. Kalsani**, P. Mal, J. W. Bats
The HETTAP Approach: Self-Assembly and Metal Ion Sensing of Dumbbell-Shaped Molecules and Clip Molecules”
Inorg. Chem. **2006**, in press.
 - 13 H. Meng, **V. Kalsani**, K. Kumar
“Fluorinated Amino Acids and Reagents in Protein Design and Biomolecule Separation” *ACS Symposium Series*, **2006**, in press.
-

Manuscripts in Preparation:

- 14 M. Schmittel, A. Ganz, M. Schlosser, H.-J. Deiseroth, S. X. Liu, **V. Kalsani**
“The HETPHEN approach - Selective Formation of HETeroleptic Cu(I) BisPHENanthroline Complexes, Racks and Spiral Assemblies: Interplay of π - π Interactions, Solvent Association, and Steric Hindrance”
 - 15 K. Kumar, **V. Kalsani**, N. Yoder
“Semifluorinated PhosphotidylCholine: Synthesis and Phase-separation at Surfaces Studied by AFM”
 - 16 M. Schmittel, **V. Kalsani**, A. Wiegrefe, C. Michel
“Heteroleptic Bisphenanthroline Metallo-Nanoscaffolds – A Model Case for the Solution State Characterisation of Supramolecular Nano-Edifices”
 - 17 **V. Kalsani**, M. Schmittel, A. Listorti, G. Accorsi, N. Armaroli
“Multi-Ligand/Metal Dynamic Rack Structures; Self-assembly, Structural Features, Absorption Spectra, Luminescence Properties”
 - 18 K. Kumar, **V. Kalsani**, L. Dafik.
“Synthesis of Semifluorinated Biotinylated Lipids and Their Interaction with Cell Membranes”
 - 19 K. Kumar, **V. Kalsani**.
“Novel Synthesis of Semifluorinated Fatty Acids; Self-Assembly in Solution and in Solid State”
 - 20 M. Schmittel, **V. Kalsani**, B. He, J. W. Bats
“A Functional Nanoscale Ladder Containing Ferrocene Units”
-

-
- 21 M. Schmittel, **V. Kalsani**, B. He, J. W. Bats
“Zn(II)/Ag(I) Nanoscale 2D Ladders Containing Pyrene Units”
- 22 M. Schmittel, **V. Kalsani**
“*Multicomponent Supramolecular Strategies*” (review)
-

Collaborations:

- 1 **Single Crystal Analysis:** Prof. Dieter Fenske, University of Karlsruhe, Germany.
Prof. H. J. Deiseroth, University of Siegen, Germany.
Prof. M. U. Schmidt, University of Frankfurt, Germany.
Dr. J. W. Bats, University of Frankfurt, Germany.
- 2 **AFM and STM Investigations:** F. Jäckel, Prof. J. P. Rabe, Humboldt University, Berlin, Germany
- 3 **TEM Investigations:** Dr. L. Kienle, Max-Planck-Institute für Festkörperforschung Heisenbergstraße 1, Stuttgart, Germany.
- 4 **Photophysical studies:** Prof. N. Armaroli, Istituto per la Sintesi Organica e la Fotoreattività, Laboratorio di Fotochimica, Bologna, Italy.
- 5 **Analytical Ultracentrifugation:** Prof. H. Cölfen, Max-Planck-Institute of Colloids and Interfaces, Golm, Germany.
-